Aerodynamic Theory

A General Review of Progress

Under a Grant of the Guggenheim Fund
for the Promotion of Aeronautics

William Frederick Durand
Editor-in-Chief

Volume IV

Div. J · Applied Airfoil Theory · A. Betz
Div. K · Airplane Body (Non-Lifting System) Drag
and Influence on Lifting System · C. Wieselsberger
Div. L · Airplane Propellers · H. Glauert
Div. M · Influence of the Propeller on other Parts
of the Airplane Structure · C. Koning

With 321 Figures

Berlin · Julius Springer · 1935

ISBN-13: 978-3-642-89630-9 e-ISBN-13: 978-3-642-91487-4
DOI: 10.1007/978-3-642-91487-4

GENERAL PREFACE

During the active life of the Guggenheim Fund for the Promotion of Aeronautics, provision was made for the preparation of a series of monographs on the general subject of Aerodynamic Theory. It was recognized that in its highly specialized form, as developed during the past twenty-five years, there was nowhere to be found a fairly comprehensive exposition of this theory, both general and in its more important applications to the problems of aeronautic design. The preparation and publication of a series of monographs on the various phases of this subject seemed, therefore, a timely undertaking, representing, as it is intended to do, a general review of progress during the past quarter century, and thus covering substantially the period since flight in heavier than air machines became an assured fact.

Such a present taking of stock should also be of value and of interest as furnishing a point of departure from which progress during coming decades may be measured.

But the chief purpose held in view in this project has been to provide for the student and for the aeronautic designer a reasonably adequate presentation of background theory. No attempt has been made to cover the domains of design itself or of construction. Important as these are, they lie quite aside from the purpose of the present work.

In order the better to suit the work to this main purpose, the first volume is largely taken up with material dealing with special mathematical topics and with fluid mechanics. The purpose of this material is to furnish, close at hand, brief treatments of special mathematical topics which, as a rule, are not usually included in the curricula of engineering and technical courses and thus to furnish to the reader, at least some elementary notions of various mathematical methods and resources, of which much use is made in the development of aerodynamic theory. The same material should also be acceptable to many who from long disuse may have lost facility in such methods and who may thus, close at hand, find the means of refreshing the memory regarding these various matters.

The treatment of the subject of Fluid Mechanics has been developed in relatively extended form since the texts usually available to the technical student are lacking in the developments more especially of interest to the student of aerodynamic theory. The more elementary treatment by the General Editor is intended to be read easily by the average technical graduate with some help from the topics comprised in Division A. The more advanced treatment by Dr. Munk will call

for some familiarity with space vector analysis and with more advanced mathematical methods, but will commend itself to more advanced students by the elegance of such methods and by the generality and importance of the results reached through this generalized three-dimensional treatment.

In order to place in its proper setting this entire development during the past quarter century, a historical sketch has been prepared by Professor Giacomelli whose careful and extended researches have resulted in a historical document which will especially interest and commend itself to the study of all those who are interested in the story of the gradual evolution of the ideas which have finally culminated in the developments which furnish the main material for the present work.

The remaining volumes of the work are intended to include the general subjects of: The aerodynamics of perfect fluids; The modifications due to viscosity and compressibility; Experiment and research, equipment and methods; Applied airfoil theory with analysis and discussion of the most important experimental results; The non-lifting system of the airplane; The air propeller; Influence of the propeller on the remainder of the structure; The dynamics of the airplane; Performance, prediction and analysis; General view of airplane as comprising four interacting and related systems; Airships, aerodynamics and performance; Hydrodynamics of boats and floats; and the Aerodynamics of cooling.

Individual reference will be made to these various divisions of the work, each in its place, and they need not, therefore, be referred to in detail at this point.

Certain general features of the work editorially may be noted as follows:

1. Symbols. No attempt has been made to maintain, in the treatment of the various Divisions and topics, an absolutely uniform system of notation. This was found to be quite impracticable.

Notation, to a large extent, is peculiar to the special subject under treatment and must be adjusted thereto. Furthermore, beyond a few symbols, there is no generally accepted system of notation even in any one country. For the few important items covered by the recommendations of the National Advisory Committee for Aeronautics, symbols have been employed accordingly. Otherwise, each author has developed his system of symbols in accordance with his peculiar needs.

At the head of each Division, however, will be found a table giving the most frequently employed symbols with their meaning. Symbols in general are explained or defined when first introduced.

2. General Plan of Construction. The work as a whole is made up of *Divisions*, each one dealing with a special topic or phase of the general

subject. These are designated by letters of the alphabet in accordance with the table on a following page.

The Divisions are then divided into chapters and the chapters into sections and occasionally subsections. The Chapters are designated by Roman numerals and the Sections by numbers in bold face.

The Chapter is made the unit for the numbering of sections and the section for the numbering of equations. The latter are given a double number in parenthesis, thus (13.6) of which the number at the left of the point designates the section and that on the right the serial number of the equation in that section.

Each page carries at the top, the chapter and section numbers.

W. F. Durand

Stanford University, California
January, 1934.

GENERAL LIST OF DIVISIONS WITH AUTHORS

Volume I.

A. Mathematical Aids

W. F. DURAND — Professor (Emeritus) of Mechanical Engineering, Stanford University, Calif., Member of the National Advisory Committee for Aeronautics.

B. Fluid Mechanics, Part I

W. F. DURAND

C. Fluid Mechanics, Part II

MAX M. MUNK — Lecturer in Aerodynamics at the Catholic University of America, Washington, D. C., and Technical Editor of the "Aero Digest".

D. Historical Sketch

R. GIACOMELLI — Lecturer in History of Mechanics at the University of Rome, Italy, and Editor of "L'Aerotecnica".

with the collaboration of

E. PISTOLESI — Professor of Mechanics at the Royal School of Engineering at Pisa, Italy, and Editor-in-Chief of "L'Aerotecnica".

Volume II.

E. General Aerodynamic Theory—Perfect Fluids

TH. VON KÁRMÁN — Director of the Guggenheim Aeronautics Laboratory, California Institute of Technology, Pasadena, Calif., and formerly Director of the Aerodynamic Institute, Aachen, Germany.

J. M. BURGERS — Professor of Aero- and Hydrodynamics at the Technische Hoogeschool at Delft, Holland.

Volume III.

F. The Theory of Single Burbling

C. WITOSZYŃSKI — Professor of Aerodynamics at the Warsaw Polytechnical School and Director of the Warsaw Aerodynamic Institute, Poland.

M. J. THOMPSON — Assistant Professor of Aeronautical Engineering at the University of Michigan, Ann Arbor, Mich.

G. The Mechanics of Viscous Fluids

L. PRANDTL — Professor in Applied Mechanics at the University of Göttingen, Germany, and Director of the Kaiser Wilhelm Institute for Fluid Research.

H. The Mechanics of Compressible Fluids

G. I. TAYLOR — Yarrow Research Professor of the Royal Society, Fellow of Trinity College, Cambridge, England.

J. W. MACCOLL — Research Officer, Department of External Ballistics, Ordnance Committee, Woolwich, England.

I. Experimental Methods—Wind Tunnels

A. TOUSSAINT — Director of the Aerodynamic Laboratory, Saint-Cyr-l'École, France.

E. JACOBS — Associate Aeronautical Engineer, in charge of the National Advisory Committee for Aeronautics' variable-density wind tunnel, Langley Field, Virginia.

Volume IV.

J. Applied Airfoil Theory

A. BETZ — Professor at the University and Director of the Aerodynamic Research Institute at Göttingen, Germany.

K. Airplane Body (Non-Lifting System) Drag and Influence on Lifting System

C. WIESELSBERGER — Professor of Aerodynamics and Director of the Aerodynamic Institute, Technische Hochschule, Aachen, Germany.

L. Airplane Propellers

H. GLAUERT [1] — Past Fellow of Trinity College, Cambridge, England; Principal Scientific Officer at the Royal Aircraft Establishment, Farnborough.

M. Influence of the Propeller on other Parts of the Airplane Structure

C. KONING — Rijks-Studiedienst voor de Luchtvaart, Amsterdam, Holland.

Volume V.

N. Dynamics of the Airplane

B. MELVILL JONES — Professor of Aeronautical Engineering in the University of Cambridge, England, Member of the Aeronautical Research Committee of Great Britain.

O. Airplane Performance

L. V. KERBER — Former Chief Aerodynamics Branch Materiel Division, U. S. Army Air Corps, and former Chief, Engineering Section Aeronautics Branch, Department of Commerce.

Volume VI.

P. Airplane as a Whole—General View of Mutual Interactions Among Constituent Systems

W. F. DURAND [2] — Professor (Emeritus) of Mechanical Engineering, Stanford University, Calif., Member of the National Advisory Committee for Aeronautics.

Q. Aerodynamics of Airships

MAX M. MUNK — Lecturer in Aerodynamics at the Catholic University of America, Washington, D. C., and Technical Editor of the "Aero Digest".

R. Performance of Airships

K. ARNSTEIN — Chief Engineer of the Goodyear Zeppelin Company, Akron, Ohio.

W. KLEMPERER — Research Engineer of the Goodyear Zeppelin Company, Akron, Ohio.

S. Hydrodynamics of Boats and Floats

E. G. BARRILLON — Director of the Naval Experimental Tank, Paris, France.

T. Aerodynamics of Cooling

H. L. DRYDEN — Physicist in the United States Bureau of Standards, Chief of the Aerodynamics Section, Washington, D. C.

---

[1] Deceased August 4, 1934.

[2] In the original plan, it was expected that this Division would be prepared by Professor M. Panetti of the R. Scuola di Ingegneria of Turin. Unfortunately, at the last, Professor Panetti found himself unable to give the needed time for this work, and in order not to delay publication, the General Editor has undertaken to prepare a brief treatment of the subject.

CONTENTS

DIVISION J

APPLIED AIRFOIL THEORY

By **A. Betz,**
Professor at the University and Director of the Aerodynamic Research Institute at Göttingen, Germany

DIVISION K

AIRPLANE BODY (NON-LIFTING SYSTEM) DRAG AND INFLUENCE ON LIFTING SYSTEM

By **C. Wieselsberger,**

Professor of Aerodynamics and Director of the Aerodynamic Institute, Technische Hochschule, Aachen, Germany

DIVISION L

AIRPLANE PROPELLERS

By **H. Glauert,**

Past Fellow of Trinity College, Cambridge, England; Principal Scientific Officer at the Royal Aircraft Establishment, Farnborough.

DIVISION M

INFLUENCE OF THE PROPELLER ON OTHER PARTS OF THE AIRPLANE STRUCTURE

By **C. Koning,**
Rijks-Studiedienst voor de Luchtvaart, Amsterdam, Holland

NOTATION

The following table comprises a list of the principal notations employed in the present Volume. Notations not listed are either so well understood as to render mention unnecessary, or are only rarely employed and are explained as introduced. Where occasionally a symbol is employed with more than one meaning, the local context will make the significance clear.

DIVISION J

X, Y	Axes, usually longitudinal and transverse
x, y	Coordinates along axes of X and Y
b	Half span of airfoil or wing
c	Chord of airfoil
f	Height of camber, II **2**
l	Length
S	Surface or area in general
α	Angle of incidence
β	Special angle in connection with Joukowski sections, II **4**
γ	Inclination of oblique motion, IV **1**
ε	Angle of decalage, III **10**
θ	Angle of a circular arc, II **2**
τ	Angle of dihedral
V	Velocity in general
u	Axial velocity, IV **2**
v	Lateral velocity, IV **2**
w	Induced or downwash velocity
ω_x	Angular velocity of roll
ω_z	Angular velocity of yaw
Γ	Circulation
D	Drag
D_i	Induced drag
D_r	Residual drag
L	Lift
M	Moment
M_q	Rolling moment
Σ	Lateral force, IV **3**
P	Force
p	Pressure
q	Dynamic pressure $= (1/2)\,\varrho\, V^2$
W	Weight
ϱ	Density
ν	Kinematic viscosity
C_D	Drag coefficient
C_f	Coefficient of friction
C_L	Lift coefficient
$C_{L\,0}$	Lift coefficient for $\alpha = 0$
$C_{D\,r}$	Coefficient of residual drag

C_M	Moment coefficient
$C_{M\,0}$	Moment coefficient referred to focus of lift parabola, II **5**
$C_{M\,q}$	Coefficient of rolling moment
C_Σ	Coefficient of lateral force, IV **3**
ε	Lift-drag ratio, III **4**
$\varkappa$	Special coefficient, II **3**, III **2**, V **10**
ξ	Used for $2\,x/c$, II **1** also y/b III **5**

DIVISION K

X, Y, Z	Axes of reference
y	Distance along axis of Y, in general along span of wing
$2\,b$	Span of wing
l	Length in general
R	Radius
S	Maximum cross section or area in general
α	Angle of incidence
δ	Special angle
V	Velocity in general
ω	Induced velocity
Γ	Circulation, vorticity
φ	Potential
D	Drag
L	Lift
q	Dynamic pressure $= (1/2)\,\varrho\,V^2$
C_D	Drag coefficient
C_L	Lift coefficient
C_F	Coefficient of friction
C_M	Moment coefficient
K_L, K_D, K_M	Special coefficients
n	Normal to a surface or line
ν	Kinematic viscosity
ϱ	Density

DIVISION L

x	Radial coordinate $= r/R$
x	Used for ratio $\Omega\,r/V$
C	Area of wind tunnel section
c	Chord
D	Diameter of propeller
H	Pitch of propeller
r	Radial distance
s	Gap between vortex sheets, VII **4**
S	Disc area of propeller
S_1	Sectional area of wake
α	Angle of incidence
γ	$tan^{-1}\,(C_D/C_L)$
φ	Angle of inclination of W to plane of rotation
θ	Blade angle, usually reckoned from plane of rotation
u	Axial velocity through propeller disc
u_1	Axial velocity in ultimate wake
u_2	Velocity outside of wake

v	Radial component of velocity
w	Tangential velocity, VI **3**
w	Total induced velocity
W	Velocity of blade element relative to fluid
V	Forward speed of aircraft
J	V/nD
Ω	Angular velocity of propeller
ω	Induced angular velocity
K	Circulation about blade
p	Pressure
p'	Pressure added at airscrew
H_0	Total pressure head of original stream
E	Kinematic energy
T	Thrust
Q	Torque (moment)
P	Power
L	Lift
D	Drag
A	Aspect ratio
C_D	Drag coefficient
C_T	Thrust coefficient
C_Q	Torque coefficient
C_P	Power coefficient
T_c	Special thrust coefficient
Q_c	Special torque coefficient
τ	Special thrust coefficient, IX
k_D	Special drag coefficient, XII **3**
C_N	Normal force coefficient
δ	Mean value of $C_D/2$
η	Efficiency
a	Axial interference factor
a'	Rotational interference factor
b	Axial slipstream factor
σ	"Solidity" of airscrew $= S/\pi R^2$, also $Bc/2\pi r$
B	Number of blades
k	Special ratio, VII **1**
λ	"Speed ratio" $V \div \Omega R$
n	Number of revolutions per second
M	Special parameter, X
N_c, N_v	Special parameters, IX
q	Special parameter, III **2**
A, B, C	Special factors, VIII (3.6)
F, G, H	Special factors, VIII (5.7), (5.8)
F, f	Special factors, XII **4**
h, k	Special factors, VIII (5.6)
α	Special factor, IX (2.9)
λ	Special factor, VI (4.3)
δ	Corrective factor for transforming C_D to infinite aspect ratio V **5**
μ	Used for $u/\Omega R$
σ	Special factor, IX (2.9)
τ	Corrective factor for transforming α to infinite aspect ratio, V **5**
τ	Special factor, VI (6.15)
ν	Kinematic coefficient of viscosity
ϱ	Density

DIVISION M

$\triangle$	As prefix implies change due to influence of propeller
0	As subscript usually implies absence of influence of propeller
x, y, z	Rectangular coordinates for axes X, Y, Z
x, r, θ	Cylindrical coordinates
ϱ, ϑ	Special radial coordinates, II **5**
t_1, t_2	Special rectangular coordinates II **5**
ζ	Used for a complex number or coordinate
t	Special complex coordinate II **5**
b	Half span of wing
c	Chord of wing
D	Diameter, also drag
n	Distance along a normal
R	Radius of propeller
R_1	Radius of slipstream boundary
S	Surface or area in general, also velocity factor
α	Geometrical angle of attack
α_e	Effective angle of attack
α_i	Induced angle of attack, I **13**
ψ	Special variable angle, II **1**
V	Velocity of undisturbed flow
V_t	Local velocity, I **12**
v_x, v_y, v_z	Components of disturbance velocities due to propeller
u, v, w	Components of disturbance velocities due to causes other than the propeller
v_x, v_t, v_r	Components of disturbance velocities in cylindrical coordinates
Ω	Angular velocity
Γ	Circulation
Φ, φ	Potential
L	Lift
D	Drag, also diameter
D_i	Induced drag
M	Pitching moment
T, Q	Thrust and torque of propeller
p	Pressure
q	Dynamic head $= (1/2)\, \varrho\, V^2$
X	Force per unit volume along axis of X
a	Axial inflow velocity factor
a'	Angular inflow velocity factor
a_n, b_n, α_n	Coefficients in Fourier series
a, b, c, d, e, f	Factors, I **21**, **22**, also parts of the flow I, **14**
C_0, C_1	Factors in the expression for lift coefficient, I **12**
C_L, C_D, C_M	Coefficients of lift, drag and pitching moment
C_T, k_T	Thrust coefficients
C_Q, k_Q	Torque coefficients
s, S	Velocity factors, I (2.1)
λ	Special coefficient, II (5.8)
n	Revolutions per second
ϱ	Density, also radial coordinate

DIVISION J

APPLIED AIRFOIL THEORY

By

A. Betz,
Göttingen

EDITOR'S PREFACE

Basic aerodynamic theory, as developed in Volume II, Division E of this series, furnishes the broad foundation for further advance in aeronautics, and in its applications to the practical problems of safe and economic air-transport. However, between the development of a broad and general body of theory and its application to the needs of aeronautic industry, there lies a very considerable domain which may properly be called "Applied Aerodynamics" and which must be concerned largely with experimental tests, full scale and model, guided on the one hand by basic theory and on the other by the continuing accumulation of the results of such experimental work.

The present Division is concerned with this middle ground between theory and practice. In Chapter I general properties of the wing are considered with special reference to the characteristics of lift, drag and moment, maximum lift and methods of increasing the same, distribution of pressure over the profile, and control of such distribution through suitable choice of profile forms.

In Chapter II the properties of profiles of various forms are discussed in detail with the results of numerous experimental observations on representative profile forms.

In Chapter III, Part A, the single wing or monoplane is considered with reference to the several variables which may affect its performance, and including the effects of slots, gaps, and other secondary features.

In Part B combinations of wings or of wings and control surfaces (fins, stabilizers, rudders, elevators) are considered with reference to their mutual reaction, stability of combination and other features of significance in their practical use. Consideration of the biplane, as a particular form of such combinations, naturally finds its place under this heading.

In Chapter IV consideration is given to various phenomena in connection with actual flight, divided under the two major types of unsymmetrical motion, side-slip and rotation. These phenomena, and including

pitching, rolling, yawing, spins and autorotation, are discussed with reference to the basic characteristics due to which they may arise, together with their mutual interactions, one upon another, all as related to stability and safety in flight.

Included with the considerable amount of experimental data presented in the text will be found references to several extended series of experimental observations on wing profiles and on other aspects of the problems here considered. These references, together with the results here presented, will furnish to the interested reader a broad domain of experimental data as a source of information regarding practical problems with which he may be concerned.

The work of translating this Division from the German has been carried out chiefly by Dr. Louis Rosenhead, Professor of Applied Mathematics at the University of Liverpool and Fellow of St. John's College, Cambridge, to whom special acknowledgments are here made for this valuable assistance.

W. F. Durand.

INTRODUCTION

In application to practice, airfoil theory must be able to solve for the designer, the problem of how airfoils must be shaped and placed in order to obtain certain desired properties of the airplane. Pure airfoil theory, as set forth in Division E, cannot completely answer this question, since certain of the phenomena on which these aeronautical properties depend cannot be given complete theoretical expression. For example, in pure airfoil theory, the resistance due to the form of the airfoil (profile-resistance) is neglected in comparison with the lift, yet this resistance is a very important quantity when the motive power is considered. Again, pure airfoil theory is able to say nothing as to the value of the maximum attainable lift on which depend the velocities of take off and landing.

Therefore, in order to realize the practical value of pure theory it is necessary to supplement it by experiment and by qualitative considerations of a theoretical nature. It is then necessary to deduce from the theory those consequences which are of practical importance. In addition it is often valuable to consider purely theoretical arguments from a somewhat different standpoint, where, with reference to practical applications, intuitive deductions may be set before strict proofs. In short it is an "applied airfoil theory", an airfoil theory adapted to practical needs, which is to be developed in the following chapters.

In continuation of Division E II, we shall first consider various airfoil cross-sections, that is, cases in which plane flow occurs, and we shall leave three-dimensional flow for discussion at a later stage.

CHAPTER I
GENERAL PROPERTIES OF THE WING

1. Lift and Moment. The connection between the shape of the cross-section of airfoils and the lift can be treated in considerable detail by theory; for simplicity the effect of the angle of incidence is included in the effect ascribed to "shape". In airplanes the lift is generally by far the predominating force; all the moments which occur depend essentially upon the lift and can therefore be calculated in great detail. The results of these theoretical considerations are discussed in Division E. In this place it is only necessary to consider the practical bearing of the results there obtained and to discuss the deviations from the predictions of pure theory.

Two methods of attack are important in the theoretical treatment: 1) the method of conformal transformation, and 2) the method of vortex fields (Division E). The first method gives exact results concerning the distribution of pressure and velocity on the surface and in the neighborhood of wings of some definite cross-section. Although this procedure could in principle be applied to a wing of any type its application is only convenient for the so-called Joukowski-profiles. The second procedure gives approximate results only; in addition to estimating velocities in the neighborhood of the airfoil it is particularly suitable for the recognition of general relations between the shape of the wing and force effects (due for example, to curvature and S-shapes, cross-sections with fixed centers of pressure, etc.).

The theoretical discussion of the cross-section of airfoils is based upon the assumption that the flows along the upper and lower sides of an airfoil meet again exactly at the trailing edge. This hypothesis is reasonably accurate for airfoils with good lift-drag ratio, but is nevertheless, not exact and deviations from the predictions of theory are for the most part due to this circumstance. These deviations will be considered in detail.

2. Resistance (Drag) of the Airfoil. Airfoil theory has but little to say concerning the resistance of the airfoil (profile-drag) and regarding the maximum attainable lift. Here it is necessary to rely chiefly on the results of experiment. Nevertheless, provided the cross-section is not too thick, statements can be made regarding the drag, which, in this case, is produced chiefly by surface friction. The laws of surface friction are better known than the considerably more complicated laws of the remaining resistances of bodies (see Division G); so that much has been attained if the drag can be reduced largely to surface friction. This fact is particularly important when determining the effects of the Reynolds number (see Division G) on the drag of the airfoil. It must not be forgotten, however, that our experimental

knowledge concerning the drag of airfoils is derived for the most part from experiments with models (Division I) and it is well known that the drags of actual airfoils of sufficiently smooth surface are nearly always considerable lower than those obtained by transforming the results obtained from models in accordance with the law of kinematic similitude.

With thin plates, well sharpened towards the front, and lying exactly along the direction of flow, drag coefficients[1] are obtained whose dependence on the Reynolds number is shown in Figs. 1 and 2 (see also Division G). These diagrams show likewise the drag coefficients for two airfoils at several angles of incidence[2]. It can be seen that for airfoils whose position and shape differ only slightly from those of thin plates lying in the direction of flow, the drag coefficients obtained are not very different from those for thin plates. However, drag coefficients which deviate considerably from those for thin plates when the Reynolds number is small, approximate more closely to the case of simple surface resistance as the Reynolds number increases. This circumstance is very fortunate since it inspires a hope that the relations obtained at high Reynolds numbers, which are very important in practice but difficult to obtain experimentally, may in time receive theoretical treatment.

The chief method adopted for the experimental determination of the drag (profile) of large airfoils consists of measurements of the loss of momentum behind the airfoil (Division G 28, 29). Unfortunately there is very scanty experimental material on this point and the available material is rather inexact. It would be extremely valuable if research in this domain could be carried on more actively. Another possible method for obtaining experimental results at high Reynolds numbers consists in the employment of high-pressure wind-tunnels (Division I). It should be noticed that the drag of thin airfoils like surface friction, exhibits minimum values for Reynolds numbers $Vc/\nu \approx 5 \times 10^5$. This Reynolds number occurs precisely in the region where many experiments with models are carried out (at Göttingen for example the standard experiments on airfoil cross-sections are carried on at $Vc/\nu = 4 \times 10^5$). We must however take into account the fact that if measurements on models give extremely small values of drag deviating only slightly from the values of surface friction, then these drags will first increase with increasing Reynolds number, and then decreasing will only reach the

[1] The drag coefficient $C_D = D/\varrho\, S\, V^2/2$ and the coefficient of surface friction $C_f = D/\varrho\, \sigma\, V^2/2$ must be carefully distinguished. The first refers to a single surface of the corresponding plate (for example, for a rectangular plate, S = length times breadth) while the second refers to the entire surface of the plate, so that each side must be included separately. For a thin plate moving in its own plane, the two values of D are the same and $\sigma = 2\, S$, whence $C_D = 2\, C_f$.

[2] Ergebnisse der Aerodynamischen Versuchsanstalt zu Göttingen, III. Lief., p. 87 (Oldenbourg, Munich, 1927).

values obtained from experiments on the model when the Reynolds number has been increased to ten or perhaps one hundred times its first value.

In general, the drag of an airfoil is greater than the surface friction. The extra resistances superimposed on the simple surface friction, are

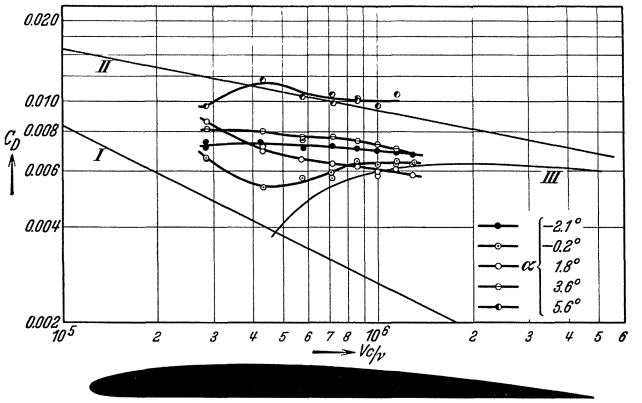

Fig. 1.

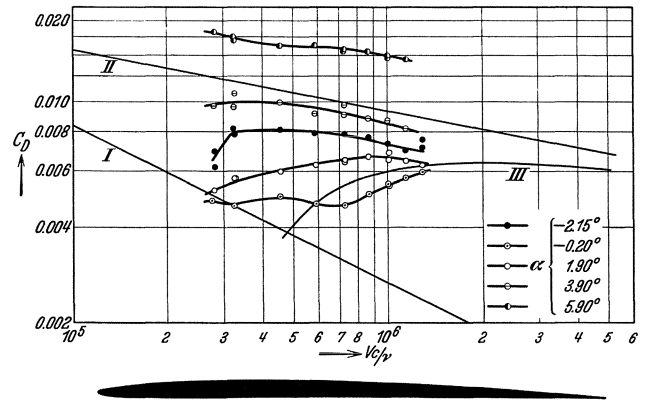

Fig. 2.

Figs. 1 and 2. Drag coefficient as a function of Reynolds number Vc/ν, for two wing forms at certain angles of incidence. For comparison also, the drag coefficient due to friction for a thin plate. Curve 1 for turbulent boundary layer, curve 2 for laminar boundary layer, and curve 3 for turbulent boundary layer over the rear part and laminar boundary layer over the front of the profile.

chiefly due to the roughness of the surface (rivet heads, fittings, unevenness, etc.) and by unfavorable flow patterns (too large a curvature of the upper side of the wing, too large angles of incidence, etc.), which thicken the boundary layer or produce separation in front of the usual position and thereby produce added drag.

Sometimes a single irregularity, insignificant in itself, such as a fitting or strut, can produce an inordinately large drag [1] (see also Division K). This is the case when the airfoil has a shape such that when no disturbance occurs the boundary layer separation is very small or negligible but the small disturbance is just sufficient to produce separation. We therefore see that the connections of the airfoil to the body of the plane deserve particular attention (Division K). The extra drag produced by the ends of the airfoil (induced drag) does not depend on the form of the airfoil and will therefore be considered separately in a later section.

3. Maximum Lift. Even less is known regarding maximum lift than regarding drag. In general maximum lift increases with the Reynolds number so that results obtained by measuring models should be on the right side. Unfortunately there are also cases in which the maximum lift noticeably decreases as the Reynolds number increases. So far this abnormal behavior of the maximum lift has not been completely explained; presumably the shape of the leading edge of the airfoil may have some effect [2].

The following general remarks can be made regarding the causes which limit the maximum lift. The typical pressure distribution on the upper side of the airfoil is approximately represented in Fig. 3. A marked decrease of the pressure and a corresponding increase of velocity, in accordance with Bernoulli's equation (Division B) near the leading edge of the airfoil, is followed by a gradual increase of the pressure and a corresponding decrease of velocity towards the trailing edge, until values are reached which do not differ greatly from the pressures and velocities of undisturbed flows. The layers of air in the immediate neighborhood of the upper surface of the airfoil are retarded by friction so that their kinetic energy is no longer sufficient to carry them forward against the increase in pressure. In normal circumstances, however, they are towed forward by the outer and faster layers through viscosity or exchanges of momentum (Division G). The towing effect produced by neighboring layers is, however, only effective if the retarded layer (boundary layer) is sufficiently thin and the increase of pressure not too great.

[1] The converse case where under certain conditions an irregularity of the surface may lower the drag, as may occur in the case of spheres, scarcely comes into the question for wing sections.

[2] Ergebnisse der Aerodynamischen Versuchsanstalt zu Göttingen, I. Lief., p. 54ff. (Oldenbourg, Munich, 1921). Some work of E. Gruschwitz (Die turbulente Reibungsschicht in ebener Strömung bei Druckabfall und Druckanstieg. Ingenieur-Archiv, Vol. II, p. 321, 1931) has brought the whole question of calculating the separation effect considerably nearer to a solution. It is now possible to obtain a picture, at least qualitatively correct, of the causes of the varying effects of Reynolds numbers.

Whenever an increase of the angle of incidence on an airfoil produces an increase of lift this is chiefly due to the fact that the sub-pressure on the upper side is made still lower. This, however, always increases the rise in pressure from the point of minimum pressure to the trailing edge, and a limiting case is reached when the entraining effect of the outer flow is eventually no longer sufficient to carry the boundary layer along against the steepened pressure gradient. If this is the case, the direction of boundary flow on the upper side of the airfoil is reversed, while the outer stream breaks off or "separates", thus altering the entire disposition of the flow (Fig. 4). This type of flow is characterized by a considerably

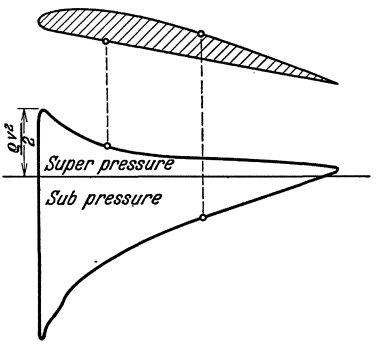

Fig. 3. Typical pressure distribution over a wing profile.

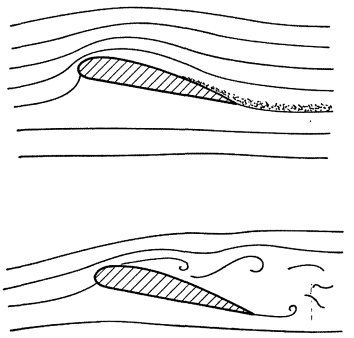

Fig. 4. Flow about a wing without and with separation.

extended region of "turbulent wake" and considerably increased drag in consequence. Moreover, the separation is usually accompanied by a decrease in the lift. There are also cases where the "separation" does not occur so suddenly, but permits a more or less continuous transition from normal flow to flow with separation (see Fig. 22). In such cases the lift may increase continuously; a fact which is important for the spin characteristics of airfoils. In most cases, however, the separation occurs rather suddenly, and if the angle of incidence is decreased, the normal conditions appear again only for angles of incidence smaller than those for which separation began. For if separation is once effected, it is much more difficult to dispose of the considerable quantity of turbulent air produced than it was to maintain the flow without mixed turbulence such as existed before the disturbance occurred. In most cases there is therefore a definite range of the angle of incidence where for each angle it is possible to have two states of flow with different values for the lift and drag. Of these, one state, that with the large lift and the smaller drag, is observed if the angle of incidence is varied by continuously increasing it from small values to larger ones; the other, when starting with the condition of separation, the angle of incidence is continuously

decreased. Very often another phenomenon can be observed in the period of transition between normal and disturbed flow, the two states of affairs continually interchanging, presenting rapidly alternating forces (jolting) whose mean value will lie nearer to the one or the other of the two boundary values of the force, according to the frequency of either the first or the second state of affairs.

If the theoretical distributions of pressure around a wing-section are calculated by the usual methods (conformal transformation for example), it is found, particularly in the case of cross-sections which are not too thick, that large angles of incidence produce extreme but sharply localized minima of pressure near the nose of the section (see the sharp point on the dotted curve in Fig. 5). The powerful increase of pressure which results usually forces the flow to separate locally, with displacement of the local pressure condition (see the continuous line of the same figure). Beyond this local disturbance which lies adjacent to the more sharply curved part of the profile, the flow usually remains in contact with the surface. The local disturbance does not in general involve the complete break-away of the flow provided the increase of pressure in the remaining portions of the upper side of the wing is within moderate bounds. Nevertheless, the maximum lift is decreased (see II 1, thin plates).

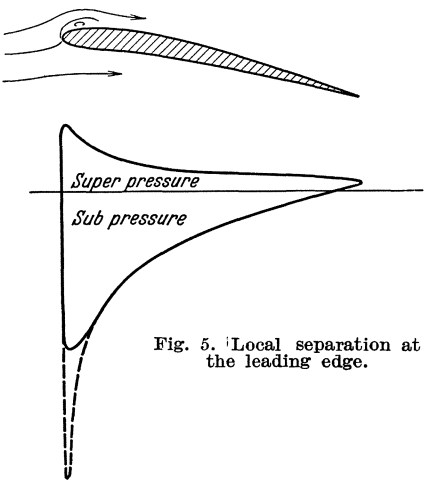

Fig. 5. Local separation at the leading edge.

It has been seen that the separation is chiefly due to a too rapid increase of pressure on the upper side of the airfoil, which in turn depends upon the maximum sub-pressure in the neighborhood of the leading edge. There are however, limits to the order of magnitude of this maximum sub-pressure and experience shows that pressure on an ordinary airfoil does not sink much below something like $-3\,\varrho\,V^2/2$, so that the velocity does not increase very much above twice the value of the velocity of general stream flow.

The sub-pressure and hence the increase of pressure are both proportional to V^2 (V = general stream velocity). But the entraining effect of the flow on the boundary layer also increases approximately as V^2, so that the limits of the separation are not materially influenced by changes of velocity. However, this proportionality is not exact, so that the Reynolds number does in general have some effect on the separation.

If the velocity is kept constant and the airfoil is uniformly increased in size, the pressure gradient per unit length decreases in inverse proportion to the chord of the wing. At the same time however, in consequence of the longer distance over which friction acts, the boundary layer becomes thicker (when compared at corresponding points of the two cross-sections), and the entraining effect is reduced approximately in the same measure as the pressure gradient. However, this adjustment is not complete so that the Reynolds number still has an effect. Since these deviations from the proportionality between the entraining effect on the one hand and V^2 or $1/c$, on the other hand, can be represented as a function of the Reynolds number and therefore as a function of Vc it follows that the laws of deviation produced by respective alterations of velocity and size are connected. The effect of a change in V is similar to the effect of a change in c. However, the deviations depend further on "roughness" which does not obey the laws of similitude.

All these considerations relate to steady motion. If the motion is not steady (as in the case of rapid increase of the angle of attack) lift-coefficients considerably higher than those previously mentioned can be produced[1]. For a discussion of abnormally high lift-coefficients for approximately rectangular airfoils (see III 7).

4. Artificial Methods for Increasing the Maximum Lift. The remarks made in the preceding sections concerning the limits of the lift apply only to ordinary wings. The maximum lift can be considerably increased above the usual values by using special measures. For several reasons there is much need for such means of lift increase; for one thing an increase of lift produces a decrease in the velocity of take-off and landing. The required effects however, are only attained if the increase of maximum lift does not at the same time produce a corresponding increase of the minimum lift best adapted to the available motor output, for otherwise the same effect could be attained quite simply by increasing the wing-chord. Wings with short chord and powerful lift have two advantages over wings of larger chord; the shorter the chord of the wing the smaller is the range over which the center of pressure moves, and on account of the larger angle of incidence, the shorter the chord the smaller is the change of lift produced by a change in the angle of incidence, and hence the less the sensitiveness to gusts. This last circumstance may, it is true, be unwelcome when large variations of angles of incidence are employed in order to produce needed changes in lift. A further advantage is found in the fact that, through increase in the maximum lift, separation of the airflow may be avoided and therewith many connected phenomena, falling into a spin for example.

[1] KRAMER, M., Die Zunahme des Maximalauftriebes von Tragflügeln bei plötzlicher Anstellwinkelvergrößerung (Böeneffekt). Zeitschr. f. Flugtechnik u. Motorl. **23**, p. 185, 1932.

Three methods are known at the present time for increasing the maximum lift:

1. The slotted wing.
2. Suction of the boundary layer.
3. Movement of the surface of the wing (rotating cylinder).

5. The Slotted Wing. Of the three methods mentioned above only the slotted wing has at the present time been utilized to any great extent in practical applications.

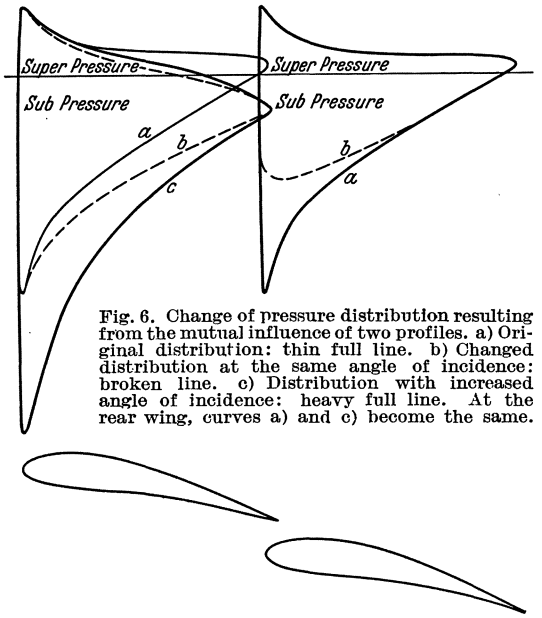

Fig. 6. Change of pressure distribution resulting from the mutual influence of two profiles. a) Original distribution: thin full line. b) Changed distribution at the same angle of incidence: broken line. c) Distribution with increased angle of incidence: heavy full line. At the rear wing, curves a) and c) become the same.

In the year 1920 Handley Page demonstrated a new type of wing provided with slots, and showing a maximum lift considerably greater than with those of conventional form[1].

In 1918 G. Lachmann in Germany had applied for a patent on a type of construction the same in principle, but in view of unfavorable conditions, the matter was not followed up immediately. This type of airfoil has therefore been called both the Lachmann wing and the Handley-Page wing. The phenomenon attracted much attention at the time of its discovery. The following[2] may serve as an explanation of the effects produced by slotting a wing.

The arrangement to be first considered consists of two approximately equal wings as in Fig. 6. The forward one itself would have had a pressure distribution represented by the continuous line *a* on the left of the diagram. When the other wing, which by itself would have had approximately the same pressure distribution, is brought near to the first one, the trailing edge of the forward wing is in a region of greater velocity and correspondingly smaller pressure, produced by the other wing. The head of the forward wing however, on account of its greater distance from the second wing, is in a region where the air is considerably less

[1] PAGE, HANDLEY, The Handley Page Aeroplane Wing. Engineering **111**, p. 274, 1921.

[2] BETZ, A., Die Wirkungsweise von unterteilten Flügelprofilen. Berichte u. Abh. der wissensch. Ges. f. Luftfahrt, Heft 6, 1922.

disturbed and the pressure is approximately normal. Hence, the presence of the after wing produces no important difference at the leading edge, but lowers the pressure at the trailing edge of the forward wing. The distribution of lift over the forward wing thus obtained is roughly represented by the broken line *b* in the diagram.

In consequence of this alteration of the pressure curve the increase of pressure on the upper side is much more gradual than before. However, it is known that the limiting values of the lift are determined by the

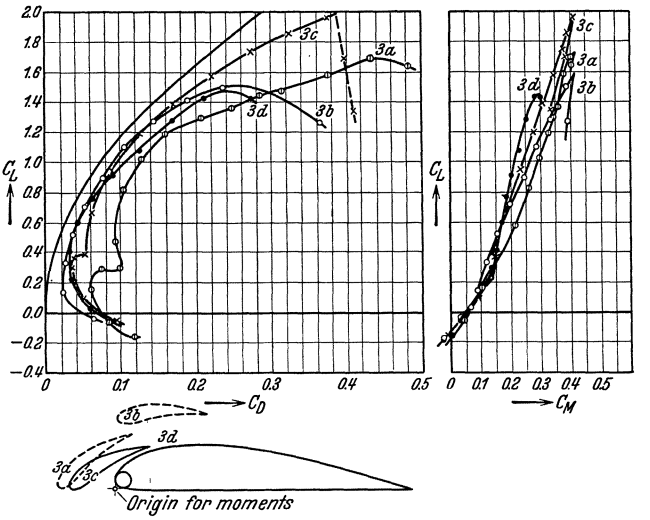

Fig. 7. Results of measurement on a wing with slot, auxiliary wing in different locations. Curve 3d gives results for same location as for 3c but with slot filled up.

steepness of the pressure curves; hence the angle of incidence can be increased again until the gradient of the pressure curve reaches its limiting value (see the continuous line *c* of the diagram). Since the velocity has increased at all points, the pressure curves can rise even more steeply than before. It is at once obvious that the lift which is represented by the area enclosed by this curve has been considerably increased.

Exactly corresponding phenomena occur at the after wing. The front wing produces a diminution of velocity and hence a reduction of the sub-pressure at the nose of the rear wing, while the trailing edge remains almost unaffected. This produces an increased pressure, chiefly on the upper side and in the neighborhood of the leading edge of the wing. The strong sub-pressure is reduced so that here too a more gradual increase of pressure occurs (dotted line *b*). Increasing the angle of incidence will again produce the former curve *a*. On the whole, this leaves the lift of the back wing sensibly unaltered, and altogether the

two wings, connected in this way, produce a greater maximum lift than if they were separated. If has been seen that this increase is to be found almost entirely at the front wing.

In order that these things should develop in the manner described, it is also necessary that the boundary layer on the upper side of the rear wing should not be disturbed by the boundary layer material leaving the after edge of the front wing. We know that whether the stream of air on the upper side separates or remains attached to the wing, depends on whether the turbulent air as formed is entrained away in sufficient quantities. Considering the work necessary to produce this effect for the rear section of the divided wing it is at once obvious that the work involved, which may be viewed either as pumping or suction work, must be supplied by the thin layer of air which has passed through the slot. This work is derived from the kinetic energy of this band of air, and if the slot is made too small the band finally becomes so narrow that its kinetic energy is not sufficient to produce its effect over the entire surface of the rear section. The air itself, issuing from the slot becomes entangled with the layers of mixed turbulence above and below, and passes into this condition itself. If the phenomena just described are considered from this standpoint they appear in quite a different light. The cross-section can now be considered as a single unit obtained from an ordinary cross-section by making connecting slots between the upper and lower sides; and this is, of course, the usual way of looking at the matter. The effect of the slots is that new energy is supplied to the boundary layer of the upper side which has been retarded by friction, thus increasing its velocity and preventing the formation of mixed turbulence. The stream of air coming from the slots has the same effect as a jet pump and thus aids the stream of air sliding along the upper side of the wing to sweep away the dead air (mixed turbulence). Since the production of lift is bound up with the output of this pumping work, and the maximum lift depends upon the restricted possibility of eliminating dead air, it is obvious that an increase of the pumping output will raise the lift-maximum. The last consideration gives a general

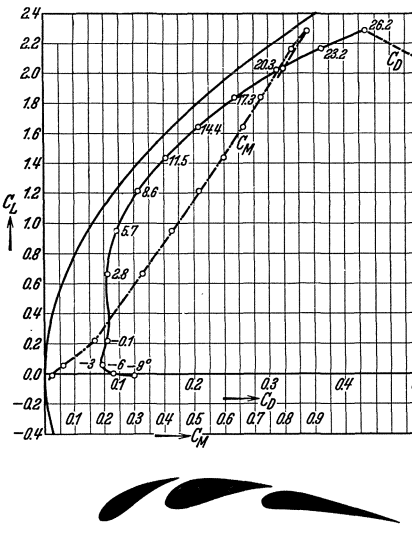

Fig. 8. Three part slotted wing.

indication as to the width of slot necessary, while from the previous statement the increase in lift can be deduced[1].

The slotted-wing is usually used in the following way: the front wing, usually called the auxiliary wing, is movable, and the slot is opened at landing and starting but closed during swift flight. The auxiliary wing is moved either by hand, or, as in the latest applications, automatically. If the angle of incidence is increased the result is to

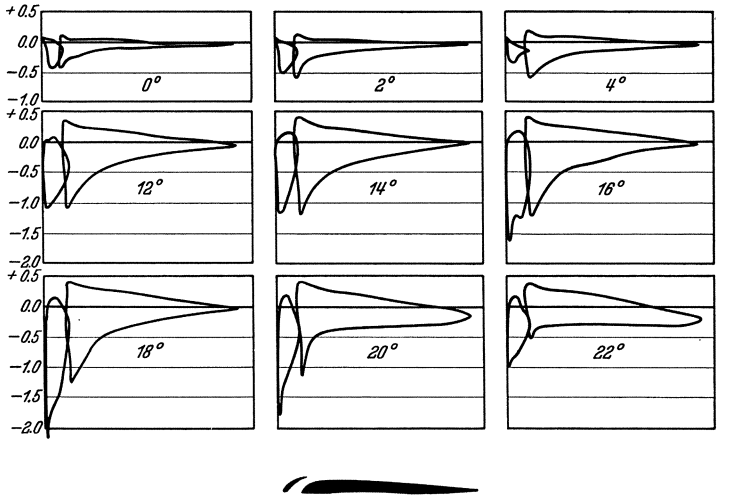

Fig. 9. Pressure distribution for a slotted wing.

produce a stronger and stronger negative pressure at the nose of the wing. This change of pressure can then be used to move the auxiliary wing hinged suitably on the principal wing in such manner as to open the slot automatically at some specific angle of incidence.

The values of the lift and resistance for a divided wing with one and with several slots are reproduced[2] in Figs. 7 and 8. Fig. 9 shows the distribution of pressure on the principal and auxiliary parts of a divided wing[3].

A method developed by A. Baumann is really connected with the phenomena associated with the slotted wing. The method employed is to blow out a stream of air at suitable points on the upper side of the

[1] An attempt to give a theoretical discussion can be found in the article by G. LACHMANN, Die Strömungsvorgänge an einem Profil mit vorgelagertem Hilfsflügel. Zeitschr. f. Flugtechnik u. Motorl. **14**, p. 71, 1923.

[2] Ergebnisse der Aerodynamischen Versuchsanstalt zu Göttingen, II. Lief., p. 58 and 64 (Oldenbourg, Munich, 1923).

[3] PAGE, HANDLEY, The Handley Page Aeroplane Wing. Engineering **111**, p. 276, 1921.

wing in order to accelerate the boundary layer. In theory the effect of this stream of air is the same as that of the stream which passes in the divided wing from the positive pressure side (lower) to the negative pressure side (upper). There is the difference however, that in Baumann's procedure the velocity of the stream of air can be chosen at will whereas in the slotted wing it depends upon the velocity which arises from the difference of pressure between the two sides of the wing. On the other hand Baumann's method involves the complications arising from the special fittings required for producing the air blast.

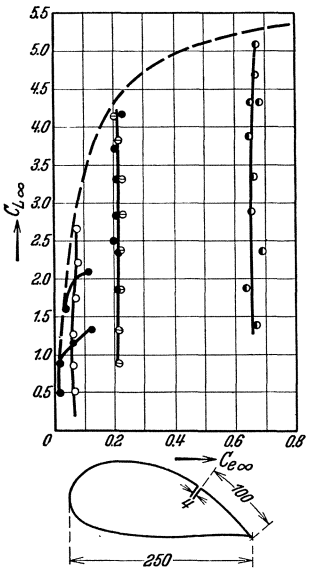

Fig. 10. Lift and efficiency coefficients for a wing with boundary layer removed by suction.

6. Suction of the Boundary Layer. The second method for increasing the lift beyond its normal value consists in sucking the boundary layer into the inside of the airfoil at those points on the upper side where it becomes sufficiently thick to induce separation. The new boundary layer produced at these places is at first thin enough to be drawn along by the outer part of the flow. If the pressure increases rapidly, suction must be repeated at several points of the upper side in order to preserve a sufficiently thin boundary layer. This method has the same disadvantage as that of Baumann, previously described, in that it requires a special fan with pipes and other auxiliary fittings. Compared with that procedure it appears to be more effective and to require a smaller power output; but too few experimental results are known for a fair judgment to be possible.

The two procedures could, of course, be combined by arranging that the air which has been sucked away and which must after all be disposed of, should emerge in such a way as to accelerate the boundary layer. The utilization of such a procedure with airplane wings should be thoroughly practicable, but thus far it does not seem to have been applied for such purposes.

Fig. 10 sets forth the results of experiments on a wing employing suction in the manner just described[1]. Owing to the abnormal circumstances the usual method of representing experimental results is no longer useful and must be modified accordingly.

The first point to be noticed is that in considering the output required during flight, the pumping output W_s, for the suction of the boundary

[1] SCHRENK, O., Versuche mit einem Absaugeflügel. Zeitschr. f. Flugtechnik u. Motorl. **22**, p. 259, 1931.

layer, is needed in addition to the propeller output W_p. The propeller output is used up in overcoming the drag and can be calculated from the drag coefficient C_D according to the formula

$$W_p = C_D \frac{\varrho V^3 S}{2}$$

C_D can therefore be regarded as an output index which determines the propeller output. In order to allow for the pumping output for wings with suction, C_D may be replaced by an output index C_e which has the same relation to the total output $(W_p + W_s)$ that the drag coefficient C_D has to the propeller output. Hence

$$W_p + W_s = C_e \frac{\varrho V^3 S}{2}$$

The induced drag (due to finite span of the wing and to the finite diameter of the wind-stream) is extremely large because the lift coefficient is large. It is therefore useful at the present stage, to consider only the profile-drag, the value of which can be directly determined by the momentum method (see Division G 28, 29). The coefficient $C_{e\infty}$ thus obtained is shown in Fig. 10.

On account of the deviation of the air flow at the wing, the lift is appreciably inclined to the direction of undisturbed flow (the cause of induced resistance). The component acting at right angles to the general direction of flow, and which thus appears as lift, is therefore diminished in the ratio of the cosine of this angle of inclination. In ordinary wings, owing to the smallness of the angle of inclination, this has no appreciable effect. Nevertheless, in order to obtain the correct relations for infinite span and infinitely extended streams of air, a corresponding correction for the lift must be introduced. The lift coefficient $C_{L\infty}$ corresponding to the corrected lift is represented in Fig. 10.

The experiments are performed in the following manner: While the number of revolutions per minute of the suction apparatus, built into the wing, is kept constant, the angle of incidence is increased by intervals of 6^0 until separation occurs. Since the pumping output is thus kept more or less constant and is usually large in comparison with the profile drag output, the points corresponding to any one fixed number of revolutions per minute are approximately in a vertical line where $C_{e\infty}$ is constant. Since the measurements take place only at intervals of 6^0, there is a possibility of an error of 6^0 in the determinations of the angle and the lift for which separation occurs. On the average, separation will take place at 3^0 beyond the last angle to be measured before the separation occurs. The limiting values of the attainable lift, estimated in this way, with a possible error of $\pm 3^0$, are connected by the broken line in Fig. 10. This curve plays the same part in estimating the effect of the wing with suction as does the polar curve of an ordinary wing corrected for infinite span.

7. Rotating Cylinder. The third procedure to prevent the separation of the boundary layer thereby producing larger lift-coefficients, consists of setting the surface of the wing into motion with approximately the same velocity as that of the general air stream. This eliminates the friction between the air and the surface of the wing, and hence the formation of the boundary layer and its separation. This procedure can hardly be realized in practice unless the wing is made in the form of a cylinder (circular cross-section) and is rotated about its axis (Magnus

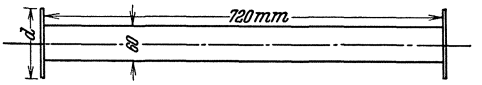

Fig. 11. Cylinder with end shields.

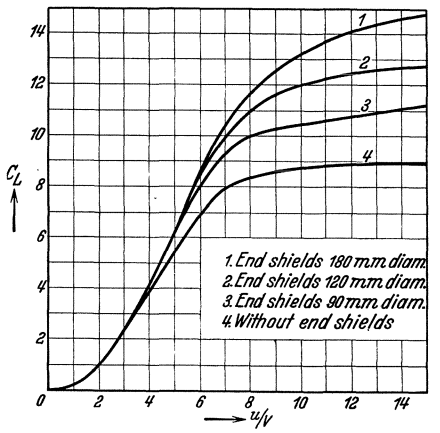

Fig. 12. Lift coefficients for a rotating cylinder as a function of the ratio between the surface velocity of the cylinder u and the wind velocity v.

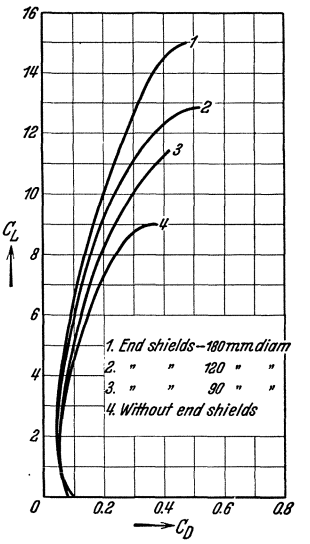

Fig. 13. Lift and drag coefficients for a rotating cylinder.

effect). This procedure is in itself by far the most effective since lift-coefficients of over 10 are obtained as compared with 1.5 for normal and something like 2 to 4 for slotted and suction wings respectively. Nevertheless, such procedure can scarcely be carried out in practice since in order to obtain such lift-coefficients the surface velocity of the cylinders must be of the order of three times the velocity of the airplane. This involves such high velocities of rotation in airplanes moving with the high speeds now usual, that the technical difficulties make the solution of the problem very difficult if not impossible.

The strong sub-pressure heads on the upper side of the rotated cylinder produce a strong tendency for air to be sucked in sideways at the ends of the cylinders. In order to prevent this effect the cylinder ends must be provided with end shields whose diameter is greater than that of the cylinder (Fig. 11). Without these precautions the air sucked

in would dislodge the main flow from the surface of the cylinder, and would hinder the production of the extremely high lift values. Figs. 12 and 13 show the results of experiments with the cylinder[1] represented in Fig. 11; Fig. 12 shows the relation between the lift-coefficient and the ratio u/V of surface velocity of cylinder (u) to wing velocity (V); Fig. 13 shows the lift and drag coefficients.

8. Effect of the Drag on Deviations From the Theoretical Lift. A potential flow produces no resistance, and the actual drag is due to the deviations of the actual flow from the potential flow. On the other hand, the theoretical discussion of lift assumes a potential flow, and the effect of the deviations of the actual flow from that theoretically postulated is to give, in practice, a somewhat smaller lift than as suggested by theory. The deviations from the potential flow involve only a minor correction of the theoretical value of the lift, whereas the drag depends entirely on the existence of these deviations. Since both phenomena, drag and deviation of the actual from the theoretical lift, can be reduced to the same cause, *viz.* deviations from the potential flow, it is to be assumed that a numerical relation connects the two.

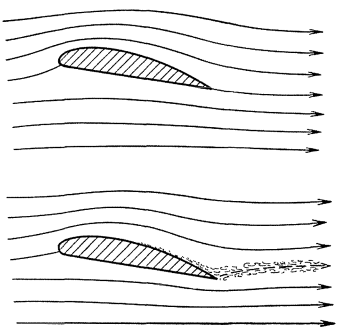

Fig. 14. Change in the flow about a wing due to "dead-water" on one side: Above, potential flow; below, flow with "dead-water".

It is possible to obtain a qualitative idea of the nature of this connecting relation from the following theoretical considerations. The deviations from the pure potential flow which produce both the drag and the diminution of the lift are due chiefly to the fact that the layers of air streaming past the wing lose a part of their energy through retardation by surface friction. These portions of the fluid produce a domain of diminished velocity behind the wing, the so-called turbulent wake. There is a comparatively simple relation between the drag on the one hand, and the extension of this wake and the diminution of velocity on the other[2]. In consequence of the higher velocities on the upper side of an airfoil experiencing lift, the loss of energy on that side is considerably greater than on the other side; hence the turbulent wake, for the most part, starts from the after part of the upper side (Fig. 14). Since the velocity is diminished in this region, less air passes

[1] BUSEMANN, A., Messungen an rotierenden Zylindern. Ergebnisse der Aerodynamischen Versuchsanstalt zu Göttingen, IV. Lief., p. 101 (Oldenbourg, Munich, 1932).

[2] For the calculation of the drag from the turbulent wake in accordance with Betz' procedure, see Division G **28, 29**.

than in the potential flow; the consequence is that neighboring stream-lines are rather more separated than in pure potential flow. In consequence of the unsymmetrical arrangement of the turbulence at the wing, the separation between the stream-lines is greater on the upper than on the lower side. The stream-lines behind the wing are therefore on the average shifted upward. The lift has approximately the same value as if the stream-lines of the pure potential flow met again, but at a point on the suction side instead of at the back edge of the wing (Fig. 14, broken stream-lines). Such a flow has, however, less circulation and

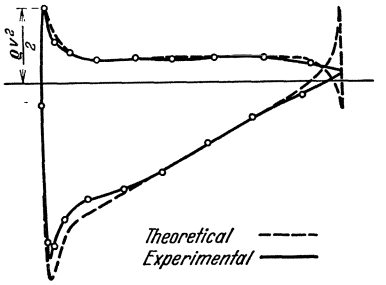

Fig. 15. Comparison between a measured pressure distribution (full line curve) and the theoretical distribution (dotted line) giving the same lift. The after stagnation point of the theoretical flow lies on the suction side with a flow about the sharp following edge where the pressure (theoretical) would be $-\infty$.

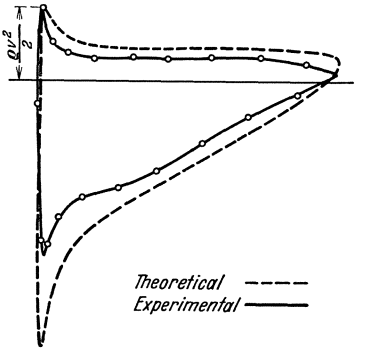

Fig. 16. Measured and theoretical pressure distribution without flow about the following edge.

therefore also less lift than that predicted in accordance with the theoretical distribution in which the stream-lines join together exactly at the after edge.

The fact that the effect of the turbulent region can be fairly well reproduced by shifting the stagnation point to the upper side of the wing can also be obtained by comparing the theoretical and observed distributions of pressure for the same lift and the same angle of incidence. Fig. 15 shows the theoretical and the experimental distributions. The rear stagnation point is so arranged in the theoretical calculation that the same lift is obtained as in the observations[1]. It is then necessary to allow a flow around the back edge which lowers the pressure in the theoretical calculations to $-\infty$. The divergences between theory and actual measurement are now concentrated in the neighborhood of the back edge where the extreme theoretical values for the pressure must be neglected. For the rest of the wing the two curves agree very well. For purposes of comparison the same observed pressure curve is reproduced in Fig. 16 together with the theoretical curve uncorrected by a displacement of the stagnation point.

[1] Betz, A., Untersuchungen einer Schukowskyschen Tragfläche. Zeitschr. f. Flugtechnik u. Motorl. VI, p. 173, 1915.

The quantitative connection between the loss of lift and the drag has not as yet been obtained. A rule which has been often used, in accordance with which $C_L = \frac{7}{8} C_L$ theor. (8.1) (see Division E I 8) should still be useful for those orders of magnitude which occur for the most part in practical applications.

C. Wieselsberger has investigated this matter in greater detail and obtained a very simple result[1]. He used an airfoil with four degrees of roughness on the upper side. The roughness simultaneously increases the drag and lowers the lift. The results of the measurements are reproduced in Fig. 17, where the four polars have been recalculated for an infinite aspect ratio (see Division E IV). The values found for equal angles of incidence (the points shown) lie, with good approximation, in parallel lines. Wieselsberger was also able to show that extrapolation to zero drag supplied almost exactly the lift required by the theory of frictionless flows. This indicates the following relation between C_D, the drag coefficient, and $\triangle C_L$ the decrease in the lift coefficient

$$\triangle C_L = 7.5\, C_D \qquad (8.2)$$

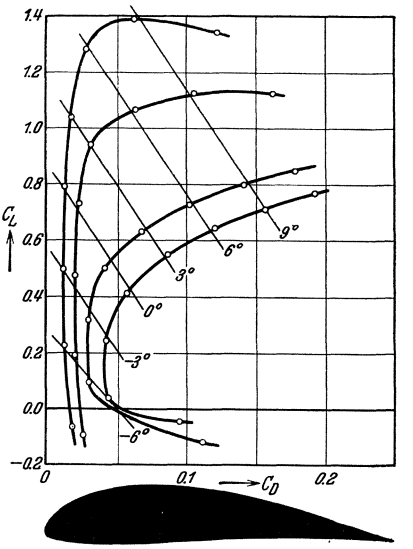

Fig. 17. Lift and drag coefficient for a wing with varying degrees of roughness on the suction side. The points which belong to the same angle of incidence lie nearly on straight lines.

This result of Wieselsberger's investigation refers only to one specific airfoil the drag of which was altered in a certain definite manner, the angles of incidence used all lying in a comparatively small region. It is easy to see that this simple result cannot hold for all cases. Considerations of symmetry show that for a symmetrical airfoil for example, $\triangle C_L$ must change its sign with the angle of incidence (or the lift) yet this is not permitted by (8.2) in which C_L is always positive. A more recent investigation[2] of this point for which Joukowski airfoils were employed and the measured values of the lift were compared with the theoretical

[1] Wieselsberger, C., Die wichtigsten Ergebnisse der Tragflügeltheorie und ihre Prüfung. Vorträge aus dem Gebiete der Hydro-Aerodynamik (Innsbruck 1922). Published by Th. von Kármán and T. Levi-Civita. Berlin: Julius Springer 1924.

[2] Betz, A., and Lotz, I., Verminderung des Auftriebes von Tragflügel durch den Widerstand. Zeitschr. f. Flugtechnik u. Motorl., 1932.

values, revealed a relation between $\triangle C_L$ and C_D as shown in Fig. 18 for two airfoils of equal mean curvature. On the whole the curves lie symmetrically about a curved mean line whose shape depends upon the airfoil curvature; this mean line for symmetrical cross-sections is straight and coincides with the C_D axis.

If the formation of a turbulent wake diminishes the lift, the question arises, does this alteration shift also the lift center of pressure, and if so, to what extent? On comparing the measured moment with the theoretical value for the *same lift coefficient* the actual measurements of the force always produce smaller moments than as required by theory. On the other hand, Schrenk[1] found, for Joukowski wings at least, in a domain where separation has not occurred, that for the *same angle of incidence*, lift and moment are reduced in approximately the same proportion when compared with the theoretical values. This means that for the same angle of incidence the center of pressure is not essentially altered. It is also permissible to deduce that in consequence of the formation of a turbulent wake, the pressure distribution curve is on the whole reduced approximately in terms of a constant ratio (see Fig. 16).

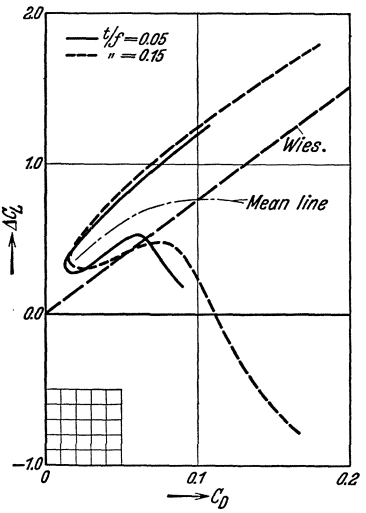

Fig. 18. Decrease of the lift coefficient as a function of the drag coefficient for two Joukowski profiles with the same mean camber (f/c = 0.1) but with different thickness (d/c = 0.05 and 0.15), where d is approximately the thickness of the profile at the middle point of the chord. Wies. = due to the formula of Wieselsberger.

9. Distribution of Pressure. The distribution of pressure over the surface of a wing is of the utmost importance for the drag, and above all for the maximum lift. As already emphasized in the discussion on maximum lift (see 3), as the pressure increases, the retarded boundary layer must be carried along by the outer flow against the increase of pressure. If, however, the pressure increases too quickly, the entraining effect is not sufficient, the boundary layer gathers together into mass turbulence, producing vortices with increased resistance and eventually leads to the separation of the stream.

In general, large lift-drag ratios and high maximum lifts are desirable for airplane wings. In order to obtain a large lift-drag ratio, the surface friction for a given lift must be kept as small as possible. This in general

[1] SCHRENK, O., Systematische Untersuchungen an Joukowski-Profilen. Zeitschr. f. Flugtechnik u. Motorl. 18, p. 225, 1927.

also makes the drag component of the normal pressure small[1]. At any point on the upper side the lift contribution is the same as the sub-pressure at that point. On the pressure side the positive pressure is a measure of the lifting force. Since the sub-pressure is connected with increased velocity and the positive pressure with diminished velocity in accordance with Bernoulli's equation (Division B), and since for equal thicknesses of the boundary layer and similar distributions of velocity the surface friction is approximately proportional to the square of the velocity, it follows that a favorable effect on the lift-drag index is obtained if the lift is effected as much as possible by pressure on the pressure side rather than by suction on the upper side. In practice, however, the greater part of the lift must be obtained by suction on the

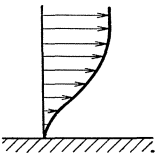

Fig. 19. Distribution of velocity in the boundary layer with pressure rise, just before separation.

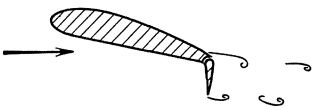

Fig. 20. Profile with sharp down turn at trailing edge.

upper side. For the maximum over pressure, $\varrho V^2/2$, occurs only at the stagnation point while a lower pressure occurs at all other points. Hence the lift which can be produced by the pressure on the pressure side is very limited. On the suction side however, the maximum negative pressure can be increased by a multiple of $\varrho V^2/2$. Hence for fairly large lifts the larger part must be supplied from the suction or upper side.

However, to obtain large maximum lift some attempt can be made to employ the pressure side as much as possible; but as already mentioned, this can be carried out to only a limited extent, and the maximum exploitation of the suction side is on the whole more important. If the pressure at the trailing edge is regarded as given, the largest area for suction is obtained if the pressure gradient toward the after edge is chosen to be everywhere as great as possible; that is, if at every point separation is almost taking place. Unfortunately we lack information regarding this favorable distribution of pressure for at the present time we have no theoretical discussion of this state. For the present we are forced to depend on practical experience which shows that certain specific distributions of pressure are favorable. The behavior of such a distribution of pressure can be obtained from Fig. 21 ($\alpha = 11.6^0$). The theoretical discussion so far described does however reveal the fact

[1] For an approximate separation of the resistance into friction and pressure components see the article by A. Betz, Untersuchungen einer Joukowski'schen Tragfläche. Zeitschr. f. Flugtechnik u. Motorl. VI, p. 173, 1915.

that at any rate a *continuous* pressure distribution is to be desired on the upper side, since every irregularity (buckling of the curve) implies an earlier separation at such a point.

The pressure gradient can be increased, without separation of the boundary layer, until a limiting value is reached for which the velocity-gradient at the surface becomes zero. A further increase of the pressure gradient would produce a reverse current and separation. The general

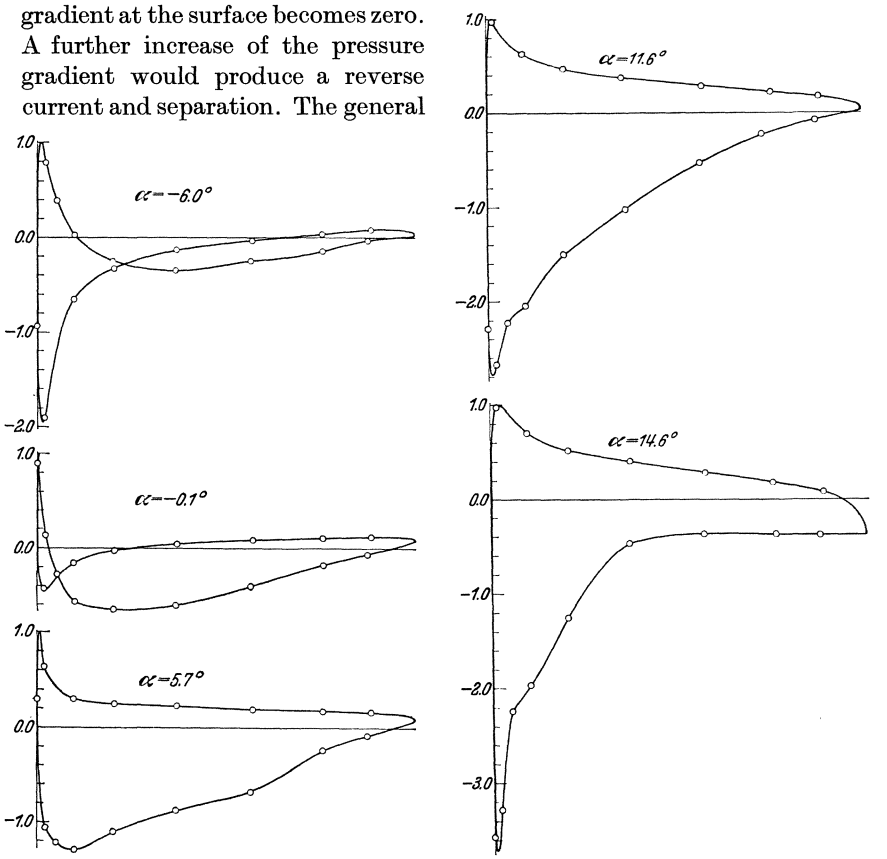

Fig. 21. Pressure distribution for profile 389 (Fig. 23) with varying angles of incidence.

distribution of air velocities in the boundary layer will then be as shown in Fig. 19. It is perhaps significant that in this limiting case the surface friction is also zero, because it is proportional to the velocity gradient. This indicates that the distribution of pressure which produces the most favorable maximum lift will also produce a favorable effect on the friction. It must however be borne in mind that a strong pressure gradient produces a comparatively large region of mixed turbulence which will increase the drag due to pressure distribution, thus more or less balancing the gain with respect to surface resistance.

In certain special cases where increase of drag and an awkward position of the center of pressure are not objectionable, the maximum lift can also be increased by lowering the pressure at the trailing edge. The effect of this is that for equal increase of pressure per unit length, the values of the sub-pressure on the upper side of the wing are correspondingly lowered (see Fig. 6). One method of producing this result is to give a sharp aileron tilt (Fig. 20), thus producing a drag with dead

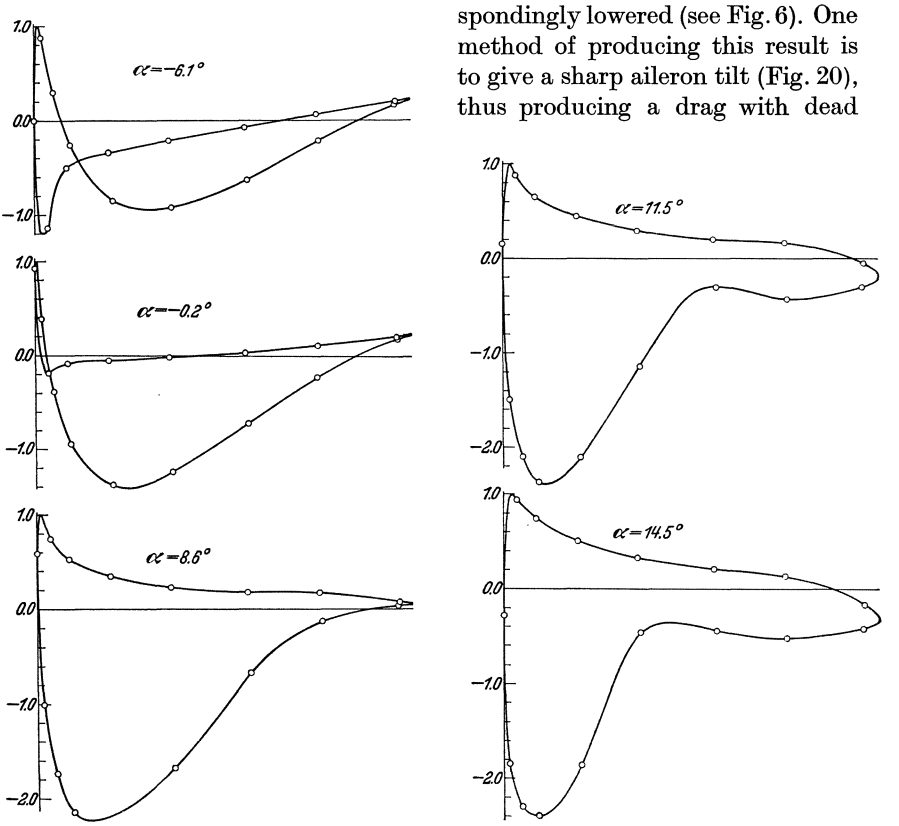

Fig. 22. Pressure distribution for profile 382 (Fig. 24) with varying angles of incidence.

air turbulence and reduced pressure. This device also produces an increase of pressure on the pressure side, thus giving a further increase of total lift[1].

[1] During the preparation of the manuscript for printing, there have appeared reports on several extended researches bearing on these matters:

Gruschwitz, E., and Schrenk, O., Über eine einfache Möglichkeit zur Auftriebserhöhung von Tragflügeln. Zeitschr. f. Flugtechnik u. Motorl. **23**, p. 597, 1932.

Weick, F. E., and Harris, Th. A., The Aerodynamic Characteristics of a Model Wing Having a Split Flap Deflected Downward and Moved to the Rear. U.S. N.A.C.A. Technical Note No. 422, 1932.

Figs. 21 and 22 show the distributions of pressure for two profiles with various angles of incidence[1].

Figs. 23 and 24 show the two profiles with the points at which pressures were measured, and the polar curves thus obtained. The aspect ratio for these airfoils was 5. The values of the angle of incidence and resistance have not been recalculated for an infinite aspect ratio. The distribution of pressure for airfoil 389 ($\alpha = 11.6^0$) represents approximately for a good profile the limiting case just before separation, and should

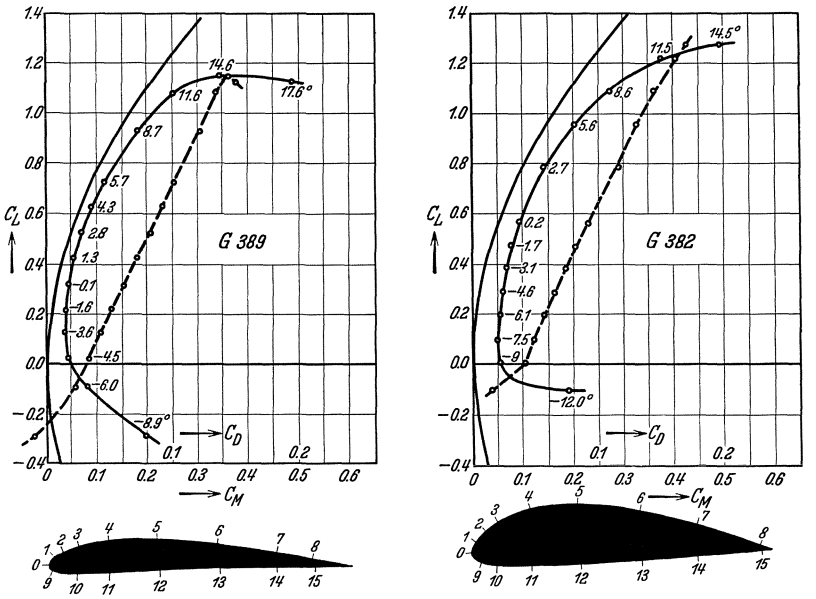

Figs. 23 and 24. Profiles 389 and 382 with points for pressure measure and the corresponding polars.

approximately correspond to the favorable distribution of pressure aimed at in the discussion just above. When the angle is increased to 14.6^0, the flow has already separated over the larger part of the suction side; the suction has collapsed and the measurements of force (Fig. 23) reveal a strong increase of the profile drag. For smaller angles of incidence the drag is less than at 11.6^0. This results from diminished sub-pressure and air velocity on the suction side, but at the same time the lift is considerably diminished. For $\alpha = -6.0^0$ the lift is approximately zero. The distribution of pressure results in a negative lift at the front part and a positive lift at the back part of the airfoil (the stagnation point is here situated on the suction side). The airfoil is therefore subject

[1] Ergebnisse der Aerodynamischen Versuchsanstalt zu Göttingen, II. Lief., p. 43 (Oldenbourg, Munich, 1923).

to an appreciable turning moment, a phenomenon which can also be observed on the thicker airfoil (382) in Fig. 22 when $\alpha = -6.1^0$. But the last mentioned wing does not exhibit the characteristic favorable distribution of pressure since the flow commences to separate at the after part of the airfoil before powerful suction has been obtained over the forward part ($\alpha = 8.6^0$). If the angle of incidence is still further increased, the position where separation occurs is shifted still further forward ($\alpha = 11.5^0$ and 14.5^0). Measurements of the forces for these angles show a gradual increase of the drag in agreement with this statement.

10. Control of the Pressure Distribution by Suitable Choice of the Profile Shape of an Airfoil. The problem of simultaneously obtaining high lift and low drag is determined by the broad features of the

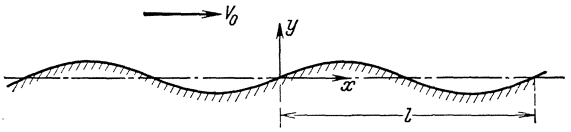

Fig. 25. Flow along a wavy surface.

distribution of pressure, a fact which however does not prevent the possibility of comparatively extensive variations depending on the shape of the airfoil (see Figs. 21 and 22). It is important in practice to know how specific alterations of the pressure distribution can be produced by suitable choices of airfoil profiles.

The simplest rule in this connection is obtained by regarding the pressure and suction (sub-pressure) respectively at the surface of the airfoil as produced by the centrifugal forces of the air currents streaming by in curved paths. For if the matter be regarded in this light it follows that to increase a convex curvature at any point of the airfoil will decrease the local pressure and to reduce such a curvature (or by application of a concave curvature) will increase the local pressure. This simple and easily comprehended rule unfortunately does not suffice for an exact calculation of the necessary alteration in shape. In order to obtain an approximate notion of the effect of alterations of shape it is useful to bear in mind the pressure distribution for the case of flow past a gently corrugated wall (Fig. 25). Let the shape of the wall be given by the equation

$$y = y_0 \sin \frac{2\pi x}{l} \tag{10.1}$$

If the air flows past with mean velocity V_0, its velocity is least in the valleys, greatest on the ridges and is given by the equation

$$V \approx V_0 \left(1 + y_0 \frac{2\pi}{l} \sin \frac{2\pi x}{l}\right) \tag{10.2}$$

The maximum differences between the velocities in the valleys or ridges and the mean velocities are given by

$$V - V_0 \approx \pm V_0 \, 2\pi \frac{y_0}{l} \tag{10.3}$$

The positive and negative pressures have therefore the limiting values

$$p \approx \pm \frac{\varrho}{2} V_0^2 \frac{4\pi y_0}{l} \approx \pm \frac{2\pi \varrho V_0^2 y_0}{l} \tag{10.4}$$

The alteration in pressure produced by a ridge therefore depends, in addition to the stagnation pressure, on the ratio of the elevation of the ridge (y_0) to its length ($l/2$).

More exact information on the effect of alteration of shape can be obtained by a conformal transformation of the airfoil cross-section to a circle. Reproduction of the alteration in the original cross-section, suitably modified by the conformal transformation, produces the so-called "almost circular" figure[1] which lends itself to further treatment with comparative ease (see Division E II **21**).

A more difficult problem is that of finding what form of profile is required to produce a given distribution of pressures. This problem has been solved[2] by the use of hodographs but the procedure involved is very laborious. It may be assumed, however, that other methods will become practically feasible[3].

CHAPTER II

PROPERTIES OF TYPICAL PROFILES

1. Thin Flat Plates. Thin flat plates are scarcely used for lifting purposes in practical applications since not only have they comparatively unfavorable aerodynamic properties but their low rigidity introduces technical difficulties in construction. The knowledge of their aerodynamic properties is nevertheless of great importance. It is important in the first place because a whole series of cross-sections, symmetrical cross-sections in particular, behave in many respects like flat plates, but above all it is important on account of the fact that many characteristics which are also present in less simple forms can be more easily understood in the case of thin flat plates. Such plates can in many respects be regarded as typical representatives of airfoils and it is often convenient to discuss features of importance using flat plates and then pass to other forms by providing a rule of transformation between such forms

[1] See also recent paper by TH. THEODORSEN, Theory of Wing Sections of Arbitrary Shape. U.S. N.A.C.A. Report No. 411, 1931.

[2] WEINIG, F., Widerstands- und Tragflügelprofile mit vorgeschriebener Geschwindigkeitsverteilung an der Oberfläche. Z. f. angew. Math. u. Mech. **9**, p. 507, 1929.

[3] BETZ, A., Änderung der Profilform zur Erzielung einer vorgegebenen Änderung der Druckverteilung. Luftfahrtforschung 11, p. 158, 1934.

and the equivalent flat plate. A discussion in some detail, of the case of thin flat plates is therefore necessary.

The flat plate can be easily treated by either of two theoretical methods: conformal transformation (Division A III **13**) and the Method of Vortex Fields (Division E II **7**). The relation obtained between the lift coefficient C_L and the angle of incidence α is

$$C_L = 2\pi \sin\alpha \approx 2\pi\alpha \qquad (1.1)$$

(For the derivation of this formula and of the two which follow see Division E II.)

If c is the breadth of the plate, y the distance of a point from the middle of the plate, and $\xi = 2y/c$, the distribution of lift over the breadth of the airfoil can be approximately expressed by the equation

$$\frac{dC_L}{dy} = \frac{2C_L}{c\pi}\sqrt{\frac{1-\xi}{1+\xi}} \qquad (1.2)$$

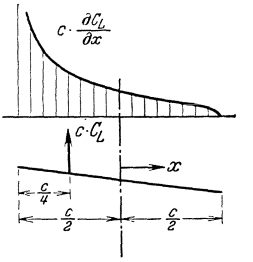

Fig. 26. Lift distribution and resulting lift for a plate placed oblique to the flow.

(see Fig. 26). The resultant of this distribution is at a distance of $c/4$ from the front edge of the airfoil; and consequently the coefficient of moment calculated for the front edge[1] is

$$C_M = \frac{1}{4}C_L = \frac{\pi}{2}\sin\alpha \qquad (1.3)$$

The theoretical discussion neglects the surface friction so that the forces deduced originate from pressure on the surface of the body. In the case of the flat plate the entire surface lies in one plane so that since the pressures are normal to the surface it must follow that the force produced by a frictionless flow over a flat plate acts perpendicularly to the surface (P in Diagram 27). This force for a finite angle of incidence α would have a drag component

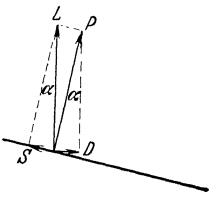

Fig. 27. Lift as resulting from normal pressure P and suction S. Decrease of suction results in an increase in drag.

$$D = P\sin\alpha \qquad (1.4)$$

in the direction of flow. This result however, contradicts the fact that in a potential flow, there can be no loss of energy and consequently no resistance to motion. In fact the force deduced by theoretical considerations should act perpendicularly to the direction of motion.

[1] If the point at a distance $c/4$ from the leading edge is chosen as center of moment, then $C_M = 0$. On account of the resulting simplicity, the "moment point" is often taken, particularly in American writings, not at the leading edge of the profile, but at a distance $c/4$ from it (see II **6**).

This apparent contradiction may be explained in the following manner[1]. The theoretical discussion commences by assuming that the air flows smoothly off the trailing edge. If, however, as in the case of thin plates, there is a forward edge, it is no longer possible to control the manner in which air streams toward this edge and in general a flow around it must be allowed. (It is indeed the back edge which practically determines the amount of circulation, the flow at the front edge being only of minor importance in this connection.)

High velocities and correspondingly low pressures occur at the curved part of a rounded edge (Fig. 28). The sub-pressures produce a corresponding force S at the curved region. The smaller the radius of curvature, the higher the velocities and in consequence the lower the pressures become. The sub-pressures vary inversely as the radius of the curvature so that the force of suction, which consists in the main of the product of sub-pressure and radius, remains constant as the radius is decreased, and has a finite value even for an infinitely small radius of curvature (sharp edge).

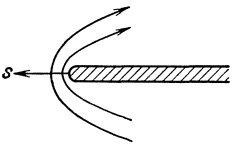

Fig. 28. Explanation of suction at leading edge.

In accordance with these considerations therefore, the flow, as theoretically calculated, will have a force of suction P_S at the leading edge of the plate (Fig. 27), which compounds with the force P_N acting normally to the surface of the plate to produce the lift L acting in a direction perpendicular to the direction of flow. In the actual state of affairs no infinitely large sub-pressures can appear, and instead, the flow separates at the sharp front edge. In that domain a small vortex region appears, restricted to the neighborhood of the front edge (Fig. 29) and therefore without any considerable effect on the remaining flow. This eliminates the suction force S in the calculated flow so that if the surface friction is neglected, the resulting force is perpendicular to the surface of the plate. At the same time the vortices formed at the front edge with the correlated phenomena of intermixing involve a loss of energy which is to be connected with the output of work required to overcome the drag.

Fig. 29. Vortex formation at the sharp leading edge of a thin plate.

From Fig. 27 the magnitude of the suction force is

$$P_S = L \sin \alpha \tag{1.5}$$

[1] KUTTA, Über eine mit den Grundlagen des Flugproblems in Beziehung stehende zweidimensionale Strömung. Sitzungsbericht d. Kgl. bayer. Akad. d. Wissenschaften, Math.-phys. Kl., 2. Abh., pp. 25 and 42, 1910.

The drag produced by the sharp front edge is

$$D = P_S \cos\alpha = L \sin\alpha \cos\alpha \approx L \sin\alpha \tag{1.6}$$

$$C_D \approx C_L \sin\alpha = 2\pi \sin^2\alpha \tag{1.7}$$

In addition allowance must be made for the effect of surface friction. This discussion has shown that the front edge of a flat plate introduces an additional drag, which is comparatively small only for small angles of incidence and correspondingly small coefficients of lift. It will therefore be desirable, when using airfoils whose shapes approximate to those of flat plates, *i. e.* thin surfaces with somewhat sharp front edges, to use only small angles of incidence if small drag is desirable (*e. g.* as in the case of tail planes). The additional drag calculated in (1.6) only reaches the value there given in the case of *infinitely thin* plates with sharp front edges. The finite thickness, which plates must always have in practical applications, introduces only a minor improvement if the front edge is sharpened off, whereas rounding off the front edge considerably reduces the drag (see the results of experiments, **6**).

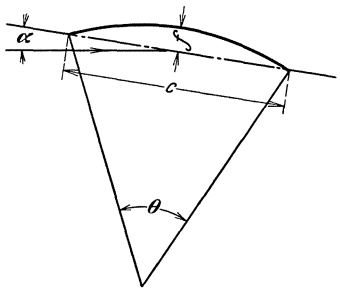

Fig. 30. Thin arched plate.

The formation of vortices at the front edge not only eliminates the force of suction P_S but also produces a diminution of lift, since it prevents the formation of the strong suction which occurs close to the front edge in the potential flow.

2. Thin Plates in the Form of Circular Arcs. This type of airfoil can also be treated quite easily by the methods of conformal transformation and vortex fields. The theoretical discussion (Division E II **10a**) provides the following equation between the lift coefficient C_L and α the angle of incidence

$$C_L = 2\pi \frac{\sin(\alpha + \theta/4)}{\cos(\theta/4)} \approx 2\pi \sin(\alpha + \theta/4) \approx 2\pi \left(\sin\alpha + \frac{2f}{c}\right) \tag{2.1}$$

In this formula θ is the angle at the center, f the height of camber, and c the chord of the circular arc (Fig. 30)

$$\theta = 8\frac{f}{c} \tag{2.2}$$

The lift vanishes for an angle of incidence

$$\alpha_0 = -\frac{\theta}{4} = -\frac{2f}{c} \tag{2.3}$$

The direction of this "null axis" of the profile is obtained by joining the middle of the profile to the back edge (Fig. 31). For the angle of incidence $\alpha = 0$, the lift coefficient is given by

$$C_{L0} = 2\pi \tan\frac{\theta}{4} \approx \frac{\pi\theta}{2} \tag{2.4}$$

The lift is, in that case, symmetrically distributed over the chord of the airfoil in accordance with the approximate equation

$$\frac{dC_{L0}}{dx} = \frac{C_{L0}}{c}\frac{4}{\pi}\sqrt{1-\xi^2} \tag{2.5}$$

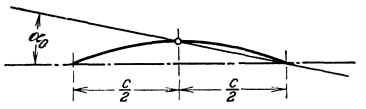

Fig. 31. Angle of incidence for an arched plate with lift zero.

The resultant lift therefore passes through the middle of the cross-section. For an angle of incidence α there is an additional lift approximately equal to the lift of a thin flat plate of the same chord and angle of incidence:

$$C_{L\alpha} = 2\pi \sin\alpha \approx 2\pi\alpha \tag{2.6}$$

and also having approximately the same distribution of lift as in the case of the flat plate [see (1.2)] and thus acting at a distance of $c/4$ from the front edge (Fig. 32). The force resulting from these two components is given by

$$C_L = C_{L0} + C_{L\alpha} \tag{2.7}$$

Its point of application is at $c/2$ when $\alpha = 0$; it approaches $c/4$ as α increases and for negative values of α shifts to the right toward ∞, which it reaches for $\alpha = -\theta/4$ with $C_L = 0$. The moment about the front edge is accordingly

$$C_M \approx \frac{\pi}{2}\sin\left(\alpha + \frac{\theta}{2}\right) \approx \frac{\pi}{2}\left(\sin\alpha + \frac{4f}{c}\right) \tag{2.8}$$

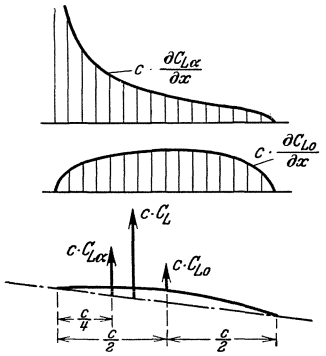

Fig. 32. Separation of the lift distribution and of the resulting lift, in parts, due each to camber (C_{L_0}) and to angle of incidence ($C_{L\alpha}$).

For curved plates, the same as in the case of flat ones, a loss occurs at the front edge when the angle of incidence is not zero; and the magnitude of this loss agrees approximately with the value for the flat plate with the same angle of incidence. There is this difference however, that curved plates already have a lift when the angle of incidence is 0 deg.; the position of least profile drag therefore moves toward larger values of C_L as the curvature increases. However, on account of the existence of lift and the dead air region at the rear end of the wing which produces the drag, there is an unsymmetrical disposition of the stream-lines, and therefore a diminution of the theoretical lift (see I 8), and therefore the smooth flow at the leading edge does not occur exactly

at $\alpha = 0$ but at a somewhat higher value. Therefore in estimating the position of least profile drag, it is useful to start from the lift rather than from the angle of incidence and to employ the approximate rule for airfoils in the shape of circular arcs, that the least profile resistance occurs approximately for $C_{L0} = 2\pi \sin \theta/4 = 4\pi f/c$. This rule is sufficiently exact for most practical purposes although in strongly curved airfoils the least drag has a rather lower position on account of the other drag component.

The preceding statements regarding thin plates apply also with good approximation to moderately thick cross-sections of equal mean curvature. Here again the amount of loss at the front edge depends very much on the extent to which it is rounded off.

3. Thin Plates with Arbitrary Curvature. The application of the method of conformal transformation to the case of cross-sections other than plane or circular form involves many difficulties. These however, are due to the additional complexity of the application of the method and not to any difficulties of principle in the theoretical discussion.

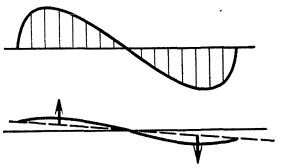

Fig. 33. Lift distribution for a profile with S-form with resultant zero lift.

The other method, employing vortex fields, permits of a simpler extension to this general case. In addition to the previous form-components, an S-shaped form must now be included. In the simplest case this is given by the equation

$$y = \frac{c}{2} \varkappa \left(\frac{\xi^3}{3} - \frac{\xi}{2} \right) \tag{3.1}$$

which corresponds to a distribution of lift over the airfoil chord in accordance with

$$\frac{dC_L}{d\xi} = -2\varkappa\xi\sqrt{1-\xi^2} \tag{3.2}$$

(see Fig. 33). The lift resulting from this component is zero and it only provides a pure moment, the coefficient of which is

$$C_M = -\frac{\varkappa\pi}{8} \tag{3.3}$$

This moment, when in conjunction with a circular curvature, produces a shift of the lift due to the circular curvature ($C_{L0} = 2\pi \cdot 2f/c$) away from the middle of the span. This shift has the value

$$\triangle s = c \frac{\varkappa}{32} \frac{c}{f} \tag{3.4}$$

If the lift be shifted in this manner to a point $c/4$ from the front edge it coincides in position with the component provided by an increasing angle of incidence, so that in this case alteration of the angle of incidence produces no displacement of the point of application. The cross-section

thus obtained is a so-called "fixed center of pressure" profile, the condition required being

$$\triangle s = \frac{c}{4} \tag{3.5}$$

It follows that

$$\varkappa_0 = \theta = \frac{8f}{c} \tag{3.6}$$

and

$$y_0 = \frac{c}{2}\,\theta\left(\frac{\xi^3}{3} - \frac{\xi}{2}\right) \tag{3.7}$$

It should be observed that the S-shaped profile of (3.1) which has no resultant lift, but a pure moment, has however, an angle of incidence (see Fig. 33), of amount

$$\alpha_S = \frac{\varkappa}{6} \tag{3.8}$$

The more general cross-sections obtained by superimposing this cross-section on to a circular arc profile of angle of incidence zero will also have an angle of incidence α_S. In order to have the ordinates still measured from the chord, it is therefore necessary to subtract the ordinates $z = -(1/2)\,c\,\alpha_S\,\xi$ of a flat plate with angle of incidence α_S. Similarly in obtaining the values of the forces and moments for an arbitrary angle of incidence α (superposition of a flat plate) it is necessary to observe that only the difference $\alpha - \alpha_S = \alpha - \varkappa/6$ is effective as an additional angle of incidence. For a cross-section whose shape is composed of a circular arc of curvature $f/c = \theta/8$ and an S-section of constant $\varkappa$, the preceding discussion supplies the equation:

$$\left.\begin{aligned} y &= \frac{c}{2}\left[\frac{\theta}{4}(1-\xi^2) + \varkappa\left(\frac{\xi^3}{3} - \frac{\xi}{2} + \frac{\xi}{6}\right)\right] = \\ &= \frac{c}{2}\left[\frac{\theta}{4}(1-\xi^2) + \frac{\varkappa}{3}(\xi^3 - \xi)\right] \end{aligned}\right\} \tag{3.9}$$

and the following coefficients of lift and moment for an angle of incidence α:

$$C_L = 2\pi\left(sin\,\alpha + \frac{\theta}{4} - \frac{\varkappa}{6}\right) \tag{3.10}$$

$$\left.\begin{aligned} C_M &= \frac{\pi}{2}\left(sin\,\alpha + \frac{\theta}{2} - \frac{\varkappa}{4} - \frac{\varkappa}{6}\right) \\ &= \frac{\pi}{2}\left(sin\,\alpha + \frac{\theta}{2} - \frac{5\varkappa}{12}\right) \end{aligned}\right\} \tag{3.11}$$

where $\theta = 8\,f/c$.

The superposition of the S-shape on the circular arc displaces the position of greatest camber height and in the shapes used in practical applications, where it is desirable to make the movement of the center of pressure as small as possible, this displacement always takes place forward. The camber height at the middle of the cross-section is not affected by the symmetrical S-shape and is simply a measure of the amount of the circular curvature, so that the camber height to be taken in the above formulae is not the maximum value, but the value at the middle

of the cross-section. The curvature of the cross-section decreases continually from the front to the back, and eventually may even become negative (S-shape). The difference between the angles ψ and φ (see Fig. 34) at the forward and after edges of the profile may be taken as a measure of the S component of the profile, while the sum $\psi + \varphi$ is a measure of the circular curvature. The following equations here apply

$$\psi - \varphi = \varkappa + 2\,\alpha_S = \frac{4}{3}\,\varkappa \tag{3.12}$$

$$\psi + \varphi = \theta = \frac{8\,f}{c} \tag{3.13}$$

The condition that a cross-section should have fixed center of pressure is $\varkappa = \theta$, giving $3\,(\psi - \varphi) = 4\,(\psi + \varphi)$

or

$$\psi = -7\,\varphi \tag{3.14}$$

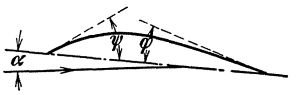

Fig. 34. End tangents for profile form.

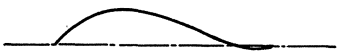

Fig. 35. Profile with fixed center of pressure.

A cross-section of this type and having fixed center of pressure is represented in Fig. 35. It has a point of inflection at $x = c/8$. The greatest camber height occurs at

$$x = \frac{c}{2}\left(\frac{1}{4} - \sqrt{\frac{19}{48}}\right) \approx = \frac{c}{2}\,(0.38)$$

The introduction of the angles φ and ψ, which are made by the tangents at the ends of the cross-section with the line joining these ends, has the disadvantage that even if their values are fixed we are still left with a range of possible shapes which the cross-section may have, and this range is too wide to allow the properties of the cross-section to be specified with any reasonable accuracy. Given the tangents at the ends, it is possible to draw different cross-sections having very different properties. The question therefore arises whether it is possible to find magnitudes characteristic of the cross-section which have a more closely determining effect on its shape. This can be effected by choosing the directions of the tangents at the points $\xi_1 = -(1/2)\sqrt{3}$, $\xi_2 = 0$, $\xi_3 = (1/2)\sqrt{3}$ as characteristics of the shape and position of the cross-section. If a contour of the fourth degree be superimposed upon the given contour of the third degree and if it be so chosen that it gives neither a lift nor a moment, it can be shown that such a superposition leaves the tangents at the three points mentioned unaltered. If γ be the angle made by tangent and chord at the point $\xi = 0$, and τ_1, τ_2 those made by the tangents at the points $\xi = \pm\,(1/2)\sqrt{3}$ respectively

with the tangent at $\xi = 0$ (see Fig. 36), the following relations hold and can be easily obtained by differentiating (3.7)

$$\gamma = \frac{\varkappa}{3} \tag{3.15}$$

$$\tau_1 = \frac{\theta}{4}\sqrt{3} + \frac{3}{4}\varkappa \tag{3.16}$$

$$\tau_2 = \frac{\theta}{4}\sqrt{3} - \frac{3}{4}\varkappa \tag{3.17}$$

These angles determine the shape of the cross-section but the ends of the profile, and hence the chord, are not quite fixed. Hence the most important quantity for the values of the force is not the usual angle of incidence α between the wind direction and the chord, but rather the position of the tangent at the point $\xi = 0$. The chord would be decisive if the shape of the cross-section were represented by (3.9), in which case $\gamma = \varkappa/3$; but if the shape of the cross-section deviates somewhat from that indicated by (3.9) the position of the chord is different. It is however possible to imagine an auxiliary chord drawn to correspond to the form of (3.9) by subtracting an angle $\gamma' = \varkappa/3$ from the tangent at the point $\xi = 0$. For a cross-section having an angle of incidence α, the tangent forms the angle $(\alpha + \gamma)$ and the auxiliary chord lies at the angle,

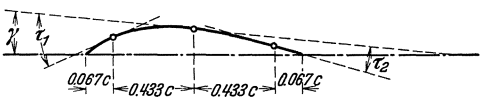

Fig. 36. Characteristic tangents for a profile.

$$\alpha' = \alpha + \gamma - \frac{\varkappa}{3} \tag{3.18}$$

with the direction of the wind. Here γ is the true angle between the tangent and chord, but on account of the uncertainty of the position of the chord it does not belong to the magnitudes which characterize the cross-section. It must therefore not be used for calculating the magnitude $\varkappa$ which does characterize the airfoil, but only for readjusting the angle of incidence. The quantities $\varkappa$ and θ are to be calculated from the characteristic angles τ_1 and τ_2 and have the values

$$\theta = \frac{2}{\sqrt{3}}(\tau_1 + \tau_2) \tag{3.19}$$

$$\varkappa = \frac{2}{3}(\tau_1 - \tau_2) \tag{3.20}$$

Hence we have the following formulae for lift and moment

$$\left.\begin{aligned} C_L \approx 2\pi\left(\sin\alpha' + \frac{\theta}{4} - \frac{\varkappa}{6}\right) \approx 2\pi\left(\alpha + \gamma - \frac{\varkappa}{3} + \frac{\theta}{4} - \frac{\varkappa}{6}\right) = \\ = 2\pi\left[\alpha + \gamma + \frac{1}{2\sqrt{3}}(\tau_1 + \tau_2) - \frac{1}{3}(\tau_1 - \tau_2)\right] \end{aligned}\right\} \tag{3.21}$$

$$C_M = \frac{\pi}{2}\left[\alpha + \gamma - \frac{\varkappa}{3} + \frac{\theta}{2} - \frac{5\varkappa}{12}\right] = \\ = \frac{\pi}{2}\left[\alpha + \gamma + \frac{1}{\sqrt{3}}(\tau_1 + \tau_2) - \frac{1}{2}(\tau_1 - \tau_2)\right] \Bigg\} \quad (3.22)$$

Cross-sections with fixed centers of pressure satisfy the condition $\varkappa = \theta$ or

$$\tau_1 - \tau_2 = \sqrt{3}(\tau_1 + \tau_2)$$

whence

$$\tau_2 = -\left(2 - \sqrt{3}\right)\tau_1 = -0.27\,\tau_1 \quad (3.23)$$

If the shape of the cross-section is expressed in this way by means of the angles τ_1 and τ_2, and the angle of incidence α is corrected by the angle γ, the properties of the cross-section are already largely determined, even if the cross-section has not quite the shape expressed by (3.9).

As in the case of flat plates an additional drag occurs at the front edge of these cross-sections if the entering flow is not smooth (without shock). Smooth entering flow is to be expected for an angle of incidence

$$\alpha_1 = \frac{\varkappa}{6} = \frac{1}{9}(\tau_1 - \tau_2) \quad (3.24)$$

and the lift coefficient

$$C_L = \pi\frac{\theta}{2} = 4\pi\frac{f}{c} \quad (3.25)$$

There is no difficulty in calculating the properties of any arbitrarily given cross-section by the method of vortex fields. In particular there are the general expressions furnished by Munk's integrals (Division E II 9).

$$C_L = 2\pi\alpha + 2\int_{-1}^{+1}\frac{y}{c}\frac{d\xi}{(1-\xi)\sqrt{1-\xi^2}} \quad (3.26)$$

$$C_M = \frac{\pi\alpha}{2} + 2\int_{-1}^{+1}\frac{y}{c}\frac{1-\xi+\xi^2}{(1-\xi)\sqrt{1-\xi^2}}d\xi \quad (3.27)$$

Munk's integral especially adapts itself to the case of a given cross-section whose shape deviates considerably from the normal and whose properties are to be estimated. If however the problem to be solved consists of finding a cross-section, or altering the shape of a given cross-section in order to obtain certain desired properties, the previously described procedure of superposition of typical forms is more suitable. For by employing that method the shape and properties of the cross-section can be defined for many requirements by the use of a small number of parameters (*e. g.*, τ_1 and τ_2 as in the example above).

In using this method however, it must be remembered that the actual value of the lift is always somewhat less than the calculated value, on account of the formation of a wake of mixed turbulence (for the connection to the drag see I 8); moreover this method can only be applied to shapes which have small drag.

4. Profiles of Finite Thickness. If a cross-section of finite thickness is treated by the method of vortex fields, the same approximations being made as in the case of thin plates, the results obtained are the same as those for a thin plate whose shape coincides with the middle line of the cross-section. Thus in order to estimate approximately the properties of a cross-section of finite thickness it may be replaced by a thin plate lying along its middle line.

It will however, be desirable to discuss in broad outline the respects in which the properties of thick cross-sections differ from those of thin cross-sections. If a circle be conformally transformed (without altering the conditions at infinity) into a straight line or a circular arc, it is found that the length of the line is exactly, and that of the circular arc is nearly, twice that of the diameter of the circle. By transforming the same circle into a cross-section of finite thickness it is possible to produce all the transitions between a circular section and a thin plate. The thicker the cross-sections the more nearly they approach the circle; the thinner they are, the more they approximate to thin plates. It follows directly from this that the cross-sections derived from the same circle, and therefore having the same lift, become shorter as they grow thicker. This means that a thick cross-section must be somewhat magnified before it is replaced by its middle line, or in other words, that the lift of a thick cross-section is rather more than that of its middle line. This effect is, however, compensated to some extent, since the drag of the cross-section increases with its thickness thereby lowering the actual lift as compared with the calculated value.

The effect of thickness in shifting the position of the center of pressure is more important. The lift of a thin plate curved into the form of a circular arc passes through the middle for angle of incidence zero and moves toward the point $c/4$ as the angle of incidence increases. For a circle, the center of the lift always passes through the center. For thick cross-sections between these two extreme cases, the shift of the center of pressure is greater than for the circle, but less than for the thin plate. In order to obtain a thick cross-section with a fixed center of pressure, a smaller S component is required for the middle line than in the case of a thin cross-section.

A point which deserves special notice in the case of thick cross-sections is the definition of the angle of incidence, which is usually referred to the chord of the section. Although the simplest relations of the properties of thin cross-sections are based on the use of angles of incidence referred to the chord of the section, thickening of the section, especially when achieved by rounding off the front edge, shifts the chord considerably. In order to apply the simple laws for thin profiles to give approximate values for sections of finite thickness, the difference in the angle so produced must be taken into account.

The relations which obtain can be best realized by considering a Joukowski cross-section. If a circle a is transformed into a circular arc a' (Fig. 37) the somewhat larger circle b transforms into the Joukowski cross-section b', a contour surrounding a'. In this case the arc a', the so-called skeleton of the Joukowski section, is obviously the aerodynamic mean line with reference to the angle of incidence. It has already been mentioned that a thin cross-section equivalent to a Joukowski cross-section must be rather larger. Especially important with reference to the angle of incidence, is the position of the foremost point relative to the after edge. The head of the Joukowski section surrounds the front end of its skeleton approximately in the shape of a parabola whose

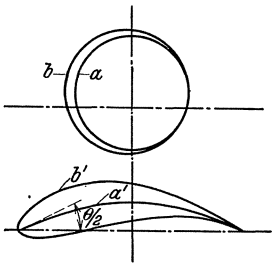

Fig. 37. Joukowski's transformation.

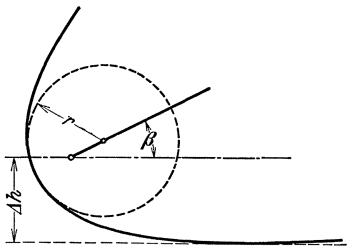

Fig. 38. Skeleton of the head of a profile.

focus is at the front edge of the skeleton (Fig. 38). If r is the radius of curvature of the leading edge of the section, the skeleton begins at a distance of $r/2$ behind the leading edge. If the deepest point of the parabola measured from the chord of the skeleton is denoted by $\triangle h$, then in accordance with known properties of the parabola (see Fig. 38)

$$\triangle h = \frac{r}{2 \sin \beta} \tag{4.1}$$

where β denotes the angle at which the front edge of the skeleton cuts the X axis (the chord of the skeleton). For skeletons in the shape of a circular arc (*e. g.* Joukowski profiles) $\beta = \theta/2$, where θ denotes, as before, the angle subtended by the circular arc at the center. But for more general cross-sections having S components, this simple relation does not hold.

The difference, $\triangle \alpha$ between the theoretical angle of incidence referred to the chord of the skeleton (X axis) and the usual angle of incidence referred to the chord of the cross-section, is obtained from the difference of height $\triangle h$:

$$\triangle \alpha \approx \frac{\triangle h}{c} = \frac{r}{2\, c \sin \beta} \tag{4.2}$$

This approximate formula holds reasonably well if $f/c > t/c$, where f means the camber of the skeleton and t the thickness of the profile. More exact

values for the difference can be obtained by drawing the corresponding cross-sections from case to case[1].

5. The Characterization of Profiles of General Form. It was found in previous paragraphs, when discussing thin cross-sections by the method of vortex fields, that the lift can be divided into two components, of which one represents the effect of curvature and the S-shape of the section and is independent of the angle of incidence, while the other is proportional to the angle of incidence and is applied at a point $c/4$ from the front edge. The moment about this point is constant for all angles of incidence, since the component which depends on the angle of incidence always passes through it and contributes nothing to the total moment. Investigations due to von Mises[2] (see Division E II **20**) have shown that this peculiarity is only a special case of a far more general law of airfoil properties. This generalized law holds not only for thin cross-sections but for boundaries of any shape, and provided a potential flow is postulated, its statement is exact and not merely approximate. *Every cross-section has a point about which the moment of the lift forces is constant, i. e., independent of the angle of incidence. The lines of action of the lift forces form the envelop of a parabola whose focus is the point about which the moment is constant*[3] (Fig. 39, focus F). Since the lift acts perpendicularly to the direction of flow and since each direction gives only one tangent to the parabola, it follows that if the parabola is known, the direction and line of application (but not the magnitude) of the lift force in every direction of flow, *i. e.* for every angle of incidence, is known. The parabola itself is fixed if the position of the focus in the cross-section, the direction of its axis, and its *focal length*, are known. For a direction of flow perpendicular to the axis of the parabola, the lift is parallel to the axis and therefore moves off to infinity and becomes zero (direction of zero lift, first axis of the cross-section). If the focal length of the parabola becomes infinitesimally small, all the forces of lift pass through the focus and the cross-section then has a fixed center of pressure.

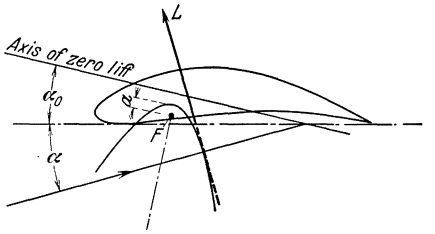

Fig. 39. Characteristic parabola for a profile.

[1] O. Schrenk has calculated these differences of angle for a series of Joukowski cross-sections. Ergebnisse der Aerodynamischen Versuchsanstalt zu Göttingen, III. Lief., p. 15 (Oldenbourg, Munich, 1927).

[2] Mises, R. von, Zur Theorie des Tragflächenauftriebes. Zeitschr. f. Flugtechnik u. Motorl. 8, pp. 11 and 157, 1917; **11**, pp. 68 and 87, 1920.

[3] See Division E **15**.

A quantity characterizing the size of the cross-section is necessary in order to determine the magnitude of the forces of lift. In theoretical work the quantity frequently used for this purpose is the radius of the circle into which the cross-section can be conformally transformed with unaltered conditions at infinity, or some other quantity connected with this transformation. For practical applications however, it is convenient to use some more obvious quantity, as for example the chord c' of an equivalent flat plate (see **1**).

The lift coefficient is then

$$C_L = 2\pi \frac{c'}{c} sin\,(\alpha + \alpha_0) \tag{5.1}$$

where c is the actual chord of the cross-section and α_0 the angle between the direction of zero lift (perpendicular to the axis of the parabola) and the chord of the cross-section, so that $(\alpha + \alpha_0)$ is the angle between the direction of flow and the direction for zero lift. The constant coefficient of moment referred to the focus F is

$$C_{M\,0} = 2\pi \frac{c'a}{c^2} \tag{5.2}$$

where a denotes the focal length of the lift parabola.

The practical applications of these important relations are chiefly connected with the solution of two problems. First, the investigation of the properties of a given cross-section, *i. e.* it is required to find the characteristic lift parabola and the equivalent chord of a given cross-section. Second, the construction of a cross-section with given properties *i. e.* it is required to find the cross-section corresponding to a given parabola and equivalent chord. The latter problem has no unique solution since any number of cross-sections can be constructed with the given properties. From these a selection must then be made in accordance with considerations regarding which theory has nothing to say. Theory assumes a potential flow in which no losses occur and has for example nothing to say regarding drag and maximum lift. Of the cross-sections which theoretically have the same properties, those will be selected which in practice have small drag and high maximum lift. The distribution of pressure obtained in accordance with theoretical considerations (see I **9**) is, however, useful for obtaining approximate values of the properties.

The methods employed in solving the above mentioned problems are described in Division E II **20**, **21** so that no further discussion is required here[1].

---

[1] See also the following articles connected with the investigations of v. MISES: W. MÜLLER, Ebene Profilströmung mit Zirkulation. Zeitschr. f. angew. Math. u. Mech. Vol. **3**, p. 117, 1923. — Zur Konstruktion von Tragflächenprofilen. *loc. cit.* Vol. 4, p. 213, 1924. — Über die Form und Auftriebsinvarianten für eine besondere

In order to obtain at least some idea of the connection between these characteristic profile magnitudes and the shape of the profile, their values will now be given for the case of a thin section with an S component, as already treated. Such an example is characterized by the angle $\theta = 8\,f/c$ for the circular arc component and the magnitude $\varkappa$ of the S component. For thin cross-sections $c' \approx c$. The focus, *i. e.* the point through which the part of the lift which is dependent on α acts, lies at a distance $c/4$ from the front edge. The lift is

$$L = \frac{\varrho}{2} V^2 c\, 2\pi \left(\alpha + \frac{\theta}{4} - \frac{\varkappa}{6}\right) \tag{5.3}$$

and the direction of zero lift is accordingly

$$\alpha_0 = \frac{\theta}{4} - \frac{\varkappa}{6} \tag{5.4}$$

The axis of the parabola is inclined to the chord at an angle

$$\frac{\pi}{2} - \alpha_0 = \frac{\pi}{2} + \frac{\varkappa}{6} - \frac{\theta}{4} \tag{5.5}$$

The moment about the focus is

$$M = \frac{\varrho\, V^2}{2} c^2 \frac{\pi}{8} (\theta - \varkappa) \tag{5.6}$$

Hence the focal length is

$$a = \frac{c}{16} (\theta - \varkappa) \tag{5.7}$$

Conversely, the constants of the thin section can be expressed in terms of the constants of the parabola

$$\varkappa = 12\,\alpha_0 - 48\,\frac{a}{c} \tag{5.8}$$

$$\theta = 12\,\alpha_0 - 32\,\frac{a}{c} \tag{5.9}$$

6. Results of Experimental Observations on Airfoils. Many types of airfoil profiles have been investigated in aerodynamic laboratories[1]. Unfortunately these experiments are often concerned with shapes which

Klasse von Flügelprofilen. *loc. cit.* Vol. 4, p. 389, 1924. — Die Ermittlung von Auftriebsinvarianten vorgegebener Profile. *loc. cit.* Vol. 5, p. 397, 1924.

F. Höhndorf, Verfahren zur Berechnung des Auftriebes gegebener Tragflächenprofile. *loc. cit.* Vol. 6, p. 265, 1926.

Theodorsen, Th., Theory of Wing Sections of Arbitrary Shape. U.S. N.A.C.A. Report No. 411, 1931.

[1] See for Example U.S. N.A.C.A. Reports Nos. 93, 124, 182, 244, 286, 315, Aerodynamic Characteristics of Airfoils (General Survey). Report 352, Large Scale Aerodynamic Characteristics of Airfoils as Tested in the Variable Density Wind Tunnel (General Survey).

Prandtl, L., and Betz, A., Ergebnisse der Aerodynamischen Versuchsanstalt zu Göttingen, Lief. I—IV (Oldenbourg, Munich 1921, 1923, 1927, 1932). In the following briefly noted as "Ergebnisse".

Jurieff, B. N., and Lessnikowa, N. P., Aerodynamical Investigations, Transaction of the Central Aero-Hydrodynamical Institute No. 33, Moscow, 1928 (Russian).

Crocco, G. A., Elementi die Aviazione, Vol. 1 (General Survey).

have accidently arisen for specific purposes and are not sufficiently distinct from one another to permit of inferences regarding the effect of individual alterations of form. In the paragraphs which follow, a selection from the great mass of experimental results will be indicated from

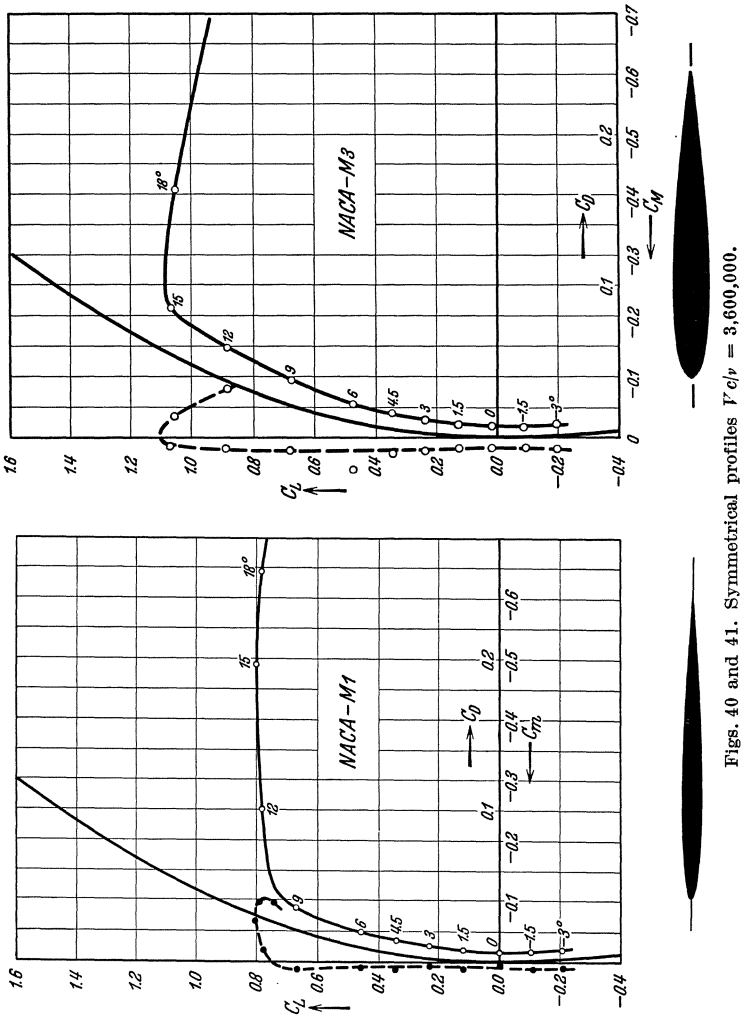

Figs. 40 and 41. Symmetrical profiles $Vc/\nu = 3{,}600{,}000$.

among those observations where the influence of systematic changes of form can be detected. Where results obtained with the variable density wind tunnel of the U.S. N.A.C.A. are available, they have been preferred for inclusion, on account of the large Reynolds numbers Vc/ν involved. These measurements have occasionally been undertaken with various

Reynolds numbers so that the effect of the Reynolds number can be detected. Where measurements with the variable density wind tunnel

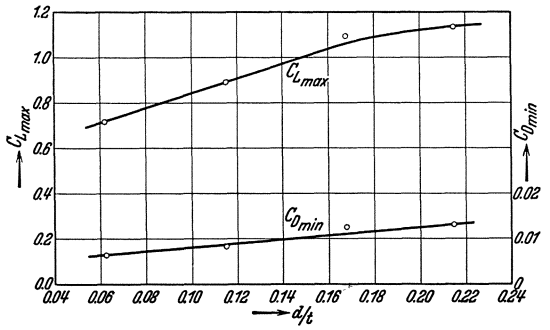

Fig. 42. Maximum lift and minimum drag for the symmetrical profile as a function of thickness ratio.

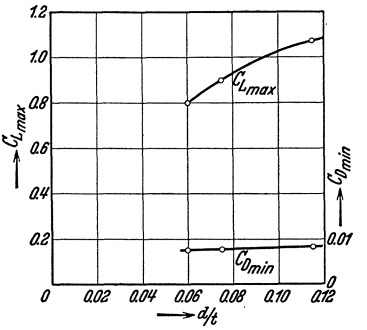

Fig. 43. Maximum lift and minimum drag for the symmetrical Joukowski profile as a function of the thickness ratio.

are not available, results obtained at the Göttingen Aerodynamic Laboratories have been included. For the former, the profiles are denoted by

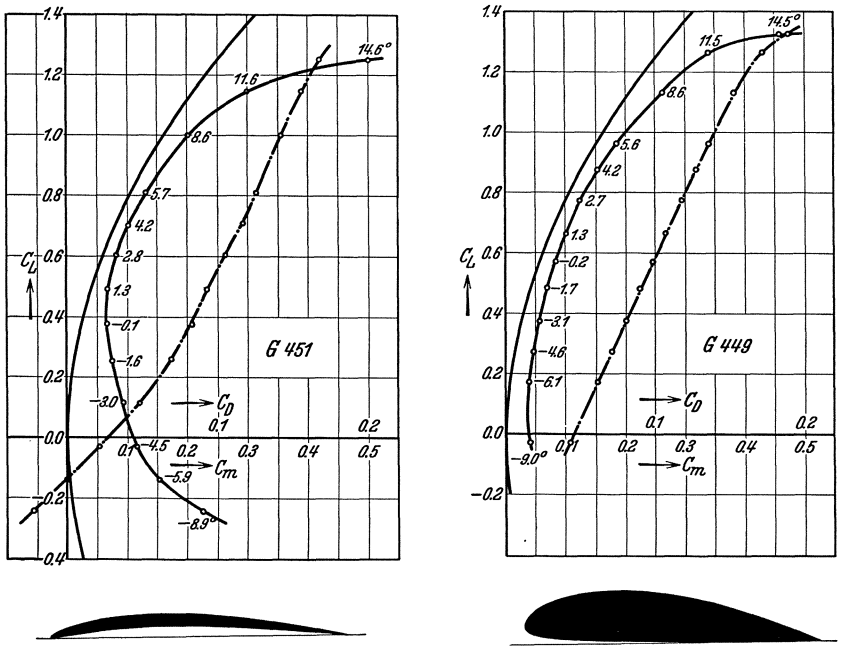

Figs. 44 and 45. Profiles with the same mean camber but different thickness: $V c/\nu = 420{,}000$.

the symbols used in the N.A.C.A. reports, and for the latter, by the numbers used in the Göttingen publication, preceded by a *G*. The

measurements taken are naturally with finite aspect ratio (Göttingen 5 : 1, N.A.C.A. 6 : 1). Instead of recalculating the results to apply to a ratio $\infty : 1$ (two-dimensional flow) the parabola of the induced drag of IV (2.10) of Division E has been introduced. The profile drag is therefore the difference between the given measurements and the parabola. The correction necessary on account of the finite diameter of the air jet has been allowed for in all cases, the adjustment being made directly

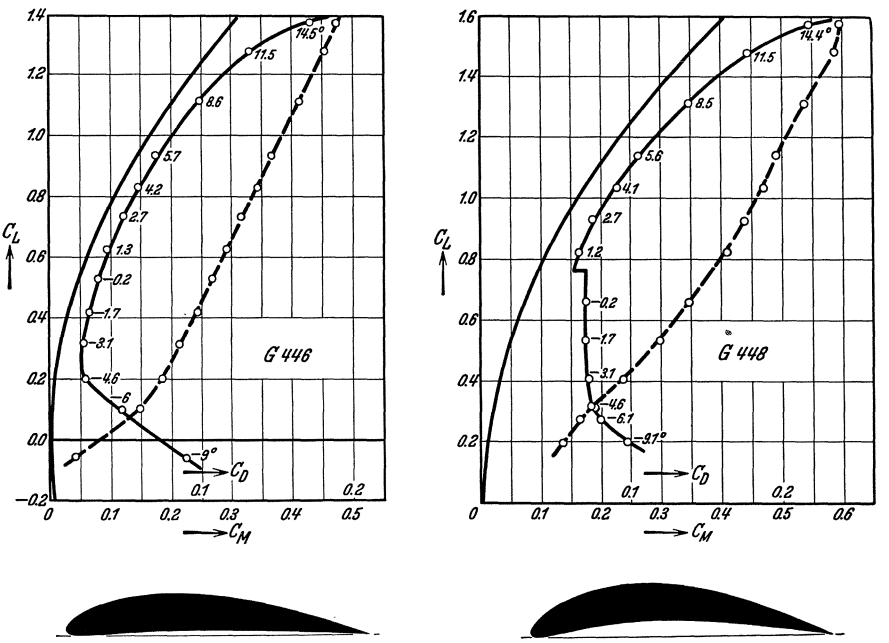

Figs. 46 and 47. Profile with the same thickness but with different mean camber: $Vc/\nu = 420{,}000$.

on the measurements provided by the Göttingen results and by altering the parabola of the American results which therefore correspond to an aspect ratio of 6.86 : 1 instead of 6 : 1.

The position of the "moment point" (*i. e.* the point about which the moment of the lift is taken) is defined as follows in the two sets of results: Göttingen: the point of the chord which lies under the nose of the cross-section (see Division E I 4); N.A.C.A.: a point of the chord $c/4$ behind the forward edge. A moment tending to increase the angle of incidence is called positive in the Göttingen results and negative in the N.A.C.A. results. There is therefore the following connection between the values of the moment in the two cases (C_{MG}, Göttingen; C_{MA}, American results)

$$C_{MG} = -C_{MA} + \frac{C_n}{4}$$

where $C_n \approx C_L$ is the dimensionless coefficient of the normal force perpendicular to the chord.

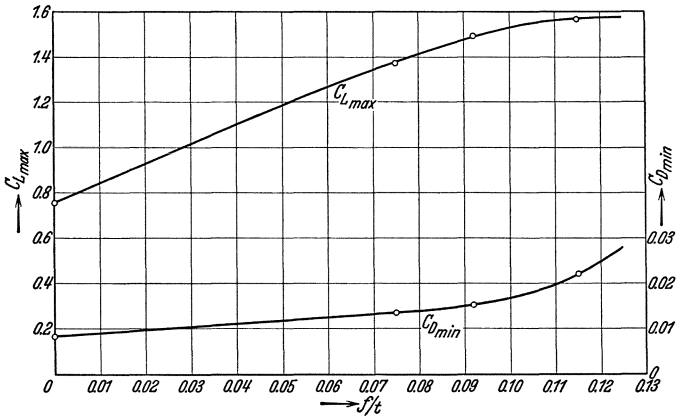

Fig. 48. Maximum lift and minimum drag for profiles of the same thickness ratio, as a function of mean camber.

Figs. 40 and 41 show two symmetrical profiles with different thickness. A further profile of this series is the American M 2 (N.A.C.A. Report

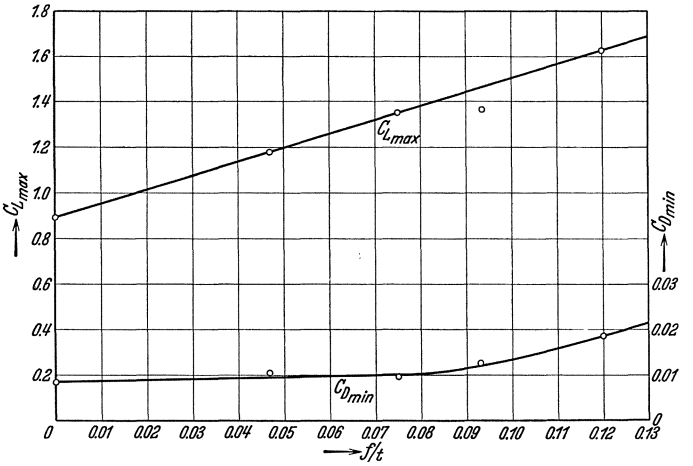

Fig. 49. Maximum lift and minimum drag for Joukowski profiles of the same thickness ratio, as a function of the mean camber.

No. 221). A similar series of symmetrical Joukowski profiles is furnished by the Göttingen G. 429, 537, 538, 539, 540, 639, 640 (Ergebnisse, Vols. III and IV). These latter are distinguished from the former series especially by the thin extended trailing edge.

The line chosen as axis of reference for the angle of incidence is in these cases the axis of symmetry. These figures assist in establishing the fundamental law that the maximum lift increases as the thickness increases but only up to a certain limiting value. In the case of thin cross-sections the maximum lift appears to be restricted by the state of affairs at the front edge (see I 3). The profile drag is least at $\alpha = 0^0$ and increases only moderately up to the neighborhood of the maximum lift. The smallest profile drags increase with the thickness. Figs. 42 and 43 show the nature of the dependence of maximum lift and least profile drag on the thickness[1]. (For the drag of thin cross-sections see **1, 2.**)

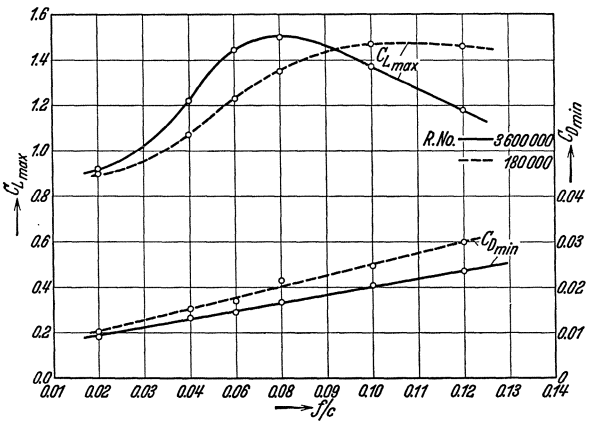

Fig. 50. Maximum lift and minimum drag for a profile with plane face, as a function of the mean camber.

Next follows a series of profiles having the same mean curvature but various thicknesses. Of these, two examples are given in Figs. 44 and 45. To the same series belongs also the intermediate profile form G. 450. Corresponding Joukowski forms are found in the Göttingen "Ergebnisse", Vols. III and IV. Essentially the same effect of thickness is shown here as in symmetrical cross-sections, but the position of least profile resistance lies not at $C_L = 0$, but at a point with finite lift (see the case of the plate in the form of a circular arc, II 2). As the thickness increases, the minimum drag increases somewhat, but so does the region in which the drag is small.

Figs. 46 and 47 show two profiles of equal thickness but of different curvatures. Between these two is also found the Göttingen profile G. 447, with a corresponding series of Joukowski profiles shown in the Göttingen "Ergebnisse", Vols. III and IV. As the curvature increases,

[1] A similar recent investigation of symmetrical cross-sections in the variable density wind tunnel can be found in Technical Note of the U.S. N.A.C.A. No. 386.

the position of minimum drag shifts toward positions with higher C_L, while at the same time the minimum drag and the maximum lift both increase. Figs. 48 and 49 show the relation between the two quantities last mentioned and the mean curvature. An intermediate position between the last two series is shown by the group of American profiles[1]

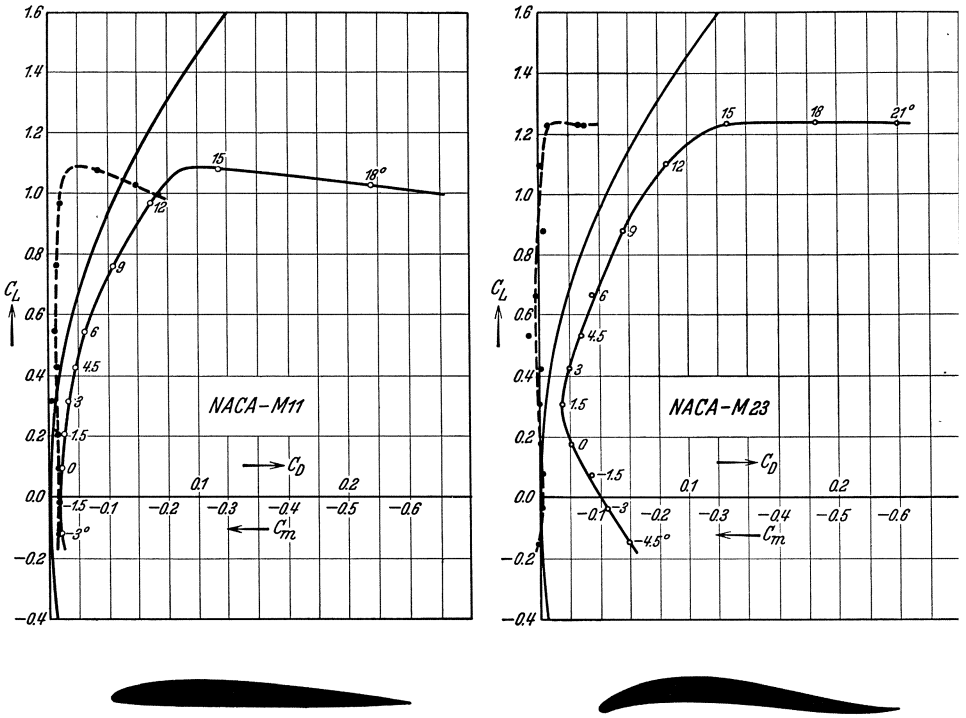

Figs. 51 and 52. Profiles of fixed center of pressure with different camber and thickness: Vc/ν = 3,860,000 and 3,370,000.

U.S. N.P.S., Nos. 1—6. These are profiles having a plane for the pressure side but with the ordinates of the other side changed in constant ratio, so that the thickness and mean curvature are altered simultaneously and in the same ratio (thickness = 2 times mean height of camber). The polars accordingly show the simultaneous effects of the alterations in thickness and curvature. Fig. 50 shows the maximum lift and minimum drag of these cross-sections as a function of their mean camber.

Of especial importance is the series N.A.C.A.—*M*., which gives results for profiles with constant center of pressure (Report No. 221). The symmetrical profiles M_1 to M_3 of this series have already been noted (see Figs. 40 and 41). The remaining members of this series are

[1] U.S. N.A.C.A. Report No. 259, 1927.

divided among groups with the same mean camber line but with three different thicknesses. If certain profiles are to be distinguished among others for small change of the center of pressure, the following groups with increasing mean camber may be noted—M_1 to M_3 (symmetrical); M_{10} to M_{12}; M_{16} to M_{18}; M_{22} to M_{24}. In Figs. 51 and 52, two examples with average thickness are shown.

CHAPTER III

AIRFOILS OR WINGS OF FINITE SPAN

A. Single Wing Monoplane

1. General Phenomena. The two-dimensional flow around a wing of finite span is disturbed at the ends of the wing. This is due to the fact that the difference of pressure between the upper and lower sides disappears at the wing boundaries and must therefore diminish to zero toward the tips. The consequent fall of pressure accelerates portions of the flow across the main direction of flow; particles above and below the wing move inward and outward respectively and form the so-called "marginal vortices".

These phenomena have the following important practical consequences:

1) There is a *diminution* in the difference of pressure between the two sides of the wing toward the ends, and hence *diminished lift and circulation* at and near these points.

2) Additional disturbing *air movements* are generated about and near the wing.

3) There is a *loss of energy*, which shows itself as an increased drag. The latter can be deduced either from the energy of the disturbing velocities or, alternatively, as a direct effect of the disturbing velocities on the airfoil itself, since it follows from the Kutta-Joukowski theorem that the combination of the vertical components of the disturbing velocities and the circulation about the airfoil produces a force in the direction opposite to that of the flow, *i. e.* a drag. This additional resistance is called the *induced drag*.

The theory of the phenomena described above is discussed in detail in Division E IV, and it will be sufficient to summarize here the most important results of that discussion. If $\Gamma = \Gamma(y)$ is the circulation along the span of the airfoil, the component vertically downward of the disturbing velocity at the point y_1 of the airfoil is given by the formula

$$w = \int_{-b}^{+b} \frac{\partial \Gamma}{\partial y} \frac{dy}{4\pi(y_1 - y)} \tag{1.1}$$

At a distance behind the airfoil these disturbing velocities increase to twice the value given by the above formula. If L is the lift on the airfoil,

$$L = \varrho V \int_{-b}^{+b} \Gamma \, d y \tag{1.2}$$

the induced drag D_i is

$$D_i = \varrho \int_{-b}^{+b} w_{(y1)} \Gamma_{(y1)} \, d y_1 = \frac{\varrho}{4\pi} \int_{-b}^{+b} \int_{-b}^{+b} \Gamma_{(y1)} \frac{\partial \Gamma}{\partial y_{(y)}} \frac{d y \, d y_1}{y_1 - y} \tag{1.3}$$

The distribution of the circulation Γ is deduced from the shape of the airfoil and the value of the disturbing velocity w. These factors are connected by the formula

$$\Gamma = \pi V c' \left(\alpha - \alpha_0 - \frac{w}{V} \right) \tag{1.4}$$

in which c' is the equivalent profile chord length $c' = (c/2\pi) \, \partial C_L / \partial \alpha$ [see II (1.1)], α the angle of incidence of the profile at the point y, and α_0 the corresponding angle of incidence for zero lift. When the shape of the airfoil is known, the two unknowns Γ and w can be calculated from (1.1) and (1.4). This involves the solution of an integral equation. It is much simpler to deduce the shape of airfoil corresponding to any given distribution of circulation. For, having solved for w by a simple integration of the right-hand side of (1.1), the equivalent chord length c' can be calculated from (1.4) by choosing arbitrary values for α and α_0. Conversely, of course, c' may be determined arbitrarily and the corresponding values of α calculated. In neither case is the solution unique for there is an infinite number of possible airfoil forms which can produce a given distribution of lift.

These forms must however satisfy some additional conditions which restrict the multiplicity of possible solutions. Even in the absence of all other restrictions α would be chosen inside a range for which the lift drag ratio of the wing is fairly good. Sometimes, the selected values of α will be as large as possible in order to minimize variations of force due to changes in the angle of incidence, while in other cases, the angle of incidence will be taken small in order to obtain large changes of force for small changes of angle or, again, in order to be sufficiently far from the maximum lift. Such varying standpoints furnish, however, only general qualitative criteria; they leave open a large field of possible values of α and are the deciding factors in selecting the average angle of incidence rather than the distribution of the angle of incidence across the span. There are, however, other considerations which provide more definite restrictions on the distribution of the angle of incidence (wing warping) over the span.

One is the behavior of the wing with respect to alterations in the total angle of incidence. If, for example, the effective angle of incidence

$(\alpha - \alpha_0)$ together with the chord length of the wing are so arranged that the former is constant across the span while the latter has a value satisfying (1.4), the change in circulation for a change in the angle of incidence of the entire wing is proportional to the circulation itself. The curves of distribution of circulation for various angles of incidence can be transformed into one another simply by multiplying the ordinates by some constant. This is easily seen if it is realized that, according to (1.1), if the ordinates of the distribution of circulation are increased in a constant ratio, $\Gamma_1 = \varkappa \Gamma$, while the velocity V is unchanged, the ordinates of the w distribution are increased in the same ratio, *i. e.* $w_1 = \varkappa w$. If this new value be substituted for w in (1.4) the requisite circulation distribution ($\Gamma_1 = \varkappa \Gamma$) can be obtained only by changing $(\alpha - \alpha_0)$ into $\varkappa (\alpha - \alpha_0)$. Since rotation of the wing as a whole can only alter the effective angle of incidence $(\alpha - \alpha_0)$ by the same amount at all points of the profile, a constant proportional increase of $(\alpha - \alpha_0)$ is only possible if $(\alpha - \alpha_0)$ is constant at all points. If this is not the case, an alteration in the angle of incidence alters the character of the circulation distribution curve. If, for example, the effective angle of incidence $(\alpha - \alpha_0)$ decreases toward the ends of the wing, the curve of circulation distribution with increase in the angle of incidence will become more full toward the ends, and with decrease in the angle, more lean.

2. Minimum Values (see Division E I **11**). If the lift L, span $2b$, velocity of flight V, and air density ϱ are given, the condition that the induced drag should be a minimum is that the lift (and hence the circulation) should have an elliptic distribution over the span, *viz.*

$$\Gamma = \Gamma_0 \sqrt{1 - \left(\frac{y}{b}\right)^2} \tag{2.1}$$

The lift is then such that

$$L = \varrho V \Gamma_0 b \frac{\pi}{2} \tag{2.2}$$

and the induced drag $$D_i = \frac{L^2}{4 \pi q b^2} \tag{2.3}$$

where $q = (1/2)\, \varrho\, V^2$. The corresponding coefficients of lift and drag satisfy the equations

$$C_L = \frac{\Gamma_0 \pi b}{V S} \tag{2.4}$$

and

$$C_{Di} = \frac{C_L^2 S}{\pi (2b)^2} \tag{2.5}$$

respectively. Here S denotes the surface area and $(2b)^2/S$ is the aspect ratio[1]; if the mean chord length is c_m, then $c_m = S/2b$ so that $(2b)^2/S = 2b/c_m$.

[1] The reciprocal of this quantity, *i. e.* $S/(2b)^2$ is also sometimes referred to as the aspect ratio.

With these values the downwash velocity w over the airfoil is constant:

$$w = V\frac{C_L}{\pi}\frac{S}{(2b)^2} = V\frac{L}{\pi q (2b)^2} \tag{2.6}$$

Since the induced drag of (2.3) and (2.5) is a minimum, its amount is not greatly altered by small divergences of the lift from the most favorable distribution represented by (2.1). Moreover, variations of the airfoil from the most favorable shape are followed only partially by the lift distribution. In general, therefore, airfoils which diverge considerably from the most favorable shape (*e. g.* a rectangular wing of constant angle of incidence as compared with a wing of elliptic contour and constant angle of incidence) may be accompanied by lift distributions not much different from the elliptic distribution, and hence by an induced drag differing only slightly from the minimum values as given by (2.3) and (2.5). (For the magnitude of the divergence see **5.**) The simple form of the minimum drag given above can therefore be used as a good approximation for almost all types of wings which occur in practice. Cases where the divergence is considerable are discussed below in **5.** We shall first consider some deductions from the formulas giving the minimum values.

3. Calculations of the Change in Drag Produced by Change of Aspect Ratio (see Division E I **12**). The formulas for the minimum induced drag are chiefly used for calculating the change in drag produced by alteration of the aspect-ratio. In doing so it is assumed that the coefficient of drag of the profile depends only on the coefficient of lift, C_L, so that if C_L is kept constant, any alteration in the total coefficient of drag is due to the induced drag alone. If C_{D1} is the coefficient of drag of a wing of aspect ratio $(2b_1)^2/S_1$, the coefficient of drag for a wing having the same profile, and the same coefficient of lift, C_L, but aspect ratio $(2b_2)^2/S_2$ is given by the formula

$$C_{D2} = C_{D1} + \frac{C_L^2}{\pi}\left(\frac{S_2}{(2b_2)^2} - \frac{S_1}{(2b_1)^2}\right) \tag{3.1}$$

[Division E I (12.7)]. It should be borne in mind that alteration of the downwash velocities also changes the effective angle of incidence, so that the value of the latter must be adjusted in order to produce the same lift. If the angle of incidence of the initial wing is α_1 the corresponding angle for the wing of altered span must be such that

$$\alpha_2 = \alpha_1 + \frac{C_L}{\pi}\left(\frac{S_2}{(2b_2)^2} - \frac{S_1}{(2b_1)^2}\right) \tag{3.2}$$

[Division E I (12.6)], the angles being measured in radians. If however, the angles are expressed in degrees the correction must be multiplied by 57.3^0.

The following relation connects C_L and α for a two-dimensional flow around an equivalent flat plate [see II (1.1)]:

$$C_L = 2\pi\alpha$$

For finite width of span on account of change of direction of relative air flow,

$$C_L = 2\pi\left(\alpha - \frac{w}{V}\right) = 2\pi\left(\alpha - \frac{C_L}{\pi}\frac{S}{(2b)^2}\right) \tag{3.3}$$

The value of the coefficient of lift for a given angle of incidence α is therefore,

$$C_L = \frac{2\pi\alpha}{\left(1 + 2\frac{S}{(2b)^2}\right)} \tag{3.4}$$

The only modification that this equation needs in order to apply to an airfoil of arbitrary profile is the multiplication of the right hand side by the ratio of c', the equivalent chord length (see II 1), to the actual chord length c, so that the equation becomes

$$C_L = \frac{c'}{c}\frac{2\pi\alpha}{\left(1 + 2\frac{S}{(2b)^2}\right)} \tag{3.5}$$

Hence the lift of a wing of finite span is reduced in the ratio $1 : \left(1 + 2\,S/(2\,b)^2\right)$.

Fig. 53 represents the polar curves[1] measured for seven wings of the same profile (G. 389) all of rectangular contour but of various aspect ratios. The same experimental results are reproduced in Fig. 54 after transformation to an aspect ratio 5 in accordance with (3.1) above. It is seen that the measured points now lie quite satisfactorily on a single curve. Systematic divergences are shown only by the values derived from airfoils of aspect ratio 1 and 2 respectively, the divergences in the latter case being somewhat smaller. Since the formulas were obtained by replacing a wing by a line bearing the whole lift, the observed divergences of forms having approximately square contours are not surprising; on the contrary, it is astonishing that the transformation formulas apply so well for such small aspect ratios. Airfoils of very large chord length are further discussed in 7.

Also the transformation of the angle of incidence in accordance with (3.2) is found to give good agreement with the results of experiment. In the same reference (see below) are given the results of plotting the lift coefficient C_L on the angle of incidence α. After transformation of the angle to correspond to a uniform value of the aspect ratio of 5, the points fall very well on the same curve, with the exception of those for ratios 1, and 2, for which the departures are somewhat greater.

In accordance with the postulates which underlie the theories under discussion, the effect of the ends of the wing is to alter the direction of approach of the flow. The effective angle of incidence remains the same for equal lifts and hence the point of application of the resultant force due to the air and the magnitude of its moment about the leading

[1] Figs. 53 and 54 together with others giving further confirmation of the transformation formula are from "Ergebnisse der Aerodynamischen Versuchsanstalt zu Göttingen", I. Lief., pp. 50 to 52 (Oldenbourg, Munich, 1921).

edge must remain the same[1]. It is therefore to be expected that the curves connecting the coefficient of moment with the coefficient of lift are identical for all aspect ratios, while the curves connecting the coefficient of moment with the angle of incidence vary with the aspect ratio. (The curves in the latter case would also coincide if the angle of incidence were transformed to apply to a single aspect ratio.) The

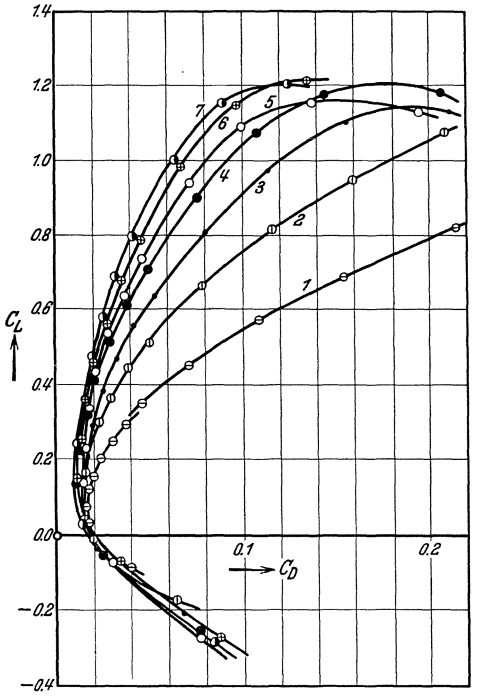

Fig. 53. Polars for airfoils of various aspect ratios. The numbers on the different curves refer to the aspect ratio $2\,b/c$.

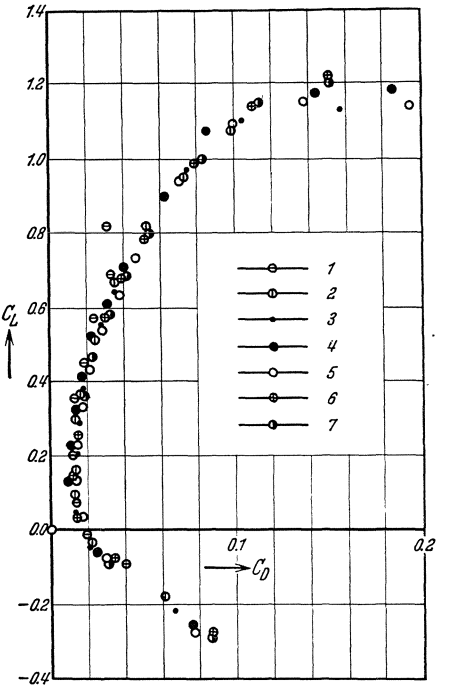

Fig. 54. The experimental results of Fig. 53 recalculated for an aspect ratio 5.

correctness of this conclusion is also shown on the basis of research measurements in the reference referred to in the footnote of p. 51.

4. Influence of the Aspect Ratio on Wing Performance. The most important result of the considerations regarding minimum values is the fact that the drag on the wing depends to a great extent on the aspect ratio $(2\,b)^2/S$, and can be reduced by increasing the aspect ratio (increase of span in comparison with chord).

[1] This simple argument however, must be corrected on account of the fact that the downwash velocities increase from the leading edge of the wing to the trailing edge. The wing is therefore in a curved flow whose effect is approximately equivalent to a decrease in the curvature of the wing. This effect is more noticeable with smaller aspect ratios.

Difficulties of construction, and in particular, consideration of the strength and rigidity of the wing, set limits to the possible increase in this direction. In order to estimate a suitable value for the aspect ratio it must be noted that only a part of the drag, *i. e.* the induced drag, depends on the aspect ratio, and is supplemented by the profile drag and, in a complete airplane, by the resistance of the remaining parts. In order to investigate the relations involved we separate the coefficient of drag, C_D of the entire airplane into the coefficients of induced drag, C_{Di} and residual drag C_{Dr} so that

$$C_D = C_{Di} + C_{Dr} \quad (4.1)$$

The relation between C_{Di} and C_L can be shown graphically for various aspect ratios in accordance with (2.5); the curves obtained are parabolas (Fig. 55). If the value of C_{Dr} is plotted from the zero point in the same diagram but in the direction opposite to that of C_{Di}, the sum $C_{Dr}+C_{Di}$ can be read off immediately as a distance. Since changes in the value of the angle of incidence produce only slight alterations in C_{Dr} the latter may be taken as constant for any given airplane and the diagram can be used to indicate the effects of various aspect ratios. Thus by drawing a tangent to the parabola corresponding to the given aspect ratio it is possible to determine the maximum lift-drag ratio and the value of the lift coefficient for which the latter is reached. An example is shown in Fig. 55: the value of C_{Dr} is given as 0.08, and $(2\,b)^2/S = 6$. The maximum value of the lift-drag ratio is then found for $C_L = 1.23$ and $C_D = 0.16$ or $(C_L/C_D)_{max} = 7.7$. From a well known property of the parabola, this condition is always found for $C_{Di} = C_{Dr}$.

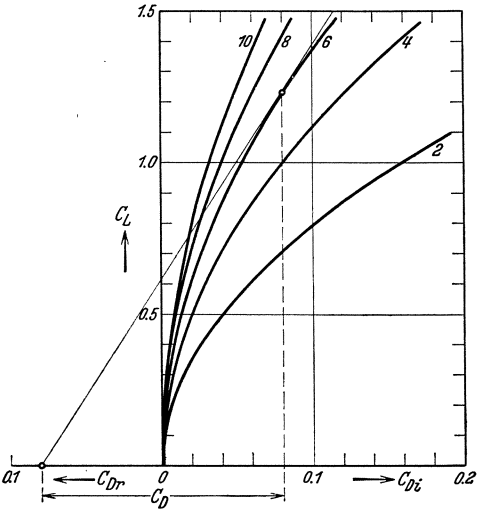

Fig. 55. Combination of induced and residual drags.

The weight W of a given airplane is essentially constant and therefore in level flight (cruising) it must have the same value as the lift. Hence for this condition

$$L = W \quad (4.2)$$

When flight occurs in the neighborhood of the maximum lift-drag ratio, then this ratio, which may be designated by ε, is approximately constant, *i. e.*, independent of the angle of incidence. Hence the drag under these conditions,

$$D = \frac{L}{\varepsilon} \quad (4.3)$$

is also approximately constant and the required propeller output,

$$P = D\,V = \frac{L\,V}{\varepsilon} \tag{4.4}$$

is directly proportional to the speed.

It should be observed that, for larger deviations from the maximum lift-drag ratio, the law connecting the induced drag D_i with the velocity V, or the dynamic pressure $q = (1/2)\,\varrho\,V^2$, is quite different in form from the corresponding law for the residual resistance D_r. In fact,

$$D_i = \frac{L^2}{\pi q\,(2b)^2} \tag{4.5}$$

while

$$D_r = C_{Dr}\,q\,S \tag{4.6}$$[1]

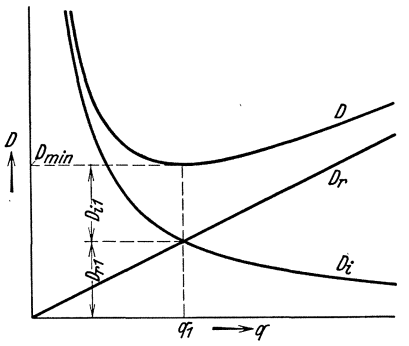

Fig. 56. Relation between induced, residual and total drags, and stagnation pressure.

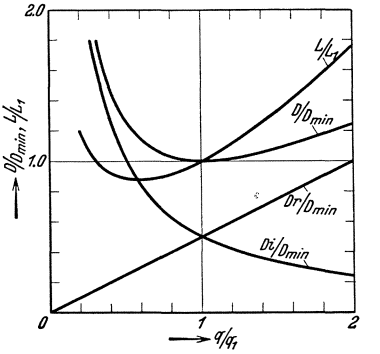

Fig. 57. General (non-dimensional) diagram of the dependence of drag and output on stagnation pressure.

If it is assumed, as previously, that C_{Dr} is approximately constant, it is seen that the residual drag is directly proportional while the induced resistance is inversely proportional to the dynamic pressure. Hence the product of the two resistances is independent of this pressure, and hence also of the velocity, and is a magnitude characterizing the airplane under consideration. Thus,

$$D_i\,D_r = \frac{L^2}{\pi\,(2b)^2}\,C_{Dr}\,S = L^2\,C_{Dr}\,\frac{S}{\pi\,(2b)^2} \tag{4.7}$$

The total resistance is

$$D = D_i + D_r = \frac{L^2}{\pi q\,(2b)^2} + C_{Dr}\,q\,S \tag{4.8}$$

and will be a minimum (with maximum lift drag ratio) for the particular value,

$$q_1 = \sqrt{\frac{L^2}{\pi\,(2b)^2}\cdot\frac{1}{C_{Dr}S}} \tag{4.9}$$

which gives,

$$D_{i1} = D_{r1} = C_{Dr}\,q_1\,S = \sqrt{\frac{L^2}{\pi\,(2b)^2}\,C_{Dr}\,S} = \sqrt{D_i\,D_r}$$

[1] The magnitude $C_{Dr}\,S$, characteristic of the particular airplane considered, is also termed the surface of equivalent drag, S_r.

Hence the minimum drag satisfies the equations

$$D_{min} = 2\sqrt{D_i D_r} = 2L\sqrt{\frac{C_{Dr}}{\pi}\frac{S}{(2b)^2}} \tag{4.10}$$

The above relationships are represented graphically in Fig. 56. A diagram applicable to all airplanes is obtained on making the drags and dynamic pressures non-dimensional. This is done by dividing these quantities by D_{min} and q_1 respectively [(4.9) and (4.10)]. In accordance with this representation, reproduced in Fig. 57,

$$\frac{D}{D_{min}} = \frac{1}{2}\frac{q_1}{q} + \frac{1}{2}\frac{q}{q_1} \tag{4.11}$$

In order to apply these results to any specific case it is only necessary to obtain from (4.9) and (4.10) the magnitudes q_1 and D_{min} characterizing the airplane in question.

The value of the cruising output (propeller output needed for level flight) satisfies the equations

$$P = V(D_i + D_r) = \frac{L^2}{\pi(2b)^2(\varrho V/2)} + C_{Dr} S \varrho \frac{V^3}{2} \tag{4.12}$$

and is a minimum for the particular value,

$$q_2 = \sqrt{\frac{L^2}{\pi(2b)^2}\frac{1}{3C_D S}} = q_1\sqrt{\frac{1}{3}} \tag{4.13}$$

or when

$$D_i = 3D_r \tag{4.14}$$

The minimum output is such that

$$\left.\begin{aligned} P_{min} &= \frac{4}{\sqrt{3}}\sqrt{D_i D_r}\sqrt{\frac{2L}{\varrho\, 2b}}\sqrt[4]{\frac{1}{3\pi C_D S}} = \\ &= 4L\sqrt{\frac{L}{3\pi(2b)^2(\varrho/2)}}\sqrt[4]{\frac{C_{Dr}S}{3\pi(2b)^2}} \end{aligned}\right\} \tag{4.15}$$

The output for the best possible lift drag ratio is given by the formula

$$P_1 = 2L\sqrt{\frac{L}{\pi(2b)^2(\varrho/2)}}\sqrt[4]{\frac{C_{Dr}S}{\pi(2b)^2}} \tag{4.16}$$

If the propeller output and the dynamic pressure are reduced to non-dimensional quantities by division by P_1 [(4.15)], and q_1 [(4.9)] respectively the form of the relation between them is independent of the type of airplane used[1]. The resulting curve is reproduced in Fig. 57.

$$\frac{P}{P_1} = \frac{1}{2}\left(\frac{q_1}{q}\right)^{1/2} + \frac{1}{2}\left(\frac{q}{q_1}\right)^{3/2} \tag{4.17}$$

[1] For examples of further applications of the above and of similar lines of development see M. SCHRENK, "Zur Berechnung der Flugleistung ohne Zuhilfenahme der Polare". Zeitschr. f. Flugtechnik u. Motorl. 18, p. 158, 1927; and "Einige weitere flugmechanische Beziehungen ohne Zuhilfenahme der Polare". *loc. cit.* 18, p. 399, 1927. Helmbold has shown that the limitation, that C_{Dr} should be independent of the angle of incidence, is unnecessary provided the symbols used are interpreted somewhat differently. (H. B. HELMBOLD, "Die generalisierten Koordinaten der Flugmechanik". Zeitschr. f. Flugtechnik u. Motorl. 18, p. 516, 1927.) The diagram of Fig. 57 remains valid for all aircraft provided the following changes

5. Influence of the Contour. From considerations of firmness and rigidity, a form of airfoil is preferred in which the chord decreases toward the wing tips (trapezoidal wing). One advantage of this is that with a given lift and given span the bending moment at the wing root is made smaller by the fact that the lift is concentrated toward the middle and the arm of the bending moment is thus made smaller. On the other hand the larger profile allows of a greater resisting moment due to the spars at the middle of the wing, at exactly the place where the bending moment is greatest. Naturally with such a contour we depart from the elliptic distribution with its minimum induced resistance, and we must discuss in somewhat closer detail the aerodynamic consequences of such deviations.

For any given airfoil the procedure developed by I. Lotz (Division E IV **12**) provides a moderately easy method for calculating the distribution of lift and hence the remaining quantities characterizing its aerodynamic behavior[1]. For present purposes, however, it is simpler to choose a suitable distribution of lift as a starting point and from it to determine the associated types of airfoil. We consider the case of a distribution of circulation characterized by the equation

$$\Gamma = \Gamma \sqrt{1 - \left(\frac{y}{b}\right)^2}\left[1 + a\left(\frac{y}{b}\right)^2\right] \tag{5.1}$$

containing an undetermined parameter a, different values of which can be used in investigating various types of airfoil.

---

are made; q_1 denotes as before the dynamic pressure at which the induced drag is equal to the residual drag (but is now no longer the dynamic pressure for which the total drag is a minimum); C_{Dr}, the coefficient of residual drag, now varies with the dynamic pressure; C_{D1} is the value of C_{Dr} when the dynamic pressure is q_1 and D_1 is the total drag for the same pressure;

$$\frac{q}{q_1} \text{ must be replaced by } \frac{q}{q_1}\sqrt{\frac{C_{Dr}}{C_{D1}}}$$

$$\frac{D}{D_{min}} \text{ by } \frac{D}{D_1}\sqrt{\frac{C_{D1}}{C_{Dr}}}$$

$$\frac{P}{P_1} \text{ by } \frac{P}{P_1}\sqrt[4]{\frac{C_{Dr}}{C_{D1}}}$$

where,

$$q_1 = \frac{L}{2b\sqrt{\pi S C_{D1}}}$$

$$D_1 = 2\frac{L^2}{\pi q_1 (2b)^2} = 2L\sqrt{\frac{C_{D1}}{\pi}\frac{S}{(2b)^2}}$$

$$P_1 = 2L\sqrt{\frac{L}{\pi (2b)^2 \varrho/2}}\sqrt[4]{\frac{C_{D1} S}{\pi (2b)^2}}$$

[1] KONING, C., and BOELEN, A., Aerodynamische Eigenschaften der Quasi-Trapezflügel mit verschiedener Breite des prismatischen Teiles. Zeitschr. f. Flugtechnik u. Motorl. **24**, p. 43, 1933.

HUEBER, J., Die aerodynamischen Eigenschaften von doppeltrapezförmigen Tragflügeln. Zeitschr. f. Flugtechnik u. Motorl. **24**, pp. 249, 269.

The formula for the lift due to the above distribution is found on calculation to be

$$L = \varrho V \int_{-b}^{+b} \Gamma \, dy = \varrho \, V \, \Gamma_0 b \, \frac{\pi}{2} \left(1 + \frac{a}{4}\right) \tag{5.2}$$

so that if L is to be constant the circulation at the center of the wing must satisfy the equation

$$\Gamma_0 = \frac{2L}{\pi \varrho \, V b \, (1 + a/4)} \tag{5.3}$$

In order to have a constant basis of comparison, the airfoil considered will always be compared with an airfoil of equal span and lift, but of elliptic distribution. Symbols referring to the latter case will be distinguished by the suffix "ell". Reference to (5.1) above shows that $a = 0$ for an elliptic distribution, so that at the middle of the wing

in the elliptic case $$\Gamma_{0\,(\mathrm{ell})} = \frac{2L}{\pi \varrho \, V b} \tag{5.4}$$

If, as a standard of comparison for the circulation, we take $\Gamma_{0\,(\mathrm{ell})}$ *i. e.* the circulation at the middle of an elliptic airfoil of equal width of span and lift, (5.3) and (5.1) can be written

$$\Gamma_0 = \frac{\Gamma_{0\,(\mathrm{ell})}}{1 + a/4} \tag{5.5}$$

$$\Gamma = \Gamma_{0\,(\mathrm{ell})} \sqrt{1 - (y/b)^2} \left(\frac{1 + a\,(y/b)^2}{1 + a/4}\right) \tag{5.6}$$

This type of distribution of circulation is illustrated in the upper part of Diagram 60 for parameter values $a = 1,\ 1/2,\ 0,\ -1/2,\ -1$. The downwash velocity on the airfoil at the point y_1 is now determined by the equations

$$w\,(y_1) = \int_{-b}^{+b} \frac{\partial \Gamma}{\partial y} \frac{dy}{4\pi (y_1 - y)} =$$

$$= \frac{\Gamma_0}{4\pi b} \int_{-b}^{+b} \frac{y/b}{(y_1 - y)\sqrt{1 - (y/b)^2}} \left[2a - 1 - 3a \left(\frac{y}{b}\right)^2\right] dy$$

$$= \frac{\Gamma_0}{4b}\left[1 - \frac{a}{2} + 3a\left(\frac{y_1}{b}\right)^2\right] = \frac{\Gamma_{0\,(\mathrm{ell})}}{4b} \frac{[1 - a/2 + 3a\,(y_1/b)^2]}{(1 + a/4)} \tag{5.7}$$

and the induced drag by

$$D_i = \varrho \int_{-b}^{+b} w \Gamma \, dy = \varrho \frac{\Gamma_0^2}{4b} \int_{-b}^{+b} \sqrt{1 - \left(\frac{y}{b}\right)^2} \left[1 + a\left(\frac{y}{b}\right)^2\right] \left[1 - \frac{a}{2} + 3a\left(\frac{y}{b}\right)^2\right] dy$$

$$= \frac{\pi \varrho \, \Gamma_0^2}{8} \left(1 + \frac{a}{2} + \frac{a^2}{4}\right) = \frac{\pi \varrho \, \Gamma_{0\,(\mathrm{ell})}^2}{8} \frac{1 + a/2 + a^2/4}{(1 + a/4)^2} \tag{5.8}$$

For elliptic distributions of lift the induced drag satisfies the formula

$$D_{i\,(min)} = \frac{L^2}{2\,\varrho\,V^2\,\pi\,b^2} = \frac{\pi\,\varrho\,\Gamma_{0\,(ell)}^2}{8} \tag{5.9}$$

and hence for given lift L and given span $2\,b$

$$\frac{D_i}{D_{i\,(min)}} = \frac{1 + a/2 + a^2/4}{(1 + a/4)^2} \tag{5.10}$$

This equation is shown graphically in Fig. 58.

The equation of the airfoil contour which corresponds to a distribution of lift satisfying (5.1) is calculated as follows: For simplicity we introduce as before

$$\xi = \frac{y}{b} \tag{5.11}$$

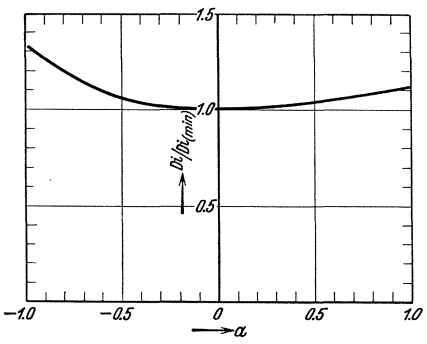

Fig. 58. Relation between induced drag and lift distribution.

and also replace the actual angle of incidence and chord length by the corresponding values for the equivalent flat plate (II 1). The new quantities are connected with those they replace by the equations

$$\alpha' = \alpha - \alpha_0 \tag{5.12}$$

$$c' = \frac{c}{2\,\pi}\frac{\delta C_L}{\delta\,\alpha} \tag{5.13}$$

Two expressions can be obtained for the circulation, for, by (1.4), its value in terms of the effective angle of incidence, $(\alpha' - w/V)$ and the chord length, c', is such that

$$\Gamma = V\,c'\,\pi\left(\alpha' - \frac{w}{V}\right) = V\,c'\,\pi\,\alpha'\left[1 - \frac{L}{2\,\varrho\,V^2\,\pi\,b^2\,\alpha'}\,\frac{1 - a/2 + 3\,a\,\xi^2}{1 + a/4}\right] \tag{5.14}$$

and, again, from (5.1) and (5.3)

$$\Gamma = \frac{2\,L}{\varrho\,V\,\pi\,b\,(1 + a/4)}\,\sqrt{1 - \xi^2}\,(1 + a\,\xi^2) \tag{5.15}$$

Then from the two equations just obtained,

$$\frac{c'}{b} = \frac{2\,L}{\varrho\,V^2\,\pi\,b^2\,\alpha'}\,\frac{1}{\pi}\,\frac{\sqrt{1 - \xi^2}\,(1 + a\,\xi^2)}{1 + a/4 - (L/2\,\varrho\,V^2\,\pi\,b^2\,\alpha')\,(1 - a/2 + 3\,a\,\xi^2)} \tag{5.16}$$

The corresponding equation for the chord at the middle of the wing ($\xi = 0$), for an elliptic distribution of lift ($a = 0$) on an airfoil of equal span and equal angle of incidence is

$$\frac{c'_{0\,(ell)}}{b} = \frac{2\,L}{\varrho\,V^2\,\pi\,b^2\,\alpha'}\,\frac{1}{\pi}\,\frac{1}{1 - L/2\,\varrho\,V^2\,\pi\,b^2\,\alpha'} \tag{5.17}$$

The mean or average chord of such an elliptic wing is

$$c'_{m\,(ell)} = \frac{S}{2\,b} = \frac{\pi}{4}\,c'_{0\,(ell)} \tag{5.18}$$

On comparing the chord length, c' of (5.16) with the mean chord length of the elliptic wing, it is seen that

$$\frac{c'}{c'_{m\,(\mathrm{ell})}} = \frac{4}{\pi}\sqrt{1-\xi^2}\,(1+a\,\xi^2)\,\frac{1-L/2\,\varrho\,V^2\pi b^2\alpha'}{1+\alpha/4-L\,(1-a/2+3a\,\xi^2)/2\,\varrho\,V^2\pi b^2\alpha'} \tag{5.19}$$

From (5.17) and (5.18), we have

$$\frac{L}{2\,\varrho\,V^2\,\pi\,b^2\,\alpha'} = \frac{c'_{m\,(\mathrm{ell})}}{b\,(1+c'_{m\,(\mathrm{ell})}/b)} \tag{5.20}$$

and hence

$$\frac{c'}{c'_{m\,(\mathrm{ell})}} = \frac{(4/\pi)\sqrt{1-\xi^2}\,(1+a\,\xi^2)}{1+\frac{a}{4}+\frac{3}{2}\,a\,\frac{c'_{m\,(\mathrm{ell})}}{2\,b}\,(1-4\,\xi^2)} \tag{5.21}$$

The parameter $2\,b/c'_{m\,(\mathrm{ell})}$ occurring in the last expression is the aspect ratio of the elliptic wing of equal lift, span and angle of incidence.

In Figs. 59 to 61 three values of the aspect ratio, *viz.*, $2\,b/c'_{m\,(\mathrm{ell})} = 4$, 8, 12, have been selected and the values of $c'/c'_{m\,(\mathrm{ell})}$ pertaining to the corresponding airfoil contours for $a = -1, -1/2, 0, +1/2, +1$, plotted in each case. The lift distributions $\Gamma/\Gamma_{0\,(\mathrm{ell})}$ which are the same for the different aspect ratios, are shown in the upper part of Fig. 60. It is seen that the deviations of the lift distribution from the elliptic form ($a = 0$) are always considerably less than the deviations of the corresponding contour from the elliptic form. Moreover, it can be seen that this difference between lift distribution and contour increases in magnitude as the aspect ratio $2\,b/c'_{m\,(\mathrm{ell})}$ decreases.

In Fig. 62 the distribution of the downwash velocity w and the induced drag $\varrho\,w\,\Gamma$ corresponding to the five parameters a are plotted against the span. The quantities w and $\varrho\,w\,\Gamma$ have been reduced to zero dimensions by division by $\Gamma_{0\,(\mathrm{ell})}/4\,b$ and $\varrho\,\Gamma^0_{2\,(\mathrm{ell})}/4\,b$ respectively. The curves vary with the parameter a but are independent of the aspect ratio $2\,b/c'_{m\,(\mathrm{ell})}$. A notable feature of these diagrams is the powerful concentration of the induced drag toward the ends or toward the middle of the airfoil respectively, according as the airfoil is more or less full than the elliptic pattern.

The simple rectangular airfoil of constant angle of incidence also exhibits a distribution of lift deviating from that for the elliptic (see Division E IV 5). The theoretical distribution of lift and induced drag is reproduced in Figs. 63 and 64[1]. Fig. 65 shows the deviations of the induced drag from the minimum value[1]. It has not as yet been possible to verify by trustworthy experiments the value of this deviation, for its amount is too small to be measured unless the aspect ratio is very large, and it is very difficult to construct wings of large aspect ratio sufficiently rigid against torsion to permit of reliable measurement of the small quantities involved.

[1] From A. Betz, Tragflügeltheorie. Berichte und Abhandlungen der wissenschaftlichen Gesellschaft für Luftfahrt I, Part 2, 1920.

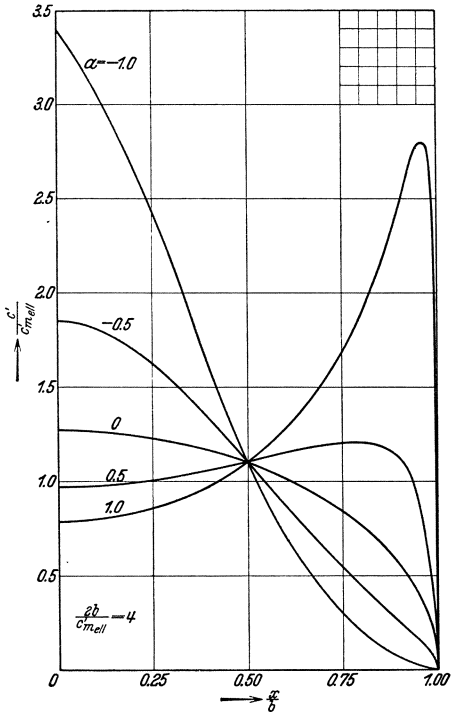

Fig. 59.

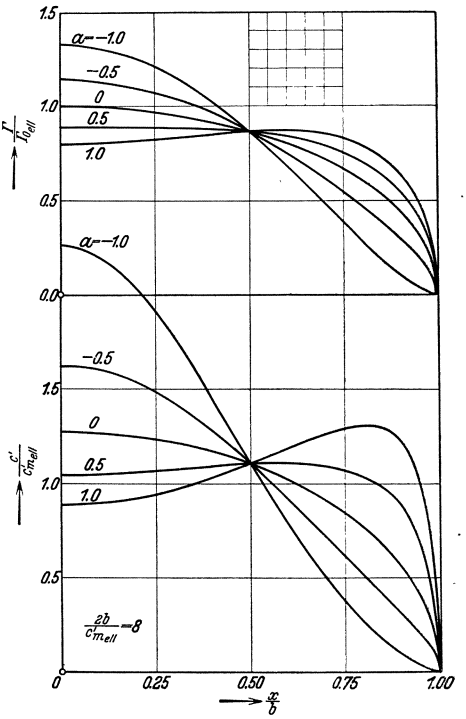

Fig. 60.

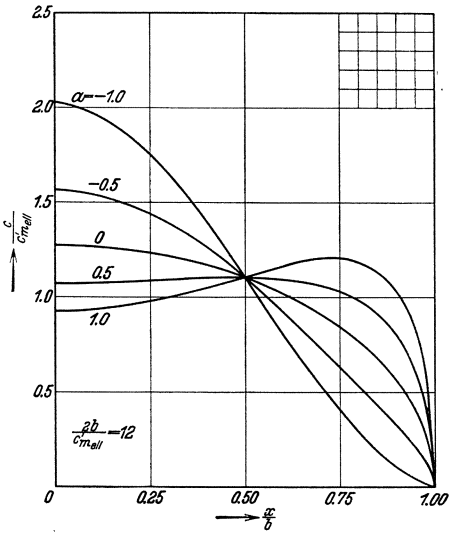

Fig. 61.

Figs. 59, 60 and 61. Various lift distributions (upper part of diagram No. 60) and the corresponding airfoil profiles.

Further data regarding the influence of the form of wing contour, including a series of wings of varying contours, have been developed at Göttingen and to the report of which reference may be made[1]. There is no noticeable difference in the behavior of the polars of the rectangular and elliptic wings respectively apart from the differences in induced drag and angle of incidence due to the different aspect ratios. Nor do the airfoils with rounded ends or of trapezoidal form produce any marked increase in drag. The only striking feature is the increase of the maximum lift in the airfoils with rounded ends. This phenomenon is probably

[1] Ergebnisse der Aerodynamischen Versuchsanstalt zu Göttingen, I. Lief., p. 63, Figs. 47—53 (Oldenbourg, Munich, 1921).

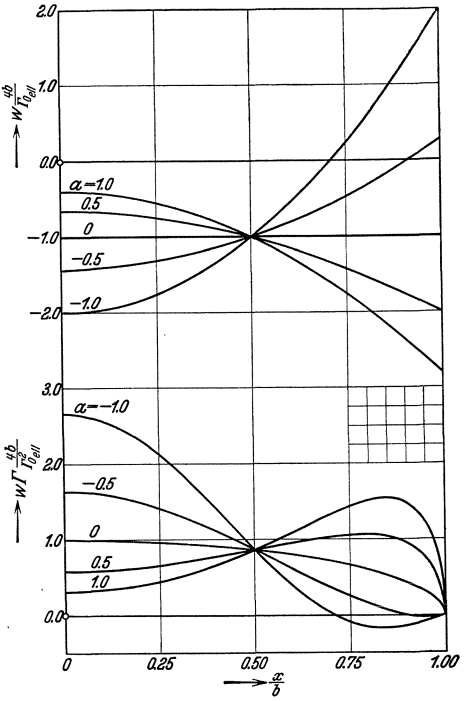

Fig. 62. Distribution of induced velocities (upper part of diagrams) and of induced drag (below) over the span, for the lift distribution shown in Fig. 60.

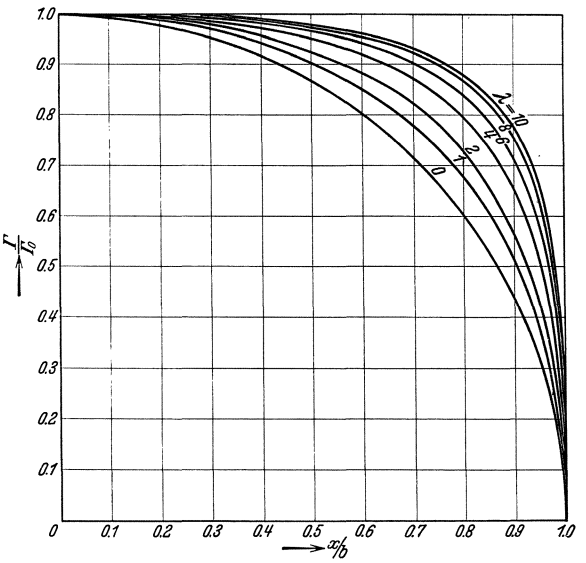

Fig. 63. Lift distribution Γ/Γ_0 across the span x/b for rectangular airfoils of constant profile and angle of incidence, for various aspect ratios. $\lambda = (2/\pi)\,(2b/c')$.

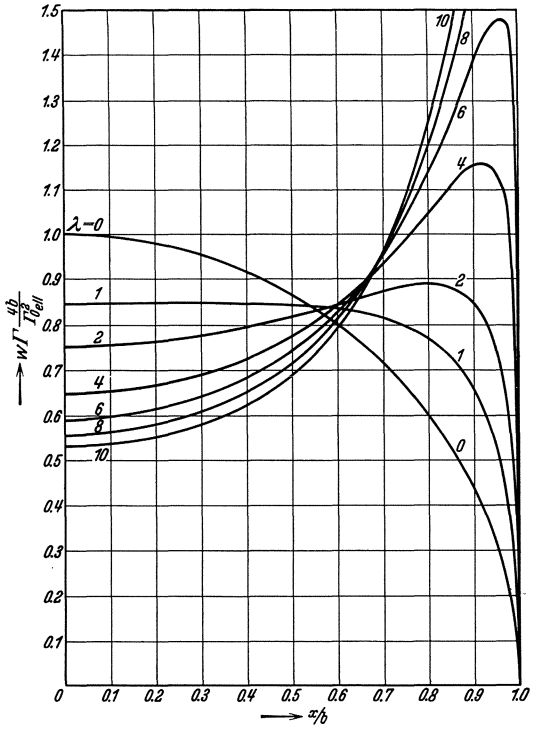

Fig. 64. Distribution of the induced drag $\varrho\, w\, \Gamma$ across the span of rectangular airfoils of constant profile and angle of incidence for various aspect ratios. $\lambda = (2/\pi)\ (2b/c')$. The lift is constant $= \varrho V \Gamma_0$ ell. $(\pi\ b/2)$.

due to the small value of the Reynolds numbers at the ends of the elliptic wing, and would probably disappear if larger airfoils were used. An airfoil with pointed ends produces far less favorable results than those already mentioned. The distribution of lift for such forms is approximately parabolic. The higher induced drag in this type of airfoil is, however, insufficient to account entirely for the increase in drag, the cause of which must be looked for in the large decrease in Reynolds number toward the ends of the airfoil, while the lower maximum lift is explained by the increased angles of incidence at the ends of the airfoil and the consequent premature separation of the flow at these ends.

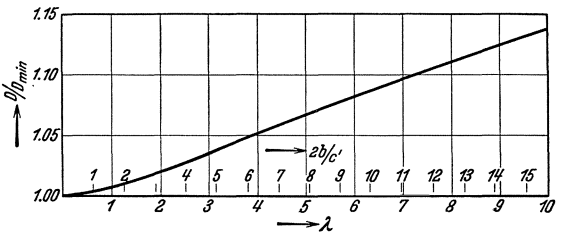

Fig. 65. Relation between the induced drag and aspect ratio of a rectangular airfoil with fixed profile and angle of incidence.

6. Wings with Gaps, Longitudinal Slots or other Disturbing Factors. Interference with the lift distribution in the middle of the wing involves more danger of increasing the drag than does interference at the ends of the wing. Such interference with the distribution of lift is, for example, often produced by cutting out portions of the wing in order to provide accommodation for the pilot or to improve his vision. It may also

occur on the upper side of the wing, *e. g.* by engine nacelles in multi-engined aircraft. The case of the complete separation of the wing into several adjacent portions by slots in the direction of the flight (longitudinal slots) though scarcely occurring at the present time, will also be discussed in the following paragraphs since the phenomena involved are simpler than for the more usual construction, and for the understanding of which they provide a useful foundation.

It might be thought possible to proceed by analogy with the previous section, *i. e.* to consider simple distributions of lift containing a depression at the central portion and then to calculate the corresponding shapes of airfoil. It appears however that in the present instance the value of the induced drag is modified so considerably by slight deviations from the basic distribution assumed, that this method gives for any

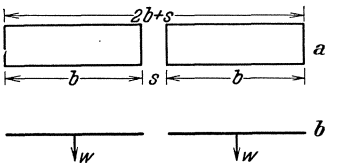

Fig. 66. Above: airfoil with longitudinal slot; below: the sheets of vorticity at the rear of the wings.

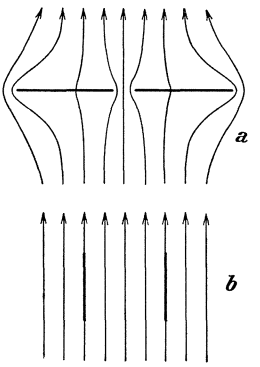

Fig. 67. Above: steady two-dimensional flow across a slotted plate; below: a conformal transformation of the same in which the two airfoil surfaces become two parallel surfaces along the direction of flow.

specified wing form, no useful results concerning the induced drag. Results of more practical value are obtained by commencing with certain boundary conditions determined by the shape of the airfoil, and then seek to determine the *minimum induced drag* under these conditions. The case which best lends itself to theoretical discussion by this method is that of a wing with longitudinal slot.

If, for example, the wing has a longitudinal slot at the center (Fig. 66a) two layers of vortices are formed behind the wing; and when the lift distribution is such that the induced drag is a minimum, the two vortex layers descend like rigid bodies with constant velocity w (Fig. 66b). This motion can be treated as steady by regarding the surfaces of discontinuity as being at rest in a flow approaching with velocity w (Fig. 67a). A method[1] exists for the solution of the latter case by transforming conformally the two surfaces at right angles to the flow into surfaces along the line of flow (Fig. 67b). The separation

[1] GRAMMEL, R., Die hydrodynamischen Grundlagen des Fluges, p. 84ff. (Brunswick, F. Vieweg, 1917).

of a wing of span $2b$ by a longitudinal slot into two halves which are kept at a distance s (Fig. 66) increases the induced drag by a factor $\varkappa$. The calculations indicated provide the following pairs of simultaneous values[1] for $s/(2b + s)$ and $\varkappa$:

$s/(2b + s)$	0	0.001	0.01	0.1	1
$\varkappa$	1.00	1.312	1.480	1.763	2

These results show that extraordinary increase in drag is produced even by very narrow slots. It should however be observed that the finite thickness of the wing with other influences, in practice somewhat reduce the increase of drag estimated by the simple theory here suggested[2]. The fact remains, however, that such discontinuities in the wing greatly increase the drag. Some physical insight into this important effect is obtained by remembering that the effect of the difference of pressure between the two sides of the wing is to cause air to flow with great velocity through any such opening in the wing and that the kinetic energy thereby lost appears as drag.

In the same manner as for longitudinal slots, any disturbance of the smooth distribution of lift produces a very great increase of drag. Such disturbance may be produced by the presence of gaps or openings in the wing form (Fig. 70). As long, however, as the flow does not separate from the connecting form across the gap, the harmful effect of the latter is small. In fact, if the distribution of lift shows only a slight local reduction the disturbing velocities produced at such a point are directed upward. Thus, the connecting bridge has larger effective angles of incidence than the rest of the profile and its lift is therefore comparatively large in spite of the diminished chord length; hence only slight deviation from the elliptic distribution results. The increased angles of incidence at the bridge, however, produce in general, premature separation of the flow, and once this condition has developed, the induced velocities upward can no longer balance the effect of reduced chord, since increase in the angle of incidence in the region of separation results in no marked increase of lift. Under such conditions there results, through the marked decrease in lift, a very considerable increase in induced drag; furthermore, separation is found to increase the profile drag of the bridge.

---

[1] PRANDTL, L., BETZ, A., Vier Abhandlungen zur Hydrodynamik und Aerodynamik, p. 52, Göttingen, 1927.

[2] MUNK, M., and CARIO, G., Flügel mit Spalt in Fahrtrichtung. Techn. Berichte der Flugzeugmeisterei, Vol. I, p. 219.

BETZ, A., Über die Vorgänge an den Schaufelenden von Kaplanturbinen. Hydraulische Probleme. Berlin. V-D-I-Verlag, p. 161, 1926.

FLACHSBART, O., Spaltverluste an Tragflügeln. Zeitschr. f. angew. Math. u. Mech. **11**, p. 411, 1931.

The magnitudes involved in these phenomena can be discussed mathematically as follows[1]. The lift in the separated portion of the flow at the bridge is approximately constant, *i. e.* independent of the angle of incidence and therefore of the induced velocities also. Over the remaining portions of the wing, the effect of the induced velocities is to build up a certain distribution of lift, for which the induced drag does not greatly exceed the minimum value for the most favorable distribution of lift over these two portions of the wing. The lift at the connecting bridge must therefore be considered apart from that over the remaining part of the wing since the two magnitudes are subject to different laws, the first being constant while the second can be evaluated by the usual methods of airfoil theory. The decomposition

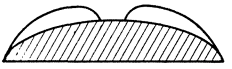

Fig. 68. Decomposition of the lift of a wing with a notch in the contour into an elliptic part and two residues.

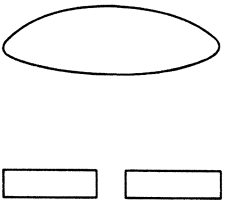

Fig. 69. An airfoil notched contour replaced by an elliptic airfoil lying in front of an airfoil with slot.

will be made by imagining the wing divided into two parts lying one behind the other[2] and such that the foremost has an elliptic distribution of lift whose maximum, at the middle of the wing, coincides with the value of the lift at the connecting bridge (hatched portions of Fig. 68). Let L_1 be the total amount of lift from this elliptic distribution. The residual lift (total amount L_2, say) has a gap at the location of the bridge and can be produced by introducing an auxiliary wing with a longitudinal slot (Fig. 69). The latter is in the downwash of the wing with elliptic flow in front of it. But the downwash is constant over the entire span so that the resulting distribution of lift on the auxiliary slotted wing is that produced by a uniform flow of somewhat different angle of incidence. Hence the known values for the induced drag on

[1] Lotz, I., Theorie von Flügeln mit Ausschnitten. Zeitschr. f. Flugtechnik u. Motorl. **23**, p. 410, 1932.

[2] In accordance with Munk's theorem any part of the lift may be arbitrarily displaced in the direction of motion without producing any alteration in induced drag, provided the magnitude of the lift and its distribution across the span is thereby unaltered. For both the lift and drag (or loss of energy) can be calculated from the field of induced velocities far behind the wing [the lift is calculated from the momentum, the loss of energy from the kinetic energy—Division E I (11.1) and (11.3)]. But the disturbing velocities are independent of their distance from the wing so that the end result of the calculations is unaffected by shifting in the direction of flow those portions of the wing which produce vortices. M. Munk, Isoperimetrische Aufgaben aus der Theorie des Fluges. Dissertation, Göttingen, 1919.

a longitudinally slotted wing can be directly applied. This drag must be supplemented by a component produced by the mutual effect of the two wings, on account of the fact that the one to the rear is subject to a downwash of magnitude

$$w = V \frac{2 L_1}{\pi q (2 b)^2} \tag{6.1}$$

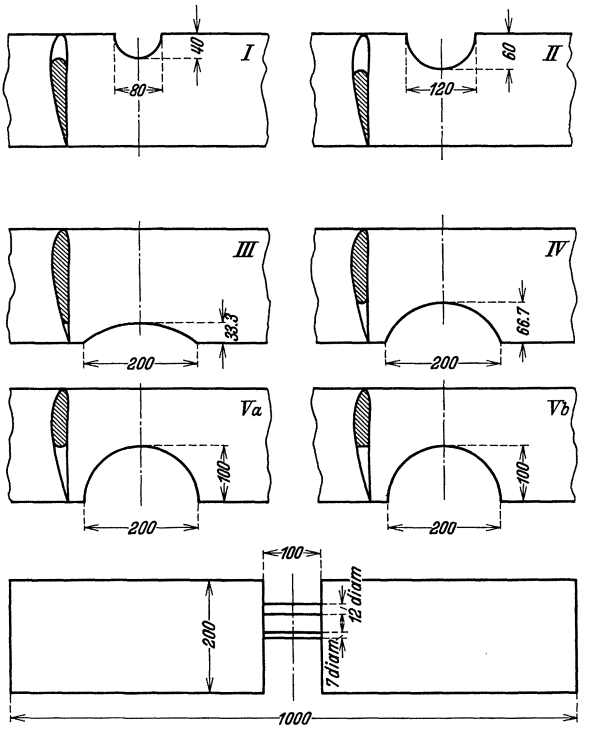

Fig. 70. Various airfoils either with gaps in contours or with longitudinal slot along the middle. The dimensions of the airfoils are 100 × 20 cm. The edges of the gaps are rounded off in all the airfoils except that labelled *V b*.

The total induced drag is therefore made up of three components

$$D_1 = \frac{L_1^2}{\pi q (2 b)^2} \tag{6.2}$$

$$D_2 = \varkappa \frac{L_2^2}{\pi q (2 b)^2} \tag{6.3}$$

$$D_3 = \frac{2 L_1 L_2}{\pi q (2 b)^2} \tag{6.4}$$

Apart from gaps in the wing, alterations in the normal distribution of lift are most often produced by disturbing bodies on the upper side of the airfoil, *e. g.* by motor supports, gondolas, etc. Such disturbances

are often deliberately introduced to lower the lift drag ratio in order to allow steeper landing[1].

In Figs. 70 to 72 measurements are shown which were made by J. Ackeret[2] on wings containing gaps or openings either at the leading or the trailing edge as well as on a wing with longitudinal slot. Openings at the leading edge produced a considerable increase in drag as soon as the flow had separated at the connecting bridge (Fig. 71). When, however, a wing with longitudinal slot was used, the increase of drag became manifest and continued to grow from the position of smallest lift. The fact that for larger lifts the curves for wings with gaps or openings approach or even intersect the curves for the wings with the longitudinal slot, can be accounted for by the considerable profile drag produced by the bridge in the latter case, which must be added to the induced drag. At the trailing edge, the principal effect of such cut out forms is to increase the profile drag (Fig. 72) with no separation at the bridge. This is due to the fact that the bluntness of the trailing edge increases the drag and hence, as already seen in I 9, increases the maximum lift (see remarks in connection with Fig. 72). The consequence is that the maximum lift at the bridge in spite of the shortening of the chord, falls only slightly[3].

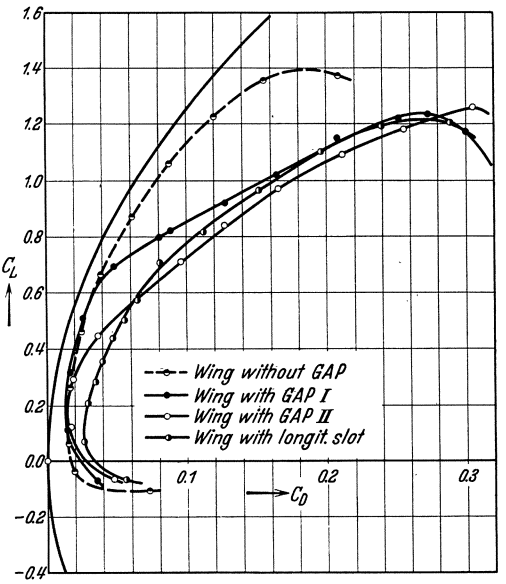

Fig. 71. Results of measurements made on wings either with longitudinal slots or notched on leading edge as shown in Fig. 70.

If the bridge is extended in such a way that, in spite of its smaller chord, its lift is equal to that of the adjacent portion of the wing, it is possible to a great extent to avoid even the harmful effects of gaps at the leading edge. To this end it is necessary first to give to the bridge

[1] Hübner, W., and Pleines, W., Das DVL-Gleitwinkelsteuer (Bauart W. Hübner). Zeitschr. f. Flugtechnik u. Motorl. **23**, p. 455, 1932.

[2] Ergebnisse der Aerodynamischen Versuchsanstalt zu Göttingen, III. Lief., p. 92 (Oldenbourg, Munich, 1927).

[3] Messungen an Profilen mit abgeschnittener Hinterkante. Ergebnisse der Aerodynamischen Versuchsanstalt zu Göttingen, III. Lief., p. 82.

a larger angle of incidence to compensate for its smaller chord, and next, to take precautions that its maximum lift in relation to its chord is correspondingly higher. If the remainder of the wing has a comparatively thin and slightly curved profile of low $C_{L\,max}$ the last condition can be satisfied simply by choosing for the bridge form a thicker and more strongly curved profile. If on the other hand the profile of the main wing is already thick and of high maximum lift, the artificial means noted in I 4 can be applied successfully in order to raise the maximum lift.

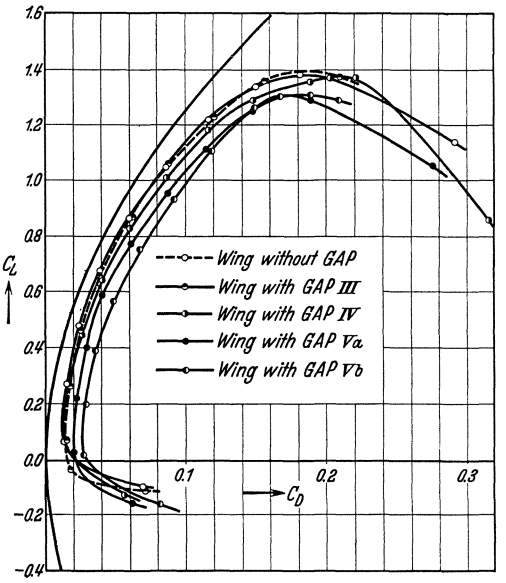

Fig. 72. Results of measurements on wings notched on trailing edge as shown in Fig. 70.

The accuracy of this reasoning has been proven through experimental research by H. Muttray [1]. These investigations showed further that another consideration needs attention in the attempt to produce an undisturbed transition of the lift distribution: the bridge must not be shifted too far in the direction of flight relatively to the remainder of the wing; the vortex lines which represent the distribution of lift over the wing must be able, in a measure, to pursue their course smoothly. The need for this condition can best be understood by considering an extreme case. If the bridge is imagined shifted so far back that it no longer has any connection with the two remaining portions of the wing, three detached wings are obtained (Fig. 73a). At the boundary of each wing the lift falls to zero and the lift distribution is, approximately, of the form shown in the lower part of Fig. 73b. If the bridge is not totally disconnected from the remainder of the wing but is shifted comparatively far in the direction of flight, the lift does not fall absolutely to zero at the transition points, but suffers a considerable decrease with consequent additional induced drag. The effect of shifting the middle of the wing in this manner, without alteration of chord has also been investigated

[1] MUTTRAY, H., Neuere Messungen an Flügeln mit Ausschnitten. Zeitschr. f. Flugtechnik u. Motorl. **20**, p. 161, 1929; and Ergebnisse der Aerodynamischen Versuchsanstalt zu Göttingen, IV. Lief., p. 85, 1932.

by Muttray [1]. It is however, impossible to state with certainty whether the harmful effect observed can be traced back to unfavorable angles of incidence on the portions displaced.

The disturbing effects of adventitious structures on the wing are illustrated by several researches carried out in the Göttingen Laboratories and to the reports of which reference may be made [2]. It will be recognized that disturbances on the upper side have a particularly unfavorable effect since they tend to produce separation and diminution of lift.

7. Wings of Large Chord. An initial assumption in the usual theory of induced drag is that the span of the wing is large compared with the chord. It is worthy of note, however, that the theoretical conclusions are also true with reasonable accuracy for wings with span approximately equal to the chord (square contour). This can be verified by reference

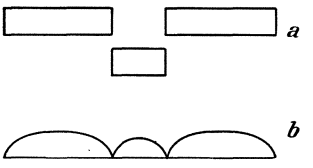

Fig. 73. Lift distribution on an airfoil the middle portion of which has been displaced toward the rear.

Fig. 74. Normal component of the velocity of approach of a plate of large chord dimension.

to Figs. 53 and 54. If the chord is large compared with the span, the effect of the flow in planes parallel to the plane of symmetry is of lesser importance than the effects of the flow at the side boundaries. In the extreme case, if the chord length is very large in comparison with the span, the flow in the longitudinal direction need be taken into account only in the neighborhood of the leading and trailing edges and even this can be neglected in comparison with the other effects on the remainder of the wing. If however, the leading and trailing edges are at a sufficient distance for their effects to be negligible, a two-dimensional transverse flow is obtained which can easily be treated by mathematical methods as follows. Let us assume that we are dealing with a flat wing:

If α is the angle of incidence on the wing and V the velocity of approach, the air has a normal velocity (see Fig. 74)

$$V' = V \sin \alpha \tag{7.1}$$

toward the wing, and exerts a force upon it of amount,

$$P = \frac{1}{2} \varrho S V'^2 C_D = \frac{1}{2} \varrho V^2 S C_D \sin^2 \alpha \tag{7.2}$$

[1] MUTTRAY, H., Messungen an einem Flügel mit versetztem Mittelteil. Ergebnisse der Aerodynamischen Versuchsanstalt zu Göttingen, IV. Lief., p. 88, 1932.

[2] Beeinflussung von Tragflächen durch Motorgondeln. Ergebnisse der Aerodynamischen Versuchsanstalt zu Göttingen, III. Lief., p. 115 (Oldenbourg, Munich, 1927).

This force is normal to the plane of the wing and can be decomposed into a lift component $L = P \cos\alpha \approx P$ (7.3)

and a drag component

$$D = P \sin\alpha = \frac{1}{2} \varrho V^2 S C_D \sin^3\alpha \tag{7.4}$$

In the above equations C_D is the coefficient of drag of a long flat plate so that C_D is approximately equal to 2. In addition, we must consider the effect of surface friction. The additional resistance is D_R where

$$D_R = \varrho V^2 S C_f \cos^2\alpha \tag{7.5}$$

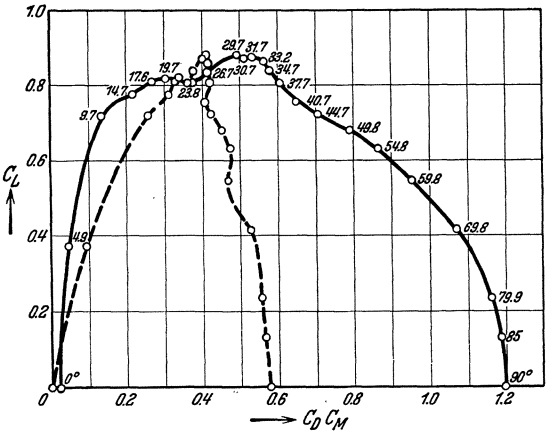

Fig. 75. Force and moment coefficients of a flat rectangular plate of aspect ratio $(2b)^2/S = 5$.

where C_f is the coefficient of surface friction[1]: $\cos^2\alpha$ is generally replaced by 1.

If the effect of surface friction is neglected the drag lift ratio has the value

$$\frac{D}{L} = \alpha \tag{7.6}$$

On calculating the most favorable drag lift ratio by applying airfoil theory to (2.3), (7.2) and (7.3) the value obtained is

$$\left(\frac{D}{L}\right)_{min} = C_D \sin^2\alpha \frac{S}{\pi (2b)^2} \tag{7.7}$$

Since $S/(2b)^2$ may be large, the theoretical minimum thus obtained is considerably higher than the minimum obtained in actual practice. This apparent contradiction is due to the fact that airfoil theory postulates a "line" airfoil. In the case under discussion, however, the projection of the wing in the direction of motion has

[1] C_f is a function of the Reynolds number. The chord length is not, however, the predominating factor in determining the value of the latter for, on account of the transverse flow, the direction of flow is not along the wing but aslant from the middle of the wing toward the edges. In this case therefore the Reynolds number of predominating effect is a function of the span and of the angle of incidence.

a considerable vertical extension since the trailing edge is considerably lower than the leading edge. In airfoil theory a wing of this kind corresponds rather to

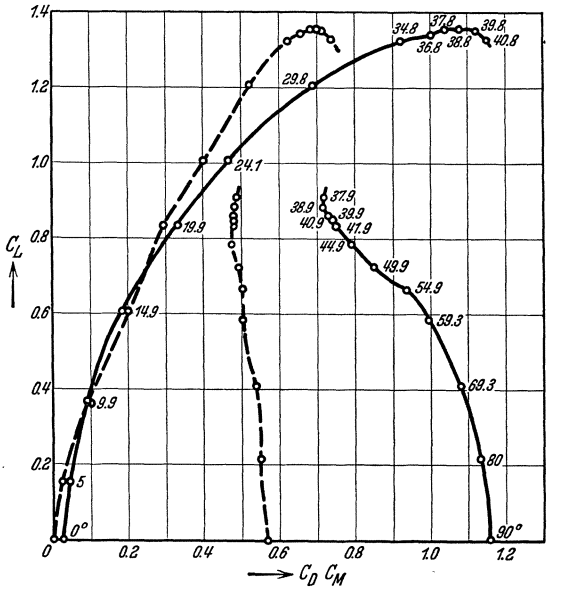

Fig. 76. Force and moment coefficients of a flat square plate.

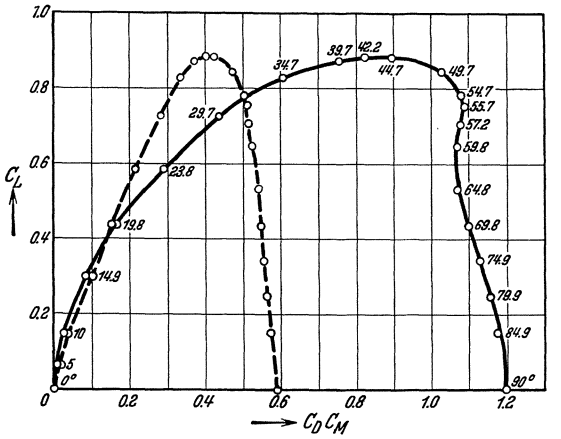

Fig. 77. Force and moment coefficients of a flat rectangular plate of aspect ratio $(2b)^2/S = 1/5$.

a "multi-plane" as discussed in Division E IV **14**. The height of the multi-plane is $h = c \sin \alpha$. If $h >> b$ the induced drag lift ratio becomes

$$\left(\frac{D}{L}\right)_{min} = \frac{L}{2\varrho V^2 h \cdot 2b} = \frac{1}{4} C_D \alpha \tag{7.8}$$

and this result is consistent with (7.6) above.

Figs. 75 to 77 show the polars for flat plates[1] of aspect ratios 1 : 5, 1 : 1 and 5 : 1. It is noteworthy that the maximum lifts for wings of approximately square contours are extraordinarily high. Exactly similar results are obtained with circular discs. There is as yet no satisfactory theoretical explanation of this abnormal phenomenon. The effect described should, however, be useful in the construction of tail-planes where premature separation must be avoided if at all possible (see **11**).

B. Combination of Wings

8. Preliminary Remarks. The combination of several wings in a single system results in peculiar properties for the system which, by proper use, may be made of great value in the problems of aircraft construction.

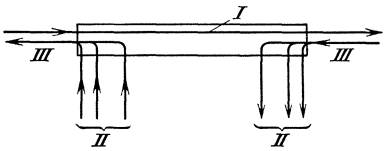

Fig. 78. The vortex system of an airfoil of finite span formed from the corresponding system of infinite span (*I*) by the addition of the vortex systems *II* and *III*. The arrow in this diagram and also in Figs. 79 and 81 indicates the sense of the vortex rotations.

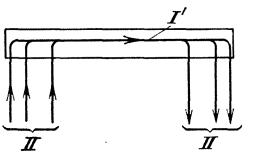

Fig. 79. Formation of the vortex system of an airfoil of finite span out of the bound vortex *I'* and the system of free vortices *II*.

The members of the system are usually arranged so closely that mutual interactions occur, the flow around each wing being disturbed by the presence of its neighbors by an amount which, as a rule, is too large to be negligible. Various contributory factors in this effect must be considered separately: in the first place, a wing of infinite span gives rise to a field of disturbance which influences the working of neighboring wings. Moreover, the fact that span is actually finite introduces a second disturbing field due partly to the vortices generated at the ends of the wing and partly to the termination of the wing at these ends (see Fig. 78 where these three factors are indicated by three systems of vortices, I, II and III, which characterize their principal respective effects). Instead of separating the three factors *viz.* infinite wing, generation of vortices, absence of the prolongations of the wing, in this fashion, it is possible to combine the first and last and to calculate the effect of a finite portion of wing (see Fig. 79 where $I' = I + III$). Such a procedure must dispense with the results of the comparatively extensive researches which have been concerned with two-dimensional flows around combinations of wings (Division E II). Whether or not it is advisable

[1] FLACHSBART, O., Messungen an ebenen und gewölbten Platten. Ergebnisse der Aerodynamischen Versuchsanstalt zu Göttingen, IV. Lief., p. 96 (Oldenbourg, Munich, 1932).

to take account of the results of these researches depends upon the extent of their influence on the total phenomena. In general, the relative importance of the two-dimensional flow increases as the distance between mutually interacting wings decreases in comparison with their span. When the latter ratio increases, the finite length of span becomes the more influential factor and the results obtained for two-dimensional flow find diminishing application.

The field of disturbance for a given body can be constructed by a known procedure out of sources, sinks and vortices. The effects of singularities which occur in pairs with opposite signs (a sink plus a source, a pair of vortices with opposite sense of rotation) diminish with distance very rapidly as compared with the effect of a single source or a single vortex. (In a two-dimensional flow, for example, the field velocity of a source or vortex varies as $1/r$, while that of a sink-source arrangement, or a vortex doublet, as $1/r^2$ for large values of r [1].) In the case of flow around an airplane wing, single vortices occur in connection with the circulation around the wing. Hence at large distances the disturbing field of an airfoil is identical with that due to a vortex having circulation equal to that around the wing. At smaller distances the effects of singularities occurring in pairs and determined by the exact shape of the wing must also be taken into account, but in the more usual cases, *e. g.* biplanes, the latter effects remain small in comparison with those produced by the circulation, and are usually neglected. If, however, it is desired to consider the special effects of the shape of the wing section, it is permissible to dispense with sources, sinks and vortices, for the shape is important only at small distances from the wing, and as the flow at some distance is sufficiently like a two-dimensional flow to be treated as such, the usual methods of two-dimensional fluid mechanics, *e. g.* conformal transformation may be employed.

Groups of wings in combination can be divided into two classes, according as the wings are arranged in fore and aft order or above and below. The first includes the so-called tandem wings (two approximately equal wings arranged in fore and aft order) which are practically obsolete at the present time but are interesting in view of their bearing on the mutual interaction of wing and tail-plane. If the distance between two such wings is made very small, arrangements are obtained which are equivalent to the combination of wing and aileron, or of fin and rudder. Although the examples given can also be treated as single wings of broken profile and might therefore have been included in the discussion of airfoil profiles in Chapter I, it has seemed more profitable, in view of their intimate connection with the combination of wing and tail-plane, to discuss them together in the present context. Slotted wings can also be regarded as combinations of wings but have already been discussed

[1] Division B II **7** and IV **10.**

in I 5. The most important member of the second class is the biplane. This case is closely connected with that of flight close to the ground, a state of affairs which is made amenable to calculation by the method of images (Division E IV Part C).

9. Stability of Wings Arranged in Tandem. If two wings are arranged fore and aft, the resultant force is the vector sum of the forces acting separately on the wings (Fig. 80). Let the two wings be assumed rigidly connected; rotation of the entire system then alters the angles of incidence on each wing always by the same amount. If the effect of this is to alter the forces on the two wings in the same ratio, the point of application of the resultant shifts only to the extent determined by the shifts of the two component forces (shift of the center of pressure on each wing). If however, increasing the angle of incidence increases the force on the rear wing by a factor greater than on the other, there will be a shift of the resultant to the rear in addition to that produced by the change in position of the centers of pressure on the wings. Conversely, if the force on the forward wing increases in relatively greater proportion than that on the rear wing, then the additional shift of the resultant will be forward. Since the forces on each wing are practically proportional to their effective angles of incidence $(\alpha - \alpha_0)$ [II (5.1)], it follows that neglecting the mutual interaction of the wings and any subsidiary phenomena, the wing for which the effective angle of incidence is smaller will show the greater proportional change in force. Hence the arrangement of two wings with appropriate *decalage*, that is with different angles of incidence for the two wings, will provide a very effective means of control for the shift of the center of pressure of the system. The shift of the center of pressure is a decisive factor in determining the stability of an aeroplane (Division N).

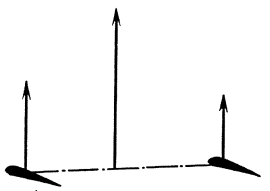

Fig. 80. Forces on two airfoils in tandem and their resultant.

If subsidiary effects such as propeller thrust, drag, height of the center of gravity above the wings are neglected, a necessary condition for equilibrium is that the line of action of the lift shall pass through the center of gravity, *i. e.* the center of gravity must lie on the line of the resultant of pressure. For if this is not the case, gravity and lift together exert a couple on the airplane. If an alteration of the angle of incidence shifts the center of pressure, equilibrium is disturbed and can be restored only by manipulating the elevator until the center of pressure and the center of gravity come again to the same vertical line. If the elevator is not used, and an increase of the angle of incidence shifts the center of pressure toward the trailing edge, the resulting couple tends to decrease the angle of incidence and equilibrium is automatically

restored. If, however, an increase of the angle of incidence carries the center of pressure forward, or a decrease carries it in the opposite direction, the resulting couple increases the initial change in the angle of incidence, and an airplane in this condition would not regain equilibrium without the use of the horizontal tail surfaces. The state of equilibrium is therefore stable or unstable according as an increase of the angle of incidence from the position of equilibrium shifts the center of pressure backward or forward. The greater the shift of the center of pressure for a given change of angle the greater the stability or instability as the case may be. If for a change in the angle of incidence the center of pressure and the center of gravity remain on the same vertical, the system is in a state of neutral equilibrium. In general it is desired to obtain a state of stable equilibrium. In general, wings by themselves are unstable, especially when lift-drag ratios are high, *i. e.* with increase of the angle of incidence the center of pressure moves forward. A condition of stable equilibrium can however, be obtained by setting the two component wings at an angle (decalage). To this end the rear wing must have a smaller effective angle of incidence than the forward wing. The magnitude of the compensating effect so produced increases with the distance between the wings and with the angle between them.

The above description of the effect of setting the two wings at an angle is, however, not quite accurate quantitively, since the mutual interaction of the wings has been neglected. The circulation around a wing produces an induced field in the neighborhood such that for positive lift induced velocities are produced the direction of which is upward in front of the wing and downward behind. As a result of the absence of indefinite lateral extension, wings of finite span give rise to induced velocities which are smaller than those produced by wings of infinite span. Vortices originating at the ends of the wing are responsible for an additional downward velocity inside a rectangular region whose width coincides with the span. In front of the wing this velocity is smaller than that on the wing itself; behind the wing it is larger. Moreover for a given angle of incidence, the finite span reduces the lift of the disturbing wing (3.4) and hence reduces the magnitude of the interference effect.

10. Measures for Obtaining Stability. In order to obtain certain general ideas on the question of stability, we shall commence with some relatively simple examples. For simplicity the actual wings will be replaced by equivalent plane wings (II 1) which will be assumed to have fixed centers of pressure, so that any shift of the resultant center of pressure must be ascribed to the arrangement of the component members of the system. We first choose two wings with span large compared with their mutual distance l, so that the effect of finite span may be neglected, and we have simply to consider the problem of

keeping the center of pressure at a fixed point between the wings. If the mutual interactions are neglected it follows that the wings must have the same angle of incidence, *i. e.* a decalage of 0^0, and the surface areas of the two wings must be in a fixed ratio. Let the surface area of the front wing be S_1', of the rear wing S_2', and let the chord lengths, c_1', c_2' respectively, be constant for each wing so that $S_1' = 2\,b_1\,c_1'$ and $S_2' = 2\,b_2'\,c_2'$. We must next investigate as to how the angles of incidence and the chords must be changed in order to obtain the same effect if the mutual interaction is taken into account. If the angle of incidence α is 0^0 the lift of each wing is zero; hence there is no interaction, no correction is required on that account and the decalage remains zero. Moreover, no restriction can be set on the chords at this angle since the lift remains zero for every possible value. If the angle of incidence is now increased to a finite value α each wing has lift and, aside from the effect of induced velocities, the coefficient of lift for each wing [II (1.1)] would be $C_L' = 2\,\pi\,\alpha$

$$\left.\begin{aligned} &\text{and the circulations} \quad \Gamma_1 = \frac{1}{2}\,C_L'\,V\,c_1' = \pi\,\alpha\,V\,c_1' \\ &\text{for the front wing and} \quad \Gamma_2 = \frac{1}{2}\,C_L'\,V\,c_2' = \pi\,\alpha\,V\,c_2' \end{aligned}\right\} \tag{10.1}$$

for the rear wing. The induced velocities associated with these circulations produce changes in the effective angles of incidence of amounts

$$\left.\begin{aligned} &\triangle\,\alpha_1 = \frac{w_1}{V} = \frac{\Gamma_2}{2\,\pi\,V\,l} = \frac{\alpha\,c_2'}{2\,l} \\ &\text{and} \quad \triangle\,\alpha_2 = \frac{w_2}{V} = -\frac{\Gamma_1}{2\,\pi\,V\,l} = -\frac{\alpha\,c_1'}{2\,l} \end{aligned}\right\} \tag{10.2}$$

respectively, so that the lift on the front wing increases while that on the rear wing decreases. In order to obtain the basic values of the circulation and the corresponding lifts for each wing, the chord of the forward wing must be decreased to c_1 and that of the rear wing increased to c_2. The values of these quantities can be obtained from the equations

$$\left.\begin{aligned} \Gamma_1 &= \pi\,(\alpha + \triangle\,\alpha_1)\,V c_1 = \pi\,\alpha\,V c_1' \\ \Gamma_2 &= \pi\,(\alpha + \triangle\,\alpha_2)\,V c_2 = \pi\,\alpha\,V c_2' \end{aligned}\right\} \tag{10.3}$$

On substituting the values for $\triangle\,\alpha_1$ and $\triangle\,\alpha_2$ from (10.2) the following equations are obtained:

$$\alpha\left(1 + \frac{c_2'}{2\,l}\right) c_1 = \alpha\,c_1' \tag{10.4}$$

$$\left.\begin{aligned} &\text{so that} \quad c_1 = \frac{c_1'}{1 + c_2'/2\,l} \\ &\text{and similarly} \quad c_2 = \frac{c_2'}{1 - c_1'/2\,l} \end{aligned}\right\} \tag{10.5}$$

The spans $2\,b_1$ and $2\,b_2$ respectively remain unchanged so that the necessary surface areas $S_1 = 2\,c_1\,b_1$ and $S_2 = 2\,c_2\,b_2$ are changed in the same ratio as the chords.

The ratio of the corrected to the original chords is independent of the angle of incidence α. Allowance for the mutual interaction of the two wings can therefore be made for all angles of incidence by replacing the chord lengths c_1 and c_2 by c_1' and c_2' respectively and assuming that the corrected wings have no interaction.

So far it has been required to hold the center of pressure at a definite point; in the case now to be considered, it is required to arrange the combination of wings so as to produce a specified shift of the center of pressure. Let ε' be the decalage (angle between the wings) necessary when mutual interaction is neglected; then with the previous notation,

$$\alpha_1 = \alpha_2 + \varepsilon' \tag{10.6}$$

Let the surface areas obtained when mutual interaction is neglected be, as above $S_1' = 2\, c_1'\, b_1$ and $S_2' = 2\, c_2'\, b_2$ for the front and back wings respectively. Since the angles of incidence of the wings now differ there will be no position where both wings have zero lift and hence no position without interference. When $\alpha_2 = 0$, α_1 becomes ε' and the coefficient of lift and circulation of the front wing have the values

$$C_{L\,1} = 2\,\pi\,\varepsilon' \tag{10.7}$$

$$\Gamma_1 = \pi\,\varepsilon'\,V c_1' \tag{10.8}$$

This wing suffers no interference since its partner has zero angle of incidence and therefore zero lift. The flow around the rear wing is, however, diverted downward by an angle

$$\triangle_2 = \frac{\Gamma_1}{2\,\pi\,l\,V} = \frac{\varepsilon'\,c_1'}{2\,l} \tag{10.9}$$

The back wing must therefore be adjusted to have an angle of incidence $\triangle_2 = \varepsilon'\, c_1'/2\,l$ in order to have zero lift. Similarly for zero angle of incidence at the front wing, the back wing will have an angle of incidence $\alpha_2 = -\varepsilon'$ and negative lift, inducing a downward flow at the front wing. Hence the angle of incidence on the front wing must be increased to

$$\triangle_1 = \frac{\varepsilon_1\, c_2'}{2\,l} \tag{10.10}$$

Since the angles of incidence have been increased by $\triangle_1$ and $\triangle_2$ respectively the alteration in decalage is $\triangle\varepsilon$, where

$$\triangle\,\varepsilon = \triangle_1 - \triangle_2 = \frac{\varepsilon'\,(c_2' - c_1')}{2\,l} \tag{10.11}$$

The required decalage is therefore

$$\varepsilon = \varepsilon' + \triangle\,\varepsilon = \varepsilon'\left(1 + \frac{c_2' - c_1'}{2\,l}\right) \tag{10.12}$$

The mutual interaction of the wings due to decalage therefore has no effect if $c_2' = c_1'$, *i. e.* if the original chord lengths uncorrected for interaction are equal. If this is not the case the decalage must be decreased or increased according as the chord of the front wing is greater or less

than the chord of the rear wing. The two possibilities are exemplified by the usual wing and tail plane type and by the "canard" type (see **13**) respectively.

The requisite chord values, c_1 and c_2, can be obtained by using the condition that for all angles of incidence the calculated values of the circulations must agree with those obtained by neglecting interaction. The equations thus obtained are:

$$\left.\begin{aligned} \Gamma_1 &= \pi\,(\alpha_1 + \triangle_1 + \triangle\,\alpha_1)\,V c_1 = \pi\,\alpha_1\,V c_1' \\ \Gamma_2 &= \pi\,(\alpha_2 + \triangle_2 + \triangle\,\alpha_2)\,V c_2 = \pi\,\alpha_2\,V c_2' \end{aligned}\right\} \tag{10.13}$$

where
$$\left.\begin{aligned} \triangle\,\alpha_1 &= \frac{\Gamma_2}{2\,\pi\,V\,l} = \frac{\alpha_2\,c_2'}{2\,l} \\ \text{and} \qquad \triangle\,\alpha_2 &= -\frac{\Gamma_1}{2\,\pi\,V\,l} = -\frac{\alpha_1\,c_1'}{2\,l} \end{aligned}\right\} \tag{10.14}$$

If the latter value for $\triangle\,\alpha_1$, and the value of $\triangle_1$ from (10.10) are inserted in (10.13), it follows that

$$\left(\alpha_1 + \varepsilon'\frac{c_2'}{2\,l} + \alpha_2\frac{c_2'}{2\,l}\right) c_1 = \alpha_1\,c_1' \tag{10.15}$$

Hence, since $\alpha_2 + \varepsilon' = \alpha_1$
$$\left(1 + \frac{c_2'}{2\,l}\right) c_1 = c_1' \tag{10.16}$$

$$\left.\begin{aligned} c_1 &= \frac{c_1'}{(1 + c_2'/2\,l)} \\ \text{and similarly} \qquad c_2 &= \frac{c_2'}{(1 - c_1'/2\,l)} \end{aligned}\right\} \tag{10.17}$$

as in the arrangement without decalage.

In the theory of the preceding paragraphs the effect of finite span and varying chord length were eliminated by postulating constant chord lengths and spans so large that the end effects were negligible. Allowance may now be made for these neglected factors by multiplying the magnitudes hitherto used by suitable coefficients. Whereas the lift of a wing of surface area S', large span, at angle of incidence α' was expressed by the formula

$$L = (1/2)\,\varrho\,V^2\,S'\,2\,\pi\,\alpha' \tag{10.18}$$

the corresponding formula for a wing of finite span becomes

$$L = (1/2)\,\varrho\,V^2\,\mu'\,S'\,2\,\pi\,\alpha' \tag{10.19}$$

where μ' expresses the reduction of lift produced by loss at the ends of the wing. For elliptic distributions, in accordance with (3.4) above

$$\mu' = \frac{1}{\left(1 + 2\,S'/(2\,b)^2\right)} \tag{10.20}$$

where $2\,b$ denotes the span as hitherto.

The previous formula for the induced velocity w at a distance l before or behind the wing of great span and constant chord length was

$$w = \mp\frac{\Gamma}{2\,\pi\,l} = \mp\frac{L}{4\,\pi\,\varrho\,V\,b\,l} \tag{10.21}$$

If a downward induced velocity is regarded as positive, the negative sign must be chosen for the value in front of the wing and the positive for that in the rear.

Furthermore, this velocity along the span of the disturbed wing was constant; for finite span, however, this is no longer the case. It is necessary in fact to replace the induced velocity w of (10.21) by a mean value $\overline{w}$ so chosen that the change of lift produced by postulating a constant velocity $\overline{w}$, equals the actual change as obtained by more detailed calculation based on actual values [see (11.3)].

The required mean value can be related to formula (10.21) by multiplying the w of that formula by a correcting factor $\varkappa$, thus,

$$\overline{w} = \mp \frac{\varkappa L}{4 \pi \varrho V b l} \tag{10.22}$$

The values of $\varkappa$ are discussed in detail in the following section but attention may be drawn at this point to two qualitative results concerning these values. In front of the wing the induced velocity is decreased by the end effect, the reverse in general being true behind the wing. It should also be observed that outside a strip of width equal to that of the span, the induced velocity due to the trailing vortices is opposite in direction to that within the same region. If, therefore, the span of one wing is considerably less than that of the other, the mean velocity $\overline{w}$ induced by it upon its neighbor is very small. Thus, for example, the interference effect of the tail-plane upon the main wing can generally be neglected.

If allowance is made for the effect of the ends of the wing, the same method which led to (10.12) and (10.17) will now give

$$\varepsilon = \varepsilon' \left[1 + \frac{1}{2 l} \left(\varkappa_2 \mu_2' \frac{S_2'}{2 b_2} - \varkappa_1 \mu_1 \frac{S_1'}{2 b_1} \right) \right] \tag{10.23}$$

$$\mu_1 S_1 = \frac{\mu_1' S_1'}{\left(1 + \dfrac{\varkappa_2 \mu_2' S_2'}{4 b_2 l} \right)}$$

$$\mu_2 S_2 = \frac{\mu_2' S_2'}{\left(1 - \dfrac{\varkappa_1 \mu_1' S_1'}{4 b_1 l} \right)} \tag{10.24}$$

Changing the surfaces S_1', S_2' into S_1, S_2 respectively also changes the aspect ratios so that the coefficient μ needs modification, as can be seen from (10.20) for elliptic distribution. The factor μ_1 therefore differs from μ_1' and μ_2 from μ_2' but the amount of the difference in general is so small that in practice it scarcely needs consideration.

11. The Induced Field in Front of and Behind a Wing: Theory. If $\Gamma(y)$ is the distribution of circulation across the span, a vortex of strength $(\partial \Gamma / \partial y)\, dy$ must originate between y and $y + dy$. If such trailing vortices are combined with those represented by the circulation around the wing, it is possible to regard the entire vortex system as

constructed of line vortices of which a representative is of strength $(\partial \Gamma/\partial y)\, dy$, bent at right angles at the points $\pm y$ (see Fig. 81). The field of such a vortex, bent at right angles at the points $\pm y_1$, induces, according to the Biot-Savart law (Division B III 2) at a point P behind the wing (Fig. 82) a downward velocity of amount dw_2. If the coordinates of P are (y_2, l) then dw_2 is given by the formula

$$dw_2 = \frac{\partial \Gamma}{\partial y_1} \frac{1}{4\pi} \left[\frac{1}{l} (\cos\varphi + \cos\psi) + \frac{1}{(y_1 + y_2)} (1 + \sin\varphi) + \frac{1}{(y_1 - y_2)} (1 + \sin\psi) \right] dy_1 \qquad (11.1)$$

where
$$\sin\varphi = \frac{l}{\sqrt{(y_1 + y_2)^2 + l^2}}, \qquad \sin\psi = \frac{l}{\sqrt{(y_1 - y_2)^2 + l^2}}$$
$$\cos\varphi = \frac{y_1 + y_2}{\sqrt{(y_1 + y_2)^2 + l^2}}, \qquad \cos\psi = \frac{y_1 - y_2}{\sqrt{(y_1 - y_2)^2 + l^2}}$$

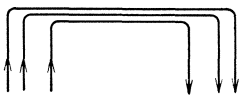

Fig. 81. Resolution of the complete vortex system of an airfoil into partial vortices at right angles.

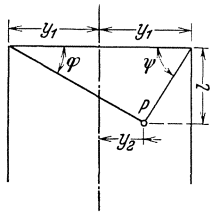

Fig. 82.

If the point P is situated in front of the wing l must be written with a negative sign. The interference effect w_2 at P, of the entire wing, is found by integrating with respect to y_1 over the half span b_1. If P is a point on the profile of the other wing of equivalent chord length c (c = the chord length of the corresponding flat plate) a portion of that wing of width dy_2 suffers a diminution of lift of magnitude $d\triangle L = w_2\, 2\pi\, c\, (1/2)\, \varrho\, V dy_2$. The whole of wing 2 lying at distance l behind wing 1 experiences a (negative) increase of lift of magnitude

$$\triangle L = -2\pi\, (1/2)\, \varrho\, V \int_{-b_2}^{+b_2} w_2\, c_2\, dy_2 \qquad (11.2)$$

The value then obtained for the mean induced velocity of the previous section is

$$\overline{w}_2 = \frac{1}{S_2} \int_{-b_2}^{+b_2} w_2\, c_2\, dy_2 \qquad (11.3)$$

where $S_2 = \int_{-b_2}^{+b_2} c_2\, dy_2$ and denotes the surface area of the rear wing.

The mean velocity $\overline{w}_1$ of the front wing under the influence of its partner can be found in similar fashion. In most cases which occur in practice the span of one of the two wings (horizontal tail surfaces) is small in

comparison with the other, and (11.1) may then be materially simplified by replacing the interference velocity w_2 (or w_1 as the case may be) by its value in the plane of symmetry. If this is done it follows that

$$\sin\varphi = \sin\psi = \frac{1}{\sqrt{l^2+y_1^2}}, \qquad \cos\varphi = \cos\psi = \frac{y_1}{\sqrt{l^2+y_1^2}}$$

and hence

$$\overline{w}_2 = w_2 = \int_{-b_1}^{b_1} \frac{\partial \Gamma}{\partial y_1} \frac{1}{2\pi} \left[\frac{1}{\sqrt{l^2+y_1^2}} \left(\frac{y_1}{l} + \frac{l}{y_1} \right) + \frac{1}{y_1} \right] d y_1 \qquad (11.4)$$

This integral has been evaluated by H. B. Helmbold[1] for elliptic lift distribution. He found that the velocity (reckoned positive downward) could be expressed as

$$w_2 = \frac{2L}{\pi \varrho V (2b)^2} [1 + \varphi (l/b)] \qquad (11.5)$$

in the region behind the wing. The corresponding formula in front of the wing is

$$w_1 = \frac{2L}{\pi \varrho V (2b)^2} [1 - \varphi (l/b)] \qquad (11.6)$$

l always being reckoned positive. The factor $2L/\pi \varrho V (2b)^2$ (which corresponds to $l = 0$) represents the downward velocity at the wing itself [see (2.6)]. Let w_0 now denote the velocity for an infinitely long wing, as obtained in (10.21). Then

$$w_0 = \mp \frac{\Gamma}{2\pi |l|} = \mp \frac{L}{4\pi \varrho V b |l|} \qquad (11.7)$$

A comparison of this formula with (11.5) and (11.6) shows that

$$\left.\begin{aligned} \varkappa_1 &= \frac{w_2}{w_0} = 2\frac{|l|}{b} [\varphi (l/b) + 1] \\ \varkappa_2 &= \frac{w_1}{w_0} = 2\frac{|l|}{b} [\varphi (l/b) - 1] \end{aligned}\right\} \qquad (11.8)$$

The values of the function $\varphi (l/b)$ can be obtained from the Table of Division E VI 6 where $(1 + \varphi)$ is denoted by φ_T/φ. The curve marked I in Fig. 83 represents $\varkappa$ as a function of l/b, the values being derived from those of φ in the table mentioned. The portions of the curve to the right and left of the origin represent respectively $\varkappa_1$ (interference on the rear tail-plane by the wing in front of it) and $\varkappa_2$ (interference on the forward tail-plane by the wing behind it).

In calculating the interference field it has been assumed that the vortices trailing from the wing move, as shown in Fig. 81, in straight lines in the direction opposite to the direction of flight. This hypothesis is justified when the interference velocities produced by the wing are very small in comparison with the velocities of flight. This assumption is usually made in applications of airfoil theory and is sufficiently near

[1] Helmbold, H. B., Über die Berechnung des Abwindes hinter einem rechteckigen Flügel. Zeitschr. f. Flugtechnik u. Motorl. **16**, p. 291, 1925. See report on this paper in Division E VI **6**.

to the facts for nearly all problems which arise; it is not, however, sufficiently accurate for the case at present under consideration, *i. e.* the problem of the mutual interaction of two airfoils. The chief reason for this exception is the fact that the band of vortices proceeding from the wing rolls up into two single vortices whose interference field differs from that of the band which existed before rolling up occurred (Division E VI 6). This effect will be understood more clearly by considering the simple case of an airfoil with elliptic lift distribution. We shall consider the effect at a point in the plane of symmetry lying so far behind the airfoil that the induction due to vortices attached to the wing itself can be neglected and that the length of the trail of free vortices extending in front of the point may be taken as infinite in the calculations. If L is the lift of the wing, the band of vortices before rolling up produces an induced velocity of amount [see (2.6)]

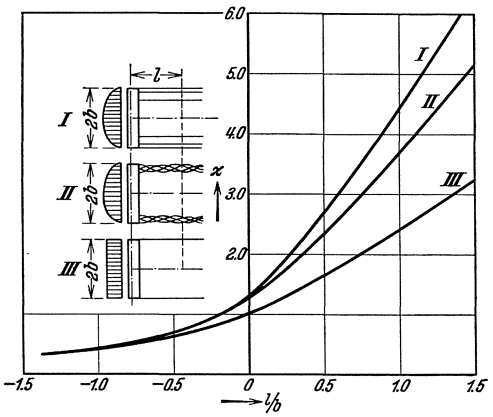

Fig. 83. Ratio of the induced velocity at the middle of a wing of finite span to the same velocity on a wing of infinite span but with equal lift per length of span, *I*, for elliptic lift distribution without rolling up of the vortex surfaces; *II*, for elliptic lift distribution with immediate rolling up of the vortex surfaces; *III*, for rectangular lift distribution.

$$w = \frac{2L}{\pi q (2b)^2} V$$

After rolling up there are two single vortices with opposite sense of rotation and with circulation (2.2)

$$\Gamma_0 = \frac{L}{\varrho V (2b) \pi/4}$$

At any instant these vortices lie at the "centers of gravity" of the two halves of the unrolled vortex band which produce them, *i. e.* at a distance

from the middle, $$b' = \frac{\pi}{4} b \tag{11.9}$$

[Division E VI (5.5)]. A vortex pair of this kind produces an induced velocity in the plane of symmetry of amount

$$w' = 2 \frac{\Gamma_0}{2b'\pi} = \frac{2L}{\pi q (2b)^2} \cdot V \cdot \frac{8}{\pi^2} \tag{11.10}$$

so that the rolling up process has reduced the induced velocity by about 20 per cent. This result is, however, only true in the plane of symmetry and the value increases toward the sides, a fact which must be considered when tail-planes of comparatively large span are used. Fig. 84 shows the velocity distribution before and after the appearance of single vortices, the first being shown by a dotted and the second by a continuous line.

If the individual vortices developed very quickly the calculations could be performed simply by replacing the actual wing and its actual lift distribution by a wing with rectangular lift distribution and correspondingly concentrated trailing vortices. Unfortunately, in most cases occurring in practice the transition into individual vortices occurs precisely in the region occupied by the horizontal tail surfaces [see Kaden's investigations, Division E VI (5.9)]. Hence the values of the downwash on the horizontal tail surfaces always lie between those for the unrolled vortex band and those for the developed vortex pair. In Fig. 83 the curves marked *I* and *II* represent the function $\varkappa$, constructed by analogy with (11.8), for the two extreme cases of vortex bands which, from their very commencement, are respectively unrolled and rolled up into a vortex pair.

Since the lift distribution of a wing is generally somewhat fuller than the ellipse, the trailing vortices before rolling up are usually concentrated more strongly at the boundary than in the example considered; this reduces the difference in the downwash before and after rolling up without, however, rendering it small enough to be negligible. The reader may be referred for a more exact account of the phenomena occurring with rectangular airfoils to the paper by H. B. Helmbold already mentioned (see footnote p. 81 and report in Division E VI 6). The limiting case for which the lift distribution is constant over the entire span is shown by curve *III* in Fig. 83. Since rolling up occurs only behind the wing the change in the induced field thereby produced is only of considerable effect in that region itself. In the space occupied by the wing and even more so in the space in front of the wing the effect of the rolling up is generally so small that it may be neglected.

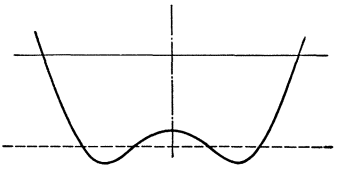

Fig. 84. Distribution of the downwash across the span.

12. Experimental Values Characterizing the Downwash Behind Wings. In consequence of the uncertainty attaching to the initial suppositions of the theory sketched in the preceding sections due, in particular, to the rolling up of the vortex layer behind the wing, the theoretical values of the induced velocities are not yet sufficiently reliable. Unfortunately, moreover, the experimental determination of the so-called downwash is rather difficult owing to the small values which have to be measured, and but few results have been obtained. One method is to measure the downwash at various points behind (or in front of) the wing by using some means for indicating the direction of flow[1]. Another is to

[1] The simplest, though not very accurate, procedure is to insert light threads into the flow which arrange themselves in the direction of flow and are then photographed. An exploration of the field behind a wing, conducted in this fashion, is published in the Technische Berichte der Flugzeugmeisterei, Vol. III, p. 10

introduce small test surfaces, and to deduce the downwash from the forces exerted upon them. The first method has the disadvantage that all accidental local interferences are included in the indications and measurements must be taken at a great many points in order to eliminate this source of error. The second method on the other hand has the disadvantage that the measurements obtained are mean values of the pressures over the testing surfaces so that alterations of the downwash in small regions, *e. g.* behind the ends of the wing, cannot be followed. If the size of the test surface is reduced, the diminished exactitude of the angular settings and the decrease in the magnitude of the forces considerably increase the difficulty and reduce the accuracy of the measurements. Also the direction sensitivity of such test surfaces is, in general, less than that of other means for direction indication.

A comprehensive survey of downwash by means of a testing surface has been made in England using a model wing of 18 inches span and 3 inches chord, and with a test plane 2-1/2 inches by 1/2 inch[1].

13. Wing and Tail-Plane. In the construction of airplanes it is usual, for reasons dictated both by considerations of strength and facility in steering, to concentrate the greater part of the lift on one wing (or otherwise, as in a multiplane, on several wings arranged in a vertical series) and to make the second wing considerably smaller in order to serve chiefly as an auxiliary stabilizing element. In general the stabilizing wing is put at the rear of the main wing but may also, as in the "canard" type, be located in front of the main wing. The "elevator" wing is usually connected to the "stabilizer" wing, the whole arrangement forming the horizontal tail structure, of which the fixed portion is the stabilizer or tail plane. If the elevator is fixed, stabilizer and elevator, *i.e.* the entire system of horizontal tail surfaces, work together as a stabilizing wing. It is often of interest to know the behavior of the airplane when the elevator is free to move; for details of the calculations of the forces on the tail-plane in the latter case, reference may be made to the following sections.

It has already been seen that the tail surface, if located behind the main wing must have a smaller effective angle of incidence than the latter. The greater this difference of angle (decalage) between the two wings the more effective is the stabilization and the smaller need be the area of the stabilizing wing or its distance from the main wing (advantages in construction). In the extreme case the stabilizing wing can be so

(M. MUNK, and G. CARIO, Luftstromneigung hinter Flügeln). A more accurate procedure involves the measurement of pressure differences by using, *e. g.* the "double tube" and the "triple tube". *c. f.* R. KRÖNER, Dissertation, Berlin (Technische Hochschule), 1915 (printed 1919).

[1] PIERCY, N. A. V., On the Flow in the Rear of an Aerofoil at Small Angles of Incidence, Br. A.R.C. R. and M. 578, 1918, 1919.

arranged as to give a negative lift (*i.e.* a downward force) during normal flight; the center of gravity of the airplane must then be situated in front of the center of pressure of the main wing. With such an arrangement, however, part of the lift is lost through the negative lift on the tail surfaces and there is also increased drag due to the induced drag of a wing with negative lift; hence the lift-drag ratio is diminished. It is more usual therefore to arrange the tail surfaces for a nearly zero lift in normal flight; small deviations from zero are comparatively unimportant and may be permitted in order to secure other favorable structural features (*e.g.* the position of the center of gravity relative to the main wing). Since the lift on the tail surfaces is in most cases in the neighborhood of zero, thin symmetrical or nearly symmetrical profiles are used in its construction.

One very important factor to be taken into account in determining the shape of the tail surfaces at the rear is the fact that the critical angle of incidence for which the lift is a maximum must first be reached at the main wing. Otherwise the separation of the flow at the tail surfaces would destroy its stabilizing effect and the airplane would become unstable for all larger angles of incidence. The thin, approximately symmetrical, tail surface profiles in general use are favorable in this respect since they have no marked critical angle of incidence. With this fact in mind the contour is frequently chosen to have an aspect ratio differing but little from one, since the lift then continues to increase for angles of incidence considerable larger than with more usual airfoil aspect ratios (Fig. 76, square plate). The large induced drag usually associated with small aspect ratios is not of importance here since the lift on the wing in its normal state is approximately zero. Often the critical angle is raised still further by the use of slots. Since the tail surfaces must work well for both positive and negative changes of angle, the normal arrangement of a slotted wing (Fig. 61) cannot be applied and instead, the space already present between stabilizer and elevator is generally used as the slot.

The working of the elevator at the rear of the main wing can be adversely affected not only by the downwash due to the circulation around the main wing, but also in serious degree by the dead air wake (mixed turbulence). In normal flight however, this wake is not of great extent and in general it is not difficult to arrange that the tail plane shall lie always outside this region. Nevertheless attention must be paid to this point since otherwise the tail surfaces may refuse to act over a given range of values of the angle of incidence. In stalled flight, however, it is much more difficult to secure for the tail surfaces a location outside the wake. In this type of flight, the flow separates from the main wing and the wake is of comparatively wide extent. It is, however, of great importance to meet this condition. At large angles of incidence the

tail-plane gives usually a positive lift. If then, as a result of separation of the flow at the main wing the tail surfaces enter suddenly into this "dead air" wake, the lift on these surfaces is decreased and an additional couple is produced tending to increase the angle of incidence. Hence in general it will not be possible to decrease the angle of incidence by manipulation of the elevator, and hence impossible, in this way, to emerge from the stalled condition. Correct choice of the position of the tail is made even more difficult by the condition that in a rapid spin about the vertical axis (flat spin), the vertical tail surfaces should not be shielded by the horizontal tail surfaces. The wake may also give rise to a condition of tail flutter with possible consequent structural damage and casualty[1].

Figs. 85 and 86 show the positions of the wake[2] at various angles of incidence of a model wing. The former diagram shows

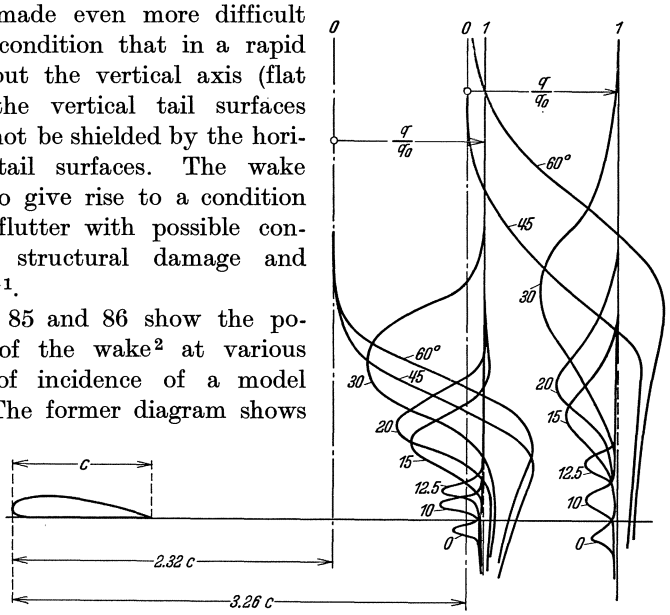

Fig. 85. Distribution of the stagnation pressure in the plane of symmetry behind a rectangular wing of aspect ratio 8.

the distribution of dynamic pressure as a function of height. Values are given for various angles of incidence at two distances in the plane of symmetry (2.32 c and 3.26 c where c = chord length). The airfoil had a rectangular contour of dimensions 736 × 92 mm.[3] (29 × 3.6 in.) and profile G. 387. The distribution curves are plotted relative to the airfoil (not relative to the wind direction) Fig. 86 indicates between

[1] DUNCAN, W. J., ELLIS, D. L., SCRUTON, C., FRAZER, R. A., FALKNER, V. M., Two Reports on Tail Buffeting, by the aerodynamics staff of the National Physical Laboratory. Br. A.R.C. R. and M. 1497, 1932.

BIECHTELER, C., Versuche zur Beseitigung von Leitwerkschütteln. Zeitschr. f. Flugtechnik u. Motorl. **24**, p. 15, 1933.

[2] According to E. PETERSOHN, Abwindmessungen hinter Tragflügeln mit abgerissener Strömung. Zeitschr. f. Flugtechnik u. Motorl. **22**, p. 289, 1931.

[3] The original paper includes results for a rectangular airfoil 1 : 4 and a trapezoidal airfoil.

lines of the same character, the boundaries of the wind shadow (wake) in the plane of symmetry, *i. e.* the region which is to be avoided for the location of the tail surfaces.

The stabilizer and elevator surfaces can also be arranged in front of the main wing ("canard" type)[1] and must then have a greater angle of incidence than the main wing, *i.e.* comparatively high lift in the normal state. Well curved profiles may therefore be used to advantage in such case, in place of those of nearly symmetrical form. It is then easy to ensure that the flow shall separate earlier and more completely at the control surfaces than at the main wing, and it is, therefore, almost impossible to stall such an airplane. This position has also the advantage that it can never be deprived of its stabilizing effect by entrance into the wake. In landing also, the ground can be approached at much greater angles of incidence and overturning is almost out of the question. The chief disadvantages lie in certain structural inconveniences (decreased visibility, installation of motor and propeller).

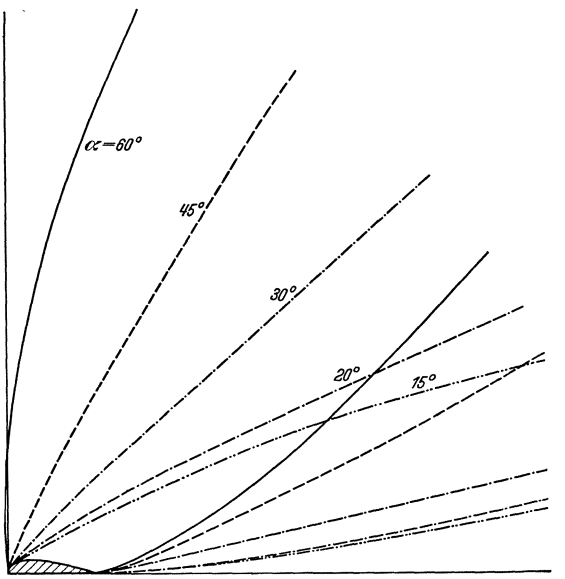

Fig. 86. Boundaries of wind shadows.

A report of research work in England[2] gives the results of extended tests on a model biplane carried out on the plane as a whole, on the plane without control surfaces and on the control surfaces alone. Reference to this report will show that the pitching moment for the entire model is not obtained by simple addition of the moments of the model minus tail surfaces and of the tail surfaces alone. The effect of the tail surfaces is less when in combination with wing than when alone, since the downwash behind the wing diminishes the lift of these surfaces (see **11**).

---

[1] KIEL, H. G., Statische Längsstabilität der Entenbauart. Zeitschr. f. Flugtechnik u. Motorl. **21**, p. 601, 1930.

[2] BRAMWELL, F. H., Experiments to determine the lift, drift and pitching moment on a model biplane and their variations with wind speed. R. and M. No. 111 (Technical Reports of the British 1913—1914), London, 1915.

14. Wing and Flap, Fixed and Control Surface. If a wing and tail-plane, as considered in the last section, are brought so close together that they are in contact, a combination is obtained which is essentially that of a wing with flap attached or a fin with rudder attached. The conclusions previously reached can therefore be partially extended to these parts of an airplane. There is however an essential difference due to the fact that the reduced distance between the two elements greatly increases their mutual interaction. A combination of this kind can therefore be regarded as a single airfoil of somewhat unusual profile as *e.g.* in the theoretical discussion of Division E II **11**, where the combination is idealized into a bent flat plate.

For experimental results of tests on this combination, reference may be made to a comprehensive report[1] on the working of a flap on the profile N.A.C.A. M6, carried out in the variable density tunnel at Langley Field and under a Reynolds number of about 4,000,000. The flap ran along the entire span and its chord was 20 per cent of the combined chord (see IV **17** for corresponding experiments with ailerons on the outer part of the wing). Similar experiments on stabilizer and elevator combinations have also been carried out in the Göttingen research laboratory, and to the reports on which, reference may be made[2]. These experiments were carried out on three combinations with varying proportions of elevator to total area, but all have the same overall form (contour and profile) for zero deflection of the elevator. The results are also compared with the theoretical values calculated with the help of Munk's integral (see II **3** and Division E II **9**). This comparison is made for the angle of incidence (α_0) at which the lift vanishes, and the agreement is good for small deflections of the elevator but for large values additional deflection produces far less effect than theory predicts, a fact which must be ascribed to separation of the flow at the rear of the wing. Similar results are found for the theoretical and measured values of the moment; the agreement is good only for small angles of incidence and small deflections of the flap.

In addition to the usual quantities, C_L, C_D, C_M for the tail-plane structure as a whole, the moment about the axis of the elevator as well as the moment coefficient

$$C_E = \frac{M_E}{S_E c_E (\varrho/2) V^2} \tag{14.1}$$

are also given. Here M_E is the moment about the axis of the elevator, S_E and c_E the surface area and chord of the elevator calculated from the

[1] Higgins, G. J., and Jacobs, Eastman N., The Effect of Flap and Ailerons on the N.A.C.A. M6 Airfoil Section. Rep. 260 (Techn. Rep. of the National Advisory Committee for Aeronautics, Washington, 1927, 1928).

[2] Ergebnisse der Aerodynamischen Versuchsanstalt zu Göttingen, III. Lief., p. 102 (R. Oldenbourg, Munich, 1927).

axis to the trailing edge. This moment is important because it determines the force which must be exerted by the pilot in moving the elevator.

For convenience of calculation in practical cases Blenk[1] has arranged results of this experiment in the following manner. The component of the force perpendicular to the plane of symmetry of the stabilizer, *i.e.* the so-called normal force N, and its non-dimensional coefficient $C_n = N/(1/2)\,\varrho\,v^2\,S$ can be expressed with good approximation by the equation

$$C_n = k\,(\alpha - \tau\,\beta) \tag{14.2}$$

where β is the angle between stabilizer and elevator (see Fig. 89). Since the normal force is almost equal to the lift, k represents essentially the known connection between the coefficient of lift and the angle of incidence of ordinary airfoils. It follows from (3.4) that the following equation is approximately true:

$$k = \frac{2\,\pi}{\left(1 + 2\,S/(2\,b)^2\right)} \tag{14.3}$$

The value of τ depends on the ratio of the surface of the elevator area to the total area of the tail-plane structure. From the results of these experiments it is possible to derive a curve connecting τ and S_E/S as shown in Fig. 87. For any given tail-plane combination, τ is a characteristic constant.

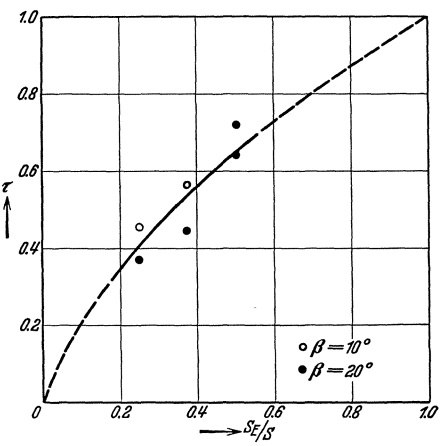

Fig. 87. Relation between the effect of the elevator on the lift and the relative surface of the elevator.

The moment of the air force about the elevator axis can be expressed approximately by the formula

$$M_E = k_1\,(\beta - \tau_1\,\alpha) \tag{14.4}$$

where $\tau_1\alpha$ is the angular movement of the elevator for which the moment vanishes. The values of $\tau_1\alpha$ are shown in Fig. 88 for the three different tail-plane combinations investigated. If the angle of incidence is not too large ($\alpha <$ about 12^0) $\tau_1\,\alpha$ is approximately proportional to the angle of incidence so that inside of this domain of values for α, τ_1 is a constant characteristic of the tail-plane. The value of this constant depends in chief degree on the surface ratio S_E/S, and a very crude approximation is $\tau_1 \approx S_E/S$.

Since definite stability is often required when the elevator is *free*, its location, in such cases, must be investigated. Stability results from the combined effect of the forces due to air and the forces otherwise

[1] Blenk, H. (see footnote p. 90).

acting on the elevator. The relations involved have been investigated in detail by H. Blenk[1]. Apart from forces due to the air the elevator is chiefly under the influence of gravitational (and possibly also inertial) forces. Insofar as these forces are due to the weight of the elevator

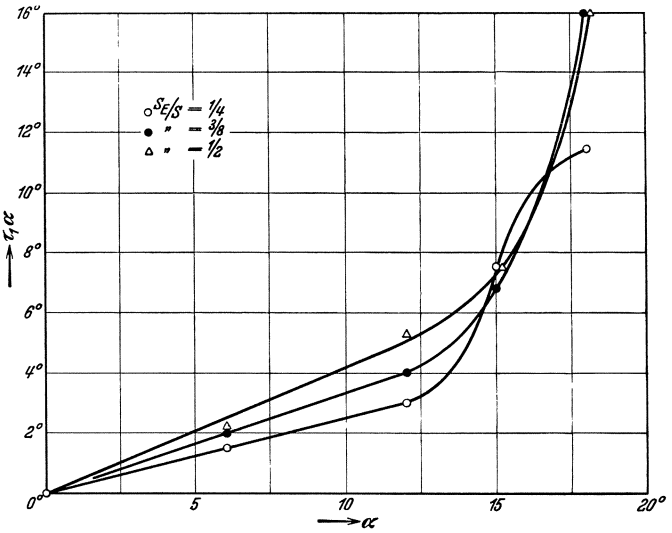

Fig. 88. Elevator displacement angle for which the moment about its axis of rotation vanishes.

itself, their moment about the axis depends on the position of the elevator with respect to the vertical (or with respect to the direction of mass forces) that is, it depends on the angle $\beta - \theta$. Here β, as hitherto, denotes the elevator deflection (angle between elevator and stabilizer) and θ the angle between the stabilizer and the horizontal (Fig. 89) Apart from the weight of the elevator itself the weight of the connecting parts, *e. g.* of the control stick must also be considered. Since the stick and rudder are usually in gear, the deflection of the former corresponding to a deflection β of the latter will be $\varkappa\,\beta$. When the elevator and stabilizer are at their zero position, *i. e.* $\theta = \beta = 0$, the stick will have an inclination ε to the vertical; hence the gravitational moments about the elevator axis can be expressed in the following form:

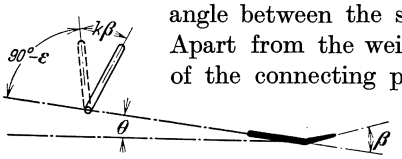

Fig. 89. Illustrating the effect of gravity on the moment about the elevator's axis of rotation.

$$M_G = M_1 \sin(\varepsilon - \varkappa\,\beta - \theta) + M_2 \cos(\beta - \theta) \qquad (14.5)$$

[1] Blenk, H., Über die Stabilität eines Flugzeuges mit losgelassenem Höhensteuer. Zeitschr. f. Flugtechnik u. Motorl. **21**, p. 189, 1930.

This moment due to the actual weights or masses must be balanced by the moment of the forces due to the air when the rudder is free. The latter moment is given by the formula

$$M_A = C_E \frac{1}{2} \varrho V^2 S_E c_E \tag{14.6}$$

and hence it is necessary that

$$M_G + M_A = 0 \tag{14.7}$$

If the angles occurring in the above formulae are small so that the sine of an angle may be replaced by the angle and the cosine by 1, it follows that, in equilibrium, the elevator deflection β_0 is such that

$$\beta_0 = \frac{[\tau_1 \alpha - m_1 (\varepsilon - \theta) - m_2]}{(1 - \varkappa m_1)} \tag{14.8}$$

where $$m_1 = \frac{M_1}{(1/2) \varrho V^2 k_1 S_E c_E} \quad \text{and} \quad m_2 \frac{M_2}{(1/2) \varrho V^2 k_1 S_E c_E} \tag{14.9}$$

In high speed aircraft special attention must be paid to the strength of the joints of the elevator since they are often subject to violent stresses caused by high negative pressures[1] in their neighborhood during quick maneuvers.

15. Biplane. Whereas the induced drag on two airfoils arranged in horizontal sequence is, in accordance with Munk's displacement theorem (I 5), independent to a first approximation of the relative arrangement of the wings (deviations being produced by the rolling up of the free vortices) an entirely different state of affairs exists when the wings are arranged one above the other. The distance between the two wings (gap) is here an essential factor in determining the induced drag of two wings arranged in the latter fashion. A detailed description of the attendant phenomena would however be superfluous at this point since the theory and calculations involved are given in detail in Division E IV Part B. It may however be mentioned that the induced drag on a biplane of span $2\,b$ may be put equal to that on a monoplane of span $2\,b'$, the two arrangements having the same induced drag for the same lift. The value of the ratio b/b' of the spans depends upon the relative arrangement of the two wings of the biplane and also upon their lift distributions. In order to characterize the essential properties of a biplane the square of the ratio mentioned above is used more often than the ratio itself, *viz.*, $\varkappa = (b/b')^2$. If the reciprocal of the biplane's aspect ratio is $S/(2\,b)^2$ then for the equivalent monoplane we shall have

$$\frac{S}{(2\,b')^2} = \varkappa \frac{S}{(2\,b)^2} \tag{15.1}$$

The most favorable allocations of the total lift between the two component wings, with the corresponding values of $\varkappa$, are tabulated in Tables 11b

[1] RHODE, R. V., The Pressure Distribution Over the Horizontal and Vertical Tail Surfaces of the F66—4 Pursuit Airplane in Violent Maneuvers, Rep. 307. U.S. N.A.C.A., 1928.

and 11a respectively of Division E IV **23**. Both wings are assumed to have elliptic lift distributions.

In calculating the connection between angle of incidence and lift of a biplane it must be noticed that in addition to the existence of a mean deviation of the flow (whose value is a predominating factor in the induced drag) this deviation is characterized by being smaller in front of the wings than behind them, so that they must be considered as acting in a curved flow. The effect of this is approximately the same as a diminution in the curvature of the wing profile. Hence for a given angle of incidence the effect of the presence of a neighboring wing is to cause the lift to decrease more rapidly than would be expected by analogy with the equivalent monoplane. In calculating angles of incidence the factor $\varkappa$ mentioned above must be replaced by a somewhat different factor, $\varkappa'$, the values of which have been calculated theoretically by N. K. Bose[1]. The following Table compares the theoretical and experimentally observed values of $\varkappa$ and $\varkappa'$ for unstaggered biplanes having the same wings above and below [g = distance between the wings (gap) c = chord, S = combined surface of both wings][2].

g/c	$2\,(b)^2/S$	$\varkappa_{\text{theor.}}$	$\varkappa_{\text{exp.}}$	$\varkappa'_{\text{theor.}}$	$\varkappa'_{\text{exp.}}$
0.8	3.0	0.794	0.852	1.447	1.221
1.1	3.0	0.754	0.819	1.110	1.049
1.4	3.0	0.721	0.754	0.9345	0.967
1.113	2.4	0.722	0.761	0.9925	0.949
1.113	1.44	0.649	0.676	0.8115	0.803

In addition to the induced drag another important feature of the biplane requiring attention is the degree of stability exhibited, although in this respect the mutual action of the two wings plays a smaller part than in the tandem arrangement. A marked effect on the stability of the combination is produced if the wings are staggered, *i. e.* if, instead of one being exactly above the other, the upper wing projects slightly forward. A relative inclination of the wings (decalage) then affects the stability in the same manner as for the tandem arrangement. The conclusions for that case remain unchanged provided that the stagger l (here) Fig. 90, is put for the gap between the wings. The quantitative determination of the mutual interaction is however somewhat different in this case (for details see Division E IV Part B).

The following difficulties arise in connection with a staggered biplane (the same as in the tandem arrangement of two wings): the front wing is exposed to a rising current of air, the rear wing to a descending current; hence in order to work with approximately equally effective angles of incidence, the forward wing should have a geometrically smaller angle

[1] Bose, N. K., and Prandtl, L., Beiträge zur Aerodynamik des Doppeldeckers. Zeitschr. f. angew. Math. u. Mech. **7**, p. 1, 1927.

[2] Ergebnisse der Aerodynamischen Versuchsanstalt zu Göttingen, II. Lief., p. 39, and III. Lief., p. 13 (correction in IV. Lief., p. 148).

of incidence than its neighbor. This however entails a relative inclination of the wings with considerable consequent instability. If, however, the relative inclination is arranged so as to increase the stability, the front wing has then a considerably higher effective angle of incidence than the rear. This effect may be measurably allowed for by choosing for the front wing a profile of greater curvature than for the rear wing, and hence the front wing will exhibit its most favorable properties at larger angles of incidence. That is, in order to obtain in a biplane favorable stability characteristics and a good lift-drag ratio at the same time, each wing must have a different profile. The choice of profiles is therefore somewhat restricted and no use can be made of the extreme properties of many profiles. It is however often desirable on other grounds to employ different profiles. Thus, for example it is possible to mitigate somewhat the effects of separation of the flow beyond the maximum lift by arranging that separation does not occur simultaneously on both wings. This diminishes the tendency to spin (see IV **11**)[1].

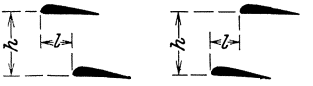

Fig. 90. Staggered biplane.

A comparison of theory with the results of experiment has been made based on the results of an experimental investigation of a series of biplane models in the Göttingen laboratory[2]. In addition to the measured polars are given also the values computed from a monoplane of the same profile and in accordance with the theory set forth in Division E IV **23**. The results show the diminution of induced drag resulting from an increase in the distance between the wings. The cause of the divergences, (generally small) between the theoretical and observed curves can perhaps be ascribed to the fact that whereas the theory is based on the assumption of elliptic lift distributions for each wing, these distributions may, in practice, diverge considerably from this form. This is especially the case if the two wings have unequal spans. In this case also the differences between theory and experiment are notably larger. In order to ascertain whether the altered lift distribution is in fact the chief cause of the divergences between the calculated and observed values, a further experiment was conducted with the same arrangement of the wings, but with unequal spans and with the wings so twisted as to give an approximately elliptical lift distribution for $C_L = 0.8$. From the results of the measurements on these distorted wings, it can be seen that the divergences have for the most part disappeared.

[1] FUCHS, R., and SCHMIDT, W., Stationärer Trudelflug. Luftfahrtforschung, Vol. III, Part I, 1929.

[2] Ergebnisse der Aerodynamischen Versuchsanstalt zu Göttingen, II. Lief. (Munich, 1926), p. 35. See among others A. BETZ, Auftrieb und Widerstand eines Doppeldeckers. Zeitschr. f. Flugtechnik u. Motorl. IV, p. 1, 1913 (measurements taken with extensively varied arrangements). Further J. C. HUNSAKER, Stable Biplane Arrangements. Engineering **7** and **14**, January, 1916.

16. Airplane Wings Near the Ground[1]. The influence of the ground (considered as a flat surface) on a nearby airplane wing may be investigated by the method of images (see Division E IV Part C). A wing near the ground and at distance h from it therefore corresponds to a wing in a flow extending to infinity at a height $2h$ above an exactly similar wing image (Fig. 91). The effect of the ground can therefore be calculated in exactly the same fashion as for the mutual interaction of the two wings of a biplane. It must however be observed that the position of the image wing is that of the underwing of a biplane when reversed, so that the effect of the flow will be of opposite sign. Moreover this method of approach will not apply to the cases of biplanes involving stagger, with different spans of the two wings, or with different lifts, since the image wing naturally lies vertically beneath the actual wing and has the same span and equal but opposite lift.

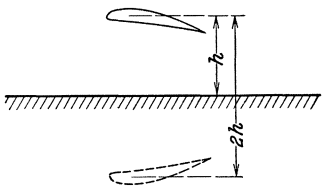

Fig. 91. The ground replaced by the image of an airfoil.

A comparison of theory with experiment in connection with this problem has been made in the Göttingen laboratory[2], based on an experimental test of a model comprising wing, fuselage and tail surfaces. The aspect ratio of the wing was $(2b)^2/S = 9.2$. The model was tested first in an unrestricted air current and then near the ground. The ratio of h, the distance from the ground, to the span in the latter case was $h/2b \approx 0.12$. It was found that the induced drag is greatly diminished in the neighborhood of the ground. The theoretical polars were calculated from the measurements in free air and corrected according to theory for the influence of the ground. For the greater part of the polar curves the theoretical amount of decrease agrees very well with experiment and the two curves diverge only for very high lifts. This divergence is due to the fact that in flow near the ground, separation commences somewhat earlier than for flow in an unrestricted air current.

CHAPTER IV

UNSYMMETRICAL AND NON-STEADY TYPES OF MOTION

1. Preliminary Remarks. The airplane and airplane combinations discussed in the previous chapter were such that all motions took place

[1] BETZ, A., Die gegenseitige Beeinflussung zweier Tragflächen. Zeitschr. f. Flugtechnik u. Motorl. V, p. 253, 1914.

[2] Ergebnisse der Aerodynamischen Versuchsanstalt zu Göttingen, II. Lief., p. 41 (Munich, 1926). See among others A. BETZ, Auftrieb und Widerstand einer Tragfläche in der Nähe einer horizontalen Ebene (Erdboden). Zeitschr. f. Flugtechnik u. Motorl. III, p. 217, 1912.

in planes parallel to an existing plane of symmetry. The resulting forces in such cases have their lines of action in the plane of symmetry and are uniquely determined by three independent quantities. For this purpose the magnitudes usually chosen are the lift, drag and moment; alternatively, it is possible to take magnitude, point of application on the chord, and direction of the resultant force, as the three independent quantities. A state of asymmetry can arise through the action of an unsymmetrical air flow upon a symmetrical airfoil or otherwise due to the asymmetry of the airplane structure itself. The condition of asymmetry in an airplane results chiefly from the use of the rudder and ailerons. However, even in such case, there is a preferred plane of reference, namely the major plane of symmetry with ailerons and rudder undeflected. This plane is called the principal plane of the airplane. In asymmetric configurations the forces which have been previously referred to as lying in the principal plane, are supplemented by further forces whose lines of action are not in that plane. These additional forces can again be determined from the values of three further data, *e. g.* the force components perpendicular to the principal plane and the moments about the vertical axis and about the longitudinal axis of the airplane. To specify the system of resultant forces completely, in magnitude, direction and point of application, six quantities are needed and these may be the components of force along the three axes of a chosen coordinate system and the moments about these axes.

In Chapters I, II and III we have considered those symmetrical motions of the airplane which affect the forces and moments without producing rotation of the airplane; such motions can be characterized by two magnitudes, the velocity and angle of incidence (*i. e.* the inclination of the velocity with respect to an axis fixed in the airplane). In defining these motions these two magnitudes may also be replaced by others, *e. g.* the two velocity components parallel and perpendicular to the axis of the airplane. The forces and moments are, however, not functions of these magnitudes alone and may be affected by the values of many other magnitudes connected with the motion, *e. g.* the acceleration of the two velocity components. In general, very little is known of these effects and in most cases their magnitudes are probably small. The effect of the angular velocity about the transverse axis is however of extreme importance. This factor comes then as a third magnitude which must be included in symmetrical motion in addition to the two velocity components mentioned above. In general, when the motion is unsymmetrical, three further principal magnitudes are required: the velocity components normal to the principal plane and the angular velocities about the vertical and longitudinal axes. The general case of unaccelerated motion is therefore determined by six quantities, which may be conveniently arranged by selecting the velocity components parallel to the

three axes of coordinates in conjunction with the angular velocities about these axes. In discussing dynamical problems of flight it is useful to have the coordinate axes coincide with the principal inertia axes of the airplane. In purely aerodynamic problems, though the axes may be chosen in any arbitrary positions, it is again more advisable to place two of them in the principal plane. A motion in which the three velocity components remain unaccelerated is a steady motion. In accordance with this definition, rotation about an axis parallel to the direction of flight is a steady motion. On the other hand rotations about other axes taken in conjunction with a forward velocity are not in general steady, for if the airplane is turning relative to the direction of motion, the angle of incidence of the flow on an axis fixed to the airplane changes with time. Rotation about the lateral axis (pitching) for example, changes the angle of incidence, and rotation about the vertical axis (yawing) changes the angle of yaw. But even in such cases the motion may be steady if the airplane describes a curve such that the change in angle of its path exactly balances that produced by its rotation; for then the angle between the path and an axis fixed in the airplane remains constant.

Since the six components of force, or moment, may each be a function of the six velocity components and, in the event of rapid changes of velocity, a function of the accelerations also, the resulting relations between the velocities and the forces which may arise are extraordinarily complicated and it is necessary from the very beginning to consider only the most important phenomena. Fortunately, in general, some of the velocity components have comparatively little influence on the force or moment components, so that in any given case it is possible to restrict consideration to the predominating influences. In such a procedure it may easily happen however, that the underestimation of certain effects, leading to their neglect, may result in wrong conclusions. Additional simplification is possible, however, if the unsymmetrical motion is small in comparison with the principal motion (flight in a slowly curving path), for the effects of unsymmetrical motions can then be treated as linear functions of these motions and the effects of the various velocity components can thus be investigated separately and compounded by simple superposition.

We will classify the motions considered according as to whether they do, or do not, involve rotation. Included in the latter are motions with a lateral velocity component, or side-slip, and those produced by asymmetric arrangements of rudders or ailerons. These phenomena can be investigated in wind tunnels with the help of the so-called "six component balance", air being directed upon a model attached to the balance in the usual way. Motions involving rotations of the airplane, however, cannot be imitated by stationary models immersed in air

currents. The model itself must be set in motion and the resulting inertial forces considerably increase the difficulty of taking measurements. We direct attention first to the effects of side-slip, and then, after a consideration of the phenomena bound up with rotational motion, conclude by examining the effects of the rudder and the associated questions of airplane steering.

A. Side-Slip

2. Side-Slip of a Simple Rectangular Wing. By analogy with the discussion of symmetrical flow, we begin by considering the *potential flow* around an *airfoil profile* set obliquely to the air flow. If the airfoil is of large span, the middle portion of a normal flow is two-dimensional. If, upon this normal flow of velocity u, we superimpose a velocity v parallel to the span of the airfoil, we obtain an oblique motion with angle of inclination γ (Fig. 92) where

$$tan\,\gamma = \frac{v}{u}$$

and the resultant velocity V is given by the equation,

$$V = \sqrt{u^2 + v^2} = \frac{u}{cos\,\gamma}$$

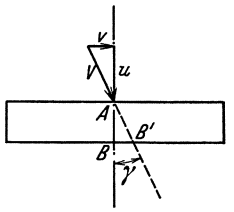

Fig. 92. Rectangular wing in side-slip.

The flow parallel to the span of the wing is a pure parallel flow of constant velocity v, undeflected by the wing except for a slight effect due to the thickness of the wing and restricted to its ends. The superposition of the transverse velocity v produces, therefore, no alteration of the pressure distribution in the region of the two-dimensional normal flow and hence no alteration in the force exerted on a given area in this region. If an airfoil of large span, therefore, is subjected to an oblique flow under an angle γ, the lift over its principal portion is independent of γ and equals the value obtained by a flow normal to the span under constant velocity u. If, on the other hand, the resultant velocity V is kept constant, the force is proportional to $u^2 = V^2\,cos^2\gamma$ and therefore for oblique flows diminishes directly as $cos^2\gamma$. The latter case arises, for example, if the wing is rotated about its vertical axis in a given stream of air. Failing a specific statement to the contrary, it will always be assumed in what follows that this is, in fact, the type of case considered; that is, the resultant relative velocity is constant.

Let us now consider the quantities connected with losses of energy, *viz.*, the drag and maximum lift. The surface friction is constant for all angles if we omit consideration of the somewhat larger Reynolds number (due to increased profile chord for oblique flows $A\,B' > A\,B$ in Fig. 92, and certain other minor effects, for the area of the surface

remains the same, the increased chord length being balanced by the diminished width of the projection of the span in the direction of motion. Since obliqueness of the flow reduces the lift, constant surface friction results in a decrease in the lift-drag ratio. The boundary layer phenomena may be similarly treated by assuming that they are not essentially modified by the superposition of a transverse flow v. A similar argument then shows that the component of drag arising from the surface pressures also decreases as $cos^2 \gamma$. A similar qualitative conclusion can be obtained by the following considerations: If it were assumed that the drag is proportional to the front elevation area (projected area in the direction of motion, corresponding to the mid-ship section in ships) it would follow from the decrease of the projection with increasing obliquity that the drag should decrease as $cos\ \gamma$; but it should be noted that the chord length of the profile is increased in the ratio $1/cos\ \gamma$ for an oblique flow (Fig. 92 $AB' = AB/cos\ \gamma$). Further, since the thickness of the profile is unchanged, the profile for oblique flow is elongated in comparison with the profile for normal flow, and hence the coefficient of drag referred to the area of front elevation should be decreased. If this diminution is proportional to the elongation ratio, *i. e.* proportional to $cos\ \gamma$, the reduction of drag becomes proportional to $cos^2 \gamma$ as in the first argument. Unfortunately, there are almost no known experimental results bearing on these questions so that practically nothing is known as to the influence of oblique flow on the separation phenomena and profile drag. But the experiments on which Figs. 97 to 105 are based, performed on a "sweepback" airfoil, indicate that the influence of obliquity of flow on the drag is comparatively small.

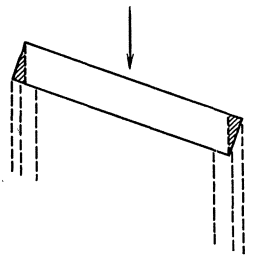

Fig. 93. Wing with vortices generated under side-slip.

Similar results are obtained by considering the maximum lift, also connected with the separation of the boundary layer. The previous considerations show that the decrease in maximum lift for varying angles of approach might be expected to be proportional to $cos^2 \gamma$, but the assumption that the superposition of a transverse velocity v does not materially affect the separation phenomena, is somewhat uncertain, with corresponding uncertainty in the conclusions obtained. Experimental evidence seems to show that the decrease of maximum lift is somewhat less than the previous reasoning would suggest; but here also the data are too few and too unreliable for conclusions to be deduced with confidence.

More important than the alteration of the properties of the profile are the changes in the disturbances produced by vortices originating at the wing edges (see III 11). Unfortunately, very little is known on

this topic also[1]. It is, however, possible to say, with some certainty, that the side of the wing which faces the oncoming stream (Fig. 93) is affected more strongly than the other side so that a couple arises which rotates the first side downward. According to Blenk[2], however, supplementary forces probably arise on the shaded triangular areas at the ends of the wing in Fig. 93 and these forces have a moment in the opposite sense. In addition, the vortices originating at the front half of the wing are displaced more strongly downward under the influence of circulation than vortices at the other side. Hence their influence on the downward disturbing velocities is reduced and the lift increased. This would produce a rolling moment tending to raise the forward wing. In addition to all these effects others are often important, especially for large angles of incidence; such are the effects connected with separation phenomena at the ends of wings in oblique flow, which may complicate seriously the resulting state of affairs[3]. In consequence of these various and oppositely directed forces, it is difficult to estimate theoretically the actual resultant moment. The experimental results given in Fig. 100 show that the sense of the resultant moment is such as to raise the front side of the wing.

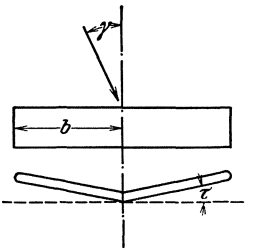

Fig. 94. Wing with dihedral.

3. The Forces and Moments on a Wing with Dihedral in Side-Slip. Effects of side-slip clearer and more marked in character are obtained if the simple rectangular wing is replaced by a wing with dihedral or sweepback, for in such cases the two halves of the wing are influenced in different ways by the transverse flow. We shall first consider the wing with dihedral (Fig. 94). An approximation to the values of the force on each half of the wing can be obtained by considering each separately and uninfluenced by the other. As previously, in the case of the simple wing, the flow in a plane perpendicular to the front edge of the wing is the predominant factor in determining the lift. For a side-slip angle γ, as in the simple wing, the velocity component of approach u varies as $\cos\gamma$ (provided the dihedral is small) and the lift therefore varies as $\cos^2\gamma$. In consequence of the dihedral however, there is the additional fact to be considered that the relative direction of

[1] In order to calculate the magnitudes here involved it is, in general, necessary to introduce the lift distribution across the chord into the calculations which are otherwise vitiated by the infinite disturbing velocities which arise. A computation of this kind has been made by Blenk: BLENK, H., Der Eindecker als tragende Wirbelfläche. Göttingen, Dissertation, 1923 (in Mss. only). Extract in Zeitschr. f. angew. Math. u. Mech. **5**, p. 36, 1925.

[2] BLENK, H., *loc. cit.*

[3] PROPOSTO, S. DEL, Über das Verhalten von Tragflächen bei Seitenwind, Aachen, Ed. Wedler and Co., 1933.

approach in this plane is changed. If the angle of incidence is α for a symmetrical flow, the corresponding angle for an asymmetric approach with angle of yaw γ is

$$\alpha' = \alpha \pm \tau\gamma \tag{3.1}$$

where τ is the angle of the dihedral (Fig. 94) and γ and τ are assumed to be small[1] [(+) for the leading wing, (—) for the following]. If L is the total lift of the wings in a symmetrical flow, each half contributes $L/2$. If α_0 denotes the angle of incidence for zero lift, then the lift for any other angle of incidence α is proportional to $(\alpha - \alpha_0)$ (see II 2). Change of the angle of incidence from α to α' changes the lift from $L/2$ to

$$\frac{L}{2} + \triangle L = \frac{L}{2}\frac{\alpha' - \alpha_0}{\alpha - \alpha_0} = \frac{L}{2}\left(1 + \frac{\alpha' - \alpha}{\alpha - \alpha_0}\right) \tag{3.2}$$

Hence the lift on the forward wing increases by

$$\triangle L = \frac{L}{2}\frac{\alpha' - \alpha}{\alpha - \alpha_0} = \frac{L}{2(\alpha - \alpha_0)}\tau\gamma \tag{3.3}$$

while the lift on the other wing is reduced by the same amount. The difference of lift on the two wings produces a moment about the longitudinal axis tending to raise the forward wing. The value of this rolling moment[2] for rectangular lift distribution is M_q where

$$M_q = b \triangle L = \frac{L b}{2}\frac{\tau\gamma}{(\alpha - \alpha_0)} \tag{3.4}$$

and the moment coefficient is

$$C_{Mq} = \frac{M_q}{\frac{1}{2}\varrho S V^2 c} = \frac{C_L}{2}\frac{b}{c}\frac{\tau\gamma}{\alpha - \alpha_0} \tag{3.5}$$

but on account of the decrease of lift toward the ends, the actual value of the moment is somewhat smaller than that indicated by the formula. In elliptic distributions for example the center of gravity of the lift distribution is at a distance $4\,b/3\,\pi \approx 0.425\,b$ from the plane of symmetry. The moment for such a lift distribution is 15 per cent smaller than for a rectangular distribution in which the distance is $0.5\,b$. The experimental results represented in Fig. 101 show that the actual influence of the dihedral is some 20 per cent less than as indicated[3] by (3.5). This difference is *inter alia* intimately connected with the effects on the velocity field of vortices generated at the wings (see the corresponding effects described in **15**).

---

[1] The corresponding formula for arbitrary values of the angles is

$$\alpha' = \alpha \pm tan^{-1}\,(tan\,\gamma\ sin\,\tau).$$

[2] Since $C_L/(\alpha - \alpha_0) \approx 2\,\pi$ (see II 2), *i.e.*, is independent of the angle of incidence α, both M_q and C_{Mq} are also independent of the angle of incidence. The same is true of the cross-wind force Σ_1 in (3.6) and (3.7).

[3] Even the dihedral $\tau = 0$ produces, in consequence of side-slip, moments and transverse forces. The values obtained for the moments and forces in accordance with the above considerations must be added to those already present when $\tau = 0$.

Since the lift components of the two wings are nearly perpendicular to the wings, *i. e.* are directed inward by angular amount τ (see Fig. 95), the changes of lift $\pm \triangle L$ produce transverse components of force which in each wing are directed from the front to the back (toward the right in Figs. 94 and 95). Let us consider this direction as negative for forces. The sum of these two horizontal components is

$$\Sigma_1 = -2 \triangle L \tau = -L \frac{\tau^2}{\alpha - \alpha_0} \gamma \tag{3.6}$$

and the corresponding coefficient of cross-wind force is

$$C_{\Sigma 1} = -C_L \frac{\tau^2}{\alpha - \alpha_0} \gamma \tag{3.7}$$

There is in addition a further lateral force connected with the flow around the boundaries of the wing. The difference of pressure between the upper and lower sides of the wing produces a flow around the side boundaries which prolongs itself behind the wing as the well-known field of trailing vortices (see III **1** and Division E III). If the distribution of lift is elliptic, *i. e.* $\Gamma = \Gamma_0 \sqrt{1 - (y/b)^2}$ [see III (2.1)] the decrease in circulation near the boundary of the wing $[(b - y) << b]$ is

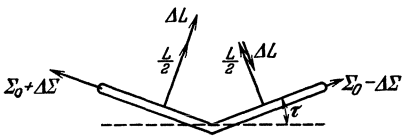

Fig. 95. Forces on a wing with dihedral.

$$\frac{\partial \Gamma}{\partial y} = \frac{-\Gamma_0}{b \sqrt{2 (b - y)/b}}$$

The circulation of the vortices between y and $y + dy$ in the vortex band behind the wing is $(\partial \Gamma / \partial y)\, dy$. When the flow associated with this vortex band occurs around a rigid body instead of around a free vortex band, the vortex distribution produces a suctional force at the edge of the surface, of amount per unit length[1]

$$z = \frac{\pi}{4} \varrho \frac{\Gamma_0^2}{2 b} \tag{3.8}$$

The lift of the wing is [see II (2.2)]

$$L = \frac{\pi}{2} \varrho V \Gamma_0 b \tag{3.9}$$

and hence

$$z = \frac{L^2}{2 \pi \varrho V^2 b^3} = \frac{L}{4} C_L \frac{S}{\pi b^3} \tag{3.10}$$

Flow around the boundaries of the wing develops only gradually. At first its amount is zero at the foremost point of the profile, but increases along the chord in proportion as the lift along the chord increases.

[1] If the band of vortices is free, this suction is not met by a resistance and produces the unfolding of the vortex band at the boundary. See KADEN, H., Aufwicklung einer unstabilen Unstetigkeitsfläche. Ing.-Arch. **2**, p. 140, 1931 (Division F IV **19** and **20**). This paper also contains a derivation of the magnitude of the suction which leads to (3.8) above.

And, in accordance with this, the suction at the boundary of the wing also increases from front to back, ultimately reaching at the rear edge the value determined by (3.8). Calculation of the total suction on the boundary therefore involves multiplication of z by a fraction of the chord length c. Usually, however, the lift distribution is not elliptic but rather fuller in form so that the consequent increase in the value of z as compared with (3.8) allows us to approximate to the total suction by writing $\Sigma_0 = z\,c$. Lifts on the two halves of the wing of amount $L/2 + \triangle L$ and $L/2 - \triangle L$ respectively, correspond then approximately to the decrease in lift of entire wings of lifts $L + 2\triangle L$ and $L - 2\triangle L$ respectively. Hence the suctions on the two boundaries are greater or less by amounts

$$\triangle \Sigma \approx \pm \frac{\partial \Sigma}{\partial L} 2 \triangle L \approx \pm \frac{L \cdot 2 \triangle L c}{\pi \varrho V^2 b^3} \tag{3.11}$$

The difference between the suctions therefore produces a resultant lateral force of magnitude

$$\Sigma_2 \approx \frac{2 L \triangle L}{\frac{1}{2} \pi \varrho V^2 b^2} \frac{c}{b} \tag{3.12}$$

directed toward the leading wing, *i. e.* in the positive direction. Substitution of the value of $\triangle L$ from (3.3) leads to the equations

$$\Sigma_2 \approx \frac{L^2}{\frac{1}{2} \pi \varrho V^2 b^2} \cdot \frac{c}{b} \cdot \frac{\tau}{\alpha - \alpha_0} \gamma \tag{3.13}$$

and

$$C_{\Sigma 2} = \frac{\Sigma_2}{\frac{1}{2} \varrho V^2 S} \approx \frac{C_L^2}{\pi} \frac{S}{b^2} \frac{c}{b} \frac{\tau}{\alpha - \alpha_0} \gamma \tag{3.14}$$

The total lateral force therefore satisfies the equation

$$\Sigma = \Sigma_1 + \Sigma_2 \approx L \left(\frac{C_L}{\pi} \frac{S}{b^2} \frac{c}{b} - \tau \right) \frac{\tau}{\alpha - \alpha_0} \gamma \tag{3.15}$$

and the coefficient of lateral force has the value

$$C_\Sigma = \frac{\Sigma}{\frac{1}{2} \varrho V^2 S} \approx C_L \left(\frac{C_L}{\pi} \frac{S}{b^2} \frac{c}{b} - \tau \right) \frac{\tau}{\alpha - \alpha_0} \gamma \tag{3.16}$$

The reader should notice that $C_{\Sigma 1}$ is proportional to $C_L \tau^2$ while $C_{\Sigma 2}$ is proportional to $C_L^2 \tau$. On account of the different effects of Σ_1 and Σ_2 this result is rather inexact, but as regards order of magnitude it agrees very well with the results of the experiments shown in Fig. 98. Similarly, it is possible to derive the value of a yawing moment from the direction of the component lifts but this moment is so strongly affected by other factors, especially by the change in profile drag, that the theoretical approximation is of small value.

4. Influence of Sweepback in Side-Slip. If the wings are arranged in sweepback form, the axes of the wings are inclined at an angle σ on each side of the direction normal to the plane of symmetry (see Fig. 96).

As pointed out in 2 the lift of a wing in oblique approach decreases approximately in proportion to the square of the cosine of the angle of obliquity. If the lift of each half of the wing is L' when isolated in a normal flow, then from 2 the corresponding lift in the sweepback formation will be $L' \cos^2 \sigma$. The lift of the combined wing formation is therefore $L_0 = 2 L' \cos^2 \sigma$. If such an arrangement is set obliquely at angle γ to the flow, the angle of yaw of the forward portion is decreased from σ to $\sigma - \gamma$ and that of the other correspondingly increased from σ to $\sigma + \gamma$. The lift on the forward half is then

$$L_1 = L' \cos^2 (\sigma - \gamma) = L' (\cos \sigma \cos \gamma + \sin \sigma \sin \gamma)^2$$
$$\approx L' (\cos^2 \sigma \cos^2 \gamma + 2 \sin \sigma \sin \gamma \cos \sigma \cos \gamma) \qquad (4.1)$$

and on the other

$$L_2 = L' \cos^2 (\sigma + \gamma) = L' (\cos \sigma \cos \gamma - \sin \sigma \sin \gamma)^2$$
$$\approx L' (\cos^2 \sigma \cos^2 \gamma - 2 \sin \sigma \sin \gamma \cos \sigma \cos \gamma) \qquad (4.2)$$

The total lift is therefore

$$L = L_1 + L_2 \approx 2 L' \cos^2 \sigma \cos^2 \gamma = L_0 \cos^2 \gamma \qquad (4.3)$$

and thus decreases as the square of the cosine of the angle of yaw, the same as for a straight wing.

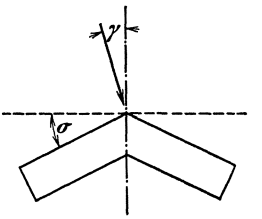

Fig. 96. Wing with sweepback.

Of more importance than the change in total lift is the difference of lift on the two portions of the wing, of amount $\pm 2 L' \sin \sigma \sin \gamma \cos \sigma \cos \gamma$, which produces a moment about the longitudinal axis in the sense tending to raise the leading wing (the left in Fig. 96). The value of this moment, on the assumption of rectangular lift distribution on each wing portion is given by the formula

$$M_q = 2 L' b \sin \sigma \sin \gamma \cos \sigma \cos \gamma = Lb \tan \sigma \tan \gamma \qquad (4.4)$$

and the moment coefficient by the formula

$$C_{Mq} = \frac{M_q}{(1/2) \varrho V^2 S c} = C_L \frac{b}{c} \tan \sigma \tan \gamma \qquad (4.5)$$

Experimental results (Fig. 102) are of the same order of magnitude but other factors (disturbances at the ends of the wings, for example) apparently produce comparable or even greater effects so that agreement with (4.5) is not as good as for the corresponding formula for a wing with dihedral.

Elementary arguments similar to those used in discussing the wing with dihedral show the existence of a lateral force and a moment about the vertical axis, but other influences are so powerful that the formulas obtained are of little practical use.

The chief purpose in using dihedral or sweepback is to produce a moment about the longitudinal axis in side-slip. Though this can be

achieved by either form, the effects so obtained differ somewhat. It must be observed in the first place, that with dihedral the moment is independent of the angle of incidence or lift, since $L/(\alpha - \alpha_0)$ is approximately constant. This is not so in the sweepback formation where the moment is proportional to the lift. With dihedral, moreover, a lateral force is produced opposing the side-slip, while the corresponding force with sweepback is smaller in magnitude or may even act in the opposing direction. During side-slip the effect of the fin is to give the airplane a yawing moment tending to turn it into the direction of motion. If the airplane hangs laterally, the side-slip with dihedral is restricted by the action of the cross-wind force and does not produce a serious yawing moment. On the other hand if use is made of sweepback, the side-slip and yawing moment are larger. There are different circumstances for which one or the other of these properties may be regarded as the more desirable (see **19**). With dihedral the moment is obtained by changing the angles of incidence of the two component wings. In the condition where the lift is near its maximum, the leading wing with dihedral may easily pass beyond this condition, with the result that the moment about the longitudinal axis suddenly decreases sharply, and in certain cases may even become negative. Consequently the forward wing tends to dip, the side-slip increases, and with such a state of affairs occurring near the ground, the result is usually a crash of the plane. With the sweepback formation, on the other hand, the moment is obtained by changing the velocity components, the values of which are the predominating factors determining the lift. This increases the lift of the forward wing, without introducing the danger of premature separation.

The effects of dihedral and sweepback are shown[1] in Figs. 98 to 106. The measurements in these diagrams refer to a rectangular wing at constant angle of incidence, having 100 cm. span, 20 cm. chord and profile G. 387. In considering the sweepback form it must be remembered that the component wings are not actually obtained by rotation of a normal wing as assumed in the theoretical discussion, but by a parallel translation of the separate profiles. The initial profile in these models is obtained by taking a section parallel to the plane of symmetry and not by a section perpendicular to the leading edge. Figs. 97, 100 and 103 respectively show the lateral force, the rolling moment and the yawing moment for a simple rectangular wing with various angles of yaw. Figs. 98, 101 and 104 show the effect of dihedral and Figs. 99—102 and 105 that of sweepback on these forces and moments. In addition to these factors, the effect of an aileron deflection of amount β is represented by thin lines (see **17**).

[1] BLENK, H., Göttinger Sechskomponentenmessungen an Flügeln mit V-Form, Pfeilform und Verwindung. Jahrbuch der Deutschen Versuchsanstalt für Luftfahrt, 1929, p. 183; or Luftfahrtforschung, Vol. 3, p. 27, 1929.

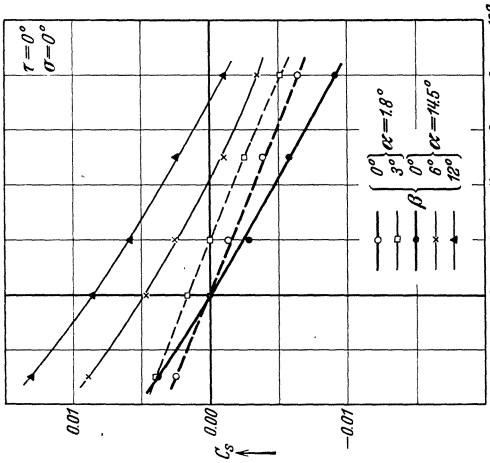

Fig. 97.

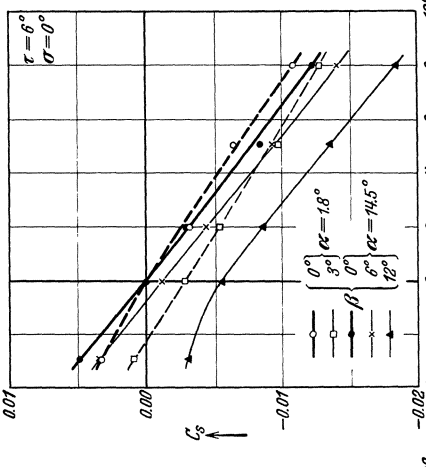

Fig. 98.

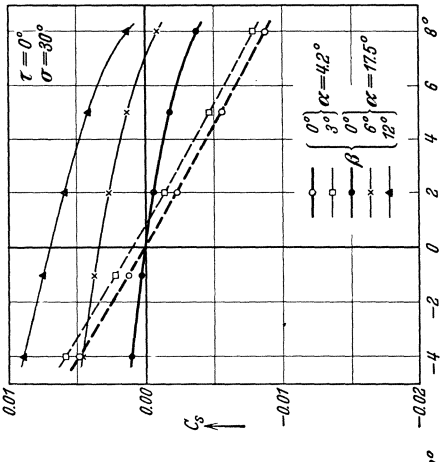

Fig. 99.

Figs. 97, 98 and 99. Relation between coefficient of lateral force and angle of yaw for various dihedral and sweepback forms.

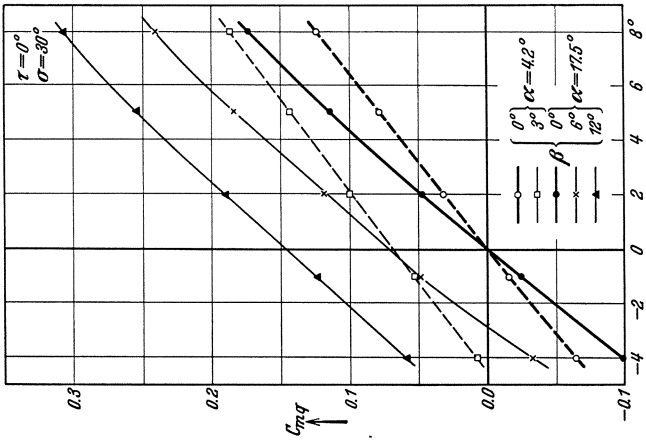

Fig. 102.

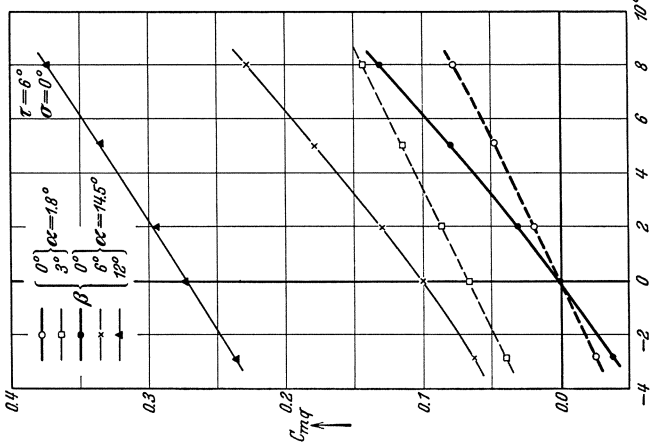

Fig. 101.

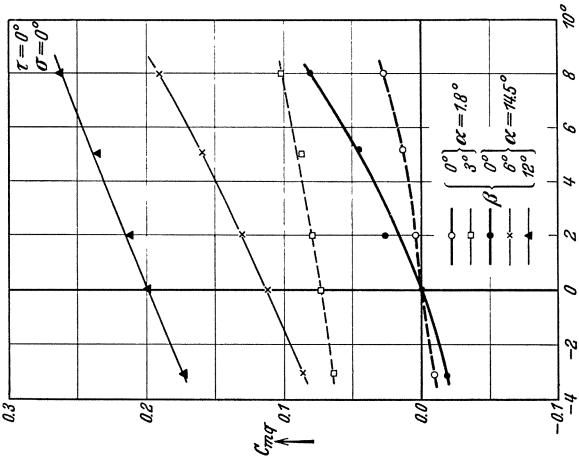

Fig. 100.

Figs. 100, 101 and 102. Relation between coefficient of rolling moment and angle of yaw for various dihedral and sweepback forms.

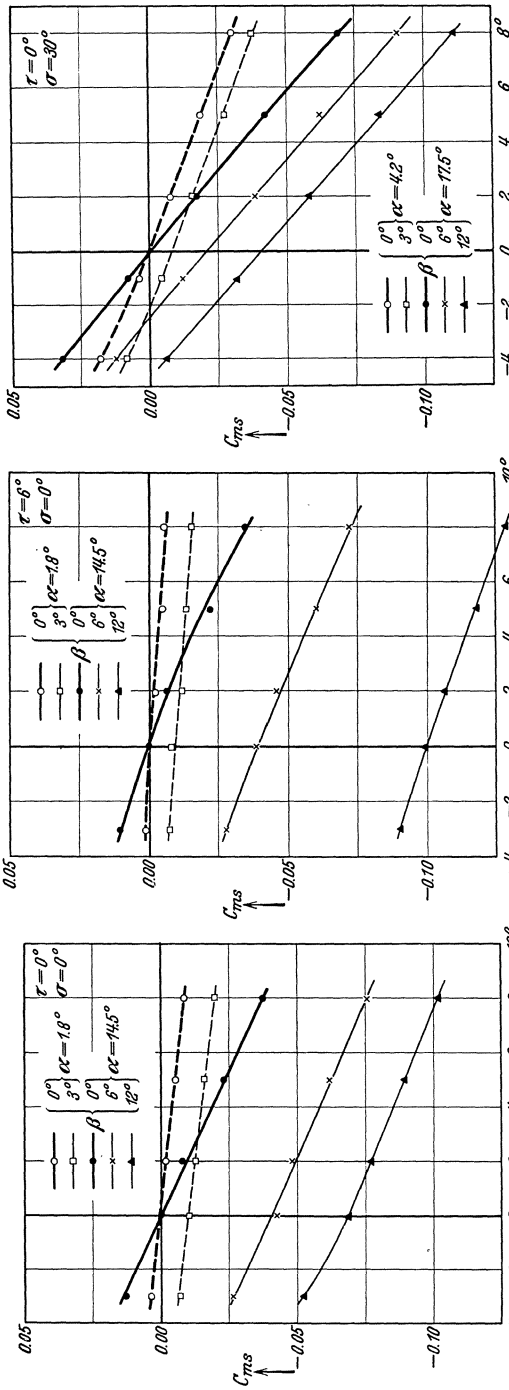

Fig. 105.

Fig. 104.

Fig. 103.

Figs. 103, 104 and 105. Relation between coefficient of yawing moment and angle of yaw for various dihedral and sweepback forms.

5. Effect of Side-Slip on an Airplane[1]. In addition to the effects of side-slip on the wings as discussed in 2, 3 and 4 above, there are, in a complete airplane, further effects produced on the fuselage, including the landing gear and other projecting parts, and especially on the vertical tail surfaces. The rolling moment is somewhat influenced by the position of the tail-plane and the landing gear or floats, though this effect, due chiefly to the relatively small moment arms of the forces acting on these parts, is not very considerable when compared with the moment due to the forces on the wings. The non-lifting system however, has a very considerable effect upon the lateral force and the yawing moment.

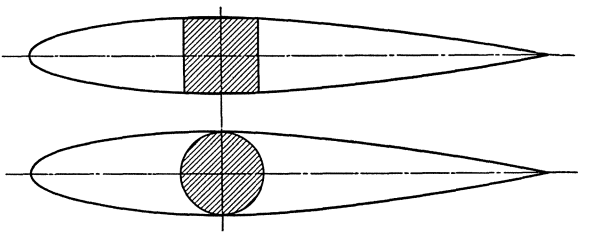

Fig. 106. Stream-line bodies with round and square sections.

The magnitude of the cross-wind force acting on the fuselage is very powerfully affected by the form of its cross-section. In Fig. 107 are shown the lift coefficients and drag coefficients of two stream-lined bodies shown in Fig. 106[2]. The distribution of the cross-sectional area along the axis is the same for both bodies. One body (an airship model) has however, a round cross-section while the other has a square cross-section. The latter body was rotated out of the wind direction, once about an axis parallel to a side of the square and once about an axis parallel to the diagonal of the square. In both cases considerably larger forces were found to act upon the angular body than upon the round one.

It is known that when an airship without stabilizing fins is subject to an oblique flow, the transverse force produced acts through a point well toward the front of the body of the airship. This produces a powerful moment tending to increase the angle between the airship axis and the direction of approach and hence to produce instability. A similar state of affairs develops in sharply rounded airplane bodies. The lateral force generally acts in front of the center of gravity and must be balanced by a sufficiently large side fin. Increasing angularity of the fuselage

[1] MATHIAS, G., Die Seitenstabilität des ungesteuerten Normalfluges und ihre technischen Vorbedingungen. 272. Bericht der Deutschen Versuchsanstalt für Luftfahrt. Zeitschr. f. Flugtechnik u. Motorl. **23**, p. 193 and 224, 1932.

[2] Ergebnisse der Aerodynamischen Versuchsanstalt zu Göttingen, Vol. II, p. 68 (Oldenbourg, Munich, 1923).

shifts the point of application of the lateral force toward the back of the airplane. This is especially the case for fuselages which transform aft into a nearly vertical face which itself acts as a fin, thus shifting the point of application of the lateral force very considerably toward the tail.

The object of the designer is, in general, to ensure that the resultant lateral force acting upon the whole airplane in side-slip shall have its point of application aft of the center of gravity. In such case, during side-slip, the airplane experiences a yawing moment which tends to turn

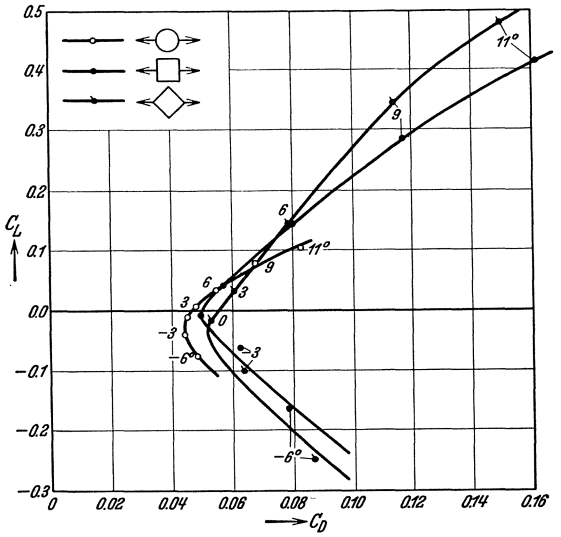

Fig. 107. Coefficients of lift and drag for the streamlined bodies of Fig. 106.

it like a weather-cock into the wind. Such an airplane is said to be statically stable with regard to its vertical axis; such stability is also known as "weather-cock stability". While an airplane possessing this kind of stability eliminates side-slip automatically, in so doing it changes its direction. Directional stability of such a kind that the airplane tends to remain in its course, cannot be obtained by purely aerodynamic measures; for since none of the various courses possible has a critical relation with respect to the directions of airflow which may arise, an alteration of course cannot induce a correcting effect. Directional stability can therefore only be achieved by special apparatus controlled by the compass (in particular by a gyroscopic compass). Nevertheless aerodynamic measures may have a powerful effect on the tendency of the airplane to deviate from its course (see **15** and **19**).

As a result of side-slip, a rolling moment is generally produced (see **2** to **4**) which inclines the airplane in such fashion that the side-slip decreases under the combined action of lift and gravity. As the result

of weather-cock stability, however, side-slip produces a yawing moment and that in turn a rolling moment in the opposite sense (see **15**). On this account, weather-cock stability must not be too greatly increased. Other properties of the airplane which influence this state of affairs are discussed in **19** below.

B. Phenomena Associated with Rotations of the Wing.

6. Preliminary Survey. If the motion of a wing consists of a rotation about the center of gravity as well as motion of the center of gravity itself, the change in the direction of the forces acting on the wing produced by such rotation will, in general, alter the course, and the center of gravity will describe a curved path. Typical examples of such motion are the change in the climbing angle produced by manipulating the elevator (especially in flattening out from a dive) and alterations in course produced by moving the rudder. The effect of displacing an aileron is first to roll the airplane, but the turn and the consequent asymmetry of the gravitational forces produces a side-slip with resultant yawing and a curved path of flight. If the roll is very rapid, these secondary effects are small and the center of gravity of the airplane describes a spiral path differing but little from a straight line. The same is true to an even greater extent when the mean path of the airplane is vertical (vertical dive or spin) for the effect of gravity in altering the direction of motion is eliminated in such cases. Motions of this sort, in which the center of gravity describes an approximately straight line while the airplane simultaneously executes a rotation about this line can be imitated with comparative success in wind tunnels. The model is fixed to an axis parallel to the wind direction and is made to rotate about this axis in the wind stream. If the axis of rotation passes through the center of gravity no asymmetry arises, either from centrifugal effects or moments due to gravity, thus disturbing the smooth rotation about the axis. In general, however, the axis of rotation will not coincide with a principal axis of inertia of the model, so that the motion will produce centrifugal moments about an axis perpendicular to the wind direction which will not only disturb the smoothness of the motion, but will interfere with measurements of the moments about this axis. It is therefore necessary to counterpoise the model so that as far as possible the axis of rotation may coincide with a principal axis of inertia in order to eliminate centrifugal moments. Clearly, the addition of counterpoises may also be used to shift the center of gravity, thus making possible the study of motions about axes which do not pass through the original center of gravity. The application of such a procedure is limited by the fact that the space available is usually comparatively small; often it is not even possible to balance the centrifugal moments completely.

In view of the fact that the axis of rotation is fixed in position, no attempt is usually made to measure the three force components, attention being restricted to the most interesting features of the situation, *viz.*, the moments about the three axes. The moment about the axis of rotation itself is the one that can be measured most easily. The question as to whether rotation tends to fade out or initiates of itself in the wind stream (autorotation) is of extreme importance; the answer is closely connected with the tendency of the plane to go into a spin.

It is scarcely possible to reproduce in wind tunnels the type of motion noted at the beginning of the section, *viz.*, that in which the center of gravity of the plane describes a curved path; for in such case it would be necessary to cause the center of gravity to execute an accelerated motion. So far, the method usually followed[1] has consisted in causing the model airplane in the wind tunnel to oscillate about the vertical or the lateral axis, and to then measure the resulting moments about the various axes. Such a procedure yields information as to the effect of the rotation but ignores that due to the acceleration of the center of gravity. Another difficulty also, lies in the fact that the angular velocity of the rotation itself is not constant.

If the curvature of the path and the rotation of the airplane combine to produce a steady motion (see **1**) it is possible to investigate the associated phenomena with the help of a "whirling table" (see **15**).

7. Pitching Moment Due to Pitching. A rotation of the airplane about the lateral axis involves a change in the angle of incidence and the higher maximum lift which can thereby be obtained has been noted in I **3**. Since a rotation of this kind is a motion in the plane of symmetry, the only moment which can arise is the pitching moment, the component forces of which lie in this plane. The yawing and rolling moments are naturally unaffected by this motion. The pitching moment due to the wing alone is small compared with that due to the horizontal tail surfaces. This follows from the length of the chord and the relatively short lever arm of the forces arising from the wing. If the airplane rotates about its center of gravity in such manner as to increase the angle of incidence α, then $\dot{\alpha}$ $[= (d\alpha/dt)]$ is positive and the center of pressure of the horizontal tail surfaces moves with velocity $l\dot{\alpha}$ downward. Here l is the distance of the center of pressure of the tail-plane from the center of gravity of the airplane (Fig. 108). The consequence of this additional downward velocity with a flight velocity V is to increase the relative angle of incidence by

$$\triangle \alpha = \frac{l\dot{\alpha}}{V} \tag{7.1}$$

Consequent on this change in the angle of incidence follows a change in the magnitude of the forces on the tail-plane. Since this change is

[1] Br. A.R.C. R. and M. 78, 1912/13; 787, 1921/22; 809, 1921/22; 848, 1922/23.

produced not by rotating the tail-plane but by rotating the direction of air approach, the lift and drag alter their directions as well as their magnitudes, for the lift and drag must be calculated in directions perpendicular and parallel to the approaching air flow. These changes are illustrated in Fig. 108. The lift changes from L to L', the drag from D to D' and the moment about the center of gravity involves consideration of the force components perpendicular to the distance l. The contribution to the lift is $\triangle L = L' - L$ and the rotation of its direction ($\triangle \alpha$, which may be assumed to be small) has a negligible effect. The change in the drag, on the other hand, is negligible while its rotation provides an effective contribution $\triangle \alpha$. Altogether, the total additional force so obtained, the direction of which is upward, is given by the equation

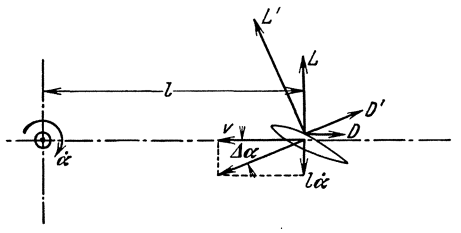

Fig. 108. Velocities and forces on the horizontal tail surfaces during pitching motion.

$$\triangle P = \triangle L + D \triangle \alpha \quad (7.2)$$

If S is the area of the horizontal tail surfaces, C_D the coefficient of drag of these surfaces, and $dC_L/d\alpha$ the rate of increase of the coefficient of lift with respect to the angle of incidence, the following relation is obtained:

$$\triangle P = \frac{1}{2} \varrho S V^2 \left(\frac{dC_L}{d\alpha} + C_D \right) \triangle \alpha \quad (7.3)$$

The force $\triangle P$ exerts a moment about the center of gravity measured by

$$M = l \triangle P = \frac{1}{2} \varrho S V \left(\frac{dC_L}{d\alpha} + C_D \right) l^2 \dot{\alpha} \quad (7.4)$$

The sense of this moment is opposed to the rotation so that a damping effect is produced. If, however, the flow separates from the tail, so that $(dC_L/d\alpha + C_D)$ is negative, a moment arises, the sense of which is the same as that of the rotation, tending therefore to augment the latter. Regard for the reliability of the elevator and stabilizer will however be reason for keeping them sufficiently far from the critical angles of incidence for which separation occurs; for the same reason types of tail-planes are preferred for which $dC_L/d\alpha$ remains positive or only slightly negative even after separation. Hence the above mentioned possibility of unstable pitching is seldom of practical significance.

The above considerations, however, imply rotation about the center of gravity while it is moving in a straight line. The lift on the main wing of an airplane in flight is considerably increased by an increased angle of incidence and the center of gravity is accelerated upward in consequence. It follows that, in addition to the rotation, an associated lateral

motion of the center of gravity is produced, which in turn involves changes of relative angle of incidence and hence of force[1]. The coupling of these two motions may produce undamped oscillations. A theoretical explanation of these phenomena was first given by C. Runge[2]. Another cause of undamped oscillations may be due to the fact that the horizontal tail surfaces, or the elevator, may not be attached with sufficient rigidity to the main structure. An increase of the oscillations may also arise as a result of a coupling between the elastic oscillation of the tail-plane and the rotational oscillations of the airplane. These dynamic phenomena are discussed in Division N.

Some notion of the order of magnitude of the damping moments which arise in such cases may be obtained by reference to an experiment performed in England some years ago with a model Bleriot monoplane[3]. The model was arranged to permit of rotation about a transverse axis through its center of gravity. It was caused, in a wind stream, to perform oscillations about its equilibrium position and the magnitude of the damping moments could then be deduced from the rate of decrease of the amplitude.

8. Rolling Moment Due to Rolling, and Autorotation. If in addition to its normal forward motion, a wing rolls about the longitudinal axis of the airplane, each end of the wing will have an additional velocity, one up and the other down. At one end, therefore, the angle of incidence of the profile relative to its direction of motion will be diminished, at the other, increased. With such changes of angle are associated changes of the impressed forces at the ends of the wings. These changes are, in general, of opposite sign, and hence a rolling moment may either increase or, as more usually, damp the rotation. The relations of the various aerodynamic quantities over a cross-section of the wing are quite similar to those arising on the horizontal tail surfaces, as discussed in the last section. The relative velocity V of the rectilinear flight is supplemented by a vertical velocity due to the rotation. This is of amount

$$w = y\,\omega_x \tag{8.1}$$

where ω_x denotes the angular velocity of the rotation, and y the distance of the profile from the plane of symmetry. The sign chosen for w is such that it is positive for a descending wing. A result of this supplementary velocity is to change the angle of incidence of the air flow upon the

[1] See the theoretical and experimental investigations of F. W. Lancester in "Aerodonetics", London, Archibald Constable and Co., 1908.

[2] Runge, C., Über die Längsschwingungen der Flugmaschinen. Zeitschr. f. Flugtechnik u. Motorl. **2**, pp. 193 and 201, 1911.

[3] Bairstow, L., and MacLachlan, L. A., The Experimental Determination of Rotary Coefficients. National Physical Laboratory, R. and M. 78, 1913.

profile. If the original angle of incidence is α then the rotation increases it[1] to α' where $\alpha' = \alpha + \triangle\alpha$

Here
$$\triangle\alpha = \frac{w}{V} = \frac{y\,\omega_x}{V} \tag{8.2}$$

If the wing is assumed to be attached to an axis of rotation fixed in the direction of the wind, as is the case in experiments on autorotation, the forces determining the couple about this axis are the components perpendicular to the axis. The change in the value of this moment, due to the changed direction of flow, is obtained in a fashion similar to that already used in discussing the pitching moment due to pitching. The change of force[1] on a portion of a wing of chord c taken between the distances y and $y + dy$ from the plane of symmetry is of amount

$$dP = \frac{1}{2}\varrho V^2 \left(\frac{dC_L}{d\alpha} + C_D\right) \triangle\alpha\, c\, dy \tag{8.3}$$

The rolling moment is deduced by multiplying by the arm y and integrating over the span. On substituting from (8.2) for the value of $\triangle\alpha$ we find that

$$M_q = \frac{1}{2}\varrho V \omega_x \int_{-b}^{b} \left(\frac{dC_L}{d\alpha} + C_D\right) y^2 c\, dy \tag{8.4}$$

In the normal working state the lift increases with the angle of incidence and $dC_L/d\alpha$ is positive. Since C_D is always positive the quantity $(dC_L/d\alpha + C_D)$ which is a measure of the autorotation, is also positive. The induced angular moment is therefore opposed to the rotation, and damps it.

If, however, the angle of incidence is increased to such an extent that the lift maximum of the wing profile is passed (stalled flight), the lift decreases with increasing angle of incidence and $dC_L/d\alpha$ is negative. If this is the case, the quantity $dC_L/d\alpha + C_D$ may become negative. The upward forces are then smaller on a descending wing than upon one which is ascending; the resulting moment increases the rotation and a wing arranged so as to permit rotation about an axis parallel to the direction of the wind, spins around like a windmill and gives an example of autorotation.

In contrast to the corresponding state of affairs in pitching, the conditions leading to an increase in the rolling motion after the position of maximum lift has been passed, are often satisfied. On account of other flight properties, most profiles are designed to have small drag and high $C_{L\,max}$; but with most profile forms the lift falls off rapidly after the critical angle of incidence has been passed.

[1] On account of the diminution of lift at the ends of the wing, the change of inclination $\triangle\alpha$ does not produce the same effect at the ends as on those parts lying nearer the middle. Hence $dC_L/d\alpha$ falls off toward the ends in much the same way as the lift on an untwisted wing.

The quantity $d\,C_L/d\,\alpha + C_D$ can be replaced by either of two good approximations, *viz.* $d\,C_n/d\,\alpha$, the rate of change of the coefficient of normal force[1] (force normal to the wing chord) with respect to angle of incidence or $d\,C_R/d\,\alpha$, the rate of change of the coefficient of the resultant force[2], either of which is a good alternative criterion of the tendency to autorotation. If these quantities are positive, damping occurs; if negative, an increase of the rotation is to be expeted.

M. Knight[3] has investigated the tendency of various wings to autorotation with reference to the shape of their polars and has compared his results with the results of experiments on rotation. He marks two regions of the angle of incidence in the polar diagram; one in which $d\,C_R/d\,\alpha$ is positive, and one in which experiments on autorotation show the wing to be unstable (*i.e.* where arbitrarily small initial rotations are sufficient to induce autorotation). In most cases, these two regions coincide with fair accuracy. In conducting experiments on autorotation several possible states of affairs require consideration; the preceding paragraphs with Knight's experiments deal with the question of deciding whether a wing or an airplane has a tendency to change from rectilinear flight to autorotation or spin. Knight has called the state of affairs in which such a tendency exists, "rotary instability". After autorotation has set in, the angular velocity at first increases until it reaches some limiting angular velocity; the condition of steady rotation thus reached, he terms, "stable autorotation". It may also occur that while the airplane shows no tendency to increase small angular velocities, which therefore die away spontaneously, forced angular velocities greater than a certain definite value may possibly increase of their own accord up to a certain equilibrium value. The limiting state of affairs in which this instability is first shown he terms "unstable autorotation".

9. Stalled Flight and Normal Spin. We have seen in the preceding section that a wing in stalled flight, that is, when the maximum lift has been passed, is unstable with respect to motion about its longitudinal axis. It inclines very easily to one side or the other. This state of affairs often occurs when an airplane takes off too suddenly. A side-slip ending in a crash nearly always results. If the airplane is stalled at a greater height, the side-slip develops into a vertical downward motion with the machine turning more and more about its longitudinal axis (normal spin). Unstable rotation may even occur when the angle of incidence is near the value corresponding to the position of maximum lift but has

[1] FUCHS, R., and SCHMIDT, W., Luftkräfte und Luftkraftmomente bei großen Anstellwinkeln und ihre Abhängigkeit von der Tragwerksgestalt. Zeitschr. f. Flugtechnik u. Motorl. **21**, p. 1, 1930.

[2] KNIGHT, M., Wind Tunnel Tests on Autorotation and the "Flat Spin". U.S. N.A.C.A. Report No. 273, 1927.

[3] KNIGHT, M., *loc. cit.*

not yet passed it; for in such a situation, there is required only the action of a sufficiently powerful impulse, as for example by the movement of an aileron causing an increase in the angle of incidence of the descending wing to the point of flow separation (see 8, "unstable autorotation").

In addition to the phenomena described in the above discussion on autorotation, it usually happens that the center of gravity itself describes a spiral path while the wing rotates about it, so that the axis of rotation does not pass through the center of gravity. More important than this eccentric position of the axis of rotation is the fact that the direction of motion of the center of gravity does not usually lie in the plane of symmetry so that in the motion one end of the wing is usually ahead of the other. A side-slip is thus superimposed upon the rotary movement, and provides an additional moment which may increase both the domain and the intensity of the unstable rotary motion. This has been shown, *inter alia* by M. Knight and J. C. Wenzinger[1].

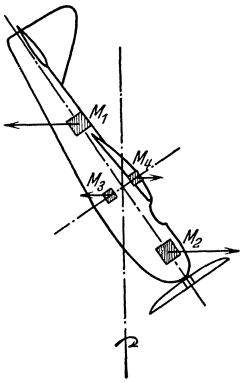

Fig. 109. Illustration of the distribution of weight on an airplane.

One way of opposing unstable rotation is by the use of the ailerons. This however, is limited by the condition that the aileron in the region of flow separation has no flow along the upper side and its effect is, in consequence, so seriously impaired that it becomes practically useless for the required purpose. To a certain point this difficulty may be overcome by slotting the aileron, fitting it with auxiliary flaps or by similar measures (see III 6 and 13).

A second method for emerging from a normal spin is to diminish the angle of incidence by means of the horizontal tail surfaces. (This is done by pushing the stick forward.) This again is opposed by centrifugal moments which arise in the course of rotation and tend to increase the angle of incidence. In Fig. 109 the distribution of mass is represented schematically by the four masses M_1, M_2, M_3 and M_4. The two masses M_1 and M_2 are large and at some appreciable distance, so as to correspond to the considerable elongation of the fuselage along the longitudinal axis; M_3 and M_4 on the other hand are relatively small and close together. If the principal axis of inertia does not coincide with the axis of rotation, the masses are eccentrically situated with regard to the latter axis and provide centrifugal forces in the directions shown by the arrows. As shown in the diagram, the effect of the masses M_1 and M_2 is to increase the angle of incidence. The

[1] KNIGHT, M., and WENZINGER, J. C., Rolling Moments Due to Rolling and Yaw for Four Wing Models in Rotation. U.S. N.A.C.A. Report No. 379, 1931.

moment of the forces due to the remaining masses M_3 and M_4, though opposite in sense, is of subordinate influence on account of the comparative smallness both of the forces involved and of their lever arms. The moment of the inertia forces increases as the square of the angular velocity. It may therefore happen that the airplane obeys the elevator as long as the rotation is small, but can no longer be controlled when the angular velocity has reached a certain value.

The tendency of an airplane to spin can be affected in three ways: 1) by distribution of the masses, 2) by the characteristics of the wing and 3) by the characteristics of the control system.

As regards the first of these, the aim should be to keep the difference between the moments of inertia about the vertical and longitudinal axes as small as possible, that is, to keep the masses M_1 and M_2 (Fig. 109) as close together, and the masses M_3 and M_4 as far apart as possible. It should also be added that the tendency of an airplane to spin decreases as the center of gravity is moved forward. As regards the control system, the end to be sought is that both elevator and aileron should be as effective as possible. For their properties reference may be made to III 14 and IV 18. The properties of the wing which are concerned in the question of stability are discussed in detail in 11 and 12 below.

10. Flat Spin. Flat spin is distinguished from the normal spin discussed in the preceding section by the fact that it occurs at much larger angles of incidence and for angular velocities which are much greater in comparison with the velocity of flight. It is not so easy to reproduce flat spin by autorotation experiments in wind tunnels. The large angular velocity and large centrifugal forces produced in consequence make considerable demands upon the rigidity of the model, demands which are increased by the fact that a high angular velocity must first be induced by an initial impulse in order to secure continuous rotation (unstable autorotation, see 8). Hence the available information concerning flat spin is not as reliable as that on normal spin. Essentially however, it should be possible to trace flat spin to the same causes as those operative in the following experiments described by Lanchester[1], Riabouchinsky[2] and others.

A bar, plane on one side and curved on the other, is arranged so as to be able to rotate about an axis perpendicular to its flat side (Fig. 110). If a current of air is directed parallel to the axis of rotation toward the bar on its flat side, the system is symmetrical and there is no reason why the bar should rotate. If however, it is given a small initial rotation in either sense it continues to turn in this direction as a windmill; that

[1] LANCHESTER, F. W., Aerodynamics, p. 44. London, Constable, 1907.

[2] RIABOUCHINSKY, D., Recherches sur la rotation des plaques symmetriques dans un courant aérien et sur la détermination de la pression qu'elles supportent. Bulletin de l'Institut l'Aérodynamique de Koutchino, Fasc. I, p. 18, Moscow, 1912.

is, it develops autorotation. The explanation is as follows (see Fig. 111): Let the velocity of approach along the axis be u. If one end of the bar is moving with velocity v then it is, effectively, in a flow which has one velocity component u and another component $-v$ at right angles to it. If v is sufficiently large in comparison with u the direction of the resultant velocity of approach V makes a small angle with the plane side of the profile. With regard to this velocity the profile acts like a wing profile. The ensuing lift L is perpendicular to the velocity of approach V and if the drag D is small enough the resulting impressed force R is such that there is a component in the direction of motion of the profile and the velocity increases.

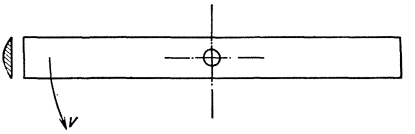

Fig. 110. Rod capable of executing auto-rotation.

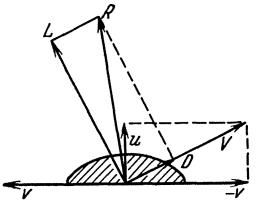

Fig. 111. Velocities and forces on the profile of a rod in auto-rotation.

In unstaggered biplanes, or biplanes with negative stagger, a very powerful tendency to flat spin is produced by the fact that at large angles of incidence the upper wing is screened by the lower. An airplane of this kind, rotating about an axis which coincides with the direction of motion, is so situated that the descending end of a wing has a much larger relative angle of incidence than the ascending end so that the descending side of the upper wing may enter the wake of the lower wing. If this occurs, the air forces on this side are considerably diminished and the rotation is accelerated. As in the case of normal spin, supplementary side-slip may increase the moments which arise; the centrifugal moments act in the same sense in either case (see Fig. 109 where the angle between the direction of motion and the principal axis of inertia is now considerably increased). Centrifugal moments, in fact, hinder attempts to restore the normal angle of incidence by the use of the elevator. An essential aid in fighting flat spin is provided by the vertical tail structure which can be used to diminish the angular velocity of the airplane. Screening of the vertical tail surfaces by the stabilizer structure may, however, adversely affect the efficiency of such measures (see III 13). The same is true if the vertical tail structure enters the "dead water" wake of a wing with separation of flow.

11. Influence of Wing Profile on the Tendency to Autorotation. Since autorotation arises from the decrease of lift consequent upon separation, it is obviously possible to reduce a tendency toward autorotation and spin by a choice of profiles for which this decrease is

as moderate as possible. In thin symmetrical or nearly symmetrical profiles, the values of the quantities $d\,C_L/d\,\alpha + C_D$ (or $d\,C_n/d\,\alpha$ or $d\,C_R/d\,\alpha$ respectively) which are the criteria for autorotation, are mostly positive, so that the danger of autorotation in such profiles is small or non-existent. Such profiles, however, have unfortunately the disadvantage that the maximum lift is small and they are associated with comparatively large drag. This disadvantage can be somewhat ameliorated by employing normal curved profiles in the middle of the wing and flat profiles only near the ends; for the forces near the middle of the wing have a smaller lever arm and play a smaller part in affecting the tendency to autorotation.

According to a proposal made by W. Schmidt[1], perforated profiles arranged at the extreme ends of the wing as in Fig. 112 are especially suitable for producing freedom from autorotation.

Fig. 112. Wing with perforated profile.

A sharp fall in the lift can be avoided in biplanes by setting the two wings so that they both do not reach their positions of maximum lift simultaneously. The fall in lift of one wing after the maximum is reached is then balanced by increase of the other wing where separation has as yet not occurred. By the time that the latter arrives and passes its position of maximum lift the first wing is in a region where the fall in lift is more gradual or where a further increase in lift may occur.

Another means of hindering a tendency to autorotation is to use the devices for increasing the maximum lift as described in I 4. Use of the slotted wing for example prevents separation until much larger angles of incidence are reached. Slots at the ends of the wing automatically opening at large angles of incidence have been found especially effective for this purpose. The effect of such a slot is shown, for example, by English experiments on an R.A.F. 31 biplane[2]. When the slot is closed strong positive moments tending to increase rotation arise for angles of incidence greater than 15^0. If, however, the slot at the end of the wing is open, the moments remain negative, that is they tend to damp rotary motion, up to comparatively high angles of incidence (about 35^0).

Suction of the boundary layer provides also a specially simple method for diminishing a tendency to autorotation[3]. At the ends of the wing,

---

[1] Schmidt, W., Beitrag zur Entwicklung eines autorotationsfreien, steil landbaren Flugzeuges. Berlin, Dissertation, 1930.

[2] Irving, H. B., Batson, A. S., Meidens, A. L., Rolling and Side-Slip Experiments on a Model Slotted Biplane of R.A.F. 31 Section. Br. A.R.C. R. and M. 1240, 1929-30.

[3] Schrenk, O., Eine Möglichkeit zur Unterdrückung der Autorotation von Tragflächen. Zeitschr. f. Flugtechnik u. Motorl. **20**, p. 553, 1929.

slits in the upper side are arranged and prolonged so as to meet in the interior of the wing (Fig. 113). If the flow separates at one side of the wing there is a less powerful negative pressure at the slit on that side than at the other side; hence air flows through the slits and through their connecting passage in the wing's interior, air being sucked into the slit on the side where separation occurs. It follows that there is a tendency to pull back a separated boundary layer or at least to prevent a boundary layer from separating as early as it otherwise would. On the other side of the wing, air streams out from the slit, disturbing the flow and tending to produce separation or at least to diminish the lift. The slits therefore effectively equalize the conditions of the flow at the two ends by increasing the lower and decreasing the greater lift. On account of the decrease of pressure at the ends of the wing, flow occurs through each slit even in normal flight, air being drawn in at the outer end and expelled at the inner end. This produces an undesired increase in drag which can, however, be reduced by subdividing the slits and joining symmetrically situated portions by special channels (indicated by dotted lines, Fig. 113). Fig. 114 gives the results of autorotation experiments on a wing similar to that shown in Fig. 113, first without, and then with, slits. The figure displays the relation between the ratio of the circulating velocity in stable autorotation (v) to the wind velocity (u), as dependent variable, and the angle of incidence as independent variable. Where autorotation did not of itself develop (rotary instability) it was initiated by forced higher revolutions (unstable autorotation) and the tendency to autorotation investigated. From the figure it is clear that the effect of the slits was to restrict considerably both the velocity of rotation and the range of values of the angle of incidence for which

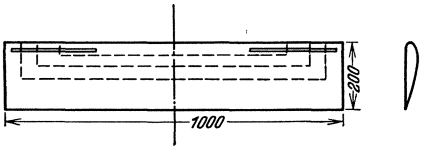

Fig. 113. Wing with slits for equalizing pressure.

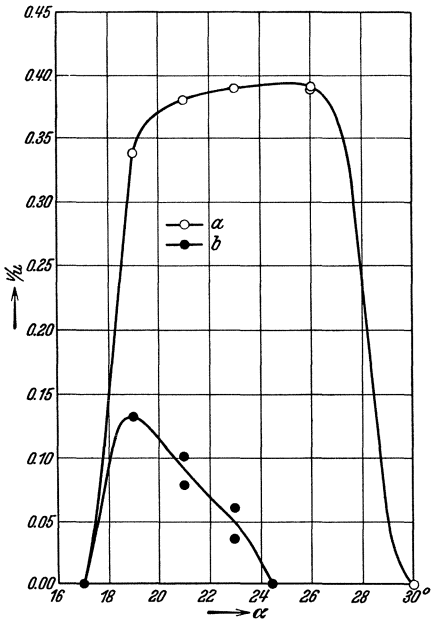

Fig. 114. Effect upon auto-rotation of slits for equalizing pressure: a) slits closed, b) slits open.

autorotation was possible. In the wing with slits, it was possible to balance the small residual unstable moments by movements of the aileron. In the wing without slits, this was not the case.

12. Influence of the Wing Contour on the Tendency to Autorotation. In addition to the effects due to shape of profile, the tendency of a wing to autorotation may be affected by the change of the profile along the span. It has already been mentioned in the preceding section that it is advisable to arrange for normal curved profiles at the middle of the wing and to change to thinner symmetrical profiles toward the ends. In the present section we shall consider, somewhat in general, the influence of this distribution of profile along the span, and in particular the influence of the form of the contour. As explained in 8, autorotation arises because the flow separates from the wing on one side so that the lift there decreases with increasing angle of incidence. The danger of this increases as the magnitude of the lift coefficient C_L at the ends of the wing becomes larger in comparison with the mean value for the wing as a whole. Conversely, the danger is diminished if the lift coefficients are smaller at the ends than in the middle. If we assume equal values of $C_{L\,max}$ for equal wing profiles, then in the latter of the two cases above noted, separation will first occur at the middle part of the wing and will, therefore, produce no considerable rolling moment. The effect of diminished lift, the horizontal tail surfaces remaining unchanged, is a tendency to reduce the angle of incidence, and the probability that this angle will increase sufficiently to produce separation at the ends is thereby very much reduced. Moreover, the strong concentration of lift over the two separated regions at the ends of the wings increases the magnitude of the induced downward velocities in these regions and thereby reduces the effective angle of incidence. The distribution of the lift coefficient is principally determined by the contour of the wing. For elliptic lift distribution and elliptic wing boundary, the chord is exactly proportional to the lift per unit length of span so that the lift coefficient is constant. If the contour of the wing is somewhat fuller than an ellipse and the angle of incidence is constant across the span, the fullness of the lift distribution curve will not increase as rapidly as that of the contour (see III 5 Figs. 59—61). The ratio of the chord to the lift per unit length increases therefore toward the ends of the wing, while the lift coefficient decreases in the same direction. For constant angle of incidence, the opposite is true if the fullness of the wing contour is less than that of an ellipse (trapezoidal form). The wing with fuller contour shows, therefore, less tendency to autorotation than one less full. In twisted wings the corresponding relationships are rather more difficult of analysis. It is possible to so arrange the twist of the wing that in spite of trapezoidal contour the coefficient of lift is smaller at the ends than

in the middle. The relationships involved and their influence on the induced drag have been investigated in detail by J. Hueber[1].

13. Influence of the General Arrangement of the Airplane Parts on the Tendency to Autorotation. The dominant factors influencing the tendency of an airplane to execute autorotation at usual angles of incidence are the wing profile and contour; these are therefore the dominant factors in determining a tendency toward normal spin. For excessive angles of incidence, corresponding to flat spin, the dominant factors are, on the other hand, the general arrangement of the wings and tail-plane structure. It has already been noted that screening of the upper wing by the lower wing of a biplane may produce a marked tendency toward flat spin. A further important factor is the damping of yaw by the fuselage and vertical tail surfaces. From the aerodynamic standpoint a large rudder and fin at a great distance from the center of gravity are advantageous in preventing flat spin. It should, however, be observed that increase in the area of the vertical tail surfaces will in general also increase the mass and the moment of inertia about the vertical axis, and this will increase the tendency to spin. Similarly, any lengthening of the fuselage intended to increase the distance of the tail-plane structure from the center of gravity involves a like unfavorable increase in the moment of inertia. Another important factor is the relative position of rudder, fin, stabilizer and elevator; for since with autorotation at large angles of incidence the tail unit is under oblique flow from beneath and from the side, the danger arises that the vertical tail surface may enter the wake of the elevator and stabilizer and thereby become ineffective. On this account it is advisable to have the rudder and fin project at least partially beneath the elevator and stabilizer and to see that the elevator is given a gap to permit of this arrangement.

14. Yawing Moment Due to Yawing. If an airplane is yawing as for example, during flight in a horizontal curve, the outer end of the wing has a larger velocity than the inner one. It follows that all impressed forces (lift and drag) are increased at the outer end, and decreased at the inner. The change in drag produces a moment opposed to the motion and therefore increases the difficulty of producing the desired turn at the same time damping undesired rotary movements. If in normal flight at speed V_0, the drag on a surface element $c\,dy$ of the wing at distance y from the plane of symmetry is denoted by $dD_0 = (\partial D_0/\partial y)\,dy$, its value for a different velocity V is approximately

$$dD = dD_0 \left(\frac{V}{V_0}\right)^2 \tag{14.1}$$

[1] HUEBER, J., Der verwundene Trapezflügel. Zeitschr. f. Flugtechnik u. Motorl. **24**, p. 307, 1933.

The change of drag is therefore given by the formula

$$d\,D - d\,D_0 = d\,D_0 \frac{V^2 - V_0^2}{V_0^2} \tag{14.2}$$

In calculating the yawing moment the change of drag must be multiplied by y, the distance of its line of action from the plane of symmetry. If further there is an angular velocity ω_z about the vertical axis, then

$$V = V_0 + y\,\omega_z \tag{14.3}$$

and the following expression is obtained for the yawing moment

$$M = \int_{-b}^{b} \frac{\partial D_0}{\partial y} \left[\left(1 + \frac{y\,\omega_z}{V_0} \right)^2 - 1 \right] y\,d\,y \tag{14.4}$$

For small angular velocities ($y\,\omega_z / V_0 << 1$) we have

$$M \approx \int_{-b}^{b} 2 \frac{\partial D}{\partial y} \frac{\omega_z}{V_0} y^2\,d\,y \tag{14.5}$$

If the total drag of the wing is therefore given we see that the moment increases according to the extent to which the drag is concentrated at the ends of the wing. The distribution of induced drag across the span (see III) is of special importance in this respect. It should, however, be noted that yawing changes the distribution of lift and hence also the vortices which are sent off, so that the effect of the various velocities considered above must be supplemented by the effect due to the variation of lift distribution. The latter produces a diminution of the yawing moment (see Wieselsberger's investigations mentioned in the following section).

In complete airplanes the rudder and fin assist the wing very considerably in hindering yawing motion. The effect is very similar to that of the elevator and stabilizer in pitching (see **7**).

15. Rolling Moment Due to Yawing. The rolling moment which arises in yawing is more important than the more or less pronounced damping moment which is brought into play. As mentioned in the preceding section the greater velocities of the outer end in a yawing turn have the result that all forces, including the lift, are increased at the outer, and decreased at the inner, end. These alterations of lift produce a rolling moment tending to raise the outer end. This property is connected with lateral instability, discussed in **19**. This rolling moment can be eliminated by ensuring angles of incidence for negative lift in the neighborhood of the ends. These parts of the wing are then subject to increased negative lift when the velocity increases and therefore produce a rolling moment in the opposite sense. On account of the larger leverage of forces at the ends of the wing a comparatively small negative lift is sufficient to compensate the moment due to the rest of the wing

so that the resulting lift is positive even when the rolling moment is completely balanced. Nevertheless this procedure decreases the lift-drag ratio very considerably and in general no attempt is made to do more than reduce the angles of incidence near the ends of the wing. The "Etrich-Taube" wing[1] designed after the seed of the *Zanonia* showed this feature very clearly. The splendid stability properties of this wing are well known. It had, however, to be abandoned with increased demands on the output of airplanes.

In determining the theoretical value of the rolling moment, an approximation can be obtained by using the lift distribution in rectilinear flight as a basis and assuming that the lift at any point during curvilinear flight is proportional to the square of the velocity at this point. If y is the distance of a point from the middle of the wing and $\Gamma(y)$ is the distribution of the circulation along the span in rectilinear flight, it follows that if the velocity of the middle of the wing is V_0 and the velocity of yawing is ω_z then the radius of curvature of the path in steady flight is R where $R = V_0/\omega_z$. Further, the velocity $V(y)$ at any point y is given by the equation

$$V(y) = V_0 + \omega_z y = V_0\left(1 + \frac{y}{R}\right) \tag{15.1}$$

and hence the lift on an element between y and $y + dy$ is given by the expression

$$\begin{aligned} dL = \varrho V_0 \Gamma(y)\left(1 + \frac{\omega_z y}{V_0}\right)^2 &\approx \varrho V_0 \Gamma(y)\left(1 + 2\frac{\omega_z y}{V_0}\right) \\ &= \varrho V_0 \Gamma(y)\left(1 + 2\frac{y}{R}\right) \end{aligned} \tag{15.2}$$

and the rolling moment is therefore of amount

$$M_q = \int_{-b}^{+b} y\, dL = 2\varrho\omega_z \int_{-b}^{b} y^2 \Gamma(y)\, dy = 2\varrho \frac{V_0}{R} \int_{-b}^{b} y^2 \Gamma(y)\, dy \tag{15.3}$$

In this expression $\varrho V_0 \int_{-b}^{b} y^2 \Gamma(y)\, dy$ is the moment of inertia of the lift distribution along the span.

The assumption on which the above is based, *viz.*, that the circulation is directly proportional to the velocity, and therefore that the lift varies as the square of the velocity, is not quite accurate, for as the circulation is changed it affects the inducing field of the vortices proceeding from the wing and this reacts upon the distribution of circulation. In consequence, the lift and circulation vary to a smaller extent than was assumed and hence the actual value

[1] ROZENDAAL, J., Die "Etrich-Taube". Zeitschr. f. Flugtechnik u. Motorl. **4**, pp. 103, 192, 258, 271, 1913; and **5**, pp. 39, 182, 204, 1914.

of the moment is smaller than as given by (15.3). In attempting to calculate the reaction of the variation of circulation upon the circulation distribution according to the usual methods of airfoil theory, it must be observed that the vortices leaving the wing travel, not in straight lines, but in paths curved to correspond to the airplane's path. Hence a more marked decrease in the effect on the circulation and also a smaller moment are produced in curved flight than in rectilinear flight. The theory of the relations involved has been developed by C. Wieselsberger[1] for a wing of elliptic outline with constant profile and angle of incidence; comparison with experimental results produced tolerable agreement. The decrease of moment was found to depend upon the aspect ratio of the wing. The calculated decrease for the wing used in Wieselsberger's experiments and having $S/(2\,b)^2 = 0.2\,(\pi/4)$ was 14-1/2 per cent while the actual observed diminution had an average value of 19 per cent.

16. Yawing Moment Due to Rolling. We have seen that if an airplane has a rotation about its longitudinal axis in addition to its principal motion, the relative angle of incidence is increased for the descending and decreased for the ascending wing. Such a change of angle of incidence produces a yawing moment in addition to the rolling moment. The former arises through the variation of profile drag with angle of incidence and on account of the fact that the oblique approaching flow changes the direction of the lift on the profile, producing a component in the direction of motion. Considerations similar to those previously used in determining the rolling moment due to rolling show that the yawing moment due to rolling is

$$M_R = \frac{1}{2}\varrho\, V\, \omega_x \int \left(\frac{d\,C_D}{d\,\alpha} - C_L\right) y^2\, c\, d\, y \tag{16.1}$$

If $(dC_D/d\,\alpha - C_L)$ is positive, the yawing moment tends to rotate the descending wing backward. For high values of the lift-drag ratio, generally $C_L > dC_D/d\,\alpha$ and hence the discriminant $(dC_D/d\,\alpha - C_L)$ is negative. It becomes positive almost without exception, however, for large angles of incidence in the neighborhood of the lift maximum. Hence the yawing moment due to rolling changes its sense when the angle of incidence has increased sufficiently. This expression may also become positive for small angles of incidence accompanied by correspondingly small values of C_L. In such cases, however, the drag diminishes somewhat with increasing angle of incidence, $dC_D/d\,\alpha$ is therefore negative, and $dC_D/d\,\alpha - C_L$ is still for the most part negative. Experimental results may be found, for example, in a report made

[1] WIESELSBERGER, C., Zur Theorie des Tragflügels bei gekrümmter Flugbahn. Zeitschr. f. angew. Math. u. Mech. **2**, p. 325, 1922. For further experiments see *e. g.* the English report L. W. BRYANT, A. T. HALLIDAY, Measurement of Lateral Derivatives on the Whirling Arm. Br. A.R.C., R. and M. 1249, 1929.

by Irving and Batson[1]. This report was especially concerned with the differences shown by wings of varying thickness. It appeared that in thicker wings the yawing moment changes sign at angles of incidence somewhat smaller than for thinner wings; the amount of yawing moment then increases rapidly, reaching values much higher than those corresponding to thinner wings in the same conditions, and then falls very quickly.

17. Effect of Ailerons. Fundamentally, an aileron is a special asymmetric arrangement of the wings with flaps as described in III **13**. Each half of the wing has its own special flap which in most cases extends only along the outer part of the wing. Both flaps are manipulated in opposite directions so that the lift is increased on one side and decreased on the other, thus producing a rolling moment under the control of the pilot. The difficulty of obtaining a quantitative estimate of the effect of ailerons is increased by the fact that their efficiency falls away at their ends. At the outer parts, in fact, the effect of ailerons diminishes approximately in proportion to the lift of the wing itself. In order to estimate the decrease at the inner ends it is possible to consider an infinitely long wing having a discontinuity in the angle of incidence at one point. The theory of the lift distribution in the neighborhood of such a discontinuity is available[2] (Division E IV **11**). It has not been possible to deduce, however, from the knowledge of single end effects any sufficiently reliable rule for calculating the combined result of two such effects[3]. For a theoretical discussion of this matter, consideration must be given to the effect of all irregularities in the form of the wing and to this class the ailerons when in action belong. This problem can be solved without serious difficulty, in view of the development by I. Lotz of a practicable procedure for calculating the lift distribution of wings with arbitrary distribution of chord and angle of incidence[4] (Division E IV **12**). Information concerning the relation between the size of ailerons and the magnitude of their effects has been supplied by experiments of Heald and Strother[5]; and further results

[1] Irving, H. B., and Batson, A. S., Rolling Experiments on an Airfoil of R.A.F. 32. Section. Br. A.R.C., R. and M. 1182, 1928.

[2] Betz, A., Petersohn, E., Zur Theorie der Querruder. Zeitschr. f. angew. Math. u. Mech., Vol. 8, p. 253, 1928.

[3] Petersohn, E., Theoretische und experimentelle Untersuchung der unter Einwirkung von Querrudern an Tragflügeln auftretenden Momente. Luftfahrtforschung, Vol. 2, p. 40, 1928.

[4] Lotz, I., Berechnung der Auftriebsverteilung beliebig geformter Flügel. Zeitschr. f. Flugtechnik u. Motorl. **22**, p. 189, 1931.

[5] Heald, R. H., and Strother, D. H., Effect of Variation of Chord and Span of Ailerons on Rolling and Yawing Moment in Level Flight. U.S. N.A.C.A. Rep. 298, 1929.

concerning the effects of ailerons are contained in the results of experiments on flaps and ailerons[1] mentioned in III **14**.

Since use of the ailerons usually also causes an airplane to side-slip, it is of interest to known how far the action of the ailerons is interfered with by side-slip. Information on this point may be obtained from the experimental results represented in Figs. 97 to 105 (thin line curves).

18. The Working of the Vertical Tail Structure (Rudder and Fin). Considered by itself the vertical tail structure works in much the same way as the horizontal tail structure (elevator and stabilizer) and as described in III **14**. There is an appreciable difference, however, when one considers the effect of this unit in relation to the whole airplane. The horizontal structure almost always acts in conjunction with a comparatively large main wing. If the airplane is turned about the lateral axis by the use of the elevator, very large changes of lift appear even with small changes of angle of incidence. These changes of lift incline the path of the airplane either up or down in such fashion that the relative angle of incidence is only slightly changed. In side-slip, however, the lateral forces appearing are generally relatively small. With use of the rudder, a lateral force appears on the tail-plane, which accelerates the airplane in a lateral direction and produces, in reaction with the inertia of the airplane, an angular moment about the vertical axis. The airplane is actually turned in direction out of its path as a result of the action of this moment; but for want of sufficient lateral force, it continues to move, in general, in its old direction; a side-slip is thus produced. The effect of this is that the vertical tail structure is subjected to a strong lateral flow and the action of the projecting rudder is more or less nullified. In this case therefore the airplane is only very slightly influenced by the rudder. In order to produce the considerable lateral force necessary to balance the centrifugal force which arises when an airplane executes a curved path in a horizontal plane, the plane must be turned about its longitudinal axis so that lift and gravity produce a resultant in a horizontal direction. This lateral inclination which is necessary for lateral steering, can be produced at will by the pilot by moving the ailerons. As already noted, however, a moment about the longitudinal axis almost always occurs in side-slip, and this automatically produces a lateral inclination in the direction necessary for lateral steering. It was seen also that this effect can be increased by using dihedral or sweepback dispositions of the wings. In addition to this, a moment which increases the lateral inclination is produced by the fact that the outer wing, in a turn, has a higher velocity than the inner wing, and therefore experiences a larger lift (see **15**).

[1] HIGGINS, G. J., and JACOBS, EASTMAN N., The Effect of Flap and Ailerons on the N.A.C.A. M-6 Airfoil Section. U.S. N.A.C.A. Rep. 260, 1927.

19. Lateral Stability. After we have analyzed the effects of the individual components of motion arising in an asymmetrical flight, we have still to form an estimate of the resultant effect of all these influences. It should, however, be emphasized that the resultant effect of various concurrently effective causes cannot in many cases be obtained by simple superposition; for the combination of such causes may involve supplementary effects. Usually, however, these additional effects are of moderate magnitudes and it is therefore possible by superposition to obtain at least a general idea of the resultant effect. The smaller the unsymmetrical movements are in comparison with the symmetrical ones, the more accurate will be the picture developed in this manner.

It was stated in **15** that the rolling moment due to yawing may easily tend to produce instability of course. We shall now examine this condition in more detail[1]. Let the airplane be supposed to have a small lateral inclination to the left. Lift and gravitation give then a resultant directed toward the left causing the airplane to side slip in the same direction. As a result of weather-cock stability, the side-slip entails a yawing turn to the left, and this in turn produces a rolling moment due to yawing and thereby increases the initial lateral inclination. The consequence of such a chain of effects would be continual increase of the unsymmetrical movement, *i. e.* marked instability. Two other effects are, however, also involved, *viz.* the rolling moment due to yaw and the yawing moment due to yawing, both of which oppose the instability. In consequence of the side-slip, the first of these moments acts to diminish the initial lateral inclination, *i. e.* to oppose the rolling moment due to yawing. Its magnitude increases with the angle of yaw. The latter is diminished by weather-cock stability (yawing moment due to yaw) but is maintained at a definite value in consequence of the damping of the motion (yawing moment due to yawing). In accordance with this, yawing moment due to yaw and rolling moment due to yawing are destabilizing factors, while the opposite is true of rolling moment due to yaw and yawing moment due to yawing. Lateral stability is present when the product of the first two moments is greater than that of the other two. As long as the moments are linear functions of the angle of yaw, or of the velocity of yaw, this criterion of stability is independent of the particular values of these quantities and is therefore a quantity characteristic of the airplane. If the condition noted is satisfied, so that the airplane is laterally stable, it will recover from a disturbance and return to rectilinear flight without the use of the controls. If the condition is not satisfied, however, a small initial disturbance tends toward continual increase, unless controlled by suitable use of the controls.

[1] MATHIAS, G., Die Seitenstabilität des ungesteuerten Normalfluges und ihre technischen Vorbedingungen. 272. Bericht der Deutschen Versuchsanstalt für Luftfahrt. Zeitschr. f. Flugtechnik u. Motorl., Vol. 23, p. 193, 1932.

Regarding this criterion of stability, the following points should be especially noted. In order to produce lateral stability, it is necessary to make the yawing moment due to yawing large and the yawing moment due to yaw small. An increase in the size of the rudder and fin increases both moments however, and thus defeats the intention of increasing one while decreasing the other. On the other hand, it is possible to increase the yawing moment due to yaw by modifying the forces on the fuselage (see 5). If a large rudder and fin are chosen in combination with a fuselage having pronounced negative weather-cock stability, the yawing moment due to yaw is the difference of the moments due to tail and fuselage, while the fuselage does little to alter the damping effect of the yawing moment due to yawing. Hence the latter moment is large as a result of the part played by the rudder and fin, while the former is small on account of the negative contribution from the fuselage.

As seen previously, it is advisable, in order to produce static lateral stability, to keep the weather-cock stability small. If too small, however, phenomena of dynamic instability often result. When this occurs the airplane performs lateral oscillations.

This subject is treated in more detail in Division N (Dynamics of the Airplane).

Bibliography.

In addition to references given in the text the reader is referred to some publications of more general character.

L. Bairstow, Applied Aerodynamics, London 1920.

R. Fuchs und L. Hopf, Aerodynamik, Berlin 1922. (2. Ed. will be published in the near future).

National Research Council Bulletin No. 84. Report of Committee on Hydrodynamics. Dryden, Murnaghan, Bateman. Washington 1932.

DIVISION K

AIRPLANE BODY (NON LIFTING SYSTEM) DRAG AND INFLUENCE ON LIFTING SYSTEM

By

C. Wieselsberger,
Aachen, Germany

EDITOR'S PREFACE

The present Division is concerned with those features of the airplane structure which, though necessary from the requirements of structure, purpose and utility, may be and usually are harmful from the standpoint of aerodynamic efficiency. Under the conditions of conventional design an airplane has a body for the accommodation of a power plant and for pilot, personnel and pay load; and likewise a landing gear to enable it to take off from and return safely, to the ground. Structurally it will have combinations of struts, wires, etc., as required for strength, but which take relatively a heavy toll in terms of increased drag and its consequences.

The Division opens with a general discussion of the problems presented by the presence of these non-lift producing elements of the structure, and including in particular a consideration of the added drag and methods for its reduction to a minimum.

One of the important items under this general heading is the influence of the airplane body on the wings and in Chapter III of the Division, consideration is given first to a theoretical approach to this problem, followed by a statement of experimental results.

From the nature of the effects due to such features as struts, wires, landing gear, etc., the chief reliance must be on experimental results and throughout the Division will be found a considerable amount of such information together with references to the original sources of the more important investigations of this character.

W. F. Durand.

CHAPTER I

DRAG OF THE BODY

1. Introduction. The body of an airplane cannot, as a rule, be formed with complete reference to the conditions for small resistance. The reason for this is found in the fact that the fuselage or body, in most cases,

carries the power plant of the structure and that the conditions for a satisfactory operation of the engines fix special requirements which are usually inconsistent with the conditions for minimum body resistance. In cases where the engines are carried in special nacelles, these particular requirements apply to the form and construction of such nacelles. In particular, the cooling of the engines requires that the part of the engine to be cooled or the cooling installation be exposed in the free airstream. This requirement which, with water cooled engines, means the installation of a radiator, or, with air cooled engines, either the projection of the cylinders beyond the body into the free streaming air, or provision for a flow of fresh air over the cylinders, has always given rise to an additional resistance of very considerable magnitude. As these matters will receive consideration in Division T, it will not be necessary here to go further into the subject.

There are, moreover, other controlling conditions which may frequently make impossible the realization of a body form with the best aerodynamic characteristics. An extreme case is, for example, the body or hull of a flying boat, for the form of which hydrodynamic conditions must largely control; because in such case, good conditions for take off and return to the surface of the water as well as provision for the necessary stability in a sea-way are absolutely essential.

In the design of the body form, due regard must also be given to those parts of the structure which connect therewith or which extend therefrom, such as wings, landing gear, empennage. Furthermore, conditions for good visibility for the pilot as well as protection for his body, place further requirements on the form of the airplane fuselage. There results, in consequence, in the design of an airplane, a body form departing more or less from that of a streamlined, geometrical form of revolution—the ideal from the viewpoint of least resistance.

If a comparison be made between the fuselage form of a number of different aircraft, even when these craft serve the same purpose and are of nearly the same size, a very great variety of fuselage form will be found with corresponding great differences in the air resistance. It thus appears that it is not possible to make any statements generally valid regarding the magnitude of the resistance of the airplane body. Furthermore, the character of the body is influenced and its resistance is modified by interaction with the wings, the propeller, and other parts of the structure. Moreover it must be noted that even in case the resistance of individual elements were known, the resistance of the structure as a whole cannot be determined by a simple addition of these individual values. The former may be greater or less than the latter. A satisfactory determination of the body resistance is to be found only by direct experimental means for each particular case. In many cases, then, when it is a matter of model experimentation, it is preferable to

deal with a model of the entire structure, because, as noted above, the mutual interference of the various elements renders unreliable any simple addition of the resistance of the individual elements.

The aircraft designer may often desire, in a preliminary way and without recourse to experimental research, to set up an approximate schedule for the drag of the structure. For this purpose it may be desirable to give, in the following paragraphs, some general statements and rules which may be employed for such purpose. On account of the large amount of material of this character available, the choice must be limited to a relatively small number.

2. The Ideal Fuselage. The ideal airplane body, which with certain groups of aircraft (racing craft, for example) may be very nearly realized, comprises a streamlined form symmetrical about the longitudinal axis, similar to approved forms for airships. The resistance coefficients for such forms are extremely small.

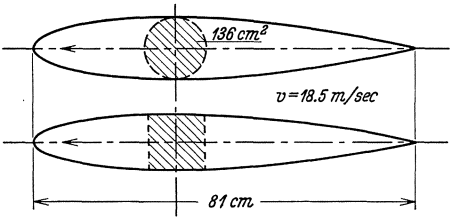

Fig. 1. Stream-line body with circular and square cross-section.

Let

D = drag.

q = dynamic pressure $= \frac{1}{2}\varrho V^2$

S = max. cross section.

C_D = drag coefficient.

Then we have,

$$C_D = \frac{D}{q\,S} \tag{2.1}$$

In this form, experiment with models gives values of this coefficient down even as low as 0.045. Such a form of streamlined body is shown in Fig. 1, in one case with circular and in the other with square cross section. The form with square section is so related to that with circular section, that at each point the section areas are the same.

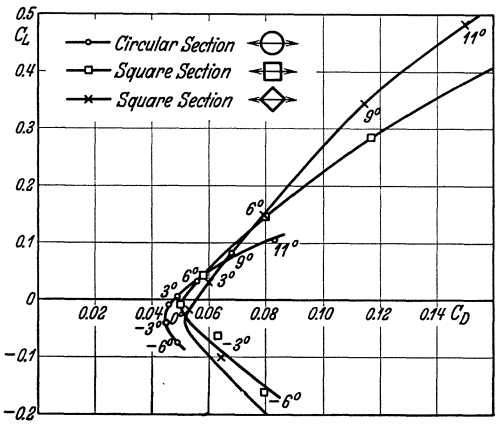

Fig. 2. Lift and drag of two stream-line bodies.

In Fig. 2 are given the results of wind tunnel measurements, carried out at a wind velocity of 18.5 m/s, showing the relation between the drag coefficient as above and the lift coefficient ($C_L = L/q\,S$, where $L = lift$) for various angles of attack. The model with square section was turned (for change of incidence) once in a plane

parallel to a side and once in a plane parallel to a diagonal. As the diagram shows, the form with circular section has the smaller resistance and experiences also a notably smaller lift than the form with square section. These indications were derived from model measurements. With full scale forms, on account of higher Reynold's numbers, somewhat lower values for the drag coefficients are to be anticipated. A formula giving approximately the reduction of drag for increase in Reynold's number is given in the following section.

3. Scale Effect. Let V denote the velocity and l some characteristic dimension of the airplane. Then, in accordance with a proposal of W. S. Diehl[1] the resistance D of the body may be expressed in the following form:

$$D = K_D (V l)^n \tag{3.1}$$

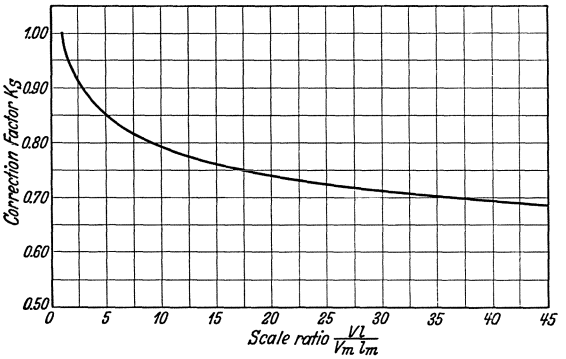

Fig. 3. Correction factor for scale effect.

where K_D is a constant peculiar to the form of the body and n is an exponent which also, in general, is different for different bodies. However, experiments show that for fuselages, engine nacelles, seaplane floats and bodies of similar form, the exponent n varies but slightly and holds a value close to 1.9 so that, for such bodies, we have:

$$D = K_D (V l)^{1.9} \tag{3.2}$$

For practical use, however, it is more convenient to write this formula in the form:

$$D = K_s D_m \left(\frac{V l}{V_m l_m}\right)^2 \tag{3.3}$$

wherein, D_m, V_m, l_m relate to the model and D, V, l to the full scale body. In this form of the equation, K_s is not a constant, but can be expressed as a function of the ratio $V l / V_m l_m$ and values can be taken in accordance with the diagram of Fig. 3. In this manner, having given the model resistance and conditions of test, the value of the full scale resistance for the proposed conditions is readily found, having regard to the influence

[1] Tests on Airplanes, Fuselages, Floats and Hulls, U.S. N.A.C.A. Report No. 236.

of scale effect. Researches regarding the difference between the resistance of full scale bodies and of models have also been carried out in Russia[1].

4. Actual Airplane Body. The actual airplane fuselage, on account of its less favorable form and especially on account of various projecting parts, will have a notably greater drag than the ideal form above considered. If to a given fuselage any other form of construction be added, there develops a reciprocal influence and, as already noted for such cases, the resultant overall drag cannot be found, having given simply the drags of the individual parts. Indeed it may be said that

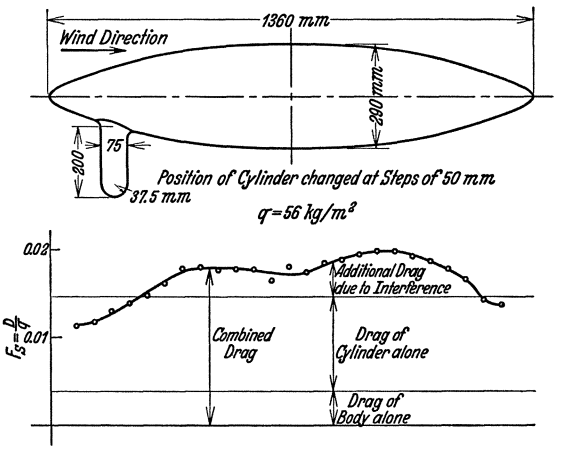

Fig. 4. Effect of appendage on a stream-line body.

by the addition of such a part of the existing fuselage, an entirely new body has been formed, the drag of which can only be determined by special research on this body itself. In order to indicate in some further detail the nature of this reciprocal influence, the results of certain researches on the subject may be given.

These researches show that in the case of an element of construction (appendage) added to a well formed streamlined body, the resultant drag will be notably increased, even to a value greater than the sum of the individual drags. The Aeronautical Research Committee has carried out at Teddington[2] measures on a streamlined body to which was added at various points, a small flat disk normal to the surface. The disk was so adjusted as to just touch the body; its area was about 1/30 the maximum section of the body and the individual drags of the body and of the disk were approximately the same.

[1] MARTYNOV, A. K., Comparative Tests on a Full-size Fuselage and its Model. Transact. of the Centr. Aero-Hydrodyn. Institute Moscou No. 430, 1931.

[2] Technical Report of the Aeronautical Research Committee, 1928-29, p. 44.

For most of the locations of the disk, the resultant overall drag was greater than the sum of the individual drags. In the location of greatest increase—just aft of the maximum body section—this additional drag amounted to 1.8 times the drag of the disk itself in a free air stream.

The observation that the overall drag, in such a case is maximum when the added body is located just aft of the major section of a streamlined form, has also been noted as the result of measurements made at the Aerodynamic Institute at Aachen, under a velocity of 30 m/s. The form of the body as well as the results of tests are shown in Fig. 4. To a streamlined figure of revolution 1360 mm. in length and 290 mm.

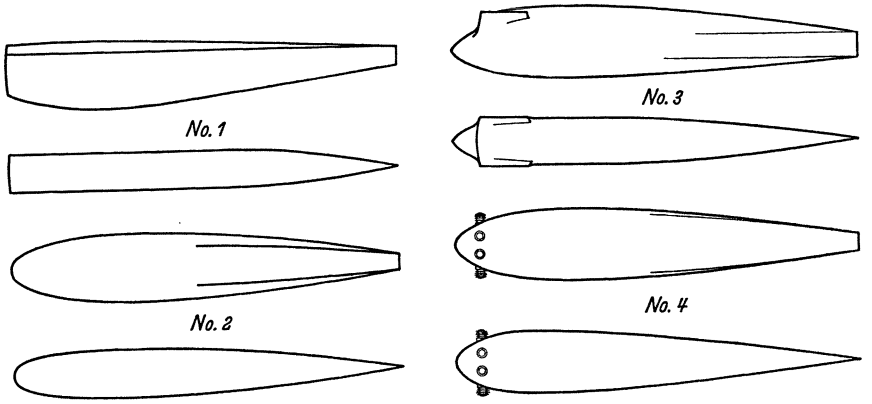

Fig. 5. Forms of fuselage.

in diameter was attached an appendage cylindrical in form 75 mm. in diameter, with axis at right angles to the direction of flow. This appendage was located first near the forward end and then at points every 50 mm. toward the after end. For each of these locations the overall drag D was measured and thence the value of the equivalent drag surface

$$F_S = \frac{2D}{\varrho V^2} \tag{4.1}$$

was found. As is seen, the overall drag varies with the location of the cylindrical appendage. It is greatest when the location is about 3/4 the length of the body from the forward end. The individual drags of streamlined body and of cylinder are also given and from these it is seen that a simple addition of the individual values in no case gives the correct result.

In Fig. 5 are shown certain fuselage forms as they must develop in practice, in part moreover with built in motors, although without other drag producing parts[1]. Model wind tunnel measurements show for these forms, drag values as given in Table 1 (p. 136).

[1] DIEHL, W. S., Engineering Aerodynamics, p. 81.

TABLE 1.

Model No.	Dimensions		Measured Drag at 40 mi/hr lb.	Absolute Drag Coefficient C_D
	Length ft.	Cross section sq. ft.		
1	1.668	0.0459	0.050	0.266
2	1.669	0.0472	0.012	0.062
3	1.663	0.0550	0.021	0.094
4	1.662	0.0662	0.068	0.251

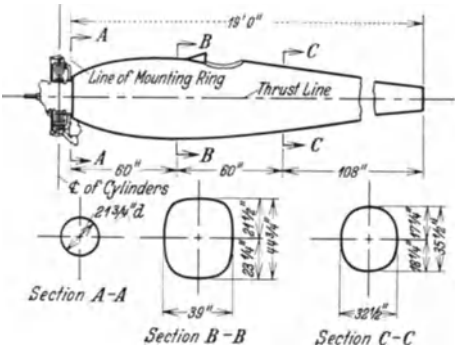

Fig. 6.

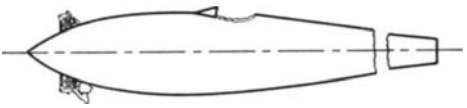

Fig. 7.

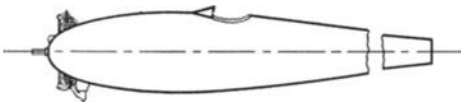

Fig. 8.

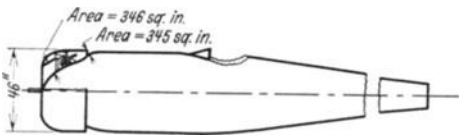

Fig. 9.

Figs. 6—9. Full scale tests with an airplane body.

The large value of the drag for model No. 1 is to be explained by the abrupt non-rounded form of the nose of this model.

Especially notable are the results of tests made in the 20 ft. wind tunnel at Langley Field on an airplane body full scale of about 20 ft. length[1]. A Wright Whirlwind air cooled engine was installed in the fuselage and the investigation was directed toward a study of the extent to which the overall drag could be reduced through forms of cowling or shrouding about the engine. The fuselage and cowling are shown in Figs. 6—9. In Fig. 6 the engine is uncowled and freely exposed. Following this, the motor was, to an increasing degree, covered by cowling and the nose rounded off, see Fig. 7. In Fig. 8 the nose is pointed and the propeller hub is provided with a spinner. Finally the engine was surrounded by a ring with airfoil section, see Fig. 9, so that the cylinders of the engine were placed in a ring formed channel through which the air streamed from front to rear. It has been shown that such a ring which is often known as N.A.C.A. cowling or the Townend Ring from the English form of this device, may in certain cases bring about a most notable reduction in the overall drag. In comparison with the drag with the uncowled

[1] WEICK, F. E., Drag and Cooling with Various Forms of Cowling for a "Whirlwind" Radial Air-Cooled Engine, II. U.S. N.A.C.A. Report No. 314.

motor, Fig. 6, such a ring may cause a decrease in the drag of about 50 per cent.

It is clear, however, that in all cases where it is desired to thus reduce the drag due to the engine, regard must be given, not alone to the reduction of the drag, but also caution must be exercised that the cooling of the engine be not unfavorably affected. Experimental research thus far carried out, together with experience gained from practical applications, show that by the use of cowling devices of the character referred to, a satisfactory cooling of the motor can be realized and abundant use of these devices in aircraft of all types has shown that such use is very advantageous. It has, however, been noted that the

TABLE 2.

No.	Fig.	Cowling	Fuselage and engine drag kg at 100 mph	Absolute drag coefficient C_D
1	6	Engine uncowled	64	0.52
2	7	Nose rounded	62	0.50
3	8	Spinner	60	0.48
4	9	Complete cowling (ring)	33	0.27
5	—	Engine and wind shields removed and cockpit covered	12.8	0.10

reduction in the drag is not, in all cases, as great as above indicated. With certain body forms, the addition of such a ring has brought only a small reduction in the drag. In any case it is very important that, through special examination, the form and proportions of such an installation be adapted to the fuselage on which it is to be placed[1].

The principal results with the fuselage above referred to are given in Table 2. The drag is here expressed in relation to the principal section of the fuselage which had an area of 10.7 sq. ft. It will be seen that the two changes noted under 2 and 3 produced but little effect, while the complete cowling ring as shown in Fig. 9 reduced the drag to about one half the uncowled value.

The notable decrease in the resistance of a circular disk fitted with a Townend ring is shown by a report of experiments carried out by the inventor of the ring[2]. The form of the ring and the decrease in the resistance, expressed as the ratio of the resistance of the disk with ring (R) to the resistance without ring (R_0) is shown in Fig. 10. It may

[1] GOUGH, M. N., Effect of the Angular Position of the Section of a Ring Cowling on the High Speed of an XF7C-1 Aeroplane. U.S. N.A.C.A. Technical Note No. 355.

[2] TOWNEND, H., The Townend Ring. Journal of the Royal Aeronautical Society, Vol. XXXIV, October, 1930.

be seen, from this diagram, that the best results are reached when the radius of the ring is about 1.5 times that of the disk. In this case, the reduction of the disk resistance is about 63 per cent. It may also be noted that the addition of a windshield and an open cockpit to a smooth body surface without motor (see No. 5 of Table) for which the drag at 100 mph is 28 lbs., causes an increase of drag of 14 lbs., that is, of 50 per cent of the smooth body drag.

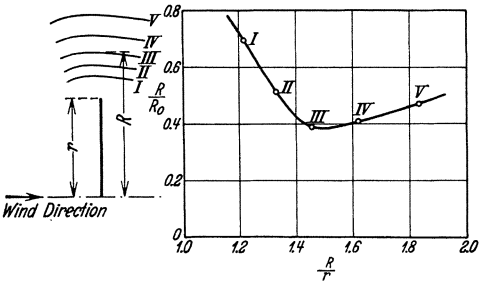

Fig. 10.
Circular disk fitted with Townend ring.

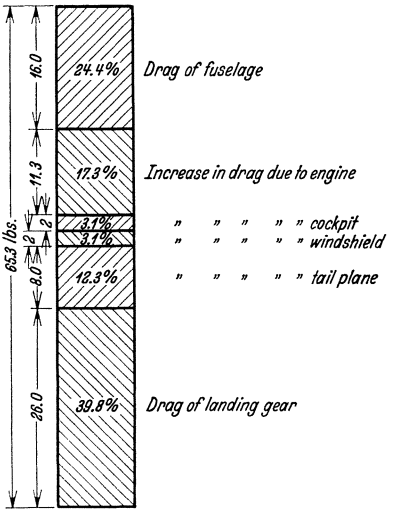

Fig. 11. Measurements of the fuselage of a Sperry Messenger plane.

A similar research regarding the influence of various forms of windshield on body drag has also been carried out by E. P. Warner and to which reference may be made[1].

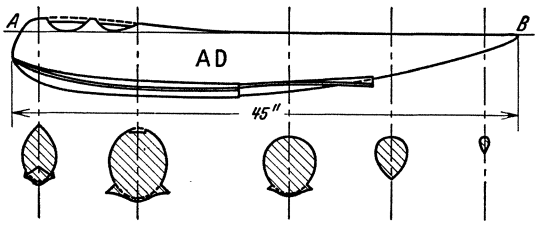

Fig. 12.

Further measurements on the fuselage of a Sperry Messenger plane, full scale, have also been carried out in the 20 ft. N.A.C.A. tunnel at Langley Field[2]. The fuselage, about 17.7 ft. in length, was fitted with an air cooled three cylinder radial engine and was further fitted with landing gear and empennage. These measurements are of especial interest and value because they serve to indicate in what manner the overall drag is made up from the drags of the individual elements.

[1] WARNER, E. P., Wind Tunnel Tests of Fuselages and Windshields, U.S. N.A.C.A. Technical Note No. 226.

[2] WEICK, F. E., Full Scale Drag Tests on Various Parts of Sperry Messenger Airplane, U.S. N.A.C.A. Technical Note No. 271.

The proportionate shares of the various parts, taken at a wind velocity of 80 mph, are shown schematically in Fig. 11. Especially notable is

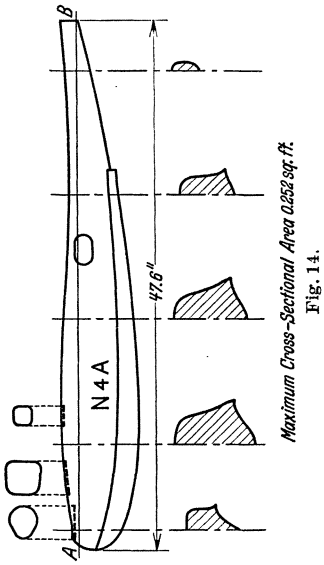

Fig. 14.

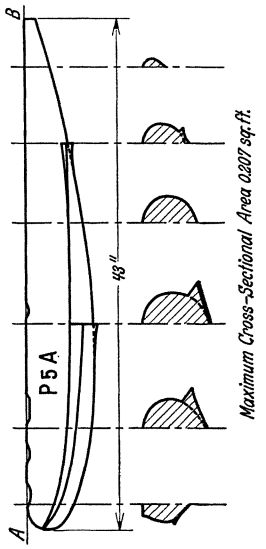

Fig. 16.

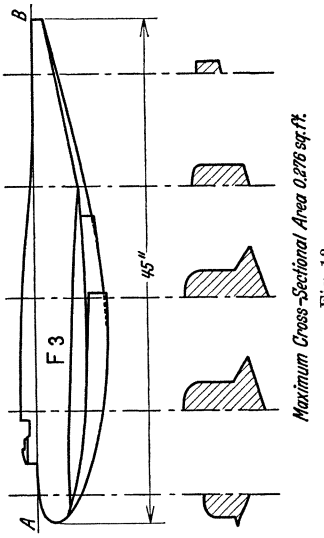

Fig. 13.

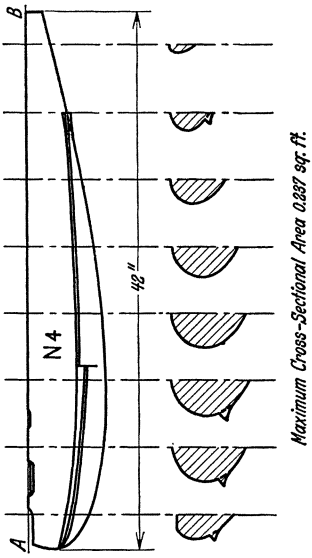

Fig. 15.

Figs. 12—16. Forms of flying boat hulls.

the high value of the drag due to the landing gear which represents nearly 40 per cent of the total. Likewise it is seen that the increase in the drag due to the engine is very considerable.

Further measurements of airplane bodies, full scale, have been carried out in the 20 ft. wind tunnel by E. F. Weick[1], O. W. Schey[2] and W. H. Herrnstein[3] giving further data of interest and value regarding fuselage drag.

In the case of flying boats the body or hull, due to hydrodynamic requirements, must be given a notably different form as compared with that for land aircraft, and in consequence different values of the drag are to be anticipated. The British Advisory Committee for Aeronautics has carried out at Teddington a number of wind tunnel measurements on models of flying boats[4] of which a brief abstract will here be given.

The models which were 35 to 48 inches long were tested almost entirely at a zero angle of incidence (line AB, Fig. 12 parallel to the

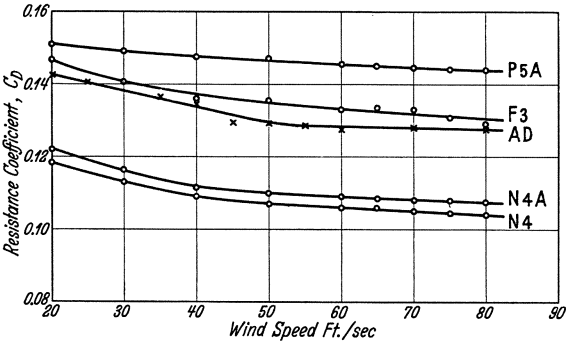

Fig. 17. Resistance of flying boat hulls.

wind). The side elevation and sections of the boat are shown in Figs. 12—16. The drag coefficient C_D (computed with reference to the principal section) in relation to velocities of the wind over the range from 20 ft/sec. to 80 ft/sec. are given in the diagram of Fig. 17. As may be noted, the values of the drag coefficient are relatively good—a result which may be referred to the smooth form without projecting parts, and in particular to the excellent rounded form at the bow. With reference to the hydrodynamic characteristics of flying boats and of floats, see Division S.

---

[1] Weick, F. E., The Drag of a J-5 Radial Air-Cooled Engine, U.S. N.A.C.A. Technical Note No. 292.

[2] Schey, O. W., Johnson, E., and Gough, M. N., Comparative Performance Obtained with XF7c-1 Airplane Using Several Different Engine Cowlings, U.S. N.A.C.A. Technical Note No. 334.

[3] Herrnstein, W. H., Full Scale Drag Tests on Various Parts of Fairchild (FC-2W2) Cabin Monoplane. U.S. N.A.C.A. Technical Note No. 340.

[4] Jones, R., and Pell, G. N., The Air Resistance of Flying Boat Hulls, Br. A.C.R. R. and M. 461, 1918-19.

CHAPTER II
PARASITIC RESISTANCES[1]

1. Drag Due to Various Parts of the Structure. In the complete structure of an aircraft are found various parts either of the structure or of the equipment which, like the body, take no part in the development of lift and the drag of which may be grouped under the general head "parasitic". A knowledge of the value of such elements of the total drag is, for the purpose of the predetermination of the performance, of very great importance. Such parts of the structure as cables, wires

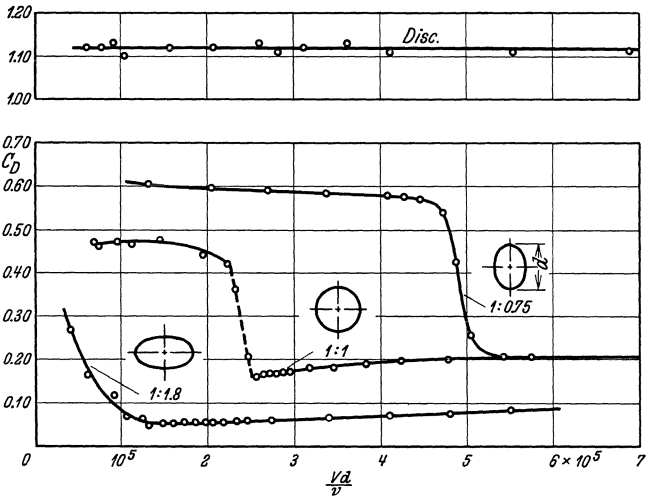

Fig. 18. Resistance of a sphere and related bodies.

and struts belong in this category. Among items of equipment mention may be made of searchlights, generators, machine-guns, etc. As such items are usually of complicated form, their drag can, in general, be found only for each special case by wind tunnel measurements. For the purposes of an approximate estimate, however, effective use may frequently be made of a knowledge of the drag of geometrically simple bodies. To this end it will be of interest to note the drag coefficients of a few bodies of simple geometrical form. In Fig. 18 are given the values of such coefficients plotted on Reynold's number for a sphere, a prolate spheroid, an oblate spheroid and a circular disk. In the case of the disk, the value is nearly independent of the Reynold's number, while for the other forms there exists a so-called "critical" value of the number at which the value of the coefficient changes more or less abruptly. In the case of plane surfaces rectangular in form, placed normal to the direction of wind flow, the coefficient is closely

[1] See also Division O Chap. II.

dependent on the ratio of breadth to length. This relation is given in the diagram of Fig. 19. While for square plates ($b/l = 1.0$) the coefficient has a value approximately 1.1, the value increases for long rectangular plates and for very long narrow forms ($b/l \cong 0$) it may reach the extraordinarily high value of 2.0.

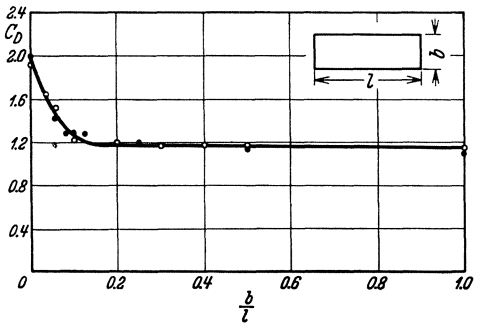

Fig. 19. Resistance of a rectangular plate.

Next in the diagram of Fig. 20 is given the value of the coefficient as a function of the Reynold's number for the case of a cylinder with circular section placed with its axis normal to the direction of the wind flow. The upper curve relates to the case of a cylinder of infinite length ($d/l \cong 0$) while for the lower curve the ratio is $d/l = 1/5$. The coefficient

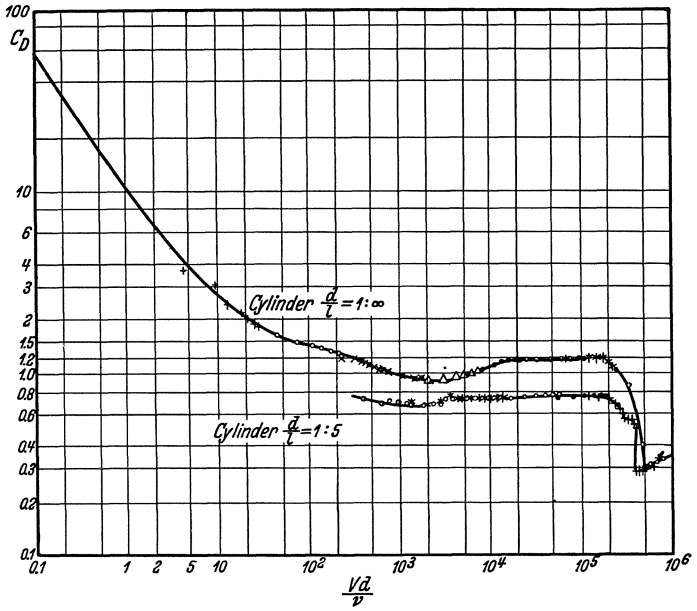

Fig. 20. Resistance of a cylinder (axis normal to wind direction).

is seen to vary in marked degree with the Reynold's number, and the same as for the sphere, there seems to exists a critical value of the number. The drag of cables made up of individual wires is not far from that for smooth wires of the same diameter. In Fig. 21 are given the

results of certain Russian measurements for two cables[1] on the value of the drag coefficient as a function of the air speed. One of the cables

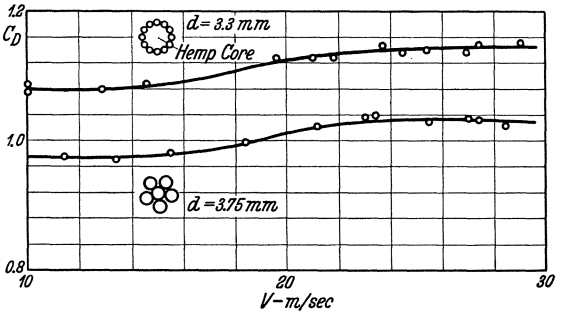

Fig. 21. Resistance of two cables.

had a diameter of 3.3 mm. and was composed of twelve single wires of a diameter of 0.7 mm. twisted over a core of hemp. The other had a diameter of 3.75 mm. and was composed of six single wires of a diameter of approximately 1.3 mm. twisted together.

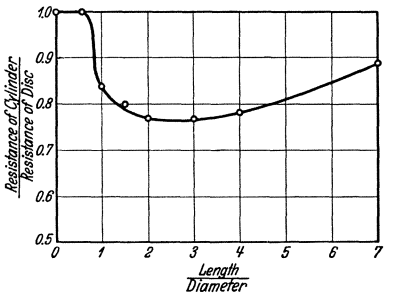

Fig. 22. Resistance of a cylinder (axis parallel to wind direction).

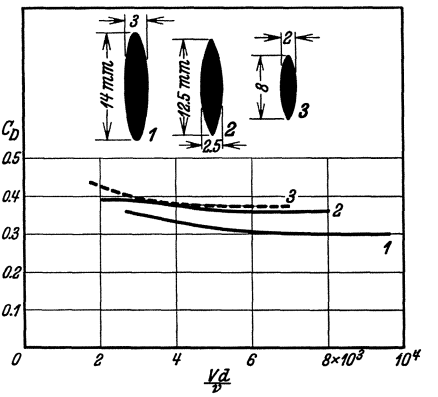

Fig. 23. Resistance of stream-line wires.

In the case of cylinders placed with the axis parallel to the direction of stream flow, the drag depends on the ratio of length to diameter. For lengths up to about half the diameter, the drag is the same as for a disk. If the length is increased, the drag decreases up to a length of about $2\frac{1}{2}$ diameters. Beyond this the drag increases with the length. In Fig. 22 are given the results of an investigation by G. Eiffel[2] showing the ratio of the drag for a cylinder to that for a disk as a function of the ratio, length of cylinder to diameter.

[1] Jurieff, B. N. and Lessnikowa, N. P., Aerodynamical Investigations. Transactions of the Central Aero-Hydrodynamical Institute No. 33, 1928.

[2] Eiffel, G., La résistance de l'air et l'aviation, Paris, 1910.

Since the drag of wires of circular cross-section is relatively high, use is now almost universally made, for all such tension members, of wire with a stream-line section—so-called stream-line wire. Values of drag coefficient for a few examples of stream-line wire are given in the diagram of Fig. 23 and it may be seen that through the use of such form of cross section the drag may be reduced to something like 1/4 the value for corresponding wire of circular section. These values, naturally hold only for the case where the long axis of the section is parallel to the direction of wind flow. For the case of oblique flow at an angle

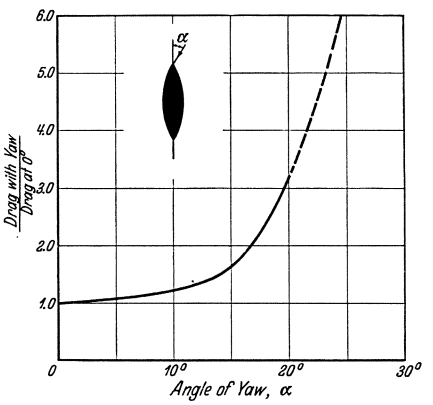

Fig. 24. Stream-line wire in oblique flow.

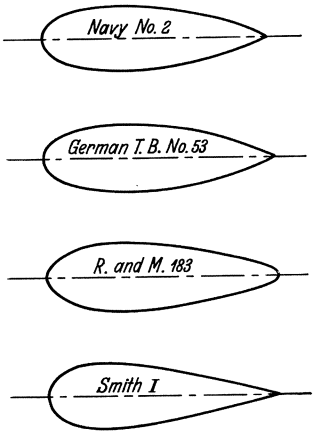

Fig. 25. Forms of airplane struts.

of incidence α, the drag is much increased as is shown by the diagram of Fig. 24. However, the change in the values up to an angle of 5^0 is not significant, and then for greater values of α, the value of the drag increases rapidly. Regarding the drag of stream-line wire including end connections—terminals or turn-buckles—reference may be made to data given by W. S. Diehl[1].

Airplane struts form an important item of the structure. Many different forms have been developed and their drag investigated. In many cases, forms of least resistance have been developed through empirical means, such as the American Navy strut No. 2, the German strut T.B. No. 53 and the English strut[2] of which the profile is given in Fig. 25. The values of the drag coefficient with symmetrical flow are given in Fig. 26. The coefficient is reckoned with reference to the area of a front elevation and the Reynold's number with reference to the thickness of the strut. To the same end, R. H. Smith has developed

[1] Engineering Aerodynamics, New York, 1928.

[2] PANNELL, J. R., and LAVENDER, T., Experiments on the Forces Acting on an Aeroplane Strut. Br. A.R.C. R. and M. 183, 1915.

forms of strut by the use of Rankine's method of combined sources and sinks[1]. The use of this method makes possible practically the determination of the velocity field in the neighborhood of the strut and the pressure distribution along the length of the strut. One of these forms of strut (Smith I) is also shown in Fig. 25 and the corresponding drag coefficient in Fig. 26. By comparison it is seen that this strut is as good as the others. Other measures of the airforces on struts have been made by Cowley, Simmons and Coales[2], by Powell[3] and by A. S. Hartshorn[4]. In these references will be found also information regarding wind forces in the case of oblique position of the struts with reference to the direction of wind flow. A large number of results of measurements on the drag of cylinders, streamline-wire, struts, etc. are also to be found in the above noted report No. 33 of the Central Aero-Hydrodynamic Institute at Moscow.

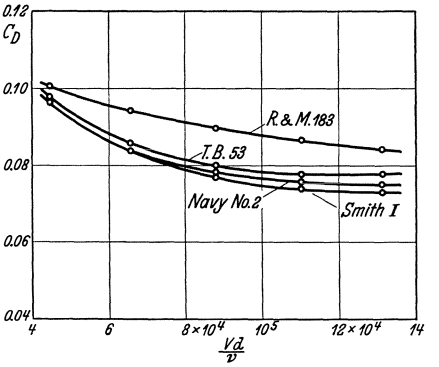

Fig. 26. Resistance of airplane struts.

Under the head of parasite resistance must also be included the resistance due to surface friction. Since the laws of frictional resistance are elsewhere considered (see Division G) it will be necessary here only to deal with actual numerical values with special reference to those surfaces which find special application in aircraft construction and first with reference to fabric covered surfaces treated with "dope" or some like substance. We may write friction drag D_F in the form:

$$D_F = C_F \varrho \frac{S' V^2}{2} \tag{1.1}$$

wherein S' = total surface in question. The coefficient of friction C_F is to be determined by experiment and is dependent on the Reynold's number. In accordance with investigations on this matter made at Göttingen[5] the coefficient C_F for fabric covered surfaces treated with six coats of dope has the value

$$C_F = 0.0375 \left(\frac{\nu}{Vl}\right)^{0.15}$$

---

[1] SMITH, R. H., Aerodynamic Theory and Test of Strut Forms, U.S. N.A.C.A. Technical Reports Nos. 311 and 335.

[2] Windforces on Aeroplane Struts and Wires. Br. A.R.C. R. and M. 256, 1916.

[3] The Resistance of Struts. Br. A.R.C. R. and M. 416, 1918.

[4] Wind Tunnel Tests of Seven Struts. Br. A.R.C. R. and M. 1327, 1929-30.

[5] PRANDTL, L., Ergebnisse der Aerodynamichen Versuchsanstalt zu Göttingen, I. Lief., p. 123.

where l is the length in the direction of flow, ν = kinematic coefficient of viscosity, V = velocity.

In Fig. 27 are given values of C_F as a function of the Reynold's number on a logarithmic scale.

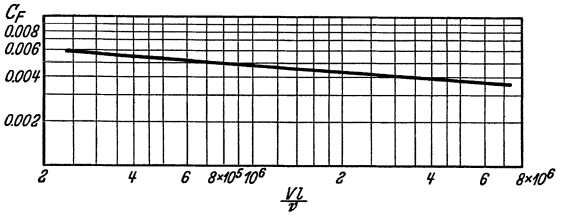

Fig. 27. Coefficient of surface friction.

2. Drag of Landing Gear and Floats. The presence of landing gear on land aircraft causes a notable increase in the parasite resistance, and the same result develops from the presence of floats of seaplanes. The forms of construction in actual practice are, however, so varied that it is hardly possible to lay down any general rules for the determination of its value in any particular case. Since a rough practical figure, which may serve for an approximate estimation of value, may however,

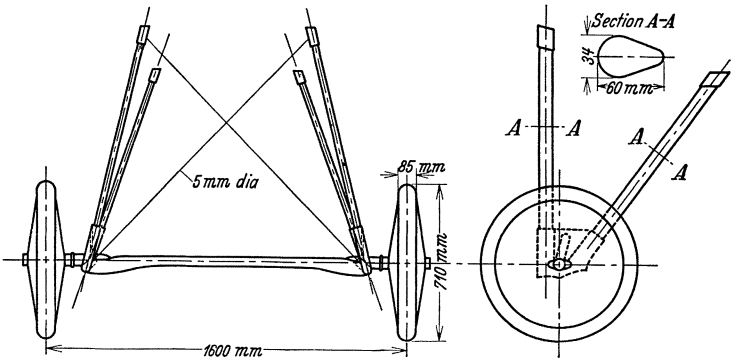

Fig. 28. Full scale landing gear.

be of use, it may be assumed that the drag of the landing gear, in normal flight, will be some 15 to 20 per cent of the total drag of the entire construction. This may be supplemented by values of the actual drag of certain forms of landing gear which have been tested full scale in a wind tunnel.

The normal type of landing gear shown in Fig. 28 was tested in the Göttingen Laboratory[1]. The drag surface $F_S = D/q$ as dependent on

[1] Technische Berichte, Bd. III, p. 275.

dynamic pressure is given in Fig. 29, once for the landing gear entire and once for the gear with the wheels removed. It is seen that the drag with the wheels is nearly double that for the landing gear otherwise. The drag of the wheels again is naturally dependent on the manner of side shrouding or fairing employed. Investigations on this subject have been made by E. A. Griffiths and J. D. Coales[1]. These investigations gave, for the wheel of Fig. 30 and with different forms of fairing, results as follows:

(1) Wheel without fairing $C_D = 0.70$.
(2) Wheel with the usual fairing from hub to rim (B—Fig. 20) $C_D = 0.43$.
(3) Wheel with complete fairing from hub to edge of tread (C—Fig. 20) $C_D = 0.23$.

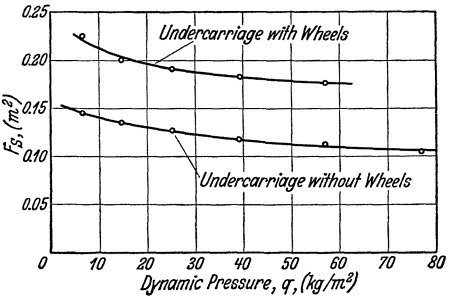

Fig. 29. Resistance of a landing gear.

The coefficient is reckoned with reference to the area of front elevation of the wheel. Certain other forms of wheel fairing have also been investigated in the Government laboratories at Amsterdam and to which reference may be made[2].

From the diagram of Fig. 29 it is seen that with a dynamic pressure of 60 kg/m² (V = 31 m/s) the drag surface of the landing gear, $F_S = 0.175$ m². Similar results are given by French measurements[3] on the landing gear of a Spad 30 and of a Spad 40 whence areas of drag surface were found equal to 0.20 m² and 0.22 m² respectively.

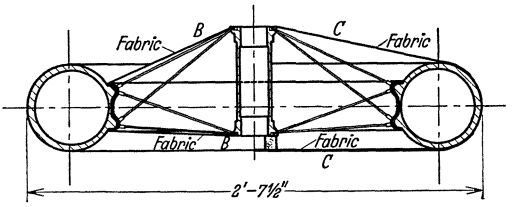

Fig. 30. Wheel with different forms of fairing.

If the total drag of complete landing gear be denoted by unity, Bairstow[4] gives for the individual parts as follows:

Wheels	0.39
Axle	0.10
Struts	0.10
Wires	0.02
Shockabsorber and resistance of joints, etc.	0.39
	1.00

[1] Br. A.R.C. R. and M. 207, 1915.
[2] Verslagen en Verhandelingen van den Rijksstudiedienst voor de Luchtvaart, 4. Teil, 1927.
[3] Bulletin technique No. 28, Aug., 1925.
[4] Bairstow, Applied Aerodynamics, p. 181.

Further note may be made of the results of measurements on the landing gear of a large airplane, the half of which is shown in Fig. 31.

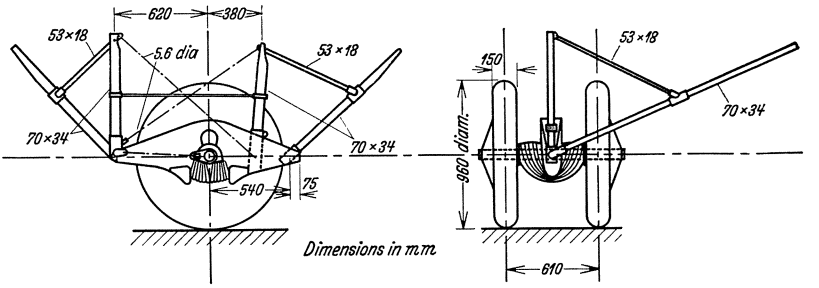

Fig. 31. Landing gear of a large airplane.

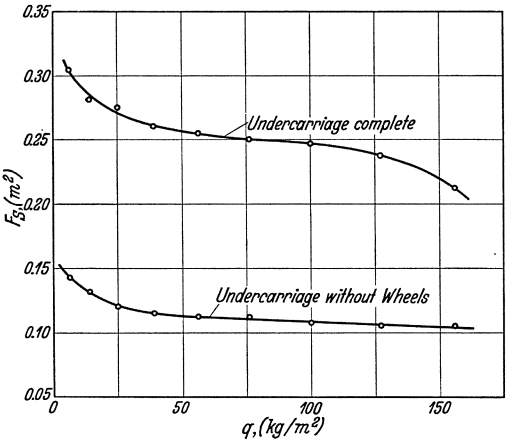

Fig. 32. Resistance of a landing gear.

The resistance area for this landing gear is given in relation to dynamic pressure, and for the two cases with and without wheels, see Fig. 32.

In the case of seaplanes, floats take the place of the landing gear and for the designer it is of importance to know the air forces to which these floats are subjected. In Fig. 33 are shown five floats of different forms which at the Göttingen

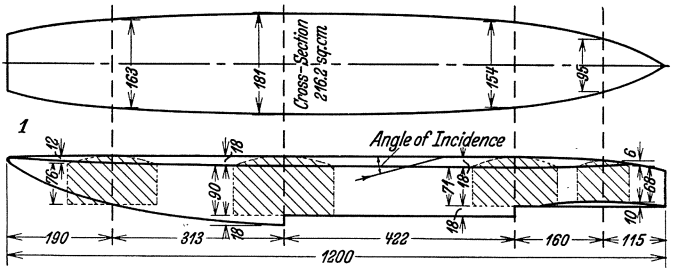

Fig. 33 (1). Forms of seaplane floats.

laboratories have been subjected to measurement for air resistance[1]. The length of the model was 1.2 m and the wind velocity 30 m/s. The

[1] PRANDTL, L., Ergebnisse der Aerodynamischen Versuchsanstalt zu Göttingen. I. Lief., p. 130.

polar and moment curves for these floats are shown in Figs. 34—38. The engle of incidence is reckoned with reference to the upper edge

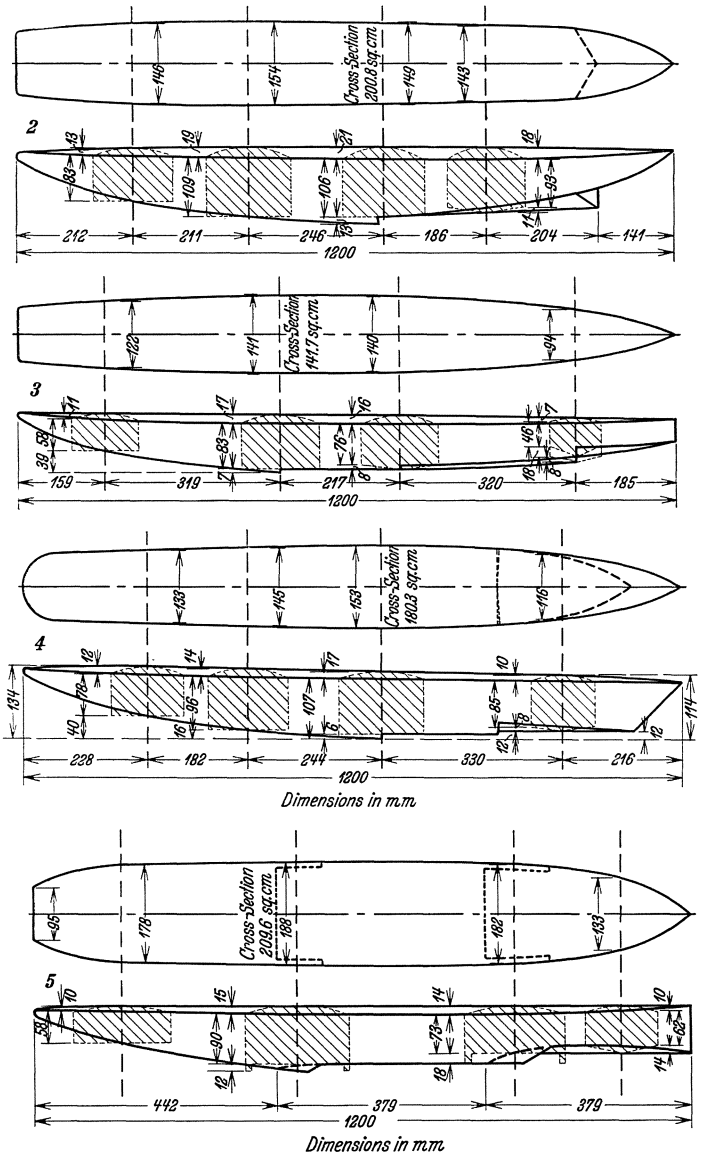

Fig. 33 (2—5). Forms of seaplane floats.

and the moment with reference to the forward point of the float. As characteristic length for the computation of the moment coefficient,

the float length 1.2 m was employed. As the capacity of a float for supporting a load on the water depends on its volume, it is more

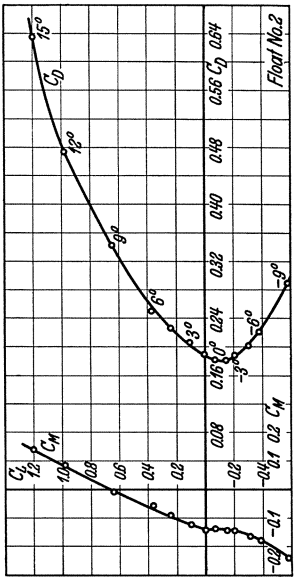

Fig. 35.

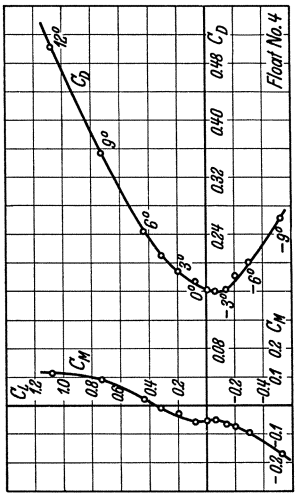

Fig. 37.

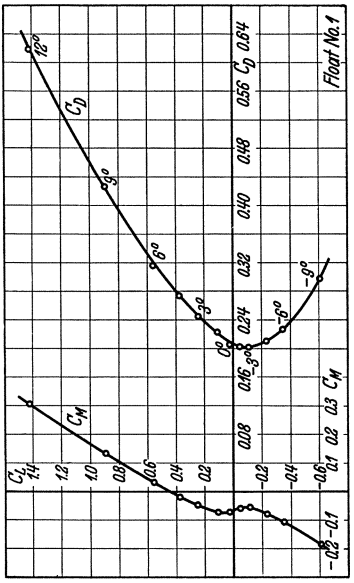

Fig. 34.

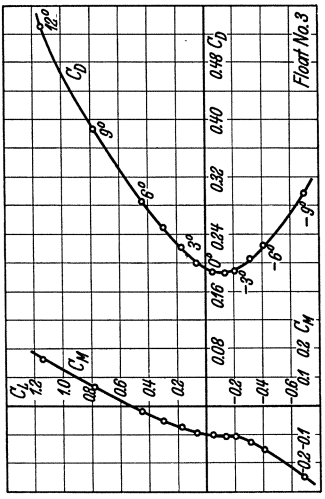

Fig. 36.

Figs. 34—37. Lift, drag and moment of seaplane floats.

commonly preferred for the comparison of floats of different form, to make use of a coefficient which does not depend on the area of

the principal section of the float, but rather on its volume. For this reason it is necessary to relate lift and drag to the 2/3 power of the volume in order to bring out the coefficient in dimensionless form.

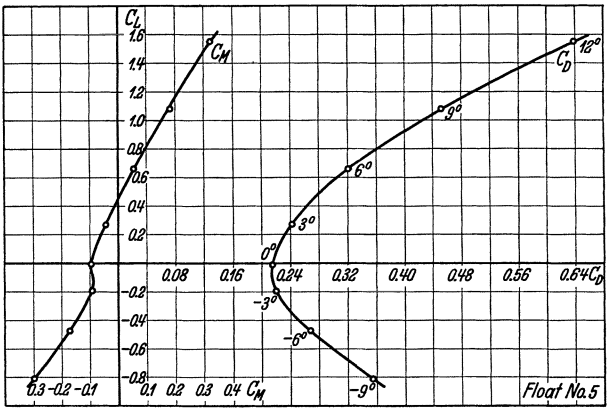

Fig. 38. Lift, drag and moment of seaplane floats.

If the volume of float be denoted by J, the new coefficients K_L, K_D, K_M are then defined through the following equations

$$\begin{aligned} &\text{Lift} && L = K_L J^{2/3} q \\ &\text{Drag} && D = K_D J^{2/3} q \\ &\text{Moment} && M = K_M J q \end{aligned}$$

Between these new coefficients and those derived from the principal section S are the following relations

$$K_L = C_L \frac{S}{J^{2/3}}$$

$$K_D = C_D \frac{S}{J^{2/3}}$$

$$K_M = C_M \frac{S l}{J}$$

These new coefficients K_L, K_D and K_M may in a simple manner be derived from the more familiar coefficients C_L, C_D and C_M. The volume, area of principal section and float length are to be taken from Table 3.

In the same manner, naturally, the air resistance coefficients for a flying boat may be related to the volume of the boat.

TABLE 3.

Float No.	Volume J cm²	$J^{2/3}$ cm²	Max. cross section S cm²	Length t cm
1	15798	629.6	216.2	120
2	15719	627.5	200.8	120
3	10644	483.9	141.7	120
4	14021	581.5	180.3	120
5	16584	650.3	209.6	120

CHAPTER III
INFLUENCE OF THE AIRPLANE BODY ON THE WINGS

1. Theoretical Development for Long Bodies[1]. The subject of the mutual influence between airplane body and wings was first investigated by J. Lennertz[2]. In order to render the problem practicable, assumption must be made of a highly idealized form of airplane body. In most cases, a cylinder was assumed with circular section with axis in the direction of flight and with ends extending infinitely beyond the wings in both directions. With these assumptions and for the case of a body long in comparison with the wing chord it may be permissible to take the flow in the neighborhood of the wings as given approximately correct.

In the development of the treatment, the methods of the Prandtl wing theory were followed. The wing area was displaced by a lifting line which produces a circulation flow of the stream around the wing area. The free vortices leaving the following edge of the wing area form a vortex band which can be taken in accordance with Prandtl's theory. The motion of the fluid is then, outside the wing area and of the free vortex band, known to be a potential flow. At the vortex band there is a sudden change in the potential which is constant along a vortex line and equal to the circulation around the wing element from which this vortex line issues.

The vortex system due to the wing induces on the body a velocity of which the component normal to the surface does not, in general, vanish. Therefore the action of an additional stream flow is necessary which causes the normal component of the velocity to vanish at the surface; but of which the influence disappears at an infinite distance from the body. This additional flow has, outside the body, a velocity potential. Since the action of this additional stream flow, for the ordinary form of airplane body is very complicated, an idealized form of the body must be taken in place of the actual. It is for this reason, that, as noted, a form of body is taken comprising a cylinder with axis in the direction of motion and stretching infinitely in both directions. The air force acting on the body is then given by application of Bernoulli's law. With the assumption of a cylindrical body of infinite length, the body will admittedly experience a lift. The influence of body on the wing arises from the fact that the additional stream flow, conditioned by the body, will in general produce a downward component of velocity on the wing surface. It will thus result that the body will cause a change in the effective angle of incidence of the wings as well as a supplementary drag for the same.

[1] This section has been contributed by Dr. Lennertz.

[2] LENNERTZ, J., Beitrag zur theoretischen Behandlung des gegenseitigen Einflusses von Tragfläche und Rumpf. Abhandlungen aus dem Aerodyn. Inst. d. Techn. Hochschule Aachen, Heft 8.

We take a Cartesian system of axes as follows. The X axis lies along the length of the body and positive in the direction of flight. The Y axis lies in the direction of the width and the Z axis upward, or in the direction of the lift.

In a simple manner, then, we may find the distribution of lift over the span as well as the total lift by application of the impulse and energy laws. In a plane stretching far behind the wing, the free vortices induce a movement about the body section. The impulse per second of this stream is equal to the lift and the rate of change of the energy is equal to the work of the air forces. We thus have, for the lift:

$$L = -\varrho V \int\int \frac{\partial \varphi}{\partial z} d y d z \tag{1.1}$$

and for the drag

$$D = -\frac{\varrho}{2} \int\int \left[\left(\frac{\partial \varphi}{\partial y} \right)^2 + \left(\frac{\partial \varphi}{\partial z} \right)^2 \right] d y d z \tag{1.2}$$

in which ϱ = density of the air, V the velocity of the basic flow and φ the potential function at a point far behind the plane of the wing. The integration is to be carried out over the entire plane outside the body and vortex band cross-section.

For the case of a uniform distribution of lift across the span, the free vortices are liberated only at the ends. The flow about the cylindrical body at a great distance behind the wing can then be found by the use of images of the free vortices relative to the body surface. Let the span be $2\,b$, the radius of the infinitely long cylindrical body be R, the height of the wing above the axis of the body, (z) be e, and the circulation about the wing, Γ. At a great distance behind the wing the values of the circulation at points $y = +\,b$, $z = e$; $y = -\,b$, $z = e$ will have the values $+\,\Gamma$ and $-\,\Gamma$ respectively. The potential function for the stream flow due to these vortices is

$$\varphi_1 = \frac{\Gamma}{2\pi} \left[tan^{-1} \frac{z-e}{y-b} - tan^{-1} \frac{z-e}{y+b} \right]$$

The images of the free vortices in the cylindrical body give two vortices of opposite sign at the points

$$y = \pm\, b \frac{R^2}{b^2 + e^2}, \qquad z = e \frac{R^2}{b^2 + e^2}$$

The potential function for these images will be

$$\varphi_2 = -\frac{\Gamma}{2\pi} \left[tan^{-1} \frac{z - e \dfrac{R^2}{b^2+e^2}}{y - b \dfrac{R^2}{b^2+e^2}} - tan^{-1} \frac{z - e \dfrac{R^2}{b^2+e^2}}{y + b \dfrac{R^2}{b^2+e^2}} \right]$$

The function $\varphi = \varphi_1 + \varphi_2$ is then the complete function in the plane at a distance behind the wing.

The lift is given by (1.1). First the integration for z is carried out. This gives the distribution for L' as follows:

$$L' = 0 \quad \text{for} \quad |y| > b$$

$$L' = \varrho V \Gamma \quad \text{for} \quad R \leq |y| \leq b$$

$$L' = \varrho V \Gamma \left[1 - \frac{1}{\pi} tan^{-1} \frac{4b(b^2+e^2-R^2)\sqrt{R^2-y^2}}{(b^2+e^2)^2+R^4-2R^2(b^2-e^2)-4(b^2+e^2)(R^2-y^2)}\right] \quad (1.3)$$

$$(\text{for} - R \leqq |y| \leqq + R)$$

Integration relative to y then gives the full lift

$$L = \varrho V \Gamma 2b \left(1 - \frac{R^2}{b^2+e^2}\right) \quad (1.4)$$

The results of actual measurements show that the influence on the lift of the height of the wing relative to the body is small. If for the airplane body, wing area of equivalent lift be substituted, the effective breadth for the total lift is found to be such that the actual span breadth is reduced by the distance between the fuselage images of the end points of the wing. For the case $e = 0$ (lifting line and body axis intersecting) and for a ratio $R/b = 1/6$, the distribution of lift over the body width is shown in Fig. 39. The lift of the body is, as appears from the diagram, less than that of the corresponding part of the wing.

Figs. 39—40. Effect of fuselage on lift distribution.

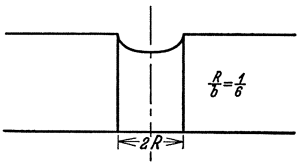

Fig. 39.

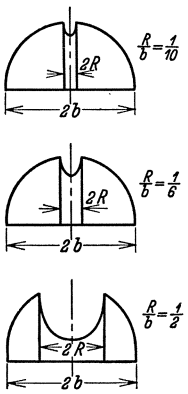

Fig. 40.

The question as to the overall drag finds, through the assumption of uniform distribution of the circulation, no satisfactory solution. In accordance with the equation of energy, the drag should be infinitely great because the velocity of concentrated vortex threads is infinitely large. However, it is possible to compute the change of wing drag as well as the change in the angle of incidence due to the influence of the body. The vortex filaments parallel to the length axis and within the body representing the images of the free vortices, induce, in fact, a flow with vertical component relative to the wing surface. The vertical velocity, by application of the Biot-Savart law, results as:

$$w_z = -\frac{\Gamma}{2\pi} b \frac{b^2+e^2}{R^2} \frac{\frac{(b^2+e^2)^2}{R^4}(y^2-e^2) + 2\frac{b^2+e^2}{R^2}e^2 - (b^2+e^2)}{\left[\frac{(b^2+e^2)^2}{R^4}(y^2+e^2) - 2\frac{b^2+e^2}{R^2}e^2 + b^2 + e^2\right]^2 - 4\frac{(b^2+e^2)^2}{R^4}y^2 b^2} \quad (1.5)$$

The effective angle of incidence on the wing will, therefore, be changed by the value $\varepsilon = -w_z/V$. Then since for any element of the wing we have $dD = \varepsilon\, dL$, the resultant effect of the body on the wing drag will follow as the result of an integration over the span. When the wing is located above or below the axis of the body, the result of the influence of the body is a small decrease in the wing drag. In such case, in fact, there will be an upward velocity in the middle of the wing caused by the vortex (image) in the interior of the body and as a consequence an increase in the angle of incidence. The largest value of the drag due to the influence of the body is found in the case where the body axis and the wing axis intersect, or otherwise for $e = 0$. This drag has the value

$$D = \frac{\varrho\, \Gamma^2}{4\pi} log\, \frac{(b+R)^4}{(b^2+R^2)^2} \tag{1.6}$$

From (1.1) and (1.2) the distribution of the circulation over the wing can be found in such manner as to give, for a stated value of the lift, the minimum value of the drag and especially for the case where the body axis and wing axis intersect. If, through the use of Stokes theorem, the surface integrals (1.1) and (1.2) be transformed into line integrals, we find

$$L = -\varrho\, V \int_{-b}^{+b} (\varphi_0 - \varphi_n)\, d\, y$$

Here $(\varphi_0 - \varphi_n)$ is the abrupt change in the potential between the upper and lower points on the body and vortex band section along a line $y = \text{const}$. This abrupt change along a vortex line of the vortex band is equal to the circulation Γ. The drag results in the form

$$D = -\frac{\varrho}{2} \int_K \varphi\, \frac{\partial\, \varphi}{\partial\, \nu}\, d\, s$$

The integration must be taken around the boundary K of the vortex band and body section, where also ν denotes the normal outward at the boundary K. Then at the body, we shall have $\partial\varphi/\partial\,\nu = 0$. If then n denotes the normal upward at the vortex band, $\partial\varphi/\partial\, n$ will remain the same for passage through the vortex band. Again remembering that by reason of the symmetry of the flow $\Gamma(y) = \Gamma(-y)$, the value of the drag becomes:

$$D = -\varrho \int_R^b \Gamma \frac{\partial\, \varphi}{\partial\, n}\, d\, y \tag{1.7}$$

The integral given above for the value of the lift can also be brought within the same field of integration. By the use of the images of the free vortices in the body, we may derive the condition that $\partial\varphi/\partial\,\nu$ vanishes at the body surface. If we put

$$\Gamma' = \frac{d\, \Gamma}{d\, y}$$

we shall have also, $$\Gamma(y) = \Gamma\left(\frac{R^2}{y}\right)$$

and $$\Gamma'(y) = -\Gamma'\left(\frac{R^2}{y}\right)$$

From (1.4) it follows that the element of lift develops from a horseshoe formed vortex of breadth $2y$ and circulation $d\Gamma$ and having the value

$$dL = 2\varrho V y\, d\Gamma\left(1 - \frac{R^2}{y^2}\right)$$

The lift is accordingly

$$L = -2\varrho V \int_R^b \Gamma'(y)\left(y - \frac{R^2}{y}\right) dy$$

Through integration by parts we find

$$L = 2\varrho V \int_R^b \Gamma(y)\left(1 + \frac{R^2}{y^2}\right) dy \tag{1.8}$$

A change $\delta\Gamma$ in the circulation will then give a change in the drag

$$\delta D = -2\varrho \int_R^b \delta\Gamma \frac{\partial\varphi}{\partial n} dy$$

and in the lift $$\delta L = 2\varrho V \int_R^b \delta\Gamma\left(1 + \frac{R^2}{y^2}\right) dy$$

The minimum value of the drag will then result, for any value of $\delta\Gamma$, if we make the condition $\delta D = \lambda\, \delta L$.

We must also have $$\frac{\partial\varphi}{\partial n} = -\lambda V\left(1 + \frac{R^2}{y^2}\right) \tag{1.9}$$

The flow corresponding to these conditions can be developed in the following manner.

A motion is determined which streams about the vortex band and the body and at a great distance has a constant velocity upward $c = \lambda V$. Then a flow about the body is superimposed, which at a great distance has a velocity c downward. The combined flows fulfill then the condition of (1.9). Such a field of flow will give, for any form of body cross-section a minimum value of the drag. In the preceding case where the body and wing axes intersect, and the body section is a circle, the field of flow about the body and vortex band results in such form that the outer surface region, outside the boundary of the body and vortex band section becomes conformally transferred into the region outside a circle. Here only the results of this method are given.

The distribution of the circulation over the wing area is

$$\frac{L'_T}{\varrho V} = \Gamma(y) = \Gamma_m \frac{b^2 + R^2}{b^2 - R^2}\sqrt{1 - \frac{b^2}{(b^2 + R^2)^2}\cdot\frac{(y^2 + R^2)^2}{y^2}} \tag{1.10}$$

The distribution of the lift over the width of the body follows in the form:

$$\frac{L'_R}{\varrho V} = \Gamma_m \frac{2b}{b^2 - R^2} \left[\sqrt{\frac{(b^2 + R^2)^2}{4b^2} - y^2} - \sqrt{R^2 - y^2} \right] \qquad (1.11)$$

In this formula, Γ_m is the circulation at the point of connection between the body and the wing. The distribution of the lift for various values of the ratio R/b is shown in Fig. 40.

The induced drag in relation to lift is furthermore given by the equation

$$D = \frac{1}{2} \frac{L^2}{\varrho V^2 \pi} \frac{b^2}{(b^2 - R^2)^2} \qquad (1.12)$$

The ratio of the body lift to the total lift, for various values of the value of b/R is given in the following Table. The figures in parenthesis give the corresponding values for the case of uniform distribution of circulation.

$\frac{b}{R} =$	2	4	6	8	10
$\frac{L_R}{L} =$	0.371 (0.333)	0.228 (0.200)	0.168 (0.143)	0.133 (0.111)	0.110 (0.091)

In connection with the overall lift and its distribution over the span, Lennertz has also carried through computations regarding the distribution of the lift along the length of the body.

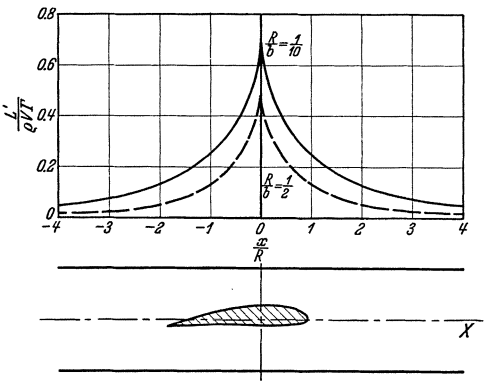

Fig. 41. Distribution of lift along cylindrical body.

The principal results only of this somewhat complicated computation will here be noted. In Fig. 41 is shown the distribution of the lift along the body for two different cases, for the ratio $R/b = 0.1$ with constant circulation over the span (full line) and for the ratio $R/b = 0.5$ with the distribution of the circulation in accordance with the requirement for minimum drag. For values of the ratio R/b between 0.0 and 0.1 there is found no sensible difference.

2. Theoretical Development for Short Bodies and Engine Nacelles. For the preceding theoretical development of the mutual influence of wing and body, use was made of a body of cylindrical form, circular section and of infinite length. In order now to free the discussion from this last assumption which limits the application of the resulting numerical values to very long airplane bodies, we shall now approach

the problem in a different manner which will give results applicable to airplane bodies of reduced length and in particular when applied to the case of engine nacelles built into the wing structure, will be able to furnish (as shown by actual experience) distinctly useful results.

The foundation of this method is found in the fact that the body (in particular a nacelle) may be viewed as a part of the wing and as such, is concerned also in the development of lift. The longitudinal sections through the body (sections given by vertical planes parallel to the axis of the body) are then to be considered as wing sections, of which the profile, angle of incidence and depth relative to the wing proper are variable. The problem then becomes one of finding the distribution of the lift for such a wing with variable section. This problem admits of solution by the use of the already established principles of wing theory.

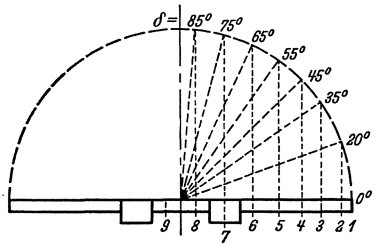

Fig. 42. Wing with two built-in nacelles.

It must first be assumed that the nearly plane flow in the neighborhood of the middle of the wing will not be disturbed by the presence of the body—that is, that the transverse component induced by the presence of the body may be neglected. For the wing, the span of which we again denote by $2\,b$, a rectangular plan form is assumed. The distance of any point of the span width from the center of the wing may be denoted by y. It is, moreover, convenient to relate the coordinate y with the angle δ through the relation, see Fig. 42.

$$y = b \cos \delta \tag{2.1}$$

The angle δ varies from 0 to π as y passes through all values from $+\,b$ to $-\,b$. In this manner each point of the span is, through the angle δ singly determined. Also let V = velocity and Γ the circulation about the wing. Then any desired distribution of the circulation over the span can be expressed in the form of a Fourier series

$$\Gamma = 4\,b\,V \sum_{n=1}^{\infty} A_n \sin n\,\delta \tag{2.2}$$

The unknown coefficients A_n must be so determined that they fulfil the conditions of wing theory. The most important of these conditions is that at each point of the span the geometrical angle of incidence α shall equal the sum of the effective angle α_e and the induced angle w/V, where w is the induced vertical velocity at that point on the wing.

We must then have:
$$\alpha = \alpha_e + \frac{w}{V} \tag{2.3}$$

But the induced vertical velocity is a function of the distribution of the circulation. At any given point x_0 it will stand, with the circulation, in the following relation:

$$w(x_0) = \frac{1}{4\pi} \int_{-b}^{+b} \frac{d\Gamma}{dx} \frac{dx}{x - x_0}$$

Now if we substitute for x in terms of the variable δ and for Γ put the expression in (2.2), the expression for the induced vertical velocity becomes

$$w(\delta_0) = \frac{V}{\pi} \int_0^{\pi} \frac{\Sigma n A_n \cos n\delta}{\cos\delta - \cos\delta_0} d\delta$$

The integration of the expression

$$J = \int_0^{\pi} \frac{\cos n\delta}{\cos\delta - \cos\delta_0} d\delta$$

has the principal value[1] $J = \pi \dfrac{\sin n\delta_0}{\sin\delta_0}$

This gives for the induced vertical velocity,

$$w(\delta_0) = V \Sigma n A_n \frac{\sin n\delta_0}{\sin\delta_0} \tag{2.4}$$

This expression must then be put into (2.3). However, before proceeding to this, it will be convenient to express the effective angle α_e in another form. We shall first note especially that the angle of incidence is always to be measured with reference to that attitude for which the lift vanishes. The lift coefficient C_L is then directly proportional to the effective angle as denoted by the equation

$$C_L = 2k\alpha_e \tag{2.5}$$

In this equation, k is a constant of which the value for very great span and for the usual form of section is not far from π (α_e is to be expressed in angular measure).

If then c denotes the wing chord, the value of the circulation can, by the Kutta-Joukowski formula, be expressed as

$$\Gamma = \frac{C_L}{2} V c$$

and by use of (2.5) and (2.2) there follows:

$$\alpha_e = \frac{\Gamma}{kVc} = \frac{4b}{kc} \sum_{n=1}^{\infty} A_n \sin n\delta$$

[1] GLAUERT, H., The Elements of Aerofoil and Airscrew Theory, p. 92.

If now this value of α_e and the value of w from (2.4) be inserted in the conditional equation (2.3), there results the following:

$$\Sigma A_n \sin n\,\delta\,(n\,\mu + \sin\delta) = \mu\,\alpha \sin\delta \tag{2.6}$$

where

$$\mu = \frac{k\,c}{4\,b}$$

The equation must hold for all values of δ between 0 and π. Aside from the coefficients A_n, all quantities in the equation are known. Practically the number of coefficients must be limited and because of the symmetry of the distribution of lift with reference to the mid point of the wing, only coefficients of odd order, A_1, A_3, $A_5 \ldots . A_i$ will enter. It thus results that the basic equation can be fulfilled only at i points of the span, δ_1, $\delta_3 \ldots . \delta_i$. If then we set up the basic equation for the angles δ_1, δ_2, $\ldots . \delta_i$, including an equal number of coefficients A_1, A_3, $\ldots . A_i$, there will result i linear equation with i unknowns from which the values of A_1, $A_3 \ldots . A_i$ may be found. Practical application to a specific case has shown that it is desirable to extend the basic equation to the end values $\delta = 0$ and $\delta = \pi$. If substitution for these values be made in this equation, there results for the wing ends

$$\Sigma\, n^2 A_n = \alpha$$

We have thus in fully written out form, the following system of equations for the determination of the coefficients $A_1 \ldots . A_i$.

$$\left.\begin{aligned}
&A_1 + 9\,A_3 + \ldots . + i^2 A_i = \alpha_1 \\
&A_1 \sin\delta_1\,(\mu + \sin\delta_1) + A_3 \sin 3\,\delta_1\,(3\,\mu + \sin\delta_1) \\
&\quad + \ldots . A_i \sin i\,\delta_1\,(i\,\mu + \sin\delta_1) = \mu\,\alpha_3 \sin\delta_1 \\
&\ldots\ldots\ldots\ldots\ldots\ldots\ldots\ldots\ldots\ldots\ldots\ldots \\
&A_1 \sin\delta_i\,(\mu + \sin\delta_i) + A_3 \sin 3\,\delta_i\,(3\,\mu + \sin\delta_i) \\
&\quad + \ldots . A_i \sin i\,\delta_i\,(i\,\mu + \sin\delta_i) = \mu\,\alpha_i \sin\delta_i
\end{aligned}\right\} \tag{2.7}$$

The solution of these equations then makes possible the determination of lift distribution for a wing of any plan form, with any distribution of profile and with any angle of incidence. The angle of incidence of the profile under consideration appears on the right hand side of (2.7) and the wing chord c is contained in the equation $\mu = k\,c/4\,b$. Furthermore this expression embodies a characteristic of the profile at the point considered, namely the magnitude

$$k = \left(\frac{d\,C_L}{d\,\alpha}\right)_{b=\infty}$$

It should also be noted that with a lift distribution symmetrical about the longitudinal axis of the plane it is only necessary to carry out the computations for one half of the wing.

In accordance with this method computations were carried out on a wing with two built in nacelles as shown in Fig. 42 while at the same time, in order to test the accuracy of the method, model tests in a wind

tunnel were carried out[1]. The points 1, 2. . . . 8 to which the basic equation was applied are also shown in the figure. The presence of a nacelle is represented by a single point only, No. 7. As a rough approximation it may be assumed that the breadth of the nacelle is determined between the mid points of the segments 6—7 and 7—8. We cannot hope that in this way an exact solution of the problem can be obtained, but to

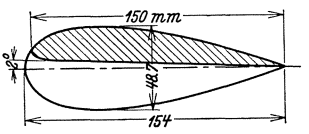

Fig. 43. Section of wing and nacelle.

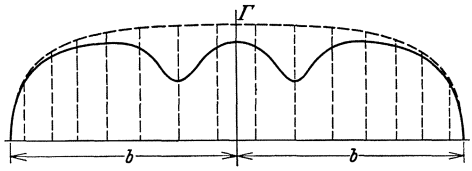

Fig. 44. Effect of nacelles on distribution of lift.

a good approximation the change in the lift distribution due to the nacelle will result. The cross sections of the wing and nacelle are shown in Fig. 43. The results of the computation, shown as the distribution of the lift along the span, are given in Fig. 44. It is thus seen that, through the presence of the nacelle, the lift distribution in the case assumed undergoes a marked change—in particular two zones of marked decrease at the points where the nacelles are located. This characteristic is in notable contrast with the distribution for the wing alone as indicated by the dotted line. The dimensions of the nacelle in this case were, on the whole, rather large in comparison with the wing and there resulted an unduly large measure of influence on the lift distribution. The departure of the lift distribution from that for the wing alone, causes also an additional induced drag, the magnitude of which, however, as the computation shows, is not of serious importance. In Fig. 45 is shown dotted the polar curve for the wing with two nacelles, deduced by theoretical means from the simple wing. The wind tunnel investigation gave the points indicated by the small circles and it is seen that the agreement between theory and experiment is quite good. Only in the

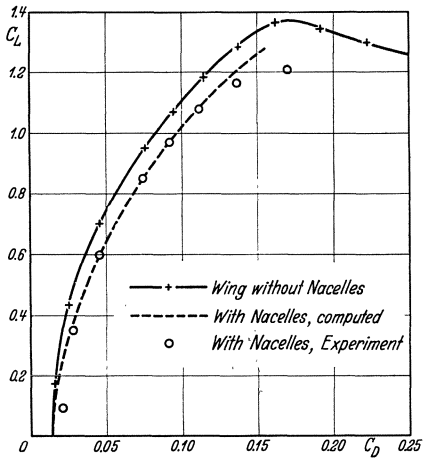

Fig. 45. Effect of nacelles on polar curve.

[1] WIESELSBERGER, C., Der Einfluß von eingebauten Motorgondeln auf die Luftkräfte eines Tragflügels. Paper No. 203 read before the Internat. Engineering Congress, Tokyo, 1929.

vicinity of the maximum lift is any marked difference to be noted. The same method can naturally be employed for an investigation of the influence of an airplane body on the lift distribution over the wing.

One disadvantage of the method is to be noted, in that the width of the body or of the nacelle is not definitely indicated. In the case employed for illustration, as already noted, the nacelle was represented only by the single point No. 7 (Fig. 42) and any change in the width, even an approach to points 6 or 8, would make no change in the results. Theoretically by an increase in the number of the points δ, the width of the nacelle may be limited more and more closely. This requires, however, an increase in the number of equations to be solved and in consequence an excessive increase in the numerical computations involved.

A method which does not have this objection and in which the basic equation is satisfied at all points of the span has been developed by S. B. Gates[1]. This method, in which the width of the body is exactly represented, leads likewise to a system of linear equations which admit of relatively ready solution.

Still another method in which the basic equation is also satisfied for all points of the span has recently been developed by I. Lotz[2]. This method may be viewed as an improvement of the one described above and is distinguished by the fact that the geometrical angle of incidence α and the wing chord c, both for any point y are developed in series. To this end we may put, for the angle $\alpha\,(y)$ multiplied by $\sin\delta$,

$$\alpha\,(y)\,\sin\delta = \Sigma\,\alpha_n\,\sin n\,\delta$$

and for the product of $c_0/c\,(y)$ by $\sin\delta$

$$\frac{c_0}{c\,(y)}\,\sin\delta = \Sigma\gamma_{2\nu}\,\cos\nu\,\delta$$

wherein c_0 denotes the chord of the wing at the point $y = 0$, and α_n, $\gamma_{2\nu}$ the generalized coefficients in the two developments. These coefficients are then determined by means of the given wing form. The carrying through of this development involves, in certain cases, considerable labor; it yields, however, a notable simplification in the later computations and leads to a system of equations, which, by the method of "iteration", may be readily solved.

3. Experimental Results. Regarding the influence of the airplane body on the wings, a large number of wind tunnel measurements have been made and from these it has appeared that through the presence of the body the drag of the wings is increased and in many cases at the same angle of incidence the lift is decreased. The increase of the drag comprises

[1] GATES, S. B., An Analysis of a Rectangular Monoplane with Hinged Tips, Br. A.R.C. R. and M. No. 1175, 1928-29.

[2] LOTZ, I., Berechnung der Auftriebsverteilung beliebig geformter Flügel. ZFM, 1931, p. 189.

in general two elements. The first element develops from the fact that by the presence of the body the flow about the wing is so changed that the profile drag of the wing is no longer the same. The second element arises from the change in the induced drag of the wing. This element develops from the fact that through the presence of the body the distribution of the lift along the wing undergoes a change and in consequence, as a general rule, the induced drag is increased.

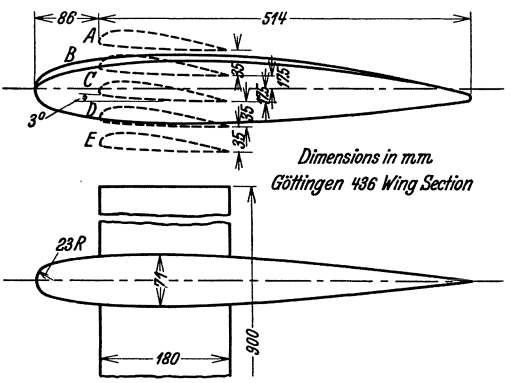

Fig. 46. Effect of wing position.

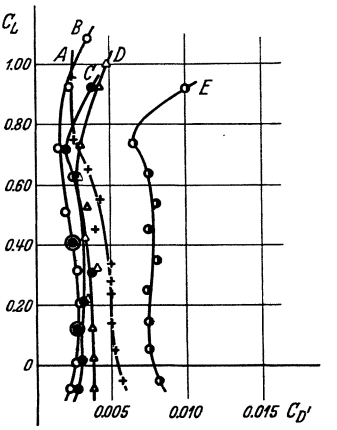

Fig. 47.

We may consider next the experimental results[1] which show the influence of change in the relative locations of wing and body. In connection with an airplane body form as shown in Fig. 46, a wing was fitted in five different locations as shown $A \ldots . E$, in each case with measurement of the polar curve. The coefficient C'_D for the difference in drag between the combination wing plus body and wing alone is shown in Fig. 47 plotted on values of the lift coefficient C_L. It is seen that the arrangements B and C give the smallest increase of drag, while the arrangement E in which the wing and body are separated by an opening, gives the greatest increase. A large number of researches with different forms of body and wings have been carried out by H. Muttray[2]. Among many other results of interest, these researches have shown that with a low wing plane with rounded body cross-section, a notable decrease in the resistance is realized when the wedge shaped space between body

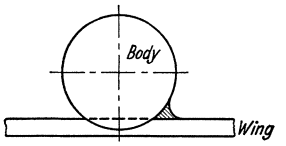

Fig. 48. Fillet between wing and body.

[1] Ergebnisse der Aerodynamischen Versuchsanstalt zu Göttingen, I. Lief., p. 118, 1925.

[2] Muttray, H., Untersuchungen über die Beeinflussung des Tragflügels eines Tiefdeckers durch den Rumpf. Luftfahrtforschung, Bd. 2, Heft 2, 1928.

and upper side of wing (Fig. 48 left) is filled in (Fig. 48 right) and in such manner that the filleting is more marked toward the following edge of the wing. M. N. Gough has also investigated full scale the influence of fillets between wing and body on drag and on propeller efficiency in the 20 ft. wind tunnel at Langley Field[1].

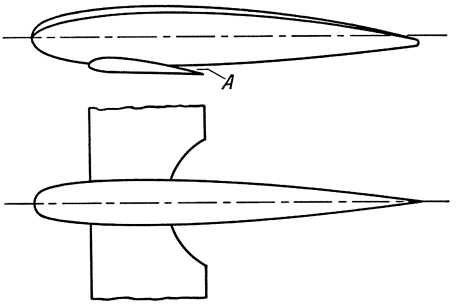

Fig. 49. Effect of wedge shaped space A.

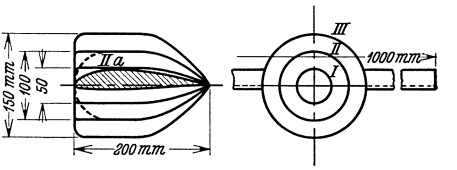

Fig. 50. Various forms of engine nacelles.

The plane was a high wing monoplane. The filleting was in consequence fitted on the pressure side of the wings and on this account only a small decrease in the drag was noted.

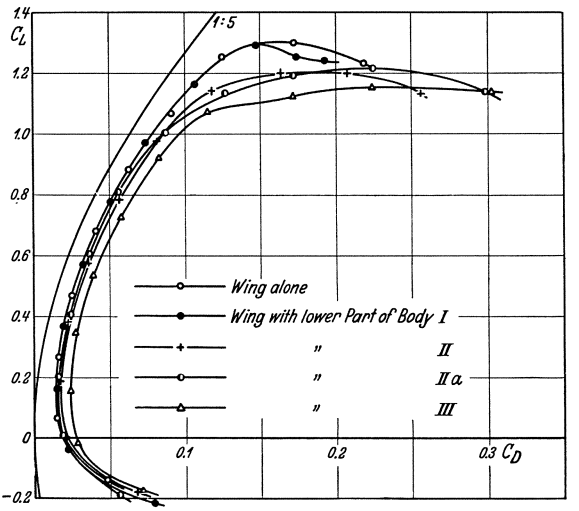

Fig. 51.

When the wing, as in Fig. 49, is so fitted to the under side of the body that between the suction side and the under side of the body, a wedge shaped space A is formed, a notable increase in the drag will

[1] Gough, M. N.: The Effect of Fillets Between Wings and Fuselage on the Drag and Propulsive Efficiency of an Airplane, U.S. N.A.C.A. Technical Note No. 299.

result. In such case, it is to be recommended that this space be eliminated by means of a section cut out from the wing, as indicated

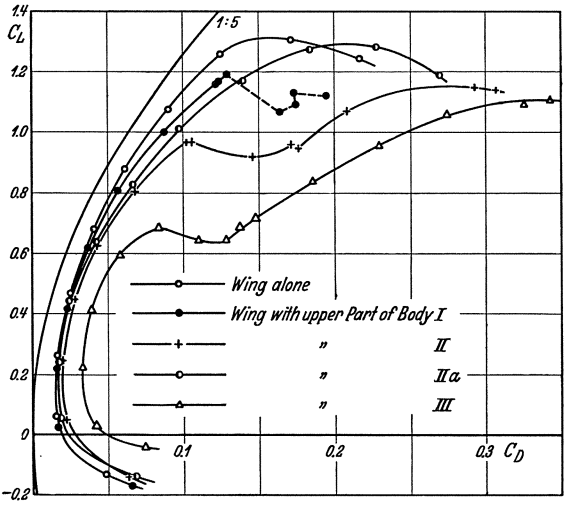

Fig. 52.

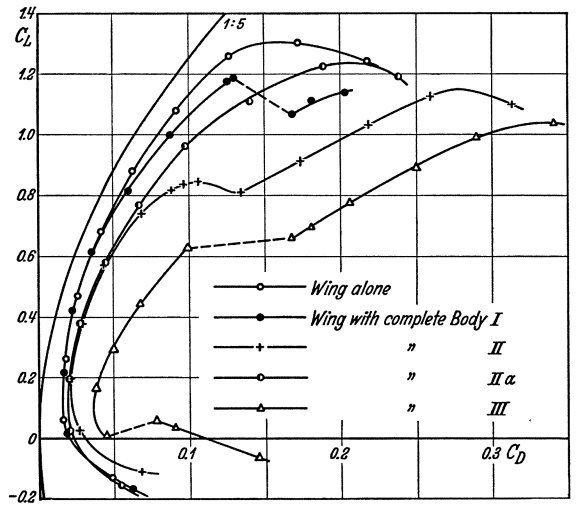

Fig. 53.

Figs. 51—53. Effect of engine nacelles on polar curve.

in the plan view of the sketch. The section cut out, however, should not be too large lest the aerodynamic characteristics of the wing be injuriously affected.

A series of researches also directed to a study of the influence of varying relative location of body and wing have been carried out by Shatswell Ober[1]. Here again, the minimum drag was found for the case where the wing was located directly on the upper side of the body (arrangement *A* of Fig. 46). Further it was shown that in the case of arrangement *B* (parasol type) the opening between wing and body can be filled in without causing thereby any marked change in the drag.

In similar fashion as by an airplane body, the airforces on the wings will be influenced by engine nacelles in the case of multimotored planes. Again here a distinction must be drawn between the case where the nacelles are built in as part of the wing structure or are separate therefrom and only connected by struts with the wings. A systematic series of researches with built-in nacelles has been carried out at the Göttingen Laboratories, the chief results of which may be indicated as follows.

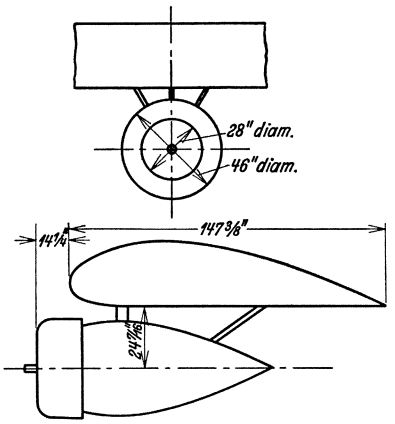

Fig. 54. Engine nacelle tested at Langley Field.

In connection with a wing of about 100 cm. span and 20 cm. chord, nacelles of circular cross-section and varying diameter were fitted (see Fig. 50). Measures were then taken of the polar curve for the three cases—upper half of the nacelle fitted to the wing, lower half fitted to the wing and finally the entire nacelle fitted to the wing. The results of these measurements are given in Figs. 51—53. It is seen that the arrangement in which the half nacelle is fitted on the suction side of the wing causes a very much greater increase of drag than when fitted on the pressure side. It is also seen that the form with rounded nose, II a, is notably better than that with flat nose of the same diameter when they are fitted on the suction side of the wing, because in this case the separation of flow on the upper forward edge of the nacelle does not occur.

A similar series of researches, in which arrangements were tested wherein the nacelle was separated from the wing and connected therewith by struts, has been carried out at Langley Field by E. N. Jacobs[2]. These researches were carried out in the variable density tunnel with a model as shown in Fig. 54, in which the wing had a span of 36 in.

[1] Ober, Shatswell, Some Studies on the Aerodynamic Effect of the Gap Between Airplane Wings and Fuselages, U.S. N.A.C.A. Technical Note No. 327.

[2] Jacobs, E. N., The Drag and Interference of a Nacelle in the Presence of a Wing. U.S. N.A.C.A. Technical Note No. 320.

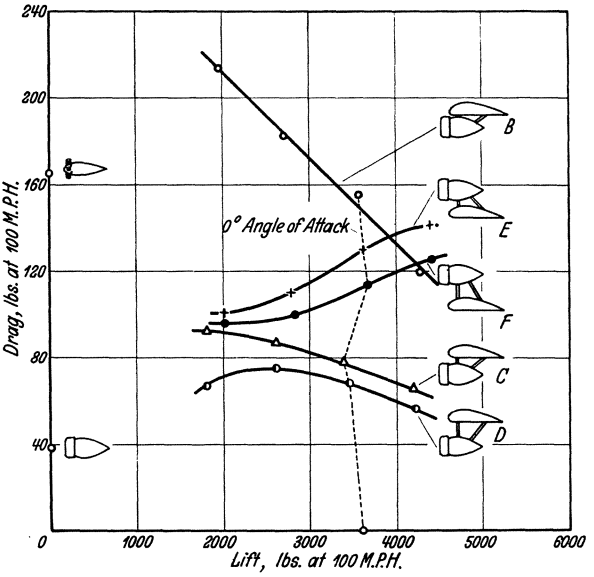

Fig. 55.

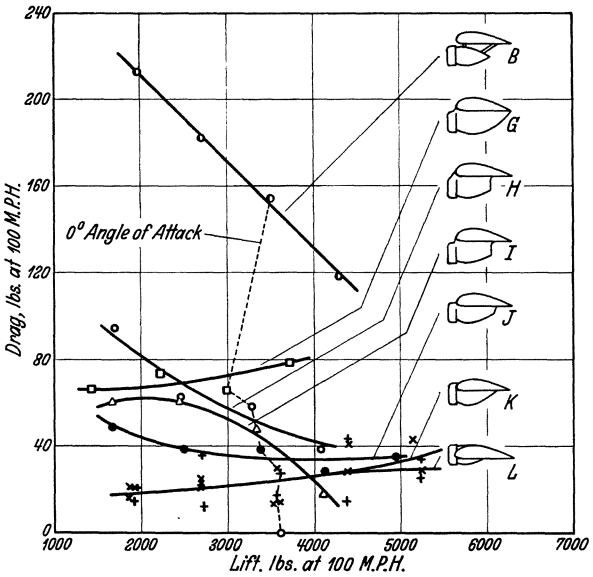

Fig. 56.

Figs. 55—56. Effect of engine nacelles on lift and drag.

Lift and drag were measured for several values of the angle of incidence. In the diagrams of Figs. 55 and 56, is shown, not the overall drag, but

the difference between the combination wing plus nacelle and wing alone, plotted on lift. Fig. 55 shows especially the influence of change in the relative position of wing and nacelle in the case where the two are completely separated. In the combinations of Fig. 56, wing and nacelle are joined in a single unit and there resulted, through a suitable union of the two forms, a most notable reduction in the increase of resistance chargeable to the nacelle (see Fig. 56) combinations *J*, *K*, *L*.

Bibliography.

In addition to the numerous references given throughout the text, the following references of a more general character may be of interest.

On fluid mechanics:

DRYDEN, MURNAGHAN, BATEMAN, Rep. of Committee on Hydrodynamics.

W. WIEN u. F. HARMS, Handbuch der Experimentalphysik, Band IV, Hydro- und Aerodynamik.

On Aeronautics (in general):

Bibliography of Aeronautics, U.S. National Advisory Committee for Aeronautics, Washington (annual volumes).

On Aerodynamics:

H. GLAUERT, The Elements of Airofoil and Airscrew Theory. Cambridge 1926.

PRANDTL-TIETJENS, Hydro- und Aeromechanik, Berlin 1931.

E. PISTOLESI, Aerodinamica, Torino 1932.

FUCHS, HOPF, SEEWALD, Aerodynamik, Berlin 1934.

DIVISION L

AIRPLANE PROPELLERS

By

H. Glauert,
Farnborough, England

EDITOR'S PREFACE

The earlier theories of the action of the screw propeller date back to the pioneer work of Rankine and Wm. Froude, the contributions of the latter continued and enlarged by R. E. Froude. These studies all related naturally to the screw propeller as applied to the problems of marine propulsion. However, there is, of course, no difference in basic theory between the propeller in its action on water and on air, and these earlier studies of Rankine and of the Froudes furnish a natural and logical historical starting point for a discussion of the theory of the screw propeller for aeronautic purposes.

The Author of the present Division, therefore, after some general introductory material in Chapter I, begins in Chapter II his treatment of the subject proper with a resumé of the Rankine-Froude axial momentum theory, leading to expressions for the ideal efficiency of a propeller as determined by the conditions of its operation. This is followed in Chapter III by a more generalized form of the momentum theory and in Chapter IV by a broader and more general discussion of propeller efficiency.

Then turning to more recent developments of the subject, Chapters V and VI are devoted respectively to a discussion of the blade element theory as developed especially by Drzewiecki, and of the vortex theory based on the developments in general airfoil theory due to Prandtl and his school during the past two decades. This is followed in Chapter VII by a discussion of propellers of the highest efficiency and of the conditions for realizing such values.

Then follows an important Chapter on body and wing interference, in which is presented a general discussion of the influence of the airplane body and wings on the performance characteristics of the propeller. This is followed in Chapter IX by a discussion of the experimental study of propellers, including reference to wind tunnel interference, scale effect and the influence of the compressibility of the medium.

In Chapter X is presented a general discussion of the theory of the helicopter screw, a field in which the pioneer work of the author will be remembered. This is followed in Chapter XI by a discussion of the theory of windmills and fans, with special reference to their aeronautic applications. The Division then closes in Chapter XII with brief discussions of certain special problems relating to the screw propeller, including with others, tandem propellers, the vortex ring state of the propeller, the effect of side-slip and pitching, and the effect of downwash behind a propeller.

The aeronautic world learned, with the most profound sorrow, of the tragic and untimely death by accident of the Author of the present Division on August 4, 1934. This sad loss to the cause of the advance of theoretical aerodynamics, to which he had been many years a most fruitful and brilliant contributor, has made necessary the preparation of this Preface by the general Editor instead of by the Author himself. Likewise the Division as printed has not had the benefit of a proof reading by the Author; but in this respect the Editor desires to acknowledge with special appreciation, the reading of the entire proof by the wife of the Author with the collaboration of Mr. R. McKinnon-Wood, for many years Head of the Aerodynamics Department at the Royal Aircraft Establishment, Farnborough, England, both of whom have been entirely familiar with the scientific work of the Author for many years. In addition it may be noted that, at the request of the Editor, the Author had, shortly before the manuscript was sent to the printer, re-read, with a few minor changes, his own copy of the work prepared somewhat earlier. The Editor believes, therefore, that the Division in its present form represents, in all important aspects, the development of this subject as it would have been left by the Author had he had an opportunity for a last revision in the Proof.

W. F. Durand.

CHAPTER I

AIRSCREW THEORY

1. Introduction. The propulsion of an aircraft is usually achieved by means of one or more propellers whose thrust overcomes the drag of the wings and structure in horizontal flight and also provides the additional force necessary to balance the component of the weight when the aircraft is climbing along a flight path inclined to the horizontal. The motion of the propeller through the air is composed of the angular velocity Ω of the blades about the axis of the propeller and of the forward speed V of the aircraft which is approximately in the direction of this axis. The aerodynamic reaction on the blades of the propeller gives a forward thrust T along the axis of rotation and a moment Q about it. The moment must be balanced by the torque of the engine

which drives the propeller, and the thrust provides the necessary force to propel the aircraft through the air. Since the power given by the engine and absorbed by the propeller is ΩQ and since the useful work done by the thrust is $V T$, the efficiency of propulsion is

$$\eta = \frac{V T}{\Omega Q} \tag{1.1}$$

A propeller is only one form of a more general class to which the term *airscrew* may be applied. An airscrew may be defined as any type of mechanism with radial blades designed to rotate about its axis during its motion relative to the air, and such airscrews may be used for a variety of purposes. The principal types of airscrew are:

(1) *Propeller.* An airscrew used for propulsion and designed to give a high thrust power $V T$ for a given torque power ΩQ.

(2) *Windmill.* An airscrew used to absorb power from its axial motion relative to the air. It is necessary to distinguish between a windmill mounted on an airplane where the drag is of importance and the axial velocity is high, and a windmill mounted on the ground where the drag is unimportant and the axial velocity is low.

(3) *Fan.* An airscrew used to give a current of air.

(4) *Anemometer.* An airscrew used to determine the relative axial velocity by measurement of the rate of rotation.

These types of airscrew all operate normally with their axes pointing in the direction of motion through the air. The propeller of an airplane, however, is fixed in position and its axis will coincide with the direction of motion at one angle of incidence only of the airplane: at other angles of incidence the relative velocity is inclined at a small angle to the axis of the propeller, and a complete account of propeller theory must therefore include the effect of such small inclinations on the characteristics of the propeller. Moreover there are types of airscrew which do not normally move through the air in the direction of their axes. These comprise the *helicopter*, which is an airscrew driven by an engine and used for sustentation, and the *autogyro* which is a freely rotating airscrew used for the same purpose. Even the cup anemometer, as used by meteorologists to determine the velocity of the wind, may be regarded as a special type of airscrew, and it may be noted that the cup anemometer has occasionally been used on an airplane as a source of power instead of a conventional windmill.

In the development of the general theory of the airscrew it is convenient to concentrate mainly on the propulsive airscrew or propeller. The theory of an airscrew follows the same lines, whatever the purpose for which it is intended, and it is proposed therefore to develop the theory of the propeller in detail and then to consider the modifications necessary for the special operating conditions of the other types of airscrew.

A propeller normally consists of a number of equally spaced identical radial blades which are maintained in uniform rotation about the axis of the propeller by the torque of the engine. The section of each blade at any radial distance has the form of an airfoil section, and each element of a blade in its motion through the air experiences the lift and drag appropriate to the airfoil section. These lift and drag forces combine to form the thrust and torque which are respectively the resultant axial force and moment experienced by the propeller. The reaction of these forces on the air produces a *slipstream* comprising all the air which has passed through the circle swept by the rotating blades of the propeller and whose motion has been modified by the reaction of the thrust and torque. In fact the thrust of the propeller is obtained by imparting a backward linear momentum to the air of the slipstream, and similarly the torque is obtained by imparting a rotational motion to the slipstream. The direct action of the thrust, however, is to give an increased pressure to the air immediately behind the disc of the propeller and a reduced pressure in front of it: the air is therefore sucked towards the front of the propeller and driven away from the back of it by the pressure system maintained by the rotating blades. The maximum axial velocity is attained only at some distance behind the propeller, but some increase of axial velocity occurs in front of the propeller. Owing to the gradual increase of the axial velocity, the slipstream contracts as it passes backward from the propeller and the type of flow can be represented diagramatically as in Fig. 1. In this figure PP represents the disc of the propeller, PS is the boundary of the contracting slipstream in which the air also has a rotational motion about the axis, and AP is the boundary of the column of air which is approaching the disc of the propeller.

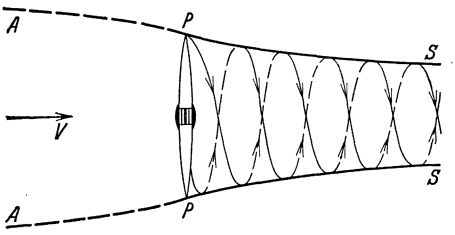

Fig. 1.

The diagram of Fig. 1 represents the normal operating condition of a propeller but other types of flow can be obtained by changing the velocity V with which the propeller is advancing through the general mass of air. The complete cycle of states of operation of an airscrew[1] is illustrated in Fig. 2, where the airscrew is assumed to be at rest in a stream of air of velocity V. The front of the airscrew is to the left and (*b*) represents the normal type of operation as a propeller. As the

[1] The first discussion of the complete cycle appears to be due to G. DE BOTHEZAT, U.S. N.A.C.A. Technical Report No. 29, 1919.

velocity of the stream increases, the thrust of the airscrew decreases and ultimately becomes a drag: the slipstream is then of the type (*a*), expanding behind the airscrew, and the airscrew acts first as a brake and then as a windmill. Type (*c*) represents the flow for zero velocity, which is the limiting condition of the normal type (*b*), but a different type of motion occurs when the stream is directed on the back of the airscrew, a vortex ring being formed as shown by type (*d*). As the velocity V increases, the flow changes to type (*e*) and then to type (*f*):

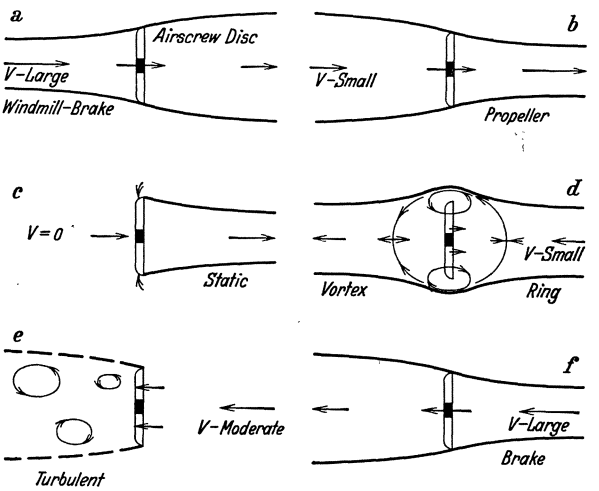

Fig. 2.

the former represents the condition when the airscrew gives rise to a turbulent wake and the latter represents a return to the initial type (*a*) but in the opposite direction. The type of flow in the vortex ring state has been investigated experimentally by C. N. H. Lock[1] by means of light streamers and the succession of types of flow illustrated in Fig. 2 is fully confirmed by these experiments.

2. Non-Dimensional Coefficients. The thrust T and the torque Q of an airscrew can be expressed as functions of the axial velocity V, the number of revolutions in unit time n, and the diameter D; and the state of operation of the airscrew is defined by the advance per revolution V/n. It is preferable, however, to express the characteristics of an airscrew in a non-dimensional form. The state of operation is therefore defined by the *advance-diameter ratio*

$$J = \frac{V}{n\,D} \tag{2.1}$$

[1] Br. A.R.C. R. and M. 1167, 1928.

and the thrust and torque are represented by the non-dimensional coefficients

$$\left.\begin{aligned} C_T &= \frac{T}{\varrho\, n^2\, D^4} \\ C_Q &= \frac{Q}{\varrho\, n^2\, D^5} \end{aligned}\right\} \tag{2.2}$$

where ϱ is the density of the fluid. At times it is useful to replace the torque Q by the power P absorbed by the airscrew, and the corresponding non-dimensional coefficient is $C_P = \dfrac{P}{\varrho\, n^3\, D^5}$ (2.3)

Since the power P is equal to $2\pi n Q$, the power and torque coefficients are related by the equation

$$C_P = 2\pi C_Q.$$

Finally the efficiency of the airscrew is

$$\eta = \frac{V\,T}{P} = J\,\frac{C_T}{C_P} \tag{2.4}$$

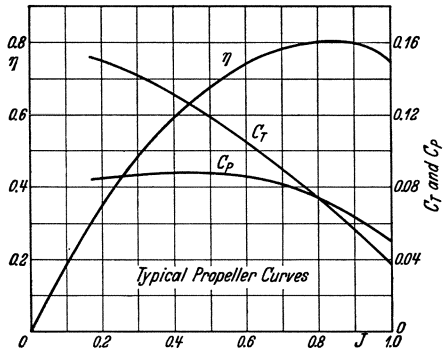

Fig. 3.

The preceding set of standard non-dimensional coefficients retains the same values whatever system of units is used to measure the individual quantities involved, but it is necessary to use a consistent system of units. Thus, for example, if the conventional engineering units are used, measuring the thrust in pounds, the diameter in feet, and the time in seconds, then the velocity must be expressed in feet per second, the power in foot-pounds per second, and the density in *slugs*[1] per cubic foot. A set of typical curves of thrust coefficient C_T, power coefficient C_P, and efficiency η against the advance-diameter ratio J are shown in Fig. 3.

Many other forms of non-dimensional coefficients have been used by different authors, involving the use of the angular velocity Ω instead of n, of the forward speed V instead of $n\,D$, and of the disc area $\pi\,D^2/4$ instead of D^2. The standard set of non-dimensional coefficients, as defined above, represents the system which has been found by experience to be most suitable for the application of propeller characteristics to aerodynamic calculations, but for the development of the theory it is preferable to use the following system:

$$\left.\begin{aligned} \lambda &= \frac{V}{\Omega R} \\ T_c &= \frac{T}{\pi R^2\, \varrho\, \Omega^2 R^2} \\ Q_c &= \frac{Q}{\pi R^2\, \varrho\, \Omega^2 R^3} = \frac{P}{\pi R^2\, \varrho\, \Omega^3 R^3} \end{aligned}\right\} \tag{2.5}$$

[1] The slug is the unit of mass on which a force of one pound causes an acceleration of one foot per second per second.

where Ω is the angular velocity of the propeller and R is its radius, so that ΩR is the rotational velocity of the tips of the propeller blades. In this system λ is the ratio of the forward speed V to the tip speed ΩR, which may be called the *speed ratio* of the propeller, and the torque and power coefficients are identical. Also the efficiency of the propeller becomes

$$\eta = \frac{\lambda T_c}{Q_c} \tag{2.6}$$

This system of non-dimensional coefficients will be used in the development of the theory, and all results will be given in terms of these coefficients. Conversion to the standard system of non-dimensional coefficients can easily be made by means of the relationships:

$$\left.\begin{aligned} J &= \pi\lambda = 3.14\,\lambda \\ C_T &= \frac{\pi^3}{4} T_c = 7.75\, T_c \\ C_Q &= \frac{\pi^3}{8} Q_c = 3.88\, Q_c \\ C_P &= \frac{\pi^4}{4} Q_c = 24.35\, Q_c \end{aligned}\right\} \tag{2.7}$$

In the discussion of these non-dimensional coefficients it has been assumed that the characteristics of a given propeller are functions of the single parameter J or λ, but the application of dimensional analysis[1] to the problem of the propeller shows that they may also depend on the Reynold's number of the motion and on the ratio of the tip speed to the velocity of sound. The Reynold's number represents the effect of the size or speed of the propeller in relation to the viscosity of the fluid in which it operates, and may be taken to be $\lambda R^2/\nu$, where ν is the kinematic coefficient of viscosity. Experience shows that the "*scale effect*" on propellers is not important in the normal states of operation, but it may become noticeable when the blades of the propeller are operating near their critical angles or when the thrust is very small. The other parameter, the ratio of the tip speed ΩR to the velocity of sound, represents the effect of the compressibility of the air on the characteristics of the propeller: this effect is unimportant with slow running propellers, but becomes increasingly important as the tip speed approaches the velocity of sound. Theory is not yet capable of dealing adequately with the effects of these two parameters and it is necessary to rely almost entirely on the results of special experimental investigations to assess their importance.

3. Airscrew Design. In defining the non-dimensional coefficients which represent the performance of an airscrew, the only geometrical constant used in the formulae was the diameter D or the radius R, but in order to describe an airscrew more fully it is necessary to specify

[1] Divisions A IV and H I 3.

also the number, B, of the blades and their geometrical shape. Apart from tilt or sweep-back of the blade as a whole, a blade can be described by considering in turn:

(1) The shape of the airfoil section at any radial distance r from the axis and its variation along the blade;

(2) The plan form of the blade, or the variation of the chord of the airfoil sections along the blade;

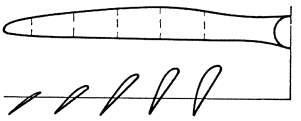

Fig. 4.

(3) The blade angles, or the inclination of the airfoil sections to the plane of rotation of the airscrew.

The airfoil sections used in airscrew design tend to be thicker than those used for airplane wings and there has been a tendency to use airfoil sections with a flat undersurface. The airfoil section is usually thinnest near the tip of the blade and increases steadily in thickness towards the root of the blade where it merges into the boss of the airscrew. A typical series of airfoil sections for an airscrew blade is shown in Fig. 4, which represents the blade of an airscrew of conventional design. In recent metal airscrews the thickness of the blades tends to be reduced but the airfoil sections remain of the same general type.

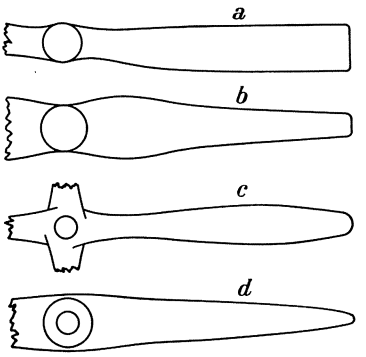

Fig. 5.

The plan form of the blade has varied widely during the development of aviation and a few typical forms are shown in Fig. 5. The first of these forms is an old type of blade with constant chord over the principal part of the blade; the second is a blade form proposed by N. E. Joukowski, and the last two are modern forms of wooden and metal propellers respectively. Experience indicates that the plan form, unless of a very peculiar design, exerts only a small influence on the characteristics of an airscrew, and the form is usually determined from structural rather than from aerodynamic considerations. Often it is not necessary to consider the exact plan form of the blade, but it is sufficient to specify merely the total blade area. It is then convenient to define the *solidity* σ of the airscrew as the ratio of the total blade area to that of the circular disc swept by the blades.

The angles at which the blade sections are set to the plane of rotation determine the *pitch* of the airscrew. If the blade section were simply a straight line set at an angle θ to the plane of rotation and the motion of the airscrew were that of a screw in a rigid medium, the blade section

would advance a distance $2\pi r \tan\theta$ during each revolution of the airscrew and this length would be the pitch of the section. In order to obtain a constant pitch H along the whole blade, the variation of blade angle θ must be adjusted according to the equation

$$2\pi r \tan\theta = H \quad \text{or} \quad \tan\theta = H/2\pi r \tag{3.1}$$

The blade angle is therefore smallest at the tip of the blade and increases steadily towards the root as indicated in Fig. 6.

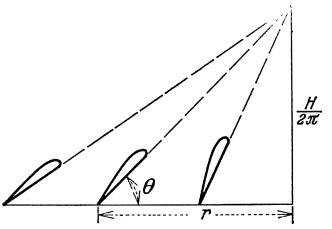

Fig. 6.

In an airscrew the blade angle θ is usually specified as the angle which the tangent to the lower surface of the airfoil section makes with the plane of rotation, and if the angles so defined vary along the blade in accordance with (3.1), the airscrew is said to have a constant geometrical pitch H. Often, however, the variation of angle along the blade does not obey the law of (3.1) and the geometrical pitch is then defined arbitrarily as the pitch of one special blade section (usually taken at $r = 0.7\ R$). The geometrical pitch

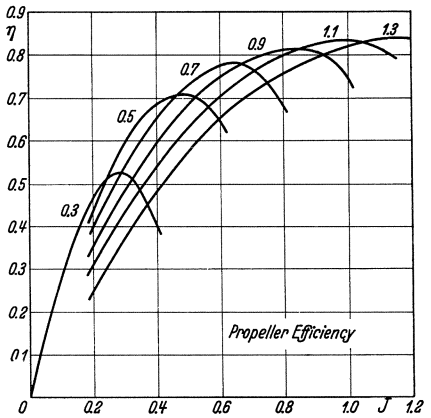

Fig. 7.

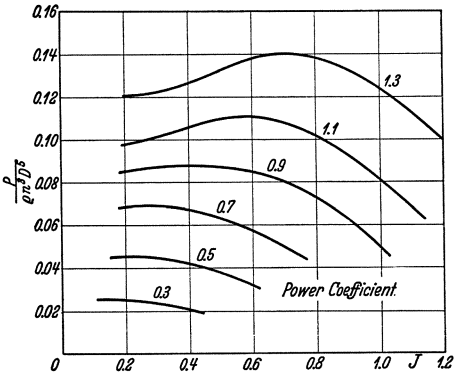

Fig. 8.

or its ratio to the diameter of the airscrew is a useful parameter for defining the members of a family of airscrews in which the blade angles are increased in some systematic manner, but in itself it has no aerodynamic significance. It would perhaps be more significant if it were based on the no lift axes of the airfoil sections instead of their tangent chords. The important aerodynamic feature is the advance per revolution at which the thrust of the airscrew becomes zero, and this advance per revolution is called the *experimental mean pitch* of the airscrew. Typical curves of efficiency and power coefficient for a family of airscrews with increasing pitch are shown in Figs. 7 and 8, the

numbers on the successive curves being the values of the geometrical pitch-diameter ratio H/D.

In general terms the form of an airscrew may be defined by specifying the number of blades, the solidity, and the pitch-diameter ratio; and for many purposes this description suffices. For more exact analysis it is necessary to specify also the shapes of the blade sections used along the blade, the plan form of the blade, and the variation of the blade angle.

4. The Development of Airscrew Theory. Though differing so much in appearance and construction, the airscrew and the marine propeller are fundamentally identical in their modes of operation, and in consequence the early stages of the development of airscrew theory must be sought in the history of ship propulsion. From an early period the development of the theory followed two independent lines of thought, which may conveniently be called the *momentum* theory and the *blade element* theory respectively.

In the momentum theory attention is directed mainly to the motion of the fluid, and the forces acting on the propeller are determined as those necessary to impart this motion to the fluid. The momentum theory was initiated by W. J. M. Rankine[1] in 1865 and was further developed by R. E. Froude[2]. It still forms a sound basis for estimating the ideal efficiency of a propeller, which is the extreme upper limit that could be obtained by the best propeller under the given conditions of operation. An important feature of the momentum theory is the conclusion that the axial velocity u of the fluid through the disc of the propeller is higher than the speed V with which the propeller is advancing through the fluid, and is in fact the arithmetic mean of the speed V and the increased axial velocity in the slipstream far behind the propeller. An extended form of the momentum theory, including the effects of the rotational motion of the slipstream, has been developed by A. Betz[3]. The momentum theory can also be extended to include the effects of the frictional drag of the propeller blades and of the interference of the body or ship on which the screw is mounted, and an estimate of these effects was included in Rankine's original paper. The defect of the momentum theory is that it gives no indication of the shape of propeller required to produce the reactions considered.

The principle of the blade element theory is to consider the forces experienced by the blades of the propeller in their motion through the fluid, and this theory is therefore intimately concerned with the geometrical shape of the propeller. The theory was initiated in a rather crude form by W. Froude[4] in 1878, but it owes its development mainly

[1] Transactions Institute of Naval Architects, Vol. 6, p. 13, 1865.
[2] Ibidem, Vol. 30, p. 390, 1889.
[3] Zeitschr. f. Flugtechnik u. Motorl. **11**, 105, 1920.
[4] Transactions Institute of Naval Architects, Vol. 19, p. 47, 1878.

to the work of S. Drzewiecki[1] and finds its complete expression in his book "Théorie générale de l'hélice" (Paris, 1920). The basis of the analysis is that the blade of the propeller is divided into a large number of elements along the radius and that each of these elements is regarded as a small airfoil moving with a velocity determined by the constant axial velocity V of the propeller and the rotational velocity Ωr, which varies from element to element along the blade. The unsatisfactory feature of this theory is the uncertainty as to the characteristics which must be assumed for the airfoil sections. In the early stages of the theory it was not perhaps realized that the characteristics of an airfoil vary with its aspect ratio, but with increasing knowledge of the behavior of airfoils and with more accurate experimental results, it became evident that it was not sufficiently accurate to assume some rather arbitrary aspect ratio for the blade elements. The question of interference between the adjacent blades of a propeller also arose, and to resolve all these uncertainties Drzewiecki proposed to derive his airfoil characteristics by analysing the observed performance of a special series of propellers. The blade element theory of a propeller was also developed by F. W. Lanchester[2] in association with his theory of the airfoil, and he endeavored to represent the mutual interference of the blades of a propeller by the analogy of an infinite staggered series or cascade of airfoils.

Apart from the incomplete solution offered by the momentum theory and the uncertainties involved in the blade element theory, there was one important point in which the theories appeared to be irreconcilable. The momentum theory determined an upper limit to the efficiency of a propeller, depending only on the thrust per unit disc area at a given speed of advance, but the blade element theory suggested that the efficiency of any propeller would tend to unity as the drag of the blades tended to zero. Also the blade element theory, using airfoil characteristics corresponding to a moderate aspect ratio, was found to represent the observed behavior of a propeller correctly in general form, but failed to give accurate numerical results. Drzewiecki hoped to overcome this difficulty by deducing his airfoil characteristics from tests of special propellers; but in Germany and England an attempt was made to modify the blade element theory by incorporating in it the conception, indicated by the momentum theory, of an increased axial velocity through the disc of the propeller. This increased axial velocity was used instead of the speed of advance of the propeller to estimate the force experienced by any blade element, and the effect of this modification was to decrease the effective angle of incidence at which the blade element operated. In Germany the effective axial velocity experienced by the blade element was taken to be the velocity determined

[1] Bulletin del'Association Technique Maritime, 1892 *et seq.*

[2] Aerodynamics; London, 1907.

by the momentum theory, and in his statement of the theory A. Betz[1] remarks that the appropriate aspect ratio for determining the lift and drag coefficients of the blade element is higher than that of an ordinary wing, tending to infinite aspect ratio but depending also on the shape of the blade: to resolve the uncertainty it is necessary to rely on experimental results. In England, on the other hand, the airfoil characteristics were still chosen to correspond to a moderate aspect ratio (usually 6), and the inflow theory of A. Fage and H. E. Collins[2] was based on an empirical estimate of the axial velocity: this theory was given in a more complete form, including also a rotational inflow velocity, by L. Bairstow[3]. The propeller theory of G. de Bothezat[4] is also in effect another statement of this inflow theory, using axial and rotational inflow velocities estimated in accordance with the momentum theory, but since he did not proceed to the conception of using airfoil characteristics corresponding to infinite aspect ratio, de Bothezat too was compelled to advocate tests of a special series of propellers to determine these characteristics.

In order to avoid the empiricism of the inflow theory, R. McK. Wood and H. Glauert[5] tried to develop a propeller theory on the conception, originally propounded by Lanchester, that the mutual interference of the propeller blades was analogous to that of a staggered cascade of airfoils; but this theory also suffered from an inadequate appreciation of the importance of aspect ratio in determining the characteristics of an airfoil or series of airfoils.

Modern airscrew theory, which reconciles and explains the discordances of the old momentum and blade element theories, rests fundamentally on the conception that the lift of an airfoil is due to a circulation of the flow around its contour. As a logical consequence of this conception, free vortices must spring from the blades of a rotating propeller and pass down stream in approximately helical paths, and it is these vortices which constitute the slipstream of the propeller. This conception of the mode of operation of a propeller was propounded by Lanchester[6], and is confirmed experimentally by Flamm's photographs[7] of the wake of a marine screw. The induced velocity due to this system of trailing vortices was investigated by N. E. Joukowski[8], but owing to the complexity of the analysis he was obliged to pass to the simplifying

[1] Zeitschr. f. Flugtechnik u. Motorl. **6**, 97, 1915.
[2] Br. A.R.C. R. and M. 328, 1917.
[3] Applied Aerodynamics; London, 1919.
[4] U.S. N.A.C.A. Technical Report No. 29, 1919.
[5] Br. A.R.C. R. and M. 620, 1918.
[6] *loc. cit.*
[7] Die Schiffschraube; Berlin, 1909.
[8] Soc. Math. Moscou, 1912; reprinted in "Théorie Tourbillonnaire de l'hélice Propulsive"; Paris 1929.

assumption of an infinite number of blades. The theory then reverts to the form of the inflow theory, using axial and rotational inflow velocities in accordance with the momentum theory but based in fact on the more reliable conception of the vortex system of the slipstream. Joukowski also proposed to employ airfoil characteristics obtained for a suitable cascade of airfoils of infinite aspect ratio, and his theory, as finally developed in 1918, is therefore in full agreement with modern airfoil and airscrew theory.

The vortex system of the slipstream was analyzed in detail by A. Betz[1] in 1919, and by assuming a lightly loaded frictionless airscrew he succeeded in establishing the system which would give the minimum loss of energy; assuming also a large number of blades, the analysis determined the best distribution of thrust along the blade. In an appendix to this paper L. Prandtl gave an approximate correction to the thrust distribution curve to represent the effect of a small number of blades, and recently S. Goldstein[2] has given a more accurate solution of this problem. More generally, however, the vortex theory of airscrews has been developed on the assumption that the number of blades is large and that the periodicity of flow associated with a small number of blades may be neglected. General airscrew theories, based on the fundamental conceptions of the vortex theory and on Prandtl's airfoil theory, have been developed by H. Glauert[3], E. Pistolesi[4], and S. Kawada[5] and the optimum distribution of thrust along the blade, as modified by the profile drag of the blade elements, has been determined by H. B. Helmbold[6], and by Th. Bienen and Th. von Kármán[7]. The important features of these developments are that, by applying the conception of induced velocity derived from Prandtl's airfoil theory, the inflow velocities at the airscrew disc have been established on a more reliable basis than was possible in the old inflow theory, and that the airfoil characteristics to be used in association with these velocities are the characteristics corresponding to an airfoil of infinite aspect ratio.

Apart from the development of the general theory, attention has constantly been devoted to the special problems associated with helicopters, windmills, tandem propellers, and the mutual interference between propeller and airplane. The analysis of these problems has not, however, modified the course of development of the general theory, but has rather followed in its wake, each successive advance in the general theory leading to a more adequate analysis of the specialized problems.

[1] Göttinger Nachr. 1919, p. 193.
[2] Roy. Soc. Proc. (A) **123**, 440, 1929.
[3] Br. A.R.C. R. and M. 786 and 869, 1922.
[4] Vorträge aus dem Gebiete der Hydro- und Aerodynamik, Innsbruck, 1922.
[5] Tokyo Imperial University, Aero. Res. Inst., No. 14, 1926.
[6] Zeitschr. f. Flugtechnik u. Motorl. **15**, 150, 1924.
[7] Zeitschr. V.D.I. **68**, 1237, 1924.

CHAPTER II

THE AXIAL MOMENTUM THEORY

1. The Rankine-Froude Theory. The function of a propeller or of any similar propulsive system is to give a forward thrust along its axis, and this thrust is obtained by imparting a backward motion to the fluid in which it operates. The production of the thrust is therefore inevitably associated with a certain loss of energy which is represented by the kinetic energy of the motion of the fluid. Additional sources of loss of energy are the rotational motion imparted to the fluid by the torque of the propeller and the frictional drag of the propeller blades in their motion through the fluid. In a first estimate of the behavior of a propeller, however, it is convenient to ignore these additional sources of loss of energy and to develop a theory for an ideal propeller which operates without any frictional drag on the blades and without any rotational motion in the slipstream. Also in this first estimate the thrust of the propeller will be assumed to be uniformly distributed over the circular disc swept by the blades of the propeller.

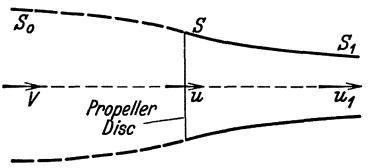

Fig. 9.

Consider a propeller of disc area S advancing through the air with the velocity V along its axis of rotation. Let P be the power required to drive the propeller and let T be the thrust along its axis, so that the useful work done by the propeller is VT and the efficiency of propulsion is

$$\eta = \frac{VT}{P} \tag{1.1}$$

By the principle of relative motion, the reaction between the propeller and the air is the same as if the propeller were rotating at a fixed point in a stream of velocity V directed along its axis, and it is convenient to consider the motion in this alternative form. Due to the reaction of the thrust on the air, a slipstream of increased axial velocity is formed behind the propeller and the general nature of the axial flow is of the form shown in Fig. 9. Let u_1 be the axial velocity in the ultimate wake, where the pressure of the air has regained its original value, and let S_1 be the cross-sectional area of the wake. Then if ϱ is the density of the air, the mass flow in unit time in the slipstream is $S_1 \varrho u_1$ and, by equating the thrust of the propeller to the increase of axial momentum in unit time,

$$T = S_1 \varrho u_1 (u_1 - V) \tag{1.2}$$

Also, since the propeller has been assumed to be at rest, the thrust does no useful work and the power P absorbed by the propeller must be equal to the increase of the kinetic energy of the slipstream in unit time, or

$$P = \frac{1}{2} S_1 \varrho u_1 (u_1^2 - V^2) \tag{1.3}$$

Alternatively, if the air is assumed to be at rest while the propeller advances with the axial velocity V, the useful work done by the thrust is VT and the kinetic energy imparted to the slipstream in unit time is

$$E = \frac{1}{2} S_1 \varrho u_1 (u_1 - V)^2 \tag{1.4}$$

since the mass flow in unit time is $S_1 \varrho u_1$ and the velocity imparted to the slipstream is $(u_1 - V)$. On this basis the power absorbed by the propeller is

$$P = V T + E \tag{1.5}$$

and it can easily be verified that this expression is consistent with the previous equations. Finally the efficiency of propulsion is:

$$\eta = \frac{V T}{P} = \frac{2 V}{u_1 + V} \tag{1.6}$$

The preceding results are all expressed in terms of the dimensions and axial velocity of the ultimate wake behind the propeller, but if u is the axial velocity through the propeller disc the condition of continuity of flow requires that

$$S u = S_1 u_1 \tag{1.7}$$

Also, regarding the propeller as at rest in a stream of velocity V, the work done on the air by the thrust of the propeller is $u T$ in unit time, and this work must be equal to the power P absorbed by the propeller and to the kinetic energy imparted to the slipstream in unit time. But from (1.2) and (1.3)

$$P = \frac{1}{2} (u_1 + V) T = u T$$

and hence

$$u = \frac{1}{2} (u_1 + V) \tag{1.8}$$

showing that the axial velocity at the propeller disc is the arithmetic mean of the axial velocity V and the slipstream velocity u_1. Also the efficiency of the propeller may now be expressed as

$$\eta = \frac{V}{u} \tag{1.9}$$

The conclusion that half the ultimate increase in the axial velocity has been attained when the air passes through the propeller disc may be derived in an alternative manner by a suitable application of Bernoulli's equation. Far in front of the propeller all the air has the same pressure p_0 and velocity V and hence also the same total pressure head $\left(p_0 + \frac{1}{2} \varrho V^2\right)$. This value of the total pressure head will be retained by the air which passes outside the slipstream, whereas the air in the wake has the same pressure p_0 but the higher velocity u_1, and hence the total pressure head of the air in the slipstream has been increased by $\frac{1}{2} \varrho (u_1^2 - V^2)$. Proceeding now to the points immediately before and behind the propeller disc, this increase of total pressure head will be manifested simply as an increase of pressure since there can be no discontinuity of velocity

as the air passes through the propeller disc. It appears therefore that there is a sudden increase of pressure behind the propeller disc and this increase of pressure, acting over the whole disc, represents the thrust of the propeller. Thus the application of Bernoulli's equation gives

$$T = \frac{1}{2} S \varrho (u_1^2 - V^2) \tag{1.10}$$

and this equation, taken in conjunction with the previous equations (1.2) and (1.7), leads to the conclusion that the axial velocity u is the arithmetic mean of the velocities V and u_1.

The representation of a propeller by a disc at which there is a sudden increase of pressure without any discontinuity of velocity was introduced by R. E. Froude[1] and is generally known as Froude's actuator disc. A physical representation of this actuator disc may be obtained by considering a close pair of tandem propellers rotating in opposite directions and so designed that the element of torque at any radial distance from the axis has the same value for each propeller, in order that there shall be no rotational motion in the slipstream: also each propeller must be assumed to have a large number of frictionless blades and to have the blade angles suitably chosen to give a uniform distribution of thrust over the whole propeller disc.

For some purposes it is convenient to present the results of the preceding analysis in a modified form. Writing

$$\left.\begin{aligned} u &= V(1+a) \\ u_1 &= V(1+b) \end{aligned}\right\} \tag{1.11}$$

where a is the axial interference factor and b is the axial slipstream factor, (1.8) shows that a is one half of b and the expressions for the thrust, power and efficiency of the propeller become

$$\left.\begin{aligned} T &= 2 S \varrho V^2 (1+a) a \\ P &= 2 S \varrho V^3 (1+a)^2 a \\ \eta &= \frac{1}{1+a} \end{aligned}\right\} \tag{1.12}$$

2. The Momentum Equation. In developing the simple Rankine-Froude theory it has been assumed that the thrust of the propeller is uniformly distributed over the whole propeller disc and that the axial velocity of the air has a constant value over this disc and over a cross-section of the ultimate wake. Also the momentum equation for the propeller has been taken to be

$$T = S_1 \varrho u_1 (u_1 - V) \tag{2.1}$$

on the basis that the right hand side of this equation represents the total increase of momentum and that the resultant pressure force on

[1] FROUDE, R. E., On the Part Played in Propulsion by Differences of Fluid Pressure. Trans. Inst. Nav. Arch., Vol. 30, p. 390, 1889.

the whole fluid is zero. To proceed further with the development of the theory it is necessary to consider the form of the momentum equation as applied to individual annular elements of the propeller, *i. e.* to the fluid which passes through the propeller disc between the radii r and $(r + dr)$, and as a preliminary step it is necessary to examine more critically the momentum equation as applied to the whole propeller. The fluid which has passed or will pass through the propeller disc forms a cylindrical column whose cross-sectional area contracts from S_0 far in front of the propeller to S at the propeller disc and finally to S_1 in the ultimate wake (see Fig. 9). The system of forces acting on the column of fluid bounded at the ends by the two sections S_0 and S_1 far before and behind the propeller comprises the thrust T, the pressure $p_0 (S_0 - S_1)$ over the ends of the column and an axial force X due to the pressure on the lateral boundary of the column which will be regarded as positive when it opposes the thrust T. The momentum equation for the column of fluid can now be expressed quite generally as

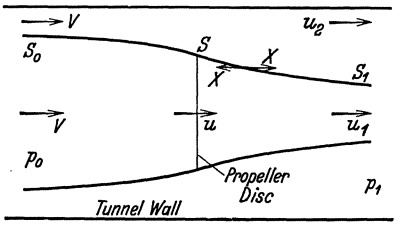

Fig. 10.

$$T - X + p_0 (S_0 - S_1) = \int \varrho\, u_1 (u_1 - V)\, dS_1 \qquad (2.2)$$

where the integral extends over the cross-section of the wake and the velocity u_1 may have different values for different annular elements. In order to establish the validity of the previous equation (2.1) it is necessary to show that the axial pressure force X on the lateral boundary of the column of fluid is equal to the pressure force $p_0 (S_0 - S_1)$ over its ends.

Consider a propeller operating in a cylindrical tunnel whose cross-section is a circle of area C. The system of velocity and pressure will be as illustrated in Fig. 10. The axial velocity V increases to u at the propeller disc and to u_1 in the wake, while the velocity outside the wake will decrease to u_2 in order to maintain the continuity of flow. The pressure far behind the propeller will have a constant value p_1 across the whole tunnel but this value will be greater than the original pressure p_0 owing to the drop of velocity outside the slipstream. Also the velocity u_2 must have the same value at all points of the section outside the slipstream, but the velocities u and u_1 may have different values for different annular elements.

The condition of continuity, applied in turn to the flow inside and outside the slipstream, gives the equations

$$V S_0 = \int u\, dS = \int u_1\, dS_1 \qquad (2.3)$$

and

$$V (C - S_0) = u_2 (C - S_1) \qquad (2.4)$$

Also if H_0 is the total pressure head of the original stream, Bernoulli's equation applied to the flow outside the slipstream gives

$$H_0 = p_0 + \tfrac{1}{2}\varrho V^2 = p_1 + \tfrac{1}{2}\varrho u_2^2$$

or
$$p_1 - p_0 = \tfrac{1}{2}\varrho (V^2 - u_2^2) \tag{2.5}$$

Inside the slipstream the total pressure head is increased to H_1 owing to the sudden increment of pressure p' which occurs at the propeller disc without any change of velocity. Considering any annular element, let v be the radial component of the velocity at the propeller disc and let p be the pressure immediately in front of the disc. Then from Bernoulli's equation applied to the flow just before and behind the propeller,

$$H_0 = p + \tfrac{1}{2}\varrho (u^2 + v^2)$$

and
$$H_1 = p + p' + \tfrac{1}{2}\varrho (u^2 + v^2)$$
$$= p_1 + \tfrac{1}{2}\varrho u_1^2$$

Hence finally
$$p' = H_1 - H_0 = \tfrac{1}{2}\varrho (u_1^2 - u_2^2) \tag{2.6}$$

and the thrust of the propeller is

$$T = \int p'\, dS \tag{2.7}$$

Now if X is the axial pressure force on the lateral boundary of the column of fluid forming the slipstream, the momentum equation for the flow outside the slipstream is

$$X + p_0 (C - S_0) - p_1 (C - S_1) = \varrho V (C - S_0)(u_2 - V)$$

from which it is possible to eliminate u_2 and p_1 by means of the equations (2.4) and (2.5). Thus

$$\begin{aligned} X &= p_0 (S_0 - S_1) + (p_1 - p_0)(C - S_1) - \varrho V (C - S_0)(V - u_2) \\ &= p_0 (S_0 - S_1) + \tfrac{1}{2}\varrho (V - u_2)[(V + u_2)(C - S_1) - 2V(C - S_0)] \\ &= p_0 (S_0 - S_1) + \tfrac{1}{2}\varrho V^2 \frac{(S_0 - S_1)^2}{C - S_1} \end{aligned}$$

and as the size of the tunnel becomes very large this equation gives the limiting value

$$X = p_0 (S_0 - S_1) \tag{2.8}$$

Similarly the momentum equation for the flow inside the slipstream is

$$T - X + p_0 S_0 - p_1 S_1 = \int \varrho u_1 (u_1 - V)\, d S_1$$

or

$$\begin{aligned} T - \int \varrho u_1 (u_1 - V)\, d S_1 &= p_0 (S_0 - S_1) + \tfrac{1}{2}\varrho V^2 \frac{(S_0 - S_1)^2}{C - S_1} - p_0 S_0 + p_1 S_1 \\ &= (p_1 - p_0) S_1 + \tfrac{1}{2}\varrho V^2 \frac{(S_0 - S_1)^2}{C - S_1} \\ &= \tfrac{1}{2}\varrho (V^2 - u_2^2) S_1 + \tfrac{1}{2}\varrho V^2 \frac{(S_0 - S_1)^2}{C - S_1} \\ &= \tfrac{1}{2}\varrho V^2 \frac{(S_0 - S_1)[C(S_0 + S_1) - 2 S_0 S_1]}{(C - S_1)^2} \end{aligned}$$

and as the size of the tunnel becomes very large this equation gives the limiting value

$$T = \int \varrho\, u_1 (u_1 - V)\, d\, S_1 \tag{2.9}$$

Thus, by considering the flow in a tunnel and then proceeding to the limiting condition of a tunnel of very large radius, it has been possible to establish the validity of the momentum equation applied to the propeller as a whole. This simple line of argument does not suffice to establish the form of the momentum equation applied to the separate annular elements of the propeller, but in the development of the theory it is customary to replace the integral (2.9) by its differential form

$$\left.\begin{aligned} d\, T &= \varrho\, u_1 (u_1 - V)\, d\, S_1 \\ &= \varrho\, u\ (u_1 - V)\, d\, S \end{aligned}\right\} \tag{2.10}$$

The validity of this equation has not been established[1] and its adoption may imply the neglect of the mutual interference between the various annular elements, but the actual deviations from the conditions represented by (2.10) are believed to be extremely small in general.

3. The Ideal Efficiency of a Propeller. The analysis of the preceding section has established that the element of thrust on an annular element of a propeller can be expressed either in terms of the increase of pressure at the propeller disc or in terms of the axial velocity in the wake as

$$d\, T = p'\, d\, S = \frac{1}{2}\, \varrho\, (u_1^2 - V^2)\, d\, S \tag{3.1}$$

since the velocity u_2 in the expression for p' given by (2.6) of the previous section becomes identical with the undisturbed velocity V when the propeller is operating in an unlimited fluid. Also the momentum equation has been accepted in the form

$$d\, T = \varrho\, u\, (u_1 - V)\, d\, S \tag{3.2}$$

Hence the equation

$$u = \frac{1}{2}\, (u_1 + V) \tag{3.3}$$

which was previously established for the whole propeller, is also true for each individual annular element. Writing

$$u = V\, (1 + a) \tag{3.4}$$

where a is the axial interference factor, the slipstream velocity u_1 becomes

$$u_1 = V\, (1 + 2\, a) \tag{3.5}$$

and (3.1) and (3.2) for the element of thrust both reduce to the same form

$$d\, T = 2\, \varrho\, V^2\, (1 + a)\, a\, d\, S \tag{3.6}$$

or for the whole propeller

$$T = 2\, \varrho\, V^2 \int (1 + a)\, a\, d\, S \tag{3.7}$$

---

[1] A discussion of this question has been given by D. THOMA, Zeitschr. f. Flugtechnik u. Motorl. **16**, 206, 1925.

The increase of kinetic energy in the slipstream in unit time, which represents a loss of energy of the propulsive system, is now

$$\left.\begin{aligned} E &= \int \tfrac{1}{2}\varrho\, u\,(u_1 - V)^2\, d\,S \\ &= 2\,\varrho\, V^3 \int (1+a)\, a^2\, d\,S \end{aligned}\right\} \tag{3.8}$$

and the ideal distribution of thrust over the disc of the propeller will be that which gives a minimum value of the energy loss E for a definite value of the useful work VT. To determine this best distribution of thrust, the axial interference factor a must be regarded as a function of the radial distance r of the annular element and the form of the function must be determined so that E is a minimum while VT remains constant.

Assume that this best distribution of thrust over the disc of the propeller has been found, so that no alteration of the distribution can reduce the loss of energy. Suppose now that the addition of a small element of thrust $\Delta\, T$ on any annulus produces a loss of energy $\Delta\, E$: if the value of $\Delta\, E$ varies with the radial distance of the annulus it is possible to obtain a new distribution of thrust with a reduced loss of energy by adding an element of thrust $\Delta\, T$ where the corresponding value of $\Delta\, E$ is small and by subtracting an equal element of thrust where $\Delta\, E$ is large. Hence the condition for the best distribution of thrust over the propeller disc is that the ratio of $\Delta\, E$ to $\Delta\, T$ shall have the same value for all annular elements of the propeller.

Now the thrust of an annular element of area $d\,S$ is

$$d\,T = 2\,\varrho\, V^2\,(1+a)\, a\, d\,S$$

and the corresponding loss of energy is

$$d\,E = 2\,\varrho\, V^3\,(1+a)\, a^2\, d\,S$$

Increasing the axial interference factor a by $\Delta\, a$, the corresponding increments of thrust and energy loss are

$$\begin{aligned} \Delta\,(d\,T) &= 2\,\varrho\, V^2\,(1+2\,a)\,\Delta\, a\, d\,S \\ \Delta\,(d\,E) &= 2\,\varrho\, V^3\,(2\,a + 3\,a^2)\,\Delta\, a\, d\,S \end{aligned}$$

The condition for the best distribution of thrust over the disc of the propeller is therefore that $\dfrac{2a+3a^2}{1+2\,a}$ should be constant, and this implies that the axial interference factor a is constant. Hence the minimum loss of energy for a given thrust occurs when the thrust is uniformly distributed over the whole propeller disc. The conditions are therefore identical with those assumed in the simple Rankine-Froude theory, and the thrust and power of the propeller are respectively

$$\left.\begin{aligned} T &= 2\,S\,\varrho\, V^2\,(1+a)\, a \\ P &= 2\,S\,\varrho\, V^3\,(1+a)^2\, a \end{aligned}\right\} \tag{3.9}$$

The efficiency of the propeller with this best distribution of thrust represents the highest efficiency which can be obtained with a propeller of disc area S advancing with the speed V and absorbing the power P: it is therefore the *ideal efficiency* of the propeller and will be denoted by η_1. The value of the ideal efficiency is

$$\eta_1 = \frac{V\,T}{P} = \frac{1}{1+a} \tag{3.10}$$

By means of (3.9) and (3.10) it is possible to eliminate the axial interference factor a and to express the thrust and power of the propeller in the form

$$\left.\begin{aligned} \frac{T}{S\,\varrho\,V^2} &= \frac{2\,(1-\eta_1)}{\eta_1^2} \\ \frac{P}{S\,\varrho\,V^3} &= \frac{2\,(1-\eta_1)}{\eta_1^3} \end{aligned}\right\} \tag{3.11}$$

and for a propeller of radius R the disc area S is simply πR^2. Table 1 gives the numerical values of the thrust and power coefficients defined by (3.11) for a wide range of values of the ideal efficiency, and the relationship between the efficiency and the power coefficient is also shown in Fig. 11. The importance of the relationship exhibited in this figure is that the ideal efficiency η_1 represents the highest efficiency which could possibly be attained with any propeller of radius R absorbing the power P at the speed V. It will be noticed that the efficiency falls as the power per unit disc area increases or as the speed decreases. On the basis of the axial momentum theory therefore the diameter of a propeller should be as large as possible.

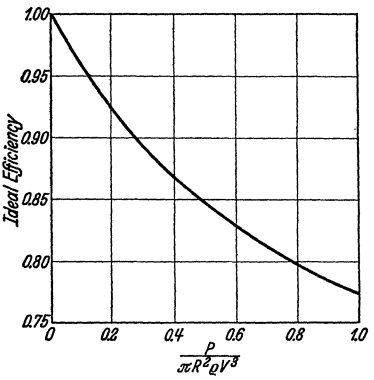

Fig. 11.

TABLE 1. Ideal Efficiency.

η_1	$T/\pi R^2 \varrho V^2$	$P/\pi R^2 \varrho V^3$	η_1	$T/\pi R^2 \varrho V^2$	$P/\pi R^2 \varrho V^3$
0.98	0.0416	0.0425	0.82	0.5354	0.6529
0.96	0.0868	0.0904	0.80	0.6250	0.7812
0.94	0.1358	0.1445	0.75	0.8890	1.185
0.92	0.1890	0.2055	0.70	1.225	1.749
0.90	0.2469	0.2743	0.65	1.657	2.549
0.88	0.3099	0.3522	0.60	2.222	3.704
0.86	0.3786	0.4402	0.55	2.975	5.410
0.84	0.4535	0.5399	0.50	4.000	8.000

The results of this general analysis can also be represented in another interesting manner. The power of an engine is a simple function of the

rate of revolution for given conditions of pressure and temperature, and it is therefore convenient to express the efficiency of a propeller in terms of a torque or power coefficient Q_c defined by the equation

$$Q_c = \frac{Q}{\pi R^2 \varrho \Omega^2 R^3} = \frac{P}{\pi R^2 \varrho \Omega^3 R^3} \tag{3.12}$$

where Ω is the angular velocity of the propeller. Denoting also the ratio of forward speed to tip speed of the propeller by λ, so that

$$\lambda = \frac{V}{\Omega R} \tag{3.13}$$

the relationship between power and ideal efficiency becomes

$$Q_c = \frac{2(1-\eta_1)}{\eta_1^3} \lambda^3 \tag{3.14}$$

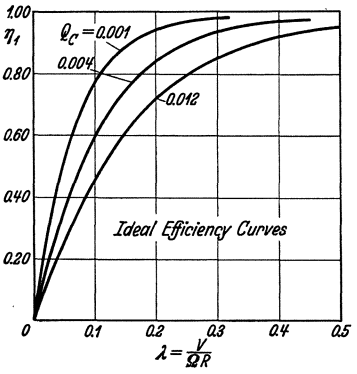

Fig. 12.

This equation has been used to calculate the relationship between λ and η_1 for a series of values of the torque coefficient Q_c. The numerical values are given in Table 2 and are shown graphically in Fig. 12. These curves show the variation of ideal efficiency with forward speed of a propeller which rotates at a definite tip speed ΩR and absorbs a definite power P. Each curve therefore represents the highest efficiency which may be anticipated from a variable pitch propeller which is driven by constant power and is adjusted to run at a constant rate of revolution. The efficiency rises with the speed ratio λ, rapidly at first and then more slowly, and tends to unity as a limit.

TABLE 2. Values of λ.

η_1	$Q_c = 0.001$	0.002	0.004	0.008	0.012
0.20	0.017	0.021	0.027	0.034	0.039
0.40	0.038	0.047	0.060	0.075	0.086
0.60	0.065	0.081	0.103	0.129	0.148
0.65	0.073	0.092	0.116	0.146	0.168
0.70	0.083	0.105	0.132	0.166	0.190
0.75	0.095	0.119	0.150	0.189	0.216
0.80	0.109	0.137	0.172	0.217	0.249
0.85	0.127	0.160	0.202	0.254	0.291
0.90	0.154	0.194	0.244	0.308	0.352
0.92	0.169	0.214	0.269	0.339	0.388
0.94	0.191	0.240	0.302	0.381	0.436
0.96	0.223	0.281	0.354	0.446	0.510
0.98	0.287	0.361	0.455	—	—

CHAPTER III

THE GENERAL MOMENTUM THEORY

1. General Equations. The axial momentum theory of the previous chapter was developed on the assumption that there was no rotational motion in the slipstream and that the propeller could be replaced by an actuator disc which produced a sudden increase of pressure in the fluid without any change of velocity. More generally the slipstream will have a rotational motion imparted to it by the reaction of the torque of the propeller and this rotational motion implies a further loss of energy. To extend the theory to include the effects of this rotational motion it is necessary to modify the qualities of the actuator disc by assuming that it can also impart a rotational component to the fluid velocity while the axial and radial components remain unaltered.

Let r be the radial distance of any annular element of the propeller disc, and let u and v be respectively the axial and radial components of the fluid velocity. Let p be the pressure immediately in front of the propeller and let p' be the increase of pressure behind the propeller, associated with an angular velocity ω. In the final wake let p_1 be the pressure, u_1 the axial velocity and ω_1 the angular velocity at a radial distance r_1 from the axis of the slipstream.

The condition of continuity of flow for the annular element is

$$u_1 r_1 \, d r_1 = u \, r \, d r \tag{1.1}$$

and the condition for constancy of angular momentum of the fluid as it passes down the slipstream is

$$\omega_1 r_1^2 = \omega \, r^2 \tag{1.2}$$

Also, since the element of torque of the propeller is equal to the angular momentum imparted in unit time to the corresponding annular element of the slipstream,

$$d Q = \varrho \, u \, \omega \, r^2 \, d S \tag{1.3}$$

Bernoulli's equation, applied in turn to the flow before and behind the propeller, gives

$$\begin{aligned} H_0 &= p_0 + \tfrac{1}{2} \varrho V^2 \\ &= p + \tfrac{1}{2} \varrho (u^2 + v^2) \end{aligned}$$

and

$$\begin{aligned} H_1 &= p + p' + \tfrac{1}{2} \varrho (u^2 + v^2 + \omega^2 r^2) \\ &= p_1 + \tfrac{1}{2} \varrho (u_1^2 + \omega_1^2 r_1^2) \end{aligned}$$

Hence

$$H_1 - H_0 = p' + \tfrac{1}{2} \varrho \, \omega^2 r^2 \tag{1.4}$$

which shows that the increase of total pressure head on passing through the propeller disc exceeds the thrust per unit area p' by a small term

representing the kinetic energy of the rotational motion imparted to the fluid by the torque of the propeller.

The expressions for the total pressure head also give

$$p_0 - p_1 = \frac{1}{2}\varrho\,(u_1^2 - V^2) + \frac{1}{2}\varrho\,\omega_1^2 r_1^2 - (H_1 - H_0)$$
$$= \frac{1}{2}\varrho\,(u_1^2 - V^2) + \frac{1}{2}\varrho\,(\omega_1^2 r_1^2 - \omega^2 r^2) - p' \qquad (1.5)$$

And in general the pressure p_1 in the slipstream is less than the external pressure p_0 owing to the rotation of the slipstream about its axis. But, applying Bernoulli's equation to the flow relative to the propeller blades which are rotating with the angular velocity Ω, the relative angular velocity decreases from Ω to $(\Omega - \omega)$ and hence the increase of pressure is

$$\left.\begin{aligned} p' &= \frac{1}{2}\varrho\,[\Omega^2 - (\Omega - \omega)^2]\, r^2 \\ &= \varrho\left(\Omega - \frac{1}{2}\omega\right)\omega\, r^2 \end{aligned}\right\} \qquad (1.6)$$

Finally, combining this result with the previous equations (1.2) and (1.5), the drop of pressure in the wake is

$$p_0 - p_1 = \frac{1}{2}\varrho\,(u_1^2 - V^2) - \varrho\left(\Omega - \frac{1}{2}\omega_1\right)\omega_1 r_1^2 \qquad (1.7)$$

The pressure gradient in the wake balances the centrifugal force on the fluid and is governed by the equation

$$\frac{d\,p_1}{d\,r_1} = \varrho\,\omega_1^2 r_1 \qquad (1.8)$$

And then differentiating (1.7) relative to r_1 and equating to (1.8) a differential equation is obtained connecting the axial and rotational velocities in the wake,

$$\frac{1}{2}\frac{d}{d\,r_1}(u_1^2 - V^2) = \frac{d}{d\,r_1}\left[\left(\Omega - \frac{1}{2}\omega_1\right)\omega_1 r_1^2\right] - \omega_1^2 r_1$$
$$= (\Omega - \omega_1)\frac{d}{d\,r_1}(\omega_1 r_1^2) \qquad (1.9)$$

The equation of axial momentum for the propeller, which can be established rigorously by a simple extension of the analysis of II 2, is

$$T = \int \varrho\, u_1 (u_1 - V)\, d\,S_1 - \int (p_0 - p_1)\, d\,S_1 \qquad (1.10)$$

and this equation is generally accepted in the differential form

$$d\,T = \varrho\, u_1 (u_1 - V)\, d\,S_1 - (p_0 - p_1)\, d\,S_1 \qquad (1.11)$$

Also from the pressure increment at the propeller disc

$$d\,T = p'\, d\,S$$
$$= \varrho\left(\Omega - \frac{1}{2}\omega\right)\omega\, r^2\, d\,S \qquad (1.12)$$

and then combining (1.1), (1.7), (1.11), and (1.12)

$$\left(\Omega - \frac{1}{2}\omega\right)\omega\, r^2 = u\,(u_1 - V) - \frac{u}{u_1}\left[\frac{1}{2}(u_1^2 - V^2) - \left(\Omega - \frac{1}{2}\omega_1\right)\omega_1 r_1^2\right]$$

or

$$u\,u_1\,(u_1 - V) - \frac{1}{2}\,u\,(u_1^2 - V^2) = u_1\left(\Omega - \frac{1}{2}\,\omega\right)\omega\,r^2 - u\left(\Omega - \frac{1}{2}\,\omega_1\right)\omega_1 r_1^2$$

which gives finally

$$\frac{1}{2}\,(u_1 - V)^2 = \left[\frac{\Omega - \frac{1}{2}\,\omega}{u} - \frac{\Omega - \frac{1}{2}\,\omega_1}{u_1}\right] u_1\,\omega_1\,r_1^2 \qquad (1.13)$$

These equations[1], though rather complex in form, suffice to determine the relationship between the thrust and torque of the propeller and the flow in the slipstream. If, for example, the angular velocity ω_1 is known as a function of the radius r_1 in the wake, (1.9) determines the axial velocity u_1 and then (1.13), taken in conjunction with (1.1) and (1.2), determines the axial and rotational velocities at the propeller disc. The thrust and torque of the propeller are then obtained from (1.12) and (1.3) respectively. Owing to the complexity of the equations, however, it is customary to adopt certain approximations based on the fact that the rotational velocity in the slipstream is generally very small.

2. Constant Circulation. An exact solution of the general equations of the preceding section can be obtained when the flow in the slipstream is irrotational except along the axis. This condition implies that the rotational momentum $\omega\,r^2$ has the same value k for all radial elements[2], *i. e.*

$$\omega_1\,r_1^2 = \omega\,r^2 = k \qquad (2.1)$$

Then by virtue of (1.9), the axial velocity u_1 is constant across the wake and it can be shown that (1.13) is satisfied by a constant value of the axial velocity u across the propeller disc: for if u and u_1 are constant, the equations of continuity (1.1) and (1.2) give

$$\frac{u_1}{u} = \frac{\omega_1}{\omega} = \frac{r^2}{r_1^2} = \frac{R^2}{R_1^2} \qquad (2.2)$$

and (1.13) then becomes

$$\frac{1}{2}\,(u_1 - V)^2 = \frac{u_1 - u}{u}\,\Omega\,k \qquad (2.3)$$

Now put

$$\left.\begin{aligned} \lambda &= \frac{V}{\Omega\,R} \\ \mu &= \frac{u}{\Omega\,R} \\ \mu_1 &= \frac{u_1}{\Omega\,R} \\ q &= \frac{u\,k}{\Omega^2\,R^3} = \frac{\mu\,k}{\Omega\,R^2} \end{aligned}\right\} \qquad (2.4)$$

and (2.3) becomes

$$q = \frac{\mu^2\,(\mu_1 - \lambda)^2}{2\,(\mu_1 - \mu)} \qquad (2.5)$$

[1] The complete series of equations appears to have been given first by N. E. Joukowski, Travaux du Bureau des Calculs et Essais Aéronautiques de l'Ecole Superièure Technique de Moscou, 1918; republished in book form as "Théorie Tourbillonnaire de l'hélice Propulsive"; Paris, 1929.

[2] This condition was used by N. E. Jouskowski as the basis of design for his special type of propeller.

Also from (1.7), since p_1 is equal to p_0 immediately inside the boundary of the slipstream,

$$\frac{1}{2}(u_1^2 - V^2) = \left(\Omega - \frac{k}{2R_1^2}\right)k$$

$$= \left(\Omega - \frac{k u_1}{2R^2 u}\right)k$$

or

$$\frac{1}{2}(\mu_1^2 - \lambda^2) = \left(1 - \frac{q\mu_1}{2\mu^2}\right)\frac{q}{\mu}$$

and eliminating q by means of (2.5)

$$\frac{1}{2}(\mu_1^2 - \lambda^2) = \left[1 - \frac{\mu_1(\mu_1-\lambda)^2}{4(\mu_1-\mu)}\right]\frac{\mu(\mu_1-\lambda)^2}{2(\mu_1-\mu)}$$

or finally

$$4(\mu_1-\mu)(2\mu-\mu_1-\lambda) = \mu(\mu_1-\lambda)^3 \tag{2.6}$$

Equations (2.5) and (2.6) determine μ and μ_1 in terms of λ and q. Also (2.6) may be written in the form

$$\mu = \frac{1}{2}(\mu_1 + \lambda) + \frac{\mu(\mu_1-\lambda)^3}{8(\mu_1-\mu)}$$

which shows that in the case under consideration

$$u > \frac{1}{2}(u_1 + V)$$

Thus the conclusion obtained in Chapter II that the axial velocity u at the propeller disc is the arithmetic mean of the axial velocity V and the slipstream velocity u_1 is not true in general when rotation also occurs in the slipstream.

Adopting the usual notation

$$\left.\begin{aligned}\mu &= \lambda(1+a)\\ \mu_1 &= \lambda(1+b)\end{aligned}\right\} \tag{2.7}$$

the expression for μ furnishes the relation

$$a = \frac{1}{2}b\left[1 + \frac{\lambda^2(1+a)b^2}{4(b-a)}\right]$$

The second term in the bracket is generally small and it is legitimate to replace b by its approximate value $2a$. Thus

$$a = \frac{1}{2}b[1 + \lambda^2(1+a)a]$$

or alternatively, to the same degree of approximation,

$$b = 2a\,[1 - \lambda^2(1+a)a] \tag{2.8}$$

Also from (2.5)

$$q = \frac{\lambda^3(1+a)^2b^2}{2(b-a)}$$

and on the same basis of approximation

$$q = 2\lambda^3(1+a)^2 a \tag{2.9}$$

The torque of the airscrew is obtained from the equation

$$\frac{dQ}{dr} = 2\pi\varrho u\omega r^3$$

$$= 2\pi\varrho u k r$$

and on integration, remembering that u and k are constant along the blade,

$$Q = \pi R^2 \varrho u k$$

The corresponding torque coefficient is

$$Q_c = \frac{Q}{\pi R^2 \varrho \Omega^2 R^3} = \frac{u k}{\Omega^2 R^3}$$

and so the parameter q defined by (2.4) and determined approximately by (2.9) is the torque coefficient of the propeller.

It is now possible to obtain an estimate of the amount by which the ratio b/a differs from the value 2 as determined by the axial momentum theory. Assuming for the torque coefficient Q_c or q the value 0.012, which is larger than any value generally obtained from a propeller, the following values of the parameter λ and of the ratio $b/2a$ are deduced from (2.8) and (2.9):

$\lambda =$	0.352	0.249	0.148
$b/2a =$	0.985	0.980	0.976

The deviation of the ratio b/a from the value 2 is therefore quite small even in this rather extreme case, and for the smaller values of the torque coefficient which are more usually obtained the deviation is quite negligible.

The condition of constant circulation k along the blade, which has been the basis of the preceding calculations, cannot be fully realized in practice since it implies that near the roots of the blades the angular velocity imparted to the air is greater than the angular velocity of the propeller itself. In any practical application of the analysis it is therefore necessary to assume that the effective part of the propeller blades commences at a radial distance not less than $\sqrt{k/\Omega}$ at which ω is equal to Ω.

3. Approximate Solution. In general the angular velocity ω imparted to the slipstream is very small compared with the angular velocity Ω of the propeller, and it is therefore possible to simplify the general equations by neglecting certain terms involving ω^2. On this basis of approximation the pressure p_1 in the wake is equal to the initial pressure p_0 of the fluid and the increase of pressure p' across the propeller disc is equal to the increase of total pressure head $(H_1 - H_0)$. The relationships connecting the thrust and axial velocity are then the same as in the simple axial momentum theory, the axial velocity u at the propeller disc is the arithmetic mean of the axial velocity V and the slipstream velocity u_1, and the element of thrust is

$$\begin{aligned} d T &= 2 \varrho u (u - V) d S \\ &= 4 \pi \varrho V^2 (1 + a) a r d r \end{aligned} \qquad (3.1)$$

Alternatively from (1.6)

$$d\,T = p'\,d\,S$$
$$= 2\,\pi\,\varrho\left(\Omega - \frac{1}{2}\,\omega\right)\omega\,r^3\,d\,r$$

and writing $\omega = 2\,a'\,\Omega$ (3.2)

this alternative expression is

$$d\,T = 4\,\pi\,\varrho\,\Omega^2\,(1 - a')\,a'\,r^3\,d\,r \tag{3.3}$$

A comparison of the two expressions for the element of thrust shows that the axial and rotational interference factors a and a' are connected by the equation $V^2\,(1 + a)\,a = \Omega^2\,r^2\,(1 - a')\,a'$ (3.4)

Finally the element of torque is obtained from (1.3) as

$$d\,Q = \varrho\,u\,\omega\,r^2\,d\,S$$
$$= 4\,\pi\,\varrho\,V\,\Omega\,(1 + a)\,a'\,r^3\,d\,r \tag{3.5}$$

and it is in these forms that it is customary to accept the equations for the thrust and torque of an ideal frictionless propeller.

4. Minimum Loss of Energy. When the rotational motion in the slipstream is ignored, the minimum loss of energy is obtained by distributing the thrust uniformly over the whole disc of the propeller and by maintaining a constant value of the axial interference factor a. The additional loss of energy due to the rotational motion is small in general, but it exerts an important influence on the best distribution of thrust over the propeller disc.

In the preceding paragraph the elements of thrust and torque have been obtained in the form

$$d\,T = 4\,\pi\,\varrho\,V^2\,(1 + a)\,a\,r\,d\,r$$

and

$$d\,Q = 4\,\pi\,\varrho\,V\,\Omega\,(1 + a)\,a'\,r^3\,d\,r$$

while the axial and rotational interference factors have been shown to be related by the equation

$$V^2\,(1 + a)\,a = \Omega^2\,r^2\,(1 - a')\,a' \tag{4.1}$$

or alternatively $V\,(1 + a)\,d\,T = \Omega\,(1 - a')\,d\,Q$ (4.2)

Writing this equation again as

$$\Omega\,d\,Q - V\,d\,T = V\,a\,d\,T + \Omega\,a'\,d\,Q$$

the left hand side represents the excess of the power absorbed by the propeller over the useful work done by the thrust, and the right hand side is an expression for the work done on the air or for the loss of energy. Thus

$$d\,E = V\,a\,d\,T + \Omega\,a'\,d\,Q$$
$$= \Omega\,d\,Q - V\,d\,T$$
$$= 4\,\pi\,\varrho\,V\,(1 + a)\,[\Omega^2\,r^2\,a' - V^2\,a]\,r\,d\,r \tag{4.3}$$

Now put
$$\left.\begin{aligned}\lambda &= \frac{V}{\Omega R}\\ x &= \frac{\Omega r}{V}\end{aligned}\right\} \tag{4.4}$$

and (4.1) becomes $$x^2 (1 - a')\, a' = (1 + a)\, a \tag{4.5}$$

while the efficiency of the annular element [see (3.3), (3.5)] is
$$\eta = \frac{1 - a'}{1 + a} = \frac{a}{a'\, x^2} \tag{4.6}$$

Thus
$$\begin{aligned} a &= x^2\, \eta\, a' \\ &= x^2\, \eta\, [1 - \eta\, (1 + a)] \end{aligned}$$

and the interference factors a and a' can therefore be expressed in terms of x and η as
$$\left.\begin{aligned} a &= \frac{x^2\, \eta\, (1 - \eta)}{1 + x^2\, \eta^2}\\ a' &= \frac{1 - \eta}{1 + x^2\, \eta^2}\end{aligned}\right\} \tag{4.7}$$

The best distribution[1] of thrust over the propeller disc is determined by the condition that the increment of loss of energy ΔE corresponding to an increment of thrust ΔT has the same value for all annular elements of the propeller, and since
$$d E = \Omega\, d Q - V\, d T$$
the increment of torque ΔQ can be used instead of the increment of energy ΔE. For an annular element of area $d S$ the increments are
$$\begin{aligned} \Delta (d T) &= 2\, \varrho\, V^2\, (1 + 2\, a)\, \Delta a\, d S \\ \Delta (d Q) &= 2\, \varrho\, V\, \Omega\, r^2\, [a'\, \Delta a + (1 + a)\, \Delta a']\, d S \end{aligned}$$
and the condition for the best distribution is therefore that
$$\frac{x^2\, [a'\, \Delta a + (1 + a)\, \Delta a']}{(1 + 2\, a)\, \Delta a}$$
has a constant value C for all values of the radial parameter x. But from (4.6), by taking finite differences Δa and $\Delta a'$,
$$x^2\, (1 - 2\, a')\, \Delta a' = (1 + 2\, a)\, \Delta a$$
and hence the condition becomes
$$\frac{x^2\, a'}{1 + 2\, a} + \frac{1 + a}{1 - 2\, a'} = C$$
or in terms of the efficiency η of the annular element
$$\frac{x^2\, (1 - \eta)}{1 + x^2\, \eta\, (2 - \eta)} + \frac{1 + x^2\, \eta}{2\, \eta - 1 + x^2\, \eta^2} = C \tag{4.8}$$

This condition is equivalent to the result obtained by A. Betz[2], who establishes the relationship between the axial interference factor a

[1] See II 3.

[2] Eine Erweiterung der Schraubenstrahltheorie. Zeitschr. f. Flugtechnik u. Motorl. 11, 105, 1920.

and the radial coordinate x and shows the variation of the interference factors a and a' along the propeller blade in a series of diagrams. The condition can, however, be simplified by assuming that the thrust per unit disc area of the propeller is small and that the efficiency is only a little less than unity. Writing

$$\eta = 1 - \varepsilon$$

where ε is small, condition (4.8) becomes

$$\frac{x^2 \varepsilon}{1 + x^2 (1 - \varepsilon^2)} + \frac{1 + x^2 (1 - \varepsilon)}{(1 + x^2)(1 - 2\varepsilon) + x^2 \varepsilon^2} = C$$

and to the first order of the small quantity ε

$$1 + 2\varepsilon = C \tag{4.9}$$

Thus to this order of approximation the best distribution of thrust over the propeller disc is such that the efficiency η has the same value for all annular elements. This simple condition applies only to a lightly loaded propeller and more generally the best distribution of thrust is determined by the condition (4.8), but there is no important difference in the variation of the interference factors a and a' along the propeller blade between the exact and the approximate solutions.

5. Constant Efficiency. The elements of thrust and torque of a propeller are respectively

$$\frac{dT}{dr} = 4\pi r \varrho V^2 (1 + a) a$$

$$\frac{dQ}{dr} = 4\pi r^3 \varrho V \Omega (1 + a) a'$$

and the interference factors a and a' are connected by the relationship

$$x^2 (1 - a') a' = (1 + a) a \quad \text{[see (4.5)]}$$

where

$$x = \frac{\Omega r}{V}$$

Also the efficiency of the annular element is

$$\eta = \frac{1 - a'}{1 + a} = \frac{a}{x^2 a'}$$

and, in accordance with the analysis of the preceding paragraph, the loss of energy of a lightly loaded propeller is a minimum when the efficiency η has a constant value along the blade.

Now

$$a = x^2 \eta a' = x^2 \eta [1 - \eta (1 + a)]$$

and hence

$$a = \frac{x^2 \eta (1 - \eta)}{1 + x^2 \eta^2}$$

$$a' = \frac{1 - \eta}{1 + x^2 \eta^2}$$

which are two equations expressing the interference factors a and a' in terms of the constant efficiency η and the radial parameter x. Using

these expressions, the thrust and torque of the propeller are obtained in the form $\frac{\eta}{\lambda R} \cdot \frac{dQ}{dx} = \frac{dT}{dx} = \pi R^2 \varrho V^2 \frac{2\lambda^2(1-\eta)}{\eta^2} G(x, \eta)$

where $$\lambda = \frac{V}{\Omega R}$$

and $$G(x, \eta) = \frac{2 x^3 \eta^3 (1 - x^2 \eta)}{(1 + x^2 \eta^2)^2}$$

The particular form chosen for the function $G(x, \eta)$ is the one which is most convenient in the subsequent analysis, and in particular the limiting value at large values of x is simply $2x$, which is independent of the efficiency η.

This function $G(x, \eta)$ defines the thrust and torque distribution along the propeller blade. Numerical values of a, a', xa' and G are given in Table 3 for two values of the efficiency η and the distribution curves in one case are shown in Fig. 13. It will be noticed that the value of the axial interference factor a rises rapidly from zero at the boss and then remains nearly constant over the outer part of the blade, while the rotational interference factor a' is very small except near the boss. The curve of xa', which represents the rotational component of the velocity, is also shown in Fig. 13. The variation of G with the radial parameter x is shown in Fig. 14 for the same value of the efficiency: the load rises slowly at first near the boss of the propeller and then increases linearly with the radius.

TABLE 3. Values of a, a', and G.

x	$\eta = 0.75$				$\eta = 0.90$			
	a	a'	xa'	G	a	a'	xa'	G
0.5	.041	.219	.110	0.10	.019	.083	.042	0.15
1.0	.120	.160	.160	0.60	.050	.055	.055	0.85
1.5	.186	.110	.165	1.49	.072	.035	.053	1.87
2.0	.231	.077	.154	2.56	.085	.024	.047	2.98
2.5	.260	.055	.138	3.68	.093	.016	.041	4.11
3.0	.278	.041	.124	4.80	.098	.012	.036	5.21
4.0	.300	.025	.100	7.02	.103	.007	.029	7.37
5.0	.311	.017	.083	9.18	.106	.005	.024	9.48
6.0	.318	.012	.071	11.30	.107	.003	.020	11.57
8.0	.324	.007	.054	15.47	.109	.002	.015	15.67
10.0	.328	.004	.044	19.56	.110	.001	.012	19.73

On integration the thrust of the propeller gives the relation

$$\frac{T}{\pi R^2 \varrho V^2} = \frac{2(1-\eta)}{\eta^2} H(\lambda, \eta)$$

where $$H(\lambda, \eta) = \lambda^2 \int_0^{1/\lambda} G \, dx$$

and, by comparison with the formulae of the axial momentum theory, it will be seen that $H(\lambda, \eta)$ represents the correction factor to the thrust at a given efficiency due to the rotational motion. Similarly for the power absorbed by the propeller we have

$$\frac{P}{\pi R^2 \varrho V^3} = \frac{2(1-\eta)}{\eta^3} H(\lambda, \eta)$$

and the torque coefficient of the propeller is

$$Q_c = \frac{P}{\pi R^2 \varrho \Omega^3 R^3} = \frac{2\lambda^3(1-\eta)}{\eta^3} H(\lambda, \eta)$$

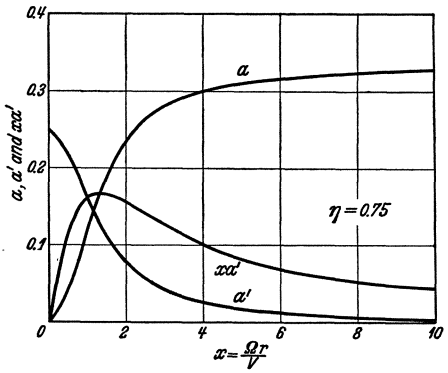

Fig. 13.

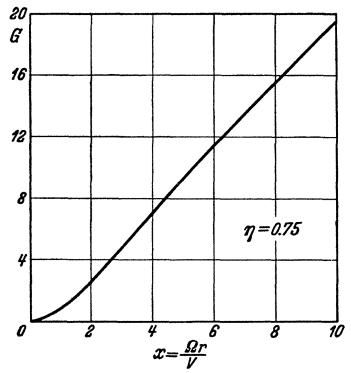

Fig. 14.

To evaluate the function $H(\lambda, \eta)$, put

$$s = x^2 \eta^2$$

and then

$$H(\lambda, \eta) = \frac{\lambda^2}{\eta^2} \int_0^{\eta^2/\lambda^2} \frac{(\eta + s)\, s}{(1+s)^2} \, ds$$

$$= \frac{\lambda^2}{\eta^2} \int_0^{\eta^2/\lambda^2} \left[1 - \frac{2-\eta}{1+s} + \frac{1-\eta}{(1+s)^2}\right] ds$$

which gives finally

$$H(\lambda, \eta) = 1 + \frac{\lambda^2(1-\eta)}{\lambda^2+\eta^2} - \frac{\lambda^2(2-\eta)}{\eta^2} \log \frac{\lambda^2+\eta^2}{\lambda^2}$$

By means of these equations the torque coefficient Q_c can be calculated as a function of λ and η, and then by drawing curves of η against Q_c for a range of values of λ it is possible to obtain the efficiency η as a function of Q_c and λ. The numerical values deduced in this manner are given in Table 4. The curves of η against λ are also shown in Fig. 15 and may be compared with the corresponding curves of Fig. 12, which were obtained from the axial momentum theory. The loss of efficiency

due to the rotational motion increases with the torque coefficient Q_c. For a moderate torque coefficient 0.004 the loss of efficiency is 2 per cent at most and for the exceptionally large torque coefficient 0.012 the loss of efficiency rises to 4 per cent. Thus the loss of efficiency due to the rotational motion is quite small in a properly designed propeller, but it may become more important if the load distribution curves depart noticeably near the boss from the form illustrated in Figs. 13 and 14.

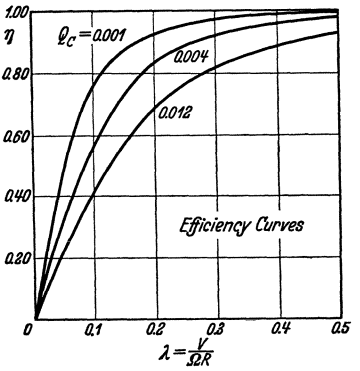

Fig. 15.

TABLE 4. Propeller Efficiency.

$Q_c=$	0.001	0.002	0.004	0.008	0.012
$\lambda=0.1$	0.763	0.669	0.570	0.475	0.422
0.2	0.935	0.893	0.828	0.739	0.680
0.3	0.978	0.958	0.922	0.865	0.820
0.4	0.989	0.978	0.958	0.924	0.893
0.5	0.994	0.988	0.975	0.951	0.930

CHAPTER IV

PROPELLER EFFICIENCY

1. The Energy Equation. The analysis of the two preceding chapters has been developed on the assumption of an ideal propeller which operates without any loss of energy due to the friction or drag of the propeller blades in their motion through the air, but the analysis can be extended without any difficulty to include this additional source of loss of energy. Ignoring the small drop of pressure in the wake owing to the rotational motion, the elements of thrust and torque of the ideal propeller have been obtained as

$$\frac{dT}{dr} = 4\pi r \varrho V^2 (1+a)\, a$$

and
$$\frac{dQ}{dr} = 4\pi r^3 \varrho V \Omega (1+a)\, a' \quad [\text{see III (3.1), (3.5)}]$$

and the corresponding energy equation is

$$(1-a')\,\Omega \frac{dQ}{dr} = (1+a)\, V \frac{dT}{dr} \quad [\text{see III (4.2)}] \qquad (1.1)$$

When the drag of the propeller blades is no longer neglected, the expressions for the elements of thrust and torque, being derived from a consideration of the momentum in the slipstream, remain unaltered, but the energy equation, (1.1), must be modified to include the loss

of energy due to the drag of the propeller blades. The energy equation may now be written as

$$(1 - a')\,\Omega \frac{dQ}{dr} = (1 + a)\,V \frac{dT}{dr} + \frac{dE}{dr} \tag{1.2}$$

where E is the additional loss of energy in unit time. Now assume that the propeller is formed of B identical blades and that c is the chord of any blade at the radial distance r. Then if W is the velocity of this blade element relative to the fluid and if C_D is the drag coefficient, the drag of the element extending a distance dr along the blade is

$$\tfrac{1}{2} C_D c \varrho W^2 dr$$

and the loss of energy in unit time from the B blade elements at the radial distance r is

$$dE = \frac{1}{2} C_D B c \varrho W^3 dr$$

or

$$\frac{dE}{dr} = \frac{1}{2} C_D B c \varrho W^3 \tag{1.3}$$

Now the axial velocity at the propeller disc is u or $V(1 + a)$, and the rotational velocity changes from zero in front of the disc to ωr behind it. Thus the mean rotational velocity relative to the blades, which are rotating with the angular velocity Ω, is $(\Omega - \frac{1}{2}\omega)\, r$ or $\Omega r\,(1 - a')$. The flow relative to the blade element at radial distance r can be represented as in Fig. 16, and if φ is the angle of inclination of the resultant velocity W to the plane of rotation

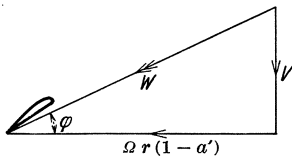

Fig. 16.

$$\left.\begin{aligned} W \sin\varphi &= V(1 + a) \\ W \cos\varphi &= \Omega r\,(1 - a') \end{aligned}\right\} \tag{1.4}$$

The velocity W is therefore known in terms of the interference factors a and a', and the loss of energy due to the drag of the blades can be determined from (1.3).

2. Approximate Solution. If it be desired to obtain the minimum loss of energy of an ideal propeller, it is necessary that the axial and rotational interference factors shall vary along the blade in the manner shown in Fig. 13, but it is to be noted that the chief variation in these factors is confined to a small region near the boss of the propeller. In deriving an approximate equation for the efficiency of a propeller it is legitimate therefore to assume mean values of a and a' along the whole blade and to replace the equations for the elements of thrust and torque by their integral forms

$$T = 2\pi R^2 \varrho V^2 (1 + a)\, a \tag{2.1}$$

and

$$P = \Omega Q = \pi R^2 \varrho V \Omega^2 R^2 (1 + a)\, a' \tag{2.2}$$

The efficiency of the propeller then is

$$\eta = \frac{V T}{P} = \frac{2 \lambda^2 a}{a'} \tag{2.3}$$

where $$\lambda = \frac{V}{\Omega R}$$

To proceed further it is necessary to evaluate the loss of energy E due to the drag of the propeller blades. In most conventional shapes of propeller blades the chord c increases slowly from the boss to a maximum value in the outer half of the blade and then decreases again towards the tip of the blade. The drag coefficient C_D of the blade section will generally have its minimum value over the principal working sections of the blade where the chord is large and will increase both towards the root owing to the increasing thickness of the blade section and towards the tip owing to the less efficient conditions of operation and possibly also to high tip speed. Thus as an approximation it is legitimate to assume a constant value of the product of chord and drag coefficient along the blade. On this basis put

$$\frac{B c}{2 \pi R} C_D = \sigma \delta \tag{2.4}$$

where $$\sigma \pi R^2 = \int_0^R B c \, dr \tag{2.5}$$

so that σ is the ratio of the total blade area to the propeller disc area and may be called the *solidity* of the propeller, while 2δ is the effective mean value of the drag coefficient C_D. The loss of energy due to the drag of the propeller blades may then be calculated as

$$E = \int_0^R \frac{1}{2} C_D B c \varrho W^3 \, dr$$

$$= \sigma \delta \pi R \varrho \int_0^R W^3 \, dr$$

Now referring to Fig. 16, let φ_1 be the value of φ at the tip of the blade, and then

$$\Omega r (1 - a') \tan \varphi = V (1 + a)$$
$$= \Omega R (1 - a') \tan \varphi_1$$

or $$r = R \tan \varphi_1 \cot \varphi$$

while the resultant velocity W is

$$W = V (1 + a) \operatorname{cosec} \varphi$$
$$= \Omega R (1 - a') \tan \varphi_1 \operatorname{cosec} \varphi$$

With these substitutions the integral for the loss of energy becomes

$$E = \sigma\,\delta\,\pi\,R^2\,\varrho\,\Omega^3\,R^3\,(1-a')^3\,f(\varphi_1) \tag{2.6}$$

where

$$f(\varphi_1) = \int_{\varphi_1}^{\pi/2} tan^4\varphi_1\,cosec^5\,\varphi\,d\,\varphi$$

and on evaluating this last integral[1]

$$f(\varphi_1) = \frac{1}{8}(2 + 5\,tan^2\varphi_1)\,sec\,\varphi_1 - \frac{3}{16}\,tan^4\varphi_1\,log\frac{1-cos\,\varphi_1}{1+cos\,\varphi_1} \tag{2.7}$$

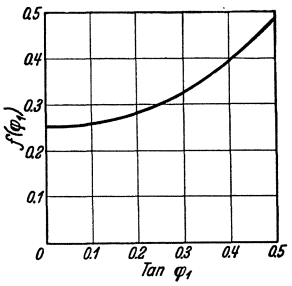

Fig. 17.

Numerical values of $f(\varphi_1)$ as a function of $tan\,\varphi_1$ are given in Table 5 and are shown graphically in Fig. 17. Also the angle φ_1 which occurs in this formula can be expressed in terms of the interference factors a and a' by the equation

$$tan\,\varphi_1 = \frac{V(1+a)}{\Omega R(1-a')} = \lambda\frac{1+a}{1-a'} \tag{2.8}$$

TABLE 5.

$tan\,\varphi_1$	0	0.10	0.20	0.30	0.40	0.50
$f(\varphi_1)$	0.250	0.258	0.282	0.325	0.393	0.488

3. Propeller Efficiency. The energy equation for the propeller, on the assumptions adopted, is

$$(1-a')\,\Omega\,Q = (1+a)\,V\,T + E \tag{3.1}$$

and the efficiency of the propeller is

$$\eta = \frac{V\,T}{\Omega\,Q}$$

It is convenient to express this efficiency η as the product of three factors

$$\eta = \eta_1\,\eta_2\,\eta_3 \tag{3.2}$$

where

$$\left.\begin{aligned}\eta_1 &= \frac{1}{1+a}\\ \eta_2 &= 1-a'\end{aligned}\right\} \tag{3.3}$$

and η_3 represents the additional efficiency factor due to the drag of the propeller blades. With these definitions the torque coefficient of the propeller is obtained from (2.2) as

$$Q_c = \frac{P}{\pi R^2\,\varrho\,\Omega^3 R^3} = \frac{\lambda(1-\eta_2)}{\eta_1} \tag{3.4}$$

and then the equation for the thrust gives

$$\eta\,Q_c = \lambda\,T_c = \frac{2\,\lambda^3(1-\eta_1)}{\eta_1^2}$$

[1] This integration is performed by means of the standard formulae

$$\int cosec^n\,\varphi\,d\,\varphi = \frac{n-2}{n-1}\int cosec^{n-2}\,\varphi\,d\,\varphi - \frac{cos\,\varphi\,cosec^{n-1}\,\varphi}{n-1}$$

and

$$\int cosec\,\varphi\,d\,\varphi = \frac{1}{2}\,log\frac{1-cos\,\varphi}{1+cos\,\varphi}$$

or alternatively, putting $\eta = \eta_1 \eta_2 \eta_3$

$$\eta_1 = 1 - \frac{1}{2} Q_c \eta_2 \eta_3 \left(\frac{\eta_1}{\lambda}\right)^3 \tag{3.5}$$

Finally the energy equation, (3.1), becomes

$$\eta_2 P = \frac{\eta}{\eta_1} P + E$$

and hence

$$\eta_2 (1 - \eta_3) Q_c = \frac{E}{\pi R^2 \varrho \Omega^3 R^3}$$
$$= \eta_2^3 \sigma \delta f(\varphi_1)$$

or

$$\eta_3 = 1 - \frac{\eta_2^2}{Q_c} \sigma \delta f(\varphi_1) \tag{3.6}$$

These last equations suffice to determine the efficiency of a propeller when the values of $\sigma \delta$, Q_c and λ are known. The shape of the propeller is not determined and the result must be regarded as the highest efficiency which can be obtained from a propeller of solidity σ designed to give the torque coefficient Q_c at the speed ratio λ when the mean drag coefficient of the blade sections is 2δ. To perform the calculation the equations are rewritten as

$$\left.\begin{aligned} \eta_2 &= 1 - \frac{\eta_1}{\lambda} Q_c \quad \text{[see (3.4)]} \\ \tan \varphi_1 &= \frac{\lambda}{\eta_1 \eta_2} \quad \text{[see (2.8)]} \\ \eta_3 &= 1 - \frac{\eta_2^2}{Q_c} \sigma \delta f(\varphi_1) \\ \eta_1 &= 1 - \frac{1}{2} Q_c \eta_2 \eta_3 \left(\frac{\eta_1}{\lambda}\right)^3 \end{aligned}\right\} \tag{3.7}$$

Starting with any assumed value of η_1/λ and given values of $\sigma \delta$ and Q_c, these equations determine in turn η_2, $\tan\varphi_1$, η_3, and η_1, from which the values of η and λ are finally obtained.

The preceding analysis is based on a consideration of the action of the propeller blades and in any exact comparison with experimental results it is necessary to make a further allowance for the drag of the propeller boss. If R_0 is the radius of this boss, which is usually of the order of one tenth of the radius of the propeller, the drag of the boss may be estimated roughly as

$$D = 0.5 \pi R_0^2 \varrho V^2$$

and this drag must be subtracted from the thrust of the propeller. The drag of the boss can therefore be represented approximately by an additional efficiency factor η_4, determined by the equation

$$\eta_4 = \frac{T - D}{T}$$

or

$$\eta_4 = 1 - \frac{1}{4} \left(\frac{R_0}{R}\right)^2 \frac{\eta_1^2}{1 - \eta_1}$$
$$= 1 - \frac{\lambda^3}{2 \eta Q_c} \left(\frac{R_0}{R}\right)^2 \tag{3.8}$$

In theoretical discussions, however, it is best to ignore the drag of the boss of the propeller and to regard the aerodynamic action of the propeller as that of the blades only.

4. Numerical Results. The equations (3.7), of the preceding section, have been used to determine the efficiency of a propeller for a suitable

TABLE 6. Calculation of Propeller Efficiency ($\sigma\,\delta = 0.0016$, $Q_c = 0.004$).

λ/η_1	η_2	$tan\ \varphi_1$	$f(\varphi_1)$	η_3	η_1	λ	η
0.15	0.973	0.154	0.269	0.898	0.482	0.072	0.421
0.20	0.980	0.204	0.283	0.892	0.782	0.156	0.683
0.25	0.984	0.254	0.302	0.883	0.889	0.222	0.773
0.30	0.987	0.304	0.327	0.873	0.936	0.281	0.807
0.35	0.989	0.354	0.358	0.860	0.960	0.336	0.816
0.40	0.990	0.404	0.396	0.845	0.974	0.390	0.815
0.45	0.991	0.454	0.439	0.828	0.982	0.442	0.805
0.50	0.992	0.504	0.493	0.804	0.987	0.494	0.787

range of the three parameters $\sigma\,\delta$, Q_c, and λ. The solidity σ of a propeller with blades of conventional shape usually ranges from 0.08 for a propeller with two blades to 0.16 for a propeller with four blades, and the value of δ, which is half the mean profile drag coefficient C_D, may vary from 0.005 for thin blade sections under favorable conditions to 0.010 or more for thicker sections under less favorable conditions. The range of values chosen for $\sigma\,\delta$ has therefore been

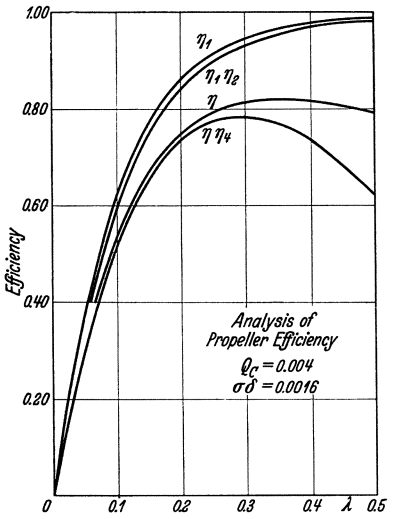

Fig. 18.

TABLE 7. Effect of Propeller Boss.

λ	η	η_4	$\eta\eta_4$
0.072	0.421	0.999	0.421
0.156	0.683	0.993	0.678
0.222	0.773	0.982	0.759
0.281	0.807	0.966	0.779
0.336	0.816	0.942	0.769
0.390	0.815	0.909	0.741
0.442	0.805	0.866	0.697
0.494	0.787	0.808	0.636

from zero to 0.0024. The torque coefficient Q_c of a propeller rarely exceeds 0.006 but the calculations have been extended to the large value of 0.012; and the range of λ considered has been from 0.1 to 0.5.

Details of the calculations in one case are given in Table 6 in order to show the varying importance of the three efficiency factors, and in Table 7 the additional loss of efficiency due to a boss of radius 0.1 R is also given. These results are illustrated in Fig. 18, the successive curves showing the values of η_1, $\eta_1 \eta_2$, η, and $\eta \eta_4$. Thus the top curve shows the ideal efficiency when all sources of loss of energy other than the axial momentum are ignored, and the distance between the following curves show the additional loss of efficiency due respectively to the rotational motion of the slipstream, the drag of the propeller blades and the drag of the boss. The chief loss of efficiency at low values of λ is due to the axial motion of the slipstream, but this loss becomes very small at higher values of λ. The loss of efficiency due to the rotational motion of the slipstream is always small and does not exceed 2 per cent. The loss of efficiency due to the drag of the propeller blades is always important, rising from 10 per cent at low values of λ to 20 per cent at the higher values. Finally the additional loss of efficiency

TABLE 8. Propeller Efficiency. Values of η in Per Cent to Nearest 0.5 Per Cent.

$\sigma\delta$	λ	$Q_c = 0.001$	0.002	0.004	0.008	0.012
0	0.10	76	66-1/2	58	48	43
	0.15	89	82-1/2	73-1/2	64	58-1/2
	0.20	94	89-1/2	83-1/2	75	69-1/2
	0.25	96-1/2	93-1/2	89-1/2	82-1/2	77-1/2
	0.30	98	96	93	87-1/2	83
	0.40	99	98	96	93	90
	0.50	99-1/2	99	97-1/2	95-1/2	93-1/2
0.0008	0.10	63	61	55-1/2	47	42
	0.15	71	74-1/2	70-1/2	63	57-1/2
	0.20	73-1/2	80-1/2	79	73-1/2	68-1/2
	0.25	74	83	84-1/2	80-1/2	76
	0.30	73	83-1/2	87	85	81-1/2
	0.40	68	82-1/2	88-1/2	89-1/2	87-1/2
	0.50	61	79-1/2	88	91	91
0.0016	0.10	48	54-1/2	55	46-1/2	41
	0.15	53	65-1/2	67	61	56
	0.20	53	71	74-1/2	71	67
	0.25	51	72	79-1/2	78	75
	0.30	47-1/2	71-1/2	81	82	80
	0.40	37	67-1/2	81	86	86
	0.50	22	60-1/2	78-1/2	86-1/2	87
0.0024	0.10	33-1/2	49-1/2	51	45-1/2	41-1/2
	0.15	34	58-1/2	64	60	55-1/2
	0.20	32	61	71	69-1/2	66
	0.25	28	61	74	75	73
	0.30	22	59-1/2	75-1/2	79	78
	0.40	6	52	74	82-1/2	83
	0.50	—	41	69	81-1/2	83-1/2

due to the propeller boss is negligible at small values of λ but becomes very important at the higher values and reduces the maximum efficiency from 81-$^1/_2$ per cent to 78 per cent.

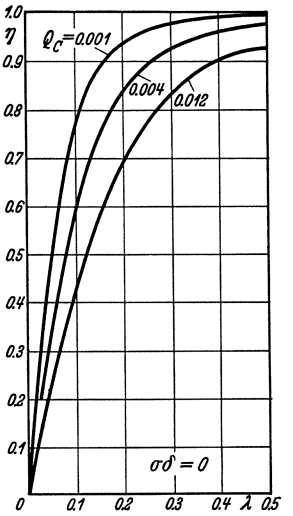

Fig. 19a.

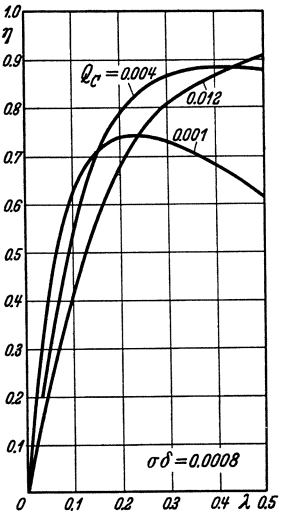

Fig. 19b.

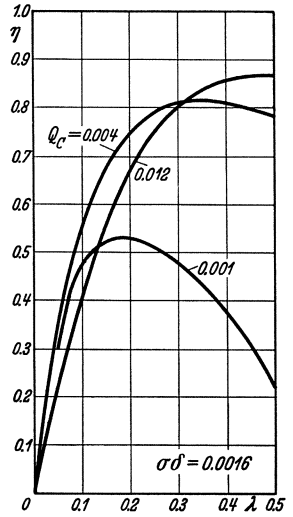

Fig. 19c.

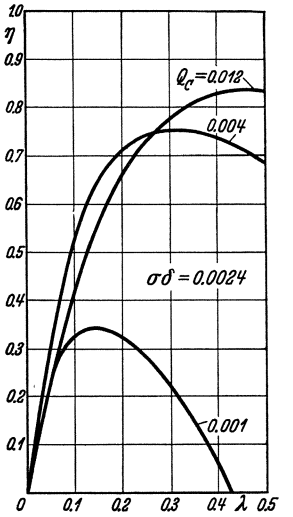

Fig. 19d.

Figs. 19a—d. Propeller efficiency curves for constant Q_c.

From detailed calculations of the type given in Table 6 curves of the efficiency η against the speed ratio λ are obtained for chosen values of the two parameters $\sigma\,\delta$ and Q_c, and from these curves the values

of the efficiency to the nearest 0.5 per cent have been read and are recorded in Table 8 above. The results are also shown graphically in Fig. 19 and Fig. 20. Fig. 19 shows the variation of the efficiency η

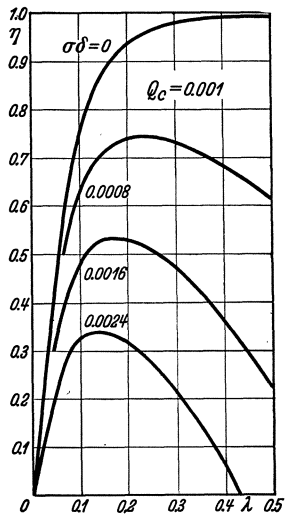

Fig. 20a.

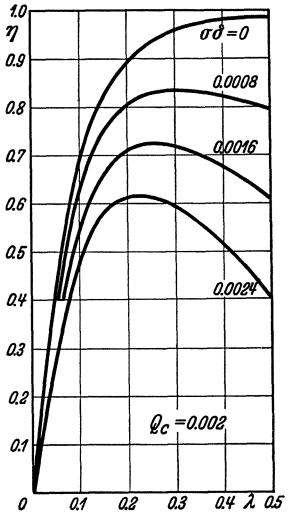

Fig. 20b.

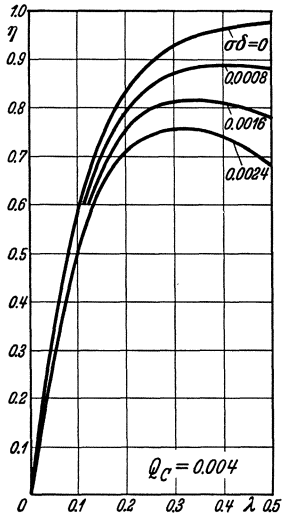

Fig. 20 c.

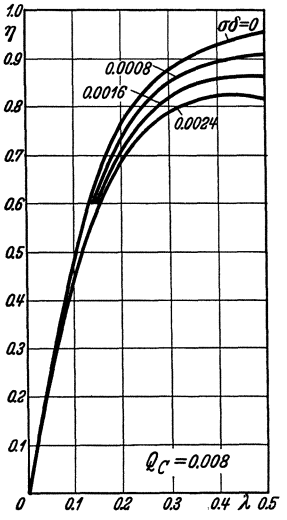

Fig. 20d.

Figs. 20a—d. Propeller efficiency curves for constant $\sigma\delta$.

with the torque coefficient Q_c for each of the four chosen values of $\sigma\,\delta$. When $\sigma\,\delta$ is zero the highest efficiency is obtained when the torque coefficient is smallest, but as the value of $\sigma\,\delta$ increases the loss of

efficiency is greatest for the lower values of the torque coefficient, and for any chosen values of $\sigma\,\delta$ and λ there is a best value of the torque coefficient which gives the highest efficiency. The effect of an increase of $\sigma\,\delta$ on the efficiency is shown more clearly in Fig. 20, and from curves of this type it is possible to estimate the efficiency for any intermediate value of $\sigma\,\delta$.

The curves of Fig. 19 for $\sigma\,\delta = 0$ may be compared with the previous curves of Fig. 15, and it can be verified that the assumption of mean values of the interference factors a and a' along the blades instead of the best distribution has not made any important difference in the efficiency calculated for given values of λ and Q_c.

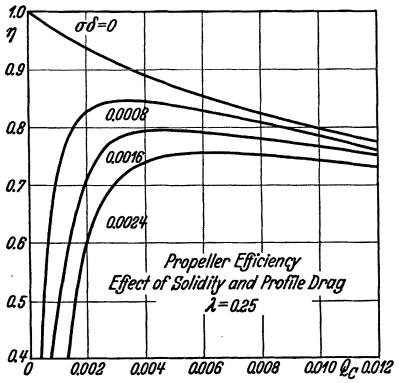

Fig. 21.

In Fig. 21 the efficiency η is plotted against the torque coefficient Q_c for the speed ratio $\lambda = 0.25$ and for a range of values of $\sigma\,\delta$. A constant value of λ means a constant ratio of forward speed to tip speed, and so the curves of this figure show the variation of efficiency with the torque coefficient when the forward speed and tip speed of the propeller remain constant. Curves of this type can therefore be used to determine the best diameter of a propeller when gearing is introduced in order to maintain a constant tip speed. Assuming an engine of 500 b.h.p., a tip speed of 800 f.p.s. and a forward speed of 200 f.p.s., the following optimum conditions are obtained, the range quoted corresponding to an efficiency which does not fall more than 0.5 per cent below the maximum possible value.

$\sigma\,\delta$	max. η	Best Q_c	Best diameter
0.0008	0.845	0.0024 to 0.0045	8 to 11 ft.
0.0016	0.795	0.0035 to 0.0061	7 to 9 ft.
0.0024	0.755	0.0051 to 0.0080	6 to 7-1/2 ft.

These numerical values show that it is best to use an airscrew of large diameter and small solidity.

In Fig. 22 the efficiency η is plotted against the torque coefficient Q_c for $\sigma\,\delta = 0.0008$ and for a range of values of the speed ratio λ. Curves of this type can be used to determine the best diameter of a propeller advancing with a definite velocity V, rotating with the angular velocity Ω and absorbing the power P. Assuming an engine power of 500 b.h.p. and a forward speed of 200 f.p.s. as in the previous numerical example, and taking a constant value of 200 for Ω (1900 r.p.m. approximately),

the following numerical values are derived. It appears that the best diameter is approximately 8 ft. for the assumed conditions of power and speed.

λ	Diameter	Q_c	η
0.15	13-1/3 ft.	0.00035	0.480
0.20	10 ft.	0.0015	0.785
0.25	8 ft.	0.0045	0.840
0.30	6-2/3 ft.	0.0112	0.825

At this stage of development of the theory it is possible to make a first rough comparison with experimental results. In Figs. 7 and 8 some experimental results are reproduced for a series of propellers of solidity 0.095, and on examining these curves it appears that the maximum efficiency of each curve occurs approximately where $Q_c = 0.011\,\lambda$. In Fig. 23 these maximum efficiencies are plotted against λ together

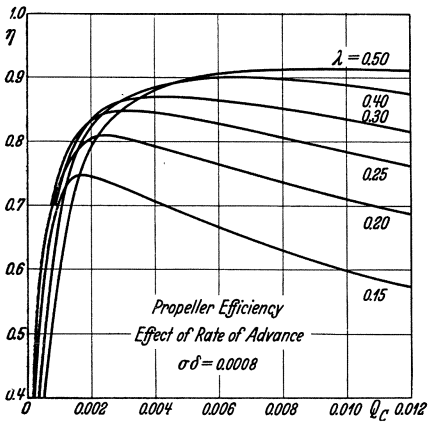

Fig. 22.

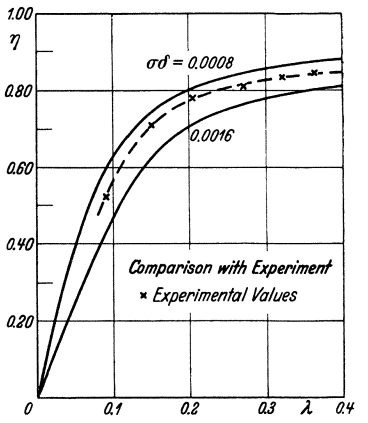

Fig. 23.

with the calculated curves of efficiency when $Q_c = 0.010\ \lambda$ for two values of $\sigma\ \delta$. It is evident that the calculated and experimental curves are of the same shape and that the experimental results correspond to a value of δ in the neighborhood of 0.010; and this value of δ would be a reasonable estimate for the blade sections used in the design of the propellers.

CHAPTER V

THE BLADE ELEMENT THEORY

1. The Primitive Blade Element Theory. The momentum theory of the propeller, which has been developed in the previous chapters, is based on a consideration of the mean axial and rotational velocity in the slipstream, and determines the thrust and torque of a propeller from the rate of increase of momentum of the fluid. The theory determines an upper limit to the efficiency of any propeller, depending

on its rate of advance and on the power absorbed, but it gives no indication of the form which must be given to the propeller to achieve this result. An alternative method of analyzing the behavior of a propeller is to estimate directly the forces experienced by the blades of the propeller due to their motion through the air. A crude attempt to estimate the force on the blade was made by W. Froude[1], but the development of the blade element theory in its true form is due almost entirely to the work of S. Drzewiecki[2].

Consider an element of a blade extending over a length dr of the radius at a distance r from the axis of rotation as shown in Fig. 24. The cross-section of this element has the shape of an airfoil section whose chord is inclined at an angle θ to the plane of rotation of the propeller, and the motion of this element is the resultant of the forward velocity V of the aircraft and the rotational velocity Ωr corresponding to the angular velocity Ω of the propeller. The resultant velocity W of the element through the air and the angle of inclination φ of this velocity to the plane of rotation are therefore determined by the equations

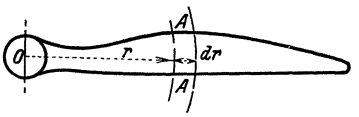

Fig. 24.

$$W^2 = V^2 + \Omega^2 r^2 \tag{1.1}$$

and

$$tan\varphi = \frac{V}{\Omega r} \tag{1.2}$$

Also the apparent angle of incidence α of the airfoil section is the excess of the blade angle θ over this angle φ, or

$$\alpha = \theta - \varphi \tag{1.3}$$

The development of the blade element theory of the propeller is based on the assumptions that the aerodynamic force acting on the blade element can be estimated as the force on a suitable airfoil of the same cross-section, advancing through the air with the uniform linear velocity W at the angle of incidence α, and that the force on the whole blade can be derived by adding the contributions of all the elements along the blade. The theory clearly admits of no interference between the successive blade elements, except in so far as such interference modifies the characteristics assumed for the airfoil section; and the validity of the theory depends intimately on the airfoil characteristics adopted for the blade elements. The discussion of this important question will be deferred to a later stage, and for the present it will be assumed that the lift and drag coefficients of each blade element are known as functions of the angle of incidence and of the shape of the cross-section.

[1] Transactions Institute of Naval Architects, Vol. 19, p. 47, 1878.

[2] Bulletin de l'Association Technique Maritime, 1892 *et seq.*

Referring to Fig. 25, the blade element will experience a lift force $d\,L$ at right angles to the direction of motion and a drag force $d\,D$ opposing this motion. Resolving at right angles to the plane of rotation, the thrust on the blade element is

$$d\,T = d\,L\cos\varphi - d\,D\sin\varphi$$

and similarly, resolving in the direction of the rotational velocity, the torque opposing the rotation of the propeller is

$$d\,Q = (d\,L\sin\varphi + d\,D\cos\varphi)\,r$$

Also, if c is the chord of the blade element, the elementary lift and drag forces can be expressed in terms of the corresponding non-dimensional coefficients as $d\,L = \frac{1}{2} C_L \varrho\, W^2 c\, d\,r$

and $d\,D = \frac{1}{2} C_D \varrho\, W^2 c\, d\,r$

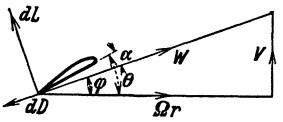

Fig. 25.

Then, adding the contributions of the corresponding elements on each of the B blades of the propeller, the elements of thrust and torque become

$$\frac{d\,T}{d\,r} = \frac{1}{2} B\,c\,\varrho\, W^2 (C_L\cos\varphi - C_D\sin\varphi) \tag{1.4}$$

and

$$\frac{d\,Q}{d\,r} = \frac{1}{2} B\,c\,r\,\varrho\, W^2 (C_L\sin\varphi + C_D\cos\varphi) \tag{1.5}$$

These two equations represent the complete solution of the behavior of a propeller according to the primitive blade element theory, and they suffice to determine the characteristics of any given propeller. The propeller is defined by the number B of its blades, by the variation of the chord c and blade angle θ along the blade, and by the shape of the blade sections: also the lift and drag coefficients of each of these blade sections are known as functions of the angle of incidence α. The state of operation of the propeller is defined by the speed ratio λ or $V/\Omega R$, and hence the angle φ is known for each successive blade element,

since $$\tan\varphi = \frac{V}{\Omega r} = \frac{\lambda R}{r}$$

The angle of incidence is then derived from (1.3) and the velocity of the blade element from (1.1), and finally the thrust and torque of the propeller can be obtained by integration of (1.4) and (1.5) along the blade. In general this integration must be performed graphically and it is only in certain special cases[1] that direct analytical integration is possible.

[1] For examples of direct integration see S. Drzewiecki, "Théorie Générale de l'Hélice"; Paris, 1920.

2. Efficiency of the Blade Element. Since the useful work done by the thrust on a blade element is $V\,d\,T$ and the power absorbed by the element is $\Omega\,d\,Q$, the efficiency of propulsion is

$$\eta = \frac{V\,d\,T}{\Omega\,d\,Q}$$

and on substituting the expressions for the elements of thrust and torque

$$\eta = \frac{V\,(C_L \cos\varphi - C_D \sin\varphi)}{\Omega\,r\,(C_L \sin\varphi + C_D \cos\varphi)} \tag{2.1}$$

It is now convenient to express the ratio of the drag and lift coefficients as

$$\frac{C_D}{C_L} = \varepsilon = \tan\gamma \tag{2.2}$$

and the formula for the efficiency of the blade element then becomes

$$\eta = \frac{1 - \varepsilon \tan\varphi}{1 + \varepsilon \cot\varphi} \tag{2.3}$$

or alternatively

$$\eta = \frac{\tan\varphi}{\tan(\varphi + \gamma)} \tag{2.4}$$

This form of expression for the efficiency of a blade element appeared first in the writings of W. Froude.

Numerical values of the efficiency deduced from this formula are given in Table 9 below, and the curves of efficiency against radial

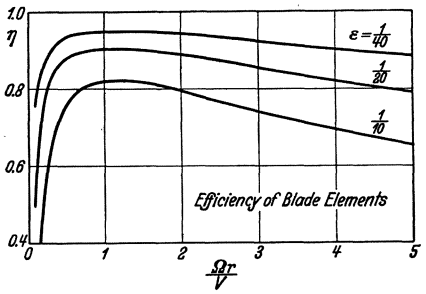

Fig. 26.

TABLE 9. Efficiency of Blade Element.

	$\varepsilon = 0.025$	0.050	0.100
$\frac{\Omega r}{V} = 0.1$	0.748	0.498	—
0.2	0.871	0.743	0.490
0.5	0.938	0.878	0.762
1.0	0.952	0.905	0.818
2.0	0.940	0.886	0.792
3.0	0.922	0.855	0.744
4.0	0.903	0.823	0.696
5.0	0.885	0.792	0.653

distance in the form $\Omega\,r/V$ are shown in Fig. 26. For any value of the drag-lift ratio ε, the efficiency is zero at the radius $\varepsilon\,V/\Omega$, rises rapidly with the radius to a maximum value, and then decreases steadily. The maximum efficiency occurs at the value of φ determined by the condition

$$\frac{d\,\eta}{d\,\varphi} = 0$$

and by logarithmic differentiation of (2.4) this condition becomes

$$\sin 2\varphi = \sin 2\,(\varphi + \gamma)$$

or

$$\varphi = \frac{\pi}{4} - \frac{\gamma}{2} \tag{2.5}$$

Thus the maximum efficiency occurs where the angle φ is slightly less than 45^0, corresponding to a radius slightly greater than V/Ω. It would therefore appear to be desirable to concentrate the principal working parts of the propeller blades about this radius, and every increase of radius of the propeller above this value will imply a reduction in the average efficiency of the propeller. The primitive blade element theory therefore indicates that the efficiency of a propeller decreases as the diameter increases above a certain optimum value, and this conclusion is an absolute contradiction of the conclusion drawn from the ideal momentum theory that the efficiency should increase with the diameter of the propeller. This discordance with the momentum theory, which is based on the fundamental laws of motion, suggests the necessity for a critical examination of the basis of the blade element theory.

That the blade element theory in its primitive form is not a satisfactory method of calculating the behavior of a propeller can be illustrated also by a direct appeal to experimental results. Fig. 27 shows the thrust and torque coefficients[1] of a series of propellers with an increasing number of identical blades, corresponding to the same speed ratio 0.162 in every case. The simple blade element theory would predict that the thrust and torque should be directly proportional to the number of blades, and the calculated relationship is also shown in the figure. There is a consistent discrepancy between the theoretical lines and the experimental curves, which suggests that the primitive blade element theory is not a complete and satisfactory explanation of the behavior of a propeller.

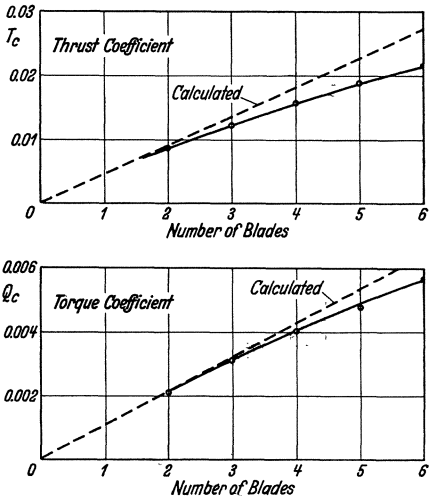

Fig. 27.

3. Blade Interference. The blade element theory is based on certain assumptions regarding the behavior of the blades, and in a critical survey of the theory it is convenient to consider in turn the following three points:—

(1) The assumption that the behavior of an element is not affected by the adjacent elements of the same blade.

[1] From Table V of Br. A.R.C. R. and M. 639, 1919.

(2) The assumption that the effective velocity of the element through the air is the resultant of the axial velocity V and the rotational velocity Ωr.

(3) The airfoil characteristics to be adopted for the element.

The independence of the blade elements, assumed in the primitive blade element theory and also in all later developments of the theory, is analogous to the assumption adopted in the momentum theory that the thrust on an elementary annulus of a propeller may be expressed as

$$d T = 2 \varrho u (u - V) d S$$

In the discussion of II 2 it was pointed out that this equation could not be established rigorously, but that the error introduced by its adoption was believed to be very small. Similarly, in the blade element theory, it is not possible to give a rigorous proof of the independence of the blade elements and the validity of the assumption must be justified by an appeal to suitable experimental results. If the assumption is valid, the thrust on the blade element at radial distance r with the blade angle θ should be independent of the variation of the blade angle along the remainder of the blade. A check of the assumption can therefore be obtained by taking two propellers of different pitch with blades of the same plan form and section, and by rotating the blades of one propeller so that the blade angles of the two propellers have the same value at a chosen radial distance r. The thrust distribution along the blades should then show the same element of thrust on the blade elements under examination. By means of a series of experiments of this nature C. N. H. Lock[1] has established the independence of the blade elements over the principal part of the blades, and a typical set of his experimental curves is reproduced in Fig. 28.

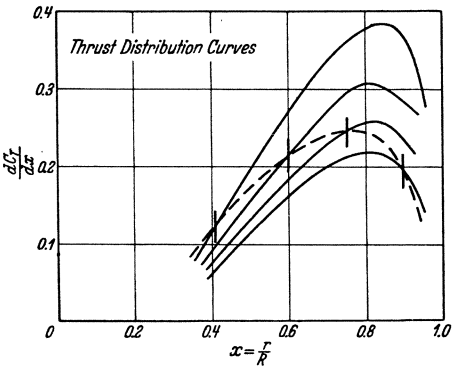

Fig. 28.

The next points to examine are the effective velocity of the blade element through the air and the airfoil characteristics to be adopted for the element. The momentum theory led to the conclusion that the axial velocity of the air relative to the propeller was increased from V to $V(1 + a)$ at the propeller disc, with a corresponding modification due to the relative rotational velocity, and it might be argued that

[1] Experiments to Verify the Independence of the Elements of an Airscrew Blade, Br. A.R.C. R. and M. 953, 1924.

the effective velocity of the blade element should be estimated in terms of these modified velocities. For simplicity the following discussion will be confined to the axial component of the velocity, but the conclusions will apply, with appropriate modifications, to the rotational component also.

Drzewiecki[1] maintained that there was no logical connection between the velocity u of the momentum theory and the velocity experienced by the blade element. In his opinion the velocity u represented only the mean value of a periodic flow, and the increased velocity at the disc of the propeller was not a general increase experienced by all the blade elements, but only a local increase concentrated around the blade elements and representing the disturbance created by them: it should not therefore be used in estimating the force experienced by the blade element. Drzewiecki therefore used the undisturbed axial velocity V and rotational velocity Ωr in estimating the force on the blade elements, and when it was found that the application of the theory failed to give accurate numerical predictions of the behavior of a propeller, he sought the cause of the discrepancy in the airfoil characteristics used for the blade elements.

In the early stages of the development of the theory no clear conception was possible of the airfoil characteristics to be used for the blade elements, since the true nature of the variation of these characteristics with the aspect ratio of the airfoil was quite unknown. Experimental results, however, showed a variation of these characteristics with aspect ratio and it was necessary to assign some suitable aspect ratio to the propeller blade in order to define the airfoil characteristics: this aspect ratio was commonly chosen to be the ratio of the length of the blade to the maximum chord and was usually in the neighborhood of 6. When his theory failed to give accurate results, Drzewiecki suggested that there might be a change in the airfoil characteristics due to the variation in thickness of the section along the blade, and he proposed to derive the appropriate characteristics from tests of a specially designed series of propellers.

A different mode of attack was adopted in other countries and several authors tried to develop a more accurate theory by incorporating the conception of an increased axial velocity. A. Betz[2] and G. de Bothezat[3] in their presentation of the blade element theory, both used the axial velocity u as determined by the momentum theory, while A. Fage

---

[1] Théorie générale de l'Hélice; Paris, 1920.

[2] Die wichtigsten Grundlagen für den Entwurf von Luftschrauben. Zeitschr. f. Flugtechnik u. Motorl. **6**, 97, 1915.

[3] The General Theory of Blade Screws. U.S. N.A.C.A. Technical Report No. 29, 1918.

and H. E. Collins[1] used an empirical fraction of the increase of velocity. It was generally recognized that the disturbance of flow at a blade element consists of one part due to the local action of the element and of another part due to the remoter action of the whole propeller, and that only this latter part should be introduced into the theory, since the local disturbance was equally present in the airfoil tests from which the airfoil characteristics were derived. This conception was sound, but the correct division of the disturbance into its two parts was impossible until the development of Prandtl's airfoil theory gave a clear explanation of the induced velocity caused by an airfoil. The theories therefore remained on an empirical basis, either as regards the magnitude of the interference flow to be adopted or as regards the appropriate airfoil characteristics to be used. Betz, using the axial velocity of the momentum theory but omitting any rotational interference flow, remarked that the appropriate aspect ratio was higher than that of an ordinary airfoil and tended towards infinite aspect ratio, depending on the shape of the blades; and de Bothezat, who used the same increased axial velocity and also introduced the rotational interference flow, adopted Drzewiecki's plan of special propeller tests to determine the airfoil characteristics. Fage and Collins, on the other hand, retained airfoil characteristics of aspect ratio 6 in their calculations and were compelled to adopt a purely empirical value for the effective axial velocity experienced by the blade element.

This general state of confusion and empiricism was inevitable until the development of a sound airfoil theory enabled a clear conception to be formed of the induced velocity experienced by an airfoil of finite span. The primitive blade element theory of Drzewiecki and the various modified theories, though correct in general structure could only be used in an empirical form, and they have now been replaced by the vortex theory which depends fundamentally on the conception that the lift of an airfoil section is associated with a circulation of the flow around its contour.

4. The Vortex System of a Propeller. According to modern airfoil theory the lift L per unit length of an airfoil section in two-dimensional motion is related to the circulation K around its contour by the equation[2]

$$L = \varrho V K \tag{4.1}$$

where ϱ is the density of the fluid and V is the uniform linear velocity of the airfoil through the fluid. Also if c is the chord of the airfoil section,

[1] Fage, A., and Collins, H. E., An Investigation of the Magnitude of the Inflow Velocity of the Air in the Immediate Vicinity of an Airscrew with a View to an Improvement in the Accuracy of Prediction from Airfoil Data of the Performance of an Airscrew. Br. A.R.C. R. and M. 328, 1917.

[2] Divisions B V 7 and E III **30**.

the lift can be expressed in terms of the non-dimensional lift coefficient as

$$L = \frac{1}{2} C_L \varrho V^2 c$$

and hence

$$K = \frac{1}{2} C_L V c \tag{4.2}$$

Applying this concept of airfoil theory to the problem of the propeller, it is evident that there must be a circulation of the flow around the blades of the propeller in order to produce the aerodynamic force experienced by the blades. In general the circulation K around the blade element will vary along the blade, but to explain the mode of action of the propeller it is simpler to assume as a first step that the circulation is constant along the whole blade. The existence of this circulation can be expressed also by the statement that there is a vortex line of strength K, bound to the blade and running along it from root to tip. But a vortex line cannot begin or end abruptly; unless it forms a closed curve in the body, it must be continued as a free vortex line in the fluid, and in this latter form it follows the general motion of the fluid as a trailing vortex behind the body. Thus the bound vortex K running along the blade of a propeller must be continued by two free vortices in the fluid, one springing from the root of the blade and the other from its tip. The free vortex springing from the roots of the propeller blades will be a straight line along the axis of the propeller and its strength will be $B\,K$ for a propeller with B blades. The tip vortices, each of strength K, will be of helical shape and will trace out roughly the paths described by the tips of the propeller blades. The system of trailing vortices of a propeller with two blades is shown diagramatically in Fig. 29. The figure represents a right hand propeller and the sense of rotation of the axial vortex is the same as that of the propeller, while the rotation of the tip vortices is of the opposite sense. These vortex lines constitute the slipstream of the propeller, and the motion of the fluid in the slipstream can be calculated as the induced velocity of this vortex system. The sense of rotation of the vortex lines is such that the fluid in the slipstream has an increased axial velocity and a rotational velocity in the same sense as the rotation of the propeller. The general nature of the flow is therefore of the same type as that postulated in the momentum theory of the propeller.

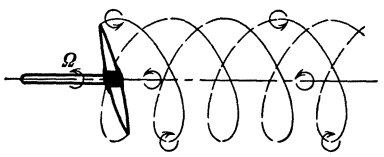

Fig. 29.

The preceding descriptive account of the vortex system of a propeller has been based for simplicity on the assumption that the circulation along the blade is constant. More generally, however, the strength of the circulation will vary along the blade, and indeed it has been shown in III 2 that the condition of constant circulation along the whole blade

is physically impossible. Due to the variation of the circulation along the blade, trailing vortices will arise, not only at the root and tip of the blade, but from every point of its trailing edge. If δK is the increase of circulation between the points r and $(r + \delta r)$ of the blade, then the strength of the helical vortex springing from this element will be $-\delta K$, the positive sense of rotation of the vortex line being that shown in Fig. 29. The vortex lines springing from one blade of the propeller form a vortex sheet in the form of a screw surface, and there will be one such surface for each blade of the propeller. The slipstream of the propeller consists of these vortex sheets and of the fluid contained between them. Owing to the contraction of the slipstream behind the propeller, the vortex sheets experience some distortion on leaving the propeller but they settle down eventually to a regular helical form in the final wake.

The disturbance of the flow caused by a propeller can be represented as the induced velocity of the complete vortex system, comprising the bound vortices of the propeller blades and the free vortex sheets of the slipstream, and the motion of the fluid relative to the propeller is the resultant of the axial velocity V and this induced velocity. It is now possible to determine the nature of the airfoil characteristics which should be used in the blade element theory of the propeller. According to the theory of airfoils of finite span developed by L. Prandtl, the behavior of an element of an airfoil is the same as in two-dimensional motion if due allowance is made for the induced velocity of the system of free vortices which spring from the airfoil. On the same basis therefore the behavior of any element of a propeller blade will be the same as in two-dimensional motion if the relative velocity of the fluid at the element is derived by including the induced velocity of the system of trailing vortices. This principle is the basis of the modern vortex theory of the propeller, which has superceded the primitive blade element theory and the empirical inflow theories. In many aspects the vortex theory is very similar to the inflow theories of Betz and de Bothezat, but it rests on a more reliable and more logical basis.

5. The Induced Velocity. Owing to the difficulty of calculating the induced velocity of the system of helical vortex sheets which constitute the slipstream of a propeller, the induced velocity is usually calculated on the assumption that the propeller has a very large number of blades. This assumption implies that the vorticity of the slipstream is distributed throughout the whole of the fluid instead of being concentrated on a few vortex sheets, and the vorticity can then be assumed to be grouped in the following manner. Considering first the condition of constant circulation along the blades, the boundary of the slipstream is a cylindrical vortex sheet as shown in Fig. 30. In place of the helical vortex lines covering the surface, the vorticity of the sheet may be considered as

a close succession of vortex rings RR whose vorticity represents the increased axial velocity of the slipstream, and a surface of vortex lines LL whose vorticity represents the rotation of the slipstream: the vortex system is completed by the axial vortex AA. More generally, with circulation varying along the blades of the propeller, the whole slipstream must be considered as full of vortex systems of this simpler type.

The induced velocity of the vortex system in the ultimate wake far behind the propeller will be an axial velocity $(u_1 - V)$ and an angular velocity ω_1, which will be functions of the radial coordinate r_1. In this wake the induced velocity of the bound vortices of the propeller blades is negligibly small. At the propeller disc also the bound vortices cannot give any component to the axial velocity owing to the symmetrical distribution of this vorticity relative to any arbitrary point of the disc, and hence the axial induced velocity $(u - V)$ will be due wholly to the trailing vortex system. To satisfy the condition of continuity of flow the axial velocities u und u_1 must be connected by the equation

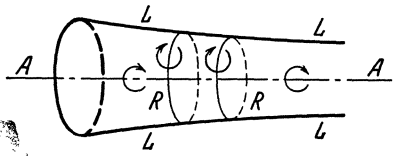

Fig. 30.

$$u\,r\,dr = u_1\,r_1\,dr_1 \tag{5.1}$$

Also, if the contraction of the slipstream can be ignored in calculating these induced velocities, it can easily be seen that the axial induced velocity at the propeller disc is half that in the ultimate wake; for the vortex system is then simply a long cylinder extending indefinitely in one direction from the propeller disc, and the induced axial velocity at a point of the wake, where the cylinder extends indefinitely in both directions, must clearly be double that at the corresponding point of the propeller disc.

Thus
$$u - V = \frac{1}{2}(u_1 - V)$$

or
$$u = \frac{1}{2}(u_1 + V) \tag{5.2}$$

which is the well known equation of the momentum theory.

The induced angular velocity ω immediately behind the propeller disc can be related to the corresponding angular velocity ω_1 in the wake by considering the constancy of circulation of the fluid. The ring of fluid of radius r immediately behind the propeller disc has the circulation $2\pi\omega r^2$, and by the laws of hydrodynamics this circulation must remain constant as the ring of fluid passes down stream. In the wake the radius of the ring has contracted to r_1 and there must therefore be an increase of the angular velocity governed by the equation

$$\omega r^2 = \omega_1 r_1^2 \tag{5.3}$$

Immediately in front of the propeller disc there can be no such circulation, since the fluid approaching the propeller is in irrotational motion. Also the bound vorticity of the propeller blades must cause equal and opposite induced angular velocities $\pm \omega'$ immediately before and behind the propeller disc, and hence the induced angular velocity of the trailing vortex system must have the value ω' at the propeller disc in order to cancel the effect of the bound vortices in front of the disc. It follows that the total induced angular velocity immediately behind the propeller disc is $2\,\omega'$, and this is the angular velocity previously denoted by ω. Hence the induced angular velocity of the trailing vortices at the propeller disc is $\frac{1}{2}\,\omega$.

It is now possible to describe the velocity experienced by the blade element. The motion of the blade element is the resultant of the axial velocity V and the rotational velocity Ωr, which are represented in Fig. 31 by NA and ON respectively. The induced velocity w of the fluid is represented by BA, and the effective relative velocity W of the blade element through the fluid is therefore represented by OB. The components of the induced velocity w are $(u - V)$ parallel to the axial velocity V and $\frac{1}{2}\,\omega r$ parallel to the rotational velocity Ωr, and hence the components of the effective velocity W are respectively u and $\left(\Omega - \frac{1}{2}\omega\right) r$. Writing as before

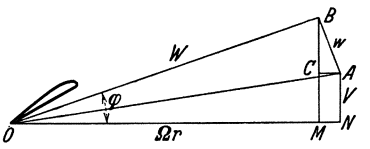

Fig. 31.

$$\left.\begin{aligned} u &= V\,(1 + a) \\ \omega &= 2\,\Omega\,a' \end{aligned}\right\} \tag{5.4}$$

and denoting by φ the angle of inclination of the effective velocity to the plane of rotation, these velocity components are

$$\left.\begin{aligned} W \sin\varphi &= u = V\,(1 + a) \\ W \cos\varphi &= \left(\Omega - \frac{1}{2}\,\omega\right) r = \Omega\, r\,(1 - a') \end{aligned}\right\} \tag{5.5}$$

6. The Airfoil Characteristics. Using the system of velocities as defined in the previous section, the airfoil characteristics must be chosen to correspond to two-dimensional motion or infinite aspect ratio, and a consideration of the implications of this conclusion explains the difficulties encountered in the primitive blade element theory and in the later inflow theories. Thus de Bothezat, using effectively the induced velocities of the vortex theory, found that airfoil characteristics of a wing of an ordinary aspect ratio were unsuitable, and was compelled to advocate special propeller tests to determine the appropriate characteristics; Fage and Collins, retaining airfoil characteristics corresponding

to an aspect ratio 6, were unable to retain the full values of the interference velocities and were compelled to reduce these velocities by an empirical factor; and Drzewiecki, who admitted no interference velocities in his theory, was also reduced to the expedient of special propeller tests, and the airfoil characteristics appropriate to his theory would have corresponded to an aspect ratio less than that of an ordinary wing.

Airfoil characteristics are usually determined from tests of a rectangular airfoil of aspect ratio 5 or 6, and before using these characteristics in propeller calculations it is necessary to correct them to infinite aspect ratio. The necessary transformation formulae have been determined by the theory of airfoils of finite span[1] but it is important that the transformation shall be made on the basis of the best known formulae for rectangular airfoils and not on the simpler hypothesis of elliptic lift distribution across the span of the airfoil. Denoting the aspect ratio of the rectangular airfoil by A and the values corresponding to infinite aspect ratio by the suffix (0), the appropriate transformation formulae[2] are

$$\left.\begin{aligned} \alpha_0 &= \alpha - \frac{C_L}{\pi A}(1+\tau) \\ C_{D0} &= C_D - \frac{C_L^2}{\pi A}(1+\delta) \end{aligned}\right\} \tag{6.1}$$

where the angle of incidence is expressed in circular measure, and the corrections to the angle of incidence and to the drag coefficient are made at definite values of the lift coefficient. The coefficients τ and δ are zero for a wing with elliptic loading, but for a rectangular airfoil they have the values given in Table 10. In this Table s_0 and s denote respectively the values of $\frac{dC_L}{d\alpha}$ for infinite aspect ratio and for the rectangular airfoil of aspect ratio A. For an airfoil of aspect ratio 6, the value of A/s_0 is approximately unity and thus, compared with the transformation formulae for elliptic loading, the correction to the angle of incidence is increased by 17 per cent and that to the drag coefficient by 5 per cent. The latter is probably unimportant, but the correction to the angle of incidence will lead to noticeable discrepancies unless the correct formulae for rectangular airfoils are used.

TABLE 10.
Transformation Constants.

A/s_0	A/s	τ	δ
0.50	0.85	0.10	0.019
0.75	1.11	0.14	0.034
1.00	1.37	0.17	0.049
1.25	1.63	0.20	0.063
1.50	1.89	0.22	0.076

Table 11 gives the results of applying the transformation formulae to a typical airfoil section[3] suitable for a propeller blade, and the

[1] See Division E IV **6.**

[2] See Division E IV (6.7), (6.10).

[3] Aerofoil No. 3 of Br. A.R.C. R. and M. 322, 1917.

TABLE 11. Transformation of Airfoil Characteristics.

Aspect Ratio 6			Infinite Aspect Ratio					
			Elliptic Loading			Rectangular Airfoil		
C_L	α	C_D	α_0	C_{D0}	ε	α_0	C_{D0}	ε
0.094	—4°	0.0294	—4.3°	0.0289	0.308	—4.3°	0.0289	0.308
0.248	—2	0.0210	—2.8	0.0177	0.071	—2.9	0.0176	0.071
0.392	0	0.0222	—1.2	0.0141	0.0360	—1.4	0.0137	0.0350
0.548	2	0.0278	0.3	0.0119	0.0217	0.1	0.0112	0.0204
0.702	4	0.0382	1.9	0.0120	0.0171	1.5	0.0108	0.0154
0.845	6	0.0515	3.4	0.0137	0.0162	3.0	0.0119	0.0141
0.980	8	0.0664	5.0	0.0154	0.0157	4.5	0.0131	0.0134
1.125	10	0.0841	6.6	0.0170	0.0151	6.0	0.0139	0.0123
1.228	12	0.1034	8.3	0.0234	0.0190	7.7	0.0196	0.0159

numerical values show clearly the importance of using the correct transformation formulae, more particularly in deducing the angle of incidence. The Table can also be used to examine another point of interest. In order to simplify calculations relating to a propeller, it is frequently assumed either that the profile drag coefficient C_{D0} is constant or that the drag-lift ratio ε is constant. The numerical values in this Table and the curves of Fig. 32 suggest that the assumption of a constant profile drag coefficient is valid over a wider range than that of a constant drag-lift ratio, and that neither assumption is quite satisfactory.

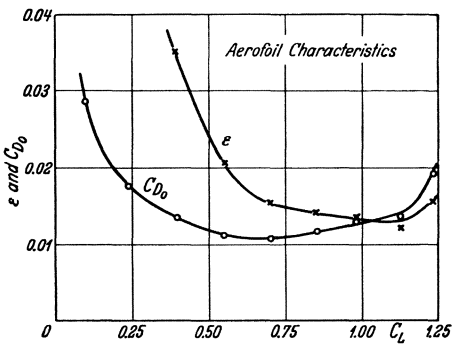

Fig. 32.

7. Multiplane Interference. The vortex theory of the propeller is based on the assumption that the blade of a propeller may be divided into a large number of elements and that each of these elements, which have the form of airfoil sections, may be regarded as in uniform linear motion through the fluid and subject to the induced velocity of the trailing vortex system of the slipstream. The velocity of a typical blade element is the resultant of an axial component V, the forward speed of the propeller through the fluid, and of a rotational component Ωr, corresponding to the angular velocity Ω of the propeller about its axis. This second component is not strictly a linear velocity, since the blade element is describing a helical path on the surface of a cylinder of radius r, whose axis is the axis of rotation of the propeller. If this cylinder is unrolled and represented on a flat surface as in Fig. 33, the elements of the blades of the propeller appear as a series of airfoil

sections along an axis AA. The distance between consecutive airfoil sections is $2\pi r/B$ and, to represent the system correctly, the set of B airfoil sections representing the B blades of the propeller must be repeated again and again so as to form an infinite series or cascade of airfoils. The axis AA represents the plane of rotation of the propeller and hence the airfoil sections are inclined to this axis at the angle θ, which is the blade angle of these elements of the propeller blade.

The motion of the blade elements, which are members of this cascade, is composed of a velocity Ωr along the axis of the cascade and of a velocity V normal to this axis, but in order to represent the behavior of the blade elements correctly by the two-dimensional flow past the cascade it is necessary to modify this system of velocities in one respect. In the two-dimensional problem the mean velocity normal to the axis of the cascade retains a constant value in order to satisfy the condition of continuity of flow, but in the actual flow past the propeller, which the cascade is to represent, there is a radial contraction of the circular annulus with a corresponding increase of the axial velocity. The two-dimensional cascade can therefore only be used to represent the flow immediately before and behind the propeller, and the velocity normal to the axis of the cascade must be taken to be the axial velocity u through the propeller disc and not simply the forward speed V of the propeller. The system of velocities relative to the airfoil sections of the cascade then assumes the form shown in Fig. 34. In front of the cascade the resultant velocity W_1 has the components u normal to the axis AA and Ωr parallel to it. The normal velocity retains the same value behind the cascade, but the tangential component is reduced to $(\Omega - \omega) r$ and the resultant velocity W_2 is therefore less than the initial velocity W_1. This reduction of velocity implies an increase of pressure and the cascade experiences a normal force Y, which corresponds to the thrust of the blade elements of the propeller. Also the change in the tangential component of the velocity is associated with a corresponding force X, so that Xr represents the torque of the blade elements.

Fig. 33.

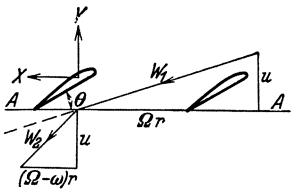

Fig. 34.

By considering the behavior of a cascade of airfoils it is possible to deduce the behavior of the corresponding blade elements of a propeller in terms of the axial velocity through the disc of the propeller. The analysis determines the rotational velocity ω imparted to the slipstream, but it is necessary to revert to the true cylindrical form of the slipstream in order to determine the relationship between the normal velocity u used in the cascade analysis and the axial velocity V of the propeller.

8. Cascade of Airfoils. Consider first a cascade of frictionless airfoils, around each of which there is a circulation K; let u be the component of the velocity normal to the axis of the cascade, and let the tangential component change from w_1 in front of the cascade to w_2 behind it. Also let s be the distance between consecutive airfoils of the cascade, and let X and Y be respectively the tangential and normal components of the force on each member of the cascade. In the corresponding propeller problem, which is represented by this cascade, the tangential velocities would be

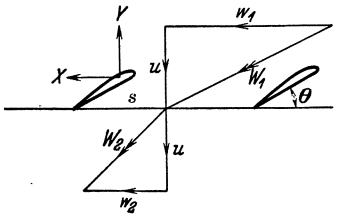

Fig. 35.

$$\left.\begin{aligned} w_1 &= \Omega r \\ w_2 &= (\Omega - \omega) r \end{aligned}\right\} \tag{8.1}$$

and the elements of thrust and torque would be respectively

$$\left.\begin{aligned} \frac{dT}{dr} &= B Y \\ \text{and} \quad \frac{dQ}{dr} &= B X r \end{aligned}\right\} \tag{8.2}$$

where B is the number of the propeller blades, and where

$$B s = 2 \pi r \tag{8.3}$$

Applying Bernoulli's equation to the flow relative to the cascade, the increase of pressure behind the cascade is obtained immediately as

$$p_2 - p_1 = \frac{1}{2} \varrho (w_1^2 - w_2^2)$$

and the normal force Y on each member of the cascade is represented by this pressure over a length s of the axis. Hence

$$Y = \frac{1}{2} \varrho (w_1^2 - w_2^2) s \tag{8.4}$$

The mass flow per unit length of the cascade is ϱu and this fluid receives a component of velocity $(w_1 - w_2)$ parallel to the axis of the cascade. Hence the tangential force per unit length of the cascade is $\varrho u (w_1 - w_2)$ and the force on each member of the cascade is

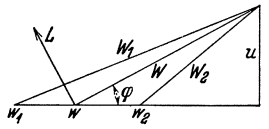

Fig. 36.

$$X = \varrho u (w_1 - w_2) s \tag{8.5}$$

These components X and Y of the force on each member of the cascade can also be derived by considering the circulation K around the section and the corresponding lift force L. The resultant velocities W_1 and W_2 in front of and behind the cascade can be represented as in Fig. 36, and the resultant velocity W experienced by the airfoil section will be intermediate between these two values. The circulation around each airfoil section is simply

$$K = (w_1 - w_2) s$$

and hence the lift L per unit length of each airfoil section is

$$L = \varrho W (w_1 - w_2) s$$

The components of this force are respectively

$$X = \varrho\, u\, (w_1 - w_2)\, s$$

and

$$Y = \varrho\, w\, (w_1 - w_2)\, s$$

This value of the tangential component X agrees with the previous expression (8.5), and a comparison of the value of the normal component with the previous expression (8.4) leads to the conclusion that

$$w = \frac{1}{2}(w_1 + w_2) \tag{8.6}$$

Thus the effective tangential component of the velocity experienced by the airfoil section is the mean of the values before and behind the cascade, and the effective resultant velocity W is the vectorial mean of the resultant velocities W_1 and W_2.

Applying these results to the problem of a propeller by means of the relationships (8.1), (8.2), and (8.3), the circulation around the blade element is

$$K = \frac{2\pi}{B}\omega r^2 \tag{8.7}$$

and in terms of this circulation the element of thrust per unit length of blade becomes

$$\frac{dT}{dr} = B\varrho K\left(\Omega - \frac{1}{2}\omega\right) r$$

$$= B\varrho K\left(\Omega r - \frac{BK}{4\pi r}\right) \tag{8.8}$$

while the corresponding element of torque per unit length of blade is simply

$$\frac{dQ}{dr} = B\varrho K u r \tag{8.9}$$

This system of equations must be completed by an additional equation expressing the relationship between the axial velocity u through the propeller disc and the forward speed V of the propeller. This equation is the well known axial momentum equation

$$\frac{dT}{dr} = 4\pi\varrho u\,(u - V)\, r \tag{8.10}$$

The system of equations (8.8), (8.9), and (8.10) suffice to determine the thrust and torque of a propeller when the distribution of circulation along the blade is known, but further analysis is necessary to relate this circulation to the shape and blade angle of the airfoil section and to allow for the profile drag of the blades. Since the lift of an airfoil section per unit length is

$$L = \varrho\, W K$$

and since this lift can also be expressed in terms of the usual non-dimensional lift coefficient C_L as

$$L = \frac{1}{2} C_L \varrho\, W^2 c$$

the circulation K is related to the lift coefficient C_L by the equation

$$K = \frac{1}{2} C_L W c \tag{8.11}$$

If this substitution is made in (8.8) and (8.9), the expressions for the elements of thrust and torque assume the forms

$$\frac{dT}{dr} = \frac{1}{2} B c \varrho W^2 C_L \cos\varphi$$

and

$$\frac{dQ}{dr} = \frac{1}{2} B c r \varrho W^2 C_L \sin\varphi$$

where

$$\tan\varphi = \frac{u}{\left(\Omega - \frac{1}{2}\omega\right) r}$$

These are the usual equations as derived in the blade element theory of the propeller with the drag of the blades omitted.

When the effect of the profile drag of the airfoil sections is included in the analysis, there will be a certain loss of total pressure head p' as the air passes through the cascade and the equation (8.4) for the normal force will assume the modified form

$$Y = \frac{1}{2} \varrho (w_1^2 - w_2^2) s - p' s \tag{8.12}$$

while the equation (8.5) for the tangential force is unaltered. Also if K is the circulation around each of the airfoil sections, the lift will still be

$$L = \varrho W K$$

but it is no longer possible to determine this circulation as $(w_1 - w_2) s$, since the tangential velocity imparted to the air as it passes through the cascade is due partly to the lift of the airfoil sections and partly to their drag in the proportion of the components of these two forces parallel to the axis of the cascade.

If D is the drag of each airfoil section, the normal and tangential components of the resultant force are respectively

$$X = \frac{u L + w D}{W}$$

and

$$Y = \frac{w L - u D}{W}$$

Eliminating the lift from these two equations and substituting for X and Y from (8.5) and (8.12), the drag is obtained in the form

$$\begin{aligned} W D &= w X - u Y \\ &= \varrho u (w_1 - w_2) s \left[w - \frac{1}{2} (w_1 + w_2) \right] + u p' s \end{aligned}$$

But $W D$ represents the rate of loss of energy due to the drag of each airfoil section and $u p' s$ is simply another measure of this loss of energy in terms of the loss of total pressure head of the air on passing through the cascade. Hence, with the other term zero we have

$$w = \frac{1}{2} (w_1 + w_2)$$

as previously obtained for the ideal cascade.

Finally, in terms of the lift and drag coefficients of the airfoil section, the elements of thrust and torque of the propeller are obtained in their usual forms

$$\frac{dT}{dr} = BY = \frac{1}{2} B c \varrho W^2 (C_L \cos\varphi - C_D \sin\varphi)$$

and

$$\frac{dQ}{dr} = BXr = \frac{1}{2} B c r \varrho W^2 (C_L \sin\varphi + C_D \cos\varphi)$$

9. Airfoil Characteristics in a Cascade. The discussion of the behavior of an infinite cascade of airfoil sections has led to the same form of equations for the thrust and torque of the blade element of a propeller as was derived previously by considering a single blade element, but it is necessary to examine whether the airfoil characteristics for the blade element in two-dimensional motion are the same for a cascade of airfoils as for a single airfoil. The general theoretical solution of this problem is not known, but the results for a cascade of straight line airfoils are available and were in fact used by Joukowski[1] in his propeller theory.

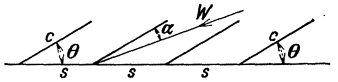

Fig. 37.

Let c be the chord of each straight line airfoil, set at an angle θ to the axis of the cascade, and let s be the spacing of the airfoils along the cascade. Also let W be the effective velocity experienced by each airfoil at an angle of incidence α: this velocity W, in accordance with the previous discussion, is to be taken as the vectorial mean of the velocities in front of and behind the cascade. Then the lift L of each airfoil can be expressed in terms of the standard non-dimensional lift coefficient C_L in the form $L = \frac{1}{2} C_L \varrho W^2 c$

and this lift coefficient is determined by the equation[2]

$$\frac{C_L}{2\pi \sin\alpha} = \frac{2 \tanh x}{\pi \sigma \sin\theta} \tag{9.1}$$

where θ is the blade angle and σ is the ratio of airfoil chord c to spacing s along the axis of the cascade, or in terms of the dimensions of the propeller,

$$\sigma = \frac{c}{s} = \frac{Bc}{2\pi r} \tag{9.2}$$

Also the subsidiary parameter x is determined in association with two additional parameters p and q by the set of equations

$$\left.\begin{aligned} \sin p &= \cos\theta \sin q \\ \sinh x &= \sin\theta \tan q \\ \frac{\pi}{2}\sigma &= x \sin\theta + p \cos\theta \end{aligned}\right\} \tag{9.3}$$

[1] Travaux de la Section de Physique de la Société des Amis des Sciences Naturelles; Moscow, 1915.

[2] These formulae are derived from Joukowski's paper with slight modification and change of notation.

For a single airfoil in two-dimensional motion the ratio $C_L/2\,\pi\,sin\,\alpha$ would be unity[1], and the importance of this analysis is to determine how far the value of this ratio is modified by the mutual interference of the airfoils in the infinite cascade. Numerical results have been deduced from these formulae and are shown in Fig. 38 as curves of the ratio $C_L/2\,\pi\,sin\,\alpha$ against the solidity σ for various blade angles (see also Table 12). The ratio never differs from unity by more than 5 per cent in the range considered, and for the usual

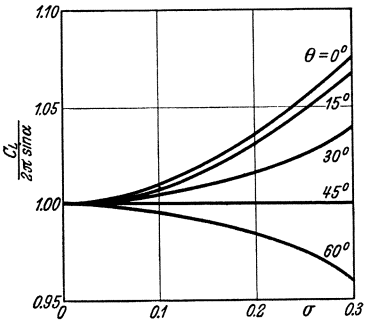

Fig. 38.

TABLE 12. Values of $\frac{C_L}{2\,\pi\,sin\,\alpha}$.

$\theta =$	0	15°	30°	45°	60°
$\sigma = 0.05$	1.002	1.002	1.001	1.000	0.999
0.10	1.008	1.007	1.004	1.000	0.996
0.15	1.019	1.016	1.009	1.000	0.991
0.20	1.033	1.029	1.016	1.000	0.984
0.25	1.051	1.047	1.025	1.000	0.975

combination of solidity and blade angle the divergence is quite small. In view of these numerical results, therefore, it appears to be legitimate to neglect the multiplane interference between the successive blades of a propeller and to adopt simply the airfoil characteristcs of a single airfoil in two-dimensional motion.

CHAPTER VI
THE VORTEX THEORY

1. The Propeller Blades. The vortex theory of the propeller is based fundamentally on the conception that trailing vortices spring from the rotating blades of the propeller and pass down the slipstream in the form of helical vortex sheets. The interference velocity experienced by the blades of the propeller must be calculated as the induced velocity of this vortex system, and the aerodynamic reaction on any blade element is derived from this modified system of velocities in association with airfoil characteristics corresponding to two-dimensional motion. The calculation of these induced velocities is very complex and the analysis is therefore usually based on the assumption that the propeller has a large number of blades. As a consequence of this simplifying assumption the velocity has a uniform value around any annulus of the propeller disc and the vortex theory becomes essentially identical with the blade element theory, including the interference velocities as determined by the general momentum theory and using airfoil characteristics

[1] See Division E II (7.4).

corresponding to two-dimensional motion. The effect of the periodicity of the flow, which actually occurs with a propeller of a small number of blades, may be estimated subsequently as a correction to this simplified form of the theory.

Consider an element of a propeller blade at the radial distance r from the axis of rotation. The effective velocity W of this blade element relative to the fluid is the resultant of an axial component u, which exceeds the forward speed V of the propeller owing to the axial induced velocity of the vortex system of the slipstream, and of a tangential component $\left(\Omega - \frac{1}{2}\omega\right) r$ where Ω is the angular velocity of the propeller and ω is the angular velocity imparted to the air immediately behind the propeller disc. Introducing the axial and rotational interference factors a and a', the effective velocity of the blade element may be illustrated as in Fig. 39 and may be defined by the equations [see V (5.5)]

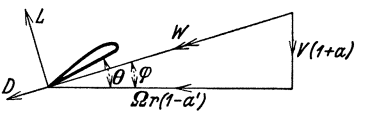

Fig. 39.

$$\left.\begin{aligned} W \sin\varphi &= u &&= V(1+a) \\ W \cos\varphi &= \left(\Omega - \tfrac{1}{2}\omega\right) r &&= \Omega r (1-a') \end{aligned}\right\} \tag{1.1}$$

The corresponding speed ratio λ of the propeller is then obtained directly as

$$\lambda = \frac{V}{\Omega R} = \frac{r}{R}\frac{1-a'}{1+a}\tan\varphi \tag{1.2}$$

The blade element experiences a lift force normal to the direction of the resultant velocity W and a drag force parallel to this direction. Expressing these forces in terms of the usual lift and drag coefficients, resolving parallel and normal to the propeller axis, and summing over all the B blades of the propeller, the elements of thrust and torque contributed by all the blade elements at the radial distance r are obtained in the same form as in the simple blade element theory. Thus

$$\frac{dT}{dr} = \frac{1}{2} B c \varrho W^2 (C_L \cos\varphi - C_D \sin\varphi) \tag{1.3}$$

and

$$\frac{dQ}{dr} = \frac{1}{2} B c r \varrho W^2 (C_L \sin\varphi + C_D \cos\varphi) \tag{1.4}$$

These equations are expressed more conveniently in a non-dimensional form. For this purpose the chord c is replaced by the solidity,

$$\sigma = \frac{Bc}{2\pi r} \tag{1.5}$$

which expresses the ratio of the total blade width of all the blade elements at radius r to the circumference of the circle on which they lie, and the thrust and torque coefficients are defined by the equations

$$\left.\begin{aligned} T &= T_c \pi R^2 \varrho \Omega^2 R^2 \\ Q &= Q_c \pi R^2 \varrho \Omega^2 R^3 \end{aligned}\right\} \tag{1.6}$$

Writing also
$$\left.\begin{aligned} C_x &= C_L \sin\varphi + C_D \cos\varphi \\ C_y &= C_L \cos\varphi - C_D \sin\varphi \end{aligned}\right\} \tag{1.7}$$
for the components of the aerodynamic force normal and parallel to the axis of the propeller, the expressions for the elements of thrust and torque become

$$R\frac{dT_c}{dr} = \sigma\left(\frac{r}{R}\right)^3 (1-a')^2 C_y \sec^2\varphi \tag{1.8}$$

and
$$R\frac{dQ_c}{dr} = \sigma\left(\frac{r}{R}\right)^4 (1-a')^2 C_x \sec^2\varphi \tag{1.9}$$

Finally the efficiency of the blade elements at radial distance r is
$$\eta_r = \frac{V\frac{dT}{dr}}{\Omega\frac{dQ}{dr}} = \frac{V\frac{dT_c}{dr}}{\Omega R\frac{dQ_c}{dr}}$$
and on substituting from the preceding equations this efficiency becomes
$$\eta_r = \frac{V}{\Omega r}\frac{C_y}{C_x} = \frac{1-a'}{1+a}\frac{\tan\varphi}{\tan(\varphi+\gamma)} \tag{1.10}$$
where
$$C_D = C_L \tan\gamma$$

These equations express the characteristics of the propeller in terms of the effective flow experienced by the blade elements, and it is necessary to introduce additional equations to determine the interference factors a and a', which represent the induced velocities at the blade elements due to the vortex system of the slipstream. The present analysis is developed on the basis that these induced velocities may be calculated on the assumption of a propeller with a large number of blades, and the appropriate equations can therefore be derived from a consideration of the energy and momentum of the air in the slipstream.

2. Energy and Momentum. The balance of energy for a propeller is considered most conveniently by assuming the propeller to be rotating with the angular velocity Ω in a stream of velocity V directed along its axis. Considering only the blade elements at distance r from the axis of rotation, the power put into the propeller is $\Omega\frac{dQ}{dr}$. This power must be equated to the work done on the air by the thrust and torque of the propeller and to the loss of energy due to the profile drag of the blade elements. The thrust operates on air moving with the axial velocity u and does the work $u\frac{dT}{dr}$ in unit time. Similarly the torque operates on air moving with the angular velocity $\frac{1}{2}\omega$ and does the work $\frac{1}{2}\omega\frac{dQ}{dr}$ in unit time. Hence if $\frac{dE}{dr}$ is the rate of loss of energy of the system, the energy equation becomes
$$\Omega\frac{dQ}{dr} = u\frac{dT}{dr} + \frac{1}{2}\omega\frac{dQ}{dr} + \frac{dE}{dr} \tag{2.1}$$

or, in terms of the interference factors a and a',

$$\frac{dE}{dr} = \Omega\,(1-a')\,\frac{dQ}{dr} - V\,(1+a)\,\frac{dT}{dr}$$

$$= W\left[\frac{1}{r}\frac{dQ}{dr}\cos\varphi - \frac{dT}{dr}\sin\varphi\right] \quad \text{[see (1.1)]}$$

Substituting the expressions for the elements of thrust and torque from the previous section, the rate of loss of energy becomes

$$\frac{dE}{dr} = \frac{1}{2}\,B\,c\,\varrho\,W^3\,C_D \tag{2.2}$$

which is the expression for the rate of loss of energy due to the profile drag of the blade elements moving with the resultant effective velocity W.

The energy of the air is represented by its total pressure head, which has a constant value H_0 in front of the propeller and is increased to a higher value H_1 in the slipstream. As the air passes through the propeller disc it receives an increase of pressure p' and an angular velocity ω without any change in the axial and radial components of the velocity, and hence the increase of total pressure head is

$$H_1 - H_0 = p' + \frac{1}{2}\,\varrho\,\omega^2 r^2 \tag{2.3}$$

This increase of energy of the air is due to the action of the thrust and torque of the propeller. Considering an annulus extending a distance dr along the blades, the energy imparted by the thrust and torque is $\left(u\,dT + \frac{1}{2}\,\omega\,dQ\right)$, and this energy is given to a volume of air $2\pi r\,u\,dr$.

Hence $$u\frac{dT}{dr} + \frac{1}{2}\,\omega\frac{dQ}{dr} = 2\pi r\,u\left(p' + \frac{1}{2}\,\varrho\,\omega^2 r^2\right)$$

But the element of thrust is clearly equal to the increase of pressure over the annulus, or

$$\frac{dT}{dr} = 2\pi r\,p' \tag{2.4}$$

and the element of torque is equal to the angular momentum imparted to the air in unit time, or

$$\frac{dQ}{dr} = 2\pi r\,\varrho\,u\,\omega\,r^2 \tag{2.5}$$

These two expressions are consistent with the previous equation for the increase of energy and show that the two terms in the expression (2.3) for the increase of total pressure head are due respectively to the thrust and torque of the blade elements.

Expressing (2.5) in its non-dimensional form

$$R\frac{dQ_c}{dr} = 4\left(\frac{r}{R}\right)^3\lambda\,(1+a)\,a'$$

$$= 4\left(\frac{r}{R}\right)^4(1-a')\,a'\tan\varphi$$

and equating this expression for the element of torque to the previous expression (1.9), the rotational interference factor a' is determined by the equation

$$\frac{a'}{1-a'} = \frac{\sigma C_x}{4 \sin\varphi \cos\varphi} \tag{2.6}$$

In order to determine the axial interference factor a it is necessary to consider the flow in the ultimate wake far behind the propeller. Denoting values in this wake by the suffix (1), the conditions of continuity of flow require that

$$\left.\begin{aligned} u\, r\, dr &= u_1\, r_1\, dr_1 \\ \omega\, r^2 &= \omega_1\, r_1^2 \end{aligned}\right\} \tag{2.7}$$

Also in the ultimate wake the pressure is governed by the equation

$$\frac{dp_1}{dr_1} = \varrho\, \omega_1^2 r_1 \tag{2.8}$$

and the total pressure head is

$$H_1 = H_0 + \tfrac{1}{2}\varrho\,(u_1^2 - V^2) + \tfrac{1}{2}\varrho\,\omega_1^2 r_1^2 \tag{2.9}$$

Owing to the contraction of the slipstream r_1 is less than r and, by virtue of the second equation (2.7), ω_1 is greater than ω and $\omega_1^2 r_1^2$ is greater than $\omega^2 r^2$. Thus, on comparing the two expressions (2.3) and (2.9) for the total pressure head, it appears that as the air passes down the slipstream the rotational energy is increased: the excess pressure behind the disc of the propeller is converted mainly into increased axial velocity but partly into increased angular velocity. Also the increase of pressure through the propeller disc can be expressed as

$$p' = \tfrac{1}{2}\varrho\,(u_1^2 - V^2) + \tfrac{1}{2}\varrho\,\omega\, r^2(\omega_1 - \omega) \tag{2.10}$$

The axial momentum equation can be derived strictly for the whole propeller only, and is [see III (1.10)]

$$T = \int_0^{R_1} 2\pi r_1 \varrho\, u_1 (u_1 - V)\, dr_1 - \int_0^{R_1} 2\pi (p_0 - p_1)\, r_1\, dr_1 \tag{2.11}$$

The solution of this system of equations is very complex but can be derived in certain special cases[1]. In general, however, the rotational motion in the slipstream is small and it is possible to neglect the angular velocity term in (2.10) and the pressure term in (2.11). With this simplification

$$p' = \tfrac{1}{2}\varrho\,(u_1^2 - V^2)$$

and, substituting in (2.4),

$$\frac{dT}{dr} = \pi r \varrho\,(u_1^2 - V^2) \tag{2.12}$$

[1] See III 2.

Now, if the contraction of the slipstream is ignored in calculating the induced velocities, the axial induced velocity $(u - V)$ at the propeller disc is half the corresponding velocity $(u_1 - V)$ in the wake; and on this basis, which is essentially the same as that adopted in simplifying (2.10), equation (2.12) for the element of thrust becomes

$$\frac{dT}{dr} = 4\pi r \varrho u (u - V)$$

or

$$R\frac{dT_c}{dr} = 4\left(\frac{r}{R}\right)\lambda^2 (1 + a)\, a \tag{2.13}$$

This result can also be derived from the axial momentum equation, (2.11), by neglecting the pressure drop in the wake and by assuming that the equation can be applied to the individual annular elements of the propeller disc. Thus

$$dT = 2\pi r_1 \varrho u_1 (u_1 - V)\, dr_1$$

and then by virtue of (2.7)

$$\frac{dT}{dr} = 2\pi r \varrho u (u_1 - V)$$

By comparison with (2.12)

$$u = \frac{1}{2}(u_1 + V)$$

which is the conclusion reached previously by considering the magnitude of the induced velocities.

Finally, combining (2.13) with (1.8), the axial interference factor a is determined by the equation

$$4\lambda^2 (1 + a)\, a = \sigma\left(\frac{r}{R}\right)^2 (1 - a')^2 C_y \sec^2\varphi$$

or, by virtue of (1.1) and (1.2),

$$\frac{a}{1 + a} = \frac{\sigma C_y}{4 \sin^2\varphi} \tag{2.14}$$

3. Propeller Characteristics. The equations of the two preceding sections suffice to determine the thrust and torque of any propeller defined by the number of blades B and by the variation of chord c and blade angle θ along the blade. The airfoil characteristics of the blade sections must also be known, *i. e.* the lift and drag coefficients of the blade sections in two-dimensional motion as functions of the angle of incidence α. The complete system of equations may be summarized as follows:—

$$\left.\begin{aligned} R\frac{dT_c}{dr} &= \sigma\left(\frac{r}{R}\right)^3 (1 - a')^2 C_y \sec^2\varphi \\ R\frac{dQ_c}{dr} &= \sigma\left(\frac{r}{R}\right)^4 (1 - a')^2 C_x \sec^2\varphi \\ \lambda &= \frac{r}{R}\frac{1 - a'}{1 + a}\tan\varphi \end{aligned}\right\} \tag{3.1}$$

where

$$\left.\begin{aligned} \sigma &= \frac{B\,c}{2\,\pi\,r} \\ C_x &= C_L \sin\varphi + C_D \cos\varphi \\ C_y &= C_L \cos\varphi - C_D \sin\varphi \end{aligned}\right\} \tag{3.2}$$

and

$$\left.\begin{aligned} \frac{a'}{1-a'} &= \frac{\sigma\,C_x}{4\sin\varphi\cos\varphi} \\ \frac{a}{1+a} &= \frac{\sigma\,C_y}{4\sin^2\varphi} \end{aligned}\right\} \tag{3.3}$$

These equations have been developed by assuming the propeller to have a large number of blades and by ignoring the contraction of the slipstream in calculating the axial induced velocity. They apply strictly therefore only to a lightly loaded propeller with a large number of blades, but experience has shown that they may be used with reasonable accuracy for any propeller. An approximate method of correcting the equations for a propeller with a small number of blades is considered later in Chapter VII.

The equations have been derived by considering the mode of operation of a propeller, but they are valid also for other working states of an airscrew. The equations can be applied without modification to determine the characteristics of a windmill, but in this application the thrust and torque, and hence also the axial and rotational interference factors, are negative. Special care must be taken in applying the equations to an airscrew with a negative rate of advance. The equations (3.1) and (3.2) are valid under all conditions, since they represent simply the aerodynamic forces on the blade elements moving relative to the fluid with a velocity whose axial and tangential components are respectively

$$u = V\,(1+a)$$

$$w = \left(\Omega - \frac{1}{2}\omega\right) r = \Omega\,r\,(1-a')$$

The equations (3.3), on the other hand, are not universally true, since they have been derived on the assumption that a slipstream of normal type exists behind the airscrew, and there are certain states of operation[1] of an airscrew in which this condition is not satisfied.

In order to examine this question, it is convenient to consider the behavior of an ordinary propulsive airscrew or propeller at different rates of advance. In the ordinary state of operation the thrust of the propeller creates a slipstream of increased velocity behind the propeller. As the speed of advance increases, at the same rate of rotation, the thrust of the propeller falls to zero and then becomes negative, and shortly afterwards the torque also becomes negative. The airscrew is then operating first as a brake and then as a windmill, and a slipstream

[1] See I 1 and Fig. 2.

of reduced velocity is formed behind the airscrew. The general equations (3.1), remain valid, but the interference factors a and a' become negative.

When the speed of advance is reduced to zero, the limiting condition of operation as a propeller is reached; the airscrew rotates without advancing through the fluid, and the application of the general equations leads to the conclusions that the air is being driven backwards through the disc of the airscrew and that the axial velocity in the ultimate slipstream is double that through the disc. If now the airscrew is assumed to move backwards slowly (V small and negative) or if a stream of low velocity is directed on the back of the airscrew, the direction of flow through the airscrew disc will still be in the same sense as in the static condition and will therefore be opposite to the direction of the general stream. The airscrew then operates in the vortex ring state, the air passing through the airscrew disc and returning backwards outside its circumference as illustrated in Fig. 2. In this condition no true slipstream is formed, and it is no longer possible to apply the equations of axial and rotational momentum as developed in VI 2. The analysis of this state of operation rests on a purely empirical basis and is considered later in Chapter XII.

As the speed of backward motion is increased, a condition is reached in which the axial velocity through the airscrew disc becomes zero, and the airscrew then acts as a centrifugal fan, sucking air towards its disc from both sides and expelling it radially. Beyond this state, at higher negative rates of advance, the flow is wholly from the back to the front of the airscrew and, after a temporary condition of turbulence, the flow passes to the same type as at high positive rates of advance. The airscrew acts as a brake, the thrust and torque are both positive, and a true slipstream is again formed downstream of the airscrew. The flow past a typical blade element in this state of operation with a stream of velocity V' directed on the back of the airscrew is illustrated in Fig. 40, where W' is the resultant effective velocity experienced by the blade element and R is the corresponding aerodynamic force. The general equations, (3.1), still represent the aerodynamic behavior of the blade element, but the axial velocity u or $V(1+a)$ is now negative, being equal in magnitude to the velocity u' of Fig. 40 but of the opposite sign. In the momentum equations, however, the velocity of flow through the airscrew disc is now u', the angular momentum equation, (2.5), must now be expressed as

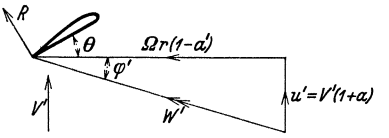

Fig. 40.

$$\frac{dQ}{dr} = 2\pi r \varrho u' \omega r^2$$
$$= -2\pi r \varrho u \omega r^2$$

and the axial momentum equation becomes

$$\frac{dT}{dr} = 4\pi r \varrho u' (V' - u')$$
$$= -4\pi r \varrho u (u - V)$$

This result is due to the fact that, in the ordinary form of the axial momentum equation [see (2.13)], $(u - V)$ represents the increase of velocity measured in the opposite direction to that of the thrust, while u represents the velocity through the airscrew disc and must be regarded as positive, whatever be the actual direction of the flow. At negative rates of advance of an airscrew, T and $(u - V)$ remain positive, but u is negative, and hence a negative sign must be introduced in the momentum equation.

The modification necessary to the momentum equations is therefore simply a change of sign, and it follows that the general equations, (3.3), must receive a similar correction and must be written as

$$\left.\begin{aligned} \frac{a'}{1-a'} &= -\frac{\sigma C_x}{4 \sin\varphi \cos\varphi} \\ \frac{a}{1+a} &= -\frac{\sigma C_y}{4 \sin^2\varphi} \end{aligned}\right\} \qquad (3.4)$$

In these equations the angle φ is negative and in general C_x and C_y are both positive. Thus the rotational interference factor a' will be positive, and the axial interference factor a will be negative.

With the substitution of equations (3.4) in place of the previous equations (3.3), the general equations can be used to calculate the performance of an airscrew at a negative rate of advance, provided that this rate of advance is sufficiently rapid to avoid the vortex ring and turbulent states of operation. The criterion that this condition is satisfied is obtained by considering the value calculated for the axial interference factor a. With a negative axial velocity V', the axial velocity through the airscrew disc is

$$u' = V' (1 + a)$$

and the axial velocity in the ultimate slipstream will be

$$u_1' = V' (1 + 2a)$$

The momentum equation presumes that the velocities V', u', and u_1' are all of the same sense, and hence the analysis is valid only if

$$a > -\frac{1}{2} \qquad (3.5)$$

Whenever the application of (3.3) or (3.4) leads to a value of the axial interference factor which is more negative than this limiting value, the equations cease to be valid, and it is then necessary to turn to the empirical analysis described in Chapter XII. The conditions of the successive states of operation may be summarized as follows:—

State of Operation	V	a	T	Q
Windmill . .	positive, large	—	—	—
Brake . . .	positive	—	—	+
Propeller . .	positive	0 to ∞	+	+
Vortex ring .	negative, small	$-\infty$ to -1	+	+
Turbulent .	negative	-1 to $-1/2$	+	+
Brake . . .	negative, large	$-1/2$ to 0	+	+

4. The Application of the Vortex Theory. The general equations of the vortex theory suffice to determine the performance of a propeller throughout its whole range of operation. To perform this calculation a few typical blade elements are chosen, suitably distributed along the blade of the propeller, and the thrust and torque of each of these blade elements is determined as a function of the speed ratio λ. Using the values of these elementary forces at any chosen value of λ, the thrust and torque distribution curves along the blade can be drawn, and the total thrust and torque of the propeller are then obtained by graphical integration. By repeating this integration at a series of values of λ, the complete curves of the thrust and torque coefficients of the propeller can be obtained.

In order to illustrate this application of the vortex theory, calculations have been made for a propeller with two blades of the shape shown in Fig. 41, and of constant pitch-diameter ratio 0.80. Five sections have been chosen along the blade, and for convenience of the numerical work the exact positions have been chosen by reference to the blade angle θ rather than to the radial coordinate r. Details of these sections are given in Table 13, and in addition it may be noted that the solidity of the propeller, *i. e.* the ratio of the total blade area to the disc area πR^2, is 0.086. The characteristics of each of these sections have been calculated according to the system of equations summarized at the beginning of 3, and full details of the calculation for the section C are given in Table 14. Starting with a series of values of the angle of incidence α, for which the lift coefficient C_L and the drag coefficient C_D of the section are known, the first step is to calculate C_x and C_y according to the equations

TABLE 13. Blade Shape.

Section	r/R	θ	c/R	σ
A	0.304	40°	0.147	0.153
B	0.500	27	0.183	0.117
C	0.700	20	0.165	0.075
D	0.833	17	0.128	0.049
E	0.950	15	0.083	0.028

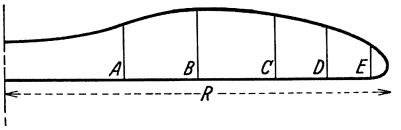

Fig. 41.

$$\left.\begin{aligned} C_x &= C_L \sin\varphi + C_D \cos\varphi \\ C_y &= C_L \cos\varphi - C_D \sin\varphi \end{aligned}\right\} \qquad (4.1)$$

The interference factors a' and a are next derived from the equations

$$\left.\begin{aligned} \frac{a'}{1-a'} &= \frac{\sigma C_x}{4 \sin\varphi \cos\varphi} \\ \frac{a}{1+a} &= \frac{\sigma C_y}{4 \sin^2\varphi} \end{aligned}\right\} \tag{4.2}$$

and finally the speed ratio λ and the elements of thrust and torque are derived from the equations

$$\left.\begin{aligned} \lambda &= \frac{r}{R}\frac{1-a'}{1+a}\tan\varphi \\ R\frac{dT_c}{dr} &= \sigma\left(\frac{r}{R}\right)^3(1-a')^2 C_y \sec^2\varphi \\ R\frac{dQ_c}{dr} &= \sigma\left(\frac{r}{R}\right)^4(1-a')^2 C_x \sec^2\varphi \end{aligned}\right\} \tag{4.3}$$

As a result of this calculation for each of the five chosen sections of the propeller blade it is possible to draw the curves of the elements

TABLE 14. Section C of Propeller. $\frac{r}{R} = 0.700$, $\theta = 20^0$, $\sigma = 0.075$.

α	C_L	C_D	C_x	C_y	a'	a	λ	$R\frac{dT_c}{dr}$	$R\frac{dQ_c}{dr}$
0	0	0.035	0.033	—0.012	0.0020	—0.002	0.255	—0.0003	0.00067
2	0.22	0.020	0.087	0.203	0.0055	0.042	0.217	0.0057	0.00171
4	0.43	0.014	0.132	0.409	0.0095	0.113	0.179	0.0112	0.00254
6	0.62	0.012	0.162	0.599	0.0130	0.238	0.139	0.0160	0.00302
8	0.80	0.013	0.179	0.780	0.0165	0.511	0.097	0.0203	0.00327
10	0.97	0.016	0.185	0.952	0.0200	1.470	0.049	0.0243	0.00330

of thrust and torque against the speed ratio λ as shown in Figs. 42 and 43, and then, reading from these curves at any chosen value of λ, it is possible to draw the thrust and torque distribution curves along the blade of the propeller. An example of these curves, for $\lambda = 0.175$, is shown in Fig. 44. The two curves are very similar in shape, rising slowly at first with the radius and reaching a maximum value at approximately four-fifths of the extreme radius. Integration of the thrust and torque distribution curves determines the thrust and torque coefficients of the propeller, and by repeating the calculation for a series of values of the speed ratio λ, the characteristics of the propeller can be determined for any range of operation. Numerical values are given in Table 15, and Fig. 45 shows the

TABLE 15. Propeller Characteristics.

λ	T_c	Q_c	η
0.100	0.114	0.00179	0.636
0.125	0.0101	0.00174	0.722
0.150	0.0085	0.00163	0.782
0.175	0.0066	0.00145	0.800
0.200	0.0047	0.00120	0.783
0.225	0.0025	0.00083	0.680

thrust and torque coefficients of the propeller and the corresponding efficiency of propulsion. The curves show that the maximum efficiency of the propeller is 0.80 and that the thrust vanishes at the speed ratio 0.256, while the torque vanishes at the slightly higher value 0.265. Thus the experimental mean pitch-diameter ratio of the propeller is $0.256\,\pi$ or 0.805, which is very slightly greater than the geometrical pitch-diameter ratio 0.800. This difference is negligibly small, and the larger difference which is generally found in experimental tests of propellers is due to the fact that the geometrical pitch of the propeller is defined by reference to the chords of the blade elements instead of the no lift axes.

Fig. 46 shows the variation of the interference factors a and a' along the blade for the speed ratio 0.175. Except at the innermost section of the blade, the rotational interference factor a' is less than 2 per cent and is unimportant compared with the axial interference factor a, which has its greatest value over the principal working parts of the blade and falls to zero at the boss and at the tip.

The calculation of the characteristics of a propeller by the detailed method described above is lengthy and laborious, and for comparative purposes it is often sufficiently accurate to consider

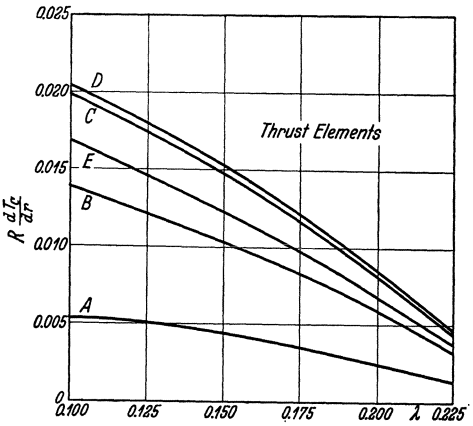

Fig. 42.

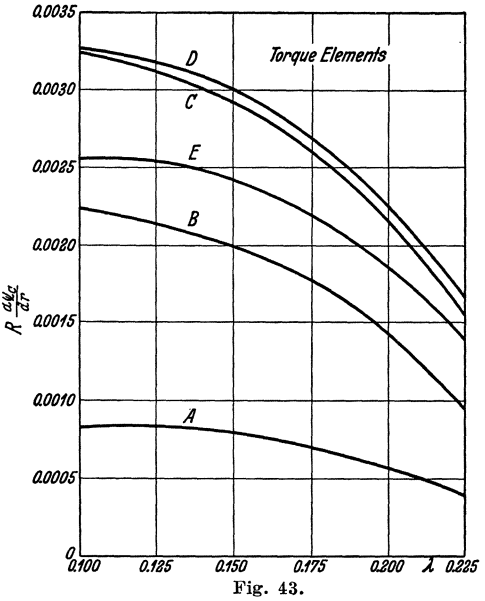

Fig. 43.

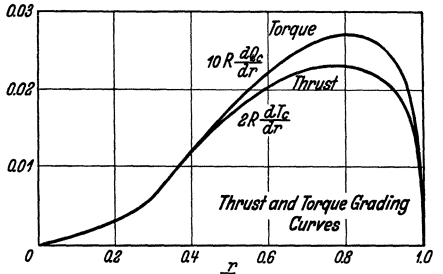

Fig. 44.

only one typical section of the propeller blade. This typical section is suitably chosen at the radius 0.7 R (Section C of Table 13) and a comparison of the results for this section with those for the whole propeller shows that the thrust and torque coefficients of the propeller are approximately 0.57 times the corresponding elements of thrust and torque for this typical section. Thus, as a rough approximation, it is legitimate to calculate the characteristics of the blade element at the radius 0.7 R and then to assume for the whole propeller

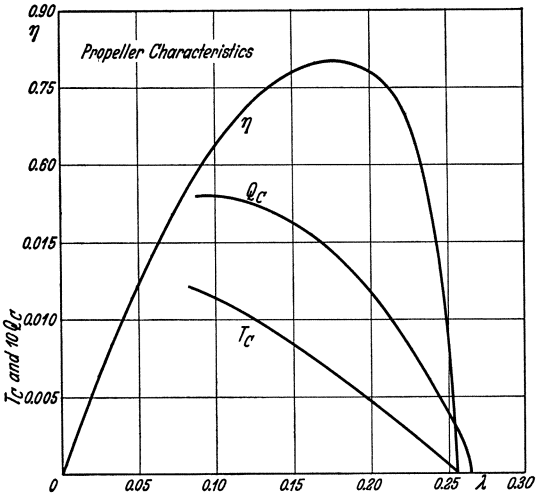

Fig. 45.

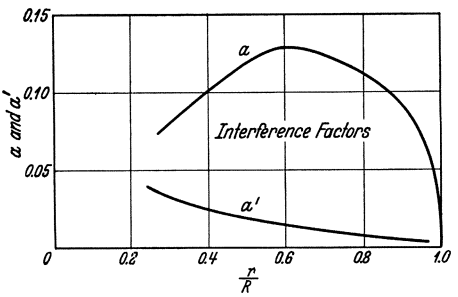

Fig. 46.

$$\left.\begin{aligned} T_c &= 0.57\, R \frac{d\,T_c}{d\,r} \\ Q_c &= 0.57\, R \frac{d\,Q_c}{d\,r} \end{aligned}\right\} \qquad (4.4)$$

The value of the numerical factor will, of course, depend on the shape of the blade and on the variation of angle along the blade. It is valid only for blades of the shape shown in Fig. 41 with constant pitch along the blade.

5. The Effect of Solidity and Pitch. Slight changes of the plan form of a propeller blade and of the variation of angle along the blade exert only a small influence on the characteristics of the propeller, and hence, to appreciate the performance of different types of propeller, it will suffice to consider blades of constant pitch and of the shape shown in Fig. 41 and defined by the numerical data of Table 13. There remain then two parameters to specify any particular propeller:—

(1) The pitch-diameter ratio.

(2) The solidity, defined as the ratio of the total blade area to the disc area πR^2.

The increase of solidity may be obtained by increasing the number of the blades or by increasing the width of the blades while the ratio

of the chords along the blade remains unchanged, since the theory indicates that these two modifications produce identical results.

In order to illustrate the influence of solidity and pitch on the characteristics of a propeller, calculations have been made for propellers of two and four blades of the form shown in Fig. 41 and for a range of pitch-diameter ratio. The corresponding solidities are respectively 0.086 and 0.172. For simplicity the calculations have been confined to the typical blade section at the radius 0.7 R and the angle at this section has been increased by steps of 5°; the corresponding values of the pitch-diameter ratio are given in Table 16. The calculations were made by the method described in the previous section and the resulting values of the thrust and torque coefficients are shown in Figs. 47 and 48, where the full lines refer to the propeller with two blades and solidity 0.086, and the broken lines refer to the propeller with four blades and solidity 0.172. If there were no induced velocities, the thrust and torque of a propeller would be proportional to the solidity, and it is convenient therefore to plot the thrust and torque per blade of the propeller instead of the total thrust and torque. This

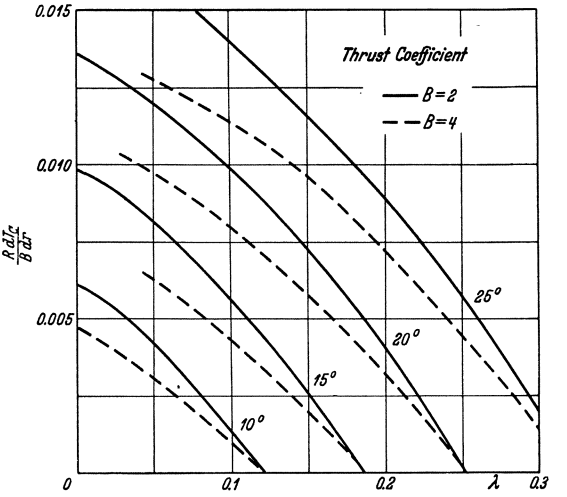

Fig. 47.

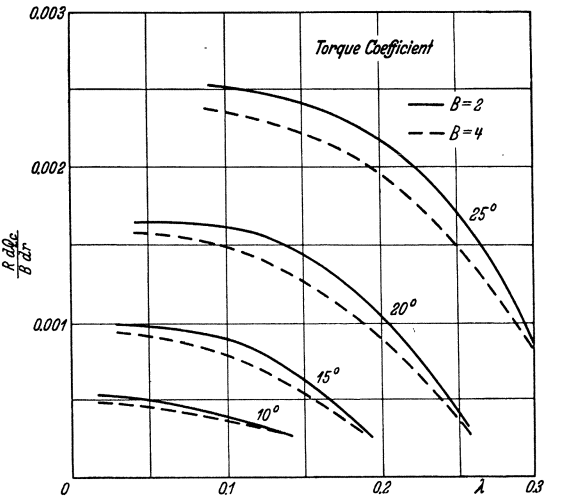

Fig. 48.

TABLE 16.

θ =	10°	15°	20°	25°
H/D =	0.39	0.63	0.80	1.03

method of plotting has been used in Figs. 47 and 48, and the deviation of the two sets of curves represents the effect of the induced velocities. The curves show only the elements of thrust and torque on the blade section at the radius 0.7 R, but in accordance with the previous discussion the total thrust and torque of the propeller may be taken to be approximately

$$T_c = 0.57\, B \left(\frac{R}{B} \frac{d\, T_c}{d\, r} \right)$$

$$Q_c = 0.57\, B \left(\frac{R}{B} \frac{d\, Q_c}{d\, r} \right)$$

The efficiency curves for the series of propellers are shown in Fig. 49, which may be compared with the set of experimental curves shown in Fig. 7. The efficiency of the propeller increases with its pitch, and there is a marked drop in efficiency when the solidity of the propeller is increased, but this drop is relatively less important for the high pitch propellers. The speed ratio, at which the maximum efficiency of any propeller is attained, appears to depend only on the pitch of the propeller and to be sensibly independent of the solidity.

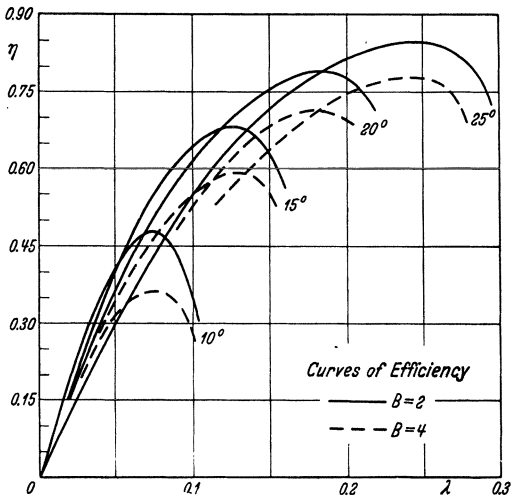

Fig. 49.

These curves can be used to indicate the change in design of a propeller which is necessary when the speed of advance is altered without any change in the rate of rotation or diameter of the propeller. Assume, for example, that a propeller of pitch-diameter ratio 0.80 ($\theta = 20^0$ at 0.7 R) and of solidity 0.172 ($B = 4$) is operating at the speed ratio 0.180 which corresponds to its maximum efficiency of 72 per cent. The corresponding value of the torque coefficient $R \frac{d\, Q_c}{d\, r}$ is 0.00107 B or 0.0043. If now the forward speed is to be increased by 35 per cent and if the propeller is to be redesigned to give the same rate of rotation and to give its maximum efficiency under these new conditions, it will be necessary to increase the pitch of the propeller so that its maximum efficiency occurs at the speed ratio 0.243. The pitch-diameter ratio required is therefore obtained

from Fig. 49 as 1.03 ($\theta = 25^0$ at 0.7 R), and from Fig. 48 the relationship between torque coefficient and solidity is as follows:—

B	σ	$\frac{R}{B}\frac{dQ_c}{dr}$	$R\frac{dQ_c}{dr}$
2	0.086	0.00180	0.0036
4	0.172	0.00155	0.0062

If the propeller is to run at the correct rate of rotation, the torque coefficient $R\,(dQ_c/dr)$ must retain its previous value 0.0043, and hence by interpolation the solidity must be reduced to 0.11 approximately. Thus the modification of the propeller to operate at the higher speed is to increase the pitch-diameter ratio from 0.80 to 1.03, which is approximately the same percentage increase as that of the forward speed, and to reduce the solidity from 0.17 to 0.11. In practice this would imply changing from a propeller with four blades of the standard shape to a propeller with two blades, each of which is increased in width by approximately 25 per cent. Although this modification has been worked out only as a special numerical example, the general conclusion is valid universally under the conditions assumed, *i. e.* that the propeller is to absorb the same power at the same rate of rotation and at the same tip speed.

6. Approximate Method of Solution. The calculation of the characteristics of a propeller by means of the general equations of the vortex theory is a straight forward process, but, owing to the nature of the equations, it is necessary to start the calculation of the characteristics of any particular blade element by assuming a series of values of the angle of incidence α, and the corresponding values of the speed ratio λ are obtained as one of the results of the calculation. The characteristics of the propeller are then determined for a range of values of the speed ratio λ. But this method of calculation is unduly elaborate if the aim of the calculation is to determine the characteristics at one chosen value only of the speed ratio. Also, if the width of the blades is increased in order to absorb more power, it is necessary to repeat the whole series of calculations from the beginning.

An approximate method of calculation, which avoids some of these difficulties, has been developed by E. Pistolesi[1] on the basis that the axial and rotational interference factors a and a' are approximately constant over the principal working part of the propeller blade. Now in general

$$\lambda = \frac{r}{R}\frac{1-a'}{1+a}\tan\varphi \qquad \text{[see (4.3)]}$$

and if a and a' are assumed to be constant, the angle φ appropriate

[1] Neue Ansätze und Ausführungen zur Theorie der Luftschrauben. Vorträge aus dem Gebiete der Hydro- und Aerodynamik, Innsbruck, 1922.

to any blade element is given in terms of these constant interference factors and of the speed ratio λ by the equation

$$\frac{r}{R} tan\, \varphi = \lambda \frac{1+a}{1-a'} = \lambda' \tag{6.1}$$

where λ' is a constant. The first step in the approximate calculation is to obtain the characteristics of the propeller for the speed ratio λ', ignoring entirely the interference velocities which actually occur. The thrust and torque, which will be denoted by accented letters, are derived from the equations

$$\left.\begin{aligned} R\frac{dT'_c}{dr} &= \sigma\left(\frac{r}{R}\right)^3 C_y\, sec^2\varphi \\ R\frac{dQ'_c}{dr} &= \sigma\left(\frac{r}{R}\right)^4 C_x\, sec^2\varphi \end{aligned}\right\} \tag{6.2}$$

which are the general equations for the elements of thrust and torque with the factor $(1-a')^2$ omitted. Since the value of the angle φ at any radius is determined from (6.1), this calculation can be made at once for any chosen value of the parameter λ', and after integration the thrust and torque coefficients of the propeller will be obtained in the form

$$\left.\begin{aligned} T'_c &= \sigma_0 f_T(\lambda') \\ Q'_c &= \sigma_0 f_Q(\lambda') \end{aligned}\right\} \tag{6.3}$$

where σ_0 is the solidity of the whole propeller, *i. e.* the ratio of the total blade area to the disc area. On this simple basis the thrust and torque coefficients are simply proportional to the solidity of the propeller, and the curves of $f_T(\lambda')$ and $f_Q(\lambda')$ against λ' apply to any propeller with the same distribution of blade angle and chord ratio along the blade, whatever the actual width or number of the blades may be.

In order to pass to the actual characteristics of the propeller, as modified by the interference velocities, it is necessary first to read the values of $f_T(\lambda')$ and $f_Q(\lambda')$ from the curves at the abscissa

$$\lambda' = \frac{1+a}{1-a'}\lambda \tag{6.4}$$

and then to reduce the thrust and torque coefficients so derived by the factor $(1-a')^2$ which was omitted in (6.2). Thus

$$\left.\begin{aligned} T_c(\lambda) &= \sigma_0 f_T(\lambda')(1-a')^2 \\ Q_c(\lambda) &= \sigma_0 f_Q(\lambda')(1-a')^2 \end{aligned}\right\} \tag{6.5}$$

The appropriate values of the interference factors a and a' are derived from the momentum equations for the whole propeller, which are

$$T = 2\pi R^2 \varrho V^2 (1+a)\, a$$

and

$$Q = \pi R^4 \varrho V \Omega (1+a)\, a'$$

or, in terms of the thrust and torque coefficients,

$$\left.\begin{aligned} T_c &= 2\lambda^2(1+a)\, a \\ Q_c &= \lambda(1+a)\, a' \end{aligned}\right\} \tag{6.6}$$

Combining these equations with the previous expressions (6.5) for the thrust and torque coefficients and with the equation (6.4), the interference factors are determined as

$$\frac{a}{1+a} = \frac{\sigma_0 f_T(\lambda')}{2\lambda'^2} \tag{6.7}$$

and

$$\frac{a'}{1-a'} = \frac{\sigma_0 f_Q(\lambda')}{\lambda'} \tag{6.8}$$

Now, starting with any value of λ' for which the values of f_T and f_Q are known, (6.7) and (6.8) determine the interference factors a and a' for any chosen solidity σ_0, and then the corresponding values of λ, T_c and Q_c are derived from (6.4) and (6.5). In general the rotational interference factor a' is very small and, unless results of high accuracy are required, it suffices to calculate only the axial interference factor a from (6.7) and then to take approximately

$$\left.\begin{aligned} \lambda &= \frac{\lambda'}{1+a} \\ T_c(\lambda) &= \sigma_0 f_T(\lambda') \\ Q_c(\lambda) &= \sigma_0 f_Q(\lambda') \end{aligned}\right\} \tag{6.9}$$

This approximate method of calculation has no advantage over the more general method developed and applied in 4 unless results are required for a series of propellers of constant pitch and increasing solidity. By a slight modification of Pistolesi's analysis, however, it is possible to derive an approximate method of calculating the effect of a change of solidity on the characteristics of a propeller. To develop this method, consider two propellers of the same pitch, with blades of the same type, but with different solidities σ_1 and σ_2. Comparing the two propellers at the same value of λ', the ratio of the thrust and torque coefficients is obtained from (6.5) as

$$\frac{T_c(\lambda_2)}{T_c(\lambda_1)} = \frac{Q_c(\lambda_2)}{Q_c(\lambda_1)} = \frac{\sigma_2(1-a_2')^2}{\sigma_1(1-a_1')^2} \tag{6.10}$$

where

$$\lambda_2 \frac{1+a_2}{1-a_2'} = \lambda_1 \frac{1+a_1}{1-a_1'} \tag{6.11}$$

and the suffixes (1) and (2) denote values appropriate to the two propellers. Also from the equations (6.7) and (6.8)

$$\left.\begin{aligned} \frac{a_2}{1+a_2} &= \frac{\sigma_2}{\sigma_1}\frac{a_1}{1+a_1} \\ \frac{a_2'}{1-a_2'} &= \frac{\sigma_2}{\sigma_1}\frac{a_1'}{1-a_1'} \end{aligned}\right\} \tag{6.12}$$

while the interference factors for the first propeller can be calculated from the equations $T_c(\lambda_1) = 2\lambda_1^2(1+a_1)a_1$

and $Q_c(\lambda_1) = \lambda_1(1+a_1)a_1'$ [see (6.6)]

Thus, starting with any value of the speed ratio λ_1 and the appropriate thrust and torque coefficients, the first step is to calculate the corresponding interference factors a_1 and a_1'. The interference factors a_2 and a_2'

for the second propeller are then calculated, and finally (6.10) and (6.11) determine the corresponding speed ratio λ_2 and the thrust and torque coefficients.

The approximation on which this method of calculation is based is the assumption of constant values of the interference factors a and a' along the blade, and it should therefore be used only for estimating the effect of a small change of solidity. The rotational interference factor a' is always very small, and it is then legitimate to make the further approximation of neglecting the rotational interference factors entirely, since these factors appear in the transformation formulae only as the ratio

$$\frac{1-a'_2}{1-a'_1}$$

which will rarely differ from unity by as much as 1 per cent. With this approximation the transformation formulae become

$$\frac{T_c(\lambda_2)}{T_c(\lambda_1)} = \frac{Q_c(\lambda_2)}{Q_c(\lambda_1)} = \frac{\sigma_2}{\sigma_1} \tag{6.13}$$

and

$$\lambda_2 = \lambda_1 \frac{1+a_1}{1+a_2} \tag{6.14}$$

Also if

$$\tau = \frac{2\,T_c(\lambda_1)}{\lambda_1^2} \tag{6.15}$$

the axial interference factor a_1 can be expressed as

$$(1+2\,a_1)^2 = 1+\tau$$

and hence

$$\frac{a_1}{1+a_1} = \frac{\sqrt{1+\tau}-1}{\sqrt{1+\tau}+1}$$

The corresponding axial interference factor a_2 for the second propeller is then obtained from (6.12)

$$\frac{a_2}{1+a_2} = \frac{\sigma_2(\sqrt{1+\tau}-1)}{\sigma_1(\sqrt{1+\tau}+1)}$$

and (6.14) for the speed ratio becomes

$$\begin{aligned}\frac{\lambda_2}{\lambda_1} &= \frac{1+a_1}{1+a_2} \\ &= \frac{\sigma_1(\sqrt{1+\tau}+1)-\sigma_2(\sqrt{1+\tau}-1)}{2\,\sigma_1}\end{aligned}$$

or

$$\frac{\lambda_2}{\lambda_1} = 1-\frac{\sigma_2-\sigma_1}{2\,\sigma_1}\left(\sqrt{1+\tau}-1\right) \tag{6.16}$$

Now, starting with any value of the speed ratio λ_1 and the corresponding thrust and torque coefficients of the first propeller, the first step is to calculate τ from (6.15). The thrust and torque coefficients of the second propeller are obtained, according to (6.13), by multiplying by the factor σ_2/σ_1, and the appropriate value of the speed ratio λ_2 is derived from (6.16). If T_c/σ and Q_c/σ are used instead of the actual

thrust and torque coefficients, the calculation is even simpler, since the only correction required is to plot these coefficients at a different value of the speed ratio λ. As an example of this method of calculation, the propeller whose characteristics are given in Table 15 and Fig. 45 has been taken as basis, and Table 17 gives the calculation for deriving the characteristics of a propeller with 20 per cent increased solidity. The corresponding curves are shown in Fig. 50, and it appears that the maximum efficiency has fallen 1-$^1/_2$ per cent which is quite consistent with the drop of 7 per cent shown in Fig. 49 when the solidity was doubled.

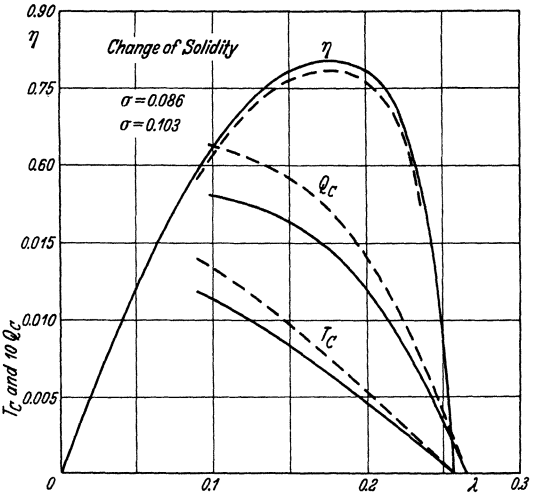

Fig. 50.

TABLE 17. Propeller of 20 Per Cent Increased Solidity.

First Propeller ($\sigma = 0.086$)				Second Propeller ($\sigma = 0.103$)		
λ	T_c	Q_c	τ	λ	T_c	Q_c
0.100	0.0114	0.00179	2.28	0.092	0.0137	0.00215
0.125	0.0101	0.00174	1.29	0.119	0.0121	0.00209
0.150	0.0085	0.00163	0.755	0.145	0.0102	0.00196
0.175	0.0066	0.00145	0.430	0.172	0.0079	0.00174
0.200	0.0047	0.00120	0.235	0.198	0.0056	0.00144
0.225	0.0025	0.00083	0.099	0.224	0.0030	0.00100

7. Effective Aspect Ratio of the Blades. In the discussion of the primitive blade element theory and the subsequent inflow theories in Chapter V, it was pointed out that one of the difficulties of the analysis was the uncertainty of the aspect ratio which should be assigned to the propeller blades in order to define their aerodynamic characteristics. This uncertainty can be resolved by examining the problem in the light of the vortex theory, and, by means of some suitable approximations, Pistolesi[1] has obtained a simple expression for the appropriate aspect ratio.

The system of velocities relative to the blade element of a propeller can be represented suitably as in Fig. 51. Here W_0 is the undisturbed

[1] Vorträge aus dem Gebiete der Hydro- und Aerodynamik, Innsbruck, 1922.

velocity far in front of the propeller, W is the velocity experienced by the blade element, and W_1 is the velocity in the ultimate wake. The effective velocity W is derived from the original velocity W_0 by the addition of the induced velocity w, and this induced velocity, being due to the reaction of the resultant force on the blade element, will be in the same direction as this force.

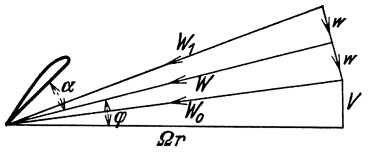

Fig. 51.

Consider now an ideal frictionless propeller. The force on the blade element, extending a distance dr along the blade, is then simply the lift dL at right angles to the velocity W and appropriate to the angle of incidence α, which is the angle between the chord of the airfoil section and the direction of the velocity W; and the induced velocity w is at right angles to the velocity W. The element of thrust contributed by the blade elements of the B blades of the propeller is

$$\frac{dT}{dr} = \frac{1}{2} B c \varrho W^2 C_L \cos\varphi$$

and the momentum equation for the thrust is

$$\begin{aligned} \frac{dT}{dr} &= 4\pi r \varrho (V + w\cos\varphi) w \cos\varphi \\ &= 4\pi \varrho \Omega r^2 w \sin\varphi \end{aligned}$$

Hence

$$\frac{w}{W} = \frac{B c W C_L}{8\pi \Omega r^2 \tan\varphi}$$

and, since the rotational interference is always small, it is legitimate to replace Ωr by $W\cos\varphi$ approximately in this equation. On this basis

$$\frac{w}{W} = \frac{B c C_L}{8\pi r \sin\varphi} \tag{7.1}$$

If the problem is considered on the lines of the primitive blade element theory, the blade element is assumed to be in the stream W_0, whose velocity is sensibly equal to the velocity W if the induced velocity w is small, and the angle of incidence is taken to be

$$\alpha_0 = \alpha + \frac{w}{W} \tag{7.2}$$

Now an airfoil of aspect ratio A, giving the same lift coefficient C_L as an airfoil of infinite span, requires a larger angle of incidence, determined by the equation[1]

$$\alpha_0 = \alpha + \frac{C_L}{\pi A} \tag{7.3}$$

and on comparing the last two equations, the effective aspect ratio of the blade element is obtained as

$$A = \frac{C_L}{\pi} \frac{W}{w}$$

[1] See Division E I (12.5).

Substituting from (7.1) for the induced velocity w this aspect ratio becomes

$$A = \frac{8\, r \sin\varphi}{B\, c} \tag{7.4}$$

This formula represents the aspect ratio which ought to be used in the primitive blade element theory to define the appropriate airfoil characteristics, and it is evident at once that this aspect ratio varies both with the position of the element along the blade and with the state of operation of the propeller. To illustrate these variations, consider a propeller with constant chord along the blade, and assume small interference velocities so that the angle φ may be determined approximately by the equation

$$\tan\varphi = \frac{V}{\Omega\, r}$$

Then

$$A = \frac{8}{\pi\, \sigma_0}\, \frac{r}{R}\, \frac{V}{\sqrt{V^2 + \Omega^2 r^2}} \tag{7.5}$$

where σ_0 is the solidity of the propeller defined by the equation

$$\sigma_0 = \frac{B\, c}{\pi\, R}$$

The form of (7.5) shows that the effective aspect ratio A is zero at the boss of the propeller and increases along the blade. The value at the tip of the blade is

$$A_0 = \frac{8}{\pi\, \sigma_0}\, \frac{\lambda}{\sqrt{1 + \lambda^2}} \tag{7.6}$$

where, as usual, λ denotes the value of $V/\Omega\, R$. Numerical values of A_0 are given in Table 18 for two values of the solidity, corresponding respectively to ordinary propellers with two and four blades, and it is evident that the assumption of an aspect ratio depending only on the shape of the blades would fail to represent correctly the behavior of the propeller. According to the conceptions of the primitive blade element theory, the appropriate aspect ratio would be R/c, or $B/\pi\, \sigma_0$. The aspect ratio, corresponding to the numerical values of Table 18, would therefore be approximately 8 according to the primitive blade element theory, and this value is correct for one state of operation of the propeller with two blades, but is always too high for the propeller with four blades, and the primitive blade element theory would therefore overestimate the efficiency of the propeller.

TABLE 18.
Effective Aspect Ratio.

$\lambda =$	0.2	0.3	0.4
$\sigma_0 = 0.08$	6.2	9.2	11.8
0.16	3.1	4.6	5.9

CHAPTER VII

PROPELLERS OF HIGHEST EFFICIENCY

1. Minimum Loss of Energy. The analysis of the preceding chapter was directed mainly to the development of a method of calculating the characteristics of a given propeller; but another problem of great interest is the determination of the design of propeller which will give

the highest efficiency. The object of a propeller is to convert the power P or torque Q of the engine into an axial thrust T. If Ω is the angular velocity of the propeller and V is its forward speed, the power absorbed is ΩQ and the useful work is VT, and hence the efficiency of propulsion η is

$$\eta = \frac{VT}{\Omega Q} \tag{1.1}$$

This efficiency depends mainly on the power absorbed, on the speed of advance, and on the diameter of the propeller, but other factors which modify the efficiency are the distribution of thrust along the blades of the propeller, the number of the blades, and the profile drag of the blade elements. Approximate formulae for the efficiency of a propeller have been developed in Chapter IV on the basis of the general momentum theory, but it is now necessary to examine, in the light of the vortex theory, the conditions which will lead to the highest efficiency of a propeller of given diameter, absorbing the power P at the forward speed V. For simplicity this problem will be considered first for an ideal frictionless propeller, and the influence of the profile drag will then be introduced as a correction to the analysis. The solution of this problem for a frictionless propeller has been obtained by A. Betz first for a lightly loaded propeller[1] of small thrust, and then more generally for any propeller[2].

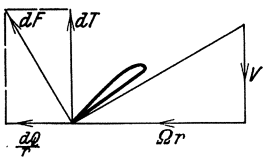

Fig. 52.

Consider the blade element at a distance r from the axis of rotation. This element has the motion composed of the axial velocity V and of the tangential velocity Ωr, and experiences a resultant force dF. Neglecting the profile drag of the blade section and the induced velocities associated with the system of trailing vortices, the force dF would be normal to the direction of motion of the element and there would be no less of energy. Also in terms of the circulation K around the blade section, the elements of thrust and torque would be

$$\left.\begin{aligned} dT &= \varrho K \Omega r \, dr \\ dQ &= \varrho K V r \, dr \end{aligned}\right\} \tag{1.2}$$

The induced velocities, which actually occur, cause a change in direction of the flow relative to the blade element, and, exactly as with an airfoil, cause an induced drag and a corresponding loss of energy. This loss of energy can be calculated from the circulation around the blade element and the appropriate induced velocities, or alternatively it can be calculated from the energy communicated to the slipstream of the propeller,

[1] Schraubenpropeller mit geringstem Energieverlust. Göttinger Nachr. 1919, p. 193.

[2] Handbuch der Physik, Vol. 7, p. 256, 1927.

and the optimum conditions which lead to the minimum loss of energy can be derived most conveniently by considering the conditions in this ultimate wake.

In order to determine the optimum condition, consider the effect of increasing the circulation around the blade element at the radius r by a small amount ΔK. This increase of circulation, produced by an increase of chord or blade angle, will modify the force experienced by the blade element itself and may also react on the other parts of the propeller, resulting in an increase of thrust ΔT and of torque ΔQ. Thus the useful work is increased by $V\Delta T$ and the power absorbed by $\Omega \Delta Q$, and it is convenient to denote the ratio of these increments by k, or

$$k = \frac{V \Delta T}{\Omega \Delta Q} \tag{1.3}$$

Now assume that the increment of circulation ΔK is chosen to give a definite value to the increment of power $\Omega \Delta Q$. If then the ratio k varies with the radius r at which the circulation is added, it is possible to keep the power constant and to increase the efficiency of the propeller by increasing the circulation around an element where k is large, and by reducing the circulation around an element where k is small. Thus the condition for the optimum distribution of circulation along the blade is that the ratio k shall have a constant value along the blade.

The calculation of the ratio k is simplified by use of Munk's displacement theorem[1], according to which it is legitimate to assume that the small increment of circulation is added in the ultimate wake instead of at the propeller disc. This theorem depends on the fact that the thrust and energy loss of a propeller can be calculated from the flow in the ultimate wake and are not modified if the elements of the blade are moved backward along the trailing vortices without change of circulation. In fact a blade element with circulation K extending a distance dr along the blade gives rise to two trailing vortices of strength K, and the whole vortex system of the slipstream can be built up by superimposing these elementary vortex systems for all the blade elements. Clearly the ultimate slipstream will not be changed if any one of these blade elements is moved backward along the lines traced by its trailing vortices, provided the circulation around this blade element and all the other elements of the propeller remains unaltered.

By virtue of this displacement theorem, the increment of circulation ΔK is assumed to be added at a point of the wake far behind the propeller. The propeller then experiences no interference from this element of circulation, and the increments of thrust and torque are due wholly to the element of circulation ΔK, situated in the velocity field

[1] Isoperimetrische Aufgaben aus der Theorie des Fluges. Göttingen, Dissertation, 1919. See also Vol. II, Division E, p. 136.

of the slipstream of the propeller. Now assume that the increment of circulation is added on an element of length dr at the radius r in the wake, where the induced velocities due to the propeller are v and ωr. The element moves with the velocities V and Ωr of the propeller, and hence the velocity of the element relative to the fluid has the components $(V + v)$ and $(\Omega - \omega) r$, which are represented by $N'A'$ and ON' in Fig. 53. Also the motion of the element is represented by OA and the motion relative to the fluid by OA', while $A'A$ represents the resultant induced velocity experienced by the element.

The increments of thrust and torque due to the element in this velocity field are

$$\Delta T = \varrho \, \Delta K \, (\Omega - \omega) \, r \, dr$$

and

$$\Delta Q = \varrho \, \Delta K \, (V + v) \, r \, dr$$

and hence

$$k = \frac{V \, \Delta T}{\Omega \, \Delta Q} = \frac{V \, (\Omega - \omega)}{(V + v) \, \Omega}$$

or

$$\frac{V + v}{(\Omega - \omega) \, r} = \frac{V}{k \, \Omega \, r} = \frac{V + v'}{\Omega \, r} \tag{1.4}$$

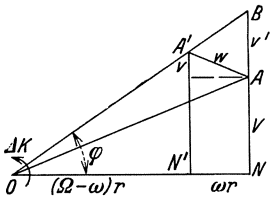

Fig. 53.

where $(V + v')$ is the velocity represented by NB in Fig. 53. The optimum condition demands that k shall have a constant value at all radii. Thus v' is constant and since the line OA forms a true screw surface of constant pitch, so also will the line OB. If there were no induced velocities, the trailing vortices would lie on the screw surface formed by OA, and under the optimum conditions the trailing vortices pass over to the screw surface formed by OB. The optimum condition for a propeller can therefore be represented by the statement that the trailing vortices in the ultimate wake lie on a screw surface of constant pitch.

The induced velocity w is not completely determined by the optimum condition, which requires only that the point A' shall lie on the line OB. If w_n is the component of w normal to OB, then the optimum condition determines the value of w_n as

$$w_n = v' \cos\varphi = \frac{1 - k}{k} V \cos\varphi \tag{1.5}$$

This condition is satisfied if the vortex sheets represented by OB in Fig. 53 form a rigid screw surface of constant pitch, which moves with the velocity v' along the axis of the propeller. A propeller with given thrust or power has minimum loss of energy and highest efficiency if the vortex sheets, after an initial limited deformation, move axially backward as rigid screw surfaces. This is Betz's general condition for a propeller of highest efficiency.

2. Lightly Loaded Propellers. The optimum condition determined by Betz establishes a relationship which must be satisfied by the trailing vortices in the ultimate wake far behind a propeller, but its application to the propeller itself is by no means simple. The condition can, however, be reduced to a simple form if the propeller is assumed to have a large number of blades and a small thrust. If the thrust is small, the contraction of the slipstream behind the propeller can be neglected, the trailing vortices from any element lie on the surface of a circular cylinder, and the system of trailing vortices can be represented as in Fig. 54. These vortex sheets are assumed to be rigid surfaces, moving backwards with the uniform velocity v'. The motion imparted to the air between these surfaces will have axial and rotational components, and in the outer parts of the slipstream there will also be a radial component owing to the tendency of the air to flow around the edges of the surfaces. If, however, the propeller has a very large number of blades, the surfaces will be close together and the radial component of the flow can be neglected.

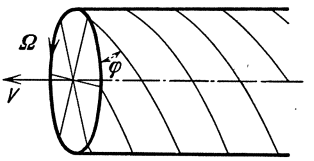

Fig. 54.

The motion imparted to the air will be normal to the vortex sheets, and since the inclination of the surface at the radius r is given by the equation

$$\tan\varphi = \frac{V}{\Omega r}$$

this normal velocity is $v' \cos\varphi$, and the axial and rotational components of the induced velocity are respectively

$$w_a = v' \cos^2\varphi = v' \frac{\Omega^2 r^2}{V^2 + \Omega^2 r^2} \tag{2.1}$$

and

$$w_t = v' \sin\varphi \cos\varphi = v' \frac{V \Omega r}{V^2 + \Omega^2 r^2} \tag{2.2}$$

Also the circulation K around each of the B blades of the propeller is obtained as

$$K = \frac{2\pi r w_t}{B} = \left(\frac{2\pi v'}{B}\right) \frac{V \Omega r^2}{V^2 + \Omega^2 r^2} \tag{2.3}$$

The velocities w_a and w_t are the induced velocities in the ultimate wake far behind the propeller and, on the assumption of zero contraction of the slipstream, the interference velocities experienced by the blades of the propeller will be half these induced velocities. Hence, in the usual notation,

$$a = \frac{w_a}{2V} = \frac{v'}{2V} \frac{\Omega^2 r^2}{V^2 + \Omega^2 r^2} \tag{2.4}$$

and

$$a' = \frac{w_t}{2\Omega r} = \frac{v'}{2V} \frac{V^2}{V^2 + \Omega^2 r^2} \tag{2.5}$$

The efficiency of the element at radius r is

$$\eta = \frac{1 - a'}{1 + a}$$

and on substituting the expressions for the interference factors a and a', this efficiency becomes approximately

$$\eta = \frac{1}{1+a+a'} = \frac{1}{1+\frac{v'}{2V}} \tag{2.6}$$

Thus the efficiency of the element is constant along the blade, and the optimum condition for a lightly loaded propeller with a large number of blades reduces simply to the condition that the efficiency is constant along the blade.

Writing

$$x = \frac{\Omega r}{V} \tag{2.7}$$

the distribution of circulation along the blade is obtained from (2.3) in the form

$$\frac{B K \Omega}{2\pi V v'} = \frac{x^2}{1+x^2} \tag{2.8}$$

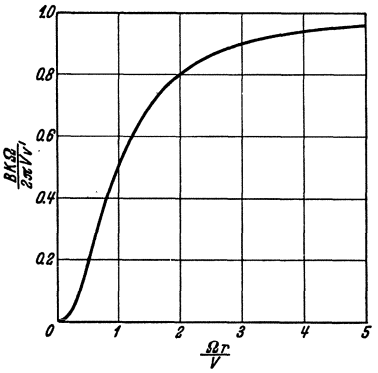

Fig. 55.

which is shown graphically in Fig. 55. This optimum distribution of circulation can also be derived[1] directly from the expression for the elements of thrust and torque in terms of the circulation around the blade element. Thus if u is the axial velocity relative to the blade element and ω is the angular velocity of the air behind the propeller disc, the expressions for the elements of thrust and torque are respectively

$$\frac{dT}{dr} = B K \varrho \left(\Omega - \frac{\omega}{2}\right) r \tag{2.9}$$

and

$$\frac{dQ}{dr} = B K \varrho u r \tag{2.10}$$

Also

$$B K = 2\pi \omega r^2 \tag{2.11}$$

and an alternative expression for the thrust is obtained from a consideration of the axial momentum as

$$\frac{dT}{dr} = 4\pi r \varrho u (u - V) \tag{2.12}$$

By equating the two expressions for the element of thrust, it appears that the axial and rotational velocities are related by the equation

$$u(u - V) = \frac{1}{2}\left(\Omega - \frac{\omega}{2}\right)\omega r^2 \tag{2.13}$$

[1] Helmbold, H. B., Zur Aerodynamik der Treibschraube. Zeitschr. f. Flugtechnik u. Motorl. **15**, 150, 1924.

Kawada, S., Theory of Airscrews. Tokyo Imperial University, Aeronautical Research Institute, Report No. 14, 1926.

and finally the loss of energy due to the action of the blade elements under consideration is

$$\frac{dE}{dr} = \Omega \frac{dQ}{dr} - V \frac{dT}{dr}$$
$$= B K \varrho r \left[\Omega (u - V) + \frac{\omega}{2} V\right] \tag{2.14}$$

Passing now to the approximation of a lightly loaded propeller, (2.13) may be taken to be

$$V (u - V) = \frac{1}{2} \Omega \omega r^2$$

or, by virtue of (2.11), $$u = V + \frac{B K \Omega}{4 \pi V} \tag{2.15}$$

and (2.9) for the element of thrust becomes approximately

$$\frac{dT}{dr} = B K \varrho \Omega r \tag{2.16}$$

Also, by virtue of (2.11) and (2.15), equation (2.14) for the loss of energy becomes

$$\frac{dE}{dr} = B K \varrho \left[\frac{B K \Omega^2}{4 \pi V} + \frac{B K V}{4 \pi r^2}\right] r$$
$$= \frac{B^2 K^2 \varrho \Omega}{4 \pi} \left[\frac{\Omega r}{V} + \frac{V}{\Omega r}\right] \tag{2.17}$$

Writing $$\gamma = \frac{B K \Omega}{2 \pi V^2} \tag{2.18}$$

these last two expressions become

$$\left.\begin{aligned} V \frac{dT}{dr} &= \frac{2 \pi \varrho V^4}{\Omega} \gamma x \\ \frac{dE}{dr} &= \frac{2 \pi \varrho V^4}{\Omega} \gamma^2 \frac{1 + x^2}{2 x} \end{aligned}\right\} \tag{2.19}$$

The optimum condition is now derived from the condition that the ratio of the increments of VT and E, due to an arbitrary small increase of γ at any radius, must be independent of the radial coordinate x. The condition is therefore

$$\gamma \frac{1 + x^2}{x} = A x$$

where A is a constant, and this condition reduces immediately to

$$\frac{B K \Omega}{2 \pi V^2} = \gamma = A \frac{x^2}{1 + x^2} \tag{2.20}$$

which is identical with the previous result (2.8) if v' is replaced by $A V$.

These results may be compared with the earlier analysis of Chapter III which was based on the general momentum theory of a propeller.

The optimum condition derived from the earlier analysis is given by III (4.8) and is

$$\frac{x^2 (1 - \eta)}{1 + x^2 \eta (2 - \eta)} + \frac{1 + x^2 \eta}{2 \eta - 1 + x^2 \eta^2} = \frac{3 - 2 \eta_0}{\eta_0 (2 - \eta_0)} \tag{2.21}$$

where η is the efficiency of the blade element at the radius r or $x V/\Omega$ and η_0 is the limit towards which η tends as x tends to infinity. In

III 5 this exact condition was replaced by the approximation of constant efficiency along the blade, which is derived from the exact condition (2.21) when the efficiency differs very little from unity, and the subsequent analysis on the basis of this approximation determines the characteristics of a lightly loaded propeller with the optimum distribution of thrust and torque along the blade.

It is interesting to examine the exact condition (2.21) and to determine the variation of efficiency along the blade. At the boss ($x = 0$) the efficiency is given by the equation

$$2\eta - 1 = \frac{\eta_0 (2 - \eta_0)}{3 - 2\eta_0}$$

or

$$\eta = \frac{3 - \eta_0^2}{2(3 - 2\eta_0)} \tag{2.22}$$

which leads to the numerical values of Table 19. There is therefore a noticeable increase of efficiency towards the root of the blade, but this increase is generally confined to a small fraction of the blade. Table 20 gives the numerical relationship between x and η when the limiting efficiency η_0 has the value 0.80. The efficiency is 0.843 at the boss, but has fallen to 0.81 when $x = 2.2$. If a propeller is operating at the speed ratio λ, the tip of the blade is represented by the coordinate $1/\lambda$ and, except for very high pitch propellers, this value is at least 5. Thus the important variation of efficiency is confined to a small part of the blade, and the approximation of assuming the optimum condition to be represented by constant efficiency along the blade is satisfactory unless the propeller has a very high pitch or a very low efficiency due to a heavy disc loading.

TABLE 19.

η_0 =	0.900	0.800	0.700	0.600
$\eta\,(x = 0)$ =	0.913	0.843	0.784	0.733

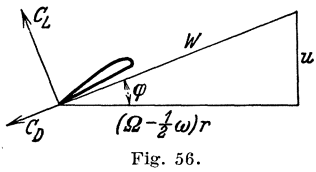

Fig. 56.

TABLE 20.
Variation of Efficiency Along the Blade.

	$\eta_0 = 0.80$					
η =	0.843	0.84	0.83	0.82	0.81	0.805
x =	0	0.32	0.79	1.30	2.21	3.38

3. The Effect of Profile Drag. The preceding analysis has been based on the assumption of a frictionless propeller. The introduction of the profile drag, assuming the same distribution of circulation along the blades, will reduce the thrust and increase the torque of the propeller, and will thus lead to a lower propulsive efficiency; but a more detailed analysis shows that the optimum distribution of circulation along the blade is also modified by the existence of the profile drag. If W is the effective velocity of the typical blade element relative to the fluid,

if c is its chord, and if C_D is its drag coefficient, then the loss of energy due to the profile drag is

$$\frac{dE_D}{dr} = \frac{1}{2} B c \varrho W^3 C_D \tag{3.1}$$

and the thrust of the element can be expressed in the usual manner as

$$\frac{dT}{dr} = \frac{1}{2} B c \varrho W^2 (C_L \cos\varphi - C_D \sin\varphi) \tag{3.2}$$

As a first approximation the effect of the profile drag on the thrust may be ignored, the angle φ may be assumed to be small, and the velocity W may be assumed to be equal to Ωr. Then, if ε denotes the drag-lift ratio of the blade section, the loss of energy due to the profile drag may be expressed approximately by the equation

$$\frac{dE_D}{dr} = \varepsilon \Omega r \frac{dT}{dr} \tag{3.3}$$

Returning now to (2.16) and (2.17), the expression for the thrust in terms of the circulation is still

$$\frac{dT}{dr} = B K \varrho \Omega r$$

but the total loss of energy becomes

$$\frac{dE}{dr} = \frac{B^2 K^2 \varrho \Omega}{4\pi} \left(\frac{\Omega r}{V} + \frac{V}{\Omega r} \right) + \varepsilon B K \varrho \Omega^2 r^2$$

or, in terms of the parameters x and γ,

$$\left.\begin{aligned} V \frac{dT}{dr} &= \frac{2\pi\varrho V^4}{\Omega} \gamma x \\ \frac{dE}{dr} &= \frac{2\pi\varrho V^4}{\Omega} \left[\gamma^2 \frac{1+x^2}{2x} + \varepsilon \gamma x^2 \right] \end{aligned}\right\} \tag{3.4}$$

The optimum distribution of circulation along the blade is now derived from the condition that the ratio of the increments of VT and E, due to an arbitrary small increase of γ at any radius, must be independent of the radial coordinate x. The condition is therefore

$$\gamma \frac{1+x^2}{x} + \varepsilon x^2 = A x$$

where A is a constant, and this condition reduces immediately to

$$\frac{BK\Omega}{2\pi V^2} = \gamma = \frac{(A - \varepsilon x) x^2}{1+x^2} \tag{3.5}$$

Thus the effect of the profile drag is to replace the constant A by $(A - \varepsilon x)$ in the formula for the circulation previously obtained for a frictionless propeller. Since ε is usually small, the variation of circulation along the blade is not changed near the root of the blade, but the circulation now reaches a maximum value as x increases and then falls to zero when x attains the value A/ε. The tip of the propeller, however, is usually reached at a lower value of x than that at which

the circulation falls to zero. A comparison of the circulation with and without profile drag is shown in Table 21 and Fig. 57.

TABLE 21. $A = 0.5$, $\varepsilon = 0.05$.

x	0.5	1	2	4	6	8	10
$\frac{A x^2}{1+x^2}$	0.100	0.250	0.400	0.471	0.487	0.492	0.495
$\frac{(A-\varepsilon x) x^2}{1+x^2}$	0.095	0.225	0.320	0.284	0.195	0.099	0

The efficiency of the blade element is obtained from the equation

$$\frac{dE}{dr} = \frac{1-\eta}{\eta} V \frac{dT}{dr}$$

and, by virtue of (3.4),

$$\frac{1-\eta}{\eta} = \gamma \frac{1+x^2}{2x^2} + \varepsilon x$$

Then, substituting from (3.5),

$$\frac{1-\eta}{\eta} = \frac{1}{2}(A - \varepsilon x) + \varepsilon x$$

$$= \frac{1}{2}(A + \varepsilon x)$$

or finally

$$\eta = \frac{1}{1 + \frac{1}{2}(A + \varepsilon x)} \tag{3.6}$$

which is identical with the result obtained by Th. Bienen[1] by a somewhat different method of analysis. To the order of approximation adopted,

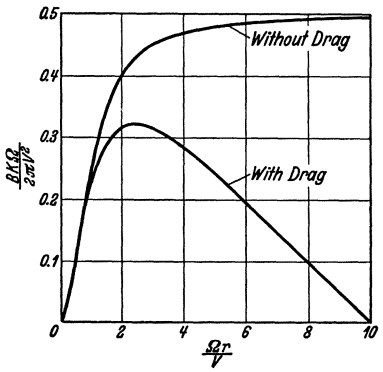

Fig. 57.

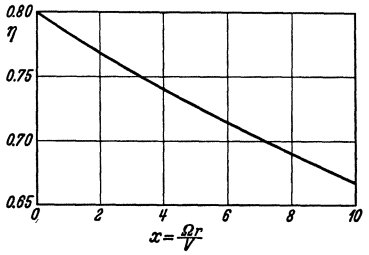

Fig. 58.

the efficiency is constant along the blade when the profile drag is neglected, but decreases outwards along the blade when this correction is introduced. Table 22 and Fig. 58 illustrate this effect by a numerical

[1] Die günstigste Schubverteilung für die Luftschraube bei Berücksichtigung des Profilwiderstandes. Zeitschr. f. Flugtechnik u. Motorl. **16**, 209, 1925.

example. It may perhaps seem anomalous that the efficiency should have fallen only to 0.667 at the point $x = 10$ where the circulation is zero, but it must be remembered that the analysis has been developed on the assumption of a constant drag lift ratio ε. Thus the drag and

TABLE 22. $A = 0.5$, $\varepsilon = 0.05$.

$x =$	0	0.5	1	2	4	6	8	10
$\eta =$	0.800	0.792	0.784	0.769	0.741	0.714	0.690	0.667

lift vanish simultaneously with the circulation, and at this point the thrust and torque are both zero. The variation of efficiency along the propeller blade due to the profile drag is most important at low rates of advance when x extends to a large value, and the effect increases with the efficiency of the propeller.

4. The Effect of Number of Blades. According to Betz's analysis the optimum condition for a propeller is obtained if the trailing vortices in the ultimate wake lie on a regular screw surface, and the appropriate velocity system of the slipstream is obtained if this vortex sheet is assumed to be a rigid membrane which moves backwards with a constant axial velocity v'. In the interior of the slipstream the velocity imparted to the air by the successive sheets of this membrane, as shown in Fig. 54, will have important axial and rotational components but the radial component will be negligibly small. Near the boundary of the slipstream, however, the air will tend to flow around the edges of the vortex sheets and will acquire an important radial velocity also. An approximate method of estimating the effect of this radial flow has been given by L. Prandtl[1].

Replace the system of vortex sheets by a series of parallel lines at a regular gap s and extending indefinitely to the left as in Fig. 59. The gap s represents the normal distance, at the boundary of the slipstream, between the successive vortex sheets, and hence

$$s = \frac{2\pi R}{B} \sin\varphi_1 = \frac{2\pi R}{B} \frac{\lambda}{\sqrt{1+\lambda^2}} \tag{4.1}$$

where B is the number of the blades of the propeller and φ_1 is the angle of the screw surface at the boundary of the slipstream, defined by the equation

$$\tan\varphi_1 = \frac{V}{\Omega R} = \lambda$$

The flow around the edges of the vortex sheets of the slipstream may then be estimated approximately from the flow around the edges of this system of straight lines, when the whole system moves downward at right angles to the lines with the uniform velocity v'.

[1] Appendix to Betz's paper, Göttinger Nachr., p. 193, 1919.

In an upward stream of velocity v' the velocity field can be expressed in terms of the complex coordinate Z as

$$u - iv = \frac{v' e^{\pi Z/s}}{\sqrt{1 - e^{2\pi Z/s}}} \tag{4.2}$$

This is a suitable form according to the general theory of flow in terms of the complex variable, it has the correct periodicity, and it gives zero normal velocity on the surface of the lines. The general type of flow is as shown in Fig. 60. Between the lines, far from the edges, the fluid is at rest, but near the edges there is a small upward flow.

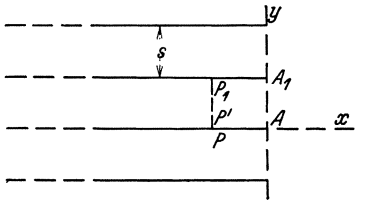

Fig. 59.

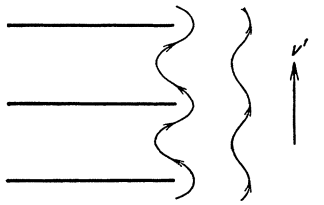

Fig. 60.

To obtain the mean upward flow on the line $P' P_1$ (Fig. 59), let $\Phi (P Q)$ denote the increase of the velocity potential from the point P to any other point Q. Then the integral of the vertical velocity v from P' to P_1 is

$$\begin{aligned} \int_0^s v\,dy &= \Phi (P' P_1) \\ &= \Phi (P' A) + \Phi (A A_1) + \Phi (A_1 P_1) \end{aligned}$$

But $\Phi (A_1 P_1)$ is equal to $\Phi (A P)$, and $\Phi (A A_1)$ is equal to $v' s$. Hence

$$\begin{aligned} \int_0^s v\,dy &= v' s - \Phi (P A) - \Phi (A P') \\ &= v' s - 2\Phi (P A) \end{aligned}$$

since the horizontal velocities at corresponding points of PA and $P'A$ are equal in magnitude and opposite in sign. Also, if a denotes the length of PA,

$$\Phi (PA) = v' \int_{-a}^{a} \frac{e^{\pi x/s} dx}{\sqrt{1 - e^{2\pi x/s}}}$$

This integral can be evaluated by substituting $\cos \theta$ for $e^{\pi x/s}$, and becomes

$$\Phi (PA) = \frac{v's}{\pi} \operatorname{arc\,cos} e^{-\pi a/s}$$

Then finally the mean vertical velocity on the line $P' P_1$ is

$$\frac{1}{s} \int_0^s v\,dy = v' \left[1 - \frac{2}{\pi} \operatorname{arc\,cos} e^{-\pi a/s} \right] \tag{4.3}$$

Now superimpose a downward velocity v' on the whole system and thus obtain the flow due to the motion of the system of lines. The mean downward velocity on the line $P'P_1$ is then

$$\bar{v} = \frac{2}{\pi} v' \, arc \cos e^{-\pi a/s} \tag{4.4}$$

In this formula a denotes the distance of the section under consideration from the edge of the lines, and must be replaced by $(R - r)$ in applying the result to the system of vortex sheets of the slipstream. Write therefore, in accordance with (4.1),

$$f = \frac{\pi a}{s} = \frac{B}{2} \frac{R-r}{R} \frac{\sqrt{1+\lambda^2}}{\lambda} \tag{4.5}$$

and

$$F = \frac{2}{\pi} arc \cos e^{-f} \tag{4.6}$$

If the lines of Fig. 59 extended indefinitely in both directions, the whole of the fluid would be carried downward with the velocity v' of the system, but owing to the flow around the edges the actual mean velocity on the line $P'P_1$ is less than v'. In fact F represents a reduction factor and can be interpreted as expressing the fraction of the velocity v' which is imparted to the air of the section $P'P_1$. In the corresponding propeller analogy, therefore, F is a reduction factor which must be applied to the momentum equation for the flow at radius r, since it represents the fact that only a fraction F of the air between the successive vortex sheets of the slipstream receives the full effect of the motion of these sheets. Applying this correction to the earlier analysis of 2, the optimum distribution of circulation along the blades becomes

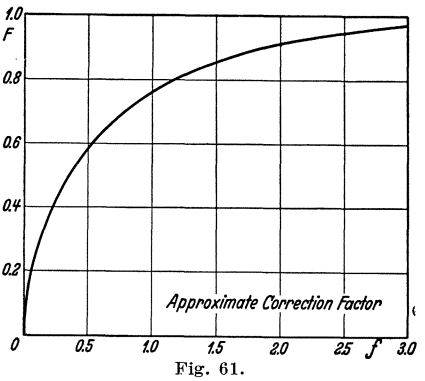

Fig. 61.

$$\frac{B K \Omega}{2 \pi V v'} = \frac{x^2 F}{1 + x^2} \tag{4.7}$$

where F is given by (4.6) and f may be expressed as

$$f = \frac{B(1 - \lambda x)\sqrt{1+\lambda^2}}{2\lambda} \tag{4.8}$$

The relationship between F and f is given in Table 23 and Fig. 61, and some examples of the optimum distribution of circulation along the blade, as modified by the factor F, are shown in Fig. 62.

TABLE 23. Reduction Factor F.

F	f	F	f	F	f
0.10	0.012	0.60	0.531	0.92	2.08
0.20	0.050	0.70	0.790	0.94	2.36
0.30	0.115	0.80	1.174	0.96	2.77
0.40	0.212	0.85	1.455	0.98	3.46
0.50	0.346	0.90	1.855	0.99	4.15

Owing to the radial flow near the boundary of the slipstream there is a drop of circulation and thrust corresponding to any chosen value of v' of the velocity of the system of vortex sheets, and hence the efficiency of the propeller, which depends only on the value of v', is associated with a lower value of the thrust. This result may be represented in another way by replacing the propeller with a finite number B of blades and the thrust T by an equivalent propeller with an infinite number of blades and with the same thrust but with a smaller radius R_e. In order to calculate this effective radius, consider again the system of parallel lines shown in Fig. 59. If the lines were indefinitely close together, the fluid between the lines would be carried downward with the velocity v' of the lines and the fluid outside the lines would be at rest. Actually some fluid flows upward around the edges of the lines and, if v is the velocity of this upward flow on the axis of x, the effective length of the lines is reduced by a, where

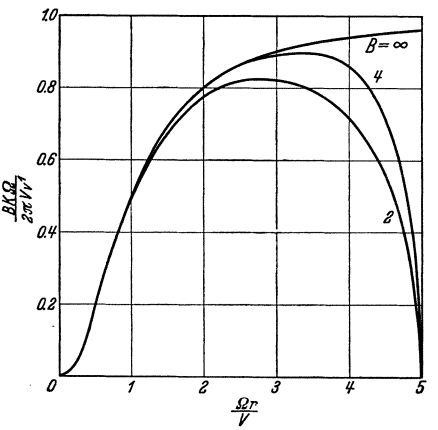

Fig. 62.

$$v' a = \int_0^\infty v \, d x$$

But from the flow function (4.2), on which a downward velocity v' must be imposed

$$\frac{v}{v'} = \frac{e^{\pi x/s}}{\sqrt{e^{2\pi x/s} - 1}} - 1$$

and hence

$$a = \int_0^\infty \left[\frac{e^{\pi x/s}}{\sqrt{e^{2\pi x/s} - 1}} - 1 \right] d x$$

To evaluate this integral, put

$$e^{\pi x/s} = \cosh \theta$$

and then

$$\frac{\pi a}{s} = \int_0^\infty (1 - \tanh \theta) \, d \theta$$

$$= [\theta - \log \cosh \theta]_0^\infty$$

Now at the lower limit this expression is zero, and when θ is large

$$\log \cosh \theta = \log \frac{1}{2} e^{\theta}$$
$$= \theta - \log 2$$

and hence
$$a = \frac{s}{\pi} \log 2 = 0.2207\, s \tag{4.9}$$

Applying this result to the analogous problem of the propeller, the effective radius is $R_e = R - 0.2207\, s$
and, substituting for s from (4.1),

$$\frac{R_e}{R} = 1 - \frac{1.386}{B} \frac{\lambda}{\sqrt{1+\lambda^2}} \tag{4.10}$$

Numerical values of this ratio are given in Table 24. Under ordinary operating conditions the ratio of the effective radius to the actual radius is of the order of 0.85 for a propeller with two blades and 0.93 for a propeller with four blades. The ratio decreases as the speed ratio of the propeller increases, and thus the tip losses of a propeller increase with its pitch-diameter ratio.

TABLE 24.
Effective Radius.
Values of R_e/R.

$V/\Omega R$	$B=2$	$B=4$
0.2	0.864	0.932
0.3	0.801	0.900
0.4	0.743	0.871

Prandtl's method of estimating the tip losses of a propeller due to the finite number of the blades by the analogy of a system of parallel lines is approximate only, and a more accurate analysis of the problem

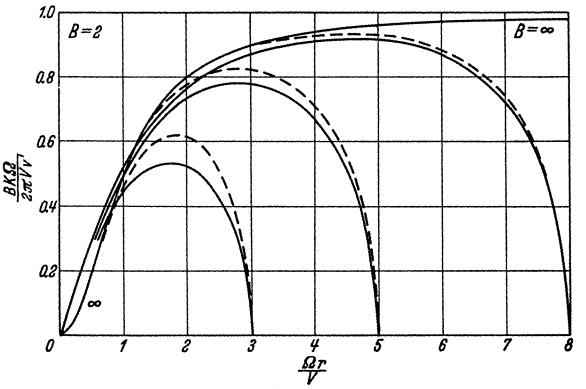

Fig. 63.

has been developed by S. Goldstein[1] by the use of Bessel functions. Goldstein's solution is a rigorous representation of Betz's optimum condition but, since it ignores the contraction of the slipstream, refers only to lightly loaded propellers. The analysis determines the circulation along the blade as a function of the radial coordinate x and the speed

[1] On the Vortex Theory of Screw Propellers. Roy. Soc. Proc. (A) **123**, 440, 1929.

ratio λ for propellers with two or four blades, but a complete reconsideration of the analysis is required when the number of blades is changed.

A comparison of the distribution of circulation for a propeller with two blades as given by Goldstein's detailed analysis and by Prandtl's approximate formula is shown in Fig. 63, where the full lines represent the exact and the broken lines the approximate solution. The agreement is satisfactory for low speed ratios ($\Omega r/V$ large), but there is an increasing divergence as the speed ratio increases. It is remarkable that this discrepancy is not confined to the outer parts of the propeller blade, but that there is a consistent difference also near the root of the blade, where the approximate formula gives no correction to the curve for an infinite number of blades.

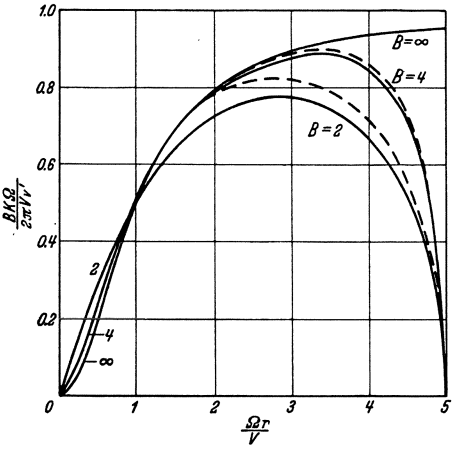

Fig. 64.

Fig. 64 shows a similar comparison for propellers with two and four blades and for a single value of the speed ratio. The difference between the exact and approximate solutions decreases rapidly as the number of blades increases, and in the light of this comparison it would appear that Prandtl's approximate formula is a sufficiently accurate representation of the tip losses of a propeller with four blades operating at an ordinary rate of advance, but that it is less reliable for propellers with two blades and for high rates of advance. The approximate formula does, however, give an indication of the tip losses which can be easily applied to any propeller, whereas Goldstein's exact analysis is too complicated for general use.

5. Applications of Prandtl's Formula. The object of the preceding analysis has been to determine the distribution of the circulation along the blade of a propeller which will lead to the minimum loss of energy or to the highest efficiency for a given thrust and for given conditions of operation of the propeller. In the course of this analysis a formula has been obtained which represents approximately the losses which arise due to the finite number of the propeller blades, and it is now necessary to consider the application of this result to the propeller theory which has been developed previously on the assumption of a large number of blades.

The development of the momentum theory in Chapters II and III led to expressions for the efficiency of a propeller in terms of the power

absorbed, of the disc area, and of the operating conditions; and the modification of this analysis to represent the effect of the finite number of the propeller blades is simply to replace the actual radius R of the propeller by the effective radius R_e which is defined by the equation

$$\frac{R_e}{R} = 1 - \frac{1.386}{B} \frac{\lambda}{\sqrt{1+\lambda^2}} \tag{5.1}$$

In order to illustrate the magnitude of this correction, consider the ideal efficiency of a propeller as determined by the axial momentum theory. According to II (3.11) this ideal efficiency η_1 is determined by the equation

$$\frac{1-\eta_1}{\eta_1^3} = \frac{P}{2\pi R^2 \varrho V^3} \tag{5.2}$$

and an ideal efficiency of 0.90 is obtained if P is equal to $0.274\pi R^2 \varrho V^3$. This value refers to a propeller with an infinite number of blades, and the corresponding ideal efficiency of a propeller with B blades must be derived from the equation

$$\frac{1-\eta_1}{\eta_1^3} = 0.137 \left(\frac{R}{R_e}\right)^2$$

Assuming a speed ratio of 0.2, *i.e.* a forward speed V of one fifth of the tip speed ΩR, (5.1) gives $\frac{R_e}{R} = 1 - \frac{0.272}{B}$

and the relationship between the ideal efficiency and the number of blades is:—

$B =$	2	4	∞
$\eta =$	0.877	0.889	0.900

Thus the efficiency drops 1 per cent for a propeller with four blades and 2-$^1/_4$ per cent for a propeller with two blades. This drop of efficiency would be doubled if the speed ratio were 0.4, and it also increases as the ideal efficiency decreases. Except for high speed ratios, however, the correction due to the finite number of the blades is always small.

Another application of the formula for the losses at the blade tips is to provide an approximate correction to the system of equations summarized in VI 3 for calculating the characteristics of any given propeller. The physical fact represented by the tip correction is virtually that the maximum increase of axial velocity, $(u_1 - V)$ or $2aV$, in the slipstream occurs only on the vortex sheets and that the average increase of axial velocity in the slipstream is only a fraction F of this velocity. Thus, to the order of approximation of the analysis, the corrected form of the axial momentum equation may be taken to be

$$\frac{dT}{dr} = 4\pi r \varrho V^2 (1+a) a F \tag{5.3}$$

The factor F has been derived for a frictionless propeller with optimum distribution of circulation along the blade, but it may probably be used also with reasonable accuracy for any propeller, since the distribution

of circulation along the blade will not depart widely from the optimum distribution in general. Similarly also the angular momentum equation may be assumed to be

$$\frac{dQ}{dr} = 4\pi r^3 \varrho V \Omega (1 + a) a' F \tag{5.4}$$

The expressions for the elements of thrust and torque in terms of the aerodynamic forces on the blade sections remain unaltered, and the only modification to the system of equations summarized in VI 3 is that the axial and rotational interference factors a and a' must now be determined from the equations

$$\left.\begin{aligned} \frac{a'}{1-a'} &= \frac{\sigma C_x F}{4 \sin\varphi \cos\varphi} \\ \frac{a}{1+a} &= \frac{\sigma C_y F}{4 \sin^2\varphi} \end{aligned}\right\} \tag{5.5}$$

The approximate formula for the factor F is

$$F = \frac{2}{\pi} \operatorname{arc\,cos}\, e^{-f} \tag{5.6}$$

where

$$f = \frac{B}{2} \frac{R-r}{R \sin\varphi_1}$$

and φ_1 is the value of the angle φ at the blade tip. This form is not very convenient for use in the method of calculating the characteristics of a propeller which is developed in VI 4, since the calculations for the typical blade element proceed without a knowledge of the corresponding value of φ_1 at the tip of the blade. In general, however, it will be sufficiently accurate to modify the expression for f by writing $r \sin\varphi$ in place of $R \sin\varphi_1$. With this modification the approximate expression for f becomes

$$f = \frac{B}{2} \frac{R-r}{r \sin\varphi} \tag{5.7}$$

The calculations then proceed exactly on the lines described in VI 4, and the effect of the tip correction is to reduce slightly the thrust and torque contributed by the elements near the tips of the blades. The effect is, however, quite small. Applied to the propeller whose characteristics are calculated in VI 4, the change in the thrust distribution at the speed ratio $\lambda = 0.175$ is given in Table 25. The difference due to the finite number of the blades would hardly be noticed in Fig. 44, but

TABLE 25. Thrust Distribution ($\lambda = 0.175$).

$\frac{r}{R}$	0.304	0.500	0.700	0.833	0.950
$R\frac{dT_c}{dr}$ $(B = \infty)$	0.0034	0.0083	0.0112	0.0115	0.0097
$R\frac{dT_c}{dr}$ $(B = 2)$	0.0034	0.0082	0.0108	0.0109	0.0090

it represents a reduction of approximately 4 per cent in the thrust coefficient. There is a corresponding but smaller reduction in the torque coefficient, and hence a small drop in the efficiency of the propeller. The correction due to the tip losses increases with pitch-diameter ratio of the propeller, and in general may be neglected except for high pitch propellers with only two blades.

A method of applying Goldstein's more accurate analysis to determine the values of the factor F has been proposed by C. N. H. Lock[1] using a series of curves for F instead of the equation (5.6).

CHAPTER VIII

BODY AND WING INTERFERENCE

1. Propeller Characteristics. Hitherto the behavior of a propeller has been considered apart from the disturbing influence of any adjacent bodies, but in practice a propeller is always attached in front of or behind an airplane body or engine car. If the diameter of this body is small compared with that of the propeller, there will be no important disturbance of the flow and the behavior of the propeller will be sensibly in accordance with the theory developed in the preceding chapters. More generally, however, the diameter of the body is comparable with that of the propeller and there is an important mutual interference: the flow around the body modifies the conditions under which the propeller operates, and the flow generated by the propeller augments the drag of the body. This mutual interference may be complicated also by the proximity of the wings of the airplane, whose lift is modified by the slipstream of the propeller.

The interference experienced by a ship's propeller was appreciated at an early date, and Rankine's original paper[2] contains an allowance for the disturbed conditions under which the propeller operates. Rankine also remarked that the change of pressure produced in the water by the action of the propeller is transmitted to some part of the ship's bottom and alters the resistance of the ship, and he gave a rather crude method of estimating this change of resistance. The problem of the mutual interference of a ship and its propeller differs very considerably from the analogous problem for the airplane. The ship's propeller is very small compared with the ship, and the thrust of the propeller is essentially equal to the drag of the ship. An airplane's propeller on the other hand has a diameter comparable with and generally greater than that of the body or car to which it is attached, and the drag of the body is only a fraction of the total drag which must be overcome by the thrust of the propeller.

[1] Br. A.R.C. R. and M. 1377, 1930.

[2] Transactions Institute of Naval Architects, Vol. 6, p. 13, 1865.

As a first step in the elucidation of the interference experienced by a propeller, consider the behavior of a propeller which is situated in the neighborhood of a large body and in a region where the velocity of the air relative to the body has been reduced from its original value V to a lower value V' by the interference of the body. If the region in which this lower velocity V' occurs is large compared with the size of the propeller, the behavior of the propeller will be sensibly the same as if it were situated in a uniform stream of this reduced velocity. Now, according to the simple momentum theory of Chapter II, the ideal efficiency η_1 of a propeller is determined as a function of the speed V, the power P, and the disc area S of the propeller by the equation

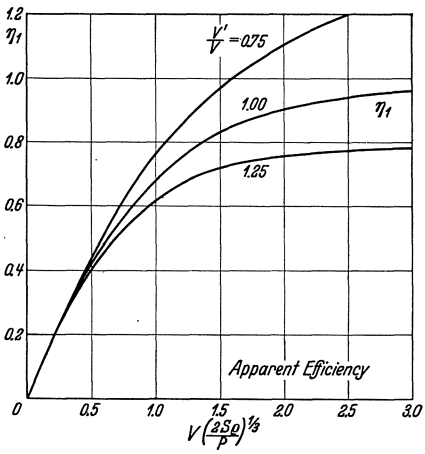

Fig. 65.

$$\frac{P}{2\,S\,\varrho\,V^3} = \frac{1-\eta_1}{\eta_1^3} \tag{1.1}$$

and this relationship is shown graphically in Fig. 11. For the present purpose, however, it is more convenient to express this relationship in the alternative form

$$\eta_1 = f(X)$$

where

$$X = V\left(\frac{2\,S\,\varrho}{P}\right)^{1/3} \tag{1.2}$$

In a stream of reduced velocity V', the ideal efficiency would be simply

$$\eta_1' = f(X')$$

where

$$X' = V'\left(\frac{2\,S\,\varrho}{P}\right)^{1/3} = n\,X$$

and

$$V' = n\,V \tag{1.3}$$

This efficiency, however, represents the ratio of the useful work $V'T$ to the power P, whereas, under the conditions assumed in the present discussion of body interference, the useful work done by the propeller is VT. Thus the efficiency of the propeller, operating in a region of reduced velocity, is apparently

$$\eta_a = \frac{V}{V'}\eta_1' = \frac{1}{n} f(n\,X) \tag{1.4}$$

The ideal efficiency η_1 increases with the speed coordinate X and hence, if n is less than unity, η_1' will be less than η_1; but, since the decrease is less rapid than that of the speed, the apparent efficiency η_a will be greater than the free efficiency η_1. The relationship between the ideal efficiency η_1 and the speed coordinate X is shown in Fig. 65, and two curves of apparent efficiency have been added, corresponding respectively

to an increase and to a decrease of speed of 25 per cent. These curves show in particular that it is possible to obtain an apparent efficiency greater than unity if the propeller operates in a region of reduced velocity. This seemingly paradoxical result is due to the fact that the reaction of the propeller on the body causes an increase of drag which has been ignored in this estimate of the behavior of the propeller.

The increase of apparent efficiency of a propeller operating in a region of reduced velocity can be illustrated in another way by considering the characteristic curves of the propeller—thrust coefficient, torque coefficient, and efficiency as functions of the advance-diameter ratio. In a free stream of velocity V these characteristics are represented by curves of the type shown by the full lines of Fig. 66. In a stream of reduced velocity V' or nV the thrust and torque coefficients are obtained by taking the corresponding values from these curves at the reduced value of the advance-diameter ratio J' or nJ, but to obtain the apparent efficiency it is necessary, in accordance with the argument developed in the previous paragraph, to increase the efficiency read from the curve at the abscissa nJ by the factor $1/n$. This process may be expressed symbolically by the equations

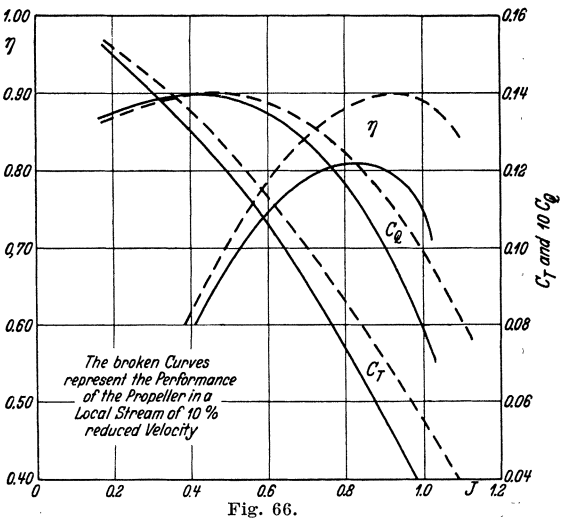

Fig. 66.

$$\left.\begin{aligned} T_a(J) &= T(nJ) \\ Q_a(J) &= Q(nJ) \\ \eta_a(J) &= \frac{1}{n}\eta(nJ) \end{aligned}\right\} \qquad (1.5)$$

In Fig. 66 the broken lines show the result of this calculation for a reduced velocity of 0.9 V, and it will be noticed that the maximum efficiency has risen from 0.81 to 0.90 and occurs at a higher value of J. The comparison between the characteristics of the propeller in a free stream and in a local stream of reduced velocity has been made on the basis of the same advance-diameter ratio J, but another interesting method of comparing the results is to consider the same conditions of flow through the propeller disc. On this basis of comparison the blade

elements of the propeller clearly experience the same forces, the propeller develops the same thrust and torque, but the advance-diameter ratio and the apparent efficiency of the propeller in the disturbed stream are higher by a factor $1/n$ than the corresponding values for the free propeller.

A typical example of some experimental curves[1] obtained from a propeller in front of an airplane body is shown in Fig. 67 together with the corresponding curves for the free propeller, and an inspection of these curves shows that the general nature of the interference experienced by the propeller must be of the type assumed in constructing the curves of the previous Fig. 66. The shift of the curves in Fig. 67

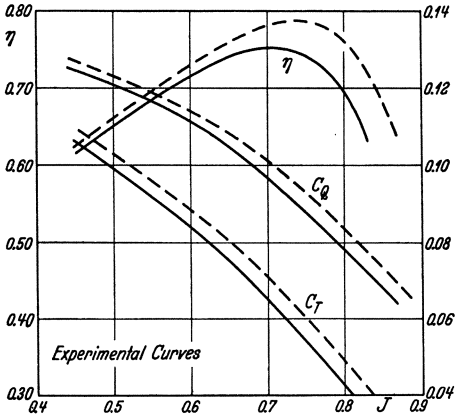

Fig. 67.

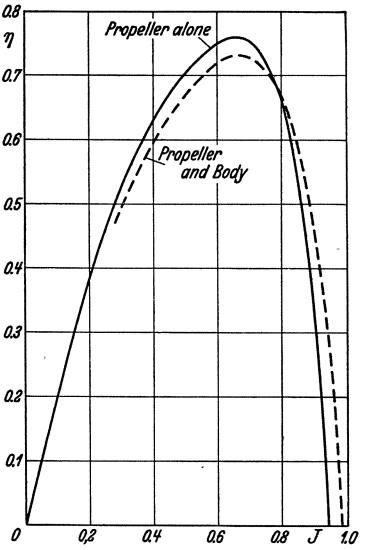

Fig. 68.

suggests that the propeller was effectively operating in a region where the velocity was reduced some 4 per cent by the interference of the body. It would appear therefore that it is possible to represent the interference experienced by a propeller in the presence of a body by a reduction in the effective velocity of advance of the propeller, but owing to the proximity of the body this effective velocity will vary for different annular elements of the propeller and the assumption of a mean effective velocity experienced by the whole propeller can only be a first rough approximation to the real conditions. Moreover, a complete solution of the problem must include also an estimate of the reaction of the propeller on the body, since, as has been suggested already, the increased apparent efficiency of the propeller finds a counterpart in an increased drag of the body.

[1] Fage, A., and Collins, H. E., An Investigation of the Mutual Interference of an Airscrew and Body of the Tractor Type of Airplane. Br. A.R.C. R. and M. 344, London, 1917.

The most suitable method of allowing for this increased drag of the body is to subtract from the thrust of the propeller, operating in front of a body, the increased drag caused on the body and any other structural parts which come within the influence of the propeller's slipstream. When the efficiency corresponding to this reduced thrust is compared with the free efficiency of the propeller, it is found that the presence of the body causes a small decrease of the maximum efficiency. Some typical experimental curves[1] are shown in Fig. 68, and in this example the maximum efficiency has been reduced by 3 per cent. The experimental curves also show that the interference of the body increases the apparent aerodynamic pitch of the propeller, since the thrust and efficiency fall to zero at a higher value of the advance-diameter ratio. Throughout the usual working range of the propeller the efficiency is reduced by the interference of the body, but at higher rates of advance there is an increase of efficiency and at some rates of advance the propeller with body interference may give a positive thrust whereas the propeller alone would experience a drag or negative thrust.

2. Propeller-Body Interference. An examination of the experimental results shown in Fig. 67 has suggested that the interference experienced by a propeller at the front of an airplane body can be represented approximately as a decrease of the effective velocity of advance of the propeller. To obtain an estimate of the interference experienced by the body it is convenient to consider first the action of a propeller on a body placed in its slipstream so far downstream that the slipstream has developed its full velocity and that the body exerts no appreciable interference on the characteristics of the propeller. The thrust of the propeller then retains its undisturbed value T and the velocity $V(1 + 2a)$ in the slipstream can be calculated from the momentum equation

$$T = 2\pi R^2 \varrho V^2 (1 + a) a$$

or

$$(1 + 2a)^2 = 1 + \frac{2T}{\pi R^2 \varrho V^2} \tag{2.1}$$

The body experiences this increased velocity $V(1 + 2a)$ and hence the drag D which it would experience in a stream of velocity V is increased to a higher value D_a according to the equation

$$D_a = D(1 + 2a)^2$$

or

$$D_a = D\left[1 + \frac{2T}{\pi R^2 \varrho V^2}\right] \tag{2.2}$$

The thrust of the propeller has not been influenced by any interference from the body, but it is reasonable to debit the propeller with the increased drag which it causes on the body. The object of the thrust

[1] DURAND, W. F., and LESLEY, E. P., Comparison of Tests of Air Propellers in Flight with Wind Tunnel Tests on Similar Forms. U.S. N.A.C.A. Technical Report No. 220, 1925.

of the propeller is to overcome the drag of the body and of any other parts of the aircraft situated outside the influence of its slipstream. If the propeller is placed in such a position that it increases the drag of the body or of any other parts of the aircraft, the thrust available for propulsion is not simply the gross thrust of the propeller but only this thrust less the increased drag caused by its slipstream. It is convenient therefore to define the *propulsive thrust* of the propeller as the apparent thrust, which is the resultant axial force on the propeller itself, less the increase of drag of the aircraft due to the interference of the propeller. When this increased drag is represented by (2.2) the propulsive thrust is

$$T_p = T - (D_a - D)$$
$$= T\left[1 - \frac{2D}{\pi R^2 \varrho V^2}\right] \qquad (2.3)$$

Since the drag D is proportional to the square of the velocity V, the propulsive thrust is a constant fraction of the apparent thrust on the assumptions made in this analysis.

In estimating the drag D in the formula (2.3) it is necessary to allow for the contraction of the slipstream behind the propeller and to include only those parts of the airplane structure which lie within the circumference of the slipstream. As a refinement also, it may be noted that the thrust is not uniformly distributed over the whole disc of the propeller. It is more accurate to use, instead of the radius R of the propeller, the effective radius[1] R_e which depends on the number of the blades of the propeller, and also to allow for a region of lower velocity around the boss of the propeller. The former of these two corrections is the more important and its effect is to increase the numerical factor 2 which occurs in the formulae (2.2) and (2.3). The increase varies with the number of the blades of the propeller and with the rate of advance, but an average value of the numerical factor for a propeller with two blades is from 2.5 to 3.0.

In the light of this discussion the following definitions and notation will be adopted as a suitable basis for considering the behavior of a propeller in the presence of a body:—

T the *free thrust* of the propeller without any interference.
D the *free drag* of the body without any interference.
T_a the *apparent thrust* of the propeller in the presence of the body.
D_a the *apparent drag* of the body in the presence of the propeller.
T_p the *propulsive thrust* of the propeller, defined as the apparent thrust less the increase of drag of the body due to the action of the propeller, or $T_p = T_a - (D_a - D)$.

Instead of the propulsive thrust it is sometimes more convenient to use the net thrust $(T_a - D_a)$ of the combined system, which can suitably

[1] See VII 4, Table 24.

be compared with the excess of the free thrust over the free drag ($T - D$) in order to assess the merit of the combination.

The analysis hitherto has been based on the assumption that the body is far behind the propeller and exerts no interference on it, but in practice the body is situated immediately behind the propeller or even includes the boss of the propeller within its nose. As the body approaches the propeller from behind, it comes under the influence of a pressure gradient, since the pressure is high immediately behind the propeller and decreases down the slipstream. The drag of the body is increased by this pressure gradient in the slipstream, and at the same time the disturbance of the flow caused by the body reacts back as an interference on the propeller. In order to analyze the nature of this mutual interference it is convenient to consider two types of body which may be called respectively stream-line and irregular bodies. In a perfect fluid no body, whatever its shape, would experience any drag owing to its motion through the fluid, and a stream-line body is one which approximates to these ideal conditions in a real fluid. The drag of a stream-line body is due mainly to the frictional force over its surface and there is only a very weak turbulent wake behind it. At the other extreme, the drag of a bluff body is due mainly to the formation of a strong turbulent wake and the surface friction is almost negligible in comparison. Bluff bodies are not normally used in association with propellers, but if the body is of irregular shape, due to projecting engine cylinders or open cockpits, the drag will be due largely to the formation of eddies, as in the case of a bluff body, and it is this condition which distinguishes the irregular bodies from the stream-line bodies.

An ideal body would experience no drag in the ultimate slipstream of a propeller, but if placed close behind the propeller in the region of decreasing pressure, a drag force will occur even in a perfect fluid. The drag due to a uniform pressure gradient can be calculated theoretically[1], but the pressure gradient behind a propeller varies in intensity and it is necessary to rely on experimental determinations of the pressure drag. The behavior of a stream-line body approximates to that of an ideal body; the drag of the body in a uniform stream is low, but there may be an important pressure drag when the body is placed close behind a propeller. Also the periodic and rotational nature of the flow in the slipstream may disturb the flow over the surface of the body and so in effect convert the stream-line body into an irregular body.

An ideal body, again, causes no loss of energy in the fluid and hence the wake far behind the propeller-body combination must be exactly

[1] MUNK, M., Some New Aerodynamical Relations. U.S. N.A.C.A. Technical Report No. 114, 1921.

GLAUERT, H., The Effect of the Static Pressure Gradient on the Drag of a Body Tested in a Wind Tunnel. Br. A.R.C. R. and M. 1158, 1928.

the same as that due to the propeller alone. If T_a is the thrust of the propeller in front of the body and if D_a is the drag of the body, the net thrust of the combination is $(T_a - D_a)$; and if this net thrust is equal to the free thrust T of the propeller alone, the combined system will cause the same loss of energy in the wake and will therefore have the same efficiency of propulsion. This argument shows that if the apparent thrust of the propeller is reduced by the pressure gradient drag of the body, the corresponding efficiency of propulsion will be the same as that of the free propeller. The combined system of a propeller and a stream-line body will nevertheless be less effective than the free propeller and free body owing to the increased frictional and eddying drag of the body in the slipstream.

The interference experienced by an irregular body is of the same general nature but the relative importance of the different components of the drag is completely changed. The frictional drag of the body is unimportant compared with the drag caused by the irregular shape and protuberances, and the action of the slipstream, instead of spoiling a good shape, may even secure a better conformity of the flow to the surface of the body. There will still be a mutual reaction between the propeller and body associated with the pressure gradient behind the propeller, but the predominant factor is the increase of drag due to the increased velocity in the slipstream.

3. Analysis of Apparent Thrust and Drag. In the light of the preceding general discussion the mutual interference between propeller and body may be divided into the following three elements:—

(1) The increase of body drag due to the increased velocity in the slipstream.

(2) The mutual reaction between the body and propeller due to the pressure gradient in the slipstream.

(3) The shielding of the nose of the body or the inclusion of the boss of the propeller inside the body.

The first effect, due to the increased velocity in the slipstream, is of the form given by (2.2) and may be expressed more generally as

$$\Delta D = f_1 \frac{D T_a}{\pi R^2 \varrho V^2} \tag{3.1}$$

where f_1 is a numerical factor. Assuming a propeller with a large number of blades and a body situated in the ultimate wake, this numerical factor f_1 has the value 2. When the body is immediately behind the propeller the full effect of the increased velocity in the ultimate wake will not be experienced by the body and the value of f_1 will tend to fall, whereas the effect of the finite number of the blades of the propeller is to increase its value.

The second effect, which would occur even with an ideal frictionless body, causes equal increments of the propeller thrust and of the body drag, and these increments may be presumed to be proportional to the apparent thrust T_a of the propeller and to the maximum cross-sectional area S of the body. Thus

$$\Delta T = \Delta D = f_2 \frac{S T_a}{\pi R^2} \tag{3.2}$$

where f_2 is a numerical factor depending mainly on the shape of the nose of the body and probably independent of its drag.

The third effect is usually of minor importance and would disappear if the free thrust of the propeller were obtained from the forces on the blades and did not include the drag of the boss. If D_B is the drag of the boss, the interference appears either as a reduction of the body drag or as an increase of the propeller thrust according as the propeller is mounted in front of the body or has its boss enclosed within the body. Adopting the former alternative as the more usual practice, the correction is

$$\Delta D = -D_B \tag{3.3}$$

Accepting these formulae as representing the total mutual interference between the propeller and body, the apparent thrust of the propeller becomes

$$T_a = T + f_2 \frac{S T_a}{\pi R^2} \tag{3.4}$$

and the corresponding apparent drag of the body is

$$D_a = D - D_B + f_1 \frac{D T_a}{\pi R^2 \varrho V^2} + f_2 \frac{S T_a}{\pi R^2}$$

which can be expressed conveniently in the form

$$D_a = D\left[A + B \frac{T_a}{\pi R^2 \varrho V^2}\right] \tag{3.5}$$

where

$$\left.\begin{aligned} A &= 1 - \frac{D_B}{D} \\ B &= f_1 + \frac{f_2}{C} \end{aligned}\right\} \tag{3.6}[1]$$

and

$$C = \frac{D}{S \varrho V^2}$$

In this formula C is the drag coefficient of the body in terms of the maximum cross-sectional area S: it is small for a stream-line body and larger for an irregular body, and hence the value of the coefficient B may be expected to increase as the drag of the body decreases. Also the coefficient A may be expected to be slightly less than unity in general, but if the body is of good stream-line shape and if the presence of the propeller disturbs the smooth flow over the body, there will be an

[1] In the development of this analysis it is convenient to adopt the English definition of drag coefficient in terms of ϱV^2 instead of the more usual definition in terms of $(1/2)\varrho V^2$.

increase of drag which will be represented by an increase of this coefficient A above the value given by this formula.

The form of the coefficient B appears to have been suggested first by R. McK. Wood[1], who obtained an upper limit to the value of the coefficient f_2 by assuming that the increase of pressure, which occurs immediately behind the propeller, acts on the whole front half of the body. The increase of pressure from the front to the back of the propeller is $T_a/\pi R^2$, and this appears half as reduced pressure before the propeller and half as increased pressure behind it. The pressure force on the body was therefore estimated to be $S T_a/2\pi R^2$, and by comparison with (3.2) the corresponding value of f_2 is 1/2. Wood's estimate for the upper limit of the coefficient B was therefore

$$B = 2 + \frac{1}{2C}$$

Adopting the expressions (3.4) and (3.5) for the apparent thrust and drag, the propulsive thrust of the propeller becomes

$$\begin{aligned} T_p &= T_a - (D_a - D) \\ &= T + D_B - f_1 \frac{D T_a}{\pi R^2 \varrho V^2} \end{aligned} \tag{3.7}$$

or, ignoring the drag of the boss and replacing the apparent thrust by the free thrust in the small correction term,

$$T_p = T(1 - f_1 C) \tag{3.8}$$

Thus the propulsive thrust is approximately a constant multiple of the free thrust of the propeller. The propulsive thrust is the force which is available to overcome the drag of the airplane, estimated without any propeller interference, and the term $f_1 C T$ represents the loss due to the mutual interference of the propeller and body. The drag coefficient C would be zero for an ideal body and there would be no loss of thrust due to the interference, and the loss which actually occurs is directly proportional to the drag of the body. It must be remembered, however, that the interference of the body will also cause a change in the torque coefficient of the propeller at a given value of the advance-diameter ratio, and that it is therefore necessary to modify the shape of the propeller slightly in order to absorb the full engine power at the correct rate of rotation.

4. Experimental Results. The validity of the analysis of the apparent thrust and drag, as developed in the previous section, may be examined by reference to experimental results on the interference between propeller and body. Numerous experiments have been made to determine the increased drag of a body behind a propeller and the results, expressed in the form

$$\frac{D_a}{D} = A + B \frac{T_a}{\pi R^2 \varrho V^2} \tag{4.1}$$

[1] Br. A.R.C. R. and M. 830, 1922.

have been analyzed by W. G. Jennings[1] to determine the relationship between the coefficient B and the drag coefficient of the body. The previous theoretical discussion has suggested the form

$$B = f_1 + \frac{f_2}{C} \tag{4.2}$$

where C is the drag coefficient $(D/S\,\varrho\,V^2)$ of the body, and the analysis of the experimental results in this form led to the numerical result

$$\frac{4}{\pi} B = 3.1 + \frac{0.323}{C}$$

or

$$B = 2.43 + \frac{0.254}{C} \tag{4.3}$$

Thus the value of f_1 is rather greater than the value 2 suggested in the theoretical discussion, due probably to the reduced effective diameter of the propeller which must be used to represent the losses at the tips of the blades, and the value of f_2 is only half the maximum possible value suggested by R. McK. Wood. The accuracy of this method of representing the increased drag of the body is illustrated in Fig. 69 which shows the experimental results[2] for a series of bodies of increasing drag.

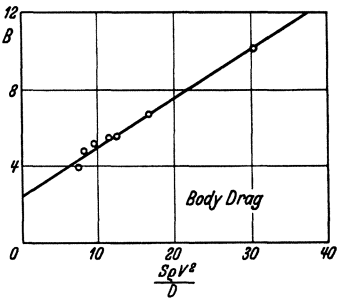

Fig. 69.

The experimental values of the coefficient A are also reasonably consistent with the theoretical ideas developed in the previous section. The value suggested for this coefficient, when the propeller boss shields the nose of the body, was

$$A = 1 - \frac{D_B}{D} \tag{4.4}$$

If the propeller boss is included in the nose of the body A should be unity, but in either case the value of A may be higher for a body of low drag if the presence of the propeller spoils the stream-line flow. Experiments[3] with a propeller in front of a airplane body gave values of A in the neighborhood of 0.85, experiments[4] with the propeller boss inclosed in the body gave values ranging from 1.0 to 1.1, and experiments[5] using a propeller with a very large boss in front of a stream-line body gave values ranging from 1.1 to 1.5 or even higher.

---

[1] Jennings, W. G., The Effects of Body Interference on Airscrew Performance. Br. A.R.C. R. and M. 1046, 1926.

[2] Br. A.R.C. R. and M. 1030, 1926.

[3] Br. A.R.C. R. and M. 334, 1917; and 393, 1918.

[4] Br. A.R.C. R. and M. 1030, 1926.

[5] Br. A.R.C. R. and M. 830, 1922.

When the propeller is mounted in front of the body, the mutual interference depends on the width of the gap between the boss of the propeller and the nose of the body. This point has been examined experimentally by W. F. Durand[1] and by C. N. H. Lock and H. Bateman[2] The latter tested a propeller in front of a body with gaps of 0.06 R and 0.17 R, and as the gap was increased the thrust and torque decreased owing to the weaker interference exerted by the body, but the excess of thrust over drag ($T_a - D_a$) remained unchanged. The experimental results are reproduced in Fig. 70: the experimental points are rather scattered, but they show

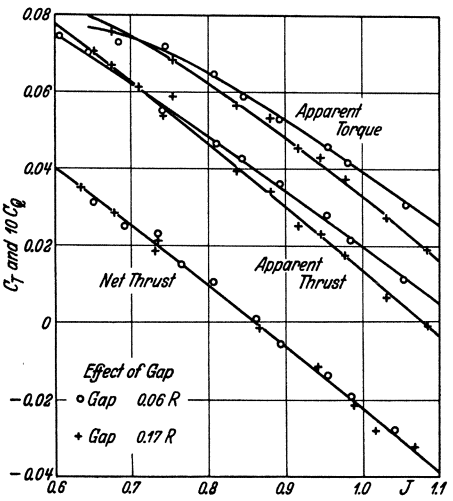

Fig. 70.

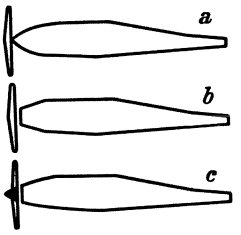

Fig. 71.

clearly the change in the apparent thrust and drag and the constancy of the net thrust. An analysis of the body drag gave the following values for the coefficients A and B of the formula (4.1):

Gap	*A*	*B*
0.06 R	1.56	11.5
0.17 R	1.36	12.3

These results are in accord with the general ideas developed in the previous section. The interference of the body on the propeller becomes weaker as the propeller is moved forward, but the reduction of the apparent thrust is balanced by an equal reduction of the apparent drag. The decrease of the value of A possibly indicates that the propeller exerts less disturbance on the stream-line flow around the body when the gap is increased.

---

[1] Interaction Between Air Propellers and Airplane Structures. U.S. N.A.C.A. Technical Report No. 235, 1926.

[2] The Effect of Gap Between an Airscrew and a Tractor Body. Br. A.R.C. R. and M. 921, 1924.

Another interesting series of experiments by A. Fage and H. E. Collins[1] shows the effect of fairing the nose of an airplane body. Fig. 71 shows the three systems examined: the propeller was mounted in turn in front of a body with a stream-line nose and with a blunt nose, and then a stream-line nose piece was fitted in front of the second combination. The results showed that the apparent efficiency of the propeller in the system (*a*) was sensibly the same as that of the free propeller without any body, the apparent efficiency in the system (*b*) was 3 per cent higher owing to the body interference, and this efficiency rose another 3 per cent in the system (*c*) owing to the shielding of the propeller boss by the stream-line nose. The combined system of propeller and body, however, showed little difference between the systems (*a*) and (*b*) since the increase of apparent thrust in system (*b*) was exactly balanced by the increase of apparent drag. The system (*c*) was superior to the others owing to the improvement in the shielding of the propeller boss. These experimental results are shown in Fig. 72 in the form of curves of net efficiency against net thrust coefficient for the three combined systems.

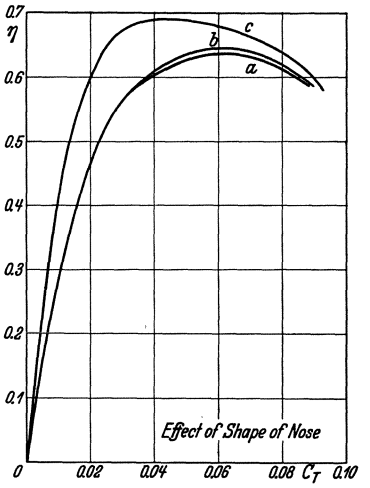

Fig. 72.

5. Apparent Thrust and Efficiency. Hitherto the interference experienced by a propeller mounted in front of a body has been discussed only in general terms, and it has been suggested that there is an increase of the apparent thrust of the propeller due to the fact that its blades operate in a region of reduced velocity. In (3.4) the apparent thrust was represented in the form

$$T_a = T + f_2 \frac{S\,T_a}{\pi R^2} \qquad (5.1)$$

where S is the maximum cross-sectional area of the body and f_2 is a numerical factor depending on the shape of the nose of the body. In order to determine the magnitude of this increase of thrust it is necessary to examine the problem in greater detail and to determine the variation along the blades of the effective velocity experienced by the propeller. A general theory of this nature, supported by a special experimental investigation, has been developed by C. N. H. Lock. In[2]

[1] An Investigation of the Mutual Interference of an Airscrew and Body of the Tractor Type of Airplane. Br. A.R.C. R. and M. 344, 1917.

[2] Analysis of Experiments on an Airscrew in Various Positions Within the Nose of a Tractor Body. Br. A.R.C. R. and M. 1120, 1927.

this theory the force on any blade element of the propeller is calculated by using the local velocity as reduced by the interference of the body, the magnitude of this interference being obtained by analysing the experimental results; and in a later paper[1] the local velocities were calculated theoretically by replacing the nose of the body by a suitable spheroid. A similar method of calculation has been used by Th. Troller[2], who represented the nose of the body by a simple distribution of sources and sinks, and calculated the performance of the blade elements in the velocity field of this system.

Consider a body whose nose is of a good stream-line shape so that the deflection of the air in the neighborhood of the propeller takes place without any loss of energy or total pressure head. Further back the body may have excrescences or irregularities of shape which cause loss of energy, and in any case there will be some such loss owing to the frictional drag of the surface. The drag which the body experiences owing to the pressure gradient behind the propeller would occur also with an ideal body and occurs without any loss of energy of the fluid. If then D_a denotes as before the total drag of the body in the presence of the propeller, and if X denotes that part of the drag which occurs without loss of energy, it follows that the total drag D_a must be inserted in the equation of axial momentum, but that only the part $(D_a - X)$ should be inserted in the equation of energy. The momentum equation for the system of propeller and body may therefore be expressed as

$$T_a - D_a = \int \varrho\, u\, (u_1 - V)\, dS \tag{5.2}$$

where dS is an element of the propeller disc, u is the axial velocity through the disc, and u_1 is the corresponding axial velocity in the ultimate wake. Also, since the increase of total pressure head in the wake is $(1/2)\, \varrho\, (u_1^2 - V^2)$, the energy equation is

$$T_a - (D_a - X) = \int 1/2\, \varrho\, (u_1^2 - V^2)\, dS \tag{5.3}$$

In order to apply the usual methods of analysis of the propeller characteristics, it is necessary to replace these integral equations by their differential equivalents, and in so doing it is necessary to assume that some appropriate fraction of the drag forces D_a and X may be associated with each annular element of the propeller disc. With this assumption the two equations become

$$dT_a - dD_a = \varrho\, u\, (u_1 - V)\, dS \tag{5.4}$$

and

$$dT_a - dD_a + dX = (1/2)\, \varrho\, (u_1^2 - V^2)\, dS \tag{5.5}$$

[1] The Application of the Theoretical Velocity Field around a Spheroid to Calculate the Performance of an Airscrew Near the Nose of a Streamline Body. Br. A.R.C. R. and M. 1239, 1928.

[2] Zur Berücksichtigung des Rumpfes beim Luftschraubenentwurf. Zeitschr. f. Flugtechnik u. Motorl. **19**, 325, 1928.

Now let
$$\left.\begin{aligned} dX &= h\,dT_a \\ dD_a &= k\,dT_a \end{aligned}\right\} \tag{5.6}$$

and
$$\left.\begin{aligned} V &= u\,(1-G) \\ u_1 &= u\,(1+H) \end{aligned}\right\} \tag{5.7}$$

Also, from the usual form of calculation for the force on the blade elements of a propeller, the thrust may be expressed in the form
$$dT_a = 2F\varrho u^2\,dS \tag{5.8}$$
where, in the usual notation,
$$F = \frac{\sigma\,(C_L \cos\varphi - C_D \sin\varphi)}{4\sin^2\varphi} \tag{5.9}$$

With these substitutions (5.4) and (5.5) become respectively
$$2F\,(1-k) = G + H$$
and
$$4F\,(1-k+h) = (G+H)\,(2-G+H)$$
and then on eliminating H,
$$G = F\,(1-k) - \frac{h}{1-k} \tag{5.10}$$

The coefficients h and k are zero for a free propeller and these equations give the result $F = G = H$

Thus the speed of advance V is determined as a function of the velocity u through the disc by the equation
$$V = u\,(1-F)$$

The interference of the body on the propeller is represented by replacing F by G in this last equation, and from the form of (5.10) it is evident that G is less than F. Thus V differs less from u when the body is present than for the free propeller.

As a first approximation when F, h and k are small, (5.10) may be expressed as $G = F - h$

or, to the same order of accuracy,
$$V\,(1-h) = u\,(1-F)$$

In this form the equation suggests that the annular element of the propeller is behaving exactly as if it were situated in a local stream of reduced velocity $V\,(1-h)$, and the analysis is therefore the same as the original simple treatment of the problem, except that the reduced velocity is now regarded as varying along the blade of the propeller instead of being represented by a general mean value.

If the body is of a good stream-line shape the drag of the body is due mainly to the pressure gradient, and the coefficients h and k are approximately equal. With this approximation (5.10) becomes
$$G = F\,(1-h) - \frac{h}{1-h} \tag{5.11}$$

The values of h were determined by Lock from this equation by analysing the observed distribution of thrust along the blade of a propeller, and the values so determined were reasonably consistent with the theoretical distribution of velocity around the nose of a spheroid representing as closely as possible the nose of the body. These values of h depend only on the shape of the body and can be used to calculate the performance of any propeller mounted in front of the body.

Hitherto the part of the body drag represented by the term X has been defined solely by the condition that this part of the drag occurs without any loss of energy. If, however, hV represents the reduction of velocity of the local stream in which the propeller operates, it would follow from the previous general discussion that $\int h dT_a$ will represent the increase of thrust and the equal increase of drag of an ideal body due to their mutual interference. This drag is represented mainly by an increase of pressure over the nose of the body and hence X may be estimated as the pressure force on the front part of the body, extending as far as the maximum cross-section. This conception was adopted by Lock and was confirmed by a further series of experiments[1].

More generally it is convenient to define the *effective* thrust of the propeller by the equation

$$T_e = T_a - X = \int (1 - h)\, dT_a \tag{5.12}$$

Previously the *propulsive* thrust was defined as

$$T_p = T_a - (D_a - D)$$

and for an ideal body of zero drag the effective and propulsive thrusts are identical. In the general discussion of **3** the apparent thrust T_a was expressed in the form

$$T_a = T + f_2 \frac{S T_a}{\pi R^2} \tag{5.13}$$

where the second term represents the increase of thrust due to the interference of the body and is balanced by an equal increase of drag. By comparison with (5.12) it would appear that the effective thrust should be sensibly the same as the free thrust of the propeller without any interference, and this conception also was confirmed by Lock's analysis when the comparison was made on the basis of a definite torque coefficient.

In the light of this analysis it is possible to lay down the guiding principles for estimating the performance of a propeller mounted at the front of a body whose nose is of a reasonably stream-line shape. As a basis for this calculation it is necessary to know the appropriate

[1] Lock, C. N. H., and Johansen, F. C., Pressure Plotting a Streamline Body with Tractor Airscrew Running. Br. A.R.C. R. and M. 1230, 1929.

airfoil characteristics of the blade sections of the propeller and the drag of the body without interference. The calculation then proceeds by the following steps:—

(1) Estimate the axial velocity $V(1-h)$ as a function of the radial distance in the plane to be occupied by the propeller. This velocity may be obtained from a test of the flow past the body, from a theoretical calculation replacing the nose of the body by a spheroid which fits it as closely as possible, from a theoretical calculation representing the nose of the body by a suitable distribution of sources and sinks, or from a comparison with any available information concerning the velocity distribution around bodies of similar shape.

(2) Calculate the thrust and torque for each annular element of the propeller in turn as if it were operating in a stream of velocity $V(1-h)$. Integration along the blades then gives the apparent thrust T_a and the apparent torque Q_a.

(3) Calculate the part of the body drag due to the pressure gradient behind the propeller as $\int h\,d\,T_a$

and the increase of body drag due to the velocity of the slipstream, in accordance with the discussion of 4, as

$$f_1 \frac{T_a}{\pi R^2 \varrho V^2}$$

where f_1 may be taken to be 2.43. The apparent drag of the body is then

$$D_a = D\left[1 + \frac{f_1 T_a}{\pi R^2 \varrho V^2}\right] + \int h\,d\,T_a \quad \text{[see (4.1)]} \tag{5.14}$$

Alternatively this apparent drag may be estimated from (4.3) as

$$D_a = D\left[1 + \frac{B T_a}{\pi R^2 \varrho V^2}\right] \quad \text{[see (3.5)]} \tag{5.15}$$

where $B = 2.43 + \frac{0.254}{C}$

and C is the drag coefficient of the body in terms of its maximum cross-section S, defined by the equation

$$D = C S \varrho V^2$$

(4) The propulsive thrust of the propeller is obtained finally in the form $T_p = T_a - (D_a - D)$

As an alternative course it is possible to calculate directly, in place of the apparent thrust T_a, the effective thrust T_e as defined by the equation $T_e = \int (1-h)\,d\,T_a$

This effective thrust, used in conjunction with the apparent torque Q_a, will lead to an efficiency sensibly equal to that of the propeller in free air. The drag of the body to be used in conjunction with the effective thrust is simply $D\left[1 + \frac{f_1 T_a}{\pi R^2 \varrho V^2}\right]$ [see (4.1)]

and in these formulae it is generally legitimate to replace the apparent thrust T_a by the effective thrust T_e. The final expression for the propulsive thrust is then

$$T_p = T_e\left[1 - \frac{f_1 D}{\pi R^2 \varrho V^2}\right] \quad \text{[see (2.2)]} \tag{5.16}$$

and this form of expression is identical with the formula (2.3) which was obtained for a propeller and a body in the ultimate wake. The only point of difference in the two results is that the corresponding torque of the propeller must be calculated to include the effects of the interference of the body.

Although in detailed calculations it is necessary to use values of the parameter h which vary along the blade of the propeller, for many purposes it is sufficiently accurate to use a suitable average effective value of h for the whole propeller. The estimation of the behavior of the propeller as modified by the interference of the body then follows quite simply from the characteristics of the undisturbed propeller by the method described in 1 and defined by (1.5) of that section. The apparent thrust and torque of the propeller in the presence of the body and at the advance-diameter ratio J are determined as the free thrust and torque of the propeller at the lower advance-diameter ratio $(1 - h)\,J$ and at the same rate of rotation. In applying this simplified method, however, it must be remembered that the average value of h associated with any definite body will decrease as the diameter of the propeller increases, and that this average value will also depend on the position of the propeller relative to the nose of the body. Experience suggests that, for the usual combination of propeller and body, the average effective value of h is approximately 0.1.

Finally one point may be noticed in connection with the design of a propeller to operate in front of a body. The reduction of velocity due to the presence of the body is greatest close to the surface and is usually negligible at the tips of the propeller blades. Thus the inner part of the propeller is virtually operating at a lower rate of advance than the outer parts: it should therefore have relatively smaller blade angles and wider blades, and, compared with a good propeller designed to operate in free air, a propeller in front of a body should have a less rapid variation of blade angle along the blade and wider chords toward the root of the blade.

6. Propeller Behind a Body. The analysis hitherto has been developed on the assumption that the propeller operates in front of the body, but a similar line of argument can be followed when the propeller is mounted behind a body or engine car. The propeller operates in a region where the velocity has been reduced by the interference and by the drag of the body, and hence, at a definite rate of advance of the propeller, the apparent thrust and torque are increased above the values which

would occur in a free stream. Fig. 73 shows some typical curves obtained from wind tunnel tests[1] of a propeller behind a body, and a comparison with the previous Fig. 67 shows that the interference experienced by the propeller is of exactly the same nature, whether the propeller is in front of or behind the body. The drag of the body is increased by the pressure gradient which is caused by the propeller, but the body, being in front of the propeller, does not experience the full force of the increased velocity of the slipstream.

To analyze the interference between a body and a propeller mounted behind it, consider first an ideal body which causes a deviation of the flow in its neighborhood but, having no drag, causes no permanent disturbance in its wake. If the propeller is far behind the body, it will cause no disturbance of the flow around the body and will itself experience no interference from the body. When the propeller is placed close behind the body, it operates in a region where the local velocity has been modified by the presence of the body, and in general this disturbance is represented by a reduced axial velocity. Simultaneously the body is situated in a region where there is a pressure gradient, owing to the reduced pressure in front of the propeller, and this pressure gradient acts as a suction on the rear of the body. The mutual interference between the body and propeller thus causes a drag force on the body and an increased apparent thrust of the propeller, and the increase of the thrust of the propeller is exactly equal to the drag of the body.

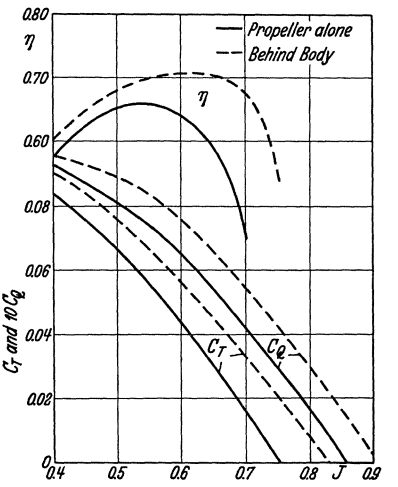

Fig. 73.

Passing next to the conditions which occur with a real body, the drag of the body causes a wake of reduced velocity and in this wake the air has lost some of its energy owing to the frictional forces on the surface of the body. The apparent thrust and torque of the propeller are therefore slightly higher than they would be with an ideal body of the same shape, and there is no corresponding reaction on the body, similar to the increased velocity over the surface which occurs when the body is behind the propeller. This argument suggests that there is a definite advantage when the body is in front of the propeller, but this conclusion must be accepted with caution. It has been derived by

[1] FAGE, A., and COLLINS, H. E., An Investigation of the Mutual Interference of Airscrews and Bodies of the Pusher Type. Br. A.R.C. R. and M. 305, 1917.

considering the behavior of a definite propeller in free air and behind the body, but the same propeller is not really suitable for these two conditions of operation. When the propeller operates behind the body, its torque coefficient at a definite rate of advance is increased, and hence the propeller, driven by a given engine, will run at a slower rate of rotation and will fail to develop the full engine power. In order to obtain the correct rate of rotation it is necessary to reduce the pitch of the propeller blades and to increase the width of the blades. These wider blades will experience a correspondingly higher frictional drag, and in this way some part of the advantage of mounting the propeller behind the body is lost. Also in practice a body in front of a propeller is almost invariably of a worse aerodynamic shape than a body behind a propeller and has a higher drag.

The apparent drag of the body in the presence of the propeller can again be represented in the form

$$D_a = D\left[A + B\frac{T_a}{\pi R^2 \varrho V^2}\right] \tag{6.1}$$

and for a body in front of a propeller the coefficient A should be unity since there is no shielding of the nose or spoiling of the flow such as may occur when the body is behind the propeller. Also, following the same line of argument which was used for a body behind a propeller, the form anticipated for the coefficient B is

$$B = f_1 + \frac{f_2}{C} \tag{6.2}$$

where

$$C = \frac{D}{S \varrho V^2}$$

and S is the area of the maximum cross-section of the body. In this expression f_1 represents the effect of the increased velocity experienced by the body. At the propeller disc the increase of axial velocity is half that in the ultimate wake, but this increase occurs in a very short distance in front of the propeller and the effective increase of velocity experienced by the body is very small. Consequently f_1 may be expected to be very small also. The coefficient f_2 represents the reduced pressure in front of the propeller, which acts as a suction on the rear of the body. This effect acts with full force and the value of f_2 may be anticipated to be sensibly the same as for a body behind a propeller. Thus, by comparison with the empirical formula (4.3) the value of the coefficient B for a body in front of a propeller would be predicted to be approximately

$$B = \frac{0.254}{C} \tag{6.3}$$

Experimental results for bodies mounted in front of a propeller are very scanty, and in general the bodies tested have also been of very bad aerodynamic shape. The results available, however, are in general

agreement with the ideas developed above. Thus, for example, tests of two pusher bodies[1] led to the values

$$A = 0.97, \quad B = 0.8, \quad C = 0.20$$

and

$$A = 1.07, \quad B = 1.9, \quad C = 0.12$$

which do not differ too widely from the values suggested by the previous general discussion; but a reliable general formula, similar to that derived for tractor bodies, cannot be obtained until further experimental results are available.

A detailed analysis of the experimental results by C. N. H. Lock and H. Bateman[2] suggests that some part of the increased drag can be explained by the suction at the rear of the body caused by the rotation of the slipstream. When the propeller is at the front of the body this rotation is reduced by any excrescences on the surface of the body, and the suctional drag is greatest if the body is smooth or if the propeller is mounted toward the rear of the body. The adverse effect can be reduced by fitting radial vanes behind the propeller to check the rotation of the slipstream.

7. Propeller-Wing Interference. The interference experienced by the propeller of an airplane is due mainly to the body on which it is mounted, but some additional interference arises also from the proximity of the wings, undercarriage or any other structural parts. The interference between the body and propeller has been considered in the previous sections and it has been tacitly assumed that the axis of the propeller was in the direction of motion and that the body was symmetrical about this axis. If this symmetry does not exist, the propeller may experience periodic aerodynamic forces, since the interference will vary with the angular position of the blades. The interference exerted by the wings of an airplane on the propeller is usually of this asymmetrical character, but the periodic fluctuations of the thrust and torque are negligible, and it suffices to consider the mean interference effects.

Regarding the wing first as an additional source of drag behind the propeller, it may be anticipated that the interference caused by the wing will be similar in character to that caused by the body but less in magnitude. The interference would then be represented by a slight reduction of the axial velocity experienced by the propeller, but there may be a small additional effect due to the fact that a wing behind the propeller will tend to check the rotation of the slipstream and this may react back on the propeller to some small extent. Some typical experimental curves[3] of the wing interference on the thrust and torque

[1] Br. A.R.C. R. and M. 305, 1917.

[2] Br. A.R.C. R. and M. No. 1445, 1931.

[3] FAGE, A., and COLLINS, H. E., An Investigation of the Mutual Interference of the Airscrew, Body, and Wings of the Tractor Aeroplane BE2E. Br. A.R.C. R. and M. 393, London, 1918.

coefficients of a propeller are shown in Figs. 74 and 75. There is a small increase of the thrust coefficient due to the presence of the wings, but no appreciable change of the torque coefficient. This conclusion is confirmed by other experiments[1], but at times there is also a small increase of the torque coefficient. These results were all obtained with the propeller axis in the direction of motion and at one angle of incidence of the wings, and it may be anticipated that the interference would increase if the wing were set at a larger angle of incidence.

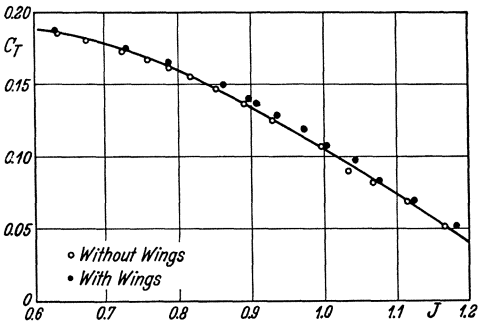

Fig. 74.

In practice the propeller axis is set at a definite angle to the chord of the wings and this axis can coincide with the direction of motion at one angle of incidence only. As the angle of incidence of the airplane is increased, the axis of the propeller will be inclined at an angle to the direction of motion, and the change of the characteristics of the propeller will be due partly to the increased interference of the wings and partly to the inclination of the propeller axis. Figure 76 shows the change of the torque coefficient of a propeller in front of a model airplane[2] as the angle of incidence is increased. The torque coefficient increases rapidly with the angle of incidence, but this increase is due more to the inclination of the propeller axis than to the interference of the wings. The change of the characteristics of a propeller due to the inclination of the axis, apart from any interference effects, is considered later in Chapter XII.

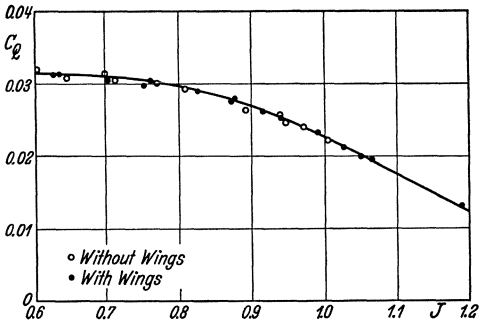

Fig. 75.

[1] FAGE, A., and COLLINS, H. E., An Investigation of the Mutual Interference of Two Model Airscrews and a Model of the Sopwith Dolphin Aeroplane. Br. A.R.C. R. and M. No. 572, 1919.

WEICK, F. E., Full Scale Tests of Wood Propellers on a VE-7 Airplane in the Propeller Research Tunnel. U.S. N.A.C.A. Technical Report No. 301, 1928.

[2] RELF, E. F., and JONES, L. J., Measurements of Lift, Drag, and Pitching Moment on the 1/5 Scale Model of the Bristol Fighter with Airscrew Running. Br. A.R.C. R. and M. No. 937, 1924.

Hitherto the wing has been regarded merely as an additional source of drag behind the propeller, but the interaction between the wing and the propeller is modified in an important manner by the lift of the wing. The effect on the propeller is due to the fact that the lift of the wing is associated with a circulation of the flow around the wing and with an upward inclination of the stream-lines in front of the wing. The propeller is therefore placed in a region where the flow is inclined to the direction of motion, and the effective inclination of the propeller axis is greater than the geometrical angle between the axis and the direction of motion. In this way the lift of the wing causes an additional increase of the thrust and torque coefficients of the propeller, and the experimental results shown in Fig. 76 must be regarded as the combined effect of the inclination of the propeller axis to the direction of motion, of the upwash due to the lift of the wings, and of the retardation of velocity due to the drag of the body and wings.

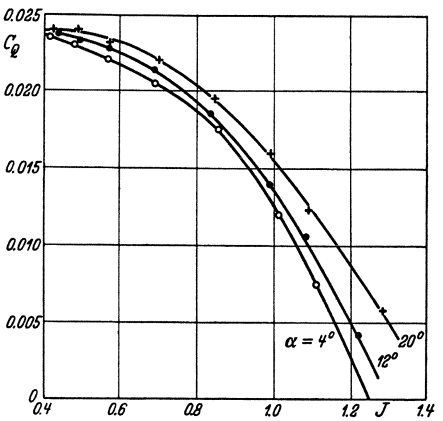

Fig. 76.

The interference of the propeller on the wings is of a very complex nature, since the increased velocity of the slipstream augments both the lift and the drag of the wing. Also the increased lift is associated with increased induced drag, and, since the slipstream acts over a small part only of the wing, the distribution of lift across the span is altered, and this alteration usually implies an additional increase of the induced drag. It is not proposed to discuss here the details of the interference experienced by the wing[1], but it is necessary to examine whether it is possible to extend the conception of propulsive thrust, which was used in analyzing the propeller-body interference, and to debit the thrust of the propeller with the increased drag of the wing.

If the extreme condition be considered of a large propeller with a small wing situated wholly in the slipstream far behind the propeller, the lift and drag of the wing will both be increased in the same ratio. By analogy with the method used in analyzing the propeller-body interference, the thrust of the propeller might be reduced by the increase of the drag, but this course is clearly unreasonable since it ignores the beneficial increase of the lift, and the increase of the drag is due mainly

[1] See Division M.

to the increase of induced drag which is inevitably associated with this increase of lift. An alternative method would be to compare the free wing and the wing in the slipstream on the basis of the same lift, reducing the angle of incidence of the wing in the slipstream to achieve this result. At small angles of incidence this comparison might be useful, but this method also breaks down because it ignores the fact that the wing in the slipstream has a higher maximum lift coefficient.

The conditions for an actual wing, which extends far beyond the boundaries of the slipstream, are even more complex, and it appears to be hopeless to attempt any separation of the propeller-wing system into its component parts. The whole question has been discussed in detail by A. Betz[1], and his conclusion is that the action of the propeller in the presence of a wing must be represented in a vector diagram. On this basis the apparent thrust T_a is reduced by the increase of drag $(D_a - D)$ to obtain the propulsive thrust

$$T_p = T_a - (D_a - D) \tag{7.1}$$

but in addition the propeller must be credited with a lift force Y at right angles to the thrust and equal to the increase of lift $(L_a - L)$ of the wing:

$$Y = L_a - L \tag{7.2}$$

These two forces may next be converted into "efficiencies" in terms of the apparent torque as

$$\eta_x = \frac{V\,T_p}{\Omega\,Q_a} \tag{7.3}$$

and

$$\eta_y = \frac{V\,Y}{\Omega\,Q_a} \tag{7.4}$$

and these two components may be plotted as coordinates of a vector diagram. The component η_x is comparable with the usual efficiency of a propeller, but the other component η_y is not an efficiency in any true sense and may have a value many times larger than η_x. The vector efficiency (η_x, η_y) is merely a convenient method of representing in one diagram the force on the propeller and the increased force on the wing due to the interference of the propeller. In general this vector efficiency is a function of two parameters, the angle of incidence of the wing and the advance-diameter ratio of the propeller, and its complete representation requires a double set of curves. A diagramatic sketch of the type of curves obtained is shown in Fig. 77, where $(\alpha_1\,\alpha_2\,\alpha_3)$ and $(\lambda_1\,\lambda_2\,\lambda_3)$ represent increasing values of the angle of incidence and of the speed ratio $(V/\Omega\,R)$ re-

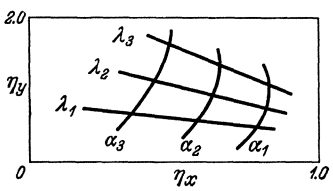

Fig. 77.

[1] Der Wirkungsgradbegriff beim Propeller. Zeitschr. f. Flugtechnik u. Motorl. **19**, 171, 1928.

spectively. No generalization of these results is possible, since they depend intimately on the relative size of the propeller and wing, on the shape of the wing and its center section, and on the inclination of the propeller axis to the wing chord. The object of the preceding discussion has been merely to explain the nature of the mutual interference between propeller and wing, and to suggest a suitable method of representing the experimental results for any particular combination of the two.

CHAPTER IX

THE EXPERIMENTAL STUDY OF PROPELLERS

1. Experimental Methods. During the course of the development of the theory of the propeller, reference has been made from time to time to experimental results, either to illustrate the significance of some aspect of the theory or to obtain empirical relationships to supplement the theoretical formulae. These experimental results are derived for the most part from wind tunnel tests of model propellers and it is necessary to consider the scope of these tests and the validity of applying them to deduce the characteristics of full scale propellers.

The simplest test of a propeller is the determination of the thrust and torque at different rates of advance, since it depends only on the measurement of the force and moment transmitted through the propeller shaft. Other methods of experiment seek to determine the distribution of thrust and torque along the blade of a propeller, either by investigating the distribution of pressure over a number of sections suitably spaced along the blade, or by investigating the pressure and velocity of the air behind the disc of the propeller. The experimental study of the pressure distribution over the blades of a rotating propeller is more complex than the corresponding experiment with a rigid wing, but it has been successfully made both on a model propeller in a wind tunnel[1] and on a full scale propeller in flight[2]. Apart from the complex and laborious nature of the work, this method of experiment suffers from the defect that it determines only the forces due to the pressure over the surface of the blades and gives no measure of the frictional forces experienced by the propeller. An alternative method of determining the distribution of thrust along the blade, proposed originally by

[1] FAGE, A., and HOWARD, R. G., A Consideration of Airscrew Theory in the Light of Data Derived from an Experimental Investigation of the Distribution of Pressure Over the Entire Surface of an Airscrew Blade, and also Over Aerofoils of Appropriate Shape. Br. A.R.C. R. and M. 681, 1921.

[2] JONES, E. T., The Distribution of Pressure Over a Section of an Airscrew Blade in Flight and the Variation of Lift Coefficient with the Speed of the Section. Br. A.R.C. R. and M. 1256, 1929.

T. E. Stanton[1], is to measure the increase of total pressure head behind the propeller, and by an extension of this method of investigation it is possible also to determine the distribution of torque along the blade. These experimental methods, which can be used either in a wind tunnel or in flight, are considered more fully in **3**.

The interpretation of the tests of model propellers raises at once the question of dynamical similarity[2]. In a frictionless incompressible fluid the thrust and torque coefficients of a propeller of given shape would depend only on the state of operation of the propeller, and would be functions of a single parameter which is usually taken to be the speed ratio $V/\Omega R$ or the advance-diameter ratio V/nD. This parameter corresponds in fact to the angle of incidence of a wing and defines the attitude of the propeller blades relative to the air through which the propeller is advancing. When, however, the actual physical properties of the air are considered, it is apparent that the characteristics of a given propeller may depend also on the viscosity and compressibility of the air.

The viscosity of the air is expressed conveniently by the kinematic coefficient of viscosity ν, which is the ratio of the coefficient of viscosity μ to the density ϱ and has the dimensions of a length multiplied by a velocity. In order to maintain dynamical similarity of the flow it is necessary to maintain a constant value of the Reynolds' number or viscosity parameter, which may be expressed in the form

$$N_v = \frac{l\,W}{\nu}$$

where l is some typical length and W is some typical velocity of the propeller. Choosing this length to be the radius of the propeller and the velocity to be the tip speed ΩR, the Reynolds' number becomes

$$N_v = \frac{\Omega R^2}{\nu} \tag{1.1}$$

Clearly it is impossible to satisfy this condition of constant Reynolds' number in any model tests, since the radius R is always less than the corresponding full scale radius and the tip speed ΩR is usually less than the full scale tip speed. Thus the use of model propellers may involve the existence of a scale effect in the characteristics of the propeller, and this scale effect can be determined only by a suitable series of comparative experiments.

The compressibility of the air can be expressed by the speed of sound V_s, which is the speed of propagation of pressure disturbances

[1] Stanton, T. E., and Marshall, D., On a Method of Estimating, from Observations on the Slipstream of an Airscrew, the Performance of the Elements of the Blades and the Total Thrust of the Screw. Br. A.R.C. R. and M. 460, 1918.

[2] Divisions A IV and H I 3.

through the air, and the effect of this compressibility on the characteristics of a propeller can be expressed in terms of another non-dimensional parameter

$$N_c = \frac{W}{V_s}$$

where W is again some typical speed of the propeller. This speed is suitably taken to be the tip speed ΩR, and hence the compressibility parameter will be taken to be

$$N_c = \frac{\Omega R}{V_s} \tag{1.2}$$

The effect of the compressibility of the air on the characteristics of an airfoil are known to be negligibly small unless the speed rises above one half of the speed of sound, but the tip speed of a propeller almost invariably exceeds this value and frequently rises as high as the speed of sound itself. It is necessary therefore to investigate the effect of the compressibility of the air on the characteristics of a propeller rotating with a high tip speed, and this effect introduces also another distinction between the behavior of model and full scale propellers, since the model propeller usually has a lower tip speed.

In spite of the uncertainty due to the unknown magnitude of the scale effect and of the compressibility effect, wind tunnel tests have provided the principal experimental method of studying the characteristics of a propeller, since these tests are comparatively easy to make and since they give more consistent results than any alternative method. The construction of the twenty foot propeller research tunnel[1] of the National Advisory Committee for Aeronautics at Langley Field has greatly extended the value of these wind tunnel tests and has gone a long way to eliminate the uncertainty associated with model experiments. Even with this tunnel, however, it is not possible to realize the actual flight conditions of the propeller of a high speed airplane, since the maximum speed in the tunnel is 110 m.p.h. and falls short of the speed of the airplane. The wind tunnel tests are usually straight forward in principle, but in interpreting the results it is necessary to consider whether the limited extent of the stream exerts any constraint on the behavior of the propeller. Moreover the conditions of test of a propeller, apart from the aircraft, frequently involve a small guard body to house the driving mechanism and, unless this body is very small, it may introduce a systematic difference between the experimental results and the performance calculated for the propeller alone.

As an alternative to the wind tunnel, a whirling arm may be used to test either a model or a full scale propeller, but although valuable results have been obtained in the past by this method, it appears to

[1] Weick, F. E., and Wood, D. H., The Twenty Foot Propeller Research Tunnel of the National Advisory Committee for Aeronautics. U.S. N.A.C.A. Technical Report No. 300, 1928.

have fallen out of use completely. A whirling arm operating in a building suffers from the defect that the air develops a circulation which complicates the interpretation of the experimental results, and a whirling arm in the open air is subjected to irregular air currents even on a fairly calm day. The same criticism applies also to a spinning tower which would otherwise provide a satisfactory method of determining the characteristics of a propeller at zero rate of advance.

Finally there remains the possibility of testing the propeller in flight on an aircraft, but such tests are difficult to make and rarely yield results comparable in accuracy with the wind tunnel tests. Measurements of the performance of an airplane are of no value since the characteristics of the propeller are inextricably entangled with the drag of the airplane and the power of the engine. It is necessary therefore to measure directly the thrust and torque transmitted by the propeller shaft, and although instruments have been designed from time to time for this purpose, they have rarely yielded results of sufficient accuracy. Moreover these instruments have been used to determine the power of the engine under different atmospheric conditions and the drag of the airplane rather than to determine the characteristics of the propeller. The investigation of the distribution of pressure over the blades of a propeller in flight is extremely difficult and laborious, but the alternative method of determining the distribution of thrust and torque along the blade by measuring the pressure and velocity behind the propeller disc can be applied in flight and should be capable of giving valuable results.

2. Wind Tunnel Interference. The problem of the constraint imposed on a propeller by the limited extent of the air stream of a wind tunnel is approached most conveniently by considering first the behavior of a propeller in a wind tunnel with a closed working section, and the magnitude of this constraint has been determined[1] by an interesting application of the axial momentum theory. The flow past the propeller is constrained by the walls of the tunnel and the uniform axial velocity V which occurs in front of the propeller in the wind tunnel differs from that which would occur in free air when the propeller is giving the same thrust and torque at the same rate of rotation. The interference may be represented in terms of an equivalent free air speed V', corresponding to the tunnel speed V. Ignoring the rotational motion of the slipstream, the thrust and torque of the propeller are determined by the axial velocity u through the propeller disc, and the equivalent free air speed V' is determined by the condition that this axial velocity u shall have the same value in the tunnel and in free air. In general the equivalent free air speed V' is less than the tunnel speed V.

[1] WOOD, R. MCK., and HARRIS, R. G., Some Notes on the Theory of an Airscrew Working in a Wind Channel. Br. A.R.C. R. and M. 662, 1920.

Consider a propeller of disc area S, Fig. 78, operating in a cylindrical tunnel whose cross-section is a circle of area C; let u be the axial velocity through the propeller disc and u_1 the axial velocity in the slipstream where the cross-section has contracted to S_1; and let u_2 be the axial velocity in the tunnel outside the slipstream. Then the conditions of continuity of the flow in the slipstream and in the region surrounding it are respectively

$$\left.\begin{aligned} u_1 S_1 &= uS \\ u_2 (C - S_1) &= VC - uS \end{aligned}\right\} \tag{2.1}$$

The total pressure head remains constant outside the slipstream, and the increase of total pressure head in the slipstream is obtained from the wake as

$$H_1 - H_0 = \tfrac{1}{2} \varrho (u_1^2 - u_2^2)$$

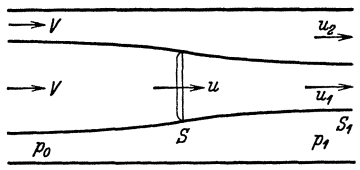

Fig. 78.

This increase of total pressure head is equal to the increase of pressure through the propeller disc, and hence the thrust of the propeller is

$$T = \tfrac{1}{2} S \varrho (u_1^2 - u_2^2) \tag{2.2}$$

Finally the momentum equation for the whole flow, both inside and outside the slipstream, is

$$T - (p_1 - p_0) C = S_1 \varrho u_1 (u_1 - V) - (C - S_1) \varrho u_2 (V - u_2) \tag{2.3}$$

and the increase of pressure in the wake is

$$p_1 - p_0 = \tfrac{1}{2} \varrho (V^2 - u_2^2) \tag{2.4}$$

Now let

$$\tau = \frac{T}{S \varrho V^2} \tag{2.5}$$

and on eliminating the velocities u_2 and u_1 by means of (2.1), expression (2.2) for the thrust becomes

$$\begin{aligned} 2\tau V^2 S_1^2 (C - S_1)^2 &= u^2 S^2 (C - S_1)^2 - (VC - uS)^2 S_1^2 \\ &= 2uS (uS - VS_1) C (C - S_1) - (uS - VS_1)^2 C^2 \end{aligned}$$

and similarly expression (2.3) for the thrust becomes

$$\begin{aligned} 2\tau V^2 S S_1 (C - S_1)^2 &= 2uS (uS - VS_1) (C - S_1)^2 \\ &\quad - 2 (VC - uS) (uS - VS_1) S_1 (C - S_1) \\ &\quad + [V^2 (C - S_1)^2 - (VC - uS)^2] C S_1 \\ &= 2uS (uS - VS_1) C (C - S_1) - (uS - VS_1)^2 C S_1 \end{aligned}$$

Eliminating in turn the two terms on the right hand sides by suitable combinations of these two equations for the thrust coefficient τ, the following pair of equivalent equations is obtained

$$\left.\begin{aligned} 2\tau V^2 S_1 (S - S_1) (C - S_1) &= (uS - VS_1)^2 C \\ \tau V^2 S_1 (CS - S_1^2) &= uS (uS - VS_1) C \end{aligned}\right\} \tag{2.6}$$

The equivalent free air speed V' has been defined as the speed which corresponds to the same values of the thrust T and of the axial velocity u.

But in free air $$T = 2 S \varrho u (u - V')$$

or $$(2u - V')^2 = \frac{2T}{\varrho S} + V'^2$$
$$= 2\tau V^2 + V'^2$$

and putting
$$\left.\begin{aligned} V &= n V' \\ x^2 &= 1 + 2\tau n^2 \end{aligned}\right\} \quad (2.7)$$

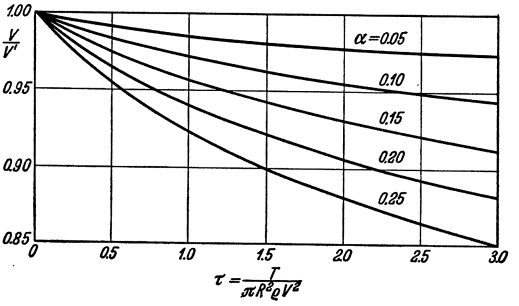

Fig. 79.

the free air condition becomes

$$u = \frac{(x+1)V}{2n} \quad (2.8)$$

Substituting these expressions for τ and u/V in terms of x and n in (2.6), and writing also for simplicity
$$\left.\begin{aligned} S &= \alpha C \\ S_1 &= \sigma S \end{aligned}\right\} \quad (2.9)$$

the wind tunnel relationships become respectively

$$4(x^2 - 1)\sigma(1 - \sigma)(1 - \alpha\sigma) = (x + 1 - 2n\sigma)^2 \quad (2.10)$$

and
$$2(x - 1)\sigma(1 - \alpha\sigma^2) = (x + 1 - 2n\sigma) \quad (2.11)$$

Squaring the second of these equations and dividing by the first, an equation is obtained to determine x as a function of α and σ,

$$\frac{x-1}{x+1} = \frac{(1-\sigma)(1-\alpha\sigma)}{\sigma(1-\alpha\sigma^2)^2} \quad (2.12)$$

Then from the second wind tunnel equation (2.11)

$$n = 1 + (x-1)\alpha\sigma^2 - \frac{(2\sigma - 1)x - 1}{2\sigma} \quad (2.13)$$

and finally from (2.7)
$$\tau = \frac{x^2 - 1}{2n^2} \quad (2.14)$$

By means of these last three equations the fraction n, which is the ratio of the wind tunnel speed V to the equivalent free air speed V', can be determined as a function of α, the ratio of the disc area S to the tunnel area C, and of τ, the thrust coefficient of the propeller referred to the wind tunnel speed V. The method of calculation is to assume a series of suitable values of σ and to calculate in turn x, n, and τ. Numerical values obtained from these equations are given in Table 26 and are shown graphically in Fig. 79 for a suitable range of the parameters α and τ. The usual size of propeller tested in a wind tunnel with closed working section corresponds to a value of α of 0.15 approximately.

Since α is usually small, an approximate formula for the equivalent free air speed can be derived from the general equations by retaining only the first power of α. On this basis (2.12) gives

$$\frac{x-1}{x+1} = \frac{1-\sigma}{\sigma}[1 + \alpha\sigma(2\sigma - 1)]$$

or
$$x(2\sigma - 1) = 1 + 2\alpha\sigma^2(1-\sigma)$$

TABLE 26. Values of V'/V.

$\tau =$	0.5	1.0	1.5	2.0	2.5	3.0
$\alpha = 0.05$	0.992	0.985	0.980	0.978	0.975	0.973
0.10	0.983	0.971	0.962	0.954	0.949	0.943
0.15	0.973	0.956	0.942	0.930	0.921	0.912
0.20	0.963	0.940	0.922	0.906	0.893	0.882
0.25	0.956	0.924	0.899	0.880	0.865	0.851

Then from (2.13) $$n - 1 = \alpha\sigma^2\left[\frac{2(1-\sigma)}{2\sigma - 1}\right] - \alpha\sigma(1-\sigma)$$
$$= \frac{\alpha\sigma(1-\sigma)}{2\sigma - 1}$$
$$= \alpha\frac{x^2 - 1}{4x}$$

and to the order of accuracy required in this equation

$$x^2 = 1 + 2\tau$$

Hence
$$n - 1 = \frac{\alpha}{2}\frac{\tau}{\sqrt{1+2\tau}}$$

or finally
$$\frac{V'}{V} = 1 - \frac{\alpha}{2}\frac{\tau}{\sqrt{1+2\tau}} \qquad (2.15)$$

If $\tau = 3.0$ and $\alpha = 0.25$, this approximate formula gives the value $V' = 0.858\ V$, which differs by less than 1 per cent from the true value, and thus the approximate formula is sufficiently accurate for most practical applications.

This method of correcting the characteristics of a propeller determined in a wind tunnel has proved quite satisfactory in practice, but unfortunately it cannot be applied when the propeller is operating in front of a body. Reverting, however, to the problem of operating in a wind tunnel, the mean axial velocity u' in the plane of the propeller but outside its circumference is given by the equation

$$u'(C - S) = VC - uS$$

or approximately
$$\frac{u'}{V} = \frac{1 - \alpha\frac{u}{V}}{1-\alpha} = 1 - \alpha\left(\frac{u}{V} - 1\right)$$

Assuming α to be small, the value of u/V in this equation may be estimated from free air conditions which give

$$\tau = 2\frac{u}{V}\left(\frac{u}{V} - 1\right)$$

or $$\frac{u}{V} = \frac{1}{2}\left(1 + \sqrt{1 + 2\tau}\right)$$

and hence the equation for the velocity u' becomes

$$\frac{u'}{V} = 1 - \frac{\alpha}{2}\left(\sqrt{1 + 2\tau} - 1\right) \tag{2.16}$$

and on expanding the expressions (2.15) and (2.16) in ascending powers of τ, which is generally a small quantity, it appears that u' and V' are equal to the first power of τ and differ only in the higher powers. This analysis suggests that a good approximation to the equivalent free air speed can be obtained by measuring the axial velocity in the plane of the propeller near the wall of the tunnel. The application of this method has proved to be satisfactory for a propeller alone and also for the combination of a propeller and body, and the accuracy of the method has been confirmed by a special series of experiments[1] in a four foot and in a seven foot tunnel.

Passing next to the problem of a propeller in a wind tunnel of the open jet type, the condition to be satisfied is simply that the pressure is constant over the boundary of the jet. The application of the axial momentum theory would suggest that there is no tunnel constraint on the characteristics of a propeller tested in an open jet, while a closer analysis of the problem[2] reveals a correction which is of the order α^2 and is small compared with the corresponding correction in a tunnel with a closed working section. This conclusion is fully substantiated by experimental evidence[3]. Tests of a propeller in jets of decreasing diameter showed no tunnel constraint until the ratio of propeller diameter to jet diameter rose to 0.67, and another series of tests with propellers of increasing diameter showed no appreciable constraint even when the ratio rose to 0.73. Thus in an open jet it is possible to test, without any correction, a propeller whose diameter is 0.6, or perhaps even 0.7, of the diameter of the jet, while an appreciable correction must be applied if the diameter of a propeller tested in a closed wind tunnel is 0.4 of the diameter of the tunnel.

No crucial experimental test of the theoretical formula for the constraint in a closed wind tunnel has been made. Comparative tests[4] of one propeller in a closed tunnel and in an open jet showed excellent

[1] LOCK, C. N. H., and BATEMAN, H., The Effect of Wind Tunnel Interference on a Combination of Airscrew and Tractor Body. Br. A.R.C. R. and M. 919, 1924.

[2] GLAUERT, H., and LOCK, C. N. H., On the Advantage of an Open Jet Type of Wind Tunnel for Airscrew Tests. Br. A.R.C. R. and M. 1033, 1926.

[3] DURAND, W. F., Experimental Research on Air Propellers. U.S. N.A.C.A. Technical Report No. 14, 1917.

[4] TOWNEND, H. C. H., and WARSAP, J. H., Tests of a Metal Airscrew in a Closed Tunnel for Comparison with American Tests in an Open Jet Tunnel. Br. A.R.C. R. and M. 1137, 1927.

agreement, and similar tests[1] of a propeller in a closed tunnel and on a whirling arm also confirm the accuracy of the wind tunnel tests, but in neither case was the tunnel correction sufficiently large for the experiments to provide a check on the accuracy of estimating the magnitude of the constraint. The method of correction has, however, proved to be entirely satisfactory for the size of propeller which it is customary to test in a closed wind tunnel.

3. Thrust and Torque Distribution. The most direct method of measuring the distribution of the aerodynamic force along the blade of a propeller is the determination of the pressure distribution around a number of sections suitably spaced along the blade. This investigation is very laborious, and the experimental technique is complicated owing to the necessity of transmitting the pressure from each observation point through the rotating boss of the propeller to a suitable manometer. Moreover the pressure distribution determines only one part of the aerodynamic force and gives no measure of the tangential frictional force on the blade section. Owing to this defect the pressure distribution cannot be used to determine the torque of the propeller, but it does give a good estimate of the thrust of the propeller and its distribution along the blade. The chief value of the experiment, however, is the confirmation which it provides of the assumption, implicit in the development of the general propeller theory, that the blade sections may be regarded aerodynamically as equivalent to airfoil sections in uniform linear motion. Owing to the complexity of the experiment it has been adopted only for a few special investigations, and the distribution of the aerodynamic force along the blade of a propeller is determined more generally by other experimental methods.

The thrust of a propeller is obtained by imparting an increased pressure to the air as it passes through the propeller disc, and hence the thrust of the propeller can be determined by measuring this increase of pressure. Experimentally it is more convenient to measure the total pressure head rather than the static pressure, and this is the method usually adopted. If p' is the increase of pressure at any radius r and if ω is the angular velocity imparted to the air immediately behind the propeller disc, then the increase of total pressure head[2] is

$$H_1 - H_0 = p' + \frac{1}{2}\varrho\,\omega^2 r^2 \tag{3.1}$$

and the corresponding element of thrust is

$$\frac{dT}{dr} = 2\pi r p' \tag{3.2}$$

---

[1] Reproduced in Br. A.R.C. R. and M. 1033, 1926.

[2] See III **1.**

Thus the increase of total pressure head is slightly greater than the increase of static pressure, but the difference is negligibly small in practice.

The experimental application of this method of investigation is simplified by the fact that the original total pressure head H_0 can be measured at any convenient point in front of the propeller, but the measurement of the total pressure head H_1 requires more care. If the observation is made at some distance behind the propeller, it is necessary to obtain an estimate of the contraction of the slipstream in order to relate the observed pressure to the corresponding section of the propeller blade. If, on the other hand, the observation is made immediately behind the propeller disc, the pitot tube may fail to record a correct mean value owing to the sudden fluctuation of the velocity and direction of the flow as the propeller blades pass in front of the pitot tube. The method of experiment relies on the fact that the reading of a pitot tube is not affected by a moderate angle of yaw, but immediately behind the propeller disc the fluctuations of angle may be excessive. In spite of these difficulties the method appears to give satisfactory results, and the integrated values of the thrust along the blade agree well with the direct measurements of the thrust.

An analogous method of investigation can be used to determine the distribution of torque along the blade of a propeller. If u is the axial component and if w or ωr is the rotational component of the velocity immediately behind the propeller disc, the element of torque is

$$\frac{dQ}{dr} = 2\pi r^2 \varrho u w \tag{3.3}$$

The determination of the torque therefore depends on the measurement of the mean value of the product uw, and if W is the resultant velocity and ψ is the angle of yaw, this product is

$$u w = \frac{1}{2} W^2 \sin 2\psi \tag{3.4}$$

The value of this product can be determined experimentally by means of a yawmeter, and two methods are available:—

(1) To measure the difference of pressure between the two arms of the yawmeter.

(2) To rotate the yawmeter until the pressure difference is zero, and to determine the velocity W by means of a pitot tube. In a steady stream both methods would be satisfactory, but owing to the fluctuations of velocity and angle which occur behind a propeller, the first method is satisfactory only if the pressure recorded by the yawmeter is proportional to $W^2 \sin 2\psi$, and the second method only if a pitot tube records a pressure proportional to $W^2 \cos 2\psi$. Actually the calibration of a pitot tube does not satisfy this latter condition and so the second method is unsatisfactory. The first method has, however, been used

successfully[1] by designing a suitable yawmeter with tubes inclined at $\pm 45^0$ to the axis of the instrument. Thus it is possible to obtain a direct measurement of the distribution of torque along the blade of a propeller. The method, however, suffers from the same difficulties as the determination of the thrust distribution, and due allowance must be made for the contraction of the slipstream in assigning the measured element of torque to the appropriate element of the propeller blade.

4. Scale Effect. Wind tunnel tests of model propellers, suitably corrected when necessary for the constraint of the tunnel walls, have hitherto been the principal experimental method of studying the characteristics of different types of propeller. In general the tip speeds of the model propeller and of the corresponding full scale propeller are not sufficiently high to introduce any important change in the characteristics due to the compressibility of the air, but owing to the lower tip speed and smaller diameter of the model propeller there may be a noticeable change due to scale effect. In order that the model should correctly reproduce the characteristics of the full scale propeller it is necessary to produce the same Reynolds' number or viscosity parameter, which is defined by the equation

$$N_v = \frac{\Omega R^2}{\nu} \tag{4.1}$$

Clearly this condition cannot be fulfilled, since the model has a smaller radius and tip speed than the actual propeller, while the kinematic coefficient of viscosity is not changed.

A propeller consists essentially of a number of radial blades whose cross-sections have the form of airfoils, and the scale effect of a propeller is therefore intimately related to the scale effect of an airfoil. Now the scale effect of a typical airfoil section shows the following characteristics: as the Reynolds' number increases, the drag coefficient of the airfoil decreases and the lift coefficient remains sensibly constant, except at very low angles of incidence where it may increase slightly, and near the critical angle where it usually increases steadily but sometimes increases to a maximum and then decreases. These changes are most noticeable at relatively small values of the Reynolds' number and may disappear almost completely on approaching the values which occur with actual aircraft. The changes in the characteristics of the airfoil sections lead to similar changes in the characteristics of a propeller. Fig. 80 shows a rather extreme example[2] of the scale effect on a propeller tested at Reynolds' numbers of 0.8×10^6 and 1.4×10^6. The scale effect shown in this figure is very large, but the lower value of the Reynolds'

[1] DOUGLAS, G. P., and COOMBES, L. P., The Measurement of Torque Grading Along an Airscrew Blade. Br. A.R.C. R. and M. 992, 1925.

[2] Ergebnisse der Aerodynamischen Versuchsanstalt zu Göttingen, III. Lief., p. 125.

number is unusually low, since a typical full scale value is 20×10^6 and a value of at least 2×10^6 is usually attained in model tests. The experimental result does, however, demonstrate the importance of making the scale of the model tests as high as possible.

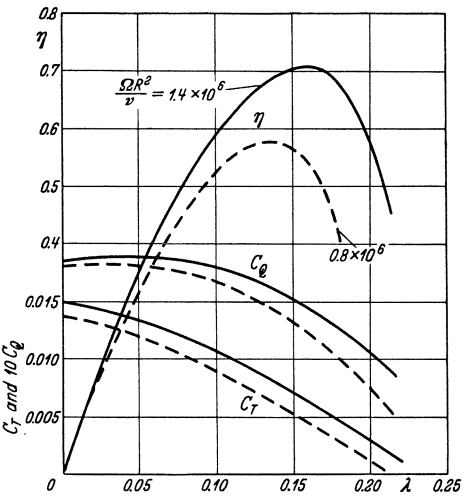

Fig. 80.

The construction of the large propeller research tunnel of the National Advisory Committee for Aeronautics has eliminated almost entirely the problem of scale effect, since it is possible to test the full scale propellers at a speed very little short of that realized in flight. The comparison of a propeller tested in this tunnel[1] with similar tests of a model propeller is shown in Figs. 81 and 82. The scale effect is small but noticeable, and is consistent with the type of scale effect which is experienced by the airfoil sections. Fig. 81 shows that the power coefficient increases with the scale of the test, particularly at low values of the advance-diameter ratio J owing to the increase of the lift coefficient of the airfoil sections near the critical angle, and also at larger values of J owing to the increase of the lift coefficient near the angle of zero lift of the airfoil sections. In the intermediate region a small increase of the lift coefficient seems to be balanced by a decrease of the drag coefficient. Fig. 82 shows the corresponding scale effect on the thrust coefficient and efficiency of the same propeller, and it is to be noted that the increase of the thrust coefficient with scale in the intermediate range, where the power coefficient was constant, is due to the fact that the small increase of the lift coefficient

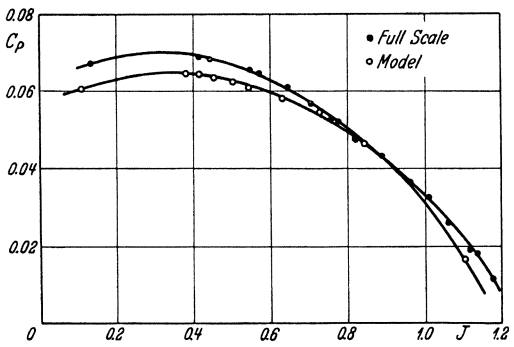

Fig. 81.

[1] Weick, F. E., Full Scale Tests of Wood Propellers on a VE-7 Airplane in the Propeller Research Tunnel. U.S. N.A.C.A. Technical Report No. 301, Washington, 1928.

and the small decrease of the drag coefficient of the airfoil sections now combine to increase the thrust coefficient. The final result of the scale effect is that the maximum efficiency of the propeller is increased by 2 per cent and that the experimental mean pitch-diameter ratio at which the thrust vanishes is increased from 1.10 to 1.16 owing to the increase of the lift coefficient of the airfoil sections near the angle of zero lift.

The propeller whose characteristics are shown in Figs. 81 and 82 has also been tested in flight and the results agree as reasonably as can be expected with the tests in the propeller research tunnel when allowance is made for the difficulty of obtaining reliable results in flight. The flight tests do, however, tend to give rather higher values of the thrust and power coefficients than the wind tunnel tests, and this discrepancy can be ascribed to a difference in the experimental conditions which occurs almost invariably in such comparative tests. A propeller is usually tested in a wind tunnel with its axis of rotation pointing in the direction of the air stream, but in flight this condition can be realized only at one speed of the airplane. At all other speeds the axis of the propeller is inclined at an angle to the direction of motion, and wind tunnel tests, which are discussed more fully in Chapter XII have shown that the effect of this inclination of the axis is to increase the thrust and torque of the propeller. Flight tests of a propeller can therefore be compared rigorously only with special wind tunnel tests in which the inclination of the axis of the propeller is varied in the same manner.

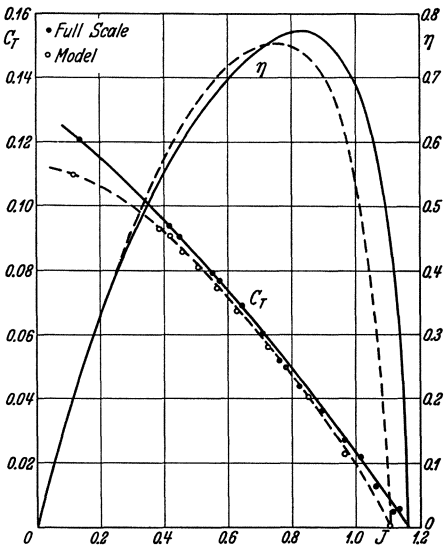

Fig. 82.

Since the scale effect of a propeller is due essentially to the scale effect of the airfoil sections which form its blades, the Reynolds' number

$$N_v = \frac{\Omega R^2}{\nu}$$

is not an entirely satisfactory parameter, and for some purposes it is more significant to consider an alternative parameter

$$N'_v = \frac{\Omega R c}{\nu} \tag{4.2}$$

where c is the maximum chord of one of the blades. The principle of dynamical similarity can be applied strictly only to two propellers which are geometrically similar in every respect, and it is then immaterial which of the alternative forms of the Reynolds' number is used. The general theory of the propeller, however, has suggested that, apart from a small effect due to losses at the tips of the blades, the characteristics of a propeller depend only on the product Bc and not on the number of blades B or on the chord c independently. If now two propellers with different numbers of blades but the same value of Bc are considered, the propeller with the larger number of blades will have the smaller value of the parameter N'_v and will therefore operate effectively at a smaller scale. It may be anticipated therefore that, of two such propellers, the one with the larger number of blades will tend to have a lower maximum efficiency and a lower experimental mean pitch-diameter ratio, and this scale effect may more than balance the effect of the tip losses which would make the maximum efficiency increase slightly with the number of the blades. This scale effect complicates the interpretation of experimental results designed to test the validity of the theoretical suggestion that the characteristics of a propeller depend essentially on the product Bc rather than on B or c separately, and the observed variation[1] of the experimental mean pitch-diameter ratio is to be ascribed purely to scale effect.

In this discussion of scale effect the terms "full scale" and "model" have been used rather loosely to describe the variation of scale between the actual propellers used in flight by modern aircraft and the smaller propellers which are tested in ordinary wind tunnels of diameter 7 ft. at most. To obtain a more precise conception of the difference of scale, it may be noted that with airfoils a Reynolds' number cV/ν of 10^6 is a convenient mark for dividing the usual model and full scale ranges, and that the important variation of the characteristics of an airfoil with scale occurs mainly in the model range so defined. If a Reynolds' number of 10^6 is attained in the test of an airfoil, it is improbable that there will be any important scale effect at the higher values which may occur with larger or faster airplanes. Turning now to the propeller and considering a typical section of a blade at 0.7 of the extreme radius, the Reynolds' number corresponding to the arbitrary dividing point chosen for the airfoils is

$$\frac{0.7\,\Omega\,R\,c}{\nu} = 10^6$$

and since the chord is usually of the order of one sixth of the radius,

[1] LOCK, C. N. H., and BATEMAN, H., Experiments with a Family of Airscrews. Analysis of the Family of Airscrews by Means of the Vortex Theory and Measurements of Total Head. Br. A.R.C. R. and M. 892, 1923.

the Reynolds' number separating the model and full scale range of operation of a propeller may be taken to be approximately

$$N_v = \frac{\Omega R^2}{\nu} = 10^7 \tag{4.3}$$

If this value is attained, important changes of the propeller characteristics with a further increase of scale are improbable, but model tests usually attain a Reynolds' number of the order of 2×10^6 only and do not therefore eliminate the possibility of further scale effect.

5. Compressibility Effect. The characteristics of a propeller at a definite rate of advance depend on the viscosity and on the compressibility of the air. The effect of the viscosity, which can be represented in terms of the Reynolds' number of the flow, has been discussed in the preceding section, and it is now necessary to consider the effect of the compressibility of the air. In an incompressible fluid any increase of pressure is transmitted instantaneously throughout the whole fluid, but in a compressible fluid the disturbance travels with a definite speed, which is the speed of sound in the fluid. The speed of sound can therefore be used as a measure of the compressibility of the fluid, and in air this speed is approximately $66 \sqrt{\theta}$ ft. per sec., where θ is the absolute temperature in the Centigrade scale. At the standard ground temperature of 15^0 C, the speed of sound is 1120 ft. per sec.

The effect of the compressibility becomes noticeable only when the speed of a body through the air is an important fraction of the speed of sound. Thus, for example, the dynamic pressure recorded by a pitot tube, which is $1/2\, \varrho\, V^2$ at low speeds, increases slowly at higher speeds owing to the effect of the compressibility of the air, and if this effect is ignored the speed deduced from the dynamic pressure exceeds the true speed by an amount which increases from 0.5 per cent at 150 miles per hour to 2 per cent at 300 miles per hour. This example suggests that the effect of compressibility can be safely neglected at the speeds which are usually encountered by the wings of an airplane, but may become important at the higher speeds experienced by the blades of a propeller.

The effect of the compressibility of the air on a propeller can be estimated from the effect on the airfoil sections of its blades. Theory is of little assistance in determining this effect, but it does suggest that the effect of the compressibility becomes apparent first as an intensification of the force experienced by the airfoil, the lift coefficient increasing with the speed as $(1 - n^2)^{-1/2}$, where n is the ratio of the speed of the airfoil to the speed of sound. This approximate formula is valid only at comparatively low speeds and breaks down as soon as the local velocity at any point of the airfoil rises to equality with the speed of sound. At higher speeds it is necessary to rely wholly on experimental

results. These experimental results have been obtained either by direct tests of very small airfoils in a high speed jet, or by analyzing the observed distribution of thrust and torque along the blade of a model propeller of low pitch rotating with a high tip speed. Unfortunately the exact significance of these results is by no means certain. The direct measurements are made with airfoils extending across a diameter of the jet and, owing to the limited extent of the jet, they do not correspond strictly to two-dimensional motion or infinite aspect ratio, but they do provide a valuable indication of the variation of the airfoil characteristics at high speeds. The derivation of

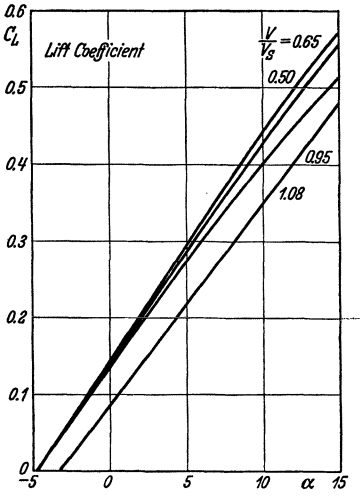

Fig. 83.

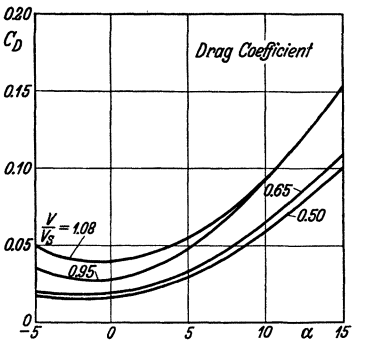

Fig. 84.

the airfoil characteristics from the test of a model propeller is even more complex, the experiments are difficult to make, and the analysis depends on the assumption that the ordinary propeller theory, which has been developed for an incompressible fluid, may be used to analyze the behavior of a propeller whose tip speed exceeds the speed of sound.

In spite of these uncertainties the general nature of the variation of the characteristics of an airfoil is now fairly well known and may be summarized as follows. The first effect of increasing speed is a gradual increase of both the lift and the drag coefficients, but with a further increase of speed the lift coefficient begins to fall and the drag coefficient increases more rapidly. These features may be illustrated by reference to the tests of airfoils in a high speed jet[1]. Fig. 83 shows the variation of the lift coefficient of a typical airfoil, and Fig. 84 shows the corresponding values of the drag coefficient. These figures illustrate the slow increase of the lift and drag coefficients at the lower speeds, followed

[1] Briggs, L. J., and Dryden, H. L., Aerodynamic Characteristics of Twenty Four Airfoils at High Speeds. U.S. N.A.C.A. Technical Report No. 319, 1929. See also Division I, Part II.

by a drop of the lift coefficient and a rapid rise of the drag coefficient. The increase of the lift coefficient at the lower speeds has also been confirmed in flight by pressure plotting over one section of a propeller blade[1].

The model experiments also show that airfoil sections of the Joukowski type are more efficient than the conventional propeller sections with flat undersurfaces, and that thin sections maintain their lift to higher speeds than thick sections. Fig. 85 shows the variation of lift coefficient at one angle of incidence for typical airfoil sections of varying thickness (0.04 c, 0.08 c, and 0.12 c), and Fig. 86 shows the variation of the minimum drag coefficient of these three airfoil sections and of three conventional propeller sections.

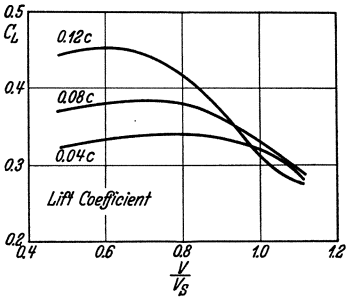

Fig. 85.

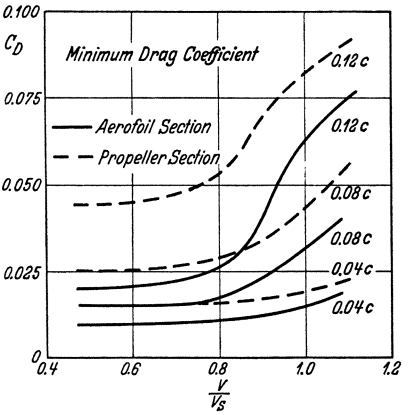

Fig. 86.

The behavior of a propeller rotating at high tip speeds can be estimated by considering the effect of these changes in the characteristics of the airfoil sections. At comparatively low speeds the lift and drag coefficients both increase, and in consequence the torque coefficient of the propeller also increases, while the thrust coefficient remains sensibly constant since the increases of the lift and drag coefficients produce opposite effects on the thrust of the propeller. This conclusion has been confirmed by flight tests[2] which showed no change of the thrust coefficient and an increase of the torque coefficient. At higher speeds the thrust coefficient would decrease owing to the decrease of the lift coefficient, but this collapse can be avoided by using thin blades of good section, and experiments in the propeller research tunnel[3] have shown no com-

[1] JONES, E. T., The Distribution of Pressure Over a Section of an Airscrew Blade in Flight and the Variation of Lift Coefficient with the Speed of the Section. Br. A.R.C. R. and M. 1256, 1929.

[2] JENNINGS, W. G., Full Scale Determination of the Effect of High Tip Speeds on the Performance of an Airscrew. Br. A.R.C. R. and M. 1173, 1928.

[3] WEICK, F. E., Full Scale Tests of a Thin Metal Propeller at Various Tip Speeds. U.S. N.A.C.A. Technical Report No. 302, 1928.

pressibility effect on a propeller with thin blades. In practice, however, the use of thin blades may introduce the danger of flutter of the blades, and some increase of the torque coefficient and some decrease of the thrust coefficient must be anticipated at high speeds.

CHAPTER X

HELICOPTER AIRSCREWS

1. Introduction. A *helicopter* may be defined as a type of aircraft in which the rigid lifting wings of a conventional airplane are replaced by one or more lifting airscrews. The primary object of a helicopter is to obtain vertical ascent, but if the helicopter ever becomes a practical type of aircraft it must also be capable of horizontal flight at a reasonable speed. The conception of the helicopter is very old; Leonardo da Vinci appears to have devoted some attention to its possibilities and to have experimented with simple models, and the last 150 years have seen a succession of experiments both with model and with full scale helicopters. Frequently the helicopters have succeeded in rising from the ground, but in general the stability and lateral control have been inadequate to ensure a safe flight of any prolonged duration. Moreover the reserve of power was usually small and the helicopter was capable of rising only a few feet from the ground.

The scope of the present discussion will be confined to the characteristics of the helicopter airscrew, and no attempt will be made to discuss the design, stability and control of the complete aircraft. A helicopter airscrew, when supporting the aircraft in the air, is merely a propeller operating at the condition of zero rate of advance, but to fulfill its specialized functions the helicopter airscrew must be designed with a large diameter and with a small pitch-diameter ratio, and owing to these special features it is possible to make some simplifications in the analysis of its characteristics. The thrust and torque of the helicopter airscrew will be expressed in terms of the same non-dimensional coefficients which have been used for the propeller, and as defined by the equations

$$\left.\begin{aligned} T &= T_c \pi R^2 \varrho \Omega^2 R^2 \\ Q &= Q_c \pi R^2 \varrho \Omega^2 R^3 \end{aligned}\right\} \tag{1.1}$$

but the efficiency of propulsion is now essentially zero and ceases to have any useful application. The merit of a helicopter airscrew can, however, be defined by a suitable non-dimensional parameter which is obtained by considering the relationship between the thrust of the airscrew and the power necessary to drive it. The thrust of the airscrew is equal to the weight which can be supported, and the power absorbed is the energy which must be expended to achieve this result. The ratio

of the thrust to the power does not provide a suitable parameter, since

$$\frac{T}{P} = \frac{T}{\Omega Q} = \frac{T_c/Q_c}{\Omega R} \tag{1.2}$$

and the ratio T/P varies inversely with the tip speed ΩR for a given design of airscrew. A suitable non-dimensional form can however, be obtained by writing $M = \frac{T}{P}\sqrt{\frac{T}{\pi R^2 \varrho}} = \frac{T_c^{3/2}}{Q_c}$ (1.3)

and the parameter M so defined will be called the *figure of merit* of the helicopter airscrew. The introduction of a coefficient of this type was due originally to C. Renard[1], but his definition involved an empirical value for the drag of a flat plate. The figure of merit is inversely proportional to the power required to lift a weight T by means of a helicopter airscrew whose disc loading is $T/\pi R^2$. Thus an increase of the figure of merit implies a reduction of the power required to lift a given weight, or an increase of the weight which can be lifted by use of an engine of given power. Also the form of the expression (1.2) shows that, with a helicopter airscrew of given design, the weight per horse power increases as the tip speed decreases, while the expression (1.3) shows that the power to support a given weight decreases as the radius increases. It is therefore advantageous to use a helicopter airscrew of large diameter rotating with a low angular velocity.

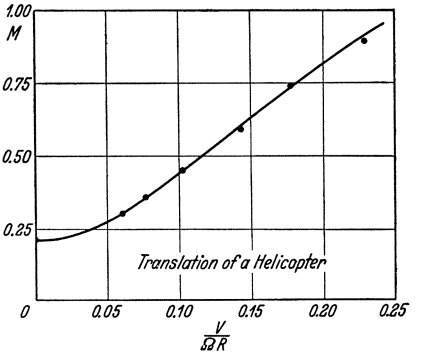

Fig. 87.

The horizontal flight of a helicopter can be achieved either by means of a propeller as in a conventional airplane or by inclining the axis of the helicopter airscrew to give a horizontal component of thrust. In either case the helicopter airscrew now has a translational velocity at right angles to its axis of rotation, and it was noticed by H. S. Maxim[2] that this translational velocity increased the thrust of the helicopter airscrew for a given power input. This increase of the figure of merit was confirmed experimentally by D. Riabouchinsky[3] and is an important factor in the horizontal flight of a helicopter. Riabouchinsky's experimental results are shown in Fig. 87. Owing to the translational motion

[1] Sur la qualité des hélices sustentatrices. Comptes Rendus, Vol. 137, p. 970, 1903.

[2] Screw Propellers Working in Air. Aeronautical Annual, 1897.

[3] Recherches sur l'hélice aérienne se mouvant dans un courant aérien dirigé perpendiculairement à l'axe de l'hélice. Bull. de l'Institut Aérodynamique de Koutchino I, 13, 1906.

the blades of the helicopter airscrew operate under different conditions, the advancing blade experiences a higher relative velocity than the retreating blade, and an aerodynamic rolling moment is experienced by the helicopter. In order to maintain equilibrium it is necessary to balance this rolling moment, and this result may be achieved by any one of the following systems, all of which have been tried in actual designs:—

(1) Two superimposed airscrews rotating in opposite senses about the same axis.

(2) Two axes rotating in opposite senses about parallel axes.

(3) Periodic variation of the blade angles during the course of each revolution.

(4) Blades hinged at the root to allow an up and down flapping motion.

The elimination of the rolling moment in the first two systems occurs automatically if the two airscrews give the same thrust and operate under similar conditions. In the third system the blade angle must be reduced where the relative velocity is high and conversely. Since the amplitude of this variation will increase with the horizontal speed of the helicopter, it must be under the control of the pilot and will thus provide a form of lateral control of the aircraft. The fourth system operates in a similar manner but is automatic in its action: the blades are hinged close to the axis of rotation and hence no rolling moment can be transmitted to the aircraft. Where the relative velocity is high, the blade rises rapidly and thus reduces its effective angle of incidence, and the amplitude of this flapping motion also will increase with the horizontal speed of the aircraft. In discussing the horizontal motion of a helicopter airscrew it will be necessary to examine the details of these alternative systems in so far as they affect the figure of merit and the horizontal drag experienced by the helicopter.

2. The Ideal Helicopter. If u is the axial velocity through the disc of the helicopter airscrew and if a' is the rotational interference factor, the momentum equations for the elements of thrust and torque are

respectively $$dT = 4\pi\varrho u^2 r\,dr$$

and $$dQ = 4\pi\varrho u \Omega a' r^3\,dr$$

Also the energy equation for the element is

$$(1 - a')\,\Omega\,dQ = u\,dT$$

Putting

$$\left.\begin{aligned} \mu &= \frac{u}{\Omega R} \\ x &= \frac{r}{R} \end{aligned}\right\} \qquad (2.1)$$

these equations become

$$\left.\begin{aligned} dT_c &= 4\mu^2 x\,dx \\ dQ_c &= 4\mu a' x^3\,dx \\ (1-a')\,a' x^2 &= \mu^2 \end{aligned}\right\} \tag{2.2}$$

These are the three fundamental equations for determining the characteristics of a helicopter airscrew by means of the momentum theory.

The simplest case to consider is that in which the rotational motion of the slipstream is ignored. The angular momentum equation for the torque is then ignored and the analysis is based on the two equations

$$dT = 4\pi\varrho u^2 r\,dr$$
$$\Omega\,dQ = u\,dT$$

or, in the non-dimensional form,

$$dT_c = 4\mu^2 x\,dx$$
$$dQ_c = 4\mu^3 x\,dx$$

The best distribution of axial velocity is obtained when μ is constant, as in the more general case of a propeller[1], and on this basis

$$T_c = 2\mu^2$$
$$Q_c = 2\mu^3$$

and the figure of merit becomes

$$M = \sqrt{2} = 1.414 \tag{2.3}$$

This value of the figure of merit is the highest which can possibly be obtained with any helicopter airscrew, since it neglects the additional energy losses which actually occur owing to the rotational motion of the slipstream and to the frictional drag of the blades.

When the rotational motion of the slipstream is no longer neglected, the analysis must be based on the general momentum equations, (2.2). The optimum distribution of axial and rotational velocities will be considered shortly, but by analogy with the analysis for a propeller as developed in III 4 and III 5, it may be anticipated that this optimum distribution will not differ greatly from that determined by the condition that $\frac{\mu}{1-a'}$ is constant along the blades. Writing

$$\frac{\mu}{1-a'} = n \tag{2.4}$$

where n is a constant, the third of (2.2) gives

$$a' x^2 = (1-a')\,n^2$$

and hence

$$a' = \frac{n^2}{n^2+x^2}$$

$$\mu = \frac{n x^2}{n^2+x^2}$$

[1] See II 3.

Also $$d\,T_c = 4\,\mu^2\,x\,d\,x$$

and hence $$T_c = \int_0^1 4\,\mu^2\,x\,d\,x$$

$$= \int_0^1 \frac{4\,n^2\,x^5\,d\,x}{(n^2+x^2)^2}$$

which gives after integration[1]

$$T_c = \frac{2\,n^2\,(1+2\,n^2)}{1+n^2} - 4\,n^4\,log\,\frac{1+n^2}{n^2} \tag{2.5}$$

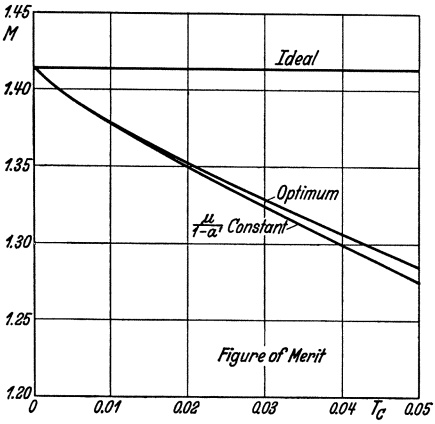

Fig. 88.

Finally the torque coefficient is obtained from (2.2) as

$$d\,Q_c = \frac{a'\,x^2}{\mu}\,d\,T_c = n\,d\,T_c$$

and hence

$$\left.\begin{aligned} Q_c &= n\,T_c \\ M &= \frac{\sqrt{T_c}}{n} \end{aligned}\right\} \tag{2.6}$$

Numerical values of the thrust coefficient and figure of merit are given in Table 27 and the curve of M against T_c is shown in Fig. 88.

TABLE 27. $\frac{\mu}{1-a'}$ constant.

n^2	0.0050	0.0100	0.0150	0.0200	0.0250	0.0300	0.0350
T_c	0.0095	0.0184	0.0266	0.0345	0.0419	0.0490	0.0558
M	1.380	1.355	1.333	1.313	1.295	1.278	1.262

The optimum distribution of the axial and rotational velocities can be determined by the method used in III 4. Starting from (2.2), the arbitrary increments of the thrust and torque coefficients are

$$\Delta\,d\,T_c = 8\,\mu\,\Delta\,\mu\,x\,d\,x$$

$$\Delta\,d\,Q_c = 4\,(a'\,\Delta\,\mu + \mu\,\Delta\,a')\,x^3\,d\,x$$

and the increments of μ and a' are related by the equation

$$(1-2\,a')\,\Delta\,a'\,x^2 = 2\,\mu\,\Delta\,\mu$$

[1] Since $$\int \frac{2\,x^5\,d\,x}{(n^2+x^2)^2} = \int\left[1 - \frac{2\,n^2}{n^2+x^2} + \frac{n^4}{(n^2+x^2)^2}\right] d\,(x^2)$$

$$= x^2 - 2\,n^2\,log\,(n^2+x^2) - \frac{n^4}{n^2+x^2}.$$

The optimum distribution is determined by the condition that the ratio of the increments of thrust and torque shall be independent of the radial coordinate x, and this condition is obtained as

$$\frac{\mu}{1-a'} + \frac{2\mu}{1-2a'} = \text{constant} \tag{2.7}$$

The analysis can now be pursued by expressing first μ and a', and then T_c and Q_c, in terms of this constant, but it becomes very complicated and the final results, which are shown in Fig. 88, differ very little from those derived from the previous simpler assumption. At a thrust coefficient of 0.050, which is very high for a helicopter airscrew, the optimum distribution gives a figure of merit only 0.6 per cent higher than the simpler assumption defined by (2.4), and hence this simple assumption suffices for all practical purposes.

3. The Effect of Profile Drag. The additional loss of energy due to the frictional drag of the blades can be estimated quite simply by the method previously used for a propeller. The rate of loss of energy E is obtained from IV (2.6) as

$$E = \sigma\,\delta\,\pi\,R^2\,\varrho\,\Omega^3\,R^3\,(1-a')^3\,f(\varphi_1)$$

and the values of $f(\varphi_1)$ are given in Table 5. As a further simplification the rotational interference factor a' will be ignored and the value of $f(\varphi_1)$ will be taken to be 0.250, since the value of $tan\,\varphi_1$ is rarely as large as 0.15 for a helicopter airscrew and is usually less than 0.10. Thus the non-dimensional coefficient of the rate of loss of energy due to the drag of the blades becomes simply

$$E_c = \frac{1}{4}\sigma\,\delta \tag{3.1}$$

When the rotational interference factor a' is ignored, the best distribution of thrust over the disc of the airscrew is obtained with a constant value of the axial velocity u, and the thrust of the airscrew is

$$T = 2\,\pi\,R^2\,\varrho\,u^2$$

or

$$T_c = 2\,\mu^2 \tag{3.2}$$

Also the energy equation is

$$\Omega\,Q = u\,T + E$$

and hence

$$Q_c = 2\,\mu^3 + \frac{1}{4}\sigma\delta \tag{3.3}$$

Finally the figure of merit of the helicopter airscrew is obtained from the equation

$$\frac{1}{M} = \frac{Q_c}{T_c^{3/2}} = \frac{1}{\sqrt{2}} + \frac{\sigma\,\delta}{4\,T_c^{3/2}} \tag{3.4}$$

If the profile drag of the blades were zero, the figure of merit would be $\sqrt{2}$, and the effect of the profile drag is to reduce this figure of merit by the factor

$$\zeta = \frac{1}{1 + \dfrac{\sigma\,\delta}{(2\,T_c)^{3/2}}} \tag{3.5}$$

Numerical values of the factor ζ are given in Table 28. If a helicopter is designed with two coaxial airscrews rotating in opposite directions, the rotational motion in the slipstream can be avoided and the figure of merit should approximate $\sqrt{2\,\zeta}$. More generally, when the rotational motion occurs, the figure of merit previously obtained and given in Table 27 must be reduced by the factor ζ to allow for the effect of the

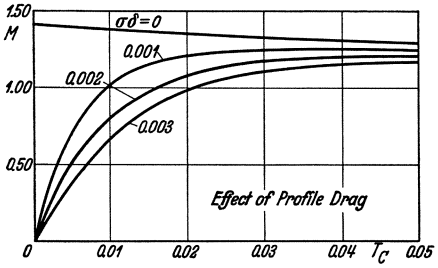

Fig. 89.

TABLE 28. Values of ζ.

$\sigma\,\delta =$	0.0010	0.0020	0.0030
$T_c = 0.005$	0.500	0.333	0.250
0.010	0.738	0.586	0.485
0.020	0.889	0.800	0.728
0.030	0.936	0.881	0.830
0.040	0.958	0.919	0.882
0.050	0.969	0.941	0.913

profile drag. The numerical values of the figure of merit estimated in this manner are given in Table 29 and are shown graphically in Fig. 89. These curves show that the effect of the profile drag is most important at small values of the thrust coefficient, and that to obtain a high figure of merit it is necessary to use either an airscrew with a large thrust coefficient, which implies an airscrew of large solidity, or a well designed airscrew of small solidity.

TABLE 29. Values of M.

$\sigma\,\delta =$	0	0.0010	0.0020	0.0030
$T_c = 0.005$	1.393	0.696	0.464	0.348
0.010	1.378	1.017	0.808	0.669
0.020	1.353	1.203	1.082	0.985
0.030	1.330	1.245	1.172	1.104
0.040	1.307	1.252	1.201	1.153
0.050	1.285	1.245	1.209	1.173

Experimental values of the figure of merit obtained with different designs of helicopter vary widely, and the highest recorded value appears to be that claimed for the Pescara helicopter[1]. The experimental results indicate a figure of merit of 1.26, obtained in association with a thrust coefficient of 0.064 by the use of a multiple airscrew of very large solidity. The helicopter comprised two coaxial biplane airscrews rotating in opposite directions, and the figure of merit therefore appears to be reasonably consistent with the theoretical estimates.

4. Blade Element Theory. The detailed calculation of the performance of any given helicopter airscrew can be made on the lines of the usual propeller calculations, but owing to the fact that the pitch-diameter

[1] Sur les resultats des essais récents d'un hélicoptère. Comptes Rendus, Vol. 172, p. 845, 1921.

ratio of the airscrew is always small, it is possible to simplify the analysis in several ways and to obtain approximate formulae for the figure of merit. By the use of such approximations H. Glauert[1] has determined the figure of merit for a helicopter airscrew of constant chord and blade angle, and for one of constant pitch; and O. Flachsbart[2] has determined the best distribution of the thrust along the blades to obtain the highest figure of merit. Flachsbart's analysis shows that the figure of merit obtained under the best conditions does not differ appreciably from that obtained when the thrust is uniformly distributed over the disc of the airscrew, and it will therefore suffice to examine the analysis when this condition is satisfied.

The momentum equation for the element of thrust is

$$\frac{dT}{dr} = 4\pi\varrho u^2 r \tag{4.1}$$

and the condition of uniform distribution of thrust over the disc of the airscrew implies that the axial velocity u has a constant value. Also the blade element equations[3] for the thrust and torque may be expressed in the approximate forms, assuming φ to be small,

$$\frac{dT}{dr} = \frac{1}{2} B c \varrho \Omega^2 r^2 C_L \tag{4.2}$$

and

$$\frac{dQ}{dr} = \frac{1}{2} B c \varrho \Omega^2 r^3 (C_D + \varphi C_L)$$

$$= \frac{1}{2} B c \varrho \Omega r^2 (\Omega r C_D + u C_L) \tag{4.3}$$

On integrating (4.1), the thrust is obtained as

$$T = 2\pi R^2 \varrho u^2$$

or

$$T_c = 2\mu^2$$

as in 2.

Also (4.3) for the torque becomes

$$\Omega \frac{dQ}{dr} = \frac{dT}{dr}\left(\Omega r \frac{C_D}{C_L} + u\right)$$

and if the drag-lift ratio C_D/C_L has the constant value ε along the blade this equation can be integrated at once to give

$$\Omega Q = \frac{4}{3}\varepsilon\pi R^3 \varrho u^2 \Omega + 2\pi R^2 \varrho u^3$$

or

$$Q_c = 2\mu^3 + \frac{4}{3}\varepsilon\mu^2$$

Finally the figure of merit is obtained as

$$\frac{\sqrt{2}}{M} = 1 + \frac{4}{3}\frac{\varepsilon}{\sqrt{2T_c}} \tag{4.4}$$

---

[1] On the Vertical Ascent of a Helicopter. Br. A.R.C. R. and M. 1132, 1927.
[2] Theorie der Hubschraube. Zeitschr. f. Flugtechnik u. Motorl. **19**, 177, 1928.
[3] See VI 1.

This result may be compared with the previous formula (3.4), which gives

$$\frac{\sqrt{2}}{M} = 1 + \frac{\sigma\,\delta}{(2\,T_c)^{3/2}} \tag{4.5}$$

and, although the two expressions differ in form, it can be shown that they are approximately equivalent. Turning to (4.2) and integrating on the assumption of a constant chord c and a mean value of C_L along the blade, the thrust is

$$T = \frac{1}{6} B\,c\,\varrho\,\Omega^2\,R^3\,C_L$$

or

$$T_c = \frac{1}{6}\sigma\,C_L \tag{4.6}$$

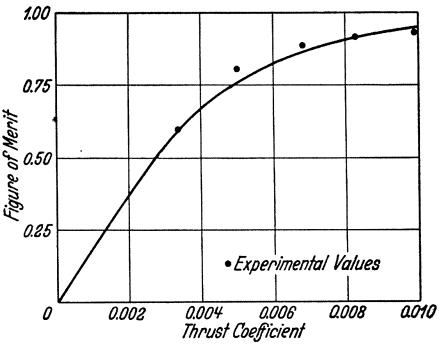

Fig. 90.

where σ is the solidity $Bc/\pi R$ of the airscrew. Using this result and remembering that δ is half the mean drag coefficient or $1/2\,\varepsilon\,C_L$, formula (4.5) becomes

$$\frac{\sqrt{2}}{M} = 1 + \frac{3}{2}\frac{\varepsilon}{\sqrt{2\,T_c}}$$

and the second term in this expression is 9/8 times the corresponding term in the formula (4.4). Thus the two methods of calculation lead to approximately the same results, but the figures of merit determined from (4.4) according to Flachsbart's analysis are slightly higher than those calculated in the previous section and shown in Fig. 89.

The validity of the approximate analysis is confirmed by the comparison[1] of theory and experiment shown in Fig. 90, where a calculated curve of figure of merit against thrust coefficient is compared with the corresponding experimental points for an airscrew of solidity 0.09 with blades of constant chord and blade angle. The agreement is quite good and shows that the theory is able to represent the experimental results reliably.

5. Horizontal Motion. Hitherto the helicopter airscrew has been considered as rotating about its axis without any translational motion relative to the general mass of air, thus representing the condition when the aircraft is hovering at a fixed point. The vertical ascent of a helicopter requires no special study since the airscrew then has a slow motion along its axis and its performance can be estimated by the usual methods of propeller theory. The horizontal motion of a helicopter however,

[1] Taken from Br. A.R.C. R. and M. 1132, 1927.

introduces some new features into the analysis[1]. In general the horizontal flight of a helicopter will be achieved with the axis of rotation inclined at a small angle to the vertical, but it will suffice to examine the rather simpler condition when the axis of rotation remains vertical and the helicopter is moving horizontally with the velocity V. In addition to the thrust and torque, the helicopter airscrew then experiences a horizontal drag H opposing the translational motion, and a rolling moment L tending to raise the advancing blade and to depress the retiring blade.

Owing to the horizontal velocity V, the slipstream of the airscrew no longer passes vertically downward, but is deflected laterally, and it is necessary to consider the form assumed by the momentum equation under these modified conditions. Assuming a uniform axial velocity u over the whole disc of the airscrew, a suitable form for this equation appears to be

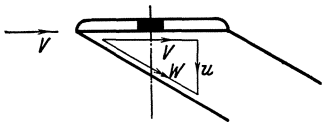

Fig. 91.

$$T = 2\pi R^2 \varrho W u \tag{5.1}$$

where W is the resultant of the horizontal velocity V and of the axial velocity u, or $W^2 = V^2 + u^2$

No rigid proof of this equation has been given, but it reverts to the correct form $T = 2\pi R^2 \varrho u^2$

when the horizontal velocity is zero; and at the other extreme, when the horizontal velocity V is large compared with the induced axial velocity u, it becomes

$$T = 2\pi R^2 \varrho V u$$

which is the standard form for the induced velocity due to an airfoil of semi-span R carrying the lift elliptically distributed across its span. The formula (5.1) may therefore be accepted as a plausible hypothesis for determining the induced velocity. Writing

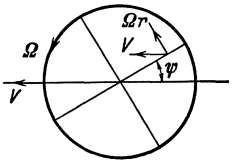

Fig. 92.

$$\left.\begin{aligned} V &= \lambda \Omega R \\ u &= \mu \Omega R \end{aligned}\right\} \tag{5.2}$$

the equation gives $T_c = 2\mu\sqrt{\lambda^2 + \mu^2}$ (5.3)

Consider now the behavior of the blade element at distance r along the blade which is at an angle ψ to the downwind position. The horizontal component of the velocity normal to the radius is

$$\begin{aligned} U &= \Omega r + V \sin\psi \\ &= \Omega (r + \lambda R \sin\psi) \end{aligned}$$

and the corresponding vertical component is simply

$$u = \mu \Omega R$$

[1] GLAUERT, H., On the Horizontal Flight of a Helicopter. Br. A.R.C. R. and M. 1157, 1928.

The inclination φ of the resultant velocity to the plane of rotation is given by the equation $\tan \varphi = \frac{u}{U}$

and the analysis will be developed on the assumption that this angle φ is small, though this approximation clearly breaks down toward the roots of the blades. Also the radial component ($V \cos \psi$) of the velocity will be ignored.

On this basis of approximation the blade element is assumed to experience a velocity W at an angle of incidence $(\theta - \varphi)$, and the force experienced by the blade element will be estimated on the assumption that the lift coefficient C_L may be taken to be

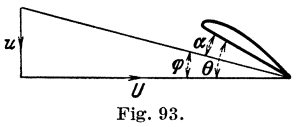

Fig. 93.

$$C_L = 6\,\alpha = 6\,(\theta - \varphi)$$

and that the drag coefficient C_D has a constant value $2\,\delta$ along the blade. The element of thrust on the typical blade element is then

$$\frac{d\,T_1}{d\,r} = \frac{1}{2}\,c\,\varrho\,(U^2 + u^2)\,(C_L \cos\varphi - C_D \sin\varphi)$$

or approximately

$$\begin{aligned}\frac{d\,T_1}{d\,r} &= 3\,(\theta - \varphi)\,c\,\varrho\,U^2 \\ &= 3\,c\,\varrho\,\Omega^2\,[\theta\,(r^2 + 2\,\lambda\,r\,R\sin\psi + \lambda^2\,R^2\sin^2\psi) - \\ &\qquad - \mu\,R\,(r + \lambda\,R\sin\psi)]\end{aligned} \tag{5.4}$$

and the corresponding element of torque is

$$\frac{d\,Q_1}{d\,r} = \frac{1}{2}\,c\,r\,\varrho\,(U^2 + u^2)\,(C_L \sin\varphi + C_D \cos\varphi)$$

or approximately

$$\begin{aligned}\frac{d\,Q_1}{d\,r} &= [\delta + 3\,(\theta - \varphi)\,\varphi]\,c\,r\,\varrho\,U^2 \\ &= c\,\varrho\,\Omega^2\,[\delta\,(r^3 + 2\,\lambda\,r^2\,R\sin\psi + \lambda^2\,r\,R^2\sin^2\psi) \\ &\qquad + 3\,\mu\,\theta\,R\,(r^2 + \lambda\,r\,R\sin\psi) - 3\,\mu^2\,r\,R^2]\end{aligned} \tag{5.5}$$

The elements of rolling moment and horizontal force are then derived as

$$\frac{d\,L_1}{d\,r} = r\sin\psi\,\frac{d\,T_1}{d\,r} \tag{5.6}$$

and

$$\frac{d\,H_1}{d\,r} = \frac{\sin\psi}{r}\,\frac{d\,Q_1}{d\,r} \tag{5.7}$$

These equations represent the forces and moments on a single blade of the airscrew, and to obtain the corresponding results for the whole airscrew it is necessary to add the contributions of all the blades in their appropriate angular positions.

6. Rigid Airscrew. Consider first a helicopter airscrew with rigid blades of constant chord c and blade angle θ. The necessary integration can then be performed quite simply, and, in the summation over the

B blades of the airscrew, all terms involving odd powers of $\sin\psi$ disappear while the mean value of $\sin^2\psi$ is 1/2. Thus for the one blade

$$T_1 = c\varrho\Omega^2 R^3\left[\theta\,(1 + 3\lambda\sin\psi + 3\lambda^2\sin^2\psi) - \mu\left(\frac{3}{2} + 3\lambda\sin\psi\right)\right]$$

and for the whole airscrew

$$T = Bc\varrho\Omega^2R^3\left[\theta\left(1 + \frac{3}{2}\lambda^2\right) - \frac{3}{2}\mu\right]$$

from which the thrust coefficient is derived as

$$T_c = \sigma\left[\theta\left(1 + \frac{3}{2}\lambda^2\right) - \frac{3}{2}\mu\right] \tag{6.1}$$

This equation, taken in conjunction with the previous formula

$$T_c = 2\mu\sqrt{\lambda^2 + \mu^2} \tag{6.2}$$

determines the values of μ and T_c for any given values of σ, θ and λ.

Similarly for the torque of the airscrew

$$Q_1 = c\varrho\Omega^2R^4\left[\delta\left(\frac{1}{4} + \frac{2}{3}\lambda\sin\psi + \frac{1}{2}\lambda^2\sin^2\psi\right) + \right.$$
$$\left. + \mu\theta\left(1 + \frac{3}{2}\lambda\sin\psi\right) - \frac{3}{2}\mu^2\right]$$

and hence

$$Q = Bc\varrho\Omega^2R^4\left[\frac{1}{4}\delta\,(1 + \lambda^2) + \mu\theta - \frac{3}{2}\mu^2\right]$$

or

$$Q_c = \frac{1}{4}\sigma\delta\,(1 + \lambda^2) + \sigma\mu\left(\theta - \frac{3}{2}\mu\right) \tag{6.3}$$

Also the rolling moment becomes

$$L = Bc\varrho\Omega^2R^4\left(\theta - \frac{3}{4}\mu\right)\lambda$$

or

$$L_c = \sigma\left(\theta - \frac{3}{4}\mu\right)\lambda \tag{6.4}$$

and the horizontal force becomes

$$H = Bc\varrho\Omega^2R^3\left(\frac{1}{2}\delta + \frac{3}{2}\mu\theta\right)\lambda$$

or

$$H_c = \frac{1}{2}\sigma\,(\delta + 3\mu\theta)\,\lambda \tag{6.5}$$

Numerical results can be derived from these equations for any airscrew defined by the values of the solidity σ and the blade angle θ. The coefficient δ may be regarded as a constant or, more accurately, it may be assumed to increase with the thrust coefficient of the airscrew, since an increase of this coefficient implies an increase of the mean lift coefficient of the blade elements. The subsequent numerical results are all based on the assumption that

$$\delta = 0.0050 + 0.25\left(\frac{T_c}{\sigma}\right)^2$$

which represents the drag coefficient of a typical symmetrical airfoil section. Table 30 gives the calculated characteristics of a helicopter airscrew of solidity 0.25 and blade angle 0.10 for a range of values of λ. The figure of merit rises rapidly with the horizontal motion of the helicopter, and the calculations thus provide an explanation of the experimental results shown previously in Fig. 87. The drag of the helicopter airscrew in the range considered is increasing slowly, but is only a small fraction of the thrust or lift of the airscrew. The rolling moment increases with the horizontal speed. The ratio L/TR represents the lateral displacement of the line of action of the thrust, and the numerical values show that this displacement is an important fraction of the radius of the airscrew.

TABLE 30.

λ	0	0.10	0.20	0.30
M	0.67	1.24	2.06	2.81
H/T	0	0.025	0.029	0.032
L/TR	0	0.185	0.281	0.364

The saving of power represented by the increase of the figure of merit in Table 30 is to some extent fictitious since it would be more economical to use a larger blade angle at the low translational velocities. A more practical comparison is given by the numerical values of Table 31 which is based on the assumption of a constant thrust coefficient. The increase of the figure of merit, though less rapid than in the previous case, is still quite important and shows that the power required for sustentation falls off rapidly as the speed of horizontal flight increases. The drag of the helicopter airscrew is approximately constant in the range of speed considered and is roughly one thirtieth of the lift of the airscrew.

TABLE 31.

λ	0	0.10	0.20	0.30	0.40	0.50
θ	0.220	0.185	0.135	0.107	0.089	0.075
M	1.16	1.46	2.19	2.84	3.29	3.57
H/T	0	0.032	0.033	0.033	0.034	0.035

7. Periodic Variation of the Blade Angle. A rigid helicopter airscrew experiences a rolling moment in horizontal flight, which must be balanced by suitable control surfaces or by the use of two airscrews rotating in opposite directions. An alternative scheme is to vary the blade angle of the airscrew periodically during the course of each revolution, reducing the angle where the thrust on a blade tends to be high and increasing it where the thrust tends to be low.

Reverting to the equations of 5, it can be shown that the rolling moment can be eliminated if the blade angle θ varies periodically according to the equation

$$\theta = \theta_0 - \theta_1 \sin \psi \qquad (7.1)$$

and if the magnitude of the variation in angle is suitably chosen. On substituting this value of θ in (5.4) and (5.5), integrating along the blade, and adding the contributions of all the blades, the characteristics

of the helicopter airscrew with periodic variation of the blade angle are found to be

$$\left.\begin{aligned} T_c &= \sigma\left[\theta_0\left(1+\frac{3}{2}\lambda^2\right)-\frac{3}{2}\mu-\frac{3}{2}\lambda\theta_1\right] \\ Q_c &= \frac{1}{4}\sigma\delta(1+\lambda^2)+\sigma\mu\left(\theta_0-\frac{3}{2}\mu-\frac{3}{4}\lambda\theta_1\right) \\ H_c &= \frac{1}{2}\sigma(\delta+3\theta_0\mu)\lambda-\frac{3}{4}\sigma\theta_1\mu \end{aligned}\right\} \qquad (7.2)$$

and the condition for zero rolling moment is

$$\theta_1\left(1+\frac{3}{2}\lambda^2\right)=\frac{8}{3}\left(\theta_0-\frac{3}{4}\mu\right)\lambda \qquad (7.3)$$

Numerical calculations, based on these equations and on the assumption of a constant thrust coefficient, have been made for comparison with the previous results given in Table 31. These results are

TABLE 32.

λ	0	0.10	0.20	0.30	0.40	0.50
θ_0	0.220	0.189	0.152	0.140	0.140	0.143
θ_1	0	0.035	0.059	0.082	0.105	0.125
M	1.16	1.44	2.02	2.52	2.88	3.14
H/T	0	0.006	0.009	0.013	0.019	0.025

given in Table 32 and the comparison of the two sets of results in Figs. 94 and 95 shows that, though the figure of merit with periodic variation of the blade angle does not rise so rapidly as that of the rigid airscrew,

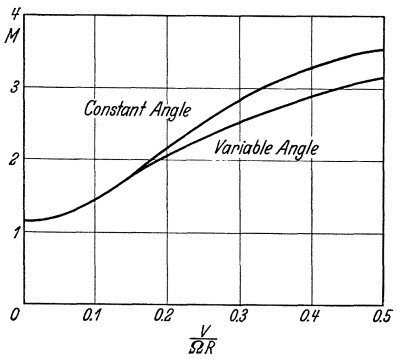

Fig. 94.

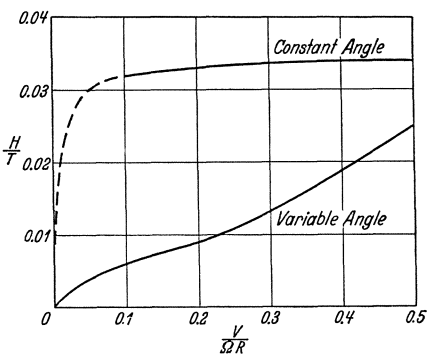

Fig. 95.

the horizontal drag is much lower. The method of variable blade angle is thus a satisfactory and economical method of eliminating rolling moment. The amplitude of the variation of angle increases with the horizontal speed, and the capacity for varying this amplitude provides a method of lateral control of the aircraft.

An alternative method of eliminating the rolling moment, which would occur with a rigid airscrew, is to hinge the blades freely at their roots and to allow them to flap up and down under the action of the aerodynamic forces. Where the thrust of the blade would be high with a rigid airscrew, the blade rises rapidly and so reduces the effective angle of incidence of the blade elements. The comparison between the method of operation of the flapping blade and the varying blade angle is shown in Fig. 96. The blade element is chosen on the advancing blade when at right angles to the direction of flight, and the angular velocity ω of the flapping motion is adjusted so that the two blade elements operate at the same effective angle of incidence α and therefore experience the same lift L. In each case the lift is inclined backward and gives a component to the horizontal force H on the airscrew, but the angle of inclination is greater for the flapping blade than for the blade with varying angle. Thus the device of flapping blades, though effective in eliminating the rolling moment, gives an increased drag force. Since the flapping blade is also incapable of providing lateral control for the aircraft, the method of periodic variation of the blade angle is to be preferred aerodynamically, though the structural details may present more difficulties than the system of flapping blades.

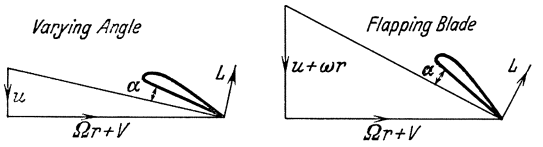

Fig. 96.

CHAPTER XI

WINDMILLS AND FANS

1. Types of Windmill. A *windmill* is an airscrew which is used to draw energy from the surrounding air and convert it into a useful form. In a propulsive airscrew or propeller the motive power supplies the torque which is necessary to maintain the rotation, and the reaction of the air on the rotating blades gives a forward thrust along the axis of rotation. In a windmill, on the other hand, the signs of the thrust and of the torque are reversed, and the aerodynamic reaction of the air on the rotating blades gives a drag force tending to check the relative axial motion and a torque which tends to increase the rotation of the windmill and which can be used as a source of power. An ordinary propeller acts as a windmill when the rate of advance is so high that the thrust and torque have both become negative, but the blade elements then operate inefficiently at negative angles of incidence. In a true windmill therefore the blades are redesigned so as to present their lower surfaces to the relative air stream, but in other respects

a windmill is essentially similar to a propeller in its design and in its mode of operation.

In discussing the characteristics of a windmill it is necessary to distinguish between a windmill mounted on an airplane as a subsidiary source of power and driven by the motion of the airplane through the air, and a windmill mounted on the ground and driven by the wind. The problem of a windmill on an airplane is very similar to that of a propeller. If D is the drag of the windmill at a speed V and if P is the power delivered by the windmill at this speed, the efficiency is

$$\eta = \frac{P}{VD} \qquad (1.1)$$

since VD is the work done by the airplane in carrying the windmill through the air and P is the useful power obtained from the windmill. Owing to the high speed of the airplane there is no difficulty in obtaining as much power as is required, but it is important that the efficiency shall be high. The efficiency is therefore the main criterion for assessing the merit of a windmill on an airplane, and this efficiency can be calculated by a direct application of the usual propeller theory, but if the equations are used in their usual forms, the thrust, torque, and interference factors will all be negative.

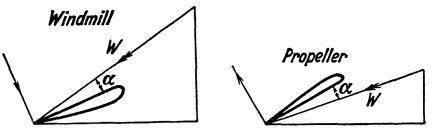

Fig. 97.

A windmill mounted on the ground presents a different problem. The drag of the windmill is of no importance, unless it becomes so high as to endanger the structure, and hence the efficiency is no longer a measure of the suitability of the windmill. The important factor is the cost of erection and maintenance, and since this cost increases with the size of the windmill it is desirable to obtain the maximum possible power from the windmill under given conditions of operation. Owing to the irregularity of the direction and strength of the wind it is necessary to provide means of regulating the windmill for the different conditions which it experiences, and owing to the occurrence of calm days it is necessary to provide means of storing sufficient energy to cover the periods during which the windmill is idle. Another difficulty in the use of a windmill as a source of power is that the rate of rotation of the windmill is usually low, and gearing must therefore be introduced into the system in order to obtain the higher rates of rotation which are required for the effective use of the power, particularly if the windmill is used to generate electricity.

The aerodynamic characterisitcs of a windmill are expressed conveniently in terms of the ratio X [1] of the tip speed ΩR to the relative

[1] Owing to the different range of operation of a windmill it is more convenient to use $\Omega R/V$ as parameter in place of $V/\Omega R$ which has hitherto been used for a propeller.

wind speed V, and of the solidity which is the ratio of the total blade area to the disc area πR^2. Windmills therefore fall into different classes according to the value of the ratio X at which they operate. Slow running windmills may operate at a value of X of the order of 1 or 2, and with the fastest running windmills in use the value of X may rise to 4. A fast running windmill requires a smaller solidity to deliver the same power as a slow running windmill, and is therefore simpler in construction. It resembles an ordinary propeller with rather wide blades, whereas a slow running windmill must be fitted with a larger number of blades. The fast running windmill also has the advantage of a high rate of rotation and requires less gearing, but on the other hand the frictional drag of its blades is high and the blades are subjected to a large centrifugal force. A fast running windmill therefore requires more careful aerodynamic and structural design than a slow running windmill.

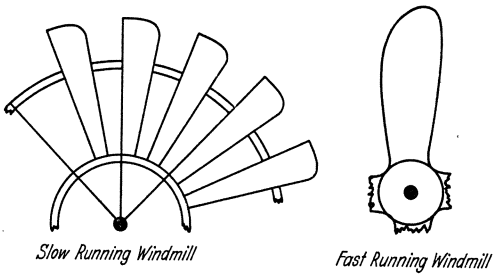

Fig. 98.

Another point of importance is the starting torque experienced by the windmill when it is at rest in a stream of air. The windmill may come to rest during a lull of the wind, and in order that it shall come into operation rapidly as the wind rises again and that it shall operate in light winds it is important that the starting torque shall be reasonably high and sufficient to overcome the internal friction of the system. The starting torque is highest for the slow running windmills and this feature may be the deciding factor in the choice of a windmill which is required to operate in light and variable winds.

2. The Ideal Windmill. If u is the axial velocity through the disc of the windmill and if ω is the angular velocity imparted to the slipstream, the momentum equations for the drag and torque are respectively

$$\frac{dD}{dr} = 4\pi r \varrho u (V - u) \qquad \text{[see V (8.10)]}$$

and

$$\frac{dQ}{dr} = 2\pi r^3 \varrho u \omega \qquad \text{[see VI (2.5)]}$$

Writing

$$u = V(1 - a)$$
$$\omega = 2\Omega a'$$

these equations become

$$\left.\begin{aligned} \frac{dD}{dr} &= 4\pi r \varrho V^2 (1 - a) a \\ \frac{dQ}{dr} &= 4\pi r^3 \varrho V \Omega (1 - a) a' \end{aligned}\right\} \qquad (2.1)$$

Also the energy equation is

$$(1 + a')\,\Omega \frac{d\,Q}{d\,r} = (1 - a)\,V \frac{d\,D}{d\,r}$$

or
$$(1 + a')\,a'\,x^2 = (1 - a)\,a \tag{2.2}$$

where
$$x = \frac{\Omega\,r}{V} \tag{2.3}$$

If the rotational motion of the slipstream is ignored the analysis must be based on the axial momentum equation

$$\frac{d\,D}{d\,r} = 4\,\pi\,r\,\varrho\,V^2\,(1 - a)\,a$$

and on the energy equation which now takes the form

$$\begin{aligned}\frac{d\,P}{d\,r} &= (1 - a)\,V \frac{d\,D}{d\,r} \\ &= 4\,\pi\,r\,\varrho\,V^3\,(1 - a)^2\,a\end{aligned}$$

Exactly as with a propeller, the best result is obtained when the axial interference factor a is constant over the whole airscrew disc, and then

$$\left.\begin{aligned}D &= 2\,\pi\,R^2\,\varrho\,V^2\,(1 - a)\,a \\ P &= 2\,\pi\,R^2\,\varrho\,V^3\,(1 - a)^2\,a\end{aligned}\right\} \tag{2.4}$$

The efficiency of the windmill, which is the ratio of the power P to the work $V\,D$ done against the drag, is simply

$$\eta = 1 - a \tag{2.5}$$

The power attains a maximum value when a is 1/3 and when η is 2/3, and this maximum power of an ideal windmill is

$$P_m = \frac{8}{27}\,\pi\,R^2\,\varrho\,V^3 \tag{2.6}$$

A useful measure of the performance of a windmill is the ratio of the power P to the maximum power P_m which would be given by an ideal windmill of the same diameter at the same speed. This ratio is

$$\zeta = \frac{P}{P_m} = \frac{27}{8}\,\frac{P}{\pi\,R^2\,\varrho\,V^3} \tag{2.7}$$

and the ideal relationship between the ratio ζ and the efficiency η is given in Table 33 and in Fig. 99. The analysis is valid only when the axial interference factor a is less than 1/2 and when the efficiency η is greater than 1/2.

The efficiency η is the important criterion for deducing the merit of a windmill mounted on an airplane, and the power ratio ζ for deducing that of a windmill on the ground. If the windmill created no disturbance of the flow, the kinetic energy of the air passing through its disc in unit time would be

$$E = \frac{1}{2}\,\pi\,R^2\,\varrho\,V^3$$

and hence ζ is 27/16 times the ratio of the power P absorbed by the windmill to this kinetic energy E.

Returning now to the more general condition when the rotational interference factor a' is retained in the analysis, the power given by the windmill is obtained from (2.1) as

$$P = \int_0^R 4\,\pi\,\varrho\,V\,\Omega^2\,(1-a)\,a'\,r^3\,dr$$

or

$$\frac{P}{\pi\,R^2\,\varrho\,V^3} = \frac{4}{X^2}\int_0^X (1-a)\,a'\,x^3\,dx \tag{2.8}$$

where

$$X = \frac{\Omega\,R}{V} \tag{2.9}$$

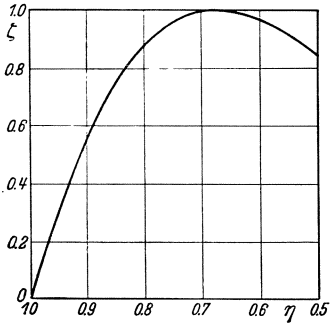

Fig. 99.

TABLE 33.

a	η	ζ	$P/\pi\,R^2\,\varrho\,V^3$
0	1.00	0	0
0.05	0.95	0.305	0.090
0.10	0.90	0.547	0.162
0.15	0.85	0.732	0.217
0.20	0.80	0.864	0.256
0.25	0.75	0.949	0.281
0.30	0.70	0.992	0.294
0.35	0.65	0.998	0.296
0.40	0.60	0.972	0.288
0.45	0.55	0.919	0.272
0.50	0.50	0.844	0.250

In order to obtain maximum power for a given speed ratio X the factors a and a' must be related by the equation

$$(1-a)\,\frac{d\,a'}{d\,a} = a'$$

while (2.2) gives also $(1+2\,a')\,x^2\,\frac{d\,a'}{d\,a} = 1-2\,a$

and hence

$$(1+2\,a')\,a'\,x^2 = (1-a)\,(1-2\,a) \tag{2.10}$$

Combining with (2.2)

$$\frac{1+2\,a'}{1+a'} = \frac{1-2\,a}{a}$$

or

$$a' = \frac{1-3\,a}{4\,a-1} \tag{2.11}$$

and then substituting back in either of (2.2) or (2.10)

$$a'\,x^2 = (1-a)\,(4\,a-1) \tag{2.12}$$

These last two equations determine the variation of the factors a and a' with the coordinate x along the blade of the windmill. This relationship is given in Table 34. For large values of x the factor a is slightly less than 1/3 and a' is very small, and for small values of x the factor a decreases to 1/4 and a' increases rapidly. Inserting these values of the interference factors in (2.8) the power given by the windmill can be

derived by graphical integration. The values of the power coefficient and of the ratio ζ of the power to the maximum possible power are given in Table 35 and the relationship between ζ and the speed ratio X is also shown in Fig. 100. In order to obtain a large fraction of the possible power it is necessary that $\Omega R/V$ shall not be too small. The speed ratio used in practice ranges from 1 to 4, and in this range the ratio ζ increases from 0.70 to 0.95.

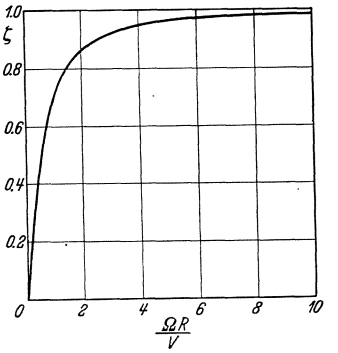

Fig. 100.

TABLE 34.

a	a'	$a' x^2$	x
0.26	5.500	0.0296	0.073
0.27	2.375	0.0584	0.157
0.28	1.333	0.0864	0.255
0.29	0.812	0.1136	0.374
0.30	0.500	0.1400	0.529
0.31	0.292	0.1656	0.753
0.32	0.143	0.1904	1.15
0.33	0.031	0.2144	2.63

TABLE 35.

$\Omega R/V$	ζ	$P/\pi R^2 \varrho V^3$	$\Omega R/V$	ζ	$P/\pi R^2 \varrho V^3$
0.5	0.486	0.144	2.5	0.899	0.266
1.0	0.703	0.208	5.0	0.963	0.285
1.5	0.811	0.240	7.5	0.983	0.291
2.0	0.865	0.256	10.0	0.987	0.292

Consider next the aerodynamic force on the blades of the windmill. The velocity experienced by the typical blade element has the components $V(1-a)$ and $\Omega r(1+a')$ as shown in Fig. 101 and, ignoring still the profile drag of the blades, the elements of drag and torque are

$$\left.\begin{aligned} \frac{dD}{dr} &= \frac{1}{2} B c \varrho W^2 C_L \cos\varphi \\ \frac{dQ}{dr} &= \frac{1}{2} B c r \varrho W^2 C_L \sin\varphi \end{aligned}\right\} \qquad (2.13)$$

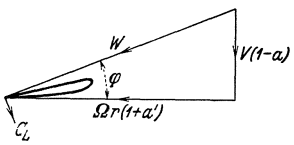

Fig. 101.

where

$$\tan\varphi = \frac{1-a}{1+a'}\frac{V}{\Omega r} \qquad (2.14)$$

Comparing these formulae with the previous momentum equations (2.1), the interference factors a and a' are obtained as

$$\left.\begin{aligned} \frac{a}{1-a} &= \frac{\sigma C_L \cos\varphi}{4\sin^2\varphi} \\ \frac{a'}{1+a'} &= \frac{\sigma C_L}{4\cos\varphi} \end{aligned}\right\} \qquad (2.15)$$

where $$\sigma = \frac{B c}{2 \pi r} \tag{2.16}$$

and eliminating a and a' from (2.14) by means of these formulae

$$x (4 \sin^2 \varphi + \sigma C_L \cos \varphi) = \sin \varphi (4 \cos \varphi - \sigma C_L) \tag{2.17}$$

In order to obtain maximum power under given conditions of operation the factors a and a' must be related by (2.11). After substituting from (2.15) this condition can be reduced to

$$\sigma C_L = 4 (1 - \cos \varphi) \tag{2.18}$$

and then combining with the previous (2.17)

$$x = \frac{\sin \varphi (2 \cos \varphi - 1)}{(1 + 2 \cos \varphi)(1 - \cos \varphi)} \tag{2.19}$$

This equation determines the optimum variation of the angle φ along the blade of a windmill, and (2.18) determines the corresponding values

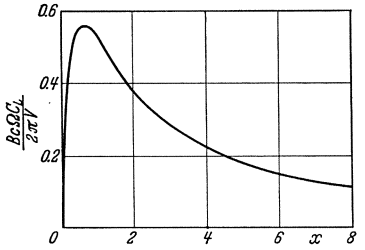

Fig. 102.

TABLE 36.

φ	x	$\frac{Bc\Omega}{2\pi V} C_L$	φ	x	$\frac{Bc\Omega}{2\pi V} C_L$
60°	0	0	20°	1.73	0.418
50	0.35	0.497	15	2.42	0.329
40	0.62	0.556	10	3.73	0.228
30	1.00	0.536	5	7.60	0.116

of σC_L. The analysis does not determine the shape of the blade uniquely but only the product of the chord and lift coefficient in the form

$$\frac{B c \Omega C_L}{2 \pi V} = x \sigma C_L = \frac{4 \sin \varphi (2 \cos \varphi - 1)}{1 + 2 \cos \varphi} \tag{2.20}$$

Table 36 gives the numerical values determined by these equations, and the relationship is also shown graphically in Fig. 102. This curve represents the shape of the blade if the blade angles are adjusted to give a constant lift coefficient. For a slow running windmill, whose blade tip is represented by $x = 1$, the chords should increase outward along the blade, but for a fast running windmill, whose blade tip is represented by $x = 4$, the chords should decrease outward along the blade except in the innermost quarter of the blade.

The total blade area S of the windmill is also defined by (2.20) if the lift coefficient has a constant value along the blade. This area is

$$S = \int_0^R B c \, dr$$

$$= \frac{2 \pi V^2}{\Omega^2 C_L} \int_0^X \frac{B c \Omega C_L}{2 \pi V} \, dx$$

and hence the solidity of the windmill is

$$\sigma_0 = \frac{S}{\pi R^2} = \frac{2}{X^2 C_L} \int_0^X \frac{B c \Omega C_L}{2 \pi V} d x$$

Numerical values of $\sigma_0 C_L$ are given in Table 37 and these are the values of the solidity when the lift coefficient C_L is unity. The solidity increases from roughly 0.2 for a fast running windmill ($X = 4$) to 1.0 for a slow running windmill ($X = 1$). Thus the fast running windmill will resemble an ordinary propeller with rather wide blades, while the slow running windmill must have a large number of blades with large blade angles.

TABLE 37.

$X =$	1	2	3	4	5
$\sigma_0 C_L =$	0.98	0.48	0.29	0.19	0.14

3. Windmill Characteristics. The discussion of the preceding section has indicated the performance which may be expected from ideal windmills of different type, but in practice the characteristics of a windmill are modified in an important manner by the frictional drag of its blades. The performance of any windmill can be calculated by the standard method used for a propeller if due allowance is made for the change of sign of the axial and rotational interference factors, or alternatively an approximate estimate can be made of the loss of power due to the profile drag of the blades by means of the analysis developed in Chapter IV. The appropriate equation for a windmill is

$$E = \sigma_0 \delta \pi R^2 \varrho \Omega^3 R^3 (1 + a')^3 f(\varphi_1) \tag{3.1}$$

where

$$\tan \varphi_1 = \frac{V}{\Omega R} \frac{1 - a}{1 + a'}$$

and σ_0 is the ratio of the total blade area to the disc area of the windmill. The values of $f(\varphi_1)$ are given in Table 5. As a rough approximation the interference factors a and a' may be neglected in this equation and the approximate expression for the loss of power due to the profile drag of the blades then becomes

$$\frac{E}{\pi R^2 \varrho V^3} = \sigma_0 \delta X^3 f\left(\frac{1}{X}\right) \tag{3.2}$$

where X denotes $\Omega R/V$. Assuming δ to be 0.01 and taking the values of the solidity from Table 37 for a lift coefficient C_L of 0.8, the numerical values of the loss of power are derived as in Table 38 and these typical numerical values suggest that the loss of power due to the profile drag of the blades is roughly proportional to the speed ratio X at which the windmill is designed to operate.

TABLE 38.

X	$f\left(\frac{1}{X}\right)$	$E/\pi R^2 \varrho V^3$
2	0.488	0.023
3	0.345	0.034
4	0.302	0.046
5	0.282	0.062

No systematic series of experiments are available to test the accuracy of these theoretical calculations, but Fig. 103 shows the observed performance of two typical model windmills[1] compared with the ideal curve of Fig. 100. The fast running windmill gives 75 per cent of the maximum possible power at its best operating condition and the efficiency of the windmill is 52-$^1/_2$ per cent. The corresponding values for the slow running windmill are 60 per cent of the maximum possible power and 29 per cent efficiency. Thus a fast running windmill is to be preferred, particularly for use on an airplane where the efficiency is important, but the slow running windmill may be more suitable on the ground since it has a larger starting torque, owing to its larger blade angles and blade area, and will therefore operate in lighter winds.

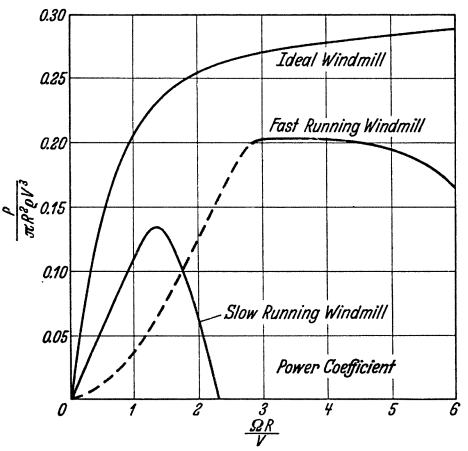

Fig. 103.

Model tests of windmills are not completely satisfactory since the models cannot reproduce correctly all the minor details of the system and since the results may suffer from an important scale effect. Full scale tests on the other hand are almost impossibly difficult owing to fluctuations of the wind velocity which cannot be accurately determined. The power delivered by a windmill depends on the cube of the velocity and the instrument which measures the mean velocity is quite unsuitable for determining the performance of a windmill. No reliance can therefore be placed on full scale tests unless they are based on a continuous record of the fluctuations of the wind velocity, but such tests as are available[2] seem to confirm the conclusions of the preceding general analysis.

4. The Lifting Windmill. A windmill used to generate power operates with its plane of rotation at right angles to its direction of motion relative to the air, but a windmill can also be used for sustentation in place of the wings of a conventional airplane if its plane of rotation is inclined at a small angle to the direction of motion. The proposal to use a windmill for sustentation is due to J. de la Cierva[3], and the application of this

[1] Ergebnisse der Aerodynamischen Versuchsanstalt zu Göttingen, III. Lief., p. 139.

[2] The Use of Windmills for the Generation of Electricity. Inst. Agric. Eng., Univ. of Oxford, Bull. No. 1, 1926.

[3] The Development of the Autogyro. Journal of the Royal Aeronautical Society, Vol. 30, p. 8, 1926.

idea has led to a novel type of aircraft which possesses several valuable features but is inferior in general performance to an airplane with fixed wings. No attempt will be made to discuss the special qualities of the aircraft, which lie outside the domain of airscrew theory, and the following analysis is confined to the determination of the characteristics of a lifting windmill.

A lifting windmill resembles in form a propeller of very low pitch with small blade angles, but it operates as a windmill, since its rotation is maintained solely by its translational motion through the air. The angle of incidence i of the windmill may be defined as the angle at which the axis is inclined backwards from the normal to the direction of motion, and the windmill may operate at any angle of incidence from a very small lower limit up to 90^0. The angular velocity Ω of the windmill is determined as a function of the translational velocity V and of the angle of incidence i by the condition that the torque Q about its axis is zero. The force experienced by the windmill may be expressed by the thrust T along its axis and by the normal component H, or alternatively by the lift L and the drag D as shown in Fig. 104. The appropriate non-dimensional coefficients which describe the characteristics of the windmill are defined by the equations

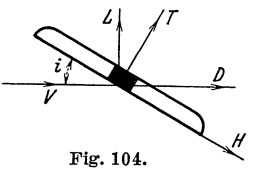

Fig. 104.

$$\left.\begin{aligned} \lambda &= \frac{V}{\Omega R} \\ T &= T_c \pi R^2 \varrho \Omega^2 R^2 \\ H &= H_c \pi R^2 \varrho \Omega^2 R^2 \\ Q &= Q_c \pi R^2 \varrho \Omega^2 R^3 \end{aligned}\right\} \tag{4.1}$$

but the lift and drag are expressed more suitably in terms of the translational velocity V instead of the tip speed ΩR, and hence

$$\left.\begin{aligned} L &= \frac{1}{2} C_L \pi R^2 \varrho V^2 \\ D &= \frac{1}{2} C_D \pi R^2 \varrho V^2 \end{aligned}\right\} \tag{4.2}$$

These lift and drag coefficients are related to the previous coefficients by the equations

$$\left.\begin{aligned} \tfrac{1}{2} \lambda^2 C_L &= T_c \cos i - H_c \sin i \\ \tfrac{1}{2} \lambda^2 C_D &= T_c \sin i + H_c \cos i \end{aligned}\right\} \tag{4.3}$$

The analysis of the performance of a lifting windmill[1] resembles very closely the analysis for the horizontal motion of a helicopter which

[1] Glauert, H., A General Theory of the Autogyro. Br. A.R.C. R. and M. 1111, 1926.

Lock, C. N. H., Further Development of Autogyro Theory. Br. A.R.C. R. and M. 1127, 1927.

is developed in Chapter X, the only important difference being that the axial velocity of the air through the disc of the airscrew is upwards for the windmill and downwards for the helicopter. This axial velocity u will be assumed to be constant over the whole disc and will be expressed non-dimensionally by the equation

$$\mu = \frac{u}{\Omega R} \tag{4.4}$$

The analysis for the aerodynamic force on the blades of a helicopter in horizontal motion can then be applied directly to the lifting windmill if the sign of μ is changed and if λ is replaced by $\lambda \cos i$ to represent the component of the translational velocity normal to the axis of the airscrew.

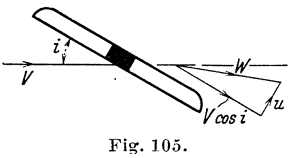

Fig. 105.

The equation for the induced velocity caused by the airscrew also needs reconsideration. The thrust of the windmill causes an induced velocity v normal to the plane of rotation, and hence the axial velocity u through the disc is

$$u = V \sin i - v$$

In accordance with the previous discussion of X **5**, the induced velocity will be determined by the equation

$$T = 2\pi R^2 \varrho \, W v$$

where W is the resultant of the components u and $V \cos i$ as shown in Fig. 105. Hence

$$T = 2\pi R^2 \varrho \, (V \sin i - u) \sqrt{u^2 + V^2 \cos^2 i}$$

or

$$\lambda \sin i = \mu + \frac{T_c}{2\sqrt{\mu^2 + \lambda^2 \cos^2 i}} \tag{4.5}$$

and this relationship replaces X (5.3) which was obtained for a helicopter.

The analysis is simplest if the windmill is assumed to be a rigid airscrew, but, as with a helicopter, there is then a rolling moment on the aircraft. The appropriate formulae are derived at once from X (6.1), (6.3), and (6.5) and are

$$\left.\begin{aligned} T_c &= \sigma\left[\theta\left(1 + \tfrac{3}{2}\lambda^2 \cos^2 i\right) + \tfrac{3}{2}\mu\right] \\ Q_c &= \tfrac{1}{4}\sigma\delta\,(1 + \lambda^2 \cos^2 i) - \sigma\mu\left(\theta + \tfrac{3}{2}\mu\right) \\ H_c &= \tfrac{1}{2}\sigma\,(\delta - 3\mu\theta)\,\lambda \cos i \end{aligned}\right\} \tag{4.6}$$

Since the torque of the lifting windmill is essentially zero, the relationship between μ and $\lambda \cos i$ is determined by the equation

$$\tfrac{1}{4}\delta\,(1 + \lambda^2 \cos^2 i) = \mu\left(\theta + \tfrac{3}{2}\mu\right) \tag{4.7}$$

Starting with a series of values of $\lambda \cos i$, for given values of θ and δ, this equation determines the corresponding values of μ. Equations (4.6) then determine the values of T_c and H_c, and (4.5) determines the angle of incidence i. Finally the lift and drag coefficients are derived from (4.3). A typical numerical solution of this system of equations is given in Table 39 and the lift and drag coefficients are plotted in Fig. 106. The calculation extends from an angle of incidence of 45° down to the angle at which the speed ratio λ is 0.5. Below this angle the approximations of the analysis cease to be valid, and above an angle of incidence of 45° the analysis is also unsatisfactory. The curve shows that the lift coefficient increases linearly with the angle of incidence at small angles and reaches a maximum value in the neighborhood of 40°. The drag is low at small angles of incidence but then increases rapidly and becomes equal to the lift at an angle of 45°.

TABLE 39. Rigid Windmill.

$\theta = 2^0$, $\sigma = 0.20$, $\delta = 0.006$					
i	λ	μ	T_c	C_L	C_D
4.9°	0.502	0.0256	0.0172	0.136	0.013
9.1	0.304	0.0234	0.0149	0.319	0.054
16.2	0.208	0.0226	0.0142	0.628	0.186
24.5	0.165	0.0224	0.0139	0.930	0.429
33.3	0.144	0.0223	0.0138	1.120	0.742
41.8	0.134	0.0222	0.0137	1.138	1.020
46.9	0.132	0.0221	0.0137	1.080	1.160

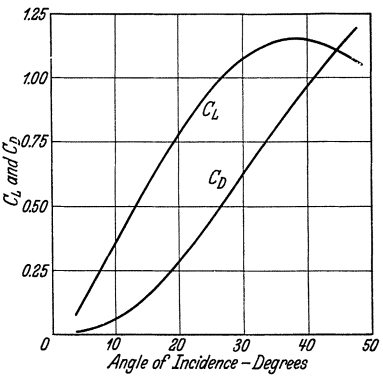

Fig. 106.

Owing to the fact that a rigid airscrew experiences a rolling moment, it is necessary to adopt a device similar to that suggested for a helicopter and to incorporate in the design a periodic variation of the blade angle, or to hinge the blades freely at their roots and to allow them to flap up and down under the action of the aerodynamic forces. The appropriate equations for periodic variation of the blade angle can be derived from the equations of X 7 by changing the sign of μ and by writing $\lambda \cos i$ in place of λ. In particular the equation for the coefficient H_c becomes

$$H_c = \frac{1}{2}\sigma(\delta - 3\theta_0\mu)\lambda \cos i + \frac{3}{4}\sigma\theta_1\mu$$

and there is therefore an increase of this force over that for the rigid windmill which leads to a corresponding increase of the drag. The drag is increased still further if the device of flapping blades is used, and the maximum lift-drag ratio of a lifting windmill with flapping blades does not exceed 8 for reasonable values of the solidity and of the profile drag coefficient of the blades.

Experimental results for lifting windmills through a large range of angle of incidence are rather scanty, and tests of small scale models are subject to an important scale effect, since a comparatively small increase of the profile drag coefficient of the blades exerts an important influence on the condition of operation of the windmill. Figure 107 shows the result of one test[1] of a small model windmill with flapping blades. The results are inferior to the calculated values of Fig. 106 owing to the small scale of the test and to the flapping motion of the blades, but they clearly indicate that the theory is a satisfactory explanation of the general behavior of a lifting windmill.

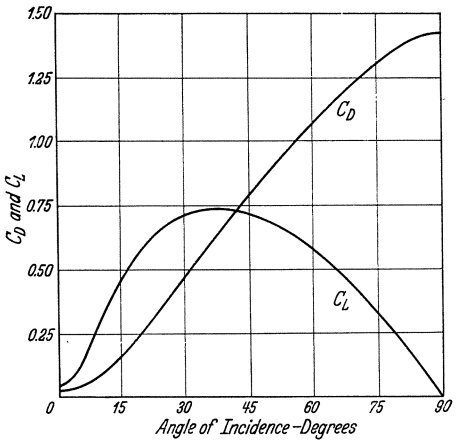

Fig. 107.

5. Windmill Anemometer. A freely rotating windmill can be used to measure the velocity of a current of air. Ignoring any friction of the bearings, the airscrew will run at the value of $V/\Omega R$ at which the torque is zero, and hence the rate of rotation is directly proportional to the air speed. Any propeller or windmill can be used in this manner, but in order to obtain satisfactory operation it is desirable that the airscrew shall respond rapidly to any changes of the air speed, and this condition can be used to determine the most suitable form of anemometer.

If a propeller is operating near the condition of zero torque, the torque coefficient may be expressed approximately as

$$Q_c = \frac{d\,Q_c}{d\,\lambda}(\lambda - \lambda_1)$$

where

$$Q = Q_c\,\pi\,R^2\,\varrho\,\Omega^2\,R^3$$

and

$$\lambda = \frac{V}{\Omega\,R}$$

and λ_1 is the value of λ at which the torque is zero. The torque of a propeller is positive when it opposes the rotation of the propeller, and the torque coefficient decreases as the speed ratio λ increases, so that $\frac{d\,Q_c}{d\,\lambda}$ is negative. In an air stream of varying speed the equation of motion of the anemometer will be

$$I\,\frac{d\,\Omega}{d\,t} = -Q = -\pi\,R^2\,\varrho\,\Omega^2\,R^3\,\frac{d\,Q_c}{d\,\lambda}(\lambda - \lambda_1)$$

[1] Caygill, L. E., and Nutt, A. E. W., Wind Tunnel and Dropping Tests of Autogyro Models. Br. A.R.C. R. and M. 1116, 1926.

where I is the moment of inertia about the axis of rotation. This equation can be expressed in the form

$$\frac{1}{\Omega}\frac{d\Omega}{dt} = a(V - k\Omega) \tag{5.1}$$

where

$$\left.\begin{aligned} a &= -\frac{\pi R^4 \varrho}{I}\frac{dQ_c}{d\lambda} \\ k &= R\lambda_1 = \left(\frac{V}{\Omega}\right)_1 \end{aligned}\right\} \tag{5.2}$$

The coefficient k is the calibration constant of the anemometer and the speed recorded in steady motion is

$$W = k\Omega \tag{5.3}$$

The equation of motion, (5.1), may therefore be taken to be

$$\frac{1}{W}\frac{dW}{dt} = a(V - W) \tag{5.4}$$

and this equation expresses the relationship between the air speed V and the corresponding speed W recorded by the anemometer.

In a steady stream the angular velocity of the anemometer determines the speed, but the usual method of using the instrument is not to obtain instantaneous readings of the angular velocity but to record the number of revolutions in a definite interval of time. Thus the anemometer is virtually an air log which records the distance travelled through the air, and the speed is derived by dividing this distance by the time interval of the measurement. In a stream of varying velocity the distance recorded by the anemometer is

$$r = \int_0^t W\,dt$$

whereas the true distance is

$$s = \int_0^t V\,dt$$

and by virtue of (5.4)

$$\begin{aligned} s &= \int_0^t \left(W + \frac{1}{aW}\frac{dW}{dt}\right) dt \\ &= r + \frac{1}{a}\Big[\log W\Big]_0^t \end{aligned}$$

or finally

$$\begin{aligned} s &= r + \frac{1}{a}\log\frac{W}{W_0} \\ &= r + \frac{1}{a}\log\frac{\Omega}{\Omega_0} \end{aligned} \tag{5.5}$$

This result shows that the difference between the true distance s and the recorded distance r depends only on the ratio of the initial and final angular velocities of the anemometer, and is independent of the intermediate conditions. In order to obtain accurate readings of a fluctuating velocity the coefficient a should be large and, by reference

to (5.2), it appears that the instrument should be of a light construction with a small value of I/R^4 and should have a rapid variation of torque coefficient with speed ratio. This second condition can be achieved by designing the anemometer with a large number of blades and with a high pitch-diameter ratio. The anemometer will then run at a low value of $\Omega R/V$ and is analogous to a slow running windmill. This form also has the advantage of a large starting torque and will therefore respond readily to low wind velocities.

The preceding discussion has ignored the frictional torque of the anemometer, but very similar conclusions can be derived when the frictional torque Q_F of the bearings is included in the analysis. The general equation of motion is now

$$I\frac{d\Omega}{dt} = -\pi R^2 \varrho \Omega^2 R^3 \frac{dQ_c}{d\lambda}(\lambda - \lambda_1) - Q_F$$

and if the frictional torque Q_F is proportional to the angular velocity Ω this equation may be written as

$$\frac{1}{\Omega}\frac{d\Omega}{dt} = a(V - k\Omega - \mu) \tag{5.6}$$

where

$$\mu = \frac{Q_F}{aI\Omega} \tag{5.7}$$

and the calibration of the anemometer is now

$$W = k\Omega + \mu \tag{5.8}$$

With this modification the distance travelled becomes

$$\begin{aligned} s &= \int_0^t V\,dt \\ &= \int_0^t \left(k\Omega + \mu + \frac{1}{a\Omega}\frac{d\Omega}{dt}\right)dt \\ &= \int_0^t W\,dt + \frac{1}{a}\log\frac{\Omega}{\Omega_0} \end{aligned}$$

or

$$s = r + \frac{1}{a}\log\frac{\Omega}{\Omega_0} \tag{5.9}$$

which is identical with the previous (5.5). It is clearly desirable that μ shall be small, and this is another reason for using an anemometer with a large number of blades and a high pitch-diameter ratio.

6. Fans. A fan is an airscrew which is used to produce a current of air and its mode of action is identical with that of a propulsive airscrew or propeller. The thrust of any type of airscrew is obtained by imparting momentum to the air which passes through its disc, and the distinction between a fan and a propeller is merely that attention is directed to the slipstream caused by the thrust rather than to the thrust itself.

An ordinary ventilating fan operates at a fixed point in the air and its characteristics may therefore be calculated by the usual theory of a propeller at zero rate of advance or of the helicopter airscrew, but the most suitable form for the fan depends on whether it is desired to obtain a large flow of air or to obtain a high speed in the slipstream. In either case the suitability of the fan can be expressed in terms of the figure of merit M which was introduced in the study of the helicopter airscrew and defined by the equation

$$M = \frac{T}{P}\sqrt{\frac{T}{\pi R^2 \varrho}} \tag{6.1}$$

If u is the mean axial velocity through the disc of the airscrew, the momentum equation for the thrust is

$$T = 2\pi R^2 \varrho u^2 \tag{6.2}$$

and the rate of flow of air down the slipstream is

$$F = \pi R^2 u \tag{6.3}$$

Eliminating the thrust and the axial velocity from these equations, the flow is obtained as a function of the power, disc area and figure of merit, in the form

$$F = \frac{1}{\sqrt{2}}\left(\frac{PM}{\varrho}\right)^{\frac{1}{3}} (\pi R^2)^{\frac{2}{3}} \tag{6.4}$$

and similarly the mean axial velocity through the disc of the fan can be expressed in the form

$$w = \frac{1}{\sqrt{2}}\left(\frac{PM}{\pi R^2 \varrho}\right)^{\frac{1}{3}} \tag{6.5}$$

In order to obtain a large flow of air the fan should have a large disc area and a high figure of merit, but in order to obtain a high speed the disc area should be small. Since the fan operates under the same conditions as a helicopter airscrew, the most suitable design to obtain a high figure of merit can be derived from the analysis given in Chapter X.

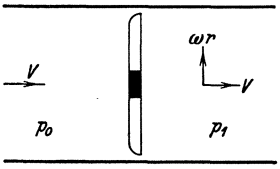

Fig. 108.

Different conditions of operation occur when a fan is used to maintain the flow of air in a wind tunnel. Assuming a cylindrical tunnel of constant radius with a uniform axial velocity V, the conditions of operation differ from those of a ventilating fan or of a propeller, since there can be no acceleration of the air behind the fan. The thrust of the fan appears solely as an increase of pressure, while the torque of the fan produces a rotation of the stream in the same sense as the rotation of the fan. Far in front of the fan there is a uniform axial velocity V and a uniform pressure p_0. Behind the fan there is the same axial velocity V with an angular velocity ω and a pressure p_1 which

vary with the radius r. The pressure in this wake is governed by the equation

$$\frac{dp_1}{dr} = \varrho\,\omega^2 r \tag{6.6}$$

and the elements of thrust and torque of the fan are respectively

$$\frac{dT}{dr} = 2\pi r\,(p_1 - p_0) \tag{6.7}$$

and

$$\frac{dQ}{dr} = 2\pi\varrho\,V\,\omega\,r^3 \tag{6.8}$$

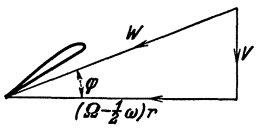

Fig. 109.

If Ω is the angular velocity of the fan, the velocity experienced by the typical blade element at the radius r is the resultant of an axial component V and a rotational component $\left(\Omega - \frac{1}{2}\omega\right) r$. Neglecting the profile drag of the blades and assuming a circulation K around the blade element, the thrust and torque of the fan are respectively

$$\frac{dT}{dr} = B\,K\,\varrho\left(\Omega - \frac{1}{2}\omega\right) r$$

$$\frac{dQ}{dr} = B\,K\,\varrho\,Vr \tag{6.9}$$

and by comparison with the previous equations (6.7) and (6.8) the circulation is

$$K = \frac{2\pi\omega r^2}{B} \tag{6.10}$$

and the increase of pressure is

$$p_1 - p_0 = \varrho\left(\Omega - \frac{1}{2}\omega\right)\omega r^2 \tag{6.11}$$

Also the increase of total pressure head behind the fan is

$$\begin{aligned} H_1 - H_0 &= p_1 + \tfrac{1}{2}\varrho\,\omega^2 r^2 - p_0 \\ &= \varrho\,\Omega\,\omega\,r^2 \end{aligned} \tag{6.12}$$

Returning now to (6.6) and substituting for the pressure from (6.11)

$$\begin{aligned} \omega^2 r &= \frac{d}{dr}\left[\left(\Omega - \frac{1}{2}\omega\right)\omega r^2\right] \\ &= 2\left(\Omega - \frac{1}{2}\omega\right)\omega r + (\Omega - \omega)\,r^2\frac{d\omega}{dr} \end{aligned}$$

or

$$(\Omega - \omega)\left[2\omega r + r^2\frac{d\omega}{dr}\right] = 0$$

and since ω is essentially less than Ω

$$r^2\frac{d\omega}{dr} + 2\omega r = 0$$

or

$$\omega r^2 = \text{constant} = k \tag{6.13}$$

Equations (6.10) and (6.12) then show that the circulation must be constant along the blades of the fan and that there is a uniform increase of total pressure head throughout the wake.

If the fan is designed to have constant circulation along the blades, the power absorbed by the fan is obtained at once from (6.8) as

$$P = \Omega Q = \pi R^2 \varrho V \Omega k$$

and hence the increase of total pressure head behind the fan is

$$H_1 - H_0 = \varrho \Omega k = \frac{P}{\pi R^2 V} \tag{6.14}$$

In practice the behavior of a wind tunnel fan deviates from the ideal conditions represented by the preceding analysis owing to the profile drag of the blades which constitute the only source of loss of energy, and the effect of this profile drag can be estimated for any fan by applying the methods of the standard propeller theory. An approximate estimate of the loss of energy can also be derived by the method developed in IV 2. Ignoring the small rotational motion of the wake and assuming $V/\Omega R$ to be small, the approximate expression for the loss of energy is

$$E = \frac{1}{8} C_D S \varrho \Omega^3 R^3 \tag{6.15}$$

where S is the total blade area and C_D is the mean profile drag coefficient of the blades, and economy of power is thus obtained by reducing the tip speed of the fan and by using a fan of relatively large solidity and high pitch.

CHAPTER XII

MISCELLANEOUS AIRSCREW PROBLEMS

1. Tandem Propellers. When an airplane is driven by a large number of engines it is often convenient to mount the engines in pairs one behind the other, and the propellers driven by these engines then form a *tandem* system. The rear propeller operates wholly or partly in the slip-stream of the front propeller, and the behavior of the front propeller is also modified by the indraught caused by the rear propeller. If the axial distance between the two propellers is very small, the tandem system is equivalent to a single propeller absorbing the total power of the two engines and the efficiency of the system can be calculated by the usual methods. In order to obtain a rough estimate of the loss of efficiency due to the use of a tandem system of propellers, Table 40 gives the ideal efficiency according to the axial momentum theory for a single propeller (η) and for a tandem system (η') absorbing double the power through the same disc area S. The appropriate values of the efficiency can be derived from the equation [see II (3.11)],

TABLE 40.

$P/S\varrho V^3$	η	η'	$\eta - \eta'$
0.2	0.922	0.870	0.052
0.4	0.870	0.797	0.073
0.6	0.829	0.748	0.081
0.8	0.797	0.712	0.085
1.0	0.771	0.682	0.089

$$\frac{P}{S \varrho V^3} = \frac{2(1-\eta)}{\eta^3} \tag{1.1}$$

or may be read from the curve of Fig. 11. The drop of ideal efficiency depends on the power loading but is of the order of 6 per cent in general.

Each member of a tandem system of propellers is usually driven by its own engine, but occasionally two propellers are mounted in close proximity on the same shaft and are driven by a single engine. The relative angular positions of these two propellers should then be adjusted so as to secure equal spacing of the blades relative to the air flow. If the two propellers were in the same plane, the blades would be equally spaced around the disc, but if the second propeller is at a small distance x behind the front propeller it is necessary to modify the relative angular positions of the two propellers in order to obtain the best results. In Fig. 110 two successive blade elements of the first propeller are shown at A_1 and A_2, and the lines L_1 and L_2 represent the flow relative to these blade elements. The blade element B_1 of the second propeller should be situated midway between the lines L_1 and L_2, and hence the angle ψ at which the blade element B_1 follows the blade element A_1 is determined by the equation

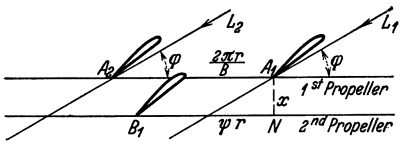

Fig. 110.

$$\psi r = \frac{\pi r}{B} + x \cot \varphi$$

where B is the number of the blades of each propeller. As a rough approximation

$$\tan \varphi = \frac{V}{\Omega r} = \frac{J R}{\pi r}$$

and hence

$$\psi = \frac{\pi}{B}\left(1 + \frac{B x}{J R}\right) \qquad (1.2)$$

The angular displacement of the two propellers from the position which they would occupy when rotating in the same plane is therefore $\frac{\pi x}{J R}$, which is independent of the number of blades and of the radial co-ordinate r, but varies with the rate of advance of the propeller. The validity of this formula is confirmed by some experiments[1] with two propellers, each with two blades, at an axial distance $0.115\ R$ apart. The efficiency of the system at the rate of advance $J = 0.62$ for various values of the angle ψ were as follows:—

$\psi =$	0	45^0	90^0	135^0
$\eta =$	0.640	0.630	0.655	0.645

According to the formula (1.2) the highest efficiency should be obtained when $\psi = 123^0$ and the lowest efficiency when $\psi = 33^0$, and this prediction is consistent with the experimental results.

[1] Fage, A., and Collins, H. E., An Investigation of the Mutual Interference of Airscrew Blades. Br. A.R.C. R. and M. 316, 1917.

Hitherto the two propellers of the tandem system have been assumed to be in close proximity, but more generally the propellers are separated by a distance of the order of the propeller diameter. If the propellers are separated by a large distance and if the rear propeller operates wholly in the slipstream of the front propeller, it is possible to obtain simple expressions for the efficiency of the tandem system. With this wide separation the front propeller does not experience any interference, but the rear propeller operates in a region of increased velocity and hence has a lower efficiency. An ideal system of this type is shown in Fig. 111. The front propeller has a disc area S_1 and the rear propeller has a smaller disc area S_2 in order to fit into the slipstream of the front propeller. The axial velocity V increases to u at the disc of the first propeller and to V' in its wake; the second propeller operates effectively in a stream of velocity V' and the velocity rises to u' at its disc. The ideal efficiency of the front propeller according to the axial momentum theory is determined by the equation

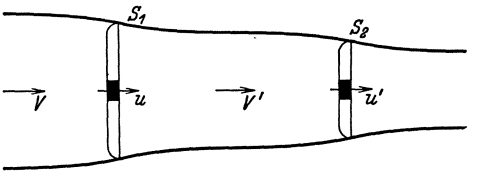

Fig. 111.

$$\frac{P}{S_1 \varrho V^3} = \frac{2(1-\eta_1)}{\eta_1^3} \tag{1.3}$$

and the fundamental equation for the rear propeller, assumed to absorb the same power P, is

$$P = u' T_2 = 2 \varrho S_2 u'^2 (u' - V')$$

The efficiency of the propeller is

$$\eta_2 = \frac{V T_2}{P} = \frac{V}{u'}$$

and hence

$$\frac{P}{S_2 \varrho V^3} = \frac{2}{\eta_2^2}\left(\frac{1}{\eta_2} - \frac{V'}{V}\right) \tag{1.4}$$

But

$$u = \frac{1}{2}(V + V')$$

and

$$u S_1 = u' S_2$$

or

$$\frac{S_1}{\eta_1} = \frac{S_2}{\eta_2}$$

and on eliminating S_2 and V' from (1.4) by means of these relationships, the equation for the efficiency η_2 of the rear propeller is obtained in the form

$$\frac{P}{S_1 \varrho V^3} = \frac{2}{\eta_1 \eta_2}\left[\frac{1-\eta_2}{\eta_2} - \frac{2(1-\eta_1)}{\eta_1}\right] \tag{1.5}$$

Numerical values derived from (1.3) and (1.5) are given in Table 41 which shows that the efficiency of the rear propeller is much lower than that of the front propeller. The efficiency of the tandem system is the

arithmetic mean of the efficiencies η_1 and η_2, and corresponds to the efficiency of a propeller of intermediate size absorbing the total power.

An improvement of the efficiency of the tandem system would be obtained by increasing the diameter of the rear propeller to that of the front propeller, but any estimate of the efficiency of the system is then complicated by the fact that the inner parts of the rear propeller experience the slipstream velocity V' of the front propeller while the outer parts experience the lower velocity V.

TABLE 41.

$P/S_1 \varrho V^3$	η_1	η_2	$\eta_1 - \eta_2$
0.2	0.922	0.804	0.118
0.4	0.870	0.704	0.166
0.6	0.829	0.637	0.192
0.8	0.797	0.589	0.208
1.0	0.771	0.554	0.217

Another method of improving the efficiency of a tandem system of propellers becomes apparent when the rotational motion of the slipstream is considered. The loss of efficiency due to this rotational motion has been considered in III 5; it depends on the torque coefficient of the propeller but is usually of the order of 2 per cent. This loss may be avoided in a tandem system if the two propellers rotate in opposite directions and if the torque distribution along the blades of the rear propeller is adjusted so as to be equal to that along the blades of the front propeller and to leave no rotational motion in the final wake.

When the distance between the two propellers is reduced, the front propeller experiences some interference owing to the acceleration of the air in front of the rear propeller, but at the same time the interference on the rear propeller is reduced since the slipstream velocity of the front propeller has not yet attained its full value. If the final wake behind the tandem system is unaltered, the efficiency of the system will also remain unaltered, but the separate efficiencies of the two propellers will differ less than is indicated by the numerical values of Table 41.

The characteristics of a tandem system, taking account of the profile drag of the blade elements, can be calculated by the standard methods of propeller theory, but unless the two propellers are widely spaced it is difficult to assign correct values to the mutual interference and therefore to design the propellers with the best blade angles. It is clear, however, that the rear propeller, which operates in a region of increased axial velocity, should be of higher pitch than the front propeller, and in order to absorb the same power the rear propeller must also have rather narrower blades.

2. Propeller with Stalled Blades. If a propeller has a high pitch-diameter ratio the angles of incidence at which the blade elements operate tend to rise above the critical angle at low rates of advance, and this fact constitutes a real difficulty in the use of propellers of

high pitch-diameter ratio, since the thrust of the propeller at low rates of advance may be insufficient to enable the airplane to take off from the ground or water. It is of some interest therefore to examine the behavior of a propeller whose blades are fully stalled.

When an airfoil is operating above its critical angle, the aerodynamic force experienced by the airfoil is approximately at right angles to the chord, and if this condition is assumed to occur on all the blade elements it is possible to obtain a simple relationship between the thrust and torque of the propeller. Let C_N be the normal force coefficient on the blade element, which experiences the effective velocity W as shown in Fig. 112. Then the expressions for the elements of thrust and torque of the propeller become simply

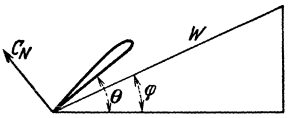

Fig. 112.

$$\frac{dT}{dr} = \frac{1}{2} B c \varrho W^2 C_N \cos\theta \tag{2.1}$$

and

$$\frac{dQ}{dr} = \frac{1}{2} B c r \varrho W^2 C_N \sin\theta \tag{2.2}$$

If now the propeller has constant geometrical pitch H along the blades, the blade angle θ is governed by the equation

$$2\pi r \tan\theta = H \tag{2.3}$$

and on substituting this relationship in (2.1) and (2.2) it appears that

$$H \frac{dT}{dr} = 2\pi \frac{dQ}{dr}$$

or after integration

$$\frac{HT}{Q} = 2\pi \tag{2.4}$$

This simple relationship for a propeller of constant pitch has been obtained on the sole assumption that the aerodynamic force on each blade element is normal to the chord, and it is quite independent of the diameter of the propeller, of the shape of the blades, and of the rate of advance. Since, however, the blades will be fully stalled only for a propeller of high pitch-diameter ratio operating at a low rate of advance, the formula is of value mainly as an estimate of the static thrust of a propeller of high pitch-diameter ratio. The torque of an engine is approximately constant under ordinary conditions of operation, and hence the formula (2.4) suggests that the static thrust which can be obtained from such an engine driving a propeller with stalled blades depends only on the pitch of the propeller and is not affected by any change of the diameter or solidity.

As a check on the validity of the formula (2.4), Fig. 113 shows the values of HT/Q at zero rate of advance for a series of propellers[1] plotted

[1] TOWNEND, H. C. H., WALKER, W. S., and WARSAP, J. H., Experiments with the Family of Airscrews in Free Air at Zero Advance. Br. A.R.C. R. and M. 1153, 1928.

against the pitch-diameter ratio. The value of HT/Q increases with the pitch-diameter ratio of the propeller to a maximum value depending on the solidity of the propeller, and then falls slowly. It would appear that the limiting value suggested by the theoretical formula (2.4) would be reached when the pitch-diameter ratio rose above the value 2.

3. Drag at Zero Torque. The propeller of an airplane normally provides the forward thrust which is necessary to maintain the motion of the airplane, but when the engine is switched off, the propeller itself experiences a drag which increases the drag of the airplane and increases its gliding angle. The drag of the propeller depends on the exact state of operation of the engine, but it is useful to have some standard of reference and this standard is provided conveniently by the condition of zero torque, which assumes that the engine is developing just enough power to overcome its own internal mechanical torque.

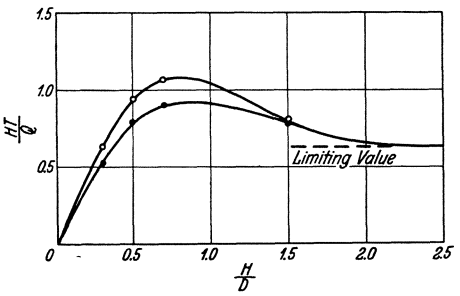

Fig. 113.

If the rotation of the propeller is stopped, the drag experienced by the propeller is approximately equal to that of a flat plate of the same projected area. Wind tunnel experiments with several model propellers have given drag coefficients ranging from 0.51 to 0.57 with a mean value of 0.55, and hence the drag coefficient of a stopped propeller may be taken to be

$$k_D = \frac{D}{\pi R^2 \varrho V^2} = 0.55\,\sigma \qquad (3.1)$$

where σ is the solidity of the propeller.

When a propeller is rotating at the condition of zero torque, the energy equation is

$$u\,D = E$$

where u is the axial velocity through the disc, and E is the energy absorbed by the profile drag of the blades. In this state of operation the axial interference velocity is very small and may be neglected in an approximate estimate of the drag of the propeller. On this basis the energy equation becomes

$$V\,D = E$$

and the loss of energy E is derived from the analysis of IV 2 as

$$E = \sigma\,\delta\,\pi\,R^2\,\varrho\,\Omega^3\,R^3\,f\,(\lambda)$$

where $f\,(\lambda)$ is a function of the speed ratio λ or $V/\Omega R$, and numerical values are as follows:—

$\lambda =$	0	0.10	0.20	0.30	0.40	0.50
$f\,(\lambda) =$	0.250	0.258	0.282	0.325	0.393	0.488

According to this analysis the drag coefficient of the propeller at zero torque will be

$$k_D = \frac{\sigma \delta f(\lambda)}{\lambda^3} \tag{3.2}$$

but in applying this formula it must be remembered that the coefficient δ may vary with the pitch-diameter ratio of the propeller. In order that the torque of a blade element shall be zero, the lift and drag coefficients of the element must satisfy the equation

$$C_L \sin\varphi + C_D \cos\varphi = 0$$

or approximately

$$C_L = -\frac{C_D}{\lambda}$$

The value of λ increases with the pitch-diameter ratio of the propeller, and the lift coefficient C_L becomes less negative. Now with ordinary airfoil sections the profile drag coefficient increases fairly rapidly as the lift coefficient becomes more negative, and thus it would appear that a high pitch-diameter ratio propeller will have a lower value of δ, which is the mean value of $1/2\, C_D$, than a low pitch propeller. This effect will tend to neutralize the increase of $f(\lambda)$ with the pitch of the propeller, and experimental results appear to suggest that in practice the product $\delta f(\lambda)$ is approximately constant.

In obtaining an empirical formula from experimental results it is convenient to use the value of $V/\Omega R$ corresponding to zero thrust rather than to zero torque, since the speed ratio at which the thrust vanishes is determined almost exactly by the pitch of the propeller blades measured from the no lift axes of the blade sections. Denoting this value of the speed ratio by λ_1, Table 42 gives the experimental values of $\lambda_1^3 k_D/\sigma$ for two series of model propellers[1]. It will be noticed that there is no systematic variation with the pitch of the propeller, and it is therefore sufficiently accurate to adopt the mean value defined by the equation

TABLE 42.

$B = 2$			$B = 4$		
λ_1	k_D	$\lambda_1^3 k_D/\sigma$	λ_1	k_D	$\lambda_1^3 k_D/\sigma$
0.214	0.0456	0.0056	0.212	0.0992	0.0059
0.282	0.0216	0.0061	0.280	0.0442	0.0061
0.379	0.0076	0.0052	0.377	0.0175	0.0059
0.550	0.0018	0.0038	0.553	0.0066	0.0070

$$k_D = \frac{0.0057\,\sigma}{\lambda_1^3} \tag{3.3}$$

or

$$k_D = \frac{0.175\,\sigma}{J_1^3} \tag{3.4}$$

The numerical value of this coefficient has, however, been derived from tests of model propellers and may be somewhat lower for full scale propellers.

[1] FAGE, A., HOWARD, R. G., and BATEMAN, H., Experiments with a Family of Airscrews. Br. A.R.C. R. and M. 829, 1922.

4. The Vortex Ring State of an Airscrew. The different states of operation of an airscrew were discussed briefly in Chapter I and are shown diagrammatically in Fig. 2, but the general aerodynamic theory has been developed essentially for a propulsive airscrew or propeller, and the possibility of applying the same system of equations to the other states of operation has been considered in VI 3. The development of the theory depends on the assumption that a true slipstream is formed behind the airscrew, and between the states of zero advance and of a high rate of negative advance of a propeller there exists a region in which this condition is not satisfied. If a propeller is moving backward slowly, the direction of the flow through the propeller disc will be in the same sense as at zero rate of advance and will be opposite to the direction of the general stream relative to the propeller. The propeller then operates in the vortex ring state, the air passing through the propeller disc and returning backward outside its circumference as shown in Fig. 114. When the speed of negative advance is increased, the direction of flow through the propeller disc is reversed, but a state of turbulence occurs before a true slipstream is again formed. The general equations of the propeller theory cannot be applied in the vortex ring state or in the turbulent state, since no true slipstream is formed and since the usual equations for the axial and rotational momentum cease to be valid. In fact no complete representation of the vortex ring state is possible without introducing the viscosity of the air by means of which the angular momentum of the rotating vortex core is transmitted to the general stream. No theory has been developed to explain the action of a propeller in these abnormal conditions, but it is possible to develop a semi-empirical method of analysis[1].

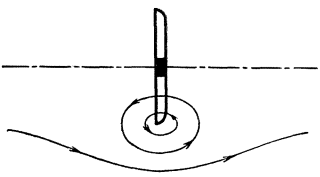

Fig. 114.

By considering the aerodynamic force on the blades, the element of thrust may be expressed as

$$\frac{dT}{dr} = 4\pi r \varrho u^2 F \tag{4.1}$$

where

$$F = \frac{Bc}{8\pi r} \frac{C_L \cos\varphi - C_D \sin\varphi}{\sin^2\varphi} \tag{4.2}$$

and

$$\tan\varphi = \frac{u}{\Omega r (1 - a')} \tag{4.3}$$

[1] LOCK, C. N. H., BATEMAN, H., and TOWNEND, H. C. H., An Extension of the Vortex Theory of Airscrews with Application to Airscrews of Small Pitch, Including Experimental Results. Br. A.R.C. R. and M. 1014, 1925.

GLAUERT, H., The Analysis of Experimental Results in the Windmill Brake and Vortex Ring States of an Airscrew. Br. A.R.C. R. and M. 1026, 1926.

In an approximate analysis the small rotational interference factor a' may be ignored, and with this simplification the above three equations determine the thrust of a propeller in terms of the axial velocity u through the propeller disc, but it is necessary to obtain another condition to relate this velocity u to the speed of advance V. If

$$\frac{dT}{dr} = 4\pi r \varrho V^2 f \tag{4.4}$$

the problem is in fact to determine a relationship between the velocities u and V, or between the coefficients F and f. In the usual propeller theory this relationship is derived from the axial momentum equation

$$\frac{dT}{dr} = 4\pi r \varrho u (u - V) \tag{4.5}$$

From (4.1) and (4.5) $V = u(1 - F)$

and then $$\frac{F}{f} = \frac{V^2}{u^2} = (1 - F)^2$$

or $$f = \frac{F}{(1-F)^2} \tag{4.6}$$

In order to extend this analysis to other states of operation in which a true slipstream is still formed, some special care is necessary with regard to the signs of the various quantities. The simplest method of generalising the analysis is to regard F and T as essentially positive, so that they represent the magnitude of the axial component of the force on the propeller irrespective of sign. The coefficient f is then also positive and the axial momentum equation must be expressed in the form[1]

$$\frac{dT}{dr} = 4\pi r \varrho |u(u - V)| \tag{4.7}$$

In the ordinary state of operation of a propeller the velocities u and V are both positive, and u is greater than V. Equation (4.7) is then identical with (4.5), and the relationship between the coefficients F and f is given by (4.6). When the propeller operates as a windmill the velocities u and V may both be positive or both negative, and u is numerically less than V. Thus (4.7) becomes

$$\frac{dT}{dr} = 4\pi r \varrho u (V - u)$$

and then by virtue of (4.1) and (4.4)

$$V = u(1 + F)$$

and $$f = \frac{F}{(1+F)^2} \tag{4.8}$$

The propeller relationship (4.6) is valid in the range of V from zero to u, or in the range of F from zero to unity. The windmill relationship (4.8) is valid in the range of V from u, which marks the transition from propeller

[1] Note that $|x|$ denotes the numerical value of x irrespective of sign.

to windmill, to 2 u, where the velocity in the final wake falls to zero and the slipstream breaks up into turbulence, and the corresponding range of F is again from zero to unity.

The relationships (4.6) and (4.8) are shown graphically by the full lines of Fig. 115, where $1/f$ is plotted against $1/F$ since this is the most convenient method of exhibiting the characteristics in the region of large values of F which represent the vortex ring and turbulent states of an airscrew. The broken curve of Fig. 115 represents an empirical extension of the characteristic curve in the region where the theory fails, and is based on the analysis of experimental tests of propellers at negative rates of advance. The extension of the windmill curve into the turbulent state is fairly well established since it is based on experiments in an open jet wind tunnel, but the form of the curve in the vortex ring state is less reliable; the experiments were made in a closed tunnel and the magnitude of the tunnel constraint is very uncertain.

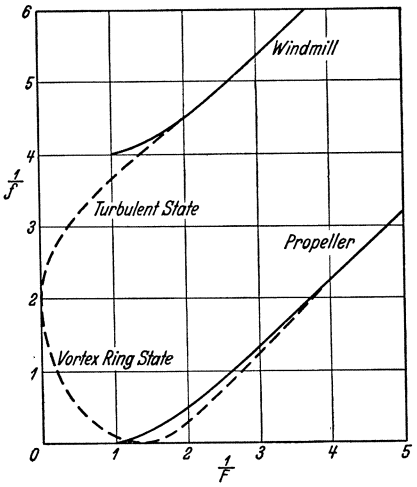

Fig. 115.

By means of the empirical characteristic curve of Fig. 115 it is possible to estimate the performance of an airscrew in any state of operation. Starting with any value of the axial velocity u through the airscrew disc, the value of the coefficient F is calculated from the aerodynamic characteristics of the blade element, the corresponding value of f is obtained from Fig. 115, and then the axial velocity V of the airscrew is calculated from the equation

$$V = u\sqrt{\frac{F}{f}} \tag{4.9}$$

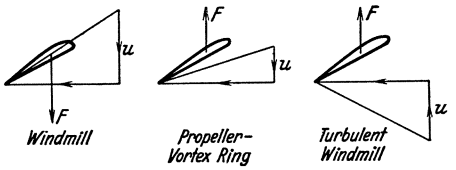

Fig. 116.

In order to decide whether the upper or the lower branch of the characteristic curve shall be used, it is sufficient to note that in the windmill and turbulent states F and u are of the same sense, and that in the propeller and vortex ring states they are of opposite senses. The possible combinations which occur in the different states of operation of an ordinary propeller are illustrated in Fig. 116. The velocity V is of the same sense as u in

every state of operation except the vortex ring state, in which V and u have opposite signs.

5. The Effect of Sideslip and Pitching. In the development of the general theory of a propeller it has been assumed that the forward motion of the propeller through the air is in the direction of the axis of rotation, but, as has been already stated in VIII 7, the propeller of an airplane can operate in this manner at one angle of incidence only, and more generally the axis of rotation is inclined at a small angle to the direction of motion. A similar effect occurs if the airplane is sideslipping; while in turns or rolls the propeller is subjected to an angular velocity which may also modify its behavior. It is necessary therefore to examine the influence of small lateral or angular velocities on the characteristics of a propeller. The theory[1] is developed in an approximate manner for small disturbances, and for more extreme conditions it is necessary to rely on experimental results.

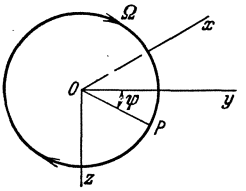

Fig. 117.

Consider a right handed propeller and choose the system of axes shown in Fig. 117 where the propeller is viewed from behind. The axis of x is taken forward along the axis of rotation, the axis of y to the right, and the axis of z downwards. Let OP represent one blade of the propeller at an angle ψ from Oy, and let the aerodynamic force on the typical element of this blade have the components $F\,dr$ parallel to the axis of x, and $G\,dr$ normal to the blade in the plane Oyz and in the sense to oppose the rotation of the propeller. Then the components of the resultant force and moment experienced by the propeller may be expressed as

$$\left.\begin{aligned} X &= \Sigma \int F\,dr & L &= -\Sigma \int G\,r\,dr \\ Y &= \Sigma \int G \sin\psi\,dr & M &= \Sigma \int F\,r \sin\psi\,dr \\ Z &= -\Sigma \int G \cos\psi\,dr & N &= -\Sigma \int F\,r \cos\psi\,dr \end{aligned}\right\} \qquad (5.1)$$

where the integration extends along the whole blade and the summation extends over all the blades of the propeller.

In uniform axial motion the thrust and torque of the propeller are respectively

$$\left.\begin{aligned} T &= X = B \int F\,dr \\ Q &= -L = B \int G\,r\,dr \end{aligned}\right\} \qquad (5.2)$$

More generally F and G are functions of the angular velocity of the blade element relative to the adjacent air and of the speed ratio λ, and

[1] HARRIS, R. G., Forces on a Propeller Due to Sideslip. Br. A.R.C. R. and M. 427, 1918.

GLAUERT, H., The Stability Derivatives of an Airscrew. Br. A.R.C. R. and M. 642, 1919.

are both of the form $\Omega^2 f(\lambda)$. The increments of F and G due to any small changes in the relative velocities can therefore be expressed in the form

$$\left.\begin{aligned} \delta F &= \frac{2F}{\Omega}\delta\Omega + \frac{\partial F}{\partial \lambda}\delta\lambda \\ \delta G &= \frac{2G}{\Omega}\delta\Omega + \frac{\partial G}{\partial \lambda}\delta\lambda \end{aligned}\right\} \tag{5.3}$$

In these expressions $\delta\Omega$ represents the increase of angular velocity of a blade element relative to the adjacent air and may be due either to a change of the angular velocity of the propeller or to a linear velocity at right angles to the blade in the plane of rotation. In the subsequent analysis the angular velocity of the propeller will be assumed to be constant, and the effects of any radial component of velocity along the blade will be ignored.

Consider now the effect of a velocity v of sideslip along the axis of y. The appropriate increments of Ω and λ are determined by the equations

$$r\,\delta\Omega = -v\sin\psi$$

and

$$\frac{\delta\lambda}{\lambda} = \frac{\delta V}{V} - \frac{\delta\Omega}{\Omega} = \frac{v\sin\psi}{\Omega r}$$

Hence according to (5.3)

$$\delta F = -\frac{2v\sin\psi}{\Omega r}\left(F - \frac{1}{2}\lambda\frac{\partial F}{\partial\lambda}\right)$$

or

$$\left.\begin{aligned} \delta F &= -\frac{2v\sin\psi}{\Omega r}\Delta F \\ \delta G &= -\frac{2v\sin\psi}{\Omega r}\Delta G \end{aligned}\right\} \tag{5.4}$$

where Δ denotes the differential operator defined by the equation

$$\Delta = 1 - \frac{1}{2}\lambda\frac{\partial}{\partial\lambda} \tag{5.5}$$

If $v X_v$ is the increment of the axial force due to sideslip and if similar expressions are used for the other force and moment components, (5.1) and (5.4) now lead to the expressions

$$\left.\begin{aligned} X_v &= -\Delta\Sigma\int\frac{2F\sin\psi}{\Omega r}dr & L_v &= \Delta\Sigma\int\frac{2G\sin\psi}{\Omega}dr \\ Y_v &= -\Delta\Sigma\int\frac{2G\sin^2\psi}{\Omega r}dr & M_v &= -\Delta\Sigma\int\frac{2F\sin^2\psi}{\Omega}dr \\ Z_v &= \Delta\Sigma\int\frac{2G\sin\psi\cos\psi}{\Omega r}dr & N_v &= \Delta\Sigma\int\frac{2F\sin\psi\cos\psi}{\Omega}dr \end{aligned}\right\} \tag{5.6}$$

If the propeller has more than two blades, the expressions involving $\sin\psi$ or $\sin\psi\cos\psi$ disappear after summation over all the blades and $\Sigma\sin^2\psi$ is equal to $1/2\,B$. If the propeller has only two blades, $\Sigma\sin\psi\cos\psi$ and $\Sigma\sin^2\psi$ contain certain periodic terms whose mean values during each revolution of the propeller are zero. These periodic terms are quite

unimportant and will be neglected in the subsequent analysis. On this basis the effect of sideslip as determined by (5.6), is to produce a lateral force derivative

$$Y_v = -\frac{B}{\Omega}\Delta \int \frac{G}{r}\,dr$$

and a pitching moment derivative

$$M_v = -\frac{B}{\Omega}\Delta \int F\,dr$$

By virtue of (5.2) this second expression can be evaluated at once as

$$M_v = -\frac{\Delta T}{\Omega} = -\frac{T}{\Omega}\left[1 - \frac{\lambda}{2\,T_c}\frac{d\,T_c}{d\,\lambda}\right] \tag{5.7}$$

but in order to evaluate the expression for Y_v it is necessary to know the form of G as a function of r. This evaluation is considered at a later stage of the analysis, and it appears that

$$B\int \frac{G}{r}\,dr = \frac{A_1 Q}{R^2}$$

or

$$Y_v = -\frac{A_1}{\Omega R^2}\Delta Q = -\frac{A_1 Q}{\Omega R^2}\left[1 - \frac{\lambda}{2\,Q_c}\frac{d\,Q_c}{d\,\lambda}\right] \tag{5.8}$$

where A_1 has the value given in Table 43.

If the sense of rotation of the propeller is reversed, the signs of Ω and Q must be changed, and then Y_v is unaltered but the sign of M_v is changed. The effect of sideslip may therefore be described by the statement that the propeller experiences a side force opposing the sideslip, and a pitching moment whose sign is determined by assuming the centroid of the thrust to move towards the point of the circumference where the blade tip is moving in the direction of the sideslip, since the sideslip increases the effective angular velocity of the blade at this point. The effect of a normal velocity w along the axis of z can be deduced directly from these preceding results. The propeller experiences a normal force opposing the normal velocity and a yawing moment due to a lateral displacement of the centroid of the thrust.

Turning next to the effect of an angular velocity q of pitch about the axis of y, the typical blade element shown in Fig. 116 experiences simply an increment of axial velocity

$$\delta V = qr\sin\psi$$

and hence $\delta\Omega$ is zero and $\dfrac{\delta\lambda}{\lambda} = \dfrac{qr\sin\psi}{V}$

Then from (5.3)

$$\left.\begin{aligned}\delta F &= \frac{qr\sin\psi}{V}\lambda\frac{\partial F}{\partial\lambda}\\ \delta G &= \frac{qr\sin\psi}{V}\lambda\frac{\partial G}{\partial\lambda}\end{aligned}\right\} \tag{5.9}$$

and the corresponding force and moment derivatives are obtained from (5.1) as

$$\left.\begin{aligned} X_q &= \lambda \frac{\partial}{\partial \lambda} \Sigma \int \frac{F r \sin\psi}{V} dr & L_q &= -\lambda \frac{\partial}{\partial \lambda} \Sigma \int \frac{G r^2 \sin\psi}{V} dr \\ Y_q &= \lambda \frac{\partial}{\partial \lambda} \Sigma \int \frac{G r \sin^2\psi}{V} dr & M_q &= \lambda \frac{\partial}{\partial \lambda} \Sigma \int \frac{F r^2 \sin^2\psi}{V} dr \\ Z_q &= -\lambda \frac{\partial}{\partial \lambda} \Sigma \int \frac{G r \sin\psi \cos\psi}{V} dr & N_q &= -\lambda \frac{\partial}{\partial \lambda} \Sigma \int \frac{F r^2 \sin\psi \cos\psi}{V} dr \end{aligned}\right\} \quad (5.10)$$

For a propeller with more than two blades the expressions involving $\sin\psi$ or $\sin\psi\cos\psi$ disappear after summation over all the blades, and the effect of the pitching of the propeller is simply to produce a lateral force derivative

$$Y_q = \frac{B\lambda}{2V} \frac{\partial}{\partial \lambda} \int G r dr$$

and a pitching moment derivative

$$M_q = \frac{B\lambda}{2V} \frac{\partial}{\partial \lambda} \int F r^2 dr$$

By virtue of (5.2) the lateral force derivative becomes

$$Y_q = \frac{\lambda}{2V} \frac{\partial Q}{\partial \lambda} = \frac{Q}{V} \left(\frac{\lambda}{2 Q_c} \frac{d Q_c}{d \lambda} \right) \quad (5.11)$$

Also the form of F as a function of r, which is discussed below, leads to an expression

$$B \int F r^2 dr = A_2 T R^2$$

and hence

$$M_q = \frac{A_2 R^2 \lambda}{2V} \frac{\partial T}{\partial \lambda} = \frac{A_2 T R^2}{V} \left(\frac{\lambda}{2 T_c} \frac{d T_c}{d \lambda} \right) \quad (5.12)$$

where A_2 has the values given in Table 43. Since Q_c and T_c both decrease as λ increases, these results show that the propeller experiences a lateral force in the direction of rotation of the blades where their forward velocity is increased by the pitching, and a pitching moment which opposes the pitching. Similar results can be deduced for the effect of an angular velocity of yawing, which produces a normal force and a yawing moment on the propeller.

In order to determine the values of the numerical coefficients A_1 and A_2 which have been introduced in the preceding analysis, it suffices to consider an ideal frictionless propeller with circulation around the blades defined by VII (2.3). Thus

$$K = K_0 \frac{x^2}{1 + x^2}$$

where

$$x = \frac{\Omega r}{V}$$

and K_0 is a constant along the blades of the propeller. Ignoring the small rotational component of the induced velocity, the thrust per unit length of the blade is

$$\frac{dT}{dr} = \varrho K \Omega r$$

or

$$\frac{dT}{dr} = \varrho K_0 V \frac{x^3}{1 + x^2}$$

and it is convenient to write this expression in the form

$$\frac{dT}{dr} = \eta A \frac{x^3}{1+x^2}$$

where η is the efficiency, which is constant along the blades, and A is another constant. The corresponding expression for the torque per unit length of the blades is then simply

$$\frac{dQ}{dr} = \frac{V}{\eta \Omega}\frac{dT}{dr} = rA\frac{x^2}{1+x^2}$$

Then by comparison with equations (5.2)

$$\left.\begin{aligned} BF &= \eta A \frac{x^3}{1+x^2} \\ BG &= A\frac{x^2}{1+x^2} \end{aligned}\right\} \tag{5.13}$$

The thrust of the propeller is

$$\begin{aligned} T &= \eta A \int_0^R \frac{x^3}{1+x^2}\,dr \\ &= \frac{\eta A V}{\Omega}\int_0^{1/\lambda} \frac{x^3}{1+x^2}\,dx \\ &= \frac{\eta A V}{2\Omega}\left[x^2 - \log(1+x^2)\right]_0^{1/\lambda} \\ &= \frac{\eta A V}{2\Omega}\left[\frac{1}{\lambda^2} - \log\frac{1+\lambda^2}{\lambda^2}\right] \end{aligned}$$

or finally

$$T = \frac{\eta A \Omega R^2}{2V}\left[1 - \lambda^2 \log\frac{1+\lambda^2}{\lambda^2}\right] \tag{5.14}$$

and similarly

$$Q = \frac{1}{2} A R^2 \left[1 - \lambda^2 \log\frac{1+\lambda^2}{\lambda^2}\right] \tag{5.15}$$

Using these expressions

$$\begin{aligned} \frac{A_1 Q}{R^2} = \int_0^R \frac{BG}{r}\,dr &= \int_0^{1/\lambda} \frac{Ax}{1+x^2}\,dx \\ &= \frac{1}{2}A\left[\log(1+x^2)\right]_0^{1/\lambda} \\ &= \frac{1}{2}A\log\frac{1+\lambda^2}{\lambda^2} \end{aligned}$$

and hence the expression for the coefficient A_1 which occurs in the formula (5.8) for Y_v becomes

$$A_1 = \frac{\log\frac{1+\lambda^2}{\lambda^2}}{1 - \lambda^2 \log\frac{1+\lambda^2}{\lambda^2}} \tag{5.16}$$

Similarly after integration

$$A_2 T R^2 = \int_0^R B F r^2 \, dr$$

$$= \int_0^{1/\lambda} \frac{\eta A V^3}{\Omega^3} \frac{x^5}{1+x^2} \, dx$$

$$= \frac{\eta A \Omega R^4}{2V} \left[\frac{1}{2} - \lambda^2 \left(1 - \lambda^2 \log \frac{1+\lambda^2}{\lambda^2} \right) \right]$$

and hence the coefficient A_2 which occurs in the formula (5.12) for M_q becomes

$$A_2 = \frac{\frac{1}{2} - \lambda^2 \left(1 - \lambda^2 \log \frac{1+\lambda^2}{\lambda^2} \right)}{1 - \lambda^2 \log \frac{1+\lambda^2}{\lambda^2}} \qquad (5.17)$$

TABLE 43.

λ	A_1	A_2
0.05	6.09	0.505
0.10	4.84	0.514
0.20	3.73	0.535
0.30	3.23	0.555
0.40	2.90	0.573

Numerical values of the coefficients A_1 and A_2 are given in Table 43 and are shown graphically in Fig. 118. These values of A_1 and A_2, though derived in an approximate manner for a

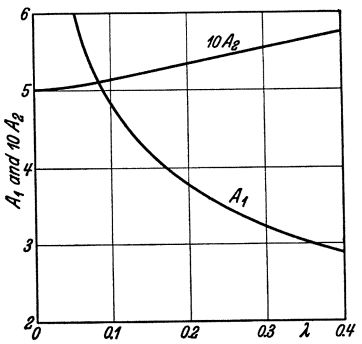

Fig. 118.

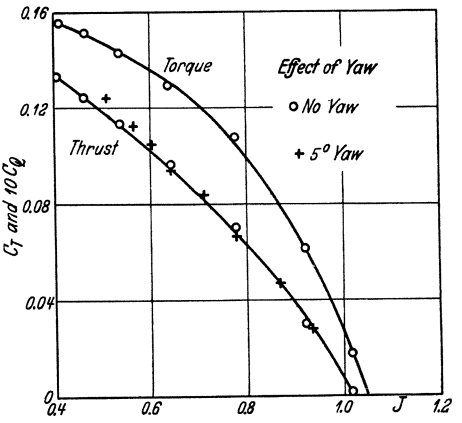

Fig. 119.

frictionless propeller, are sufficiently accurate for determining the force and moment experienced by a propeller due to sideslip or pitching.

One conclusion which follows from the preceding analysis is that the thrust and torque of a propeller are not altered by a small velocity of sideslip or angle of yaw. This conclusion is confirmed by experimental results[1]. Fig. 119 shows the thrust and torque coefficients of a model

[1] BRAMWELL, F. H., RELF, E. F., BRYANT, L. W., Experiments to Determine the Lateral Force on a Propeller in Sidewind. Br. A.R.C. R. and M. 123, 1914.

propeller, and the corresponding thrust coefficients when the propeller axis was set at 5^0 to the wind stream. Fig. 120 shows the side force on the propeller, and the experimental points agree well with the theoretical curve deduced from (5.8). Although no experimental confirmation of the other formulae is available, it would appear from this comparison that the theory is probably a sufficiently accurate representation of the actual conditions.

At larger angles of yaw the analysis ceases to be valid. Figure 121 shows the torque curve of a propeller tested at large angles of yaw[1], and it appears that there is a noticeable increase of the torque coefficient when the angle of yaw is 10^0 and that the torque coefficient increases rapidly with a further increase of the angle of yaw.

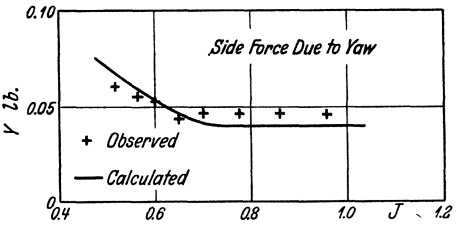

Fig. 120.

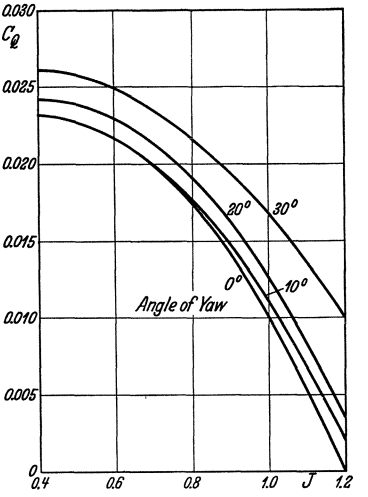

Fig. 121.

6. Downwash Behind a Propeller. When a propeller operates with its axis along the direction of motion, the effect of the thrust is simply to create a slipstream of increased axial velocity, but when the axis is inclined to the direction of motion the propeller produces also a deflection of the air stream, and thus the propeller of an airplane may modify the angle of downwash which is experienced by the tailplane. If the axis of the propeller is inclined at a small angle θ to the velocity V, the thrust of the propeller is not altered but there is a small lateral force Y, and it is the resultant of the thrust T and of the lateral force Y, resolved normally to the direction of motion, which determines the angle of downwash.

Considering first the action of the thrust only, the system of velocities is as shown in Fig. 122. The thrust is associated with an added velocity $2w$ along the axis of the propeller and the velocity in the wake is the

[1] RELF, E. F., and JONES, L. J., Measurements of Lift, Drag, and Pitching Moment on the 1/5 Scale Model of the Bristol Fighter with Airscrew Running. Br. A.R.C. R. and M. 937, 1924.

resultant of this added velocity and of the original velocity V. Hence the angle of deflection ε_1 of the stream in the wake is determined by the equation

$$\frac{2w}{\sin \varepsilon_1} = \frac{V}{\sin(\theta - \varepsilon_1)}$$

or approximately

$$\frac{\varepsilon_1}{\theta} = \frac{2w}{V + 2w}$$

where, according to the axial momentum equation,

$$T = 2\pi R^2 \varrho (V + w) w$$

Writing as usual $w = a V$

the angle of downwash becomes

$$\frac{\varepsilon_1}{\theta} = \frac{2a}{1 + 2a} \tag{6.1}$$

where $(1 + 2a)^2 = 1 + 2\tau$

and $\tau = \dfrac{T}{\pi R^2 \varrho V^2}$ (6.2)

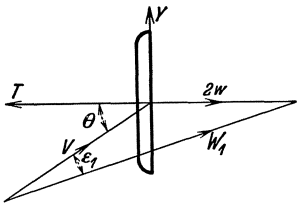

Fig. 122.

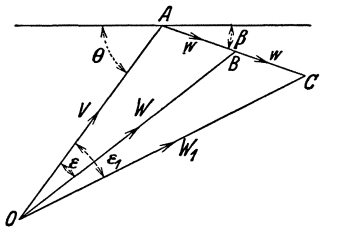

Fig. 123.

These formulae ignore the fact that the existence of the sideforce Y implies an increased angle of downwash. If

$$Y = \beta T$$

the system of velocities will be as shown in Fig. 123, where W represents the resultant velocity at the propeller disc and W_1 the corresponding velocity in the wake. From the triangles OAB and OAC the angles of downwash at the disc and in the wake are now obtained in the form

$$\frac{\varepsilon}{\theta + \beta} = \frac{w}{V + w} = \frac{a}{1 + a}$$

and

$$\frac{\varepsilon_1}{\theta + \beta} = \frac{2w}{V + 2w} = \frac{2a}{1 + 2a}$$

The lateral force Y is due to an effective angle of yaw $(\theta - \varepsilon)$ of the propeller, and according to the analysis of 5 this lateral force is of the form

$$Y = K(\theta - \varepsilon)$$

where

$$K = \frac{A_1 \lambda Q}{R}\left[1 - \frac{\lambda}{2 Q_c}\frac{d Q_c}{d \lambda}\right]$$

But from the previous definition

$$Y = \beta T$$

and hence

$$\beta = k(\theta - \varepsilon)$$

where

$$k = \frac{A_1 \lambda Q}{T R}\left[1 - \frac{\lambda}{2 Q_c}\frac{d Q_c}{d \lambda}\right] \tag{6.3}$$

Substituting back this expression for β in the equations for the angle of downwash, the final formulae become

$$\frac{\varepsilon}{\theta} = \frac{a(1+k)}{1 + a(1+k)} \tag{6.4}$$

and

$$\frac{\varepsilon_1}{\theta} = \frac{2a(1+a)(1+k)}{(1+2a)[1+a(1+k)]} \tag{6.5}$$

The importance of the factor k in these formulae depends on the speed ratio at which the propeller is operating, and in general k increases with the speed ratio.

The angles of downwash for one propeller, calculated according to these formulae, are shown by the curves of Fig. 124, and a few experimental points[1] are added for comparison. The experimental values represent the mean angle of downwash observed by means of a tailplane in the wake of the propeller, and, although the points are rather scattered, the comparison of Fig. 124 suggests that the slipstream velocity had not yet attained its full value. In any case it is difficult to attach a precise meaning to the angle of downwash behind a propeller, since the direction of motion varies across the slipstream owing to the rotation caused by the torque. Moreover the propeller is usually situated in front of the wings of the airplane and the slipstream suffers a further deflection on passing the wings. The ultimate deflection, due to the propeller and wings, is of a very complex nature and it is necessary to rely wholly on experiments to determine the direction and velocity of the flow experienced by the tailplane of an airplane.

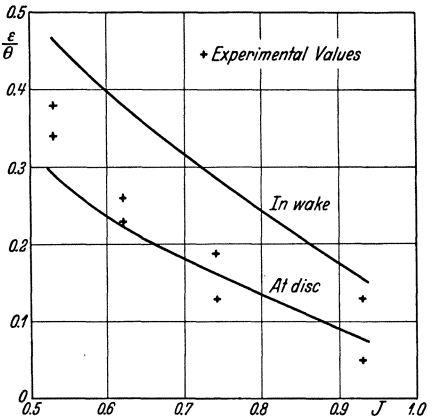

Fig. 124.

[1] SIMMONS, L. F. G., and OWER, E., Investigation of Downwash in the Slipstream. Br. A.R.C. R. and M. 882, 1923.

Bibliography

Books

DRZEWIECKI, S., Théorie Générale de l'Hélice Propulsive. Paris, 1920.

GLAUERT, H., The Elements of Aerofoil and Airscrew Theory. Cambridge, 1926.

JOUKOWSKI, N. E., Théorie Tourbillonnaire de l'Hélice Propulsive. Paris, 1929.

WEICK, F. E., Aircraft-Propeller Design. New York, 1930.

Papers, etc.

BETZ, A., Schraubenpropeller mit geringstem Energieverlust. Göttinger Nachr., 1919 — reprinted in Vier Abhandlungen über Hydro- und Aerodynamik. Prandtl u. Betz. 1927.

— Eine Erweiterung der Schraubenstrahltheorie. Z.F.M. 11, 105, 1920.

— Der Wirkungsgradbegriff beim Propeller. Z.F.M. 19, 171, 1928.

PISTOLESI, E., Neue Ansätze und Ausführungen zur Theorie der Luftschrauben. Vorträge aus dem Gebiete der Hydro- und Aerodynamik. Innsbruck, 1922.

GLAUERT, H., An Aerodynamic Theory of the Airscrew. Br. A.R.C., R. and M. 786 (1922).

— and LOCK, C. N. H., The Accuracy of the Vortex Theory of Airscrews in the Light of Recent Experimental Work and its Application to Airscrew Design. Br. A.R.C., R. and M. 1040 (1926).

BIENEN, TH. u. TH. v. KÁRMÁN, Zur Theorie der Luftschrauben. Z. V.D.I. 68, 1237 (1924).

DURAND, W. F., and LESLEY, E. P., Experimental Research on Air Propellers. U.S., N.A.C.A., Reports 14, 30, 64, 109, 113, 139, 141, 196, 220, 235, 237 (1917—1926).

FAGE, A., LOCK, C. N. H., HOWARD, R. G., and BATEMAN, H., Experiments with a Family of Airscrews, Including the Effect of Tractor and Pusher Bodies. Parts I and II. Br. A.R.C., R. and M. 829 and 830 (1922—1923).

FAGE, A., and LOCK, C. N. H., Experiments with a Family of Airscrews. Part III. Br. A.R.C., R. and M. 892 (1923).

DOUGLAS, G. P., and PERRING, W. G. A., Wind Tunnel Tests with High Speed Airscrews. Br. A.R.C., R. and M. 1086, 1091, 1123, 1124, 1134, 1174, 1198 (1927—1928).

GOLDSTEIN, S., On the Vortex Theory of Screw Propellers. Royal Society Proc. (A), 123, 440 (1929).

LOCK, C. N. H., The Application of Goldstein's Airscrew Theory to Design. Br. A.R.C., R. and M. 1377 (1930).

— Theory of Airscrew and Body Interference. Br. A.R.C., R. and M. 1378 (1930).

Autogyro Theory

CIERVA, J. DE LA, The Development of the Autogyro. Journal of the Royal Aeronautical Society, 30, 8 (1926).

GLAUERT, H., A General Theory of the Autogyro. Br. A.R.C., R. and M. 1111 (1926).

LOCK, C. N. H., Further Development of Autogyro Theory. Br. A.R.C., R. and M. 1127 (1927).

GLAUERT, H., and LOCK, C. N. H., A Summary of the Experimental and Theoretical Investigations of the Characteristics of an Autogyro. Br. A.R.C., R. and M. 1162 (1928).

DIVISION M

INFLUENCE OF THE PROPELLER ON OTHER PARTS OF THE AIRPLANE STRUCTURE

By

C. Koning,

Amsterdam, Holland

EDITOR'S PREFACE

The ideal presented by the more general treatment of wing and airplane theory contemplates an airplane or airfoil moving relative to a body of undisturbed air. In the actual case with the usual disposition of the propeller, a part of the wings and most or all of the control surfaces will be under the influence of an additional velocity, more or less turbulent in character, and formed by the wake of the propeller. Moreover even outside the wake proper the action of the propeller will be accompanied by a change of the flow and hence of the forces acting on a part of the airplane. Obviously no complete theory, including in detail the effects of a turbulent wake, can at present be hoped for and in order to secure any approach to a theoretical discussion of the influence of the propeller on the remainder of the structure, various simplifying assumptions must be made.

The present Division is concerned with a discussion of these problems based on such assumptions as can reasonably be made and by means of which the treatment becomes possible without involving too extreme a complexity of detail.

In the approach to a discussion of this problem it must be remembered that not only does the propeller affect the remainder of the airplane structure, but in turn is affected by it. The interaction is mutual, but here only those questions will be discussed in which the influence on the propeller of the part of the airplane considered may be neglected or at least supposed to be known. The other side of the problem, the mutual interference between the propeller and the parts of the airplane in its neighborhood, has been treated in Division L.

Chapter I opens with a discussion of the flow about a propeller in the absence of other bodies, followed by a consideration of the influence of the simplifying assumptions introduced and then by a general discussion of the theory of its action on the wing system. The treatment of the latter problem is based on the vortex theory of the airfoil.

In Chapter II the applications of this theory to various problems are considered in detail. This discussion covers both the wing of finite span in different positions relative to the propeller and the wing of infinite span crossing the slipstream boundary, together with a comparison of theoretical and experimental results.

This is followed by closing sections on certain interference effects not covered by the theory of Chapter I and by a consideration of the influence of propeller action on the control surfaces, especially as affecting stability and controllability. W. F. Durand.

CHAPTER I

DEVELOPMENT OF THEORETICAL ASPECTS OF THE PROBLEM

A. Introduction

1. The Problems to be Discussed. A propeller, introduced in a flow of air, will change this flow by its action. This change will be called the disturbance of the flow caused by the propeller. If there are other bodies present, the change of the flow will be accompanied in general by a change of the forces acting on them. This change may be called the influence of the propeller on the bodies. On the other hand the introduction of a body will change in general the forces acting on the propeller.

The problems concerning the interference between the propeller and the other parts of the airplane may thus be divided into two groups. The first is formed by those cases in which the attention is directed primarily to the influence of other bodies on the propeller, whereas the second includes those relating to the influence of the propeller on other parts of the structure. Problems belonging to the first group can be attacked satisfactorily only by considering the mutual interference between the propeller and other adjacent bodies, and must be treated in close connection with the theory of the propeller. As these questions, the most important of which is the interference between the propeller and the fuselage or nacelle placed just behind or in front of it, have been treated already in Division L of this work, no special attention will be paid to them here.

The most important problem, which remains after elimination of that of the propeller-body interference, for the reason noted, is that of the influence of the propeller on a wing. This problem is the only one of the second group a theoretical discussion of which may be given for the moment. It will be seen that it is not only important from the point of view of the influence on the wings of the airplane, but that it has also a bearing on its stability.

Besides this, a short discussion of some other questions will be given.

2. Coordinates and General Notations. According to the special problem to be treated, rectangular coordinates x, y, z or cylindrical coordinates x, r, θ, as indicated respectively in Figs. 1*a* and 1*b*, will be used. In both cases the origin coincides with the center of the propeller disc. The axis of x is directed downstream parallel to the direction of the undisturbed flow. The positive sense on the other axes is chosen such as to have a right hand system of coordinates. In the case of the isolated propeller, the direction of the axes of y and z is arbitrary. On the other hand, in discussing the influence of the propeller on a wing, the axis of y, or with cylindrical coordinates the axis $\theta = 0$, will be taken parallel to the wing, whereas the axis of z is directed downward.

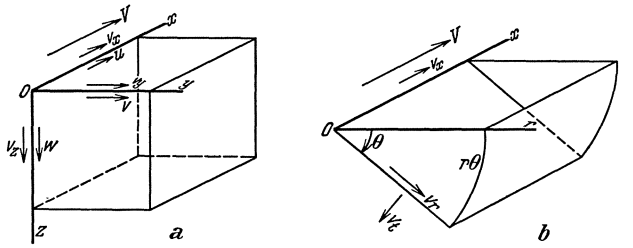

Fig. 1. Coordinates and components of velocity: a) rectangular, b) cylindrical.

Though a list of symbols is given at the beginning of this Division, it may be well to note here the meaning of certain of them to be used most frequently.

The velocity of the undisturbed flow will be indicated by V; the components of the disturbance velocity, due directly to the action of the propeller by v_x, v_y and v_z, rectangular coordinates being used. On the other hand, the components of any other deviation from the undisturbed flow, *e. g.* caused by the presence of a wing, will, for these coordinates, be denoted by u, v and w. If cylindrical coordinates are used, the components of any disturbance velocity will be indicated by v_x, v_t and v_r.

The axial component v_x, as defined above, may, for any point in the slipstream, be given also in the form $s\,V$ and the sum of this component with V by $S\,V$. This gives the relation,

$$S = 1 + s \tag{2.1}$$

The value of s at the propeller disc being important as a reference quantity, the special symbol a will be used for it.

The thrust and torque of the propeller will be given by T and Q respectively and may be expressed in non-dimensional coefficients by means of:

$$\left.\begin{aligned} T &= C_T\,\varrho\,V^2D^2 \\ Q &= C_Q\,\varrho\,V^2D^3 \end{aligned}\right\} \tag{2.2}$$

in which, apart from the quantities defined already, ϱ is the density of the air and D the diameter of the propeller.

Occasional reference will also be made to coefficients k_T and k_Q defined as follows:

$$\left.\begin{aligned} T &= k_T \varrho\, n^2\, D^4 \\ Q &= k_Q \varrho\, n^2\, D^5 \end{aligned}\right\} \tag{2.3}$$

These C and k coefficients are related thus:

$$k_T = C_T\,(V/nD)^2 \qquad k_Q = C_Q\,(V/nD)^2$$

Lift, drag and pitching moment of a wing will be denoted by L, D and M respectively[1], the non-dimensional coefficients for these quantities being defined in the usual way by:

$$\left.\begin{aligned} L &= C_L \tfrac{1}{2} \varrho\, V^2 S \\ D &= C_D \tfrac{1}{2} \varrho\, V^2 S \\ M &= C_M \tfrac{1}{2} \varrho\, V^2 S\, c \end{aligned}\right\} \tag{2.4}$$

Here S denotes the wing area and c the chord of the wing.

Properties, related to the case in which the propeller is absent will be indicated by the suffix 0, whereas the prefix $\triangle$ will be used to denote the change in any property caused by the action of the propeller.

B. The Flow Around a Propeller in the Absence of Other Bodies

3. The "Ideal Propeller". The best way to study the change of the flow associated with the action of a propeller is to realize that this change is caused by the forces which it exerts on the air. The problem in its most general form is very complex, for, the propeller being a solid body, the exact solution would have to satisfy certain conditions at its boundary. But what is wanted here is rather a simple approximate solution, such that its general characteristics only are the same as those of the real flow. Such a solution may be obtained, neglecting the conditions mentioned above, if the system of external forces acting on the air is similar, again in its main properties only, to that for the real propeller.

Since the most important function of the propeller is to give a force in the direction of its axis, it is to be expected that the axial components of the general force system will dominate and be mainly responsible for the character of the flow. Now going a step further in simplification by supposing that there are only axial forces acting over a thin disc substituted for the propeller, and that they have a constant value per unit area over the whole airscrew circle, we come to the so-called "ideal propeller", a notion introduced for the first time by Froude.

In general the simplified picture of the flow, obtained in this way, will approximate the real flow sufficiently close to be used as a basis

[1] The use of the same symbol D to denote both diameter and drag will not be found to introduce any confusion, since both will not occur in the same equation.

for the solution of various problems. But, owing to the assumptions introduced, there will be differences between the idealized flow and the real one which may be of some importance. A short discussion of these will be given in 8 and 9.

4. The Flow Around the Ideal Propeller. General Solution[1]. In the following discussion the influence of the viscosity and compressibility of the air will be neglected and the disc, representing the propeller, will be taken to be normal to the direction of the undisturbed flow.

If now the components of the change in velocity, caused by the action of the propeller, are supposed to be small compared with the velocity V of the undisturbed flow, the equations of motion take the form:

$$\left.\begin{aligned} \varrho V \frac{\partial v_x}{\partial x} &= -\frac{\partial p}{\partial x} + X \\ \varrho V \frac{\partial v_y}{\partial x} &= -\frac{\partial p}{\partial y} \\ \varrho V \frac{\partial v_z}{\partial x} &= -\frac{\partial p}{\partial z} \end{aligned}\right\} \tag{4.1}$$

$$\frac{\partial v_x}{\partial x} + \frac{\partial v_y}{\partial y} + \frac{\partial v_z}{\partial z} = 0 \tag{4.2}$$

According to the assumptions discussed in 3, the external forces will have the component X only, which moreover will be zero everywhere except in the region occupied by the disc.

Integration of the first of (4.1) over a line parallel to the axis of x from x_1 to x_2 leads to

$$\varrho V (v_{x2} - v_{x1}) = -(p_2 - p_1) + \int_1^2 X \, dx$$

If the point 1 is taken just in front and the point 2 just behind the propeller disc and the latter is supposed to be infinitely thin, then for reasons of continuity, v_{x1} will be equal to v_{x2}, so that

$$p_2 - p_1 = \int_1^2 X \, dx$$

The expression $(p_2 - p_1)$ represents a sudden increase in pressure, observed in passing through the propeller disc and $\int_1^2 X \, dx$ is the total amount of axial force acting per unit area. The latter having a constant value over the whole disc and the sum of all axial forces being equal to the thrust T of the propeller, the pressure difference may, if the first of (2.2) is used, be given by:

$$p_2 - p_1 = \frac{T}{\pi R^2} = \frac{8}{\pi} C_T q \tag{4.3}$$

[1] A more exact discussion of this problem is given by J. M. BURGERS in Proc. Kon. Ak. v. Wet. Amsterdam, Vol. 32, No. 9, p. 1278, 1929.

In the region outside the disc the pressure will be continuous, all external forces being absent. By eliminating v_x, v_y and v_z from (4.1) and (4.2), the equation

$$\frac{\partial^2 p}{\partial x^2} + \frac{\partial^2 p}{\partial y^2} + \frac{\partial^2 p}{\partial z^2} = 0 \tag{4.4}$$

is obtained. Being identical with the equation of Laplace, it shows that p will be a potential function. From the discussion given above, it follows that at the propeller disc this function will show a sudden increase of $(p_2 - p_1)$ in passing from the negative to the positive side of the disc.

As is known from general theory [1], such a potential may be obtained by covering the surface of the disc with double sources (doublets) distributed continuously and having the intensity $(p_2 - p_1)$ per unit area. Now at any point A, which is not situated on the disc, the value of p will be given by

$$p = + \frac{p_2 - p_1}{4\pi} \int_S \frac{\partial}{\partial n}\left(\frac{1}{\omega}\right) dS$$

in which n denotes the positive normal to the disc and ω the distance from any point of the disc to the point A. The integral above is to be taken over the whole disc.

By introducing cylindrical coordinates, so that $x_1 = 0$, r_1, θ_1 indicate any point of the disc and x, r, θ, the point A, the result is then obtained in the form

$$\left.\begin{aligned} p &= \frac{p_2 - p_1}{4\pi} \int_0^R \int_0^{2\pi} r_1 \frac{\partial}{\partial x_1}\left(\frac{1}{\omega}\right) d r_1 \, d\theta_1 = \\ &= \frac{p_2 - p_1}{4\pi} \int_0^R \int_0^{2\pi} \frac{x \, r_1 \, d r_1 \, d\theta_1}{[r_1^2 + r^2 + x^2 - 2 r_1 r \cos(\theta_1 - \theta)]^{3/2}} \end{aligned}\right\} \tag{4.5}$$

Now p being determined, the values of the components v_x, v_y, v_z might be calculated with the aid of the equations (4.1).

It may be proved, that both inside and outside the slipstream boundary, the flow has a velocity potential. This "slipstream boundary" is a surface of revolution, extending in the positive direction from the edge of the propeller disc to infinity, at which v_x shows a discontinuity.

The solution obtained does not lend itself to an easy application in the problems to be treated afterward. Therefore in the next section an approximation will be given, derived from it by introducing certain simplifying assumptions. This simplification will be based on the fact that within the slipstream boundary the values of v_x will be relatively large and in any cross-section, they will not differ greatly from that on the axis $r = 0$.

[1] See Riemann-Webers Differentialgleichungen der Physik, Vol. I, Chap. XIV, Braunschweig, 1925.

Use will be made of one result only obtained here, that for the value of p at $r = 0$, which is,

$$p = \frac{p_2 - p_1}{4\pi} \int_0^R \int_0^{2\pi} \frac{x\, r_1\, d\, r_1\, d\, \theta_1}{(r_1^2 + x^2)^{3/2}} = \frac{p_2 - p_1}{2} \left(\frac{x}{\sqrt{x^2}} - \frac{x}{\sqrt{R^2 + x^2}} \right)$$

In this expression the roots are to be taken positive, so that the result may be given in the form:

$$\left.\begin{aligned} r = 0, x < 0 \qquad p &= \frac{p_2 - p_1}{2} \left(-1 - \frac{x}{\sqrt{R^2 + x^2}} \right) \\ r = 0, x > 0 \qquad p &= \frac{p_2 - p_1}{2} \left(+1 - \frac{x}{\sqrt{R^2 + x^2}} \right) \end{aligned}\right\} \tag{4.6}$$

5. The Flow Around the Ideal Propeller. Approximate Solution. The axial component v_x of the velocity due to the action of the propeller must vanish at $x = -\infty$ and be continuous at the propeller disc. So, from the first of (4.1) and equations (4.6) it may be seen at once that for $r = 0$, it is given by

$$-\infty < x < +\infty: \quad v_x = \frac{p_2 - p_1}{2\varrho V} \left(1 + \frac{x}{\sqrt{R^2 + x^2}} \right)$$

By introducing the value of $v_{x\,(x=0)} = a V$ at the airscrew disc, the so-called "inflow velocity", as the governing factor instead of $(p_2 - p_1)$, this result may be written in the form:

$$v_x = a V \left(1 + \frac{x}{\sqrt{R^2 + x^2}} \right) \tag{5.1}$$

With the aid of (4.3) the following relation between a and the thrust coefficient C_T may be obtained:

$$a = \frac{p_2 - p_1}{2\varrho V^2} = \frac{2}{\pi} C_T \tag{5.2}$$

Owing to the simplifications introduced above, this value of a is only approximate. In general, therefore, it will be better to use the more exact value

$$a = \frac{1}{2} \left(-1 + \sqrt{1 + \frac{8}{\pi} C_T} \right) \tag{5.3}$$

as given by the momentum theory of the propeller[1].

Now the simplifying assumption is made that (5.1) not only gives v_x for $r = 0$, but for each point of the slipstream as well. The name "slipstream" is to be taken here in the generalized sense, indicating the region occupied by the fluid which has passed or is to pass through the propeller disc.

Tangential forces being absent, the velocity will have no tangential component, so that, both inside and outside the slipstream,

$$v_t = 0 \tag{5.4}$$

[1] This relation may be obtained by introducing the first of (2.2) in the first of equations (1.12) of Division L II.

The radial component v_r of the velocity in the slipstream may be found by using the equation of continuity:

$$\frac{1}{r}\frac{\partial}{\partial r}(r\,v_r) + \frac{1}{r}\frac{\partial v_t}{\partial \theta} + \frac{\partial v_x}{\partial x} = 0$$

and introducing in it the values for v_x and v_t given by (5.1) and (5.4). As v_r must vanish at $r = 0$, we shall have

$$v_r = -\frac{1}{2}\frac{a\,V\,R^2\,r}{(R^2 + x^2)^{3/2}} \tag{5.5}$$

The determination of the components v_r and v_x in the region outside the slipstream is based on the conditions that here the flow shall have a potential and that at the boundary of the slipstream the radial component of the velocity must be equal to that given by (5.5). Taking the diameter $2\,R_1$ of this boundary equal to that of the propeller disc ($2\,R$) everywhere, these conditions will be satisfied by the flow due to a sink of intensity $2\pi\,R^2 a\,V$ at the origin. Hence the disturbance flow in the region considered will have the potential

$$\varphi = \frac{a\,V\,R^2}{2\sqrt{x^2 + r^2}}$$

and the components of its velocity are

$$\left.\begin{aligned} v_x &= -\frac{1}{2}\,a\,V\,R^2\frac{x}{(x^2 + r^2)^{3/2}} \\ v_r &= -\frac{1}{2}\,a\,V\,R^2\frac{r}{(x^2 + r^2)^{3/2}} \end{aligned}\right\} \tag{5.6}$$

Taking the results given by (5.1) to (5.6) together and introducing rectangular coordinates, the components of the velocity of the flow due to the action of the propeller, are:

inside the slipstream $[(y^2 + z^2) < R_1^2]$:

$$\left.\begin{aligned} v_x &= a\,V\left(1 + \frac{x}{\sqrt{R^2 + x^2}}\right) \\ v_y &= -\frac{1}{2}\,a\,V\frac{R^2\,y}{(R^2 + x^2)^{3/2}} \\ v_z &= -\frac{1}{2}\,a\,V\frac{R^2\,z}{(R^2 + x^2)^{3/2}} \end{aligned}\right\} \tag{5.7}$$

outside the slipstream $[(y^2 + z^2) > R_1^2]$:

$$\left.\begin{aligned} v_x &= -\frac{1}{2}\,a\,V\frac{R^2\,x}{(x^2 + y^2 + z^2)^{3/2}} \\ v_y &= -\frac{1}{2}\,a\,V\frac{R^2\,y}{(x^2 + y^2 + z^2)^{3/2}} \\ v_z &= -\frac{1}{2}\,a\,V\frac{R^2\,z}{(x^2 + y^2 + z^2)^{3/2}} \end{aligned}\right\} \tag{5.8}$$

The boundary of the slipstream is a surface of revolution with the axis $r = 0$. Its radius R_1 at any section x may be determined by considerations of continuity, since the volume of fluid flowing through

it must be the same as that which has passed the airscrew disc. So by introducing v_x from the first of (5.7) we get:

$$\pi R_1^2 (V + v_x) = \pi R_1^2 V \left[1 + a \left(1 + \frac{x}{\sqrt{R^2 + x^2}}\right)\right] = \pi R^2 V (1 + a)$$

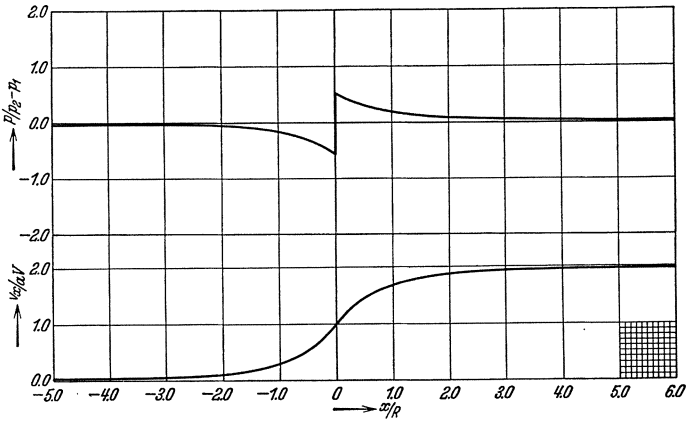

Fig. 2. The pressure p and the velocity component v_x of the propeller flow in the propeller axis ($r = 0$).

or, taking account of the fact that second and higher powers of a may be neglected,

$$R_1 = R \sqrt{\frac{1 + a}{1 + a\,(1 + x/\sqrt{R^2 + x^2})}} \simeq R \left(1 - \frac{a\,x}{2\sqrt{R^2 + x^2}}\right) \qquad (5.9)$$

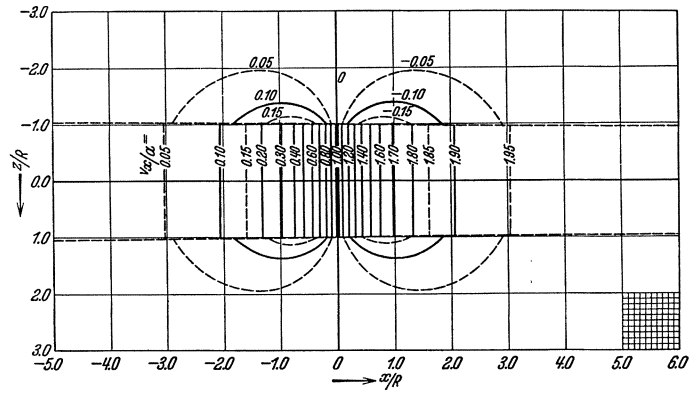

Fig. 3. The axial component v_x of the velocity of the propeller flow in the plane $y = 0$.

6. Numerical Values. As an illustration of the results obtained in 5 the numerical values of the most interesting quantities are given in Figs. 2—5.

Figure 2 shows the pressure and axial velocity for the line $r = 0$. According to the first of (4.1) there is a close relation between these two quantities. The main differences in character are, that v_x has no

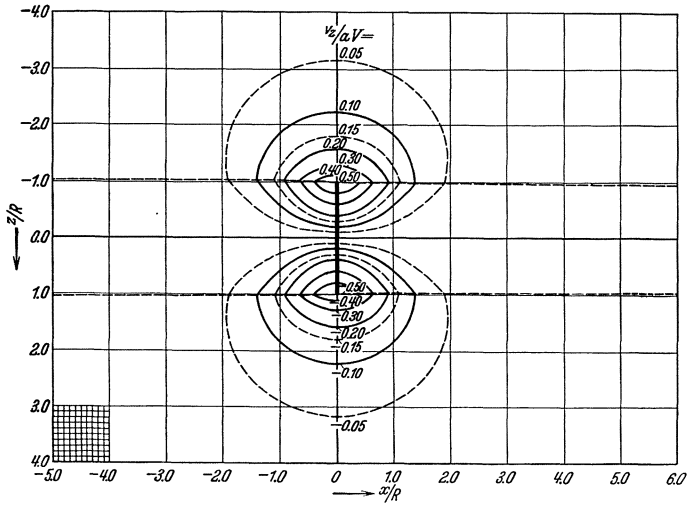

Fig. 4. The component v_z of the velocity of the propeller flow in the plane $y = 0$.

discontinuity at the propeller disc ($x = 0$) and converges at large positive values of x to a value twice that at the disc. For both quantities the gradient is steepest in the neighborhood of the propeller.

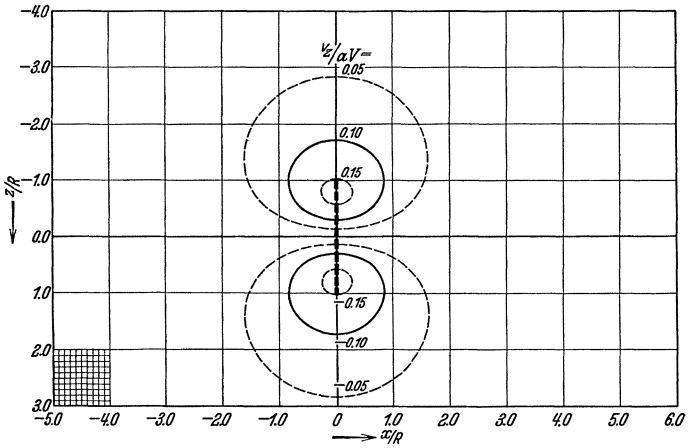

Fig. 5. The component v_z of the velocity of the propeller flow in the plane $y = 1.1\,R$.

In Fig. 3 the values of v_x, the axial component, are given for the plane $y = 0$. After the discussion of Fig. 2, little need be said regarding the slipstream region. Outside this region, the values of v_x are much

smaller, $v_x/a\,V$ amounting here to something more than 0.15 at most. From the character of the flow in this region (due to a sink at the origin) it is evident that v_x changes sign in passing through the plane $x = 0$ and decreases rather rapidly for increasing distances from the propeller.

The values of v_z, the other component of importance, are given in Figs. 4 and 5 for the planes $y = 0$ and $y = 1.1\,R$ respectively. In both cases, as in the whole flow, v_z is symmetrical about the plane $x = 0$, and anti-symmetrical about the plane $z = 0$, being positive in the region above the propeller axis. The largest values occur at the edge of the propeller disc in the plane $y = 0$, v_z/aV being here 0.50. In the plane $y = 1.1\,R$, the curves show a character similar to that of those in the plane $y = 0$, but the values of v_z are much smaller.

Fig. 3 shows a discontinuity in velocity at the slipstream boundary both in front and behind the propeller. In the first region this discontinuity is fictitious and due to the simplifications introduced. There is some similarity with the real flow, in that, in front of the propeller, the discontinuity in v_x is in general rather small compared with that behind it.

Thus far the values of $(p_2 - p_1)$ and a have been left out of the discussion. To give an idea of these quantities, they are shown in Fig. 6, together with the corresponding values of the thrust coefficients C_T and k_T. The values of the latter are taken from experiments by Fage, Lock, Howard and Bateman[1] with the model of a propeller which may be considered as representative of those in normal use (two blades with constant pitch $P = 0.70\,D$ and a maximum blade width of $0.082\,D$). For a both the exact value calculated from (5.3) and the approximate one according to (5.2) are given, showing that there may be a rather important difference between these two. The normal working range of a propeller, such as is considered here, will be from about $V/nD = 0.4$

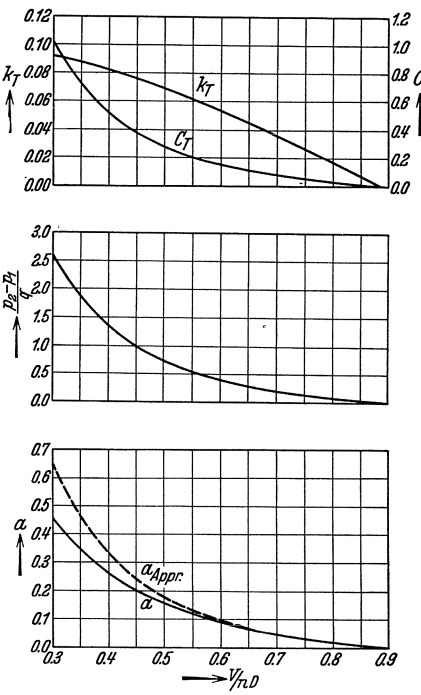

Fig. 6. Values of $(p_2 - p_1)$ and a for a two-bladed propeller with pitch $P = 0.7D$ and maximum blade width $c = 0.082\,D$.

[1] Experiments with a Family of Airscrews, Part I. Br. A.R.C. R. and M. 829, Vol. I, 1922-23.

to $V/nD = 0.8$. Hence the greatest value of a to be expected here under normal conditions, will be about 0.26, a value which justifies the assumption that in most cases the disturbance velocity, due to the action of the propeller will be small compared with V.

7. Experimental Results. As rather drastic simplifications have been introduced in developing the theory of the flow around the ideal propeller, it is desirable to compare the results obtained with those of experiments. As will be discussed in 8 and 9, the general assumptions, especially those

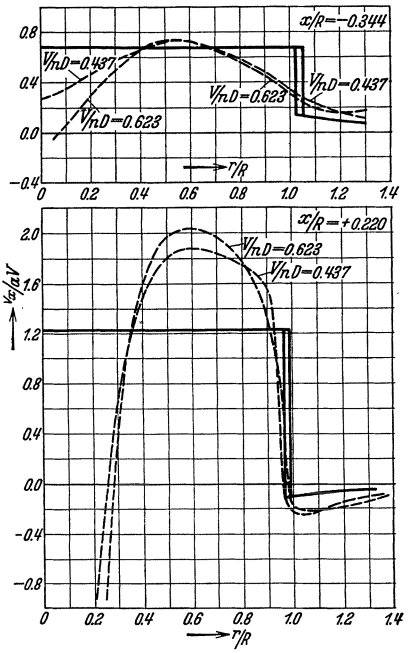

Fig. 7. Calculated and experimental values for the axial component v_x of the velocity of the propeller flow. Continuous line—calculated, broken line—experimental.

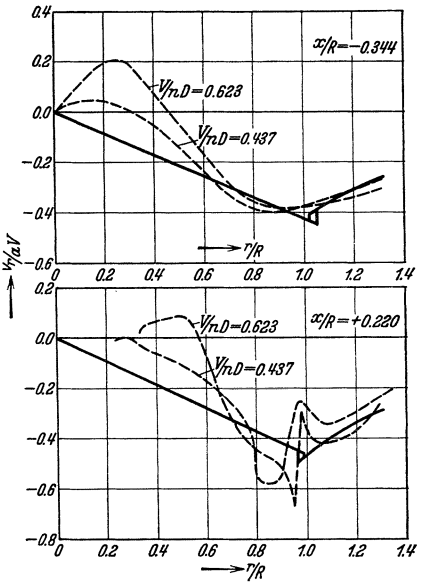

Fig. 8. Calculated and experimental values for the radial component v_r of the velocity of the propeller flow. Continuous line—calculated, broken line—experimental.

relating to the forces acting on the air, will cause some fundamental differences, but in many of the problems to be treated their influence is small or negligible. For the moment, therefore, attention will be paid rather to the question of prime importance, namely, whether there is a sufficient agreement in the mean values of the velocity components v_x and v_r.

For a satisfactory quantitative comparison the results of the exploration of the whole flow around an isolated propeller are needed. But, thus far, exact measurements of the components of the velocity have been made in the neighborhood of the propeller only, the purpose being rather to check the performance calculation of the propeller.

Experiments of this kind have been made by Lock and Bateman[1] with a model propeller which was closely related to that mentioned in 6, the only difference being that here a four-bladed model was used. The experimental values of v_x and v_r for a plane in front and a plane behind the propeller are given in Figs. 7 and 8, together with the corresponding calculated values. The experiments were made with a body behind the propeller, the diameter of which was about 1/3 D. A primitive correction has been applied for its influence by subtracting from the values measured, those for the body without propeller. It will be evident, that, due to interference effects, even with such correction, the experimental and calculated values are not comparable in the strict sense. Bearing this in mind the agreement may, however, be called satisfactory. Though, owing to the fact that more exhaustive experimental information is lacking, the check of the calculated values is very incomplete, it will be assumed that, apart from the differences to be discussed in 8 and 9, the flow around the ideal propeller may be considered as a satisfactory approximation to the real flow around an isolated airscrew. Hence it may be used as a basis for the determination of the influence of the propeller on the parts of an airplane, if only the form and situation of these parts are such that their interference with the action of the propeller is not important and that the influence of other parts of the airplane is negligible.

8. Influence of the Simplifying Assumptions. Besides possible discrepancies in the mean values of v_x and v_r, some of the assumptions introduced may lead to differences in character between the real flow and the calculated one. The main causes of these differences are the assumptions relating to the axial forces and the omission of the effects due to viscosity and the tangential forces.

For the real propeller the axial force will in general be a non-constant function of r and even change sign in the region occupied by the boss. This will result in a value of v_x which in the slipstream is a function of r too, but for the problems to be treated here this deviation will, in general, be of secondary importance.

Somewhat more serious is the fact, that, due to the finite number of blades, the forces are concentrated on a number of rather narrow strips moving with the angular velocity of the airscrew. Hence the flow will not be steady but will have a periodic character. This phenomenon has been investigated by Townend[2] and by Lock and Yeatman[3], respectively from the experimental and the theoretical sides. It has been

[1] The Measurement of Airflow Around an Airscrew. Br. A.R.C. R. and M. 955 Vol. II, 1924-25.

[2] Hot Wire and Spark Shadowgraphs of the Airflow Through an Airscrew. Br. A.R.C. R. and M. 1434, 1931-32.

[3] Periodic Flow Behind an Airscrew. Br. A.R.C. R. and M. 1483, 1932-33.

shown by the latter authors that there is a good agreement between the real flow and that due to a certain system of vortex sheets. This system is a simplification of the helical vortex sheets springing off the trailing edges of the blades, the existence of which may be predicted from the circulation theory of the airscrew (see Division L VI). Moreover there will be other causes tending to destroy the steadiness of the flow, such as the vortices related to the profile drag of the blades and the resistance of the boss. The generation of the latter vortices is due to viscosity.

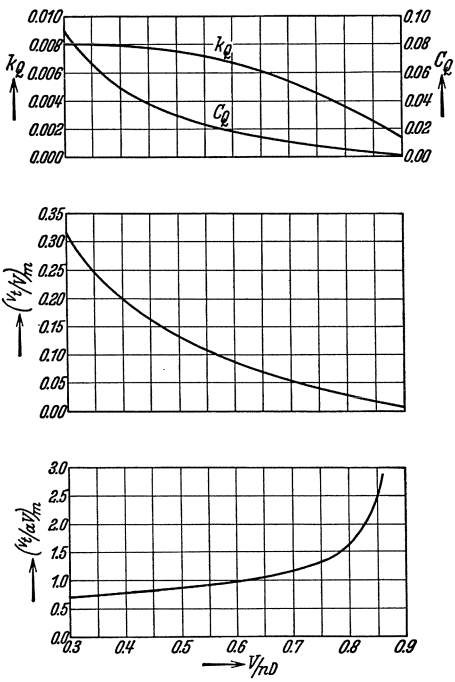

Fig. 9. Values of $(v_t/V)_{max}$ and $(v_t/aV)_{max}$ for a two-bladed propeller with pitch $P = 0.7\,D$ and maximum blade width $c = 0.082\,D$.

Another effect of viscosity will be observed at the boundary of the slipstream. Whereas the theory of the ideal propeller assumes a surface of discontinuity, in the real flow, instead of such a surface, a region will be observed in which the velocity changes more or less rapidly. Due to the diffusion of vorticity, the radial thickness of this region will increase with increasing distance behind the propeller.

9. Influence of the Simplifying Assumptions (Continued). The forces in a tangential direction, exerted on the air by the real propeller, will cause a rotation of the slipstream. As was indicated by Taylor[1] for the first time, the circulation in any fluid line which has not passed through the propeller disc will be zero. Hence, both in front of the propeller and in the region behind it but outside the slipstream, the mean value of the tangential velocity will be zero likewise. To obtain a rough approximation of the tangential velocity in the slipstream, the following calculation may be made, based on the assumption that the whole mass of air which has passed through the airscrew disc rotates like a solid cylinder.

The angular velocity of the airscrew being $\Omega = 2\,\pi\,n$, that of the cylinder may be taken in the form $2\,a'\,\Omega$, whereas the axial velocity of the air at the propeller disc is $(1 + a)\,V$. The torque of the propeller

[1] The "Rotational Inflow Factor" in Propeller Theory, Br. A.R.C. R. and M. 765, 1921-22.

will be equal to the moment of momentum impressed on the air passing through it per unit time; hence,

$$Q = \int_0^R 2\,a'\,\Omega\,r \cdot r \cdot \varrho\,(1+a)\,V \cdot 2\,\pi\,r\,dr = \frac{\pi}{16}\,\varrho\,\Omega\,V D^4\,(1+a)\,a'$$

or, by introducing the coefficient C_Q from the second of (2.2)

$$a' = \frac{16\,Q}{\pi\,\varrho\,\Omega\,V D^4\,(1+a)} = \frac{8}{\pi^2}\,\frac{C_Q}{1+a}\,\frac{V}{nD}$$

The maximum value of the tangential velocity v_t will occur at the slipstream boundary, and hence will be given approximately by

$$v_{t\,max} = 2\,a'\,\Omega\,R = \frac{16}{\pi}\,\frac{C_Q}{1+a}\,V \tag{9.1}$$

or, to make this result directly comparable with the velocities for the ideal propeller, as in **6**,

$$\frac{v_{t\,max}}{a\,V} = \frac{16}{\pi}\,\frac{C_Q}{a\,(1+a)} \tag{9.2}$$

In Fig. 9 the values of $v_{t\,max}/V$ and $v_{t\,max}/a\,V$ are given together with the corresponding values of the coefficients k_Q and C_Q for the same propeller, the results of which have been discussed already in **6** in relation with Fig. 6. The absolute value of v_t/V is seen to decrease rapidly with increasing values of $V/n\,D$, but its relative importance (compared with a) increases, slowly at first, but more rapidly in the neighborhood of the point of zero thrust. As is known from **6** (Fig. 4), the maximum value of the component v_z in the flow around the ideal propeller is $0.5\,aV$. The maximum value of v_t may therefore surpass it greatly.

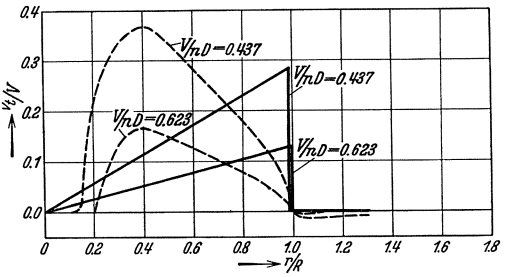

Fig. 10. Calculated and experimental values for the tangential component v_t of the velocity of the propeller flow. Continuous line—calculated, broken line—experimental.

A comparison between the values of v_t, calculated in the manner indicated above and those taken from the experiments of Lock and Bateman[1] is given in Fig. 10. It shows that the calculated results are a rough approximation only, but that the maximum values, though occurring at quite different values of r, do not differ greatly.

The rotation in the slipstream will be accompanied by a pressure gradient along the radius which will cause a negative change of the pressure in its interior.

[1] See footnote, p. 373.

C. The Influence of the Propeller on the Wing System

10. Introduction. In the preceding Part B, it appeared practical to divide the disturbances of the flow, due to the action of the propeller, into two groups. The reason for this was that, by introducing certain simplifications, the problem took a form admitting of an approximate numerical solution. This solution may be regarded as representing the first and most important part of the disturbances mentioned. For the second part, including all differences between the idealized flow and the real one, such a solution is not possible. For a part of these differences, only a rough approximation could be given, and for a part, even this is impossible.

As a consequence, in analyzing the influence of the propeller on the wing system, a similar division of the effects is desirable. For, numerical results on the flow around the ideal propeller being available, we have the opportunity to study in some detail its influence on the properties of a wing. On the other hand, no consistant numerical values on the disturbances included in the second group are available. Hence it is evident that it is not possible to give even an approximate numerical treatment of the effects caused by them; moreover, such a treatment would involve other serious difficulties.

It should be remarked that the boundary line between the two groups of phenomena chosen here, is not entirely in accord with that introduced in treating the flow around the propeller, as effects due to changes in pressure will be excluded from the first group here.

This division of the effects, prescribed by the possibility of analytical treatment, is somewhat parallel to a division based on their practical importance. The effects of the first group will exist in every case and may be important. On the contrary, those of the second group will in general be less important or exist only in special cases, such as wings at a large angle of attack.

In dealing with this subject, the theory of the influence of the ideal propeller on the wing system will be given first, **12—26**, followed in Chapter II, Part A, by its application to the problem in the different forms in which it may be encountered, together with a comparison with some experimental results. Whereas in the present chapter the form of the wing system will be arbitrary and the influence of the propeller on lift, drag and pitching moment will be considered, in Chapter II, Part A, for the sake of brevity, the discussion will be restricted mainly to wings of a special, simple form, and to the lift only, the latter furnishing the most interesting aspect from a theoretical point of view. Finally in Chapter II, Parts B and C certain questions will be discussed which are not covered by the theory developed in the present chapter.

11. Statement of Problem. The treatment of the problem will be based on the three-dimensional airfoil theory, as it has been developed in Division E III, IV. A summary of the assumptions taken from that theory is given in **12**.

Anticipating the more exact formulation of the problem to be treated here, which will be given in **14**, it can be characterized best by indicating the fundamental difference which exists between it and the similar one which is solved by airfoil theory. The latter theory supposes the wing system to be situated in a flow of air in which, in its absence, the velocity would have the same magnitude and direction at every point. On the other hand, we must here deal with a flow in which, even in absence of the wing system, the velocity is varying from point to point both in magnitude and direction.

The problem in its most general form, that is to say that of the wing in an arbitrary flow, presents serious difficulties, but there are circumstances here which make it unnecessary to attack it in this general form.

In the absence of the wing and without the action of the propeller, the velocity of the flow is constant both in magnitude and direction. As has been indicated already in Part B, the changes in velocity due to the action of the propeller, may be supposed to be small. This will result in simplifications, being similar to those encountered in the theory of the lightly loaded wing.

Here, as in the latter theory, the disturbance velocities due to the action of the wing will play an important role in the determination of the circulation for a wing of given form. If now the changes in flow caused by the action of the propeller were small, but otherwise arbitrary, it would be difficult to determine these velocities. On the other hand, the flow in the absence of the wing being such as to have a continuous velocity potential everywhere, these difficulties would disappear entirely and in calculating the velocities mentioned, use could be made of the methods known from airfoil theory. Now our problem lies midway between these two extreme cases, since here we have to do with two regions, in both of which a velocity potential exists, but which are separated by a surface of discontinuity. Hence we shall have to investigate the influence of such a discontinuity, which will show itself to be important, as it not only exists in the case in which the wing crosses the slipstream boundary, but also in that for the wing situated entirely within or without such boundary.

12. General Assumptions. Although most of the assumptions are taken from basic airfoil theory and so have been discussed in Division E, it may be well to summarize them here.

The change of the undisturbed flow, caused by the action of the wing, is identical with that related to a system of vortices. This system consists of two parts: a rectilinear line vortex, taking the place of the

wing, the so-called "lifting vortex" and a layer of "trailing vortices" extending from the lifting vortex to infinity. The lifting vortex will be normal to the plane $x\,z$, whereas the trailing vortices are parallel to the axis of x. The vortex strength of the lifting vortex will in each point be equal to the circulation around the corresponding element of the wing. The total strength of the trailing vortices, starting from any part of the lifting vortex, will correspond with the change in circulation of the latter in the part considered.

The distance from the wing to the point in which the velocity is to be determined, being rather large, the vortex system thus indicated may be replaced by a more simple one, the so-called "horseshoe vortex", consisting of a lifting vortex of constant strength and two trailing line vortices extending from its ends.

The velocity caused by the action of the wing will be so small that, if any function of its components is expanded in a power series, only the lowest powers need be taken into account.

The force acting on an element of the wing will, apart from its dimensions and aerodynamic properties, depend on the local velocity only. This "local velocity" is the component, normal to the axis of y, of the velocity which would exist in the point at which the element is located, if this element were taken away but everything else left unaltered. The components of the force, normal and parallel to the local velocity, are equal respectively to the lift and drag which would act on it if it formed part of a wing of infinite span in two-dimensional flow. In the latter case, the angle of attack and the velocity, taken in the usual sense, should be equal respectively to the aerodynamic angle of attack and the local velocity for the element considered. A definition of the "aerodynamic angle of attack" is given in **13**.

The component dL of the force normal to the local velocity, may be expressed either in terms of the circulation around the element, or in terms of its lift coefficient.

The first relation is given by the generalized law of Kutta-Joukowski:

$$dL_\infty = \varrho\, V_t\, \Gamma\, dy \tag{12.1}$$

the second by

$$dL_\infty = C_{L\infty}\, (1/2)\, \varrho\, V_t^2\, c\, dy \tag{12.2}$$

in which

dL_∞ = component of the force considered;
ϱ = mass density of the air;
Γ = circulation around the element;
V_t = local velocity;
dy = "span" of the element;
c = chord of the element;
$C_{L\infty} = C_0 + C_1\, \alpha_\infty$ = lift coefficient for the wing of infinite span at the same aerodynamic angle of attack, C_0 and C_1 being constants, depending on the properties of the wing section only.

The component dD_∞ of the force parallel to the local velocity, being the profile drag of the element, will be small compared with the normal component and independent of the angle of attack.

For each element of the wing the axis about which the pitching moment dM is defined, may be taken such as to make it independent of the angle of attack.

Besides these well-known assumptions the following new ones will be here introduced.

The ratio between any of the components of the velocity due to the action of the propeller and the undisturbed velocity, will be small compared with unity. Hence, if any regular function of them or of the "inflow factor" a is expanded in a power series, only the terms of the order zero and one are to be retained.

In working out the results of the theory, the components of the velocity will be introduced in the form given in **5**. On the other hand in the general discussion, use will be made of the fact that the exact solution for the disturbance flow due to the action of the propeller, will have a velocity potential both inside and outside the slipstream boundary (see **4**).

13. Some General Definitions. For the sake of brevity the name "airfoil theory" will be used to indicate that part of this theory which treats the wing in an unbounded parallel flow and which is based on the assumptions discussed in **12**.

Fig. 11. Angles of attack. α = geometrical; α_e = aerodynamic; α_i = induced.

For the same reason, the system of vortices which may be substituted for the wing (see **12**), will be called the "vortex system of the wing". Likewise the name "cross components" will indicate the components of any velocity in a plane normal to the axis of x.

The prefix "induced", taken from airfoil theory, will be used here in a more general sense. In airfoil theory its meaning is, that the property considered, resistance for example, is related to the change of flow caused by the action of the wing. Here it will be used to indicate a property related to all disturbances taken together. For instance, in calculating a component of the induced velocity, the summation should be taken of the components due to the disturbances caused by the action of both the wing and the propeller.

Taking the "induced angle of attack" α_i in this sense, such as to give at any element of the wing the angle between the direction of the undisturbed flow and of the local velocity, it is evident that the relation

$$\alpha_i + \alpha_e = \alpha \tag{13.1}$$

is still valid here (see Fig. 11). The "aerodynamic angle of attack" α_e is the angle between the local velocity and a reference line fixed to

the wing section, *e. g.* the chord. The "geometrical angle of attack" α is the angle between this reference line and the direction of the undisturbed flow.

An "element of the wing" will always be the part of the wing situated between two planes normal to the axis of y, their separation being dy.

14. General Discussion of the Problem. After the introduction given in the preceding sections, a more exact statement of the problem can be given than was possible in **11**. The resulting flow which will exist, both the propeller and the wing being present, may be decomposed into different parts. To distinguish them, the following names will be used:

a) "undisturbed flow": the flow in the absence of wing and propeller, being a parallel flow with constant velocity V;
b) "propeller flow": the difference between *a* and the flow which would exist if the propeller were acting in absence of the wing;
c) "airfoil flow": the change in flow caused by the action of the wing when introduced into *a*, the propeller being absent;
d) "additional airfoil flow": the disturbance flow, related directly to the change in circulation around the wing, caused by the action of the propeller;
e) "additional flow": the difference between the resulting flow *f* and the flow which would be obtained by simple superposition of *a*, *b*, *c* and *d*;
f) "resulting flow": the flow existing with both propeller and wing present and in action.

It should be remarked at once, that this decomposition has only a kinematic character and does not assume that each part can exist as an independent flow.

As to the meaning of the three first mentioned parts, little need be said. Flow *b* is the change in flow due to the action of the propeller, as discussed in **4—6**, whereas flow *c* is the disturbance flow considered by airfoil theory. The vortex system of the wing being given, the velocity of the latter flow at any point may be calculated by using the well-known formula of Biot and Savart.

In the absence of the propeller, the flow around the wing consists of parts *a* and *c* only. Introduction of the propeller action leads to a change in flow, which, the form of the wing being unaltered, will in general result in a change in the circulation for each element of the wing. The resulting vortex system may be considered as consisting of two parts; the first is identical with the original ("original vortex system"), whereas the second part ("additional vortex system") incorporates all changes due to the introduction of the propeller action. The character of these two systems is the same, the only differences arising from a different distribution of the circulation along the lifting vortex and a corresponding difference in the strength and distribution of the trailing vortices. Now, starting from the additional vortex system, a flow may be constructed, related to it in exactly the same way as the airfoil

flow to the original vortex system, and this will be the additional airfoil flow d.

But, as will be discussed in more detail in the next section, the flow obtained by a superposition of a to d cannot exist. So, to obtain the resulting flow f, still another, the additional flow e, must be added.

The circulation being known, the calculation of the aerodynamic properties of the wing will not present fundamental difficulties. Hence the main problem will be the determination of the change in circulation. This change, depends directly on both the propeller flow and the additional flow; the determination of the latter is important and is to be first considered.

15. The Superposition of Potentials with Singularities. In the theory of irrotational fluid motion, use is often made of the superposition of potentials[1]. Such a superposition is always permitted, if only in the region considered, both φ_1 and φ_2 are free from singularities.

A discussion of the different kinds of singularities which may be encountered in hydrodynamic theory may be omitted here, as we shall have to deal with two kinds only, which are closely related. Either the singularities will be situated on a line or on a surface. In the first case their character is such that, in approaching the line, the value of the velocity tends to infinity, whereas the circulation around the line differs from zero (line vortex). In the second case, the velocity has a finite, but different value and/or direction on the two sides of the surface, so that a discontinuity in velocity occurs here (vortex sheet, surface of discontinuity).

If now the potential functions have singularities, the question whether superposition is permitted requires special attention.

In some of these cases, it may be shown that superposition is indeed permitted, but that the existence of the flow having the potential obtained in this way, will only be possible if external forces are applied to the fluid. A well-known example is the following case which is of direct present interest. Both the undisturbed flow a and the airfoil flow c, as they have been defined in **14**, have a potential. The potential φ_a of the first flow has no singularities whatever, whereas that of the second, φ_c, has singularities coinciding with the vortex system of the wing. As is known from airfoil theory, the flow obtained by superposition can exist only if certain external forces act on the fluid in the line occupied by the lifting vortex.

If now the propeller flow b is superposed, the situation is altered. The fact that the vortex system of the wing is changed does not present a fundamental difficulty, as the flow related to it (the additional airfoil flow d) has exactly the same character as the original airfoil

[1] See Division A VII **2**.

flow c. Hence an addition of its potential φ_d will result only in a change of the forces necessary to act in the lifting vortex. A more important point is the fact that the potential φ_b of the propeller flow has its singularities also, located on the boundary of the slipstream, the surface on which there is a discontinuity in tangential velocity. This surface may be considered as a vortex layer, but here the introduction of external forces would conflict with the physical meaning of the problem. Hence we must approach from a different direction, by investigating what mechanical conditions (boundary conditions) are to be satisfied for an element of fluid situated on the boundary.

In general, the flow given by the potential φ_1, which is obtained by a simple addition of φ_a, φ_b, φ_c and φ_d (uncompensated potential) will not satisfy these conditions. We therefore make use of the possibility of superposing still another potential φ_e (additional potential). The latter may have quite a different character in the regions situated inside and outside the slipstream boundary, but in both it should be free from singularities. On the other hand, singularities at the boundary will be permitted and even necessary. Moreover it is to be chosen such that the potential of the resulting flow, φ_f (compensated potential) $= \varphi_1 + \varphi_e$ satisfies the boundary conditions.

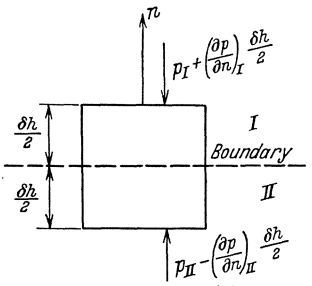

Fig. 12. Pressure condition at the boundary.

16. Conditions at the Boundary of the Slipstream: General Form. The conditions to be satisfied at the boundary of the slipstream may be given in the following form:

a) the pressure shall have the same value on each side of the boundary,

b) the component of the velocity, normal to the boundary, shall be the same on both sides and in our special case, in which the flow will always be supposed to be steady, equal to zero.

The necessity of equality of pressure may be demonstrated in the following way. Let us take an element of fluid, bounded by a small cylindrical surface crossing the boundary (Fig. 12). The base of this cylinder is taken parallel to the boundary, whereas its generating lines are normal to it. The height of the cylinder is δh. External forces being absent, the equation of motion of the element in the direction of the normal n to the boundary will contain inertial and pressure terms only. The inertial terms will be all proportional to δh, the pressure terms take the form:

$$-p_I + p_{II} - \left[\left(\frac{\partial p}{\partial n}\right)_{II} + \left(\frac{\partial p}{\partial n}\right)_I\right]\frac{\delta h}{2}$$

The suffixes I and II indicate respectively whether the property considered is related to the region outside or inside the boundary. If

now δh converges to zero, it will be seen at once that, if $(p_{II} - p_I)$ was not equal to zero, the acceleration of the fluid would be infinite at the boundary. Hence the first boundary condition is

$$p_I = p_{II} \tag{16.1}$$

The second condition is one of continuity and has the meaning that at the boundary no fluid should disappear or be generated. The boundary being a surface of revolution the normal component of the velocity is (see Fig. 13)

at side I: $V_{nI} = V_{rI} \cos\beta + V_{xI} \sin\beta$

at side II: $V_{nII} = V_{rII} \cos\beta + V_{xII} \sin\beta$

in which β is the angle between the normal n to the boundary and a plane normal to the axis of x. The symbol V is used here to indicate the total value of any component of the velocity for the flow considered.

As noted above, both V_{nI} and V_{nII} must be equal to zero, which, by elimination of β, results in the second boundary condition

$$\left(\frac{V_r}{V_x}\right)_I = \left(\frac{V_r}{V_x}\right)_{II} \tag{16.2}$$

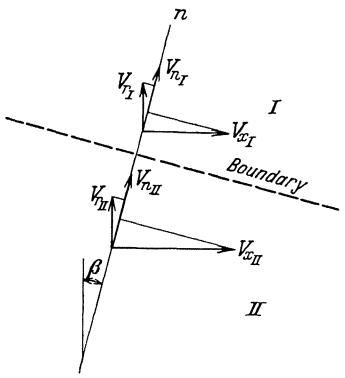

Fig. 13. Condition of continuity at the boundary.

17. Conditions at the Boundary of the Slipstream: Special Form. By (16.1) and (16.2) the boundary conditions are given in their most general form for a steady flow, but another form will be more suitable for the solution of the problem indicated in **15**.

To obtain this form, the somewhat simplified case will be considered in which the propeller flow b consists only of a constant increase $(V_{II} - V_I)$ in axial velocity inside the slipstream boundary. Moreover in the absence of the wing, the latter will be a circular cylinder with radius R_1, the axis of which coincides with the axis of x and which extends from $x = -\infty$ to $x = +\infty$. Hence the flow $(a + b)$ will be a parallel flow with the velocity $V = V_I$ outside and V_{II} inside the slipstream boundary.

Introduction of the wing will influence the form of this boundary; but, the disturbance velocities being small, it will deviate only slightly from the original form specified above. Hence it will be permissible to seek a solution for which the boundary conditions are not satisfied at the real boundary, but at the idealized one represented by the cylinder.

Both inside and outside the slipstream, the flow will be irrotational, so that the pressure is given by:

$$p + \frac{1}{2}\varrho[(V + u)^2 + v^2 + w^2] = C$$

Here, in distinction from the general use, V indicates the velocity of the flow $(a + b)$. C will be constant both inside and outside the slipstream, but will have a different value in these two regions.

The velocities u, v and w will be small, so that their squares may be neglected. Moreover at $x = -\infty$, u_I and u_{II} will vanish and p_I and p_{II} will have the value p_0. Hence the pressure equation may be reduced to the form

$$\begin{aligned} &\text{outside:} \quad p_I = p_0 - \varrho\, V_I\, u_I \\ &\text{inside:} \quad p_{II} = p_0 - \varrho\, V_{II}\, u_{II} \end{aligned}$$

By substitution of these results, (16.1) becomes

$$r = R_1\colon\ V_I\, u_I = V_{II}\, u_{II} \tag{17.1}$$

The flow existing in the absence of the wing and having the potential $(\varphi_a + \varphi_b)$, satisfies the boundary conditions. Hence, in introducing the potential in these conditions, only the part $(\varphi_c + \varphi_d + \varphi_e)$ (see **14**) need be considered, and (17.1) may be written in the form

$$r = R_1\colon\ V_I \frac{\partial\,(\varphi_c + \varphi_d + \varphi_e)_I}{\partial\, x} = V_{II} \frac{\partial\,(\varphi_c + \varphi_d + \varphi_e)_{II}}{\partial\, x} \tag{17.2}$$

Now the relation

$$\varphi\,(x_1) = \int_{-\infty}^{x_1} \frac{\partial\,\varphi}{\partial\, x}\, d\, x + \varphi\,(-\infty)$$

may be used. Owing to the fact that the cross components v and w of the velocity will vanish at $x = -\infty$, $\varphi\,(-\infty)$ will be an arbitrary constant here, independent of y and z. Hence in integrating (17.2) $\varphi\,(-\infty)$ may be omitted as having no physical meaning and the first boundary condition is obtained in the form

$$r = R_1\colon\ V_I\,(\varphi_c + \varphi_d + \varphi_e)_I = V_{II}\,(\varphi_c + \varphi_d + \varphi_e)_{II} \tag{17.3}$$

The velocity u being small, it may be neglected in the second boundary condition (16.2), so that this becomes

$$r = R_1\colon\ \left(\frac{v_r}{V}\right)_I = \left(\frac{v_r}{V}\right)_{II}$$

or, again introducing the potential,

$$r = R_1\colon\ V_{II} \frac{\partial\,(\varphi_c + \varphi_d + \varphi_e)_I}{\partial\, r} = V_I \frac{\partial\,(\varphi_c + \varphi_d + \varphi_e)_{II}}{\partial\, r} \tag{17.4}$$

18. Determination of the Additional Flow. The result of the discussion in the preceding sections may be summarized as follows. The flow obtained by superposing on the undisturbed flow a the disturbances caused by the action of the propeller (propeller flow b) and that of the wing (airfoil flow c + additional airfoil flow d) cannot exist. The cause of this is the fact that the mechanical conditions which should be satisfied for each element of the fluid are violated at the boundary of the slipstream. Hence another flow (additional flow e) must be added. The

latter must satisfy the following conditions: Both inside and outside the boundary mentioned, it must have a velocity potential, which, except at this boundary, has no singularities. If the boundary is supposed to have the special form introduced in **17**, this potential should be determined such that, together with those of the airfoil flow and the additional airfoil flow, it satisfies conditions (17.3) and (17.4). At a large distance from the wing, the velocity of the airfoil flow vanishes, except in the region behind the wing. Hence this should also be the case with the velocity of the additional flow.

Potential theory provides means by which a complete solution of this problem might be obtained, if such a solution were wanted. But it will be shown here, that owing to certain peculiarities of our special problem, a partial solution will be sufficient.

Though similar questions are encountered in airfoil theory, a short discussion of them, in view of their importance, will be given here.

For simplicity the lifting vortex of the wing is supposed to be situated in the plane $x = 0$, an assumption which does not introduce any restriction.

The behavior of an element of the wing depends only on the magnitude and direction of the local velocity. Moreover the value of the velocity component u of the airfoil flow (and likewise of the additional airfoil flow) is small, so that its influence may be neglected. Owing to the relation between airfoil flow and additional flow, this will also be the case for the component u of the latter. Hence the component w of the velocity of the additional flow in the plane $x = 0$ is the only quantity required.

Moreover, as will be shown in the next section, both for the potential and for the cross components of the velocity, an important and simple relation exists between their values at corresponding points in the planes $x = 0$ and $x = +\infty$. The name "corresponding points" indicates here, as in the following discussion, points having the same values of y and z.

19. Determination of the Additional Flow (Continued). The vortex system of the wing being given, the velocity of the airfoil flow may be determined by means of the formula of Biot and Savart. As given by this formula, the element of induced velocity due to a rectilinear part of a vortex line is parallel to a plane normal to this line. Hence in calculating the component u, only the lifting vortex need be taken in account, the trailing vortices contributing to the cross components of the velocity only. As a consequence the values of u will be symmetrical about the plane $x = 0$:

$$u(-x) = u(+x) \tag{19.1}$$

Of course u is a function of the coordinates y and z also, but the omission of these in the notation will indicate that corresponding points are considered.

Now the difference between the value of the potential at two arbitrary points x_1 and x_2 situated on a line parallel to the axis of x is

$$\varphi(x_2) - \varphi(x_1) = \int_{x_1}^{x_2} \frac{\partial \varphi}{\partial x} dx = \int_{x_1}^{x_2} u\, dx \tag{19.2}$$

Bearing in mind the result given by (19.1), it follows at once that, for any value of x, we have the relation

$$\varphi(0) - \varphi(-x) = \varphi(+x) - \varphi(0)$$

or

$$\varphi(+x) = 2\varphi(0) - \varphi(-x) \tag{19.3}$$

If in (19.2) either x_1 or x_2 tends to infinity, this expression remains valid, as it may be shown that for large values of x, u takes the form x^{-n}, in which n is larger than unity. The same is true for (19.3) and it becomes

$$\varphi(+\infty) = 2\varphi(0) - \varphi(-\infty)$$

At $x = -\infty$ the cross components of the velocity will vanish, so that $\varphi(-\infty)$ will be a constant, independent of y, z. As a constant term in the potential has no physical meaning, it may be omitted with the result

$$\varphi(+\infty) = 2\varphi(0) \tag{19.4}$$

This relation is valid for each set of values of y and z. Hence for the cross components of the velocity, being the derivatives of the potential, the analogous relations will exist. For instance for the most important components of the velocity, we have

$$\left.\begin{aligned} w(+\infty) &= 2w(0) \\ v_r(+\infty) &= 2v_r(0) \end{aligned}\right\} \tag{19.5}$$

In this discussion no special assumptions were made regarding the vortex system of the wing, so that results (19.4) and (19.5) are valid both for the airfoil flow and the additional airfoil flow. Now considering the boundary conditions as they are given by (17.3) and (17.4), it is obvious that for the additional flow, the analogous relations will exist between the values of the potential and of the components of the velocity in the planes $x = 0$ and $x = +\infty$.

At large values of x both u and its derivative $\partial u/\partial x$ will vanish. Hence at $x = +\infty$, the potentials of the airfoil flow, the additional airfoil flow and the additional flow will be functions of y and z only, which moreover satisfy the equation

$$\frac{\partial^2 \varphi}{\partial y^2} + \frac{\partial^2 \varphi}{\partial z^2} = 0$$

and hence are two-dimensional potential functions.

Summarizing the results obtained, the conclusion is that the problem of the influence of the additional flow is reduced to the determination of the component w of a plane potential flow, satisfying the boundary conditions (17.3) and (17.4). This reduction is an important one, as now the more simple and powerful means provided by two-dimensional

potential theory may be used. One of these, leading in many cases to a simple method for calculating the velocity component w of the additional flow, the so-called "method of images", will be discussed in some detail in the following sections.

20. Method of Images (Introduction). In the preceding section the question of the influence of the additional flow for the simplified case introduced in **17**, has been reduced to an investigation of this flow in the plane $x = +\infty$. In this plane both the airfoil flow and the additional airfoil flow, which should be "compensated" by it, have the character of a plane potential flow related to a layer of vortices (or, in simplified cases, a set of line vortices) the axes of which are perpendicular to it. Hence a general solution will be found easily, if only the additional flow related to an isolated line vortex is known.

The similarity of this problem with that of the influence of the walls of a wind tunnel, as treated by airfoil theory, suggests the use here of the method of images, a method which, in the former case, has led to simple results.

First, some general definitions and formulae may be given.

The "image" of a line vortex (original vortex) parallel to the axis of x and crossing the plane considered at a point A, is a similar vortex crossing that plane at the point which is the "image" of A. Stress should be laid here on the fact that this definition does not include anything regarding the vortex strength of the image. For the circle with radius R_1, the center of which coincides with the point $y = 0$, $z = 0$, the relation between the coordinates of the point A (y_1, z_1) and those of its image (y_i, z_i) may, by using complex coordinates, be given in the form

$$\zeta_i = \frac{R_1^2}{\overline{\zeta_1}} \tag{20.1}$$

in which

$$\zeta_i = y_i + iz_i$$
$$\overline{\zeta_1} = y_1 - iz_1$$

Hence, returning to rectangular coordinates, those of the image are

$$\left.\begin{aligned} y_i &= \frac{R_1^2 y_1}{y_1^2 + z_1^2} \\ z_i &= \frac{R_1^2 z_1}{y_1^2 + z_1^2} \end{aligned}\right\} \tag{20.2}$$

As may be shown without difficulty, both (20.1) and (20.2) indicate that the point A and its image are interchangeable.

In the following discussion, it will be assumed that $z_1 = 0$, so that the coordinates of the image are:

$$y_i = \frac{R_1^2}{y_1}; \quad z_i = 0 \tag{20.3}$$

an assumption which does not introduce any restriction in the problem.

The potential of the flow around a line vortex through the point $y = y_1$, $z = 0$, the circulation of which is $+1$, is:

$$\Phi_1 = \frac{1}{2\pi} tan^{-1} \frac{z}{y - y_1} \tag{20.4}$$

In considering the boundary conditions, the value of the potential and of its normal derivative are wanted for the circle $r = R_1$. They are:

$$\Phi_{1\,(r=R_1)} = + \frac{1}{2\pi} tan^{-1} \frac{R_1 \sin\theta}{R_1 \cos\theta - y_1} \tag{20.5}$$

$$\left(\frac{\partial \Phi_1}{\partial r}\right)_{r=R_1} = - \frac{1}{2\pi} \frac{y_1 \sin\theta}{R_1^2 + y_1^2 - 2 R_1 y_1 \cos\theta} \tag{20.6}$$

θ being the angular coordinate given in Fig. 1b. These results are valid independent of whether $y_1 < R_1$ or $y_1 > R_1$, and hence both for a vortex lying inside or outside the slipstream boundary.

By introducing $y_i = R_1^2/y_1$ for y_1, the potential is obtained for the image of the vortex, its strength being supposed for the moment to be $+1$ also:

$$\Phi_2 = \frac{1}{2\pi} tan^{-1} \frac{z}{y - R_1^2/y_1} \tag{20.7}$$

At the boundary, its values and that of its normal derivative are

$$\Phi_{2\,(r=R_1)} = + \frac{1}{2\pi} tan^{-1} \frac{\sin\theta}{\cos\theta - R_1/y_1} \tag{20.8}$$

$$\left(\frac{\partial \Phi_2}{\partial r}\right)_{r=R_1} = - \frac{1}{2\pi} \frac{y_1 \sin\theta}{R_1^2 + y_1^2 - 2 R_1 y_1 \cos\theta} \tag{20.9}$$

Still a third potential will be needed, that of a vortex coinciding with the axis of x, again with circulation $+1$. Here y_1 being equal to zero, this potential is

$$\Phi_3 = \frac{1}{2\pi} tan^{-1} \frac{z}{y} \tag{20.10}$$

and the values at the boundary are

$$\Phi_{3\,(r=R_1)} = \frac{1}{2\pi} \theta \tag{20.11}$$

$$\left(\frac{\partial \Phi_3}{\partial r}\right)_{r=R_1} = 0 \tag{20.12}$$

Between the results given by (20.4) to (20.12) two relations exist, the first being

$$\Phi_{1\,(r=R_1)} + \Phi_{2\,(r=R_1)} = \Phi_{3\,(r=R_1)} \tag{20.13}$$

This may be proved easily by using the well-known trigonometric relation

$$\alpha + \beta = tan^{-1} \frac{tan\,\alpha + tan\,\beta}{1 - tan\,\alpha\, tan\,\beta}$$

and substituting

$$\alpha = 2\pi \Phi_{1\,(r=R_1)}, \qquad \beta = 2\pi \Phi_{2\,(r=R_1)}$$

By comparing (20.6) and (20.9), the second relation is seen at once to be:

$$\left(\frac{\partial \Phi_1}{\partial r}\right)_{r=R_1} = \left(\frac{\partial \Phi_2}{\partial r}\right)_{r=R_1} \tag{20.14}$$

21. Method of Images (Vortex Outside). If the original vortex is situated outside the boundary of the slipstream ($y_1 > R_1$) and has a circulation $\Gamma = +1$, let us suppose that the potential of the additional flow may be given by:

$$\left.\begin{array}{ll} \text{outside } (r \geqq R_1): & \varphi_{eI} = a\,\Phi_2 + b\,\Phi_3 \\ \text{inside } (r \leqq R_1): & \varphi_{eII} = c\,\Phi_1 \end{array}\right\} \tag{21.1}$$

Here Φ_1, Φ_2 and Φ_3 have the values given by (20.4), (20.7) and (20.10) respectively, whereas a, b and c are constants to be determined with the aid of the boundary conditions.

As the singularities of Φ_1 are situated outside, and those of Φ_2 and Φ_3 inside the slipstream circle, the potential of the additional flow, given in the form (21.1), satisfies the condition that it should be free of singularities in both regions.

For the reason given in **17**, in considering the boundary conditions, the potential of the undisturbed flow and of the propeller flow may be left out of account, so that the uncompensated flow may be taken to be that around the original vortex and to have the potential:

$$\left.\begin{array}{ll} \text{outside } (r \geqq R_1): \\ \text{inside } (r \leqq R_1): \end{array}\right\} (\varphi_c + \varphi_d)_{I,\,II} = \Phi_1 \tag{21.2}$$

Introduction of $(\varphi_c + \varphi_d)$ and φ_e, as they are given by (21.2) and (21.1), and of $S = V_{II}/V_I$ in the boundary conditions (17.3), (17.4), leads to:

$$(S + S\,c - 1)\,\Phi_{1\,(r=R_1)} - a\,\Phi_{2\,(r=R_1)} - b\,\Phi_{3\,(r=R_1)} = 0$$

$$(S - c - 1)\left(\frac{\partial \Phi_1}{\partial r}\right)_{r=R_1} + a\,S\left(\frac{\partial \Phi_2}{\partial r}\right)_{r=R_1} + b\,S\left(\frac{\partial \Phi_3}{\partial r}\right)_{r=R_1} = 0$$

or, taking account of the relations (20.12), (20.13) and (20.14):

$$(S - b + S\,c - 1)\,\Phi_{1\,(r=R_1)} - (a + b)\,\Phi_{2\,(r=R_1)} = 0$$

$$(S + S\,a - c - 1)\left(\frac{\partial \Phi_1}{\partial r}\right)_{r=R_1} = 0$$

Now the latter conditions are to be satisfied at each point of the boundary. As $\Phi_{1\,(r=R_1)}$, $\Phi_{2\,(r=R_1)}$ and $\left(\frac{\partial \Phi_1}{\partial r}\right)_{r=R_1}$ are non-constant functions of θ, and as the first two are linear independent, this will only be possible if a, b and c satisfy the equations:

$$\begin{aligned} b - Sc &= +S - 1 \\ a + b &= 0 \\ Sa - c &= -S + 1, \end{aligned}$$

the solution of which leads to:

$$a = -\frac{S^2 - 1}{S^2 + 1}; \qquad b = +\frac{S^2 - 1}{S^2 + 1}; \qquad c = -\frac{(S-1)^2}{S^2 + 1}$$

The result obtained may be summarized as follows: the uncompensated flow being that around a line vortex with circulation $+\Gamma$, the potential of the additional flow takes the form:

$$\text{outside } (r \geqq R_1): \quad \varphi_{e\,I} = -f_1(S)\,\Gamma\Phi_2 + f_1(S)\,\Gamma\Phi_3 \tag{21.3}$$

$$\text{inside } (r \leqq R_1): \quad \varphi_{e\,II} = -f_2(S)\,\Gamma\Phi_1 \tag{21.4}$$

in which Φ_1, Φ_2 and Φ_3 have the values given by (20.4), (20.7) and (20.10) respectively, whereas

$$f_1(S) = +\frac{S^2-1}{S^2+1} \tag{21.5}$$

$$f_2(S) = +\frac{(S-1)^2}{S^2+1} \tag{21.6}$$

The vortex system of any wing may be considered as composed of a number of horseshoe vortices, so that at $x = +\infty$, we shall have to do with pairs of vortices with equal circulation, but having opposite signs. As a consequence, the term containing Φ_3, which is the potential of the flow around a vortex situated always in the axis of x, is of no practical importance and may be left out of account.

Now considering the other terms, it is seen that outside the boundary, the compensated flow, as far as the direct influence of the original vortex is concerned, is unaltered and the additional flow has the character of that around an image of the original vortex. The strength and sign of this image depend on the value of S and hence on the ratio between the original velocity inside and outside. On the other hand, inside the boundary, the resulting flow has the character of the flow around the vortex coinciding with the original one, the circulation of which is changed from $+\Gamma$ to $+[1-f_2(S)]\,\Gamma$. As the value of $f_2(S)$ will be always positive (except for $S = 1$), the boundary decreases, for the region inside it, the influence of a vortex situated outside.

There are three values of S which may be used for checking the results obtained. For $S = 1$, the additional potential will vanish, as there is no boundary. For $S = \infty$ and $S = 0$ the boundary is identical with a rigid one and with a "free jet surface" respectively, and the results are in accordance with those known for these two cases from the theory of tunnel wall interference.

22. Method of Images (Vortex Inside; Summary of Results). For the original vortex with $\Gamma = +1$ situated inside the boundary, the potential of the additional flow may be given in the form:

$$\text{outside } (r \geqq R_1): \quad \varphi_{e\,I} = d\,\Phi_1 + e\,\Phi_3 \tag{22.1}$$

$$\text{inside } (r \leqq R_1): \quad \varphi_{e\,II} = f\,\Phi_2 \tag{22.2}$$

As, compared with the foregoing case, the original vortex and its image have changed their position, here again the condition of freedom of singularities is satisfied.

Now introduction of (21.2), (22.1) and (22.2) in the boundary conditions leads, in the same way as in **21**, to the equations:

$$\begin{aligned} d + e &= +S - 1 \\ e - Sf &= 0 \\ Sd - f &= -S + 1 \end{aligned}$$

having the solution:

$$d = -\frac{(S-1)^2}{S^2+1}; \quad e = +\frac{S(S^2-1)}{S^2+1}; \quad f = +\frac{S^2-1}{S^2+1}$$

Hence, for the uncompensated flow around a line vortex with circulation $+\Gamma$, the potential of the additional flow will be here:

$$\text{outside } (r \geqq R_1): \quad \varphi_{e\,I} = -f_2(S)\,\Gamma\Phi_1 + S f_1(S)\,\Gamma\Phi_3 \tag{22.3}$$

$$\text{inside } (r \leqq R_1): \quad \varphi_{e\,II} = +f_1(S)\,\Gamma\Phi_2 \tag{22.4}$$

Φ_1, Φ_2 and Φ_3 have here again the values given by (20.4), (20.7) and (20.10) respectively, whereas $f_1(S)$ and $f_2(S)$ are the functions defined by (21.5) and (21.6).

The meaning of this result is similar to that discussed in **21**. For the region in which the original vortex is situated, the additional flow is that around a vortex, which is the image of the original one. In the other region, leaving the potential Φ_3 out of discussion for the reason mentioned already, the resulting flow has the same character as that around the original vortex, but at each point the value of the potential and so that of the velocity, is decreased by the influence of the boundary.

Here too the results may be checked by the introduction of $S = 1$, $S = 0$, and $S = \infty$, but it should be remarked that, owing to the meaning of S, the physical interpretation of the cases $S = 0$ and $S = \infty$ is interchanged.

The results obtained are indicated schematically in Fig. 14. This figure gives, from left to right, the uncompensated flow, the compensated flow outside the slipstream boundary and the compensated flow inside the boundary. In each case the flow is indicated by the vortices, to which it is related. Vortices, situated in the region considered are indicated by full line, the others by dotted arrows.

Thus far, both in the deduction of the boundary conditions and in the determination of the additional flow, S has been considered an arbitrary constant. As in applying the results it will be assumed that $(V_{II} - V_I)$ is small compared with V_I, S will differ only slightly from unity. Now introducing $S = 1 + s$

and neglecting second and higher powers of s, we get:

$$f_1(S) = +s; \quad f_2(S) = 0; \quad S f_1(S) = +s$$

and the results, given in their general form by (21.3), (21.4) and (22.3), (22.4) take the following simplified forms:

The uncompensated flow being that around a vortex with circulation $+\Gamma$ and $s = (V_{II}/V_I) - 1$ being small, the potential φ_e of the additional flow is given:

a) If the original vortex is situated outside the boundary of the slipstream, by:

$$\text{outside } (r \geqq R_1): \quad \varphi_{eI} = -s\Gamma\Phi_2 + s\Gamma\Phi_3 \tag{22.5}$$

$$\text{inside } (r \leqq R_1): \quad \varphi_{eII} = 0 \tag{22.6}$$

b) If the original vortex is situated inside the boundary mentioned, by:

$$\text{outside } (r \geqq R_1): \quad \varphi_{eI} = +s\Gamma\Phi_3 \tag{22.7}$$

$$\text{inside } (r \leqq R_1): \quad \varphi_{eII} = +s\Gamma\Phi_2 \tag{22.8}$$

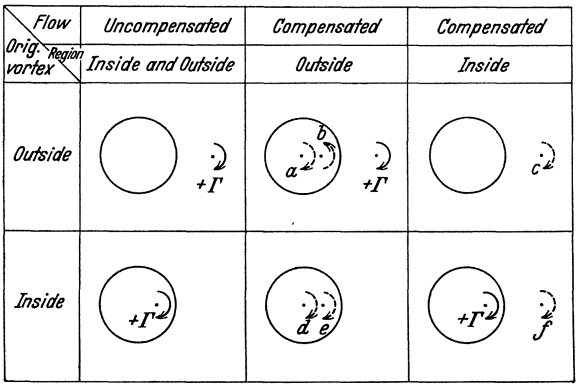

Fig. 14. Images of vortices
Continuous line = vortices in the region considered
Broken line = vortices outside the region considered

a $= +f_1(S)\,\Gamma$ d $= +Sf_1(S)\,\Gamma$
b $= -f_1(S)\,\Gamma$ e $= +[1 - f_2(S)]\,\Gamma$
c $= +[1 - f_2(S)]\,\Gamma$ f $= +f_1(S)\,\Gamma$

Here, as before, Φ_1, Φ_2 and Φ_3 indicate the potentials, as they are given by (20.4), (20.7) and (20.10) respectively. Hence, for small values of s, the influence of the images in the region in which the original vortex is situated remains, but that of the boundary on the flow in the other region vanishes.

23. The Equation for the Change in Circulation. General Form. In treating the influence of the ideal propeller on the properties of the wing, the central part of the problem is the determination of the change in circulation. The fundamental equation for this change will be derived here; the way in which a solution may be obtained will be given later in discussing the different forms of the problem.

After the foregoing discussion leading to the introduction of the additional flow, it is evident that it is not allowable to calculate the change in circulation by considering only the change in local velocity which is directly related to the propeller flow.

To derive the equation for the change in circulation, let us start with the problem of a wing situated in an arbitrary flow, which in its absence, would have the velocity components $V + v_x$, v_y and v_z. No restrictions bearing upon the magnitude of these components or the general character of the flow will for the moment be introduced.

The dimensions, aerodynamic properties and geometrical angle of attack α of an element of the wing being given, the force acting on it depends on the direction and magnitude of the local velocity only. As has been noted in **13**, the angle α is the sum of the induced and effective angles of attack:

$$\alpha = \alpha_i + \alpha_e \tag{23.1}$$

The induced angle of attack has to be taken in the generalized sense, as was indicated in **13**, and is given by:

$$\alpha_i = tan^{-1} \frac{v_z + w(\Gamma)}{V + v_x} \tag{23.2}$$

The symbol $w(\Gamma)$ calls for some explanation. It is used to represent the velocity component w at the point considered, as it is caused by the action of the wing in the resulting flow. Hence, using the terminology introduced in **14**, it is equal to the sum of the components w of the airfoil flow, the additional airfoil flow and the additional flow. It will depend both on the vortex system of the wing (in the resulting flow) and on the values of v_x, v_y and v_z throughout the entire field of flow. Moreover it will be a function of the coordinates of the wing element.

The effective angle of attack α_e may be expressed by the circulation Γ around the element, bearing in mind that on the one hand the force normal to the local velocity is equal to:

$$dL_\infty = \varrho \, \Gamma \, V_t \, dy$$

on the other to:

$$dL_\infty = C_{L\infty} \, (1/2) \, \varrho \, V_t^2 \, c \, dy = (C_0 + C_1 \, \alpha_e) \, (1/2) \, \varrho \, V_t^2 \, c \, dy$$

as noted in **12**. Equating these expressions we have,

$$\alpha_e = \frac{2\,\Gamma}{C_1 \, V_t \, c} - \frac{C_0}{C_1} \tag{23.3}$$

Introduction of (23.2) and (23.3) in (23.1) leads to the general equation for the circulation:

$$tan^{-1} \frac{v_z + w(\Gamma)}{V + v_x} + \frac{2\,\Gamma}{C_1 \, V_t \, c} = \alpha + \frac{C_0}{C_1} \tag{23.4}$$

It should be remarked that in the symbol $w(\Gamma)$, Γ indicates the whole vortex system of the wing, whereas in the second member it means the circulation at the point considered.

24. The Equation for the Change in Circulation. Special Form. In the foregoing deduction, the velocity components v_x, v_y and v_z were considered to be arbitrary. Now coming to the case in which they are the velocity components of the propeller flow, we know from the discussion given in **5**, that they are proportional to a parameter a.

Hence they may be given in the form $(v_x/a)\,a$, $(v_y/a)\,a$ and $(v_z/a)\,a$, the fractions (v_x/a), etc. being functions of the coordinates x, y, z and the propeller radius R only. Moreover the values of these fractions are finite at every point.

It follows that Γ and $w(\Gamma)$ will be functions of a also and we will suppose that these functions are regular in the neighborhood of $a = 0$, so that they may be expanded in power series of a. For the circulation this series takes the form:

$$\Gamma = \Gamma_0 + \Gamma_1 a + \ldots \text{ higher powers of } a \tag{24.1}$$

In expanding $w(\Gamma)$, account should be taken of the fact that both the vortex system, indicated by Γ, and the relation between a given vortex system and the velocity component w, as indicated by the functional operator $w(\ )$, depend on a. This results in a series of the form:

$$w(\Gamma) = w_0(\Gamma_0) + w_1(\Gamma_0)\,a + w_0(\Gamma_1)\,a + \ldots \text{ higher powers of } a \tag{24.2}$$

The meaning of the symbols introduced here is the following:

$w_0(\Gamma_0)$: the component w of the disturbance velocity due to the action of the wing, a being zero, in the absence of the propeller, and Γ_0 indicating the vortex system of the wing in this case;

$w_1(\Gamma_0)a + w_0(\Gamma_1)a$: the total change of w caused by the action of the propeller for small values of a, a change which may be decomposed into the two parts:

$w_1(\Gamma_0)a$: the change of w which would occur if the propeller was introduced, but the vortex system of the wing was left unaltered;

$w_0(\Gamma_1)a$: the change of w in the case that, in the flow without the propeller, the vortex system of the wing was changed in such a way as to make it identical with that in the resulting flow with the propeller.

Or again, speaking in the terminology introduced in **14**, $w_0(\Gamma_0)$ is the velocity component w of the airfoil flow, $w_0(\Gamma_1)\,a$ that of the additional airfoil flow and $w_1(\Gamma_0)\,a$ that of the additional flow. As to the latter, it should be remarked that only the influence of that part of the additional flow is taken in account which is related to the airfoil flow. The second part, depending on the additional airfoil flow is neglected as it depends on second and higher powers of a only.

25. The Equation for the Change in Circulation. Special Form (Continued). As is known from **6**, a may be considered a small quantity, so that its second and higher powers may be here neglected. Moreover, for the same reasons as in airfoil theory, $w(\Gamma)$ may also be taken to be a small quantity.

Now first expanding α_i from (23.2) in terms of v_x and v_z and afterward introducing their values and that of w given in **24**, we find:

$$\left.\begin{aligned}\alpha_i = \frac{w(\Gamma)}{V} + \frac{v_z}{V} - \frac{w(\Gamma)}{V^2}v_x = \frac{1}{V}w_0(\Gamma_0) - \frac{w_0(\Gamma_0)}{V^2}\frac{v_x}{a}a + \\ + \frac{1}{V}\frac{v_z}{a}a + \frac{1}{V}w_1(\Gamma_0)\,a + \frac{1}{V}w_0(\Gamma_1)\,a + \ldots\end{aligned}\right\} \tag{25.1}$$

As, according to the definition given in **12**,

$$V_t = [(V + v_x + u)^2 + (v_z + w)^2]^{1/2} = V + \left(\frac{v_x}{a}\right) a + \ldots \qquad (25.2)$$

expansion of α_e from (23.3) leads to:

$$\alpha_e = \frac{2}{C_1 c}\frac{\Gamma_0}{V} - \frac{C_0}{C_1} + \frac{2}{C_1 c}\frac{\Gamma_1}{V} a - \frac{2}{C_1 c}\frac{\Gamma_0}{V^2}\left(\frac{v_x}{a}\right) a + \ldots \qquad (25.3)$$

Now, putting (25.1) and (25.3) in (23.1) and separating the terms in 1 and a, we obtain, instead of equation (23.4), the two equations:

$$\frac{w_0(\Gamma_0)}{V} + \frac{2}{C_1 c}\frac{\Gamma_0}{V} = \alpha + \frac{C_0}{C_1} \qquad (25.4)$$

$$\frac{w_0(\Gamma_1)}{V} + \frac{2}{C_1 c}\frac{\Gamma_1}{V} = \frac{1}{V^2}\left[w_0(\Gamma_0) + \frac{2}{C_1 c}\Gamma_0\right]\frac{v_x}{a} - \frac{1}{V}\frac{v_z}{a} - \frac{w_1(\Gamma_0)}{V} \qquad (25.5)$$

As was to be expected, the first of these is identical with that given by airfoil theory for the determination of the circulation of a given wing.

Comparison of (25.4) and (25.5) leads to the conclusion that the change in circulation caused by the action of the propeller is identical with that which would result from a certain change in the angle of attack for the wing located in the undisturbed flow.

Equation (25.5) being linear in Γ_1, the influences of v_x, v_z and $w_1(\Gamma_0)$ may be treated separately.

In treating the different forms in which the problem may be encountered, the methods of solution for (25.5) will be discussed. In advance, the following should be noted here. Whereas v_x and v_z are independent of Γ_0, this is not the case for $w_1(\Gamma_0)$. Hence, to obtain a complete solution for Γ_1, it is necessary first to determine the solution of the equation (25.4) or at least a vortex system which will approximate sufficiently that for the wing in the absence of the propeller. This being done, $w_1(\Gamma_0)$, being a component of the additional flow, is to be determined by a method based on the principles given in **18**—**22**.

26. The Changes in Lift, Drag and Pitching Moment. According to **12** the component normal to the local velocity, of the force acting on the element is given by: $dL_\infty = \varrho\,\Gamma\,V_t\,dy$

and its component parallel to that velocity, by dD_∞. The angle between local and undisturbed velocity is α_i. As this angle is small and moreover dD_∞ is small compared with dL_∞, the lift dL and drag dD, being the components respectively normal and parallel to the undisturbed velocity, are:

$$dL = \varrho\,\Gamma\,V_t\,dy \qquad (26.1)$$

$$dD = \varrho\,\Gamma\,V_t\,\alpha_i\,dy + dD_\infty \qquad (26.2)$$

When the second and higher powers of a are neglected, introduction of Γ and V_t, as they are given by (24.1) and (25.2) in (26.1) leads to:

$$dL = \varrho\,\Gamma_0\,V\,dy + \varrho\left(\Gamma_1 V + \Gamma_0\frac{v_x}{a}\right) a\,dy$$

The lift in the absence of the propeller is:

$$d\,L = \varrho\,\Gamma_0\,V\,dy$$

So the total change in lift, caused by the action of the propeller, is given by

$$d\,\triangle L = \varrho\left(\Gamma_1\,V + \Gamma_0\frac{v_x}{a}\right)a\,dy \tag{26.3}$$

This result shows that the change in lift consists of two parts, the first of which is related to the change in circulation, whereas the second depends directly on the component v_x of the propeller flow. As is indicated by equation (25.5) the change in circulation is a function of v_x too, so that, unlike v_z, this quantity influences the lift in two different ways.

The drag of the element, as it is given by (26.2) is composed of two parts: the induced resistance $d\,D_i = \varrho\,\Gamma\,V_t\,\alpha_i\,dy$ and the profile drag $d\,D_p = d\,D_\infty$.

The change in induced resistance may be obtained in the following way. According to (25.1) α_i may be written in the form:

$$\alpha_i = \alpha_{i0} + \alpha_{i1}\,a,$$

in which:

$$\alpha_{i0} = \frac{w_0(\Gamma_0)}{V}; \qquad \alpha_{i1} = -\frac{w_0(\Gamma_0)}{V^2}\frac{v_x}{a} + \frac{1}{V}\frac{v_z}{a} + \frac{w_1(\Gamma_0)}{V} + \frac{w_0(\Gamma_1)}{V}$$

By introducing this result, together with the values of Γ and V_t from (24.1) and (25.2), and neglecting once more the second and higher powers of a, we have,

$$d\,D_i = \varrho\,\Gamma_0\,V\,\alpha_{i0}\,dy + \varrho\left(\Gamma_0\frac{v_x}{a}\alpha_{i0} + \Gamma_0\,V\,\alpha_{i1} + \Gamma_1\,V\,\alpha_{i0}\right)a\,dy$$

The original induced resistance being

$$d\,D_{i0} = \varrho\,\Gamma_0\,V\,\alpha_{i0}\,dy$$

the change in this part of the drag, caused by the action of the propeller, becomes,

$$d\,\triangle D_i = d\,D_i - d\,D_{i0} = \varrho\left(\Gamma_0\frac{v_x}{a}\alpha_{i0} + \Gamma_0\,V\,\alpha_{i1} + \Gamma_1\,V\,\alpha_{i0}\right)a\,dy \tag{26.4}$$

As the profile drag is independent of the angle of attack, the change in this quantity will be equal to

$$d\,\triangle D_p = \left(\frac{V_t^2}{V^2} - 1\right)d\,D_\infty = 2\,\frac{v_x}{a}\,\frac{a}{V}\,d\,D_\infty \tag{26.5}$$

Considering the changes in the two parts of the drag as they are given by (26.4) and (26.5), we come to the conclusion that the change in total resistance may be decomposed into three parts:

a) both the induced resistance and the profile drag are increased by the increase in local velocity due to v_x [(26.5) and first term in (26.4)];

b) the induced resistance is increased owing to the fact that the force acting originally on the element is turned backward through an angle $\alpha_{i1}\,a$ [second term in (26.4)];

c) the induced resistance is increased by the increase of the normal force, the latter being taken in its original direction [third term in (26.4)].

In this latter discussion it was supposed that v_x, α_{i1} and Γ_1 are positive; otherwise, signs should be changed accordingly.

In analogy with the increase of the lift, here the part c) depends partly on v_x. This is an explanation of the fact that, whereas the increase of the profile drag contains the factor 2, the part a) of the increase of induced resistance does not.

For an element of the wing the axis about which the pitching moment is determined may be always chosen such as to make this moment independent of the angle of attack. In this case, the change of the pitching moment will, by analogy with that of the profile drag, be

$$d \triangle M = 2 \frac{v_x}{a} \frac{a}{V} d M \tag{26.6}$$

It should be remarked that in general for the different elements of the wing, the axes defined above will not coincide. Hence the change in pitching moment for the whole wing must be calculated from the changes in the lift and moment for the elements as they are given by (26.3) and (26.6).

CHAPTER II

APPLICATIONS OF THEORY AND EXPERIMENTAL RESULTS

A. Application to Influence on Wing

1. General Method of Solution for the Wing of Finite Span. The circulation Γ_0 in the absence of the propeller and the change in circulation $\triangle \Gamma$, due to its action, are determined by the equations:

$$\frac{w_0(\Gamma_0)}{V} + \frac{2}{C_1 c} \frac{\Gamma_0}{V} = \alpha + \frac{C_0}{C_1} \tag{1.1a}$$

$$\frac{w_0(\triangle \Gamma)}{V} + \frac{2}{C_1 c} \frac{\triangle \Gamma}{V} = \left(\alpha + \frac{C_0}{C_1}\right) \frac{v_x}{V} - \frac{v_z}{V} - \frac{a\, w_1(\Gamma_0)}{V} \tag{1.1b}$$

Whereas the first one is I (25.4), the second is obtained by multiplying I (25.5) by a, introducing $\triangle \Gamma = a \Gamma_1$ and changing the right hand member with the aid of I (25.4).

Both these equations being identical with the equation for the circulation of a wing, the form and angle of attack of which are given, the method of Lotz (see Division E IV 3) may be used for their solution.

The discussion will be here restricted to the special case of the elliptic wing with constant geometrical angle of attack. Moreover only the change in lift will be considered, but an extension of the method to other wing forms and to other aerodynamic properties will not present difficulties.

First, the variable ψ is introduced, defined by

$$y = -b \cos\psi \tag{1.2}$$

in which b is the semi-span of the wing.

As $$w_0(\Gamma_0) = \frac{1}{4\pi}\int_{-b}^{+b} \frac{d\Gamma_0}{dy_1}\frac{dy_1}{y-y_1} = \frac{1}{4\pi b}\int_0^{\pi} \frac{d\Gamma_0}{d\psi_1}\frac{d\psi_1}{\cos\psi_1 - \cos\psi}$$

and $$c = c_0 \sin\psi$$

in which c_0 is the chord of the median section of the wing, the solution of (1.1a) is found to be

$$\Gamma_0 = \frac{1}{2} V c_0 C_1 \frac{8b}{8b + c_0 C_1}\left(\alpha + \frac{C_0}{C_1}\right)\sin\psi \tag{1.3}$$

This result leads to the lift L_0 and lift coefficient C_{L0} for the wing in the absence of the propeller

$$L_0 = \int_0^{\pi} \varrho\, \Gamma_0\, V b \sin\psi\, d\psi = \frac{\pi}{4}\varrho\, V^2 b c_0 C_1 \frac{8b}{8b + c_0 C_1}\left(\alpha + \frac{C_0}{C_1}\right)$$

$$C_{L0} = \frac{L_0}{\frac{1}{2}\varrho V^2 \frac{\pi}{2} c_0 b} = C_1 \frac{8b}{8b + c_0 C_1}\left(\alpha + \frac{C_0}{C_1}\right) \tag{1.4}$$

By introducing (1.4) in (1.3), Γ_0 may be written in the form

$$\Gamma_0 = \frac{1}{2} V c_0 C_{L0} \sin\psi \tag{1.5}$$

a form which will be used in the following.

Equation (1.1b) is solved in an analogous way by introducing

$$\left.\begin{aligned} \triangle\Gamma &= \frac{1}{2} V c_0 C_1 \sum_1^{\infty} a_n \sin n\psi \\ \left[\left(\alpha + \frac{C_0}{C_1}\right)\frac{v_x}{V} - \frac{v_z}{V} - \frac{a\, w_1(\Gamma_0)}{V}\right]\sin\psi &= \sum_1^{\infty} \alpha_n \sin n\psi \end{aligned}\right\} \tag{1.6}$$

in which

$$\alpha_n = \frac{2}{\pi}\int_0^{\pi}\left[\left(\alpha + \frac{C_0}{C_1}\right)\frac{v_x}{V} - \frac{v_z}{V} - \frac{a\, w_1(\Gamma_0)}{V}\right]\sin\psi \sin n\psi\, d\psi \tag{1.7}$$

Equation (1.1b) now takes the form,

$$\frac{c_0 C_1}{8b}\sum_1^{\infty} n a_n \sin n\psi + \sum_1^{\infty} a_n \sin n\psi = \sum_1^{\infty} \alpha_n \sin n\psi$$

so that for each value of n, the coefficient a_n is given by

$$a_n = \frac{8b}{8b + n c_0 C_1}\alpha_n \tag{1.8}$$

For the determination of the lift, only the first term of the series (1.6) is of interest. Hence, making use of (1.6), (1.8), (1.7) and (1.4), $\triangle \Gamma$ may be written in the form,

$$\left.\begin{aligned}\triangle \Gamma = \frac{1}{\pi} V c_0 \sin\psi \Big[C_{L0} \int_0^\pi \frac{v_x}{V} \sin^2\psi \, d\psi - \\ - \Big(\frac{d C_L}{d\alpha}\Big)_0 \int_0^\pi \Big(\frac{v_z}{V} + \frac{a w_1(\Gamma_0)}{V}\Big) \sin^2\psi \, d\psi \Big] + \\ + \frac{1}{2} V c_0 C_1 \sum_2^\infty a_n \sin n\psi\end{aligned}\right\} \quad (1.9)$$

It should be remembered that the meaning of $(d C_L/d\alpha)_0$ is the change in lift coefficient with geometrical angle of attack for the wing of finite span and without propeller.

From I (26.3) it is known that the increase of lift consists of two parts, which for the moment will be indicated by $\triangle_A L$ and $\triangle_B L$, being given for the element by

$$d \triangle_A L = \varrho V b \triangle \Gamma \sin\psi \, d\psi$$
$$d \triangle_B L = \varrho v_x b \Gamma_0 \sin\psi \, d\psi$$

For the wing the value of the first part is obtained by introduction of $\triangle \Gamma$ from (1.9) and integration over the span:

$$\left.\begin{aligned}\triangle_A L = \frac{1}{2} \varrho V^2 b c_0 \Big[C_{L0} \int_0^\pi \frac{v_x}{V} \sin^2\psi \, d\psi - \\ - \Big(\frac{d C_L}{d\alpha}\Big)_0 \int_0^\pi \Big(\frac{v_z}{V} + \frac{a w_1(\Gamma_0)}{V}\Big) \sin^2\psi \, d\psi \Big]\end{aligned}\right\} \quad (1.10)$$

the second by introduction of Γ_0 from (1.5) and integration:

$$\triangle_B L = \frac{1}{2} \varrho V^2 b c_0 C_{L0} \int_0^\pi \frac{v_x}{V} \sin^2\psi \, d\psi \quad (1.11)$$

Taking the two parts together and proceeding to the lift coefficient, the final result is obtained

$$\left.\begin{aligned}\triangle C_L = \frac{\triangle_A L + \triangle_B L}{\frac{1}{2} \varrho V^2 \frac{\pi}{2} c_0 b} = \frac{2}{\pi} \Big[2 C_{L0} \int_0^\pi \frac{v_x}{V} \sin^2\psi \, d\psi - \\ - \Big(\frac{d C_L}{d\alpha}\Big)_0 \int_0^\pi \Big(\frac{v_z}{V} + \frac{a w_1(\Gamma_0)}{V}\Big) \sin^2\psi \, d\psi \Big]\end{aligned}\right\} \quad (1.12)$$

Comparison of (1.10) and (1.11) shows that, so far as the influence of v_x is concerned, just one half of the increase in lift is caused by the change in circulation, the other half directly by v_x.

The right hand member of (1.1b) has been supposed to be known, but the determination of $a\,w_1\,(\Gamma_0)$ is still to be discussed. The character and importance of the influence of this component of the additional flow depend on the relative position of the wing and slipstream boundary. Three cases, in which this position is fundamentally different, will be treated here separately: the wing in front of the propeller plane (see 2), the wing behind the propeller plane, but outside the slipstream boundary (see 3), and the wing crossing the slipstream boundary (see 8). As an introduction to the latter case the more simple problem of the wing of infinite span will be first considered (see 4—7).

2. The Wing in Front of the Propeller Plane. In contrast with the approximate solution for the propeller flow given in I 5, the real flow will be continuous in the entire region in front of the propeller. Hence the surface of discontinuity, which according to the discussion in I **15** is responsible for the existence of the additional flow, is situated entirely behind the wing. Now this part of the flow may be considered to be related to a change in the vortices which form the boundary of the slipstream. Hence its component w will die out rather rapidly upstream of the propeller. Moreover, for the wing which does not cross the surface of discontinuity, in general the influence of the additional flow will not be very important compared with the direct influence of v_x and v_z. Together this gives sufficient reason for the assumption that for the wing in front, the influence of the additional flow may be neglected altogether, so that here we may write $a\,w_1\,(\Gamma_0) = 0$.

From I 5 it is known that both v_x and v_z have a quite different form in the regions $r > R_1$ and $r < R_1$. Hence in calculating the change in lift coefficient, as in (1.12), it is practical to separate these two regions, thus leading to

$$\triangle C_L = \triangle_1 C_L + \triangle_2 C_L + \triangle_3 C_L + \triangle_4 C_L \tag{2.1}$$

in which the parts are respectively due to: v_x in the region $r > R_1$ ($\triangle_1 C_L$), v_x in the region $r < R_1$ ($\triangle_2 C_L$), v_z in the region $r > R_1$ ($\triangle_3 C_L$) and v_z in the region $r < R_1$ ($\triangle_4 C_L$). This notation will be maintained and extended in the following.

Taking the coordinates of the centre of the wing to be x_0, 0, z_0, introduction in (1.12) of the values of v_x and v_z, as they are given by the first and last equations of I (5.7) and (5.8) leads to

$$\triangle_1 C_L = -2\,a\,C_{L\,0}\,\frac{x_0}{(x_0^2 + b^2 + z_0^2)^{1/2}}\,f_1\,(x_0, z_0, b, R, \psi_1) \tag{2.2a}$$

$$\triangle_2 C_L = 4\,s\,C_{L\,0}\,f_2\,(\psi_1) \tag{2.2b}$$

$$\triangle_3 C_L = a\left(\frac{d\,C_L}{d\,\alpha}\right)_0 \frac{z_0}{(x_0^2 + b^2 + z_0^2)^{1/2}}\,f_1\,(x_0, z_0, b, R, \psi_1) \tag{2.2c}$$

$$\triangle_4 C_L = a\left(\frac{d\,C_L}{d\,\alpha}\right)_0 \frac{R^2 z_0}{(R^2 + x_0^2)^{3/2}}\,f_2\,(\psi_1) \tag{2.2d}$$

with

$$f_1(x_0, z_0, b, R, \psi_1) = \frac{2}{\pi}\frac{R^2}{b^2}\left[-F(k,\psi_1) + \frac{x_0^2+b^2+z_0^2}{x_0^2+z_0^2}E(k,\psi_1) - \right.$$
$$\left. - \frac{1}{2}\frac{b^2}{x_0^2+z_0^2}\frac{\sin 2\psi_1}{\sqrt{1-k^2\sin^2\psi_1}}\right]$$

$$f_2(\psi_1) = \frac{1}{\pi}\left(\frac{\pi}{2} - \psi_1 + \frac{1}{2}\sin 2\psi_1\right)$$

$$F(k,\psi_1) = \int_0^{\psi_1} \frac{d\psi}{\sqrt{1-k^2\sin^2\psi}}$$

$$E(k,\psi_1) = \int_0^{\psi_1} d\psi \sqrt{1-k^2\sin^2\psi}$$

$$k^2 = \frac{b^2}{x_0^2+b^2+z_0^2}$$

$$\psi_1 = \cos^{-1}\frac{y_1}{b} = \cos^{-1}\frac{(R_1^2-z_0^2)^{1/2}}{b}$$

$$s = a\left[1 + \frac{x_0}{(R^2+x_0^2)^{1/2}}\right]$$

y_1 is the value of y for the point in which the wing cuts the circle $r = R_1$ and ψ_1 is the corresponding value of ψ.

If $|z_0| > R_1$, so that the wing is situated entirely outside the region $r \leqq R_1$, $\triangle_2 C_L$ and $\triangle_4 C_L$ are zero and ψ_1 should be taken equal to $\pi/2$.

3. The Wing Behind the Propeller Plane and Outside the Slipstream Boundary. For the wing behind the propeller plane and $|z_0| > R_1$, as before, the partial changes in C_L due to v_x and v_z are respectively equal to $\triangle_1 C_L$ and $\triangle_3 C_L$ as they are given by (2.2a) and (2.2c) with $\psi_1 = \pi/2$, whereas $\triangle_2 C_L$ and $\triangle_4 C_L$ are zero.

In contrast with the case treated above, the influence here of the additional flow must be taken into account. To make it possible to calculate the corresponding part of the change in C_L, we will assume that the influence of the real boundary is the same as that of a cylindrical boundary coaxial with the original one and extending from $x = -\infty$ to $x = +\infty$. The radius of this cylinder is equal to R_1, the change in axial velocity sV at its surface, become v_x, as given by I (5.9) and the first of I (5.7) respectively for the section $x = x_0$.

Now according to the discussion given in I **19—22**, the component w of the velocity of the additional flow may be calculated for any distribution of the circulation Γ_0 by considering the images of the trailing vortices of the wing. But, to simplify the calculation, we will replace the vortex system of the wing by a horse-shoe vortex, the latter having the same span $2b$ and a circulation $\Gamma = (\pi/8)\, C_{L0}\, V c_0$ such as to make the lift equal in both cases. Hence in the plane $x = +\infty$ the component w considered is due to a pair of vortex images with the coordinates

$$y_i = \pm R_1^2\, b/(b^2 + z_0^2), \qquad z_i = + R_1^2\, z_0/(b^2 + z_0^2)$$

and the circulation $\Gamma_i = (\pi/8)\, s\, C_{L0}\, V c_0$ (see I **20** and **22**). This gives

$$w = \frac{\Gamma_i}{2\pi}\left[\frac{y - y_i}{(y - y_i)^2 + (z_0 - z_i)^2} - \frac{y + y_i}{(y + y_i)^2 + (z_0 - z_i)^2}\right]$$

whereas according to the first equation of I (19.5),

$$a w_1(\Gamma_0) = (1/2)\, w$$

Introduction of this result in (1.12) leads to the change in lift coefficient due to the additional flow:

$$\triangle_5 C_L = - s\, C_{L0} \left(\frac{d C_L}{d\alpha}\right)_0 \frac{c_0}{b} f_5(z_0, b, R_1) \tag{3.1}$$

with

$$f_5(z_0, b, R_1) = - \frac{1}{8b}\left[y_i + R\left(i\sqrt{b^2 - \zeta_i^2}\right)\right]$$

in which ζ_i is the complex number given by

$$\zeta_i = y_i - i\,(z_0 - z_i)$$

and $R\left(i\sqrt{b^2 - \zeta_i^2}\right)$ is the real part of $i\sqrt{b^2 - \zeta_i^2}$.

Moreover y_i and z_i have the values as above, both having positive signs.

The case of the wing, situated entirely inside the slipstream boundary has not been considered here, but it might be treated in a similar way.

4. The Wing of Infinite Span Crossing the Slipstream Boundary. In the determination of the velocity component w of the additional flow for the wing outside the slipstream boundary, only the influence of the trailing vortices had to be taken in account. As a consequence, for a wing of infinite span with constant circulation and hence without trailing vortices, the additional flow will vanish and there will be no influence of the slipstream boundary.

If the wing crosses the slipstream boundary, the situation is changed. Even if the wing is such as to have a constant circulation at each section, the mere fact that at both sides of the boundary the circulation and hence the velocity component u has the same value, violates the boundary condition of equal pressure [see I (17.1)]. The latter will be satisfied only by a flow in which a sudden change in circulation occurs at the boundary, such that the circulation is inversely proportional to the velocity. This involves the existence of an additional flow having a corresponding change in w.

Before treating the more complicated problem of the wing of finite span, a simple case will be discussed, as indicated schematically in Fig. 15a. The wing of infinite span, the lifting vortex of which coincides with the axis of y, is prismatic. The propeller flow has the simplified character introduced in I **17**. Hence the slipstream boundary is a circular cylinder, extending from $x = -\infty$ to $x = +\infty$, with its axis coinciding with the axis of x, its radius being R_1. The velocity component v_z is zero everywhere and the component v_x is zero in the region outside

the boundary, whereas inside, it has the constant value sV, s being small compared with unity.

The determination of the circulation will be based on the results obtained in I **19**, which enable us to reduce the problem to one of a two-dimensional flow in the plane $x = +\infty$.

From airfoil theory it is known that on a surface behind the wing, formed by lines parallel to the axis of x and extending from the wing to infinity, the potential of the flow shows a discontinuous change equal to the circulation for the corresponding section of the wing (see Division E I **7**). This surface of discontinuity and the slipstream boundary divide the plane $x = +\infty$ into four regions (see Fig. 15b). To distinguish the potential in these regions double suffixes will be introduced:

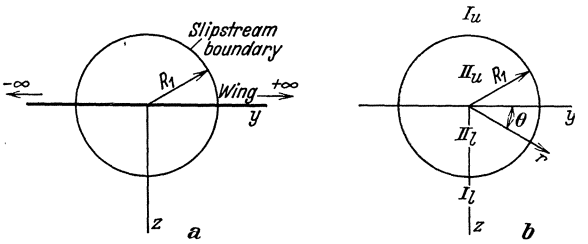

Fig. 15. The wing of infinite span crossing the slipstream boundary: a) the plane $x = 0$, b) the plane $x = +\infty$.

I and II indicate whether the part considered is situated outside or inside the slipstream boundary, whereas u ("upper") and l ("lower") are used for the region respectively above or below the surface of discontinuity behind the wing.

At the boundaries $z = 0$ and $r = R_1$ the potential has to satisfy certain conditions which lead to eight relations from which it is to be determined.

The first two relations, which are obtained at once from the condition that the normal velocity shall be continuous at the boundary $z = 0$, are:

$$z = 0,\ r > R_1: \frac{\partial \varphi_{Iu}}{\partial z} = \frac{\partial \varphi_{Il}}{\partial z} \tag{4.1a}$$

$$z = 0,\ r < R_1: \frac{\partial \varphi_{IIu}}{\partial z} = \frac{\partial \varphi_{IIl}}{\partial z} \tag{4.1b}$$

The second set of two relations may be derived from the equation for the circulation [see I (23.4)]. As $w(\Gamma)$ is small and v_z zero, it may be written in the form,

$$\frac{w(\Gamma)}{V + v_x} + \frac{2\Gamma}{C_1 c (V + v_x)} = \alpha + \frac{C_0}{C_1} \tag{4.2}$$

As indicated above, between the circulation and the change in potential there exists the relation,

$$\Gamma = (\varphi_u - \varphi_l)_{z=0} \tag{4.3}$$

Moreover it follows from the first equation of I (19.5), that

$$w(\Gamma) \equiv w(0) = \frac{1}{2} w(+\infty) \equiv \frac{1}{2} \left(\frac{\partial \varphi_u}{\partial z} \right)_{z=0} \tag{4.4}$$

Introduction of these results in (4.2) leads to

$$z = 0,\ r > R_1: \frac{1}{2V} \frac{\partial \varphi_{Iu}}{\partial z} + \frac{2(\varphi_{Iu} - \varphi_{Il})}{C_1 c V} = \alpha + \frac{C_0}{C_1} \tag{4.1c}$$

$$z = 0,\ r < R_1: \frac{1}{2V} \frac{\partial \varphi_{IIu}}{\partial z} + \frac{2(\varphi_{IIu} - \varphi_{IIl})}{C_1 c V} = (1+s)\left(\alpha + \frac{C_0}{C_1}\right) \tag{4.1d}$$

The remaining four conditions, which are to be satisfied at the boundary of the slipstream, follow from the boundary conditions I (17.3) and (17.4). The potential indicated by $(\varphi_c + \varphi_d + \varphi_e)$ is identical with the potential φ as it is used here. Hence they result in

$$r = R_1,\ 0 < \theta < \pi: \quad \varphi_{Il} = (1+s)\,\varphi_{IIl} \tag{4.1e}$$

$$r = R_1,\ \pi < \theta < 2\pi: \quad \varphi_{Iu} = (1+s)\,\varphi_{IIu} \tag{4.1f}$$

$$r = R_1,\ 0 < \theta < \pi: \quad \frac{\partial \varphi_{IIl}}{\partial r} = (1+s)\frac{\partial \varphi_{Il}}{\partial r} \tag{4.1g}$$

$$r = R_1,\ \pi < \theta < 2\pi: \quad \frac{\partial \varphi_{IIu}}{\partial r} = (1+s)\frac{\partial \varphi_{Iu}}{\partial r} \tag{4.1h}$$

5. The Wing of Infinite Span Crossing the Slipstream Boundary (Continued). If s is zero, the conditions (4.1) are satisfied by:

$$\varphi_{0Iu} = \varphi_{0IIu} = +\frac{1}{4} C_1 c V \left(\alpha + \frac{C_0}{C_1}\right) \tag{5.1a}$$

$$\varphi_{0Il} = \varphi_{0IIl} = -\frac{1}{4} C_1 c V \left(\alpha + \frac{C_0}{C_1}\right) \tag{5.1b}$$

the suffix 0 indicating, as before, the absence of slipstream influence.

According to (4.3), the circulation will be,

$$\Gamma_0 = \varphi_{0u} - \varphi_{0l} = \frac{1}{2} C_1 c V \left(\alpha + \frac{C_0}{C_1}\right) \tag{5.2}$$

For the general case, in which s differs from zero, φ is introduced in the form

$$\varphi = \varphi_0 + \triangle \varphi \tag{5.3}$$

of which the first part is equal to the value of φ_0 given by (5.1). The value of s being small, $\triangle \varphi/\varphi_0$ will be small of the same order. Hence, after expansion of the conditions (4.1) in power series of s and $\triangle \varphi/\varphi_0$, only the terms of order 0 and 1 are to be retained, so that two sets of equations are obtained. The first set contains only φ_0 and as it leads again to the solution (5.1), no further discussion of it is needed. As $(\partial \varphi_0/\partial r)_{r=R_1}$ is zero for all regions, in using the results (5.1) and (5.2) the second set takes the form:

$$z = 0, r > R_1: \frac{\partial \triangle \varphi_{Iu}}{\partial z} = \frac{\partial \triangle \varphi_{Il}}{\partial z} \tag{5.4a}$$

$$z = 0, r < R_1: \frac{\partial \triangle \varphi_{IIu}}{\partial z} = \frac{\partial \triangle \varphi_{IIl}}{\partial z} \tag{5.4b}$$

$$z = 0, r > R_1: \frac{C_1 c}{4} \frac{\partial \triangle \varphi_{I\,u}}{\partial z} + \triangle \varphi_{I\,u} - \triangle \varphi_{I\,l} = 0 \tag{5.4c}$$

$$z = 0, r < R_1: \frac{C_1 c}{4} \frac{\partial \triangle \varphi_{II\,u}}{\partial z} + \triangle \varphi_{II\,u} - \triangle \varphi_{II\,l} = s\,\Gamma_0 \tag{5.4d}$$

$$r = R_1,\ 0 < \theta < \pi: \quad \triangle \varphi_{I\,l} - \triangle \varphi_{II\,l} = -\frac{1}{2} s\,\Gamma_0 \tag{5.4e}$$

$$r = R_1,\ \pi < \theta < 2\pi: \quad \triangle \varphi_{I\,u} - \triangle \varphi_{II\,u} = +\frac{1}{2} s\,\Gamma_0 \tag{5.4f}$$

$$r = R_1,\ 0 < \theta < \pi: \quad \frac{\partial \triangle \varphi_{II\,l}}{\partial r} = \frac{\partial \triangle \varphi_{I\,l}}{\partial r} \tag{5.4g}$$

$$r = R_1,\ \pi < \theta < 2\pi: \quad \frac{\partial \triangle \varphi_{II\,u}}{\partial r} = \frac{\partial \triangle \varphi_{II\,l}}{\partial r} \tag{5.4h}$$

From these conditions $\triangle \varphi$ is to be determined. This is done most conveniently by taking the plane $x = +\infty$, considered thus far, to

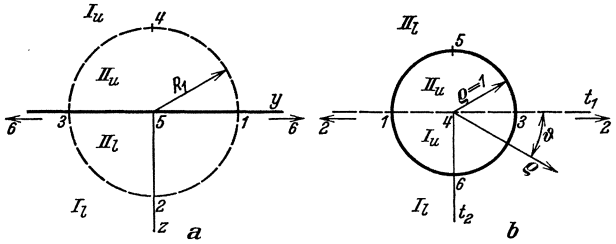

Fig. 16. The transformation $\zeta = -R_1\,(t + i)/(i\,t + 1)$; a = ζ plane, b = t plane.

be the plane of the complex variable $\zeta = y + iz$ and transforming it in the plane of the variable $t = t_1 + it_2$ by:

$$\zeta = -R_1 \frac{t + i}{it + 1} \tag{5.5}$$

Now the real axis of the ζ plane ("wing") becomes the circle with radius 1 and centre $t = 0$ in the t plane and the circle with radius R_1 ("slipstream boundary") the real axis. The relation between the different regions in both planes and between certain points which are of interest, is indicated in Fig. 16.

For the real axis $z = 0$ of the ζ plane, (5.5) takes the form

$$y = -R_1 \frac{\cos \vartheta}{1 - \sin \vartheta} \tag{5.6}$$

in which ϑ is the angular coordinate in the t plane, whereas here the absolute value of the differential coefficient of the transformation function is

$$\left| \frac{d\,t}{d\,\zeta} \right| = \frac{1 - \sin \vartheta}{R_1} \tag{5.7}$$

In the conditions (5.4), both $\partial \triangle \varphi/\partial r$ and $\partial \triangle \varphi/\partial z$ are the differential coefficients of $\triangle \varphi$ in the direction normal to the boundary considered. Moreover, taking in account (5.7), for $z = 0$ this coefficient will be

$$\frac{\partial \triangle \varphi}{\partial z} = \left|\frac{dt}{d\zeta}\right| \frac{\partial \triangle \varphi}{\partial \varrho} = \frac{1}{R_1}(1 - \sin\vartheta)\frac{\partial \triangle \varphi}{\partial \varrho}$$

ϱ being the radial coordinate in the t plane (see Fig. 16b).

Hence the conditions to be satisfied by $\triangle \varphi$ in the t plane result from (5.4) as follows:

$$\varrho = 1; 0 < \vartheta < \pi: \quad \frac{\partial \triangle \varphi_{Iu}}{\partial \varrho} = \frac{\partial \triangle \varphi_{Il}}{\partial \varrho} \tag{5.8a}$$

$$\varrho = 1; \pi < \vartheta < 2\pi: \frac{\partial \triangle \varphi_{IIu}}{\partial \varrho} = \frac{\partial \triangle \varphi_{IIl}}{\partial \varrho} \tag{5.8b}$$

$$\varrho = 1; 0 < \vartheta < \pi: \; 2\lambda(1 - \sin\vartheta)\frac{\partial \triangle \varphi_{Iu}}{\partial \varrho} + \triangle \varphi_{Iu} - \triangle \varphi_{Il} = 0 \tag{5.8c}$$

$$\varrho = 1; \pi < \vartheta < 2\pi: 2\lambda(1 - \sin\vartheta)\frac{\partial \triangle \varphi_{IIu}}{\partial \varrho} + \triangle \varphi_{IIu} - \triangle \varphi_{IIl} = s\Gamma_0 \tag{5.8d}$$

$$\vartheta = 0, \pi; \varrho > 1: \triangle \varphi_{Il} - \triangle \varphi_{IIl} = -\frac{1}{2} s\Gamma_0 \tag{5.8e}$$

$$\vartheta = 0, \pi; \varrho < 1: \triangle \varphi_{Iu} - \triangle \varphi_{IIu} = +\frac{1}{2} s\Gamma_0 \tag{5.8f}$$

$$\vartheta = 0, \pi; \varrho > 1: \frac{\partial \triangle \varphi_{IIl}}{\partial \vartheta} = \frac{\partial \triangle \varphi_{Il}}{\partial \vartheta} \tag{5.8g}$$

$$\vartheta = 0, \pi; \varrho < 1: \frac{\partial \triangle \varphi_{IIu}}{\partial \vartheta} = \frac{\partial \triangle \varphi_{Iu}}{\partial \vartheta} \tag{5.8h}$$

with $\lambda = C_1 c/8 R_1$.

We now introduce $\triangle \varphi$ in the form:

$$\triangle \varphi_{Il} = s\Gamma_0 \left(a_0 + \sum_1^\infty a_n \varrho^{-n} \cos n\vartheta + \sum_1^\infty b_n \varrho^{-n} \sin n\vartheta \right) \tag{5.9a}$$

$$\triangle \varphi_{IIl} = s\Gamma_0 \left(\frac{1}{2} + a_0 + \sum_1^\infty a_n \varrho^{-n} \cos n\vartheta + \right.$$
$$\left. + \sum_1^\infty b_n \varrho^{-n} \sin n\vartheta \right) \tag{5.9b}$$

$$\triangle \varphi_{Iu} = s\Gamma_0 \left(-a_0 - \sum_1^\infty a_n \varrho^n \cos n\vartheta - \sum_1^\infty b_n \varrho^n \sin n\vartheta \right) \tag{5.9c}$$

$$\triangle \varphi_{IIu} = s\Gamma_0 \left(-\frac{1}{2} - a_0 - \sum_1^\infty a_n \varrho^n \cos n\vartheta - \sum_1^\infty b_n \varrho^n \sin n\vartheta \right) \tag{5.9d}$$

a form which satisfies both the differential equation of Laplace:

$$\frac{\partial^2 \triangle \varphi}{\partial t_1^2} + \frac{\partial^2 \triangle \varphi}{\partial t_2^2} \equiv \frac{1}{\varrho} \frac{\partial}{\partial \varrho} \left(\varrho \frac{\partial \triangle \varphi}{\partial \varrho} \right) + \frac{\partial^2 \triangle \varphi}{\varrho^2 \partial \vartheta^2} = 0$$

and the conditions (5.8a), (5.8b) and (5.8e), (5.8f), (5.8g), (5.8h).

The coefficients a and b are to be determined from the remaining conditions (5.8c, d). The latter may be considered as one condition which is to be satisfied in the interval $0 < \vartheta < 2\pi$. Introduction of (5.9) and separation of the parts which are symmetrical and antisymmetrical about $\vartheta = \pi$ leads to

$$\left.\begin{aligned} a_0 + \sum_1^\infty (n\lambda + 1)\, a_n \cos n\vartheta - \\ - \lambda \sin\vartheta \sum_1^\infty n\, b_n \sin n\vartheta = -\frac{1}{2} \quad 0 < \vartheta < 2\pi \end{aligned}\right\} \tag{5.10a}$$

$$\left.\begin{aligned} -\lambda \sin\vartheta \sum_1^\infty n\, a_n \cos n\vartheta + \\ + \sum_1^\infty (n\lambda + 1)\, b_n \sin n\vartheta = \begin{cases} +\frac{1}{2} & 0 < \vartheta < \pi \\ -\frac{1}{2} & \pi < \vartheta < 2\pi \end{cases} \end{aligned}\right\} \tag{5.10b}$$

It follows from the general character of the problem, that $\triangle \varphi$ will be symmetrical about the axis $y = 0$ (see Fig. 16a). Hence the solution in the form (5.9) must be symmetrical about $\vartheta = \pi/2$ and $\vartheta = 3\pi/2$, with the result that the coefficients a_n will be zero for all odd values of n and the coefficients b_n for all even values of n.

Taking this into account and introducing

$$\sum_1^\infty \frac{2}{(2n-1)\pi} \sin(2n-1)\vartheta = \begin{cases} +\frac{1}{2} & 0 < \vartheta < \pi \\ -\frac{1}{2} & \pi < \vartheta < 2\pi \end{cases}$$

the following set of equations is obtained for the determination of the coefficients

$$\left.\begin{aligned} 2a_0 - \lambda b_1 &= -1 \\ 2\lambda a_2 + 2(\lambda + 1) b_1 &= +\frac{4}{\pi} \\ n \geqq 1 \begin{cases} 2(2n\lambda + 1) a_{2n} + \lambda(2n-1) b_{2n-1} - \\ \qquad - \lambda(2n+1) b_{2n+1} = 0 \\ -\lambda 2n a_{2n} + \lambda(2n+2) a_{2n+2} + \\ \qquad + 2[\lambda(2n+1) + 1] b_{2n+1} = +\frac{4}{(2n+1)\pi} \end{cases} \end{aligned}\right\} \tag{5.11}$$

Taking the question strictly, both the number of equations and of unknown coefficients is infinite. But for practical application, it will be sufficient to consider the set formed by the first m equations only, m being a finite number fixed by the degree of approximation desired.

Now the number of unknowns is $(m+1)$, a fact, which may be used to choose a value for one of them, say a_0 or b_1, such as to obtain good convergence.

6. The Wing of Infinite Span Crossing the Slipstream Boundary (Continued). The changes in the aerodynamic properties of the wing due to the influence of the slipstream may be calculated from $\triangle\varphi$ as it is given by (5.9). Attention should be paid to the fact that in the latter formulae, $\triangle\varphi$ is given in the coordinates ϱ and ϑ of the t plane. As has been discussed above, ϱ will be equal to 1 for any point of the wing, the relation between y and ϑ being given by (5.6).

In analogy with (5.3) Γ may be decomposed into Γ_0 and $\triangle\Gamma$. Now introduction of (5.3), (5.2) and (5.9) in (4.3) results in

$$r > R_1: \triangle_I \Gamma = -2\,s\,\Gamma_0 \left(a_0 + \sum_1^\infty a_n \cos n\vartheta + \sum_1^\infty b_n \sin n\vartheta \right) \tag{6.1a}$$

$$r < R_1: \triangle_{II} \Gamma = -2\,s\,\Gamma_0 \left(\frac{1}{2} + a_0 + \sum_1^\infty a_n \cos n\vartheta + \sum_1^\infty b_n \sin n\vartheta \right) \tag{6.1b}$$

According to the assumptions introduced in **4**, v_x is zero outside the slipstream, whereas inside its value is $s\,V$. Hence I (26.3) leads to the change in lift $d\triangle L$ for the element dy:

$$\left.\begin{aligned} r > R_1: d\triangle_I L &= \varrho\, V \triangle_I \Gamma\, dy = \\ &= -2\varrho\, s\, V \Gamma_0 \left(a_0 + \sum_1^\infty a_n \cos n\vartheta + \sum_1^\infty b_n \sin n\vartheta \right) dy \end{aligned}\right\} \tag{6.2a}$$

$$\left.\begin{aligned} r < R_1: d\triangle_{II} L &= \varrho\, V (\triangle_{II} \Gamma + s\,\Gamma_0)\, dy = \\ &= -2\varrho\, s\, V \Gamma_0 \left(a_0 + \sum_1^\infty a_n \cos n\vartheta + \sum_1^\infty b_n \sin n\vartheta \right) dy \end{aligned}\right\} \tag{6.2b}$$

The total increase in lift $\triangle_I L$ for the part of the wing situated outside the slipstream is:

$$\triangle_I L = \int_{-\infty}^{-R_1} d\triangle_I L + \int_{+R_1}^{+\infty} d\triangle_I L$$

After introduction of (6.2a) and the variable ϑ instead of y, use is made of the relation,

$$a_0 + \sum_1^\infty a_n \cos n\vartheta + \sum_1^\infty b_n \sin n\vartheta = \\ = -\lambda (1 - \sin\vartheta) \left(\sum_1^\infty n\, a_n \cos n\vartheta + \sum_1^\infty n\, b_n \sin n\vartheta \right)$$

obtained by introduction of (5.9a), (5.9c) in (5.8c). The result is:

$$\left.\begin{aligned}
\triangle_I L &= -2\varrho\, s\, V\, \Gamma_0 R_1 \int_0^{\pi} \left(a_0 + \sum_1^{\infty} a_n \cos n\vartheta + \right. \\
&\qquad \left. + \sum_1^{\infty} b_n \sin n\vartheta \right) \frac{d\vartheta}{1-\sin\vartheta} = \\
&= 2\varrho\, s\, V\, \Gamma_0 R_1 \lambda \int_0^{\pi} \left(\sum_1^{\infty} n\, a_n \cos n\vartheta + \right. \\
&\qquad \left. + \sum_1^{\infty} n\, b_n \sin n\vartheta \right) d\vartheta = \\
&= 4\varrho\, s\, V\, \Gamma_0 R_1 \lambda \sum_1^{\infty} b_n = 2\, s\, \lambda\, L_{0\,II} \sum_1^{\infty} b_n
\end{aligned}\right\} \quad (6.3\text{a})$$

in which $L_{0\,II} = 2\varrho\, V\, \Gamma_0\, R_1$ is the lift on the part of the wing situated inside the slipstream in the absence of the latter.

In a similar way the total increase in lift $\triangle_{II} L$ for the part of the wing inside the slipstream is shown to be:

$$\triangle_{II} L = 4\varrho\, s\, V\, \Gamma_0 R_1 \left(1 - \lambda \sum_1^{\infty} b_n \right) = 2\, s\, L_{0\,II} \left(1 - \lambda \sum_1^{\infty} b_n \right) \quad (6.3\text{b})$$

Taken together, (6.3a), (6.3b) give the change in lift L for the whole wing

$$\triangle L = \triangle_I L + \triangle_{II} L = 2\, s\, L_{0\,II} \quad (6.4)$$

This shows the remarkable result, that the total increase in lift is equal to that, which would be obtained by elementary calculation taking into account only the direct influence of v_x. On the other hand (6.3a), (6.3b) indicate that the distribution of this increase in lift is different here, as both the parts of the wing inside and outside the slipstream contribute to it. Such a deviation from the results of the elementary calculation is only possible if w differs from zero. Its value may be calculated either from $(\partial \triangle \varphi / \partial \varrho)_{\varrho = 1}$ or from the change in lift given by (6.2a), (6.2b), either way leading to the result:

$$\left.\begin{aligned}
r > R_1\colon \quad w_I &= \frac{1}{2} \frac{s\, \Gamma_0}{R_1 \lambda} \left(a_0 + \sum_1^{\infty} a_n \cos n\vartheta + \sum_1^{\infty} b_n \sin n\vartheta \right) = \\
&= 4 \frac{s\, \Gamma_0}{C_1 c} \left(a_0 + \sum_1^{\infty} a_n \cos n\vartheta + \sum_1^{\infty} b_n \sin n\vartheta \right)
\end{aligned}\right\} \quad (6.5\text{a})$$

$$\left.\begin{aligned}
r < R_1\colon \quad w_{II} &= \frac{1}{2} \frac{s\, \Gamma_0}{R_1 \lambda} \left(1 + a_0 + \sum_1^{\infty} a_n \cos n\vartheta + \sum_1^{\infty} b_n \sin n\vartheta \right) = \\
&= 4 \frac{s\, \Gamma_0}{C_1 c} \left(1 + a_0 + \sum_1^{\infty} a_n \cos n\vartheta + \sum_1^{\infty} b_n \sin n\vartheta \right)
\end{aligned}\right\} \quad (6.5\text{b})$$

This quantity w is not identical with the velocity component $a w_1 (\Gamma_0)$ of the additional flow, but is this component together with the corresponding one of the additional airfoil flow (see I 14). The value of s being small, the induced angle of attack is, for both regions,

$$\alpha_i = \frac{w}{V} \tag{6.6}$$

in which w has the value given by (6.5).

As $\alpha_{i0} = 0$ and $\alpha_{i1} a = \alpha_i$, I (26.4) leads here to the induced resistance for the element

$$d D_i = d \triangle D_i = \varrho \Gamma_0 V \alpha_i d y \tag{6.7}$$

Introduction of (6.6) and (6.5a), (6.5b) and integration over the whole wing results in

$$D_i = \triangle D_i = 0 \tag{6.8}$$

As squares and higher powers of s have been neglected, this result does not indicate that D_i is exactly equal to zero, but only that if this quantity is expanded in a power series of s, the term in s^1 will vanish.

7. The Wing of Infinite Span Crossing the Slipstream Boundary. Numerical Results. The equations (5.11) show that the values of the coefficients a_n, b_n depend only on the parameter $\lambda = C_1 c/8R_1$. Now, as may be seen from the results given in 6, these coefficients determine the character of the changes in the aerodynamic properties of the wing. Hence it will be sufficient to consider here these changes for some values of λ which are of practical interest. As such were chosen, $\lambda = 1, 2, 3$. Taking C_1 to have the normal value 5, the range of c/R_1 covered by them is from 1.6 to 4.8.

The coefficients a_n and b_n have been calculated up to $n = 40$ and introduced in (6.1)—(6.5). The results are given in Figs. 17 and 18. For comparison there has been included the results obtained by taking the circulation proportional to the local velocity ("elementary calculation").

At the slipstream boundary the circulation (Fig. 17a) shows the sudden change which has been predicted in 4. For the part of the wing inside the boundary the circulation is much lower than would be expected from the results of the elementary calculation. For $\lambda = 2$ or 3 it even falls below Γ_0 in the whole region; for $\lambda = 1$, this is only the case in the neighborhood of the boundary. On the other hand outside the boundary the circulation is increased.

In contrast to $\triangle \Gamma$ the lift (Fig. 17b) is continuous, whereas its increase is positive for the whole wing. Compared with the result of the elementary calculation the lift curves show a considerable flattening out due to induction, resembling that observed for a wing having a sudden change in the angle of attack along its span. This effect increases with increasing values of λ. Its importance is still better shown in Fig. 18 which gives the total increase of the lift for the two parts

of the wing separately. It shows that the share of the outer part is important and that it even surpasses that of the inner part for $\lambda > 1.4$.

The values of w (Fig. 17c) are representative for α_i and dD_i also, as is shown by (6.6) and (6.7). As to the signs it should be remarked that α_i and dD_i will be positive for positive values of w.

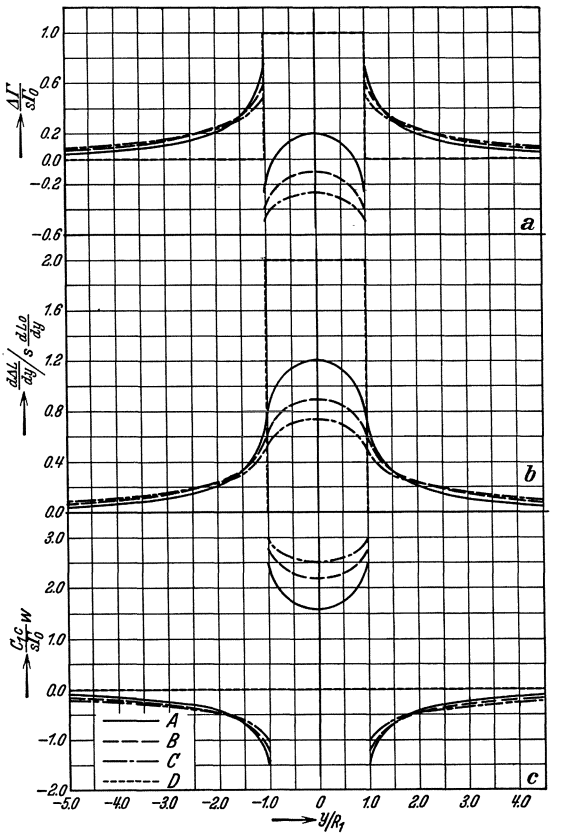

Fig. 17. Changes in circulation, lift and induced velocity due to the action of the slipstream; A: $\lambda = 1$, B: $\lambda = 2$, C: $\lambda = 3$, D: elementary.

Besides the effects considered thus far, the change in aerodynamic angle of attack accompanying α_i may be important from another point of view (see **13**). It may be calculated by using I (13.1), (6.6) and (5.2):

$$\triangle \alpha_e = -\alpha_i = -\frac{s}{2}\left(\alpha + \frac{C_0}{C_1}\right)\frac{C_1 c}{s\Gamma_0} w \qquad (7.1)$$

Now Fig. 17c shows that, for the values of λ considered here, $(C_1 c/s\Gamma_0)w$ ranges from -1.5 to $+3$. Introduction of these values, together with $s = 0.4$ and $(\alpha + C_0/C_1) = 10^0$ in (7.1) leads to the result that changes

in the aerodynamic angle of attack from about -6^0 to $+3^0$ may be found in normal cases.

In treating the wing of finite span, use will be made of the values of w obtained here. As the form in which they are given is too complicated, the following approximations will be used:

$$|y| > R_1: \; w_I = s\frac{\Gamma_0}{4R_1} w_I^*\left(\frac{y}{R_1}, \lambda\right) \tag{7.2a}$$

$$|y| < R_1: \; w_{II} = s\frac{\Gamma_0}{4R_1} w_{II}^*\left(\frac{y}{R_1}, \lambda\right) \tag{7.2b}$$

in which
$$w_I^*(y/R_1, \lambda) = b_{2\,I}(R_1/y)^2 + b_{4\,I}(R_1/y)^4 \tag{7.2c}$$
$$w_{II}^*(y/R_1, \lambda) = b_{0\,II} + b_{2\,II}(y/R_1)^2 + b_{4\,II}(y/R_1)^4 \tag{7.2d}$$
$$b_{2\,I} = -1.320 + 0.590\lambda - 0.086\lambda^2$$
$$b_{4\,I} = -0.183 + 0.326\lambda - 0.072\lambda^2$$
$$b_{0\,II} = +1.149 - 0.415\lambda + 0.057\lambda^2$$
$$b_{2\,II} = +0.381 - 0.235\lambda + 0.041\lambda^2$$
$$b_{4\,II} = +0.633 - 0.433\lambda + 0.077\lambda^2$$

The values of the coefficients were obtained in the following way. For the region I they were calculated for each value of λ separately, so as to make the exact and approximate values equal at the points $\vartheta = 0^0$, 30^0, corresponding with $y/R_1 = \pm 1, \pm 1.732$. After that they were expressed in polynomials of λ. For the region II the procedure was the same, the points considered being $\vartheta = 270^0$, 330^0, 360^0 ($y/R_1 = 0, \pm 0.577, \pm 1$).

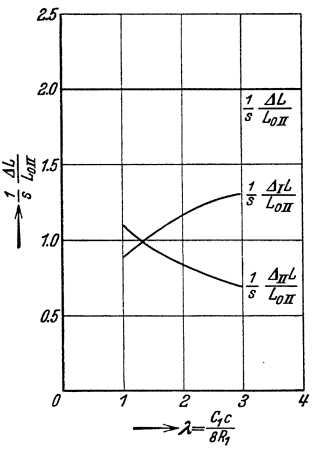

Fig. 18. Increase in lift on the part of the wing outside ($\triangle_I L$) and inside ($\triangle_{II} L$) the boundary.

8. The Wing of Finite Span Crossing the Slipstream Boundary. For the wing of finite span crossing the slipstream boundary the change in lift coefficient, due to the direct influence of v_x and v_z may be calculated by the method developed in **1**. This calculation leads again to $\triangle_1 C_L$, $\triangle_2 C_L$, $\triangle_3 C_L$ and $\triangle_4 C_L$, as they are given respectively by (2.2a, b, c, d).

The question of the influence of the term $a w_1(\Gamma_0)$ in (1.1b) or as it may be called, the influence of the slipstream boundary, is more complicated. After the discussion in **4**—**7**, it is evident that the fact that the wing crosses the boundary will cause an effect of the same character as in the case of the wing of infinite span. But, apart from this "direct influence" of the boundary, there will still be another effect "indirect influence", as here the original vortex system of the wing has trailing vortices, which will interact with the boundary.

Treating the latter question first, we introduce again the assumptions given in **3** in discussing the same subject for the wing outside the slip-stream boundary. Thus the boundary is replaced by a cylinder extending from $x = -\infty$ to $x = +\infty$ and the original vortex system of the wing by a horse-shoe vortex. The trailing vortices of the latter will be situated outside the boundary. From I **22** it is known that in this case the value of $a w_1 (\Gamma_0)$ in the region outside the boundary may be calculated by making use of the images of the trailing vortices, whereas inside the boundary it is zero. A rather lengthy calculation along the lines indicated already in **3** leads to the change in lift coefficient $\triangle_5 C_L$, due to the indirect influence of the boundary on the part of the wing situated outside it,

$$\triangle_5 C_L = -s C_{L0} \left(\frac{d C_L}{d \alpha}\right)_0 \frac{c_0}{b} f_5 (z_0, b, R_1, \psi_1) \tag{8.1}$$

with:

$$f_5 (z_0, b, R_1, \psi_1) = \\ = \frac{1}{8 \pi b} \left\{ -2 y_i \psi_1 + R \left[\sqrt{b^2 - \zeta_i^2} \log \frac{\left(\zeta_i \sqrt{b^2 - y_1^2} + y_1 \sqrt{b^2 - \zeta_i^2}\right)^2}{b^2 (y_1^2 - \zeta_i^2)} \right] \right\}$$

in which, as in **3**:

$$\zeta_i = y_i - i (z_0 - z_i)$$

$$y_i = \frac{R_1^2 b}{b^2 + z_0^2}$$

$$z_i = \frac{R_1^2 z_0}{b^2 + z_0^2}$$

$R [\ ]$ = real part of the complex number between brackets.

The change in lift coefficient $\triangle_6 C_L$, due to the indirect influence of the boundary on the part of the wing inside it, is always

$$\triangle_6 C_L = 0 \tag{8.2}$$

The calculation of the direct influence of the boundary will be based on the results given in **7** for the wing of infinite span. The velocity component w given there is the sum of the components of the additional flow and of the additional airfoil flow, corresponding with the terms $w_0 (\triangle \Gamma) + a w_1 (\Gamma_0)$ in (1.1 b).

As it is not possible to separate the two parts, we have to deviate from the way followed thus far and introduce the somewhat bold assumption that the quantity w is the same for the wing of finite span "wing a" and for the wing of infinite span "wing b" under the following conditions. For wing b the relative situation of wing and boundary is that given in **4**, but the radius R_1 of the boundary is equal to y_1, being the value of y for the point at which wing a crosses the boundary. The circulation Γ_0 and chord c of wing b are equal to that of wing a at the section $y = y_1$. Moreover s has the value calculated from the first equation of I (5.7) by introduction of the coordinate x_0 for the centre of wing a.

Now the change in lift coefficient $\triangle_7 C_L$, due to the direct influence of the boundary on the part of the wing outside it, is determined in the following way.

According to our assumptions, equation (1.1b) takes the form:

$$\frac{2}{C_1 c} \triangle_7 \Gamma = - w_I$$

Introduction of the value of w_I given by (7.2a) with

$$\Gamma_0 \to \Gamma_0 (y_1) = \frac{1}{2} C_{L0} V c_0 \sin \psi_1$$

$$R_1 \to y_1 = b \cos \psi_1$$

leads to $$\triangle_7 \Gamma = - \frac{1}{16} s C_{L0} C_1 \frac{c_0}{b} V c_0 \tan \psi_1 w_I^* \left(\frac{y}{y_1}, \lambda \right) \sin \psi$$

in which $w_I^* (y/y_1, \lambda)$ has the form given by (7.2c).

From this result the increase $\triangle_7 L$ is obtained by multiplication with ϱV and integration over the parts of the wing outside the boundary, resulting in the change in lift coefficient,

$$\triangle_7 C_L = s C_{L0} C_1 \frac{c_0}{b} f_7 (\psi_1, \lambda) \tag{8.3}$$

in which

$$f_7 (\psi_1, \lambda) = - \frac{1}{4\pi} \left[b_{2I} (1 - \cos 2\psi_1 - \psi_1 \sin 2\psi_1) + \right.$$
$$\left. + \frac{1}{12} b_{4I} (3 - 4 \cos 2\psi_1 + \cos 4\psi_1) \right]$$

and the coefficients b_{2I} and b_{4I} have the form given in 7.

The change in lift coefficient $\triangle_8 C_L$, due to the direct influence of the boundary on the part of the wing inside it, is determined in the same way, the difference being only that w_{II} and w_{II}^* from (7.2b, d) are used and the change in lift is integrated over the other part of the wing. The result is:

$$\triangle_8 C_L = s C_{L0} C_1 \frac{c_0}{b} f_8 (\psi_1, \lambda) \tag{8.4}$$

with

$$f_8 (\psi_1, \lambda) = - \frac{1}{8\pi} \tan \psi_1 \left\{ b_{0\,II} \left[2 \left(\frac{\pi}{2} - \psi_1 \right) + \sin 2\psi_1 \right] + \right.$$
$$+ \frac{1}{8} \frac{b_{2\,II}}{\cos^2 \psi_1} \left[4 \left(\frac{\pi}{2} - \psi_1 \right) + \sin 4\psi_1 \right] + \frac{1}{48} \frac{b_{4\,II}}{\cos^4 \psi_1} \left[12 \left(\frac{\pi}{2} - \psi_1 \right) - \right.$$
$$\left. \left. - 3 \sin 2\psi_1 + 3 \sin 4\psi_1 + \sin 6\psi_1 \right] \right\},$$

the coefficients b having again the form given in 7.

It should be remarked that, according to the assumptions introduced above, the value of λ is here to be calculated from

$$\lambda = \frac{C_1 c_0}{8 b} \tan \psi_1 \tag{8.5}$$

9. Summary of the Results for the Wing of Finite Span. The discussions given in 2, 3 and 8, have shown that, in the most general case,

the increase in lift coefficient $\triangle C_L$, due to the action of the propeller, may be decomposed into eight parts, indicated by $\triangle_1 C_L$ to $\triangle_8 C_L$. It may be useful to sum up the causes to which these parts are related:

$\triangle_1 C_L$, $\triangle_2 C_L$: direct influence of v_x,
$\triangle_3 C_L$, $\triangle_4 C_L$: direct influence of v_z,
$\triangle_5 C_L$, $\triangle_6 C_L$: indirect influence of the slipstream boundary,
$\triangle_7 C_L$, $\triangle_8 C_L$: direct influence of the slipstream boundary.

Odd suffixes indicate the part contributed by the part of the wing situated outside the region $r < R_1$, even suffixes that by the part inside this region.

The formulae by which the different parts are to be calculated, are indicated in Table 1.

TABLE 1.

	Wing in front of the propeller plane		Wing behind the propeller plane	
	$\lvert z_0 \rvert > R_1$	$\lvert z_0 \rvert < R_1$	$\lvert z_0 \rvert > R_1$	$\lvert z_0 \rvert < R_1$
$\triangle_1 C_L$	(2.2a), $\psi_1 = \frac{\pi}{2}$	(2.2a)	(2.2a), $\psi_1 = \frac{\pi}{2}$	(2.2a)
$\triangle_2 C_L$	0	(2.2b)	0	(2.2b)
$\triangle_3 C_L$	(2.2c), $\psi_1 = \frac{\pi}{2}$	(2.2c)	(2.2c), $\psi_1 = \frac{\pi}{2}$	(2.2c)
$\triangle_4 C_L$	0	(2.2d)	0	(2.2d)
$\triangle_5 C_L$	0	0	(3.1)	(8.1)
$\triangle_6 C_L$	0	0	0	0
$\triangle_7 C_L$	0	0	0	(8.3)
$\triangle_8 C_L$	0	0	0	(8.4)

The numbers in parenthesis relate to the formulae in question. If necessary the value of ψ_1, which is to be used in the special case, is added. Any part being zero, it is indicated by 0.

The meaning of the symbols in the formulae was explained as they were introduced, but it may be desirable to draw attention to two points of interest. The coordinate y_1 fixes the point at which the lifting vortex of the wing crosses the circle $r = R_1$, at which point the character of the velocity components changes (see I 5), whereas ψ_1 is determined by $\psi_1 = cos^{-1} y_1/b$. Again, a and s are the values of the ratio v_x/V, respectively at the propeller disc and at the plane $x = x_0$ through the lifting vortex.

For practical application it is important that the parts $\triangle_3 C_L$ and $\triangle_4 C_L$ do not depend on C_{L0}, whereas the others are proportional to it. Hence the total increase in lift may be written in the form:

$$\triangle C_L = b_0 + b_1 C_{L0} \tag{9.1}$$

in which

$$b_0 = \triangle_3 C_L + \triangle_4 C_L$$

$$b_1 = \frac{1}{C_{L0}} (\triangle_1 C_L + \triangle_2 C_L + \triangle_5 C_L + \triangle_6 C_L + \triangle_7 C_L + \triangle_8 C_L)$$

If now, for the wing in the absence of the propeller, C_L is given by:

$$C_{L0} = a_0 + a_1 \alpha \tag{9.2a}$$

the influence of the propeller changes it into

$$C_L = (a_0 + b_0 + a_0 b_1) + a_1 (1 + b_1)\alpha \tag{9.2b}$$

Two quantities which will be used in comparing experimental and calculated results, may be derived at once. They are:

The lift coefficient for the angle of attack at which C_{L0} is zero

$$(C_L)_{C_{L_0}=0} = b_0 \tag{9.3a}$$

and the change in slope of the lift,

$$\triangle \frac{dC_L}{d\alpha} = \frac{d \triangle C_L}{d\alpha} = b_1 a_1 \tag{9.3b}$$

It should be remarked that, of course, the coefficients a, b used here, have nothing to do with those introduced in 5.

10. Experimental Results. Most experiments with propeller and plane together, have been carried out with models in which a body was present, so that they do not give the influence of the propeller on an isolated wing, the theory of which has been developed in the foregoing sections. Hence only a few experimental results are available to check this theory.

The most complete series is that described by Wieselsberger[1]. These experiments were made with a rectangular wing ($2b = 0.960\,m$, $c = 0.160\,m$) and a propeller, the diameter of which was rather large ($D = 0.265\,m$). The wing was situated at a normal distance either in front of or behind the propeller. The distance z_0 from the wing to the propeller axis, which was always parallel to the direction of the undisturbed flow, varied from about $-0.2\,m$ to $+0.2\,m$ in both cases. Apart from the measurements without propeller, the latter was acting at one value of C_T only.

For comparison with the calculated results, the experimental results were considered in the range over which the relation between C_L and α is linear (in general about $-9^0 < \alpha < +9^0$).

Though the theory might be extended to the case of the rectangular wing without fundamental difficulties, the comparison will be based here on the assumption that the influence of the propeller is equal to that on the elliptic wing with equal span and aspect ratio (S/b^2). The lifting vortex is taken at one quarter chord behind the leading edge. For some quantities which varied slightly in the experiments, mean

[1] Ergebnisse der Aerodynamischen Versuchsanstalt zu Göttingen. I. Lief., p. 112, 1921.

values were introduced in the calculations which are given in Table 2. For the experimental results, the values of z_0, showing small variations with α, were taken constant and equal to their value at $\alpha = 0$.

In Figs. 19—23 both the experimental and the calculated results are given for the quantities $(C_L)_{C_{L_0}=0}$ and $\triangle (dC_L/d\alpha)$ [see (9.3a), (9.3b)], which are representative of the influence of the propeller on the wing in the range of α here considered. For the case in which the elementary calculation (taking only the direct influence of the increase in velocity in the slipstream into account) leads to a result differing from zero, this result has been included for comparison (Fig. 22).

TABLE 2.

	Wing	
	in front	behind
x_0	$-0.170\ m$	$+0.105\ m$
C_T	0.201	0.196
a	0.115	0.112
s	0.024	0.182

The first impression of these figures is, that there is a quite satisfactory agreement in $\triangle (dC_L/d\alpha)$ for the wing behind the propeller

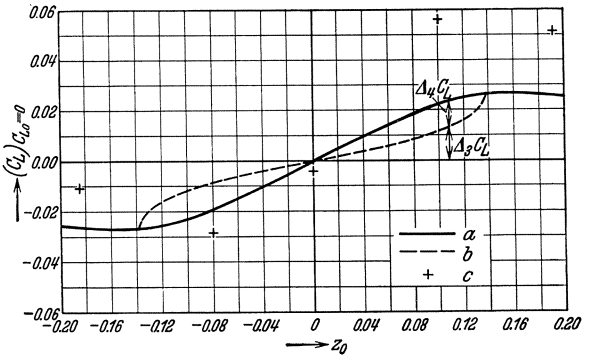

Fig. 19. Wing in front of the propeller, $(C_L)_{C_{L_0}=0}$
a, b = calculated. c = experimental.

and crossing the slipstream boundary (Fig. 22), whereas there are rather large discrepancies in some other cases. But, as the experimental results given are the small differences between relatively large quantities, these discrepancies may, at least partly, be attributed to the unavoidable inaccuracy of the experiments. The fact that the experimental points are rather scattered, points in the same direction.

Hence the final conclusion is that, though a more elaborate experimental check is urgently needed, the theory, for the moment may be considered as giving a picture of the real phenomena sufficiently accurate to serve as a basis for further investigation.

To give an impression of the relative importance of the different parts in which $\triangle C_L$ may be decomposed (see 9), their values are

included in the figures, except in Fig. 22, in which case they are given separately in Fig. 23. As was to be suspected in the latter case, $\triangle_2 (dC_L/d\alpha)$ which is equal to the result of the elementary calculation indicated above, dominates. Both $\triangle_1 (dC_L/d\alpha)$ and $\triangle_5 (dC_L/d\alpha)$ are

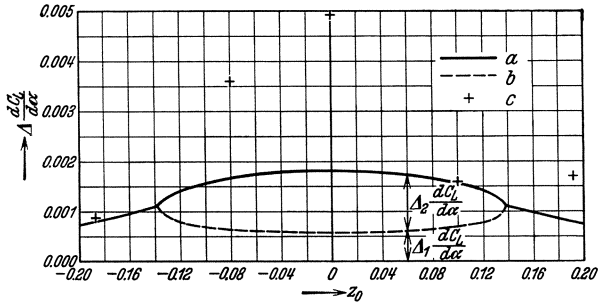

Fig. 20. Wing in front of the propeller, $\triangle (dC_L/d\alpha)$
a, b = calculated, c = experimental.

relatively unimportant here. Hence the main cause of the deviation between the results of the elementary and exact calculation is the difference between $\triangle_7 (dC_L/d\alpha)$ and $\triangle_8 (dC_L/d\alpha)$, which for $z_0 = 0$ is equal to about 30% of the total value of $\triangle (dC_L/d\alpha)$.

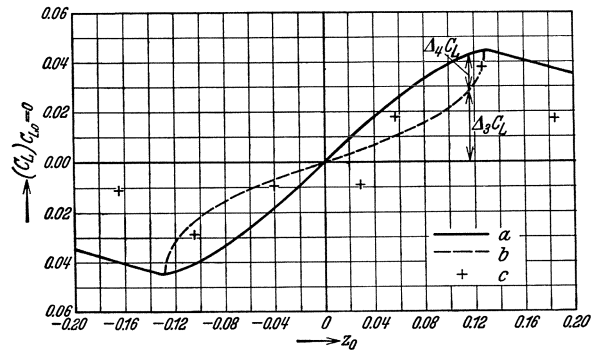

Fig. 21. Wing behind the propeller, $(C_L)_{C_{L_0}=0}$
a, b = calculated, c = experimental.

Considering again the results given in 7 this effect may be explained somewhat superficially in the following way. For the wing of infinite span, the increase in lift on the outer and the decrease on the inner part of the wing, corresponding respectively to $\triangle_7 C_L$ and $\triangle_8 C_L$, balance each other so as to make the total increase equal to the result of the elementary calculation. Now the wing of finite span may be considered to be derived from the wing of infinite span by cutting off its extreme ends. Though this will result in other minor changes in

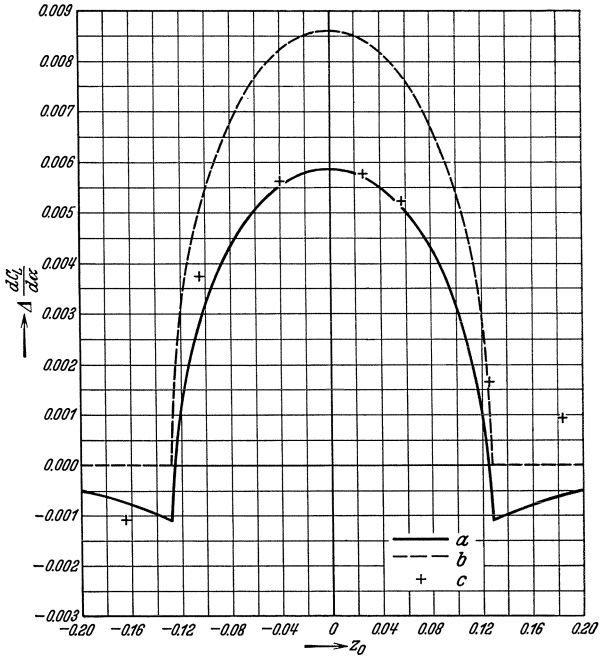

Fig. 22. Wing behind the propeller, $\triangle (dC_L/d\alpha)$
a = calculated, b = calculated (elementary), c = experimental.

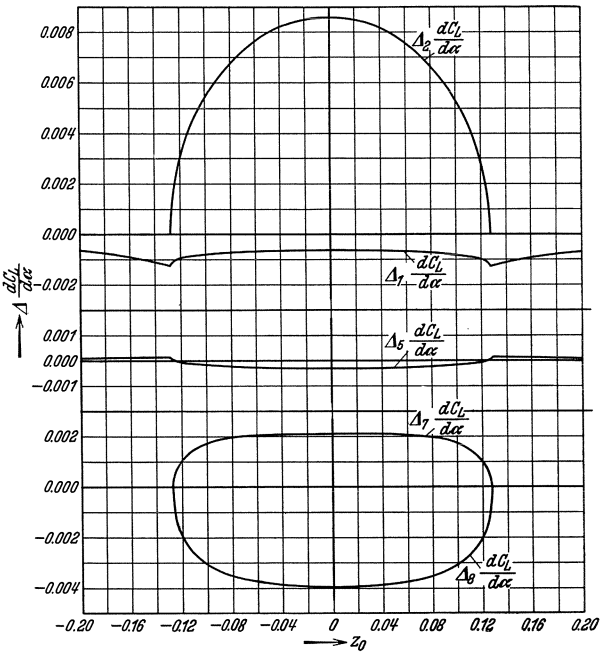

Fig. 23. Wing behind the propeller. Parts of $\triangle (dC_L/d\alpha)$.

$\triangle \Gamma$ too, the dominant fact will be, that $\triangle_7 C_L$ decreases, whereas $\triangle_8 C_L$ remains nearly unaltered.

The result that $\triangle C_L$ may be much less than would be predicted by the elementary calculation is confirmed by experiments of Bradfield[1] and also by some experiments by the Rijks-Studiedienst voor de Luchtvaart, the results of which have not yet been published.

As to $(C_L)_{C_{L_0}=0}$ it may be remarked, that here its maximum values of 0.026 (wing in front) and 0.044 (wing behind) correspond with changes in the angle of attack for the wing without propeller of about 0.35^0 and 0.6^0 respectively.

B. Interference Effects on Wings not Covered by the Theory of I C

11. Introduction. The theory developed in I C and II A starts from simplifying assumptions bearing upon both the properties of the propeller flow and those of the wing. Hence there may be discrepancies due to these simplifications between the results, the calculation of which is based on the theory and the experimental results. Though but little in the way of consistent experimental values are available on this subject a short discussion of the matter may be of interest.

The main differences between the real propeller flow and the simplified flow, on which the theory is based, have been discussed already in I 8 and 9. It will therefore be sufficient here to sum them briefly. They are: differences in the axial and radial components of the velocity, rotation in the slipstream, periodicity and eddying character of the flow, presence of a boundary region of finite thickness between the slipstream and the outer region. Another point, passed over without discussion thus far, is the fact that in general the propeller axis will not be parallel with the direction of the undisturbed flow. Moreover, the changes in pressure, due to the action of the propeller, have been left out of account.

As to the airfoil, it has been assumed that the aerodynamic properties of the wing section will not be changed by the influence of the propeller (see I 12). Even if this assumption is valid at small angles of attack, it is doubtful whether it is true at large angles, at which separation occurs. This question being the one of greatest interest it will be discussed separately (see 13) after some remarks on other effects (see 12).

12. Effects Not Connected with Separation. The fact that the propeller axis is not parallel to the direction of the undisturbed flow may be of practical importance. The main problem to be solved in extending the theory in this direction is the determination of the changes in the propeller flow due to this cause and the approximation of the results in such

[1] Preliminary Tests on the Effect on the Lift of a Wing of the Position of the Airscrew Relative to It. Br. A.R.C. R. and M. 1212, 1928-29.

a form that they may be used in calculation. The first part of this problem has been treated already by Misztal[1] both from the theoretical and experimental side; but, as his calculation is rather long, starting from the blade element theory of the airscrew, reference may preferably be made to the original publication.

Before proceeding to the influence of the other differences between the real and the calculated flow, a remark should be made on their general importance. As, together with another effect which will be indicated in **13**, these differences are responsible for discrepancies between calculated and experimental values, the results discussed in **10** may be considered to give an indication that in normal cases they will not be of prime importance.

The differences in the values of the velocity components, including those due to the rotation in the slipstream and to the gradual change in velocity at the slipstream boundary, will affect three different sides of the problem.

First of all they conflict with some of the assumptions on which the theory is based, *e. g.* that of the flow having a velocity potential everywhere except at the surface of discontinuity. But, if the propeller flow is not too irregular in this sense, this question will be of theoretical interest only.

A second point is the assumption that the properties of the wing section are equal to those of the same section in a parallel flow (see I **12**). It is evident that these properties may be altered by the propeller influence, as now both the magnitude and the direction of the velocity change from point to point. But it appears that the resulting effect will not be serious, if only the situation of the lifting vortex representing the wing is taken such as to give suitable mean values for the velocity components. As such, the position at one quarter chord was quite satisfactory in the case described in **10**.

The remaining point is the direct influence of the differences in the values of the velocity components to be introduced in the calculation. The most serious point in this respect is the fact, indicated already in I 8 that v_x will not be constant over the propeller disc, but may fall off sharply in the neighborhood of its axis. A first step to comply with this peculiarity is the following: The slipstream is considered to be composed of a central core, surrounded by the slipstream proper, both coaxial with the propeller. In the core, corresponding with the region of the propeller disc $[r < (1/2)\, D_1]$, occupied by the boss and less effective parts of the blade roots, v_x is zero. In the outer part, as before, v_x depends on a, which is constant in this region. As may be shown without difficulty, the latter quantity may be calculated from

[1] Zur Frage der schräg angeblasenen Propeller. Abh. a. d. Aerodyn. Inst. a. d. Techn. Hochsch., Aachen, Heft 11, 1932.

I (5.3) if only instead of C_T the value of the ratio $C_T : [1 - (D_1/D)^2]$ is introduced. This leads to an increase of v_x for that part of the wing which is situated in the outer region of the slipstream, but the effect may be partly balanced by the influence of the core in which v_x is zero. If we take $D_1 = 0.3\,D$, a rather large value, the result will be an increase of about 10 per cent in a and a corresponding increase of roughly 10 per cent in $\triangle C_L$, the wing being taken as situated outside the central core.

As has been indicated in I **9** the change in the velocity component v_z, due to the rotation in the slipstream, may surpass the value of this component in the idealized propeller flow. But as it will be antisymmetrical and occur in the slipstream region only, its influence, at least on the lift, will be negligible.

Though it is possible that the periodic and eddying character of the flow may influence the properties of the wing section, for the moment there are no results known which clearly show such an effect at small angles of attack.

The pressure gradient due to the action of the propeller will result in a kind of buoyancy, so that the resulting force depends on the volume of the body. Now for a wing the volume of the part situated in the region in which large pressure gradients exist, will be relatively small so that this effect may be left out of account.

Though lying somewhat outside of the problems discussed here, another interference effect should be mentioned. It is the influence of a stopped propeller on the lift and drag of a wing behind it. The results of experiments by Perring and Callen[1] show that this effect is most marked for the propeller directly ahead of and parallel to the wing, but that it exists also when the propeller is placed above or below the wing.

13. The Influence of the Propeller on Separation. The general characteristics of the phenomenon known under the name "separation" and the conditions which govern it, have been discussed in Division G. We may therefore start at once with the special points which are of present interest.

The flow around the wing in the presence of the propeller embodies three features which may influence separation: changes in angle of attack, changes in pressure gradient and turbulence.

In the absence of the propeller, separation will start at a certain angle of attack and a further increase of that angle for the whole wing leads in general to an increase of the region over which it takes place. If now the aerodynamic angle of attack of only a part of the wing is

[1] The Influence of a Stopped Airscrew on the Lift and Drag of an Aerofoil. Br. A.R.C. R. and M. 1347, 1930-31.

increased, a similar effect is to be expected. It should be remarked that this statement does not imply that the separation at any element of the wing depends only on its aerodynamic angle of attack, as it is influenced also by the flow around the elements in the neighborhood. Hence, as the interference effects involve local changes in the angle of attack, we have to face the possibility that the separation is influenced by them. The changes mentioned may result from different causes, such as the contraction of the flow, the rotation in the slipstream and the effects indicated by the terms "direct" and "indirect" influence of the slipstream boundary (see 8).

The general theory of separation shows that it depends on the pressure gradient along the surface of the body, a positive increase of pressure stimulating the separation. So the negative pressure gradient, due to the action of the propeller (see I, 6), may delay separation.

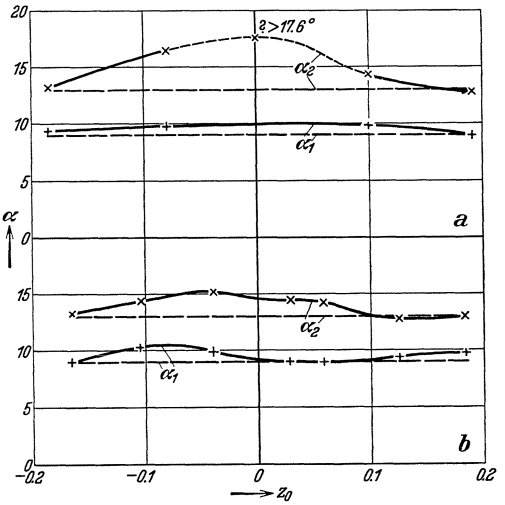

Fig. 24.
Influence of the propeller on separation. a) wing in front, b) wing behind. Continuous line—with propeller. Broken line—without propeller.

As has been pointed out by von Kármán[1], turbulence of the flow around the wing may change the character of the flow in the boundary layer and so influence the separation. This has been confirmed by the experiments of Millikan and Klein[2]. The results of these tests which were carried out with different degrees of turbulence, show clearly its important influence at those angles of attack at which separation occurs. The irregularities in the flow around the propeller may differ from the small and rapid fluctuations usually called turbulence, but this does not exclude the possibility that they may cause similar effects.

Since theoretical considerations lead to the conclusion that the propeller may influence separation, it is desirable to examine some experimental results from this point of view. Here again the results given by Wieselsberger[3] are used. From them the values of α_1 and α_2

[1] Quelques problèmes actuels de l'aérodynamique. Journées Tech. Intern. de l'Aéronautique, 1932.

[2] The Effect of Turbulence. Aircraft Engineering, p. 169, August, 1933.

[3] See footnote, p. 416.

were determined, being respectively the angle of attack at which the deviation from the linear relation between C_L and α starts, and that angle at which C_L reaches its maximum value. As the distance between successive angles of attack, for which the results are given, is rather large, the values obtained, especially for α_1, are somewhat uncertain. Hence they will represent the general character of the effect only. The results given in Fig. 24 show clearly that here the propeller influences both α_1 and α_2, an effect which, for the latter angle, is most marked for the wing in front of the propeller and close to its axis. For $z_0 = 0$ the angle α_2 even falls outside the region covered by the experiments. Though it is not possible to say what part of the effect should be attributed to the different causes discussed above, the results for the wing in front give ground for the belief that the influence of the pressure gradient may be important.

In this respect it is interesting to note the coincidence of large values of α_2 (Fig. 24) and of large discrepancies between the experimental and calculated results at small angles of attack (Fig. 20) for the wing in front at $z_0 = 0$ and $z_0 = -0.08$. These features suggest the possibility of attributing such discrepancies to the influence of the pressure gradient on the properties of the wing section.

The results of experiments made at the Rijks-Studiedienst voor de Luchtvaart by van der Maas[1], indicate that at full scale also, the propeller may have an influence similar to that discussed above. In these experiments the maximum value of C_L was determined both in gliding flight and at full throttle. In some cases these two values show differences much larger than would be predicted from the theoretical results given in Part A.

C. Influence of Propeller on Remaining Parts of Structure

14. Introduction. The influence of the propeller on those parts of the airplane which have not been considered thus far, will be due to the same causes as those which influence the wing structure, but their relative importance may be greatly different. So, for instance, the influence on tail-plane will show a marked resemblance with that on a wing, whereas in other cases, such as airplane bodies, the direct influence of the increase in axial velocity and effects due to the pressure gradient will dominate.

Here, more than in the problem treated previously, the question is important, whether the propeller flow may be represented by the simplified picture developed in I B. For, in the region behind the wing structure, the flow may be disturbed greatly by the influence of

[1] Unpublished.

the wings and body. Fig. 25, giving a result of early experiments at the Royal Aircraft Factory, Farnborough[1], illustrates this statement. It gives the square of the ratio (total velocity/airplane velocity) in a plane in front of the tail-plane for a single engined tractor airplane at low velocity and full throttle. Though in modern clean airplanes the flow may be less irregular, it still represents a condition which should not be overlooked.

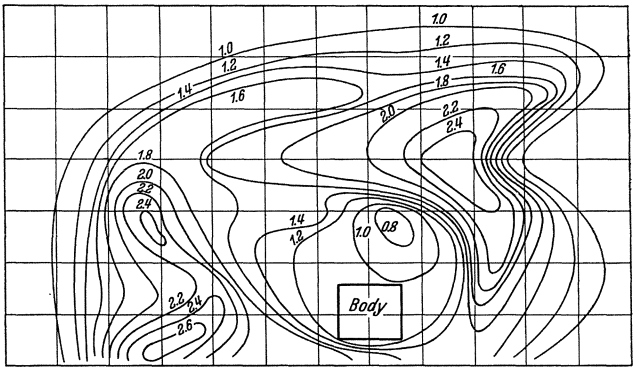

Fig. 25. Change in velocity $(V_t/V)^2$ in front of the tail-plane due to the action of the propeller.

15. The Influence of the Propeller on Stability and Controllability. Though, as has been indicated in the preceding section, the flow in the neighborhood of the tail-planes may be very irregular, it still remains attractive to investigate what may be learned from the theory developed in I C. Its applicability is based on the fact that, in their general behaviour, tail-planes are identical with wings. As this problem has not yet been worked out in detail, the discussion must be restricted to some general remarks.

First of all the influence of the propeller in a "skeleton airplane", consisting of a tail-plane and a propeller only, will be considered. As the tail-plane is far behind the propeller, it may be assumed to be at infinity. So, from the idealized flow around the propeller, as described in I 5, only the increase in axial velocity (v_x) need be taken into account. Other factors which may influence the action of the tail-plane are: the change in the propeller flow due to the obliquity of the propeller axis, the rotation in the slipstream and the eddying character of the flow (see **12**, and I **9** and **8**). The increment v_x will increase the normal force on the part of the tail-plane situated inside the slipstream. But, due to the influence of the boundary, this increase will be less than

[1] Exploration of the Airspeed in the Airscrew Slipstream of a Tractor Machine. Br. A.R.C. R. and M. 438, 1917-18.

would be expected from elementary calculation (see Fig. 26a). On the other hand, the boundary causes an increase in normal force for the tail-plane outside the slipstream (see Fig. 26b, c). Thus the boundary influence results in a flattening out of the effects, somewhat similar to that discussed previously for the wing (see 7). A change in angle of the elevator (or rudder) being accompanied by a change in normal force, a similar effect is to be expected in the action of the controls. Whether this part of the interference is important and whether it will increase or decrease the stability of the airplane are questions which for the moment cannot be definitely answered.

The most important change in the propeller flow due to the obliquity of the propeller axis is the existence of a velocity component v_z in the

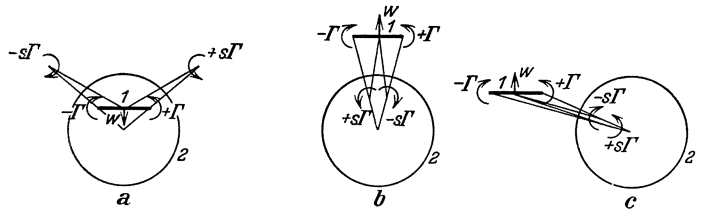

Fig. 26. Influence of the slipstream boundary on the tail-plane.
a) tail-plane inside, b), c) tail-plane outside. 1. tail-plane, 2. slipstream boundary.

slipstream. For positive "angles of attack" of the propeller axis, v_z will be positive and so its influence on the tail-plane will be identical with that due to an increase in downwash. As this effect will increase with the angle of attack, it results in a decrease of the longitudinal stability.

The influence of the rotation will be most marked for a tail-plane (for instance the fin) situated eccentrically in the slipstream.

The less favourable form which the section of a tail-plane may have when the control angle differs from zero, has given rise to the suspicion that such a section might be more liable than one of normal form to changes in its properties caused by the eddying character of the flow. Experiments in this direction made by the author have, however, failed to confirm this supposition.

In the complete airplane, the direct influence of the propeller on the tail-plane will be similar to that discussed above. But, as the propeller wing interference causes a change of the flow also, still other effects are to be considered here. As has been discussed in I 14, this change of flow may be decomposed into two parts, the additional airfoil flow d and the additional flow e. For the sake of brevity, the corresponding parts of the interference effect for the tail-plane will be indicated here by d and e also. The effect d depends on the additional vortex system of the wing, so that it may be calculated only after this system has been determined in detail. As to the effect e, the problem is less complicated.

The relative increase in velocity in the slipstream (s) being small, it is sufficient to consider only the additional flow related to the original vortex system of the wing; and then a further simplification may be obtained by substituting the corresponding horse-shoe vortex for this. Applying the results given in I 22, it is seen that inside the slipstream, the effect considered here is zero, whereas outside it this effect may be determined by using the images of the tip vortices of the wing. Fig. 27 indicates the result in the latter case: for the tail-plane above or below the slipstream (Fig. 27 a), w will be negative and if situated at the side (Fig. 27 b), it will be positive. Since here Γ and hence the absolute value of w increase with the angle of attack, the additional flow has the

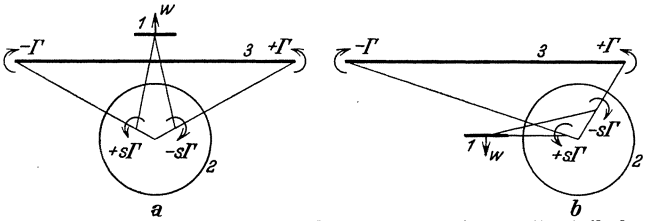

Fig. 27. Influence of the additional flow of the wing on the tail-plane.
a) tail-plane above
b) tail-plane sideways of } slipstream.
1. tail-plane, 2. slipstream boundary, 3. wing.

tendency to increase the stability in the case mentioned first (tail-plane above or below) and to decrease it in the latter case (tail-plane at the side). It should be remarked that in the exact calculation, the position of the tail-plane relative to the slipstream will enter and as it changes with the angle of attack, this introduces a new element influencing the stability.

16. The Influence of the Propeller on Stability and Controllability (Continued). Experimental results on the influence of the slipstream on longitudinal stability have been compiled by Bradfield[1]. They are analyzed in such way as to express the changes in downwash and in velocity at the tail-plane. After the discussion in the preceding section, it is evident that these changes will be apparent ones and that in general they need not agree with the mean values which would be obtained by direct measurement. This question has been discussed in some detail by Koning and Boelen[2], who give a method for determining these quantities from test results by using measurements with different elevator settings.

[1] Wind Tunnel Data on the Effect of Slipstream on the Downwash and Velocity at the Tail Plane. Br. A.R.C. R. and M. 1488, 1932-33.

[2] The Influence of the Aeroplane on the Action of the Tail Plane. Report A 363, Verslagen en Verhandelingen. RSL, Amsterdam. Vol. VI, p. 129.

The results given by Bradfield, including those of tests on twelve models of different type, always show an increase in downwash and in velocity due to the action of the propeller; that in downwash increasing with the angle of attack. The first effect will decrease the stability, whereas in general the latter tends to increase it. So these two will balance each other partly. The sign and value of the resulting effect will not only depend on the form and relative disposition of the parts of the airplane, but also on its angle of attack. A change in the latter may even result in a reversal of sign.

Some tests with models of two and three engined airplanes made by the author, the results of which are not available for publication at the moment, clearly show a decrease in longitudinal stability, due to the influence of the slipstream.

Thus far, static stability, a measure of which is the change in pitching moment with angle of attack at a constant value of C_T, has been considered. If instead of this criterion of stability, the stability of control, as introduced by van der Maas[1], is used, the direct influence of the propeller thrust should be taken into account. For, as here the change in moment coefficient with the angle of attack (and so with flight velocity) is considered at constant throttle, the value of C_T will not be constant and there will be a change in the part contributed by the thrust in the pitching moment.

The dynamic stability may be influenced by the action of the propeller in different ways, as both the forces and moments acting on the propeller and the slipstream influence on the remaining part of the airplane will show changes due to the motion of the airplane. Instead of entering here upon a discussion of these questions, reference may be made to the publications of the Royal Aircraft Establishment[2], Glauert[3] and Hartshorn, Hirst and Midwood[4] dealing with these problems.

17. Miscellaneous Questions. After the discussion on the influence of the propeller on the wing and tail-plane, little need be said regarding its influence on the remaining parts of the structure, since, for reasons already mentioned in the introduction, the propeller-body interference is left out of present account. The modern trend toward "cleaner" design leads to a reduction of the number and size of the parts considered here and thus makes the question of the influence of the propeller on

[1] Elevator Curves, Their Determination by Means of Flying Tests and Their Significance for the Judgment of the Stability. Verslagen en Verhandelingen, RSL, Amsterdam. Vol. V, p. 140.

[2] The Behaviour of the Slipstream on a Phugoid Oscillation. Br. A.R.C. R. and M. 464, 1918-19.

[3] The Stability Derivatives of an Airscrew. Br. A.R.C. R. and M. 642, 1919-20.

[4] Wind Tunnel Tests on a Model of the "Wapiti" Including the Effect of the Slipstream on Certain Derivatives, Br. A.R.C. R. and M. 1419, 1931-32.

them one of lesser importance. As a consequence, this influence will in general be of interest only for those parts which are situated in the slipstream, this being the region in which the changes in the flow due to propeller action are most marked.

It is evident that there will be an increase in drag over these parts, due to increased velocity. Furthermore the body considered being of good stream-line shape and having its plane or axis of symmetry parallel to the direction of the undisturbed flow, the change in direction due to the propeller action may, by spoiling the flow, cause a considerable increase in resistance. In this respect special attention should be paid to the rotation in the slipstream.

Experiments such as those by Dryden and Kuethe[1] and Lyon[2] have shown that turbulence of the flow may influence the drag of a stream-line body considerably, an effect due to a change in flow in the boundary layer. There is, therefore, a possibility that a similar effect may result from the irregularities in the propeller flow, but there is no experimental evidence confirming this. It is true that the results of tests of Lock and Johansen[3] and of Bateman and Johansen[4] on propeller body interference together with the analysis by Lock and Bateman[5] show the existence of a spoiling effect, but this may be due to quite different causes. First of all, the rotation in the slipstream may result in a rather high suction on the tail of the body, causing an increase in its resistance. The importance of this effect is demonstrated by the experiments of Johansen[6] in which the rotation was decreased by radial vanes, leading to a definite decrease in body drag.

Moreover, if in these cases a part of the spoiling effect is due to an influence of the propeller on the flow in the boundary layer, it should be noted that we have here to do with two questions which are fundamentally different. In the experiments mentioned, the blade roots of the propeller crossed the boundary layer of the body and so influenced it directly. On the other hand the possible effect, ascribed above to the eddying character of the flow, would not be due to a solid body in direct contact with the boundary layer, but to the irregularities of the flow

[1] Effect of Turbulence in Wind Tunnel Measurements, U.S. N.A.C.A. Technical Report No. 342, 1930.

[2] The Effect of Turbulence on the Drag of Airship Models. Br. A.R.C. R. and M. 1511, 1932-33.

[3] Pressure Plotting a Streamline Body with Tractor Airscrew Running. Br. A.R.C. R. and M. 1230, 1928-29, and R. and M. 1284, 1929-30.

[4] Pressure and Force Measurements on Airscrew-Body Combinations. Br. A.R.C. R. and M. 1380, 1931-32.

[5] Analysis of Experiments on the Interference Between Bodies and Tractor and Pusher Airscrews. Br. A.R.C. R. and M. 1445, 1931-32.

[6] Improvement of Airscrew Body Performance by Means of Radial Vanes. Br. A.R.C. R. and M. 1495, 1932-33.

caused by the presence of a body (here the propeller) at some distance. It is evident, that in these two cases the effect may be quite different.

Thus far, in discussing the influence of the propeller on the parts of the airplane, it has been assumed tacitly that these parts behave like isolated bodies. But in the actual airplane, even in absence of the propeller, there will be interference effects among these parts. As to the question how these effects are influenced by the propeller, little is known for the moment. The only experiments made with the special aim of investigating this part of the propeller airplane interference are those by Ower, Warden and Jones[1]. They were carried out with a model consisting of a stream-line body, propeller and wing, the latter in different positions. The results of these tests which were restricted to small angles of attack, show that the propeller did not alter the interference effects greatly. For the positions of the wing showing bad interference effects without propeller, it caused a slight improvement. On the other hand there are indications that the propeller may spoil the flow for other positions of the wing. Moreover a spoiling effect, due to the rotation in the slipstream, was observed. It is thought that the improvement due to the propeller action may be caused by the negative pressure gradient in the slipstream preventing separation.

[1] The Effect of a Tractor Airscrew on Body-Wing Interference. Br. A.R.C. R. and M. 1512, 1932-33.

INDEX

Printed by Universitätsdruckerei H. Stürtz A.G., Würzburg.

Turbulenz. **Physikalische Statistik und Hydrodynamik.** Von Dr. **Hans Gebelein,** VDI, Stuttgart. Mit 40 Textabbildungen. VIII, 177 Seiten. 1935. RM 12.50; gebunden RM 14.—

Das vorliegende Werk ist das Ergebnis von Forschungen über das Turbulenzproblem, die der Verfasser 1932 in Göttingen bei Professor Prandtl in Angriff genommen hat. Das Ziel war, durch Heranziehung statistischer Schlußweisen, die in den letzten Jahrzehnten auf vielen Gebieten der Physik mit großem Erfolg angewendet worden sind, die theoretische Hydrodynamik so zu entwickeln oder zu begründen, daß sie die Erscheinungen der Turbulenz umfaßt. Bei den vorliegenden Untersuchungen erscheint daher die Hydrodynamik als ein Zweig der physikalischen Statistik. Daher wechseln in dieser Abhandlung Abschnitte mehr statistischen Inhalts und solche mehr hydrodynamischen Inhalts miteinander ab. Das mathematische Rüstzeug sind in erster Linie die Methoden der Wahrscheinlichkeitsrechnung. Da die Wahrscheinlichkeitsrechnung bis heute in den Ingenieurwissenschaften noch kaum Anwendung gefunden hat, können ihre Grundtatsachen nicht als bekannt vorausgesetzt werden. Daher bringt das erste Kapitel eine kurze Einführung in die Wahrscheinlichkeitsrechnung. Im zweiten Kapitel schließt sich dann eine Darstellung der Grundlagen der physikalischen Statistik an, wobei im Mittelpunkt der Untersuchungen das Problem des Zusammenhanges zwischen deterministischer Mechanik und physikalischer Statistik steht. Nachdem auf diese Weise die Grundlagen für die Behandlung der Strömungsvorgänge in statistischer Auffassung gewonnen sind, wird in den folgenden drei Kapiteln die statistische hydrodynamische Theorie entwickelt. Der systematische Aufbau führt zu drei hydrodynamischen Theorien, die sich gegenseitig ergänzen und deren Gültigkeitsbereiche in klar erkennbarer Weise einander ablösen. Es ist dies die Theorie der idealen, der zähen und der turbulent fließenden Flüssigkeit. Die Theorie der idealen Flüssigkeit entsteht durch Außerachtlassen der statistischen Streuungen, die Theorie der zähen Flüssigkeit aber durch deren Berechnung mit Hilfe der Vorstellungen des Maxwell-Boltzmannschen Gasmodells. Die dritte, neue Theorie endlich entsteht auf Grund einfacher hydrodynamischer Tatsachen, die zur Theorie des Turbulenztensors und zu den Grundgleichungen der „statistischen Hydrodynamik" führen. So sind als Ergebnis des fünften Kapitels Gleichungen gewonnen, von denen vermutet werden kann, daß sie die turbulenten Strömungsvorgänge umfassen. Dies nachzuweisen ist eine der Aufgaben der nächsten beiden Kapitel, in denen nun die Verbindung mit der experimentellen Turbulenzforschung hergestellt wird. Dabei wird in erster Linie in Kapitel VI auf die umfangreichen Versuche im Kreisrohr Bezug genommen. Besonders geben die Experimente auch Aufschluß über diejenigen Konstanten, die in die Theorie eingehen, so daß die Untersuchungen bis zu einem gewissen Abschluß geführt werden können.

Das Gebiet der turbulenten Strömungsvorgänge, das von der Theorie der „statistischen Hydrodynamik" beherrscht wird, erweist sich als ein Erscheinungsgebiet mit durchaus eigenen Gesetzmäßigkeiten. Zu ihnen den Weg zu zeigen und dieses bisher geheimnisvolle Gebiet der theoretischen Erkenntnis zu erschließen, ist das Ziel dieser Untersuchungen.

Theorie der Luftkräfte. Von Professor Dr. **Richard Fuchs,** Berlin. Mit 224 Abbildungen im Text und in einem Anhang. VIII, 310 und 24 Seiten. 1935. Gebunden RM 30.—

Inhaltsübersicht: Mathematische Hilfsmittel. — Ergebnisse der klassischen Hydrodynamik. — Zweidimensionale Strömungsvorgänge. Der Tragflügel von unendlicher Breite. Besondere Tragflügelprofile bei zweidimensionaler Strömung. — Der Tragflügel von endlicher Breite. — Auftriebsverteilung bei gegebener Tragflügelgestaltung. — Der Mehrdecker. — Theorie des Widerstandes ohne Berücksichtigung der Reibung. Entstehung der Zirkulation. — Widerstand und Zähigkeit. — Namen- und Sachverzeichnis. — Abbildungsanhang.

Mechanik des Flugzeugs. Von Professor Dr. **L. Hopf,** Aachen. Unter teilweiser Mitwirkung von S. del Proposto. Mit 268 Textabbildungen. VIII, 339 Seiten. 1934. Gebunden RM 30.—

(Band II und I des Werkes: „Aerodynamik" von R. Fuchs, L. Hopf und Fr. Seewald.)

Hydro- und Aeromechanik nach Vorlesungen von L. Prandtl. Von Dr. phil. **O. Tietjens,** Mitarbeiter am Forschungs-Institut der Westinghouse Electric and Manufacturing Co., Pittsburgh Pa., U.S.A. Mit einem Geleitwort von Professor Dr. **L. Prandtl,** Direktor des Kaiser Wilhelm-Institutes für Strömungsforschung in Göttingen.

Erster Band: **Gleichgewicht und reibungslose Bewegung.** Mit 178 Textabbildungen. VIII, 238 Seiten. 1929. Gebunden RM 15.—*

Zweiter Band: **Bewegung reibender Flüssigkeiten und technische Anwendungen.** Mit 237 Textabbildungen und 28 Tafeln. VIII, 299 Seiten. 1931. Gebunden RM 23.—

---

* The books published before July 1, 1931 are sold with a price reduction of 10%.

PUBLISHER: JULIUS SPRINGER · BERLIN

Die Grundlagen der Tragflügel- und Luftschraubentheorie.

Von **H. Glauert,** M. A., Fellow of Trinity College Cambridge. Übersetzt von Dipl.-Ing. **H. Holl,** Danzig. Mit 115 Textabbildungen. VI, 202 Seiten. 1929. RM 12.75; gebunden RM 13.75*

Zweck des Buches ist eine Darstellung der Tragflügel- und Luftschraubentheorie auch für solche Leser, die keine strömungstechnischen Vorkenntnisse besitzen. Das Werk beginnt daher mit fünf Kapiteln Einführung in die Strömungslehre; es folgt die konforme Abbildung, die ebene Tragflügelströmung, der Einfluß der Widerstandswirbel und der Zähigkeit, sowie die Grenzschichttheorie und die Zirkulation, sodann die Wirkung der Wirbelzöpfe bei verschiedenen Formen des Eindeckers, die gegenseitige Beeinflussung von Tragflügeln und die Störungen durch den Windkanal. — Für die Treibschraube wird die Strahltheorie, die Tragflügeltheorie und das Verhalten im Windkanal betrachtet. — Die Darstellung ist klar und leicht lesbar, die Übersetzung so gut, daß man nur gelegentlich die englische Quelle spürt..... *„Nachrichten für Luftfahrer."*

(German translation of H. Glauert, The elements of aerofoil and airscrew theory. Cambridge, 1926.)

Angewandte Hydromechanik.

Von Dr.-Ing. **Walther Kaufmann,** o. Professor der Mechanik an der Technischen Hochschule München.

Erster Band: **Einführung in die Lehre vom Gleichgewicht und von der Bewegung der Flüssigkeiten.** Mit 146 Textabbildungen. VIII, 232 Seiten. 1931. RM 12.50; gebunden RM 14.—*

Zweiter Band: **Ausgewählte Kapitel aus der technischen Strömungslehre.** Mit 210 Textabbildungen. VII, 293 Seiten. 1934. RM 16.50; gebunden RM 18.—

Mathematische Strömungslehre.

Von Dr. **Wilhelm Müller,** Privatdozent an der Technischen Hochschule Hannover. Mit 137 Textabbildungen. IX, 239 Seiten. 1928. RM 18.—; gebunden RM 19.50*

Vorträge aus dem Gebiete der Aerodynamik und verwandten Gebieten

(Aachen 1929). Herausgegeben von **A. Gilles, L. Hopf, Th. v. Kármán.** Mit 137 Abbildungen im Text. IV, 221 Seiten. 1930. RM 18.50; gebunden RM 20.—*

Vorträge aus dem Gebiete der Hydro- und Aerodynamik

(Innsbruck 1922). Herausgegeben von **Th. v. Kármán** und **T. Levi-Civita.** Mit 98 Abbildungen im Text. IV, 251 Seiten. 1924. RM 18.—*

Theorie des Segelfluges.

Von Dr.-Ing. **W. Klemperer.** („Abhandlungen aus dem Aerodynamischen Institut an der Technischen Hochschule Aachen", Heft 5.) Mit 17 Abbildungen im Text. 78 Seiten. 1926. RM 6.90*

Aufgaben aus der Flugzeugstatik.

Im Auftrage der Deutschen Versuchsanstalt für Luftfahrt, E. V., Berlin-Adlershof, herausgegeben von Professor Dr.-Ing. **K. Thalau** und Dr.-Ing. **A. Teichmann,** Berlin-Adlershof. Mit 90 Einzelaufgaben, 106 Tabellen und 291 Textabbildungen. XI, 345 Seiten. 1933. RM 26.50; gebunden RM 28.—

---

* The books published before July 1, 1931 are sold with a price reduction of 10%.